

Design of Polymeric Materials: Novel Functionalized Polymers for Enhanced Oil Recovery & Gas Sorption Applications

by

Alison Jean Scott

A thesis
presented to the University of Waterloo
in fulfillment of the
thesis requirement for the degree of
Doctor of Philosophy
in
Chemical Engineering

Waterloo, Ontario, Canada, 2019

© Alison Jean Scott 2019

Examining Committee Membership

The following served on the Examining Committee for this thesis. The decision of the Examining Committee is by majority vote.

| | |
|--------------------------|--|
| External Examiner | Mehrab Mehrvar Professor Department of Chemical Engineering, Ryerson University |
| Supervisor | Alexander Penlidis Professor Department of Chemical Engineering, University of Waterloo |
| Internal Members | Ali Elkamel Professor Department of Chemical Engineering, University of Waterloo |
| | Xianshe Feng Professor Department of Chemical Engineering, University of Waterloo |
| Internal-external Member | Susan Tighe Professor Department of Civil and Environmental Engineering, University of Waterloo |

Author's Declaration

This thesis consists of material all of which I authored or co-authored: see Statement of Contributions included in the thesis. This is a true copy of the thesis, including any required final revisions, as accepted by my examiners.

I understand that my thesis may be made electronically available to the public.

Statement of Contributions

Throughout my PhD, I have been fortunate to have my own research work (and work accomplished in a collaborative manner) published in several reputable peer-reviewed journals. A full list of publications (and how they relate to the contents of this thesis) is provided in Chapter 10, Section 10.2. For publications where I am listed as the first author, I collected and analyzed the data and wrote the original draft of the manuscript; any material published elsewhere and used in this thesis is my own work. For papers where I am a co-author, my specific contributions are stated below.

A.J. Scott, V.A. Gabriel, M.A. Dubé and A. Penlidis (2019). “Making the Most of Parameter Estimation: Terpolymerization Troubleshooting Tips”, *Processes* (Special Issue: Computational Methods for Polymers), vol. 7, no. 7, p. 444.

- In this collaborative project with the University of Ottawa, I handled the data analysis, interpreted the results, and wrote the original draft of the manuscript. V.A. Gabriel and M.A. Dubé contributed experimental data and provided insights about the analysis of results.
- Selections from this paper are included in Chapter 5 (specifically, the case studies and discussion presented in Section 5.2).

K.M.E. Stewart, **A.J. Scott** and A. Penlidis. “Evaluation of Doped and Undoped Poly (o-anisidine) as Sensing Materials for a Sensor Array for Volatile Organic Compounds”, Accepted in *Polymers for Advanced Technologies*, September 2019.

- My role in this project was to help collect sorption data (using the experimental procedures described in Section 7.4), to analyze the data sets using principal component analysis, and to contribute to the explanation of results. K.M.E. Stewart collected the majority of the experimental data and wrote the first draft of the paper.
- Parts of this paper are included in Chapter 6 (specifically, the case study presented in Section 6.3.1).

Abstract

As material requirements for particular applications become more specific and strict, using a targeted approach to design polymeric materials becomes a necessity. Following a general design framework prevents researchers from using trial-and-error approaches or shoehorning materials into applications for which they are non-optimal. To obtain polymer products with desirable properties (both fundamental characteristics and for a specific application), one must always begin with an awareness of existing materials and methods. This background knowledge informs preliminary design of experiments, which in turn provides insight for additional experiments to synthesize (and characterize) optimally designed materials.

A general framework for the design of polymeric materials has been developed in this thesis, and the specific aspects are grounded in two independent case studies. These two distinct (yet related) case studies have been selected to demonstrate that the framework is not limited to a particular industry or application, nor to a specific type of polymeric material. In Case Study #1, water-soluble terpolymers (and related polymerization kinetics) are investigated for use in polymer flooding during enhanced oil recovery (EOR). In contrast, Case Study #2 examines a variety of polymeric materials that have the potential to be used for acetone gas sensing (for diabetic applications). Both case studies use the same general design framework in a sequential, iterative manner to move towards optimally designed materials for each target application.

Polymers are already used in EOR; the most common synthetic material used for polymer flooding is partially hydrolyzed polyacrylamide (HPAM). In many cases, polymers for EOR are exposed to high temperatures, high shear rates, and high concentrations of salt in the reservoir. The shortcomings of HPAM include poor thermal stability, poor shear stability, and poor brine compatibility. As a result, HPAM can degrade during EOR, thus lowering molecular weight averages and reducing oil recovery efficiency. Therefore, the target for Case Study #1 is to build on existing knowledge to improve acrylamide-based polymers for enhanced oil recovery.

Important characteristics of polymeric materials for EOR include good viscosity modification (achieved through water solubility, high molecular weight averages and the incorporation of carboxylate ions), reasonable chemical stability (achieved by incorporating high levels of amide groups into the polymer), and a good distribution of ions along the polymer backbone (that is, a targeted sequence length distribution). HPAM (a copolymer of acrylamide (AAm) and acrylic acid (AAc)) meets these requirements, but the thermal and shear stability concerns described above have not been considered. Therefore, a third comonomer, 2-acrylamido-2-methylpropane sulfonic acid (AMPS) can be added to the polymer formulation, as the bulky sulfonic acid groups are expected to improve thermal stability and protect the main chain from shear degradation. When a multi-component polymer like AMPS/AAm/AAc is being considered for any application,

understanding and manipulating ternary reactivity ratios (which are related to both the cumulative terpolymer composition and the sequence length distribution) is essential.

Therefore, once the AMPS/AAm/AAC terpolymer is selected for enhanced oil recovery, relationships between (experimental) synthesis conditions and polymer properties can be researched, verified and exploited. First, a comprehensive study (involving both an examination of the literature and a series of designed screening experiments) is performed to establish the effect of synthesis conditions (like pH, ionic strength, monomer concentration and feed composition) on the terpolymerization kinetics and product terpolymer properties. Deliberate design of screening experiments (designed considering the ‘rule-of-thumb’ for ternary reactivity ratio estimation) makes it possible to establish that the key factors within the experimental range studied are ionic strength (which affects cumulative terpolymer composition and sequence length distribution), monomer concentration (which affects molecular weight averages) and feed composition (which, of course, impacts the cumulative composition of the terpolymer product).

Given the results of the screening experiments, two optimal terpolymers of AMPS/AAm/AAC are designed, synthesized, characterized and tested. The designed terpolymers have polymer properties that agree with model predictions, but (more importantly) show excellent EOR performance. In a series of sand-pack flooding experiments (simulating enhanced oil recovery in a reservoir), the designed terpolymers perform much better than reference materials. The newly synthesized terpolymers achieve an overall oil recovery of (on average) 78.0% for one optimal material and 88.7% for the second optimal material. In contrast, the commercially available reference material allows for an overall oil recovery of 59.8%. Therefore, the design framework has allowed us to converge upon optimal terpolymer formulations with excellent EOR application performance.

The same general framework is applied to inform the design, synthesis and characterization of polymeric sensing materials for acetone detection. Highly concentrated breath acetone measurements are correlated with high levels of blood glucose, so detecting acetone gas could be useful in a non-invasive breath sensor for diabetic applications. In this case, key design considerations (to inform potential backbone selection) include operational temperature (and the glass transition temperature of candidate polymeric materials), surface morphology, and the chemical behaviour of the target analyte. Solubility parameters, for example, can be used to provide insight about the compatibility of the target analyte (acetone) and potential sensing materials. For polymeric sensing materials, the most important characteristics are sensitivity and selectivity. Sensitivity studies provide information about how well the target analyte sorbs onto the polymeric material (that is, whether there is a strong affinity towards acetone), and selectivity measures how well the target analyte sorbs in the presence of other interferent gases.

After preliminary screening (based on a detailed literature review), three polymer backbones and three metal oxide dopants are selected as promising candidates for acetone sensing. Polyaniline, polypyrrole and poly(methyl methacrylate) are doped with varying quantities of SnO₂, WO₃ and ZnO nanoparticles. In a series of screening experiments, 30 materials are synthesized and evaluated in terms of acetone sorption (using a uniquely designed gas sensing set-up and a highly specialized gas chromatograph). The most promising materials are evaluated further, both in terms of surface morphology and in terms of selectivity (measurement of acetone sorption in the presence of acetaldehyde, ethanol and benzene). In general, pure polyaniline and pure polypyrrole show the most promise of the materials studied; poly(methyl methacrylate) does not sorb acetone at all, and metal oxide doping (using these dopants and up to 20 wt% doping) does not improve application performance.

In the customized experiments, adjustments are made to polymer synthesis steps in an attempt to improve the properties of the polymeric sensing materials (especially in terms of selectivity). One customization option that is investigated is the acid-doping of polyaniline (synthesis in an aqueous oxalic acid solution) to change the backbone charge, thereby taking advantage of the polarity of acetone. Another customization option involves the synthesis of copolymers of polyaniline and polypyrrole (both in water and in oxalic acid solution) by combining the two monomers in a single formulation. Product characterization shows some improvement over the original (screening) materials, but further improvement is still possible. Therefore, this target application can continue to benefit from sequential, iterative steps towards optimality.

Ultimately, both case studies overlap when the general design framework is considered. An awareness of existing materials and methods can inform statistically designed preliminary experiments, which eventually lead to optimally designed materials for specific (targeted) applications. The contents of this thesis (especially the two major case studies) and several related publications demonstrate that this framework is useful and relevant for design of polymeric materials. The effectiveness is visible throughout the research process, but it is especially evident in the application performance of the final (optimal) product, along with the flexibility of the design approach with respect to expanding into new areas, at the same time by minimizing time and effort.

Acknowledgements

It has been an honour to work under the supervision of Prof. Alex Penlidis. I have grown as a researcher and as an individual over the past many years, largely thanks to his guidance and support. I am so grateful for the mentorship that he has provided, and I feel very fortunate to have had this experience.

Throughout my studies, I have benefited immensely from the knowledge and experience of many friends and colleagues. Kate Stewart, Yasaman Amintowlieh, Nicole Francis, Hadi Izadi, Niousha Kazemi, Noushin Majdabadifarahani, Afsaneh Nabifar, Marzieh Riahinezhad and Pouyan Sardashti have all influenced my research journey, and I am thankful for each of them. I have also appreciated the support of the Chemical Engineering department – special thanks to Ralph Dickhout and Bert Habicher for their problem-solving expertise.

I have been fortunate to collaborate with (and learn from) many individuals beyond the Chemical Engineering department at the University of Waterloo. I am especially grateful to Prof. Eihab Abdel-Rahman, Mohamed Arabi, Prof. Marc Dubé, Vida Gabriel, Dr. Nina Heinig, Prof. Neil McManus, Prof. Laura Romero-Zerón and Jan Venne. I would also like to acknowledge the financial support from the Natural Sciences and Engineering Research Council (NSERC) of Canada and OMNOVA Solutions, USA.

Finally, I am extremely thankful for my friends and family. They have helped me to maintain perspective and have supported me throughout this journey. I am blessed beyond measure.

Table of Contents

| | |
|--|-------|
| Examining Committee Membership..... | ii |
| Author’s Declaration..... | iii |
| Statement of Contributions..... | iv |
| Abstract..... | v |
| Acknowledgements..... | viii |
| List of Figures..... | xiii |
| List of Tables..... | xviii |
| Chapter 1. Introduction..... | 1 |
| 1.1 Problem Statement..... | 1 |
| 1.2 Research Hypotheses..... | 2 |
| 1.3 Research Objectives..... | 3 |
| 1.4 Thesis Organization..... | 4 |
| Chapter 2. Literature Background for Case Study #1 – Enhanced Oil Recovery..... | 7 |
| 2.1 Enhanced Oil Recovery..... | 7 |
| 2.1.1 Existing Materials and Methods..... | 9 |
| 2.1.2 Application Requirements..... | 14 |
| 2.1.3 Backbone Selection..... | 20 |
| 2.1.4 Product Customization..... | 22 |
| 2.2 Kinetics of Free Radical Polymerization..... | 22 |
| 2.2.1 Free Radical Copolymerization..... | 23 |
| 2.2.2 Free Radical Terpolymerization..... | 25 |
| 2.3 Reactivity Ratio Estimation..... | 28 |
| 2.3.1 Design of Experiments for Reactivity Ratio Estimation..... | 28 |
| 2.3.2 Reactivity Ratio Estimation using the Error-in-Variables Model..... | 33 |
| 2.4 Terpolymerization Kinetics of AMPS/AAm/AAc..... | 46 |
| 2.4.1 Effect of pH..... | 48 |
| 2.4.2 Effect of Ionic Strength..... | 50 |
| 2.4.3 Effect of Monomer Concentration..... | 51 |
| 2.4.4 Effect of Feed Composition..... | 53 |
| Chapter 3. Experimental Methodology for Case Study #1 – Enhanced Oil Recovery..... | 54 |
| 3.1 Materials..... | 54 |
| 3.2 Polymer Synthesis..... | 54 |
| 3.2.1 Screening Experiments..... | 54 |
| 3.2.2 Optimally Designed Experiments..... | 56 |
| 3.3 Characterization of Polymer Properties..... | 57 |

| | | |
|------------|--|-----|
| 3.3.1 | Conversion | 57 |
| 3.3.2 | Composition..... | 57 |
| 3.3.3 | Molecular Weight | 58 |
| 3.3.4 | Sequence Length Distribution..... | 59 |
| 3.3.5 | Thermal Stability | 60 |
| 3.3.6 | Additional Characterization | 60 |
| 3.4 | Characterization of Application-Specific Properties..... | 60 |
| 3.4.1 | Rheology..... | 60 |
| 3.4.2 | Enhanced Oil Recovery | 60 |
| Chapter 4. | Results and Discussion for Case Study #1 – <i>Enhanced Oil Recovery</i> | 67 |
| 4.1 | Screening Experiments..... | 67 |
| 4.1.1 | Effect of pH..... | 67 |
| 4.1.2 | Effect of Ionic Strength..... | 71 |
| 4.1.3 | Effect of Monomer Concentration | 82 |
| 4.1.4 | Effect of High NaCl Content | 85 |
| 4.1.5 | Concluding Remarks on Terpolymerization Screening Experiments..... | 92 |
| 4.2 | Optimally Designed Experiments | 93 |
| 4.2.1 | Justification of Experimental Conditions..... | 93 |
| 4.2.2 | Investigation of Polymer Properties..... | 95 |
| 4.2.3 | Investigation of Application-Specific Properties..... | 108 |
| 4.2.4 | Concluding Remarks on Optimally Designed Terpolymers for EOR | 124 |
| Chapter 5. | An Aside: Comparison of Binary and Ternary Reactivity Ratio Estimates | 126 |
| 5.1 | Using Appropriate Estimation Procedures..... | 126 |
| 5.1.1 | Case Study: Terpolymerization of AN/Sty/MA | 127 |
| 5.1.2 | Direct Comparison of Binary and Ternary Systems (AMPS/AAm/AAC)..... | 128 |
| 5.1.3 | Concluding Remarks on Appropriate Estimation Procedures | 137 |
| 5.2 | Terpolymer Troubleshooting Tips | 138 |
| 5.2.1 | Addressing Composition Restrictions & Ill-Conditioned Systems | 139 |
| 5.2.2 | Improved Performance with Ternary Data | 147 |
| 5.2.3 | Concluding Remarks on Terpolymer Troubleshooting Tips | 158 |
| 5.3 | Concluding Remarks | 159 |
| Chapter 6. | Literature Background for Case Study #2 – <i>Polymeric Sensing Materials</i> | 161 |
| 6.1 | Polymeric Sensing Materials for Detection of Acetone..... | 161 |
| 6.1.1 | Existing Materials and Methods | 161 |
| 6.1.2 | Application Requirements | 164 |

| | | |
|------------|--|-----|
| 6.1.3 | Backbone Selection..... | 167 |
| 6.1.4 | Product Customization..... | 173 |
| 6.2 | Extensions to Detection of Additional VOCs | 178 |
| 6.2.1 | Detection of Formaldehyde - Project Background | 179 |
| 6.2.2 | Significant Contributions | 180 |
| 6.3 | Sensing Material Array for Volatile Organic Compounds..... | 182 |
| 6.3.1 | Case Study: Evaluation of Doped and Undoped PoANI as Materials for a Sensing Array | 182 |
| Chapter 7. | Experimental Methodology for Case Study #2 – <i>Polymeric Sensing Materials</i> .. | 189 |
| 7.1 | Materials..... | 189 |
| 7.2 | Polymer Synthesis for Acetone Detection | 189 |
| 7.2.1 | Synthesis of PANI..... | 190 |
| 7.2.2 | Synthesis of PPy | 190 |
| 7.2.3 | Preparation of PMMA..... | 191 |
| 7.2.4 | Customized Synthesis: Acid Doping and Copolymerization..... | 191 |
| 7.3 | Characterization of Polymer Properties | 194 |
| 7.4 | Characterization of Application-Specific Properties..... | 195 |
| 7.4.1 | Deposition of Materials for Analysis of Sorption..... | 195 |
| 7.4.2 | Experimental Set-Up for Sorption Studies | 195 |
| Chapter 8. | Results and Discussion for Case Study #2 – <i>Polymeric Sensing Materials for Acetone Detection</i> | 197 |
| 8.1 | Screening Experiments: Metal Oxide-Doped Polyaniline, Polypyrrole and Poly(methyl methacrylate)..... | 197 |
| 8.1.1 | Sensitivity – Acetone Sorption | 197 |
| 8.1.2 | Selectivity – Mixtures of 4 Gases | 211 |
| 8.1.3 | Concluding Remarks on Screening Experiments for Acetone Sensing..... | 216 |
| 8.2 | Customized Experiments: Acid-Doped Polymers and Copolymers | 217 |
| 8.2.1 | Investigation of Polymer Properties..... | 217 |
| 8.2.2 | Investigation of Application-Specific Properties..... | 224 |
| 8.2.3 | Concluding Remarks on Customized Materials for Acetone Detection | 229 |
| Chapter 9. | Commonalities between Case Studies – <i>Design of Polymeric Materials: Synthesis of Design Prescriptions</i> | 231 |
| 9.1 | Design Framework | 231 |
| 9.2 | Awareness of Existing Materials and Methods..... | 235 |
| 9.3 | Design of Preliminary Experiments | 237 |
| 9.4 | Design of Optimal Materials | 239 |

| | | |
|-------------|--|-----|
| 9.5 | Extensions and Concluding Remarks..... | 241 |
| Chapter 10. | Overall Thesis Conclusions, Main Thesis Contributions, and Recommendations | 242 |
| 10.1 | Overall Thesis Conclusions..... | 242 |
| 10.2 | Main Thesis Contributions..... | 244 |
| 10.3 | Recommendations for Future Work..... | 246 |
| 10.3.1 | Short-Term Recommendations..... | 246 |
| 10.3.2 | Long-Term Recommendations..... | 248 |
| References | | 251 |
| Appendix A. | Derivation of Equations for Multi-Component Polymerization Kinetics..... | 271 |
| A.1 | Derivation of the Alfrey-Goldfinger Model..... | 271 |
| A.2 | Original Derivation of the Recast Alfrey-Goldfinger Model (from Ratios)..... | 272 |
| A.3 | New Derivation of the Alfrey-Goldfinger Model (from Kinetics)..... | 273 |
| Appendix B. | Computational Package for EVM..... | 277 |
| B.1 | Computational Package Demonstration..... | 277 |
| B.2 | Relevant Statistical Principles for the Error-in-Variables Method..... | 280 |
| B.2.1 | Additive and Multiplicative Error..... | 280 |
| B.2.2 | Calculation of G as an EVM Program Output..... | 282 |
| Appendix C. | Relevant Data & Calculations for Case Study #1..... | 283 |
| C.1 | Sample Gravimetry Calculations..... | 283 |
| C.2 | Sample Elemental Analysis Calculations..... | 285 |
| C.3 | Molecular Weight Analysis (Supplemental Information)..... | 287 |
| C.4 | Thermal Gravimetric Analysis (Supplemental Information)..... | 292 |
| C.5 | Additional Rheology Data..... | 295 |
| C.6 | Sand-pack Flooding Experimental Details..... | 297 |
| Appendix D. | Relevant Data & Calculations for Case Study #2..... | 299 |
| D.1 | Sample Gas Chromatography Analysis..... | 299 |
| D.2 | Experimental Data from Sensitivity and Selectivity Studies..... | 303 |
| D.3 | Comparison of Acetone Sorption Performance..... | 307 |

List of Figures

| | |
|--|----|
| Figure 2.1: Simplified Schematic of Polymer Flooding Process for Enhanced Oil Recovery | 9 |
| Figure 2.2: Incremental Oil Recovery vs. Amount of Polymer Injected | 10 |
| Figure 2.3: Comparison of Sweep Efficiency in (a) Water Flooding and (b) Polymer Flooding [22]..... | 18 |
| Figure 2.4: Temperature Distribution of Global Oil Fields (as of 1998) [45] | 19 |
| Figure 2.5: Linking Application Requirements to Polymer Properties | 21 |
| Figure 2.6: Terminal Model for Free-Radical Copolymerization..... | 23 |
| Figure 2.7: Effect of Sequentially Designed Experiments for the Copolymerization of BA/MMA | 31 |
| Figure 2.8: Optimally Designed Experiments for Ternary Reactivity Ratio Estimation (as per [60])..... | 33 |
| Figure 2.9: Nested-Iterative Algorithm for the Error-in-Variables-Model (EVM) | 34 |
| Figure 2.10: Graphical Representation of EVM (inspired by [67])..... | 35 |
| Figure 2.11: Fineman-Ross Plots for the Copolymerization of MDO/VAc with (a) $M_1 = \text{MDO}$ ($r_{\text{MDO}} = 1.06$; $r_{\text{VAc}} = 1.83$) and (b) $M_1 = \text{VAc}$ ($r_{\text{MDO}} = 1.96$; $r_{\text{VAc}} = 2.03$) | 39 |
| Figure 2.12: EVM-obtained RR Estimates and JCRs for the Copolymerization of MDO/VAc with (a) $M_1 = \text{MDO}$ ($r_{\text{MDO}} = 1.19$; $r_{\text{VAc}} = 1.87$) and (b) $M_1 = \text{VAc}$ ($r_{\text{MDO}} = 1.01$; $r_{\text{VAc}} = 1.72$)... .. | 40 |
| Figure 2.13: Comparison of Prediction Performance for RR Estimates Obtained by (a) F-R and (b) EVM | 41 |
| Figure 2.14: Prediction Performance of RR Estimates for HEA/DCP Copolymerization (Obtained by Linear RRE Techniques)..... | 42 |
| Figure 2.15: EVM-obtained RR Estimates and JCRs for the Copolymerization of HEA/DCP using the Instantaneous Model ($r_{\text{HEA}} = 1.28$; $r_{\text{DCP}} = 0.56$) and the Cumulative Model ($r_{\text{HEA}} = 1.32$; $r_{\text{DCP}} = 0.55$) | 43 |
| Figure 2.16: Prediction Performance of RR Estimates Obtained using EVM..... | 44 |
| Figure 2.17: Comparison of Results for the Copolymerization of BMA/BA using the Instantaneous Model ($r_{\text{BMA}} = 2.11$; $r_{\text{BA}} = 0.49$) and the Cumulative Model ($r_{\text{BMA}} = 2.11$; $r_{\text{BA}} = 0.50$) | 46 |
| Figure 3.1: Optimally Designed Experiments for Ternary Reactivity Ratio Estimation (Constrained Design for AMPS/AAm/AAC Terpolymerization) | 55 |
| Figure 3.2: Experimental Set-Up for Sand-pack Flooding Tests..... | 61 |
| Figure 3.3: Particle Size Distribution of Sand for Sand-pack Flooding Tests..... | 62 |
| Figure 4.1: Comparison of Reactivity Ratio Estimates for AMPS/AAm/AAC at pH 5, 7 and 9.. | 68 |
| Figure 4.2: Predicted Cumulative Composition from Screening Experiments for AAm-rich Terpolymer at pH 5, 7 and 9 | 69 |
| Figure 4.3: Comparison of Reactivity Ratio Estimates for AMPS/AAm/AAC | 72 |
| Figure 4.4: Reactivity Ratio Estimates for AMPS/AAm/AAC at IS = 1.5 M; Comparison of Results at Constant/Varying pH and [M]..... | 73 |
| Figure 4.5: Cumulative Composition for AMPS-rich Terpolymer at IS = 0.9 M and 1.5 M..... | 75 |
| Figure 4.6: Cumulative Composition for AAm-rich Terpolymer at IS = 0.9 M and 1.5 M..... | 76 |
| Figure 4.7: Prediction of Instantaneous ‘Blocky’ Triad Fractions at IS = (a) 0.9 M and (b) 1.5 M | 78 |
| Figure 4.8: Optimized Instantaneous Triad Fractions for Enhanced Oil Recovery at (a) IS = 0.9 M and (b) IS = 1.5 M ($A = f_{\text{AMPS},0}$, $B = f_{\text{AAm},0}$, $C = f_{\text{AAC},0}$)..... | 80 |

| | |
|---|-----|
| Figure 4.9: Cumulative Terpolymer Composition Predictions from Optimized Triad Fractions at (a) IS = 0.9 M and (b) IS = 1.5 M..... | 82 |
| Figure 4.10: Comparison of Reactivity Ratio Estimates for AMPS/AAm/AAc at [M] = 0.5 M, 1.0 M and 1.5 M..... | 83 |
| Figure 4.11: Effect of Monomer Composition on Peak Average Molecular Weights for $f_{AMPS,0}/f_{AAm,0}/f_{AAc,0}$ = (a) 0.8/0.1/0.1, (b) 0.1/0.2/0.7 and (c) 0.1/0.8/0.1 | 84 |
| Figure 4.12: Effect of High NaCl Content on the Conversion Level of AMPS/AAm/AAc ($f_{AMPS,0}/f_{AAm,0}/f_{AAc,0}$ = 0.1/0.8/0.1 and [M] = 1.0 M); with data from Scott et al. [80] | 86 |
| Figure 4.13: Poor Dissolution of Solids in PAAm5 | 87 |
| Figure 4.14: Effect of High NaCl Content on the Conversion Level of PAAm at [M] = 1.0 M.. | 88 |
| Figure 4.15: Conversion Level Adjustment (NaCl Consideration) for PAAm at [M] = 1.0 M ... | 89 |
| Figure 4.16: High NaCl Mass Adjustment for the Conversion of AMPS/AAm/AAc ($f_{AMPS,0}/f_{AAm,0}/f_{AAc,0}$ = 0.1/0.8/0.1 and [M] = 1.0 M); with data from Scott et al. [80] | 90 |
| Figure 4.17: Repeatability of Gravimetric Results for Optimal Terpolymers; $f_{AMPS,0}/f_{AAm,0}/f_{AAc,0}$ = | 96 |
| Figure 4.18: Cumulative Terpolymer Composition for Terpolymer Opt1 ($f_{AMPS,0}/f_{AAm,0}/f_{AAc,0}$ = 0.21/0.69/0.10)..... | 97 |
| Figure 4.19: Cumulative Terpolymer Composition for Terpolymer Opt2 ($f_{AMPS,0}/f_{AAm,0}/f_{AAc,0}$ = 0.10/0.75/0.15)..... | 98 |
| Figure 4.20: Effect of Conversion on (a) Peak Average Molecular Weight, (b) Weight Average Molecular Weight and (c) Bulk Intrinsic Viscosity (and Comparison to Reference Polymer Alcoflood 955) for Optimal Terpolymers..... | 103 |
| Figure 4.21: ^{13}C -NMR Spectra of Terpolymer #1 in Buffer/D ₂ O at 68°C | 104 |
| Figure 4.22: ^{13}C -NMR Spectra of Terpolymer #2 in Buffer/D ₂ O at 68°C | 105 |
| Figure 4.23: Thermal Behaviour (from Thermal Gravimetric Analysis) for Optimally Designed Terpolymers, Reference Material, and a Designed AAm/AAc Copolymer | 106 |
| Figure 4.24: Sample Results (from Terpolymer #1) for Strain Sweep Test at 10 Hz (solution concentration of 0.01 g/mL in water) | 109 |
| Figure 4.25: Complex Viscosity Profiles for AMPS/AAm/AAc Terpolymers in Water and Buffer for (a) Terpolymer #1 and (b) Terpolymer #2 | 111 |
| Figure 4.26: Elastic and Loss Modulus for AMPS/AAm/AAc Terpolymers in Water for | 113 |
| Figure 4.27: Elastic and Loss Modulus for AMPS/AAm/AAc Terpolymers in Buffer for..... | 114 |
| Figure 4.28: Dynamic Mechanical Loss Tangent ($\tan\delta$) for Designed Terpolymers and Reference Polymer | 115 |
| Figure 4.29: Resistance Factor (RF) from Polymer Flow Performance Testing | 117 |
| Figure 4.30: Residual Resistance Factor (RRF) from Polymer Flow Performance Testing | 118 |
| Figure 4.31: Sand-pack System Pressure throughout Heavy Oil Displacement Testing for | 121 |
| Figure 5.1: Experimental [125] and Predicted Terpolymer Composition for the AN/Sty/MA Terpolymer, using (a) Binary and (b) Ternary Reactivity Ratio Estimates for Prediction (Inspired by [135])..... | 128 |
| Figure 5.2: Comparison of Reactivity Ratio Estimates for Comonomers AMPS/AAm using Copolymerization Data (Binary Estimates) and Terpolymerization Data (Ternary Estimates) . | 130 |
| Figure 5.3: Comparison of Reactivity Ratio Estimates for Comonomers AMPS/AAc using Copolymerization Data (Binary Estimates) and Terpolymerization Data (Ternary Estimates) . | 130 |
| Figure 5.4: Comparison of Reactivity Ratio Estimates for Comonomers AAm/AAc using Copolymerization Data (Binary Estimates) and Terpolymerization Data (Ternary Estimates) . | 131 |

| | |
|---|-----|
| Figure 5.5: Experimental [80] and Predicted Terpolymer Composition for the AMPS/AAm/AAC Terpolymer using (a) Binary and (b) Ternary Reactivity Ratio Estimates for Prediction..... | 133 |
| Figure 5.6: Experimental [80] and Predicted Terpolymer Composition for the AMPS-rich Terpolymer ($f_{AMPS,0}/f_{AAm,0}/f_{AAc,0} = 0.8/0.1/0.1$)..... | 134 |
| Figure 5.7: Experimental and Predicted Terpolymer Composition for Sub-Optimal AMPS/AAm/AAC Terpolymerizations, using (a) Binary and (b) Ternary Reactivity Ratio Estimates for Prediction..... | 135 |
| Figure 5.8: Experimental and Predicted Terpolymer Composition for the Sub-Optimal Terpolymer ($f_{AMPS,0}/f_{AAm,0}/f_{AAc,0} = 0.5/0.1/0.4$)..... | 136 |
| Figure 5.9: HOST/EAMA/PAG Terpolymer Composition Prediction for $f_{1,0}/f_{2,0}/f_{3,0} = 0.4/0.5/0.1$ (Experimentally Measured Composition for TPF10 from Pujari et al. [138]) | 141 |
| Figure 5.10: HOST/EAMA/PAG Terpolymer Composition Prediction for $f_{1,0}/f_{2,0}/f_{3,0} = 0.1/0.1/0.8$ | 142 |
| Figure 5.11: Feed Compositions for the BA/BMA/lim Terpolymer, as Reported by Ren et al. [134]..... | 143 |
| Figure 5.12: Ternary Reactivity Ratio Estimates for the Terpolymerization of BA(1)/BMA(2)/lim(3), with Data from Ren et al. [134]..... | 145 |
| Figure 5.13: Ternary Reactivity Ratio Estimates for the Terpolymerization of BA/MMA/EHA for (a) $M_1/M_2/M_3 = BA/MMA/EHA$ and (b) $M_1/M_2/M_3 = MMA/EHA/BA$, with Instantaneous Data from [137]..... | 149 |
| Figure 5.14: Ternary Reactivity Ratio Estimates for the Terpolymerization of BA/MMA/EHA for (a) $M_1/M_2/M_3 = BA/MMA/EHA$ and (b) $M_1/M_2/M_3 = MMA/EHA/BA$, with Cumulative Data from [137]..... | 151 |
| Figure 5.15: Prediction of Cumulative Terpolymer Composition for BA/MMA/EHA ($f_{BA,0}/f_{MMA,0}/f_{EHA,0} = 0.1/0.1/0.8$) (Experimental Data and Binary Predictions from [137])..... | 153 |
| Figure 5.16: Comparison of Residuals for Sty/MMA/MA Terpolymer Composition Predictions | 155 |
| Figure 5.17: Terpolymerization Feed Compositions for AN/Sty/MMA (Data from [143]) | 156 |
| Figure 5.18: Ternary Reactivity Ratio Estimates (RREs) for the Terpolymerization of AN/Sty/MMA with Data from Brar and Hekmatyar [143] | 157 |
| Figure 6.1: Five Oxidation States of PANI (from [189]) | 169 |
| Figure 6.2: Conductive and Non-Conductive Forms of PANI (from [190]) | 169 |
| Figure 6.3: Polyaniline and Sample Derivatives (a) PANI, (b) PoANI and (c) P25DMA | 170 |
| Figure 6.4: Similarity of Chemical Structures of (a) Phosgene, (b) Formaldehyde and (c) Acetaldehyde..... | 179 |
| Figure 6.5: Deposition of Polymeric Material onto Sensor Plate | 181 |
| Figure 6.6: Sensor (a) Before and (b) After Polymer Deposition..... | 181 |
| Figure 6.7: Sensor Array for Individual Gases; Methanol (M), Ethanol (E), Acetone (A) and Benzene (B) | 184 |
| Figure 6.8: Sensor Array for All Possible Gas Mixture Combinations of Methanol (M), Ethanol (E), Acetone (A) and Benzene (B)..... | 184 |
| Figure 6.9: Sensor Array for All Gas Combinations of Methanol (M), Ethanol (E) and Acetone (A)..... | 186 |
| Figure 6.10: Sensor Array for All Gas Combinations of Ethanol (E), Acetone (A) and Benzene (B)..... | 186 |

| | |
|---|-----|
| Figure 6.11: Sensor Array for All Gas Combinations of Methanol (M), Acetone (A) and Benzene (B) | 187 |
| Figure 6.12: Sensor Array for All Gas Combinations of Methanol (M), Ethanol (E) and Benzene (B) | 187 |
| Figure 7.1: Comparison of Qualitative Observations during PANI (left) and ox-PANI (right) Synthesis | 193 |
| Figure 7.2: Comparison of Qualitative Observations during PANI (left) and ox-PANI (right) Synthesis | 194 |
| Figure 7.3: Experimental Set-Up for Evaluation of Sensing Materials, where MFC represents Mass Flow Controller and FM represents Flow Meter (adapted from [257]) | 196 |
| Figure 8.1: Sorption of Acetone for PANI, PPy and PMMA (source: 5 ppm acetone in nitrogen) | 197 |
| Figure 8.2: Surface Morphology of (a) PANI, (b) PPy and (c) PMMA from SEM at 500X Magnification | 199 |
| Figure 8.3: Surface Morphology of (a) PANI, (b) PPy and (c) PMMA from SEM at 5000X Magnification | 200 |
| Figure 8.4: Surface Morphology of (a) PANI, (b) PANI doped with 10 wt% SnO ₂ , (c) PANI doped with 10 wt% WO ₃ (typical result), (d) PANI doped with 10 wt% WO ₃ (metal oxide cluster), and (e) PANI doped with 10 wt% ZnO | 203 |
| Figure 8.5: Sorption of Acetone for PANI-based Polymeric Materials (formulations #1-#10; source 5 ppm acetone in nitrogen) | 205 |
| Figure 8.6: Surface Morphology of (a) PPy doped with 20 wt% SnO ₂ , (b) PPy doped with 20 wt% WO ₃ , and (c) PPy doped with 20 wt% ZnO | 207 |
| Figure 8.7: Sorption of Acetone for PPy-based Polymeric Materials (formulations #11-#20; source 5 ppm acetone in nitrogen) | 208 |
| Figure 8.8: Surface Morphology of PMMA doped with 10 wt% SnO ₂ | 210 |
| Figure 8.9: Sorption of Acetone for PMMA-based Polymeric Materials (formulations #21-#30; source 5 ppm acetone in nitrogen) | 210 |
| Figure 8.10: Sorption of Acetaldehyde, Ethanol, Acetone and Benzene for PANI-based Polymeric Materials (formulations #1, #3, #5 and #10); source ~1 ppm each analyte in nitrogen) | 212 |
| Figure 8.11: Sorption of Acetaldehyde, Ethanol, Acetone and Benzene for PPy-based Polymeric Materials (formulations #11, #13, #15 and #18); source ~1 ppm each analyte in nitrogen) | 214 |
| Figure 8.12: Sorption of Acetaldehyde, Ethanol, Acetone (A) and Benzene for Pure PANI and Pure PPy (formulations #1 and #11); source ~1 ppm each analyte in nitrogen or A-rich gas mixture)..... | 215 |
| Figure 8.13: XRD for pure PANI (formulation #31) and ox-PANI (formulation #32); characteristic peaks reported by Noby et al. [271] | 218 |
| Figure 8.14: Replicated XRD for pure PPy (formulation #11); characteristic peak range reported by Chougule et al. [273] and Waghuley et al. [274]..... | 219 |
| Figure 8.15: XRD for the copolymer of PANI/PPy (formulation #33); characteristic peak range reported by Hammad et al. [234] | 220 |
| Figure 8.16: XRD for the copolymer of ox-PANI/PPy (formulation #34) compared to PANI/PPy (formulation #33); characteristic peak range (for PANI/PPy copolymer) reported by Hammad et al. [234]..... | 220 |

| | |
|---|-----|
| Figure 8.17: XRD for PMMA (formulation #21); characteristic peaks reported by Abdelrazek et al. [275]..... | 221 |
| Figure 8.18: Surface Morphology of (a) PANI (b) ox-PANI, (c) PANI/PPy and (d) ox-PANI/PPy from SEM at 5000X Magnification | 223 |
| Figure 8.19: Sorption of Acetone for Customized Polymers (source: 5 ppm acetone in nitrogen) | 225 |
| Figure 8.20: Sorption of Acetone in the Presence of Acetaldehyde for Customized Polymeric Materials (formulations #31 to #34); source ~2 ppm each analyte in nitrogen)..... | 226 |
| Figure 8.21: Sorption of Acetone in the Presence of Ethanol for Customized Polymeric Materials (formulations #31 to #34); source ~3 ppm each analyte in nitrogen)..... | 227 |
| Figure 8.22: Sorption of Acetone in the Presence of Benzene for Customized Polymeric Materials (formulations #31 to #34); source ~ 2 ppm each analyte in nitrogen)..... | 227 |
| Figure 8.23: Sorption of Acetone and Sorption of Benzene for Customized Polymers (analytes evaluated individually; source: 5 ppm acetone in nitrogen or 5 ppm benzene in nitrogen) | 229 |
| Figure 9.1: Overall Experimental Plan for Related Copolymerization Study (based on [41])... | 232 |
| Figure 9.2: Practical Prescriptions for the Selection of Polymeric Sensing Materials (from [182]) | 233 |
| Figure 9.3: General Framework for the Design of Polymeric Materials for Custom Applications | 234 |
| Figure B.1: ‘QuickStart’ Menu | 277 |
| Figure B.2: ‘Preliminary Estimates’ Prompt | 278 |
| Figure B.3: ‘Copolymerization Data’ Prompt | 278 |
| Figure B.4: ‘Default Settings’ Prompt..... | 279 |
| Figure B.5: Sample Data File for Computational Package..... | 280 |
| Figure C.1: Sample Analysis from GPC; (a) Sample Chromatograms, (b) Sample Peaks and (c) Distribution Plots for the AAm/AAc Reference Copolymer | 288 |
| Figure C.2: Peak Average Molecular Weight and Weight Average Molecular Weight for Optimal Terpolymer Samples (compared to Reference Polymer Alcoflood 955)..... | 291 |
| Figure C.3: Bulk Intrinsic Viscosity (IV) and Peak Average Molecular Weight for Optimal Terpolymer Samples (compared to Reference Polymer Alcoflood 955)..... | 291 |
| Figure C.4: Bulk Intrinsic Viscosity (IV) and Weight Average Molecular Weight for Optimal Terpolymer Samples (compared to Reference Polymer Alcoflood 955)..... | 292 |
| Figure C.5: Synthesis and Characterization Replicates of TGA for Terpolymer #1 | 293 |
| Figure C.6: Expansion of Terpolymer #1 Sample during TGA..... | 293 |
| Figure C.7: Synthesis Replicates Analyzed with TGA for Terpolymer #2 | 294 |
| Figure C.8: Thermal Gravimetric Analysis Results for Reference Material (Alcoflood 955) ... | 294 |
| Figure C.9: Thermal Gravimetric Analysis Results for a Designed AAm/AAc Copolymer..... | 295 |
| Figure C.10: Comparison of Frequency Sweep Results at 1% Strain and 10% Strain for Reference Polymer (solution concentration of 0.01 g/mL in water) | 296 |
| Figure D.1: Sample Chromatograms (red = no sensing material; black = PPy) from GC for ~1 ppm Mixture of Acetaldehyde, Ethanol, Acetone and Benzene; (a) Full Chromatogram, (b) Acetaldehyde Response, (c) Ethanol Response, (d) Acetone Response and (e) Benzene Response | 301 |
| Figure D.2: Sample GC Results for ~1 ppm Mixture of Acetaldehyde, Ethanol, Acetone and Benzene; (a) Blank System and (b) with Polypyrrole | 302 |

List of Tables

| | |
|---|-----|
| Table 1.1: Parallel Case Studies for Thesis Organization..... | 4 |
| Table 2.1: Polyacrylamide-Based Materials for Polymer Flooding EOR | 11 |
| Table 2.2: Potential Biopolymers for Polymer Flooding EOR (adapted from [15]) | 13 |
| Table 2.3: Summary of Reactivity Ratio Estimation (RRE) Studies for 2-methylene-1,3-dioxepane (MDO; monomer 1)/Vinyl Acetate (VAc; monomer 2) Copolymerization..... | 37 |
| Table 2.4: RRE Data for the Copolymerization of MDO (Monomer 1)/VAc (Monomer 2) [77] | 38 |
| Table 2.5: Summary of RRE Results for Hydroxyethyl Acrylate (HEA; Monomer 1)/4-(3-(2,4-dichlorophenyl)-3-oxoprop-1-enyl) Phenylacrylate (DCP; Monomer 2) Copolymerization | 41 |
| Table 2.6: Summary of RRE Results for <i>n</i> -Butyl Methacrylate (BMA; Monomer 1) and <i>n</i> -Butyl Acrylate (BA; Monomer 2) Copolymerization..... | 45 |
| Table 2.7: Effect of pH on AAm/AAc Polymerization Kinetics | 50 |
| Table 3.1: Definitive Screening Design for Terpolymerization of AMPS/AAm/AAc | 56 |
| Table 3.2: Optimally Designed Experiments for Terpolymerization of AMPS/AAm/AAc | 57 |
| Table 3.3: Sand-pack Characteristics and Experimental Conditions..... | 62 |
| Table 3.4: Composition of Synthetic Brine | 63 |
| Table 3.5: Composition of Reference Polymer for EOR Testing..... | 63 |
| Table 4.1: pH Effects on Ternary Reactivity Ratio Estimates for AMPS/AAm/AAc ($M_1/M_2/M_3$) | 67 |
| Table 4.2: Reactivity Ratio Estimates at pH 7 with Varying and Constant IS and [M] | 70 |
| Table 4.3: Ionic Strength (IS) Effects on Ternary Reactivity Ratio Estimates for AMPS/AAm/AAc ($M_1/M_2/M_3$) | 71 |
| Table 4.4: Ionic Strength (IS) Effects on Ternary Reactivity Ratio Estimates; Varying and Constant pH and [M] | 74 |
| Table 4.5: Possible Triad Fractions for the AMPS/AAm/AAc Terpolymer | 77 |
| Table 4.6: Optimized Triad Fractions for Enhanced Oil Recovery | 79 |
| Table 4.7: [M] Effects on Ternary Reactivity Ratio Estimates for AMPS/AAm/AAc ($M_1/M_2/M_3$) | 82 |
| Table 4.8: NaCl Addition for the AMPS/AAm/AAc Terpolymerization Screening Design | 85 |
| Table 4.9: PAAm Salt Study Experiments | 87 |
| Table 4.10: Analysis of Elemental Contributions for Run S7 | 91 |
| Table 4.11: Adjusted Analysis of Elemental Contributions for S7 | 91 |
| Table 4.12: Analysis of ICP Results for S7-10..... | 92 |
| Table 4.13: Comparison of Molecular Weight Averages for Opt2-1 using ‘Measured’ and ‘Expected’ Sample Concentrations..... | 99 |
| Table 4.14: Reproducibility/Repeatability of Molecular Weight Averages for Opt1 | 101 |
| Table 4.15: Reproducibility/Repeatability of Molecular Weight Averages for Opt2 | 101 |
| Table 4.16: Comparison of Cumulative Terpolymer Composition from ^{13}C -NMR and EA..... | 105 |
| Table 4.17: Points of Interest from Thermal Gravimetric Analysis Results..... | 107 |
| Table 4.18: Summary of Shear Viscosities for Terpolymer Solutions | 112 |
| Table 4.19: Sand-pack Properties for Sand-pack Flooding Tests..... | 116 |
| Table 4.20: Summary of Reservoir Flow Properties for Terpolymer Solutions..... | 119 |
| Table 4.21: Sand-pack Properties and Initial Conditions for Heavy Oil Displacement Tests.... | 120 |
| Table 4.22: Oil Recovery Efficiency Results from Heavy Oil Displacement Tests..... | 122 |

| | |
|--|-----|
| Table 5.1: Comparison of Binary and Ternary Reactivity Ratio Estimates AN(M ₁)/Sty(M ₂)/MA(M ₃) | 127 |
| Table 5.2: Comparison of Binary and Ternary Reactivity Ratio Estimates AMPS/AAm/AAC. 129 | 129 |
| Table 5.3: Reactivity Ratio Estimates for HOST(1)/EAMA(2)/PAG(3) (Data from [138]) | 140 |
| Table 5.4: Reactivity Ratio Estimates for Terpolymerization of BA(1)/BMA(2)/lim(3) with Experimental Data from Ren et al. [134]..... | 143 |
| Table 5.5: Reactivity Ratio Estimates for Terpolymerization of BA(1)/BMA(2)/lim(3) with Supplemental Data (Experimental Data from [134] and Simulated Data from Current Work) . | 147 |
| Table 5.6: Reactivity Ratio Estimates for Terpolymerization of BA/MMA/EHA from Low Conversion Data (Experimental Data from [137]) | 148 |
| Table 5.7: Reactivity Ratio Estimates for Terpolymerization of BA/MMA/EHA from All Terpolymerization Data (Experimental Data from [137]) | 150 |
| Table 5.8: Reactivity Ratio Estimates for Terpolymerization of Sty(1)/MMA(2)/MA(3) (Experimental Data from [128]) | 154 |
| Table 5.9: Comparison of Model Predictions for the Sty/MMA/MA Terpolymerization (Experimental Data and Original Predictions from [128]) | 155 |
| Table 5.10: Analysis of (a) Composition and (b) Microstructure for AN/Sty/MMA (Experimental Data from [143]) | 158 |
| Table 6.1: Breath Acetone Detection Studies; Summary of Sensing Materials | 163 |
| Table 6.2: Hildebrand Solubility Parameters for Target Analyte, Interferents, and Potential Sensing Materials (from [185] unless otherwise stated)..... | 168 |
| Table 6.3: Potential Dopants, Based on Prior Breath Acetone Studies | 175 |
| Table 7.1: Experimental Design of Polymeric Materials for Acetone Detection | 190 |
| Table 7.2: Experimental Design of Polymeric Materials for Acetone Detection: Part II..... | 192 |
| Table 8.1: Measured Metal Incorporation for PANI-based Polymeric Materials | 201 |
| Table 8.2: Measured Metal Incorporation for PPy-based Polymeric Materials | 206 |
| Table 8.3: Average Selectivity of Customized Polymeric Materials for Three Distinct Interferent Gases | 228 |
| Table C.1: Analysis of Elemental Contributions for S5 (no NaCl added)..... | 285 |
| Table C.2: Confirmation of GPC Accuracy for Polyelectrolytes using AAm/AAC Reference Copolymer..... | 287 |
| Table C.3: Effect of Sample Filtration on Concentration of GPC Samples (see Section 4.2.2.3) | 289 |
| Table C.4: ANOVA Table for Comparisons between Opt1 Samples (see Section 4.2.2.3)..... | 290 |
| Table C.5: ANOVA Table for Comparisons between Opt2 Samples (see Section 4.2.2.3)..... | 290 |
| Table C.6: Summary of Shear Viscosities for Terpolymer Solutions (extended version of Table 4.18) | 297 |
| Table C.7: Experimental Plan for Phase I of EOR Study | 298 |
| Table C.8: Experimental Plan for Phase II of EOR Study..... | 298 |
| Table C.9: Dead Volume Values for Phase II of EOR Study..... | 298 |
| Table D.1: GC Retention Times for Molecules of Interest..... | 302 |
| Table D.2: Experimental Acetone Sorption Data for PANI-based Polymeric Materials (formulations #1 through #10; supplemental to Figure 8.5) | 303 |
| Table D.3: Experimental Acetone Sorption Data for PPy-based Polymeric Materials (formulations #11 through #20; supplemental to Figure 8.7) | 303 |

| | |
|---|-----|
| Table D.4: Experimental Acetone Sorption Data for PMMA-based Polymeric Materials (formulations #21 through #30; supplemental to Figure 8.9) | 304 |
| Table D.5: Experimental Acetone Sorption Data for Customized Polymeric Materials (formulations #31 through #34; supplemental to Figure 8.19) | 304 |
| Table D.6: Experimental Selectivity Data from ~1 ppm Analyte Gas Mixture ((a) Acetaldehyde, (b) Ethanol, (c) Acetone and (d) Benzene; supplemental to Figure 8.10 and Figure 8.11) | 305 |
| Table D.7: Experimental Selectivity Data from Acetone-Rich Analyte Gas Mixture (containing Acetaldehyde, Ethanol, and Benzene; supplemental to Figure 8.12) | 306 |
| Table D.8: Experimental Selectivity Data from ~2 ppm Analyte Gas Mixture of Acetone and Acetaldehyde; supplemental to Figure 8.20..... | 306 |
| Table D.9: Experimental Selectivity Data from ~2 ppm Analyte Gas Mixture of Acetone and Ethanol; supplemental to Figure 8.21 | 307 |
| Table D.10: Experimental Selectivity Data from ~2 ppm Analyte Gas Mixture of Acetone and Benzene; supplemental to Figure 8.22..... | 307 |
| Table D.11: ANOVA Comparing SnO ₂ Dopant Levels in PANI..... | 308 |
| Table D.12: ANOVA Comparing WO ₃ Dopant Levels in PANI | 308 |
| Table D.13: ANOVA Comparing ZnO Dopant Levels in PANI..... | 308 |
| Table D.14: ANOVA Comparing Pure PANI to ‘Best’ Doped PANI | 309 |
| Table D.15: ANOVA Comparing SnO ₂ Dopant Levels in PPy..... | 309 |
| Table D.16: ANOVA Comparing WO ₃ Dopant Levels in PPy | 309 |
| Table D.17: ANOVA Comparing ZnO Dopant Levels in PPy..... | 310 |
| Table D.18: ANOVA Comparing Pure PPy to ‘Best’ Doped PPy | 310 |
| Table D.19: ANOVA Comparing Customized Materials (from Section 8.2) | 310 |

“Trust in the LORD with all your heart, and do not lean on your own understanding.
In all your ways acknowledge Him, and He will make straight your paths.”
~Proverbs 3:5-6

Chapter 1. Introduction

1.1 Problem Statement

The wide variety (and subsequent versatility) of available polymeric materials is extremely attractive from a design standpoint. Polymers are typically inexpensive (in terms of both materials cost and processing cost), lightweight, and have tailorable application properties. As a result, they are employed as foams, fibres, films, and bulk molded materials.

The range of polymeric materials available for engineering applications can be overwhelming. Technical data are typically available once a material is selected, but how is that initial selection made? How can that material be tailored for a specific application? Many scientists and engineers use trial-and-error approaches; often the synthesis is the priority, and finding a suitable application is an afterthought. In other cases, researchers may have an application in mind, and they try various recipes until they are satisfied with the result. However, both of these approaches are ineffective. Not only are valuable experimental resources wasted during the trial-and-error stage, but there is also no guarantee that the polymer products have been optimized for the specific application.

The overarching motivation for this work is to make full use of available resources and to efficiently work towards the identification, synthesis, characterization, and eventual application of polymer products with optimal properties. Therefore, the design of materials (through exploring structure-property relationships and making use of established design frameworks) is essential. To demonstrate the importance (and the potential for success) of using a systematic design (plan) for the synthesis of polymeric materials, two related (yet distinct) case studies are considered. Case Study #1 uses design principles to improve on existing materials for enhanced oil recovery (EOR), while Case Study #2 employs design prescriptions to select optimal polymeric sensing materials for gaseous acetone detection.

For the enhanced oil recovery investigation (Case Study #1), the challenge is to design a water-soluble polymer that performs better than the materials that are currently available. Typically, primary oil recovery, which forces the crude oil to the surface as a result of the natural reservoir energy, only extracts up to 10% of the total oil in the reservoir. The secondary oil recovery process, in which an additional 25% to 30% of the oil is extracted, typically uses water flooding to displace the oil [1]. In some cases, up to 75% of the oil remains in the reservoir, even after primary and secondary oil recovery has occurred [2]. Thus, there is significant motivation to advance to tertiary oil recovery. While tertiary oil recovery is more expensive than the previous stages, it has the potential to extract an additional 20% to 30% of the oil. Tertiary oil recovery processes include thermal recovery, gas injection, and chemical injection.

The chemicals injected during tertiary oil recovery are often polymeric materials; adding small quantities of polymeric material to the flood water improves mobility control and ultimately improves the efficiency of the oil recovery process. In general, the most widely used synthetic polymers for EOR are polyacrylamide and polyacrylamide-based materials (such as hydrolyzed polyacrylamide, HPAM). Polyacrylamide-based materials are relatively inexpensive, easily obtained, and perform fairly well in EOR applications. Specifically, HPAM is widely used in polymer flooding because it provides good control over viscosity and effective permeability. However, there is room for improvement when the mechanical and thermal stability of HPAM are considered. It would be extremely beneficial (in terms of application performance) to minimize shear degradation of the polymer backbone, especially at the high temperatures and high salinities characteristic of oil reservoirs.

In Case Study #2, the aim is to detect gaseous acetone. Breath acetone concentration is correlated with blood glucose levels, which is especially important for people living with diabetes. If this relationship can be exploited, the physiological change could be detected through a simple and non-invasive breath test. Therefore, the goal is to design polymeric sensing materials that have the properties necessary to detect acetone. The versatility of polymeric materials and the range of available options (in terms of polymer backbones) make them a very attractive option for sensing applications. Compared to the metals and metal oxides that are typically used as sensing materials, polymers are more cost effective, can operate at room temperature, provide better selectivity [3], and can easily be customized. Therefore, an opportunity exists here to improve on what is currently available for the application, especially using prior knowledge and a framework for designing polymeric materials [4, 5].

1.2 Research Hypotheses

This research aims to pursue several hypotheses, which range from general statements to more specific concepts. However, all hypotheses eventually converge to the common focal point of a more rational and systematic design of polymeric materials.

(1) Design of polymeric materials (using a targeted approach and exploiting existing knowledge) is necessary for the synthesis of polymeric materials with optimized and desirable properties for specific applications.

(2) A general design framework (valid for any number of applications) should exist to guide researchers in their pursuit of optimal polymeric materials.

(3) Design principles (and, specifically, accurate reactivity ratios for multi-component polymers) can be employed to understand and manipulate the properties of synthetic water-soluble polymers for enhanced oil recovery.

(4) Design prescriptions can be advantageous in the development of polymeric sensing materials, especially when prior knowledge exists to inform new investigations.

1.3 Research Objectives

The goal of this thesis is to use statistical design principles to optimize polymeric materials for specific applications. There are known connections between polymerization kinetics and polymer properties, and between those properties and application requirements/performance. If these links are well-understood, it becomes possible to essentially ‘reverse-engineer’ the polymeric material; the researcher can start with known application requirements and synthesize polymers with tailor-made properties using an optimized recipe (according to the polymerization kinetics).

Since the number of applications for polymeric materials is essentially limitless, the current work will feature two specific case studies. The first examines water-soluble polymers for viscosity modification in enhanced oil recovery (EOR), while the second investigates polymeric sensing materials for acetone detection. In the specific research objectives outlined below, items 1 through 4 relate to Case Study #1 (materials for enhanced oil recovery) and items 5 through 7 relate to Case Study #2 (polymeric sensing materials). Item 8 is more general, as it relates to design principles applied to polymeric materials and is linked to both case studies.

- (1) Identify important attributes of synthetic polymeric materials for improved enhanced oil recovery performance.
- (2) Research, characterize and exploit relationships between (experimental) synthesis conditions and properties of the terpolymer products.
- (3) Design, synthesize, characterize and test optimal terpolymers for the enhanced oil recovery application.
- (4) Demonstrate the importance of statistically correct experimental techniques and subsequent analyses, especially as they relate to copolymers and terpolymers.
- (5) Identify important attributes of synthetic polymeric materials for gas sensing applications, with specific emphasis on acetone sensing for diabetic applications.
- (6) Research and characterize relationships between polymeric sensing materials and dopants as they relate to analyte sensitivity and selectivity.
- (7) Design, synthesize, characterize and test optimal polymers for detection of acetone gas.

(8) Demonstrate the advantages of a design framework (considering physicochemical behaviour, statistical design principles, and product requirements) for polymer synthesis and application performance.

1.4 Thesis Organization

Based on the work conducted throughout this research period, the thesis includes 10 chapters. The nature of the project (with two related yet independent case studies) necessitates that the thesis be divided into two major (parallel) sections. Chapters 2 through 5 are specific to the enhanced oil recovery project (Case Study #1), whereas Chapters 6 through 8 focus on the polymeric sensing material project (Case Study #2). Both case studies follow the same general outline, as shown in Table 1.1. The two major sections are bookended by chapters that are relevant to both projects; Chapter 1, Chapter 9 and Chapter 10 are intended to draw links between the two case studies through more general tips on the design of polymeric materials.

Table 1.1: Parallel Case Studies for Thesis Organization

| | Case Study #1: Enhanced Oil Recovery | Case Study #2: Polymeric Sensing Materials |
|---|---|---|
| Introduction | Chapter 1 | |
| Literature Background | Chapter 2 | Chapter 6 |
| Experimental Methodology | Chapter 3 | Chapter 7 |
| Results and Discussion | Chapter 4 | Chapter 8 |
| ‘An Aside’ | Chapter 5 | -- |
| Commonalities between Case Studies | Chapter 9 | |
| Overall Conclusions, Main Contributions & Recommendations | Chapter 10 | |

Chapter 1 is the introductory chapter. It provides a problem statement (which is three-fold and related to design of materials, polymers for enhanced oil recovery, and polymeric sensing materials for acetone detection), the research hypothesis and associated objectives. Chapter 1 also provides a brief outline of subsequent chapters.

In **Chapter 2**, background information from the literature is provided for the enhanced oil recovery (EOR) project (Case Study #1). The chapter begins with a review of existing EOR methods, but it also takes a critical look at the literature in order to identify application requirements (both in terms of polymer properties and application-specific performance), establish potential polymer backbones, and investigate techniques for product customization (note here the parallelism with Chapter 6, to be discussed shortly). Part of the design process is to build on existing knowledge, so Section 2.1 provides a comprehensive overview. Because this case study ultimately employs

multi-component polymers for the application, Sections 2.2 and 2.3 provide details and examples related to multi-component polymerization kinetics (copolymerization and terpolymerization) and reactivity ratio estimation (for both binary and ternary systems). Finally, Section 2.4 looks more specifically at how properties of the material selected for EOR (the terpolymer of 2-acrylamido-2-methylpropane sulfonic acid, acrylamide and acrylic acid) can be manipulated. A preliminary understanding of formulation effects on the polymerization kinetics is available from the literature and is exploited herein.

The experimental methodology (from synthesis to characterization) for the EOR project (Case Study #1) is presented in **Chapter 3**. Two related investigations were performed: a screening study and an optimally designed study (based on knowledge acquired from the screening experiments). The synthesis procedure was similar for both investigations, and relevant details are provided in Section 3.2. In general, polymer properties (characterized as described in Section 3.3) were evaluated for the screening experiments and the optimally designed experiments. However, since evaluating the application-specific properties involves more rigorous procedures, they were only performed for the optimally designed experiments. The techniques employed are explained in Section 3.4.

Chapter 4 contains results and related discussion from the enhanced oil recovery project (Case Study #1). The chapter is divided into two major sections: Section 4.1 provides all of the results that are related to the screening experiments, while Section 4.2 is focused on the optimally designed experiments. Since the purpose of the screening experiments was primarily to determine the effects of potentially influential factors on the product terpolymer, the effects of pH, ionic strength, monomer concentration, and high salt (NaCl) content on the terpolymerization kinetics and terpolymer properties are critically evaluated. These results inform the synthesis of custom AMPS/AAm/AAC terpolymers, obtained from optimally designed experiments. The selected polymerization conditions are justified in Section 4.2.1, and the characteristics of the terpolymer products are expounded in the following sections (4.2.2 and 4.2.3).

While this thesis is composed of two parallel case studies, **Chapter 5** acts as an ‘intermission’ chapter. The terpolymerization research associated with the enhanced oil recovery project required additional investigation, specifically related to ternary reactivity ratio estimation. Terpolymerization systems are intrinsically linked to their analogous copolymers, and some researchers suggest that binary reactivity ratios (from copolymerization systems) can be used to describe ternary systems. Therefore, to elucidate the importance of ternary reactivity ratio estimation (and to justify this portion of the research), a direct comparison of binary and ternary reactivity ratios became necessary. Our findings are presented in the first half of Chapter 5 (Section 5.1). The second half of the chapter (Section 5.2) is dedicated to a series of terpolymerization troubleshooting tips (again related to ternary reactivity ratio estimation) and describes many of the lessons learned over the course of this project through a series of smaller case studies.

Chapter 6 marks the beginning of the acetone sensing project (Case Study #2) and has parallel features to Chapter 2. Here, background information is provided about existing materials and methods for acetone sensing, and application requirements are deduced from the literature. As for the first case study, polymer properties and application-specific requirements are considered, potential polymer backbones are reviewed, and some common techniques for product customization are considered. This chapter also demonstrates how to extend the design process to additional volatile organic compounds (here, formaldehyde) and provides a brief introduction to sensor arrays.

In **Chapter 7**, the experimental methodology for Case Study #2 is presented. As before (in Chapter 3 for Case Study #1), the process involved two phases: a design of experiments for introductory tests and a customization phase. The detailed synthesis procedure for each polymer backbone is provided in Section 7.2 and characterization techniques are described in Sections 7.3 and 7.4.

Like Chapter 4, the results and discussion shown in **Chapter 8** are divided into two related sections. In Section 8.1, the preliminary (screening) experiments are evaluated in terms of sensitivity and selectivity towards acetone, and select polymer properties are considered to justify the results. The conclusions based on these experiments inform the study described in Section 8.2. To better appreciate the custom materials, the polymer samples are again characterized in terms of polymer properties (namely crystallinity and surface morphology) and application performance.

The purpose of **Chapter 9** is to further highlight the parallels between the two main case studies, and to bring the focus back to the overarching concept of design of polymeric materials. The chapter outlines the design framework that was used for both case studies (based on best practices) and describes the process for creating links between polymer properties and application performance. Ultimately, the goal is to use foundational knowledge (polymerization kinetics, application chemistry, and so on) to manipulate the properties of the product polymer and provide desirable properties (and design tips) for a specific application.

Finally, **Chapter 10** contains concluding remarks, identifies the main contributions of this work, and presents recommendations for future work.

Appendices have also been included in this thesis to provide additional (supplemental) information. The four appendices include details regarding terpolymerization kinetics and the Alfrey-Goldfinger model (Appendix A), a computational package developed to simplify reactivity ratio estimation (developed during this PhD project and described in Scott and Penlidis [6], Appendix B), relevant data and sample calculations for Case Study #1 (Appendix C) and the same for Case Study #2 (Appendix D).

Chapter 2. Literature Background for Case Study #1 – Enhanced Oil Recovery

2.1 Enhanced Oil Recovery

Typically, oil is extracted from reservoirs through a sequence of recovery methods. Although specific methods are largely dependent on the properties of the reservoir, the same general procedures are generally followed. Primary oil recovery exploits the natural energy of an oil reservoir. Oil expansion, expansion of gases within the reservoir, migration of naturally pressurized water, or gravitational effects (for high elevation reservoirs) may contribute to the natural expulsive forces that promote primary recovery. Primary oil recovery can continue until the natural reservoir pressure has been depleted and may be supplemented with pumping. However, this primary stage will only be pursued while it is economically reasonable; eventually, the primary recovery will not be sufficient to justify the resources being used.

During primary oil recovery, there is loss of most natural reservoir energy. However, a substantial volume of crude oil remains in the reservoir (often more than 90% of the original oil in place, especially for conventional crude oil) [7]. Thus, when feasible, secondary recovery methods are employed immediately after the natural reservoir energy has been exhausted. The objective at this stage is to inject a fluid (like water, brine, or natural gas) into the reservoir. Fluid injection repressurizes the system (which ‘revives’ the expulsive forces that are characteristic of primary oil recovery) and the fluid injected will sweep through the reservoir (transporting more crude oil towards the production well). The combination of increasing pressure and promoting fluid flow allows for further oil recovery. Water flooding is the most commonly used secondary oil recovery method, but the efficiency is dependent on the reservoir characteristics and oil viscosity. Water flooding essentially forces water through the reservoir and ‘pushes’ residual oil with it. However, if there is a clear path of least resistance (that is, reservoir segments with better permeability), the water will not sweep the whole reservoir. As a result, large volumes of oil are bypassed and remain in the reservoir. Similar behaviour is observed when the oil is much more viscous than the water; the water will simply flow around the oil that it is meant to displace. When water begins channeling through the reservoir (rather than sweeping the full reservoir volume), the production efficiency is much reduced. When this occurs (or when secondary methods become uneconomical), tertiary oil recovery methods are considered.

Tertiary oil recovery methods are also called enhanced oil recovery (EOR) techniques, and supplement the oil recovery achieved in the first two stages. Many different EOR approaches exist, but can be divided into three main categories: thermal methods, miscible methods (where whatever is injected is miscible with the oil) and chemical flood methods (where the chemicals injected promote oil flow towards the production well). The most efficient approach for a particular

situation will depend on several factors including reservoir characteristics, crude oil characteristics, and economic considerations.

Thermal methods are designed to assist with the removal of heavy and viscous crude oils, as the viscosity of oil can decrease significantly when temperature is increased. This allows residual oil to flow more easily towards a production well, which improves the recovery efficiency of the process. Typically, thermal methods involve the injection of steam or hot water, which simultaneously reduces the viscosity and increases the pressure; this acts as a driving force for oil production. Alternatively, thermal methods can involve the generation of thermal energy within the reservoir via oil combustion. In this case, injected air allows for the ignition of the residual oil, which in turn generates heat and produces combustion gases. Thermal methods are the most commonly used EOR methods worldwide (producing ~2 million barrels of oil per day) [8], but present major challenges including poor sweep efficiency, loss of thermal energy underground, poor injectivity of steam, negative environmental impacts, and poor control of in situ combustion reactions [7, 9].

Miscible methods, in which the injected fluid dissolves in the crude oil to modify viscosity, are also commonly used in EOR. Many fluids including alcohols, carbon dioxide, and petroleum gases (containing ethane, propane, butane and/or pentane) have been employed [7], but CO₂ injection is by far the most common [8]. The advantage of using CO₂ is two-fold: the viscosity of the crude oil is reduced (therefore oil recovery can occur more easily) and greenhouse gases are consumed. To ensure that the CO₂ is miscible with oil, the reservoir is usually repressurized (with water) before the CO₂ injection. Typically, complete miscibility of the CO₂ and the oil is only achievable when the reservoir temperature and pressure ensure the presence of supercritical CO₂. Therefore, reservoirs deeper than 2,000 feet are preferable for CO₂ flooding [10]. An additional advantage of using CO₂ for EOR is the fluid behaviour upon exiting the production wells. As the supercritical CO₂ returns to its gas state, it provides a 'gas lift' to enhance the recovery efficiency (as would occur during the primary oil recovery stage). That said, the main disadvantage of CO₂ injection is the viscosity of CO₂ under reservoir conditions (0.03 cP to 0.10 cP) compared to viscous crude oil (up to 50 cP) [7]. This can result in significant channeling (and reduced recovery) in the reservoir, similar to what was described previously as a limitation of water flooding.

The final tertiary recovery method (or EOR method) discussed herein is chemical flooding. Chemical EOR uses additives like polymers, alkalis, or surfactants to improve the mobility control of the injected water and/or to reduce the interfacial tension between the oil and the reservoir pores. Polymer flooding is arguably the most common form of chemical EOR [8] and has been used effectively in Chinese oilfields [11, 12]. In Daqing, for example, up to 10% incremental oil recovery (and up to 53% overall oil recovery) was achieved using high molecular weight partially hydrolyzed polyacrylamide [12]. However, one of the main shortcomings of polymer flooding is the instability of materials at high temperature and high salinity conditions that are characteristic

of oil reservoirs [13-15]. In spite of this challenge, polymer flooding is still more widely used than alkali or surfactant flooding. Alkalis tend to be problematic as they introduce scaling and plugging [8], and both alkalis and surfactants become less efficient as they flow through porous media due to adsorption effects [15].

Polymer flooding is of particular interest because it is a developing field that still has significant room for improvement. As natural resources are being consumed, it is more important than ever to focus on overall (long-term) oil recovery rather than ‘easy’ (immediate) oil recovery. Therefore, it is worth investing in materials (such as optimally designed polymers) that will promote maximum oil recovery. In order to design new polymeric materials for enhanced oil recovery, a good understanding of the technique and the application requirements is essential. Taking advantage of prior knowledge will assist with identifying potential polymer backbones and can influence product customization. This will be described in what follows.

2.1.1 Existing Materials and Methods

During polymer flooding, a dilute aqueous polymer solution is slowly injected into the reservoir, which forces residual oil out of the reservoir and into a production well (see Figure 2.1). The viscosity increase (compared to regular water flooding) and the properties of the polymeric material ensure that channeling (that is, finding the path of least resistance) through the reservoir is minimal. Thus, more of the reservoir is exposed to the displacing fluid and less oil is left behind.

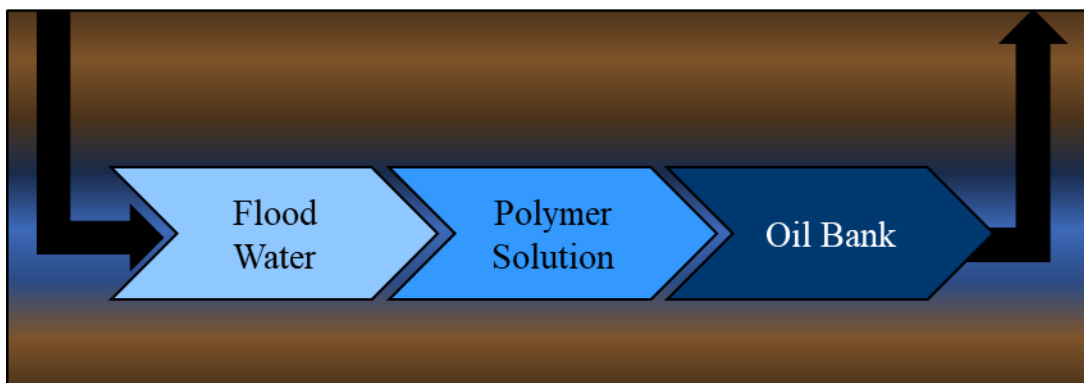


Figure 2.1: Simplified Schematic of Polymer Flooding Process for Enhanced Oil Recovery

Two main classes of polymeric materials are used in EOR: synthetic polymers and biopolymers. The most widely used synthetic polymer for polymer flooding is partially hydrolyzed polyacrylamide (HPAM), which is a linear water-soluble polymer. It can either be synthesized through the copolymerization of acrylamide and acrylic acid (or sodium acrylate) or by partially hydrolyzing polyacrylamide (that is, converting amide groups to carboxyl groups). HPAM is inexpensive, readily soluble in water, and provides good mobility control. Also, the anions on the carboxyl groups promote polyelectrolyte behaviour, which increases viscosity and decreases

adsorption within the reservoir. The oil recovery efficiency of a particular polymer is typically dependent on the degree of hydrolysis (which typically ranges from 15% to 35% [15]) as well as the molecular weight (which can be varied up to about 30×10^6 g/mol, as reported by [16]).

However, as mentioned already in Chapter 1 (Section 1.1), HPAM is known to be shear sensitive at high temperatures and high salinities. If the polymeric material begins to degrade, the viscosity modification effects are reduced, as is the EOR efficiency. As a result, other synthetic polymers, many of which are derivatives of polyacrylamide, have also been considered for polymer flooding [17]. These include branched polyacrylamide [18, 19] and N,N-dimethyl acrylamide [20], as well as acrylamide-based copolymers containing 2-acrylamido-2-methylpropane sulfonic acid [20-23], n-vinyl pyrrolidone [21], and others. These types of materials have been studied in great detail, so only an overview of polyacrylamide-based materials for polymer flooding is presented herein. Many investigations synthesize new materials that show desirable properties for the EOR application, but EOR testing is not pursued. Similarly, many large-scale projects use proprietary materials with unknown characteristics. Polymer properties and resulting performance (including incremental oil recovery) available from recent studies are listed in Table 2.1. Also, an informative figure showing the incremental oil recovery of known polymer flooding projects (both pilot and large-scale applications) has been compiled by Sheng et al. [24]; this is provided in Figure 2.2.

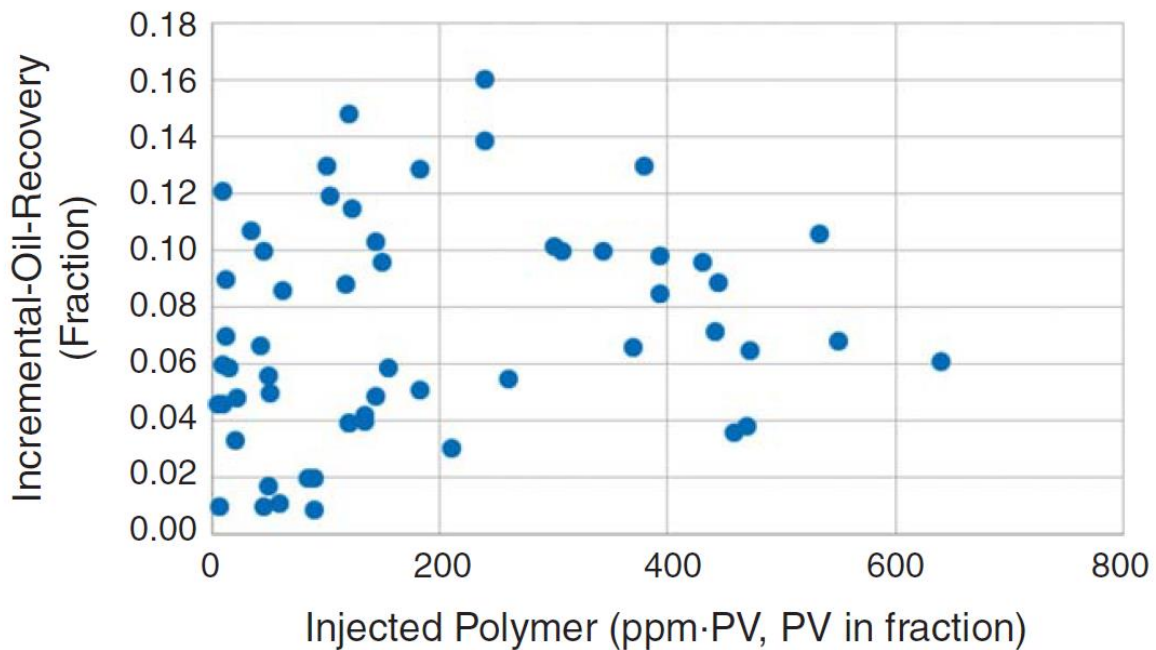


Figure 2.2: Incremental Oil Recovery vs. Amount of Polymer Injected (where PV represents Pore Volume; from [24])

Table 2.1: Polyacrylamide-Based Materials for Polymer Flooding EOR

| Ref. | Polymeric Material | Polymer Properties | Polymer Performance |
|----------|--|--|---|
| [20, 23] | AAm copolymers and NNDAM copolymers with AAc or AMPS | \bar{F}_{AAm} or $\bar{F}_{NNDAM} \sim 0.60$; \bar{F}_{AAc} or $\bar{F}_{AMPS} \sim 0.40$ | <ul style="list-style-type: none"> NNDAM/AMPS had superior brine compatibility, shear stability, and thermal stability Flooding with NNDAM/AMPS allowed for incremental oil recovery up to ~11% (using 2000 ppm polymer solution) |
| [25] | AAm/AMPS/VN terpolymer | $\bar{F}_{AAm} \sim 0.89$; $\bar{F}_{AMPS} \sim 0.10$ (low concentrations of VN); low MW | <ul style="list-style-type: none"> Experimental evidence of temperature-thickening, pseudoplastic behaviour, anti-shearing behaviour and brine compatibility |
| [21] | AAm copolymers with AAc, AMPS or NVP | <p>AAm/AAc copolymer: $\bar{F}_{AAm} \sim 0.72$; MW = 18.5×10^6 g/mol</p> <p>$\bar{F}_{AAm} \sim 0.67$; MW = 12×10^6 g/mol</p> <p>AAm/AMPS copolymers: $\bar{F}_{AAm} \sim 0.95$; MW = 6×10^6 g/mol $\bar{F}_{AAm} \sim 0.75$; MW = 8×10^6 g/mol</p> <p>AAm/NVP copolymer: $\bar{F}_{AAm} \sim 0.50$; MW = $6-8 \times 10^6$ g/mol</p> | <ul style="list-style-type: none"> Higher molecular weight polymers were more shear sensitive AAm/AMPS had highest shear stability (larger AMPS proportion improved shear stability) AAm/NVP and AAm/AAc had similar shear stability (not as good as AAm/AMPS, but better than PAAm) |
| [26] | AAm/AMPS copolymer (AN125) | MW = 12×10^6 g/mol | <ul style="list-style-type: none"> 0.2 wt% polymer solution in seawater exhibited RRF values up to 2.2; no plugging observed |
| [27] | HPAM and AAm/AAc/NAE terpolymer | <p>HPAM: MW = 5×10^6 g/mol</p> <p>AAm/AAc/NAE terpolymer synthesis conditions: [AAm] = 16wt%, [AAc] = 4wt%, [NAE] = 0.3wt% (balance water)</p> | <p>Incremental oil recovery from 1 g/L polymer solution (in brine at 65°C):</p> <ul style="list-style-type: none"> HPAM: 4% Terpolymer: 7.6% |
| [18] | PAAm with controlled molecular architectures | Linear, star, and comb structures; MW ranging from 2.8×10^4 g/mol to 5.9×10^5 g/mol | <ul style="list-style-type: none"> Molecular architecture impacts polymer solution viscosity Comb-like structures have higher viscosity and more elasticity than linear or star-like equivalents |

| | | | |
|----------|--|--|---|
| [28] | AAm/SAM/NABI terpolymer | AAm/NABI copolymer sulfonated with HCHO and NaHSO ₃ ; $\bar{F}_{AAm} > 0.95$ | <ul style="list-style-type: none"> Incremental oil recovery up to 10.6% in brine at 60°C (using 7 g/L polymer solution) |
| [29, 30] | Crosslinked AAm/DBSV copolymer | MW = 1.2×10 ⁶ g/mol | <ul style="list-style-type: none"> Incremental oil recovery up to 20.8% (using 2 g/L polymer solution) |
| [19] | Salt-resistant HPAM derivatives with modified molecular architecture | Comb-shaped, branched, star-shaped and hydrophobic associating polymers Degree of hydrolysis ~25%; MW ranging from 10×10 ⁶ g/mol to 25×10 ⁶ g/mol | <ul style="list-style-type: none"> Modified polymers have better salt tolerance (viscosifying ability, long term stability, flow properties) than linear HPAM Some materials have been used in EOR, but results are not reported |
| [14] | HPAM and proprietary hydrophobically modified AAm-based copolymer | HPAM: Degree of hydrolysis = 5% MW = 8×10 ⁶ g/mol Proprietary copolymer: MW = 6×10 ⁶ g/mol | <ul style="list-style-type: none"> Improved performance for proprietary copolymer over HPAM (more elastic properties, reformability, high mobility control) Significant polymer retention in sand-pack tests (RRF = 165) |
| [31] | PAAm and AAm/AH copolymer | PAAm: MW = 5.0×10 ⁶ g/mol AAm/AH copolymer: $\bar{F}_{AAm} \sim 0.66$; MW = 5.6×10 ⁶ g/mol | <ul style="list-style-type: none"> Incremental oil recovery up to 20.0% with 2000 ppm copolymer solution in water (at 30°C); achieved 18.7% in brine (at 80°C) Incremental oil recovery up to 18.8% with 2000 ppm PAAm solution in water (at 30°C); only 11.8% in brine (at 80°C) |
| [32] | AAm/AAc copolymer (HPAM) | Polymer 1: $\bar{F}_{AAm} = 0.67$; MW = 6.0×10 ⁶ g/mol Polymer 2: $\bar{F}_{AAm} = 0.93$; MW = 4.5×10 ⁶ g/mol Commercial HPAM: $\bar{F}_{AAm} = 0.92$; MW = 4.0×10 ⁶ g/mol | Incremental recovery from 1wt% polymer solution: <ul style="list-style-type: none"> Polymer 1: 20.11% Polymer 2: 29.68% Commercial HPAM: 15.07% |
| [33] | Hydrophobically associating HPAM-based water-soluble polymer | AAm-rich multi-component polymer containing functional monomers (ACMO, HDDE, AMPS, IBOMA) | <ul style="list-style-type: none"> Experimental evidence of heat resistance, salt tolerance, and good antimicrobial degradation performance |

AAc = acrylic acid; AAm = acrylamide; ACO = N-acryloyl morpholine; AH = acryloyl hydrazide; AMPS = 2-acrylamido-2-methylpropane sulfonic acid; DBSV = 4-dodecyl-benzenesulfonate-1-vinylimidazol-3-ium-divinyl sulfone; HDDE = N,N'-((2-hydroxy-4,5-dimethyl benzene-1,3-diyl) dimethanediyl) bisprop-2-enamide; IBOMA = isobornyl methacrylate; NABI = N-allylbenzamide; NAE = N-allyloctadec-9-enamide; NNDAM = N,N-dimethyl acrylamide; NVP = n-vinyl pyrrolidone; PAAm = polyacrylamide; SAM = sodium (acrylamido) methanesulfonate; VN = 2-vinylnaphthalene

Many researchers have also considered combining polymer flooding with other chemical flooding techniques (for example, alkaline-surfactant-polymer (ASP) flooding), but those processes are beyond the scope of this work; detailed reviews have been conducted recently [34, 35]. Nevertheless, many of the polyacrylamide-based materials described in Table 2.1 could, in theory, be used in combination with alkalis and/or surfactants to further increase incremental oil recovery.

Alternatively, the most common (natural) biopolymer for enhanced oil recovery is xanthan gum. Xanthan gum is less shear sensitive and more brine compatible than HPAM, but does not increase the viscosity to the same extent (and is therefore less efficient than HPAM). Several reviews of biopolymers that have been investigated for EOR applications have been compiled recently (including [15, 36]), and key points are summarized in Table 2.2.

Table 2.2: Potential Biopolymers for Polymer Flooding EOR (adapted from [15])

| Biopolymer | Advantages | Disadvantages |
|------------------------|--|--|
| Carboxymethylcellulose | <ul style="list-style-type: none"> • Environmentally friendly • Water-soluble | <ul style="list-style-type: none"> • Oxidative decomposition • Thermal degradation |
| Cellulose | <ul style="list-style-type: none"> • Thermal stability • Shear stability | <ul style="list-style-type: none"> • Not water-soluble • Heterogeneous swelling |
| Guar Gum | <ul style="list-style-type: none"> • Environmentally friendly • Good salt compatibility | <ul style="list-style-type: none"> • Potential for plugging • Thermal degradation • Weak elasticity |
| Hydroxyethylcellulose | <ul style="list-style-type: none"> • Water-soluble • Thermal stability • Shear stability • Good viscosity modification | <ul style="list-style-type: none"> • Biodegradation |
| Lignin | <ul style="list-style-type: none"> • Environmentally friendly • Low cost | <ul style="list-style-type: none"> • Not water-soluble • Biodegradation • Oxidative decomposition |
| Schizophyllan | <ul style="list-style-type: none"> • Thermal stability • Good salt compatibility • Good viscosity modification • Non-toxic | <ul style="list-style-type: none"> • Biodegradation |

| | | |
|--------------|--|---|
| Scleroglucan | <ul style="list-style-type: none"> • Thermal stability • Shear stability • Good viscosity modification | <ul style="list-style-type: none"> • Biodegradation • Oxidative decomposition • Poor filterability of material in porous media |
| Welan Gum | <ul style="list-style-type: none"> • Long-term stability • Good viscoelastic properties | <ul style="list-style-type: none"> • Affected by inorganic cations in reservoir |
| Xanthan Gum | <ul style="list-style-type: none"> • Thermal stability • Shear stability • Good salt compatibility • Long-term stability | <ul style="list-style-type: none"> • Biodegradation • Oxidative decomposition • Potential for plugging |

2.1.2 Application Requirements

Since enhanced oil recovery has been studied in great detail, there is already a lot of information in the literature about current best practices. However, there are some general application requirements that must still be considered as part of the design process. It may seem evident, but one of the most important requirements for polymer flooding materials is that the polymer is water-soluble. As mentioned previously, the two most widely used polymers for enhanced oil recovery are HPAM and xanthan gum, both of which meet this requirement.

While water-soluble polymers come from a variety of sources, the current work focuses on synthetic polymers. This makes it possible to examine the design process from the initial synthesis (and recipe optimization) to applications, rather than modifying a pre-existing polymer. Free-radical polymerization is the primary synthesis technique, mainly due to its simplicity and versatility.

The application requirements for polymer flooding materials can be divided into two subsections: polymer properties and application-specific properties. Ultimately, to achieve desirable application-specific properties, one must first be able to understand and control the (microstructural and bulk) polymer properties. Therefore, they will be discussed separately.

2.1.2.1 Polymer Properties

A polymer's ability to increase the aqueous solution viscosity depends largely on the hydrodynamic volume of said polymer. The hydrodynamic volume, in turn, is influenced by the polymer's conformational rigidity and its molecular weight [37]. Therefore, the key properties for designing polymers for EOR are chemical composition (especially for multi-component polymers), sequence length distribution, and molecular weights.

One must first establish the reactivity ratios for the system to predict polymer composition and the resulting polymer microstructure. Reactivity ratios provide information about the degree of

incorporation of each comonomer into the resulting polymer and can be estimated by applying the error-in-variables method to experimental data (namely, conversion, initial composition and cumulative copolymer composition). The importance of using appropriate estimation techniques has been strongly emphasized in previous work; specific details about reactivity ratio estimation for binary and ternary polymerization systems can be found in recent work by Scott and Penlidis [38], and are also discussed in Section 2.3 of this thesis.

A significant advantage of using multi-component polymers (that is, copolymers or terpolymers) in EOR is the ability to tailor the product for the application requirements. Copolymers can incorporate the desirable properties of several components simultaneously, which ultimately improves the overall performance of the polymer [39]. The proportions of comonomers to be included in the recipe can be selected based on the expected degree of incorporation (that is, reactivity ratio estimates) and the known properties of their specific end groups. For example, high levels of amide (CONH₂) groups are known to increase stability, while high levels of carboxylate ions (COO⁻) will increase viscosity and decrease adsorption in the reservoir [22]. These behaviours are related not only to the functional groups, but also to their charges; this will be discussed further during the ‘Backbone Selection’ step in Section 2.1.3.

Knowledge of the terpolymerization reactivity ratios also provides information about the terpolymer microstructure, namely sequence length distribution and triad fractions. In some cases, two copolymers may have the same cumulative composition, but the distribution of the comonomers (and therefore functional groups) along the polymer backbone may differ. The structure of the copolymer (block, alternating, random, etc.) affects its viscoelastic properties (consider chain flexibility, for example), and will also affect the charge density in polyelectrolytes. For enhanced oil recovery, the microstructure can significantly affect the conformation of polymer chains in solution (that is, coiling or uncoiling). Since conformation affects the solution viscosity and EOR sweep efficiency, the distribution of the acidic comonomers is an important design consideration.

Sequence length distribution can be evaluated using probability functions, given the reactivity ratios and the composition of the polymerizing mixture [40]. For the copolymer case, the mole fraction (N_i) of monomer i sequences of length l can be calculated according to Equation 2.1:

$$N_i(l) = (p_{ii}^{l-1})(p_{ij}) = (p_{ii}^{l-1})(1 - p_{ii}) \quad 2.1$$

Where p_{ij} represents the probability that a growing radical ending with unit i adds monomer j (and is presented in Equations 2.2 and 2.3).

$$p_{ii} = \frac{r_i f_i}{f_j + r_i f_i} \quad 2.2$$

$$p_{ij} = \frac{f_j}{f_j + r_i f_i} \quad 2.3$$

The three-component case is presented in Equations 2.4 through 2.6, but the concept can be extended to any number of comonomers.

$$p_{ii} = \frac{f_i}{f_i + \frac{f_j}{r_{ij}} + \frac{f_k}{r_{ik}}} = \frac{r_{ij} r_{ik} f_i}{r_{ij} r_{ik} f_i + r_{ik} f_j + r_{ij} f_k} \quad 2.4$$

$$p_{ij} = \frac{r_{ik} f_j}{r_{ij} r_{ik} f_i + r_{ik} f_j + r_{ij} f_k} \quad 2.5$$

$$p_{ik} = \frac{r_{ij} f_k}{r_{ij} r_{ik} f_i + r_{ik} f_j + r_{ij} f_k} \quad 2.6$$

Alternatively, polymer microstructure can be quantified using instantaneous triad fractions, A_{ijk} . These values are also statistically based and can be calculated as a function of feed composition, given the associated reactivity ratios (see Equations 2.7 through 2.9). Note that only the i -centered triads are presented in the equations, but that the expressions can easily be extended to j -centered triads (thus, there are 6 possible triad fractions for the copolymer system).

$$A_{iii} = p_{ii}^2 = \left(\frac{r_{ij} f_i}{r_{ij} f_i + f_j} \right)^2 \quad 2.7$$

$$A_{jij} = p_{ij}^2 = \left(\frac{f_j}{r_{ij} f_i + f_j} \right)^2 \quad 2.8$$

$$A_{iij} = A_{jii} = p_{ii} p_{ij} = p_{ii} (1 - p_{ii}) = \frac{r_{ij} f_i f_j}{(r_{ij} f_i + f_j)^2} \quad 2.9$$

As expected, multi-component polymers are more complex, but the triad fractions can still be estimated from reactivity ratios. As an example, there are 18 possible triad fractions for the terpolymer case. The probability functions defined in Equations 2.10 through 2.15 must be used to ensure that all three comonomers are taken into account. Again, only the i -centered triads are presented herein, with obvious extensions to the j - and k -centered triads.

$$A_{iii} = p_{ii}^2 = \left(\frac{r_{ij} r_{ik} f_i}{r_{ij} r_{ik} f_i + r_{ik} f_j + r_{ij} f_k} \right)^2 \quad 2.10$$

$$A_{jij} = p_{ij}^2 = \left(\frac{r_{ik} f_j}{r_{ij} r_{ik} f_i + r_{ik} f_j + r_{ij} f_k} \right)^2 \quad 2.11$$

$$A_{kik} = p_{ik}^2 = \left(\frac{r_{ij} f_k}{r_{ij} r_{ik} f_i + r_{ik} f_j + r_{ij} f_k} \right)^2 \quad 2.12$$

$$A_{iij} = A_{jii} = p_{ii}p_{ij} = \left(\frac{r_{ij}r_{ik}f_i}{r_{ij}r_{ik}f_i + r_{ik}f_j + r_{ij}f_k} \right) \left(\frac{r_{ik}f_j}{r_{ij}r_{ik}f_i + r_{ik}f_j + r_{ij}f_k} \right) \quad 2.13$$

$$A_{iik} = A_{kii} = p_{ii}p_{ik} = \left(\frac{r_{ij}r_{ik}f_i}{r_{ij}r_{ik}f_i + r_{ik}f_j + r_{ij}f_k} \right) \left(\frac{r_{ij}f_k}{r_{ij}r_{ik}f_i + r_{ik}f_j + r_{ij}f_k} \right) \quad 2.14$$

$$A_{jik} = A_{kij} = p_{ij}p_{ik} = \left(\frac{r_{ik}f_j}{r_{ij}r_{ik}f_i + r_{ik}f_j + r_{ij}f_k} \right) \left(\frac{r_{ij}f_k}{r_{ij}r_{ik}f_i + r_{ik}f_j + r_{ij}f_k} \right) \quad 2.15$$

The cumulative triad fractions, \bar{A}_{ijk} , are perhaps more useful, as they characterize the final polymer product as a function of conversion, X (given the initial feed composition and reactivity ratios); the relevant equation is shown in Equation 2.16.

$$\frac{d(X\bar{A}_{ijk})}{dX} = A_{ijk} \quad 2.16$$

While these calculations are theoretical in nature, previous research has shown promising agreement between predicted triad fractions and experimental results from ^{13}C NMR [41].

High molecular weight polymers increase the solution viscosity and the permeability reduction factor (that is, the ability for EOR polymers to adsorb onto the porous well walls, reducing channeling effects and increasing sweep efficiency). This means that high molecular weight polymers allow more of the reservoir to be exposed to the displacing fluid and less oil is left behind [22]. The increased viscosity and permeability reduction factor both increase the oil recovery factor (compared to the same amount of a lower molecular weight polymer), which means that a high molecular weight polymer solution requires less polymeric material to achieve a designated recovery factor. The advantage of using less polymeric material in the EOR process is evident, both in terms of environmental and economic implications.

If the molecular weights are too high, there will be additional complications associated with the EOR application. One of the major issues is the potential degradation of the polymer, as high molecular weight chains tend to be more shear sensitive (especially in typical EOR conditions). Another concern is that the viscosity of the polymer flooding solution may end up being too high; this could lead to problems with reduced injectivity (where injectivity is the ratio between injection rate and pressure drop) and slower fluid throughput in the reservoir (largely due to plugging) [42].

Therefore, molecular weight control is important during the design and synthesis of EOR polymers. In free radical polymerization, the molecular weight can be controlled through careful selection of monomer concentration and feed composition (in the multi-component case); these techniques will be discussed further in Section 2.4. Most researchers studying acrylamide-based polymers for enhanced oil recovery agree that a target molecular weight on the order of 10^6 g/mol is appropriate [21, 32, 43].

2.1.2.2 Application-Specific Properties

Good control over the polymer properties is essential, especially since they are expected to have a significant effect on the application performance. Quantitative structure-property relationships will be pursued throughout this study, but the specific application requirements must first be understood. For the sake of discussion, these requirements will be presented in terms of flow behaviour, polymer stability and EOR performance.

The flow behaviour in enhanced oil recovery is characterized using a mobility ratio, M (see Equation 2.17). Ideally, the mobility ratio, which compares the displaced fluid (oil) to the displacing fluid (water), should be less than unity.

$$M = \frac{\lambda_w}{\lambda_o} = \frac{k_w/\mu_w}{k_o/\mu_o} \quad 2.17$$

Where λ represents mobility, k represents effective permeability, and μ represents viscosity for w , water and o , oil.

Typically, lower mobility ratios lead to better EOR efficiency. Adding polymeric material to the flood water has significant potential to decrease the mobility ratio, as the polymer will increase the flood water viscosity (μ_w) and reduce the effective permeability (k_w). Effective permeability is reduced as EOR polymers tend to adsorb onto the porous well walls, which ultimately reduces channeling effects and increases sweep efficiency. That is, more of the reservoir is exposed to the displacing fluid, and less oil is left behind, as demonstrated in Figure 2.3.

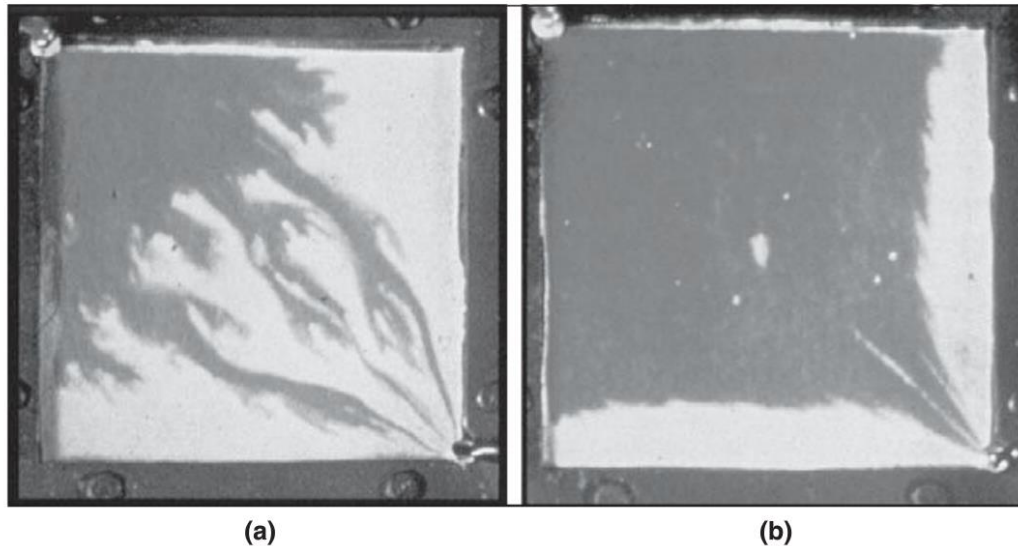


Figure 2.3: Comparison of Sweep Efficiency in (a) Water Flooding and (b) Polymer Flooding [22]

Depending on the polymer being used, the flow behaviour can be significantly influenced by the application conditions. For example, the effects of polymer concentration, salinity, pH, and temperature on polyacrylamide flow behaviour have been reported recently [44]. As expected,

increased polymer concentration decreases the mobility ratio (and therefore increases efficiency), as it alters the viscosity and the permeability of the polymer flood water. Salinity also has a significant impact on the flow behaviour, for two main reasons: first, some EOR polymers precipitate in high salinity reservoirs, and second, the dissolved salts affect the polymer chain conformation (due to charge effects) [41]. Thus, brine compatibility must be considered when the EOR polymer is being designed.

Polymer stability (mechanical, chemical, etc.) is also an important consideration in EOR, as the polymer-containing flood water is often subjected to hostile conditions. One of the biggest mechanical concerns, especially for acrylamide-based polymers, is the shear stability of the material; the polymer is typically exposed to high flow rates (and therefore high shear stresses), which is known to cause backbone degradation. This ultimately reduces the molecular weight of the polymer, which in turn reduces the viscosity (and efficiency) of the polymer flood water.

The chemical stability of the application polymer should also be considered, as there may be short-term (contaminant) and long-term (hydrolysis) concerns. In the short-term, polymers may be susceptible to redox reactions in the presence of contaminants, like oxygen or iron, which lead to viscosity loss [22]. These issues are typically addressed during the polymer flooding stage. However, the long-term concerns should be considered as the material is being designed. The oil reservoir may be at a high temperature level, which is known to lead to hydrolysis. A study performed by Ryles [13] showed that high temperatures lead to faster and more severe polymer degradation (in both synthetic and bio-based EOR polymers). As shown in Figure 2.4, the majority of oil fields are below 120°C, but polymer materials for enhanced oil recovery should be stable until at least 200°C [45].

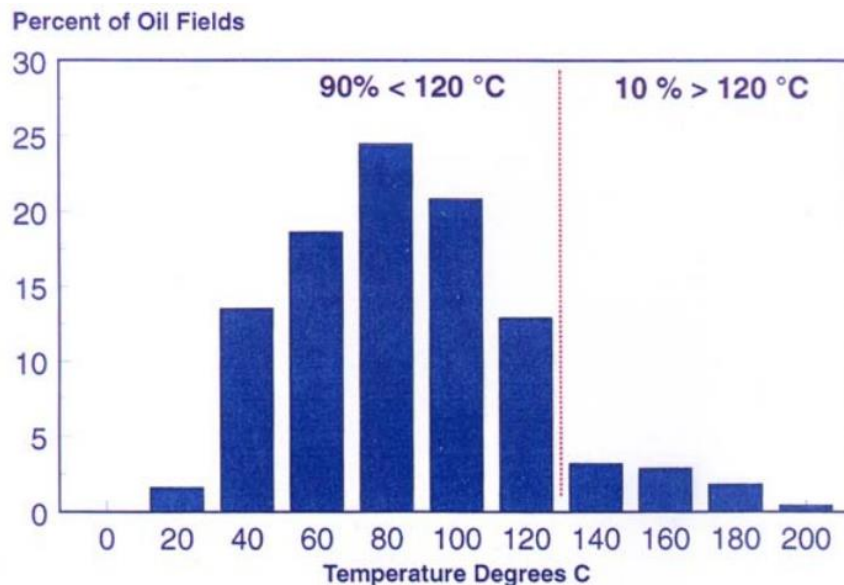


Figure 2.4: Temperature Distribution of Global Oil Fields (as of 1998) [45]

Finally, perhaps the most important application requirement is the EOR performance. The main goal for an EOR polymer is to maximize the amount of heavy oil recovery, while also taking environmental and financial considerations into account. This requires some level of optimization; injecting more polymer into the well (that is, increasing the polymer concentration in the flood water) will increase operating costs, but will likely increase the heavy oil recovery.

The tailor-made polymer should manipulate polymer properties to ensure good flow behaviour and satisfactory stability, so that the oil recovery process can be as efficient as possible. The original oil in place (OOIP) recovered during polymer flooding can be determined using sand-pack flooding experiments (to be discussed in Section 3.4.2), and is defined as the ratio between the volume of oil that has been recovered over the original amount of oil in the sand-pack (reservoir equivalent).

2.1.3 Backbone Selection

According to Ashby and Johnson [46], design materials may be selected by analysis, synthesis, similarity and/or inspiration. In the case of selecting a backbone for an optimized EOR polymer, the first three selection methods are relevant. However, the key here is selection by similarity. As mentioned previously, there are already many synthetic polymers employed in enhanced oil recovery, so these can act as a starting point for the design process.

The most widely used synthetic polymer for EOR is polyacrylamide (and other acrylamide-based polymers). Polyacrylamide and its derivatives are widely available, relatively inexpensive, and perform fairly well in EOR applications. However, polyacrylamide has a positive charge in acidic conditions, so partially hydrolyzed polyacrylamide (HPAM) is often preferred. Since HPAM loses some of the amide groups during hydrolysis, partially hydrolyzed polyacrylamide is essentially a copolymer of acrylamide and acrylic acid. Not only does the incorporation of the acrylic acid comonomer improve the electrostatic properties of the polymer, but the addition of the carboxylate groups also increases the solution viscosity.

As outlined in Section 2.1.2, the EOR polymer should be designed with certain properties in mind; this is where Ashby's selection by analysis becomes relevant. For the application, the polymer should have good flow behaviour (consider viscosity and effective permeability) and reasonable stability, which lead to excellent oil recovery properties. These requirements are linked to the polymer properties in Figure 2.5.

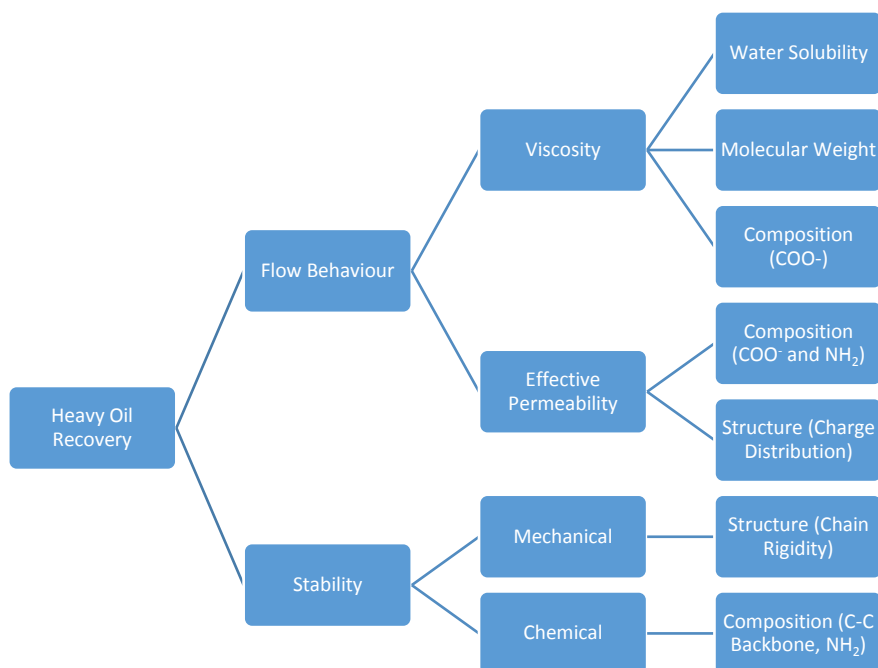


Figure 2.5: Linking Application Requirements to Polymer Properties

From Figure 2.5, it is clear that good control over viscosity, effective permeability, and chemical stability can be obtained with a tailor-made copolymer of acrylamide and acrylic acid. However, the missing component is the mechanical stability; it is important to minimize shear degradation by increasing the chain rigidity. Thus, a third component must be considered for the backbone: one that is compatible with the other application requirements, but that will also protect the polymer backbone from shear degradation.

Two comonomers have been considered: 2-acrylamido-2-methylpropane sulfonic acid (AMPS) and *n*-vinyl-pyrrolidone (NVP). However, since NVP has very poor additivity with acrylamide and acrylic acid, AMPS seems to be the better choice. Previously, it has been suggested that the bulky sulfonic acid group will protect the main chain (due to steric hindrance) and increase viscosity [20, 21]; also, strong hydrogen bonding will increase the polymer's solubility in water. Recent studies have also shown that copolymers containing AMPS are more stable in conditions of high temperature and high salinity [20, 47].

Several groups have recently become interested in the terpolymer of AMPS with acrylamide (AAm) and acrylic acid (AAc) [21, 48-51]. However, the polymerization kinetics are often ignored; the primary focus tends to be on synthesis, characterization, and potential applications for this terpolymer. As mentioned previously, the characteristics (and application requirements) of the EOR polymer can be directly related to its microstructure. Therefore, it is important to have a clear understanding of the terpolymerization kinetics. Since this information is not available in the literature, reliable reactivity ratios for this AMPS/AAm/AAc system will be determined experimentally as part of this research.

2.1.4 Product Customization

The key application requirements, both in terms of polymer properties and application-specific properties have been outlined in the previous sections. Now, it becomes necessary to understand how experimental conditions (that is, the pre-polymerization recipe) can be used to control the polymer product. The polymer properties (polymer composition, sequence length distribution and molecular weight) can all be optimized by selecting optimal reaction conditions. The most influential variables, herein called the ‘design variables’, are pH, ionic strength, monomer concentration and feed composition [41]. The first three design variables are known to affect the reactivity ratios (which in turn affect polymer composition and sequence length distribution). Additionally, molecular weight can typically be controlled with monomer concentration and feed composition.

Once these relationships are established, there is significant potential to tailor kinetics (and, subsequently, to achieve the required polymer properties) by selecting optimal reaction conditions. A good understanding of the terpolymerization kinetics of AMPS/AAm/AAC is essential to designing optimal materials for enhanced oil recovery, so a more detailed review of the literature (especially in terms of how these design variables affect the product terpolymer) is presented in Section 2.4. Then, quantitative relationships can be developed through chemical understanding, statistical design of experiments, and relevant analysis of results. These will be discussed in what follows.

2.2 Kinetics of Free Radical Polymerization

Many polymers, including some of the polymeric systems investigated herein, are produced via free radical polymerization (FRP). FRP is a type of chain polymerization which involves four main steps: initiation, propagation, chain transfer and termination.

The kinetics of free radical polymerization are well understood, and standard equations are readily available to provide information about polymerization rate [52]. The overall rate of polymerization, R_p , describes the rate of consumption of monomer ($-d[M]/dt$), with the majority of the monomer molecules consumed in the propagation step (long chain approximation).

$$R_p = k_p[M][R^\bullet] = k_p[M] \left(\frac{R_i}{k_t} \right)^{1/2} = k_p[M] \left(\frac{2fk_d[I]}{k_t} \right)^{1/2} \quad 2.18$$

Where f = initiator efficiency, k_d = initiator decomposition rate constant (very sensitive to temperature), k_p = propagation rate constant (also sensitive to temperature), k_t = overall termination rate constant, $[M]$ = monomer concentration, $[R^\bullet]$ = total free radical concentration, R_i = rate of initiation, R_p = rate of polymerization, and $[I]$ = initiator concentration.

A good understanding of free radical polymerization kinetics has the potential to be used to control synthesis reactions for specific applications. Kinetics can be directly linked to design, especially for copolymerizations (Section 2.2.1) and terpolymerizations (Section 2.2.2).

2.2.1 Free Radical Copolymerization

2.2.1.1 Terminal Model

When two comonomers are included within a single recipe, the kinetics become more complex. The typically used terminal model assumes that the reactivity of the propagating radical only depends on the terminal monomer unit (that is, the radical at the reactive end of the propagating chain) [53].

The terminal model assumes that there are four possible propagation reactions:

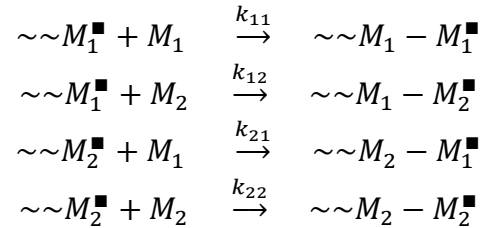


Figure 2.6: Terminal Model for Free-Radical Copolymerization

In this series of reactions, M_i^\blacksquare represents a radical species with monomer i at the chain end ($i = 1, 2$). Similarly, M_j represents monomer j that is being added to the chain end ($j = 1, 2$). Each of the four reactions has a rate constant, k_{ij} (radical i adding monomer j).

Two parameters, monomer reactivity ratios (r_1 and r_2), can be used to describe the potential for homopropagation relative to the potential for cross-propagation.

$$r_1 = \frac{k_{p11}}{k_{p12}} \quad \text{and} \quad r_2 = \frac{k_{p22}}{k_{p21}} \quad 2.19$$

Reactivity ratios can be estimated using experimental data and a copolymerization model, if the unreacted monomer composition in the polymerizing mixture and the copolymer composition are known. Techniques used for reactivity ratio estimation will be discussed in Section 2.3

The Mayo-Lewis equation, also called the instantaneous copolymer composition equation, is the most widely used copolymerization model. Two forms of this classical equation are shown below. Equation 2.20 is the differential form of the model, which is written in terms of monomer concentration in the polymerizing mixture ($[M_i]$). This assumes constant volume, which may not always be an accurate assumption.

$$\frac{d[M_1]}{d[M_2]} = \left(\frac{[M_1]}{[M_2]} \right) \left(\frac{r_1[M_1] + [M_2]}{[M_1] + r_2[M_2]} \right) \quad 2.20$$

Equation 2.21 can be used to determine the instantaneous mole fraction of monomer 1 incorporated into the copolymer (F_1) given the comonomer composition in the polymerizing mixture (as mole fractions, f_i). It is important to note that the Mayo-Lewis equation provides the instantaneous copolymer composition, which means that the model is only applicable for low conversion data (typically <5%, where composition drift is minimal).

$$F_1 = \frac{r_1 f_1^2 + f_1 f_2}{r_1 f_1^2 + 2f_1 f_2 + r_2 f_2^2} \quad 2.21$$

In order to analyze polymerization data for medium or high conversion levels, a cumulative form of the copolymer composition model becomes necessary. Two cumulative composition models (one derived using numerical integration and one derived using analytical integration) are available.

Direct numerical integration (DNI) requires solving an instantaneous mole balance and a cumulative mole balance (after reaching a certain conversion level, X_n) simultaneously [54]. The instantaneous mole balance (Equation 2.22), is an ordinary differential equation, for which f_i can be found at any conversion level if reactor volume is constant (initial conditions $f_i = f_{i,0}$ at $X_n = 0$). The cumulative mole balance at X_n gives the well-known Skeist equation, which is shown in Equation 2.23.

$$\frac{df_1}{dX_n} = \frac{f_1 - F_1}{1 - X_n} \quad 2.22$$

$$\bar{F}_1 = \frac{[M_{1,0}] - [M_1]}{[M_{1,0}] + [M_{2,0}] - [M_1] + [M_2]} = \frac{f_{1,0} - f_1(1 - X_n)}{X_n} \quad 2.23$$

DNI employs a direct approach and does not rely on model transformations or other potentially restrictive assumptions. This is a significant advantage over other copolymerization models, including the analytical integration technique discussed next.

Analytical integration of the Mayo-Lewis model (Equation 2.21) results in the Meyer-Lowry model (Equation 2.24), which is applicable for low to medium conversion levels (up to 20-40%) [55]. However, since X_n cannot be measured directly during experimentation, a rearranged version of the Skeist equation (Equation 2.23) is used to express conversion as a function of feed composition (f_i) and cumulative copolymer composition (\bar{F}_1).

$$X_n = 1 - \left(\frac{f_1}{f_{1,0}} \right)^\alpha \left(\frac{f_2}{f_{2,0}} \right)^\beta \left(\frac{f_{1,0} - \delta}{f_1 - \delta} \right)^\gamma = \frac{f_1 - f_{1,0}}{f_1 - \bar{F}_1} \quad 2.24$$

Where $\alpha = \frac{r_2}{1-r_2}$; $\beta = \frac{r_1}{1-r_1}$; $\gamma = \frac{1-r_1 r_2}{(1-r_1)(1-r_2)}$; $\delta = \frac{1-r_2}{2-r_1-r_2}$

It is important to note that molar conversion (X_n) is used in Equations 2.22 through 2.24, but that mass conversion (X_w) is typically measured experimentally. Molar conversion and mass conversion can be related using monomer molecular weights, as shown in Equation 2.25.

$$X_n = X_w \frac{MW_1 f_{1,0} + MW_2 f_{2,0}}{MW_1 \bar{F}_1 + MW_2 \bar{F}_2} = X_w \frac{MW_1 f_{1,0} + MW_2 (1 - f_{1,0})}{MW_1 \bar{F}_1 + MW_2 (1 - \bar{F}_1)} \quad 2.25$$

Where MW_1 and MW_2 are the molecular weights of monomer 1 and monomer 2, respectively.

An additional point of interest in copolymerization kinetics is establishing the azeotropic composition (if it exists) for the system. At the azeotropic point, the feed composition (f_i) and the instantaneous copolymer composition (F_i) are equivalent. If the reactivity ratios are known, the instantaneous copolymerization equation (Equation 2.21) can be used to examine F_i as a function of f_i and to establish the azeotropic point. By setting $F_i = f_i$, Equation 2.21 can be simplified, as shown in Equation 2.26.

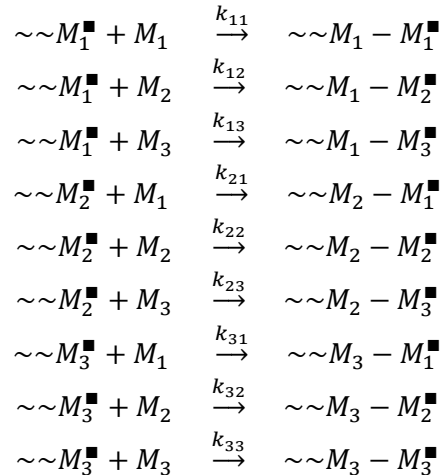
$$F_1 = f_1 = \frac{1 - r_2}{2 - r_1 - r_2} \quad 2.26$$

2.2.2 Free Radical Terpolymerization

Terpolymerization systems (and multi-component polymerizations in general) are part of an interesting and growing area of research, since there are countless combinations of monomers to be discovered. However, because of the wide range of possibilities, terpolymerization systems have not been studied as thoroughly as copolymerization systems.

2.2.2.1 Traditional Alfrey-Goldfinger Model

The kinetics of terpolymerization systems were first described by Alfrey and Goldfinger [56]. Given that there are three different possibilities for the terminal monomer (on the growing radical), and three options for the added monomer, nine different propagation steps are possible according to the terminal model:



Based on these propagation steps, Equations 2.27, 2.28 and 2.29 can be written in a form that is equivalent to the Mayo-Lewis equation (Equation 2.20), modified for a three-component system. The derivation is provided in Appendix A, Section A.1.

$$\frac{d[M_1]}{d[M_2]} = \left(\frac{[M_1]}{[M_2]} \right) \left(\frac{[M_1]/r_{31}r_{21} + [M_2]/r_{21}r_{32} + [M_3]/r_{31}r_{23}}{[M_1]/r_{12}r_{31} + [M_2]/r_{12}r_{32} + [M_3]/r_{32}r_{13}} \right) \left(\frac{[M_1] + [M_2]/r_{12} + [M_3]/r_{13}}{[M_2] + [M_1]/r_{21} + [M_3]/r_{23}} \right) \quad 2.27$$

$$\frac{d[M_1]}{d[M_3]} = \left(\frac{[M_1]}{[M_3]} \right) \left(\frac{[M_1]/r_{31}r_{21} + [M_2]/r_{21}r_{32} + [M_3]/r_{31}r_{23}}{[M_1]/r_{13}r_{21} + [M_2]/r_{23}r_{12} + [M_3]/r_{13}r_{23}} \right) \left(\frac{[M_1] + [M_2]/r_{12} + [M_3]/r_{13}}{[M_3] + [M_1]/r_{31} + [M_2]/r_{32}} \right) \quad 2.28$$

$$\frac{d[M_2]}{d[M_3]} = \left(\frac{[M_2]}{[M_3]} \right) \left(\frac{[M_1]/r_{12}r_{31} + [M_2]/r_{12}r_{32} + [M_3]/r_{32}r_{13}}{[M_1]/r_{13}r_{21} + [M_2]/r_{23}r_{12} + [M_3]/r_{13}r_{23}} \right) \left(\frac{[M_2] + [M_1]/r_{21} + [M_3]/r_{23}}{[M_3] + [M_1]/r_{31} + [M_2]/r_{32}} \right) \quad 2.29$$

As before, $[M_i]$ represents the concentration of monomer i ($i = 1, 2, 3$) in the system, and the r_{ij} values represent (binary) monomer reactivity ratios. In this case (given nine propagation steps), there are 6 unique reactivity ratios which can be estimated simultaneously given sufficient terpolymerization data. The estimation of these ternary reactivity ratios will be discussed further in Section 2.3.

$$r_{12} = \frac{k_{11}}{k_{12}} \quad r_{13} = \frac{k_{11}}{k_{13}} \quad r_{21} = \frac{k_{22}}{k_{21}} \quad r_{23} = \frac{k_{22}}{k_{23}} \quad r_{31} = \frac{k_{33}}{r_{31}} \quad r_{32} = \frac{k_{33}}{k_{32}} \quad 2.30$$

Again, these equations can be rearranged to form expressions for instantaneous terpolymer composition (F_i) as a function of unreacted monomer mole fractions in the feed (f_i) (in a way analogous to Equation 2.21 for copolymerization). Typically, this form of the Alfrey-Goldfinger model uses ratios of mole fractions (i.e. F_i/F_j) as responses (see Appendix A). However, measurements taken from experimental work are typically single mole fractions, not ratios, which means that evaluating F_i/F_j results in lost information and a distorted error structure.

2.2.2.2 Recast Alfrey-Goldfinger Model

To avoid the limitations associated with the traditional Alfrey-Goldfinger model (described above), the terpolymerization equations were re-derived from basic polymerization kinetics for this study, so that each terpolymer mole fraction is presented as a single response (see Equations 2.31 to 2.33; the derivation is presented in Appendix A, Section A.3). This formulation is an improvement over the original Alfrey-Goldfinger model, as it eliminates symmetry issues and error structures are not distorted. It also agrees with recent work published by Kazemi et al. [57], in which the ‘recast’ version of the Alfrey-Goldfinger model was developed using the ratio-based equations as a starting point (presented in Appendix A, Section A.2 for reference).

$$F_1 - \frac{f_1 \left(\frac{f_1}{r_{21}r_{31}} + \frac{f_2}{r_{21}r_{32}} + \frac{f_3}{r_{31}r_{23}} \right) \left(f_1 + \frac{f_2}{r_{12}} + \frac{f_3}{r_{13}} \right)}{f_1 \left(\frac{f_1}{r_{21}r_{31}} + \frac{f_2}{r_{21}r_{32}} + \frac{f_3}{r_{31}r_{23}} \right) \left(f_1 + \frac{f_2}{r_{12}} + \frac{f_3}{r_{13}} \right) + f_2 \left(\frac{f_1}{r_{12}r_{31}} + \frac{f_2}{r_{12}r_{32}} + \frac{f_3}{r_{13}r_{32}} \right) \left(f_2 + \frac{f_1}{r_{21}} + \frac{f_3}{r_{23}} \right) + f_3 \left(\frac{f_1}{r_{13}r_{21}} + \frac{f_2}{r_{23}r_{12}} + \frac{f_3}{r_{13}r_{23}} \right) \left(f_3 + \frac{f_1}{r_{31}} + \frac{f_2}{r_{32}} \right)} = 0 \quad 2.31$$

$$F_2 - \frac{f_2 \left(\frac{f_1}{r_{12}r_{31}} + \frac{f_2}{r_{12}r_{32}} + \frac{f_3}{r_{13}r_{32}} \right) \left(f_2 + \frac{f_1}{r_{21}} + \frac{f_3}{r_{23}} \right)}{f_1 \left(\frac{f_1}{r_{21}r_{31}} + \frac{f_2}{r_{21}r_{32}} + \frac{f_3}{r_{31}r_{23}} \right) \left(f_1 + \frac{f_2}{r_{12}} + \frac{f_3}{r_{13}} \right) + f_2 \left(\frac{f_1}{r_{12}r_{31}} + \frac{f_2}{r_{12}r_{32}} + \frac{f_3}{r_{13}r_{32}} \right) \left(f_2 + \frac{f_1}{r_{21}} + \frac{f_3}{r_{23}} \right) + f_3 \left(\frac{f_1}{r_{13}r_{21}} + \frac{f_2}{r_{23}r_{12}} + \frac{f_3}{r_{13}r_{23}} \right) \left(f_3 + \frac{f_1}{r_{31}} + \frac{f_2}{r_{32}} \right)} = 0 \quad 2.32$$

$$F_3 - \frac{f_3 \left(\frac{f_1}{r_{13}r_{21}} + \frac{f_2}{r_{23}r_{12}} + \frac{f_3}{r_{13}r_{23}} \right) \left(f_3 + \frac{f_1}{r_{31}} + \frac{f_2}{r_{32}} \right)}{f_1 \left(\frac{f_1}{r_{21}r_{31}} + \frac{f_2}{r_{21}r_{32}} + \frac{f_3}{r_{31}r_{23}} \right) \left(f_1 + \frac{f_2}{r_{12}} + \frac{f_3}{r_{13}} \right) + f_2 \left(\frac{f_1}{r_{12}r_{31}} + \frac{f_2}{r_{12}r_{32}} + \frac{f_3}{r_{13}r_{32}} \right) \left(f_2 + \frac{f_1}{r_{21}} + \frac{f_3}{r_{23}} \right) + f_3 \left(\frac{f_1}{r_{13}r_{21}} + \frac{f_2}{r_{23}r_{12}} + \frac{f_3}{r_{13}r_{23}} \right) \left(f_3 + \frac{f_1}{r_{31}} + \frac{f_2}{r_{32}} \right)} = 0 \quad 2.33$$

In spite of the advantages associated with these newly derived equations, they are only valid for the instantaneous case. Using low conversion data makes it possible to assume that the terpolymer composition drift is negligible (that is, at low conversions, the measurable cumulative copolymer composition is approximately equal to its instantaneous value). However, this restrictive assumption introduces additional sources of error, including significant experimental difficulties.

As an alternative, a cumulative ternary composition model can be used to analyze data over the full conversion trajectory. The cumulative model (essentially the Skeist equation applied to terpolymerization), shown in Equations 2.34 through 2.36, relates the cumulative terpolymer composition for each monomer (\bar{F}_i) to the mole fraction of monomer in the initial feed ($f_{i,0}$), the mole fraction of unreacted monomer (f_i) and the molar conversion (X_n). Note that these are analogous to Equation 2.23 for the copolymer case.

$$\bar{F}_1 = \frac{f_{1,0} - f_1(1 - X_n)}{X_n} \quad 2.34$$

$$\bar{F}_2 = \frac{f_{2,0} - f_2(1 - X_n)}{X_n} \quad 2.35$$

$$\bar{F}_3 = \frac{f_{3,0} - f_3(1 - X_n)}{X_n} \quad 2.36$$

If one cannot assume constant composition (that is, composition drift is no longer negligible), f_i must be evaluated over conversion X_n , according to the model in ordinary differential equation form (shown in Equations 2.37 through 2.39). Given the initial conditions $f_i = f_{i,0}$ at $X_n = 0$, a numerical solution can be used to evaluate terpolymer compositions along the full conversion trajectory. Here, the analogous equation for the copolymer case is Equation 2.22.

$$\frac{df_1}{dX_n} = \frac{f_1 - F_1}{1 - X_n} \quad 2.37$$

$$\frac{df_2}{dX_n} = \frac{f_2 - F_2}{1 - X_n} \quad 2.38$$

$$\frac{df_3}{dX_n} = \frac{f_3 - F_3}{1 - X_n} \quad 2.39$$

2.3 Reactivity Ratio Estimation

As mentioned earlier, reactivity ratios are important parameters for multi-component polymerization, since they provide information about the degree of incorporation of each comonomer into the resulting polymer product. Reactivity ratios can be estimated using experimental data and a polymerization model, if the free (unreacted) monomer composition in the polymerizing mixture and the bound (incorporated) monomer composition in the polymer chains (i.e., copolymer composition) are known.

Two important considerations for reactivity ratio estimation are careful (statistically informed) design of experiments and selection of appropriate parameter estimation techniques. Therefore, in this thesis section, design of experiments (Section 2.3.1) and reactivity ratio estimation (Section 2.3.2) are described for both copolymer and terpolymer systems.

2.3.1 Design of Experiments for Reactivity Ratio Estimation

A common source of error in reactivity ratio estimation is poorly designed (or undesigned) experiments. When too few (usually unreplicated) data points are chosen at random, it can be difficult to draw accurate information from experimental results. Thus, design of experiments is an important consideration in reactivity ratio estimation studies. When a series of experiments is designed in an optimal way, it becomes possible to minimize the number of experiments while increasing the information content from those experiments. Optimally designed experiments typically have much smaller joint confidence regions (JCRs), which is indicative of higher precision reactivity ratio estimates [58].

The error-in-variables model (EVM) can be used for model-based design of experiments, which increases the precision of parameter estimates through optimally designed experiments. EVM considers error in all terms, so using a design of experiments technique within the EVM context helps to account for the error in both the independent variables (feed compositions) and the dependent variables (copolymer or terpolymer compositions). EVM can also take into account any experimental limitations, which ensures that the mathematical results of the design of experiments are physically viable. Details have been presented previously [59, 60], but the key points are briefly revisited below. The following is applicable to any multi-component system, but details specific to binary and ternary systems are outlined in Sections 2.3.1.1 and 2.3.1.2, respectively.

The EVM design criterion aims to maximize the determinant of the information matrix (\underline{G}), which is the inverse of the variance-covariance matrix of the parameters.

$$\underline{G} = \sum_{i=1}^n r_i \underline{Z}'_i (\underline{B}_i \underline{V} \underline{B}'_i)^{-1} \underline{Z}_i \quad 2.40$$

Here, r_i is the number of replicates at the i^{th} trial (out of n trials), \underline{Z}_i is the vector of partial derivatives of the model function with respect to the parameters (in this case, the partial derivatives of the copolymerization/terpolymerization model with respect to the reactivity ratios), \underline{B}_i is vector of partial derivatives of the model function with respect to the variables (in this case, the partial derivatives of the copolymerization/terpolymerization model with respect to the feed (f) and copolymer/terpolymer (F) compositions), and \underline{V} is variance-covariance matrix of the variables (which provides information about measurement error and possible correlation of the variables involved).

During experimentation, either initial or sequential design schemes may be used. The initial design is employed when no prior information is known about the system; the design is based solely on a certain number of trials (usually chosen arbitrarily or at random, so they may or may not be optimal), and is a function of the number of parameters in the model. Alternatively, when some prior information is available for the system, a sequential design is employed. As the name suggests, the sequential design is an iterative process, and is repeated until the desired level of precision is obtained for the parameter estimates being studied [59]. Sequential design schemes typically provide smaller JCRs, which indicates that the reactivity ratio estimates are more reliable than those obtained from initial designs (a case study demonstrating this concept is shown in Section 2.3.1.1). Thus, to the extent possible, the sequential technique will be used to design experiments.

2.3.1.1 Design of Experiments for Binary Reactivity Ratio Estimation

Two common design of experiments techniques for copolymer systems are the Tidwell-Mortimer [61] and EVM (described above and elsewhere [59]) methodologies. Both use preliminary reactivity ratio estimates to suggest the initial feed compositions for subsequent runs [62].

Tidwell and Mortimer presented one of the earliest (mechanistic model-based) techniques for designing reactivity ratio estimation experiments [61]. The Tidwell-Mortimer methodology applies an approximate D-optimality criterion to the Mayo-Lewis copolymerization equation (Equation 2.21) to determine ‘optimal’ feed compositions at which to run reactivity ratio estimation experiments. The Tidwell-Mortimer design gives the following experimental conditions as optimal suggestions:

$$f_{2,0} = \frac{r_1}{2 + r_1} \qquad f_{2,0} = \frac{2}{2 + r_2} \qquad 2.41$$

Where $f_{2,0}$ is presented twice to denote the feed composition of monomer 2 for two distinct experiments. Preliminary reactivity ratio estimates (r_1 and r_2) are typically obtained from the literature or from some type of preliminary experimentation.

The Tidwell-Mortimer (T-M) equations are recognized as practical tools for the design of optimal experiments in reactivity ratio estimation. However, the method does have some limitations. The T-M design cannot take composition constraints into account, and is only applicable to binary systems. In a recent comparison of T-M and EVM design techniques, both techniques yielded similar parameter estimates. However, those obtained from the EVM-designed data gave parameter estimates with a higher degree of confidence [62].

To demonstrate the importance of sequential design of experiments for reactivity ratio estimation, we will briefly review a case study presented by Scott and Penlidis [6]. This was published as part of a Feature Paper in *Processes*, which demonstrated a user-friendly computational package for reactivity ratio estimation using EVM. Details about the computational package are shown in Appendix B (Section B.1), but the case study below provides an excellent example of the benefit of sequential design of experiments.

This case study employs experimental data for the copolymerization of butyl acrylate (BA; monomer 1) and methyl methacrylate (MMA; monomer 2). The original investigation by Dubé and Penlidis [63] was a detailed, multi-step analysis, but only data from the first step are used in the current exhibit.

In investigating the effect of experimental design on the confidence in our estimation results, there are two important pieces of information to consider. If the preliminary estimates of r_1 are smaller than r_2 , then (1) uncertainty in r_1 will seem much lower than uncertainty in r_2 (the same relative error will have a larger absolute value in r_2 compared to r_1) and (2) the Tidwell-Mortimer design will suggest recipes rich in monomer 1. As shown in Figure 2.7 (black JCR; 2 feed compositions), $r_1 < r_2$ for the BA/MMA system and there is more uncertainty in r_2 (that is, in the vertical direction). Generally speaking, the JCR is ‘stretched’ along the axis of the larger reactivity ratio estimate, which is due to both the absolute error and the selected feed compositions.

Since the absolute error is experiment-dependent, it is a fact of life that one has to live with. Thus, this case study focuses on item (2) described above: how do the feed compositions (selected randomly or via design of experiments) affect the reactivity ratio estimates and associated JCRs? In the case of BA/MMA copolymerization (given preliminary estimates $r_1 = 0.51$ and $r_2 = 2.38$ from Grassie et al. [64]), the Tidwell-Mortimer criterion suggests the following feed compositions: $f_{1,0} = 0.543$ and $f_{1,0} = 0.798$, where monomer 1 is butyl acrylate [63]. Based on this criterion, all of the experimental data collected are rich in monomer 1, which provides more certainty in r_1 (see again Figure 2.7; black JCR; 2 feed compositions).

At the next step, EVM-based sequential design of experiments can be employed [59]. This allows for further refinement of the reactivity ratio estimates, a higher degree of certainty and therefore smaller JCRs. The procedure is described below:

- (1) EVM is applied to instantaneous (low conversion) data (from [63]) to estimate reactivity ratios. Feed compositions are selected according to Tidwell-Mortimer design and four runs are done at each level: $f_{1,0} = 0.543$ and $f_{1,0} = 0.798$.
- (2) Parameter estimation results from EVM are recorded. Specifically, reactivity ratio estimates (r_1 and r_2) and the \underline{G} matrix (as defined in Equation 2.40) are required for sequential design of experiments.
- (3) The EVM-based sequential design of experiments program (using data from step (2), as well as the preliminary feed compositions from step (1)) is employed. Details on the design have been reported by Kazemi et al. [59].

From the sequential design of experiments, the next ‘best’ feed composition for analysis of the BA/MMA copolymerization is $f_{1,0} = 0.100$. This indication that more monomer 2-rich data is required is very reasonable, since all data collected to this point has been rich in monomer 1. By introducing experimental data rich in monomer 2, the uncertainty in r_2 should decrease.

In the absence of experimental data for $f_{1,0} = 0.100$, data were simulated using the instantaneous copolymerization model and random error was added (based on the variance reported in the original study). As was the case for the other feed compositions, four data points at $f_{1,0} = 0.100$ were added to the analysis. These new data points, along with the original data were then used to re-estimate the reactivity ratios with EVM. The results are shown alongside the original analysis in Figure 2.7 (red JCR; 3 feed compositions).

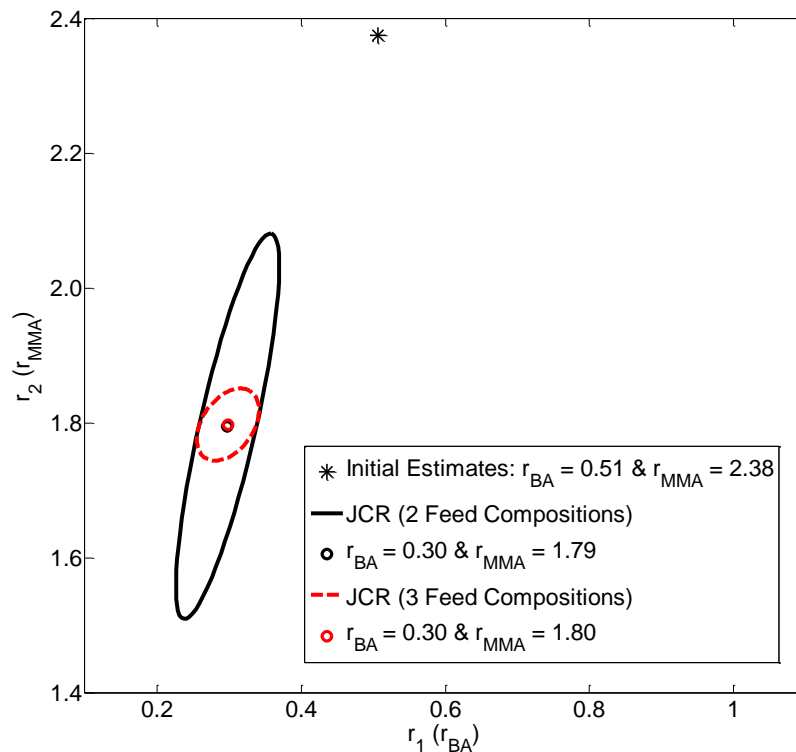


Figure 2.7: Effect of Sequentially Designed Experiments for the Copolymerization of BA/MMA

The inclusion of data rich in monomer 2 drastically improves the degree of certainty in the reactivity ratio estimates. While the point estimates are unaffected, the error in r_2 is significantly reduced. This is as expected: when data rich in monomer 2 are available, one can have greater confidence in r_2 .

This result demonstrates the importance of design of experiments for reactivity ratio estimation. Design of experiments makes it possible to maximize the information content from a minimal number of runs and to decrease the degree of uncertainty in parameter estimates. Sequential designs are extremely useful and revealing, and minimize the overall experimental effort.

2.3.1.2 Design of Experiments for Ternary Reactivity Ratio Estimation

As explained in previous work by Kazemi et al. [60], three optimal experiments are sufficient to estimate terpolymerization reactivity ratios. In the terpolymerization problem, the EVM model consists of three equations (see again Equations 2.31 to 2.33) and five variables (f_1, f_2, F_1, F_2, F_3); only 2 of the 3 feed compositions are independent ($f_3 = 1 - f_1 - f_2$) and the terpolymer compositions are measured independently. Therefore, for the terpolymerization, there are two independent variables (5 variables – 3 equations = 2) and six (6) parameters (reactivity ratios). The number of optimal experiments needed can be calculated by dividing the number of parameters by the number of independent variables (see Bard [65] and Duever et al. [66]), hence $6 \div 2 = 3$.

Of particular note is a practical heuristic for designing experiments for ternary reactivity ratio estimation, which suggests that (statistically speaking) the optimal feed compositions always fall into the same range [60]. When a multiplicative error structure is assumed and there are no other process constraints, the optimal feed compositions are as shown (in the shaded areas) in Figure 2.8. Three terpolymerization formulations, each rich in one comonomer, are sufficient to estimate ternary reactivity ratios [60]. In a recent study (also presented in Section 5.1.2 of this thesis), this was further confirmed while investigating the terpolymerization kinetics of 2-acrylamido-2-methylpropane sulfonic acid, acrylamide and acrylic acid [38].

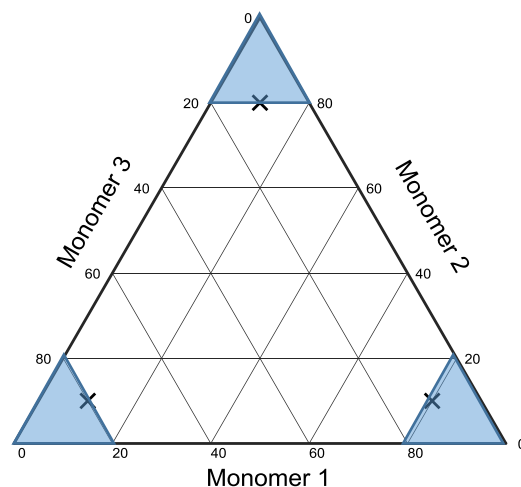


Figure 2.8: Optimally Designed Experiments for Ternary Reactivity Ratio Estimation (as per [60])

2.3.2 Reactivity Ratio Estimation using the Error-in-Variables Model

Linear regression techniques, including the Mayo-Lewis method (method of intersections), the Fineman-Ross method and the Kelen-Tudos method, have traditionally been used for reactivity ratio estimation [52]. However, by examining the instantaneous copolymer composition models shown in Equation 2.21 (for the 2-component system) and Equations 2.31 to 2.33 (for the 3-component system), one can see that the kinetic models are clearly non-linear in the parameters! While linearization provides computational simplicity (which, incidentally, is no longer necessary thanks to technological advancements), it also requires making imprecise and invalid assumptions. The problems associated with linear methods for parameter estimation have been thoroughly discussed in the literature [54, 67], and an additional relevant case study is provided in the following section (see Section 2.3.2.1).

Therefore, non-linear reactivity ratio estimation techniques should always be employed [67-70]. While some researchers choose to use a non-linear least squares approach, the error-in-variables-model (EVM) method is the most statistically correct technique. EVM forces the experimenter to consider all sources of error, including the error associated with independent variables (such as feed composition).

To obtain estimates of the ‘true’ values of both the independent variables and the parameters, EVM uses a nested-iterative approach (this is represented schematically in Figure 2.9, with variables defined in the discussion below) [69]. The inner loop searches for ‘true’ values of the independent variables, since there is inevitably some error associated with the measured values. Mathematically, one can relate the vector of known measurements (\underline{x}_i) to the vector of their unknown ‘true’ values ($\underline{\zeta}_i$) and an error term ($k\varepsilon_i$), according to Equation 2.42. In the error term, k

is a constant that represents the magnitude of the error and $\underline{\varepsilon}$ (error) is a random variable that is typically uniformly distributed on the interval $[-1, 1]$ (an additional explanation is included in Appendix B, Section B.2 for the interested reader). At the same time, the outer loop uses a copolymerization model (such as the instantaneous copolymer composition model, Equation 2.21) to relate the ‘true’ variables and the parameter (reactivity ratio) estimates, as shown in Equation 2.43.

$$\underline{x}_i = \underline{\xi}_i(1 + k\underline{\varepsilon}_i) \text{ where } i = 1, 2, \dots, n \quad 2.42$$

$$\underline{g}(\underline{\xi}_i, \underline{\theta}) = 0 \text{ where } i = 1, 2, \dots, n \quad 2.43$$

In both Equations 2.42 and 2.43, i represents the trial number (out of n trials), and underlined terms are either vectors or matrices.

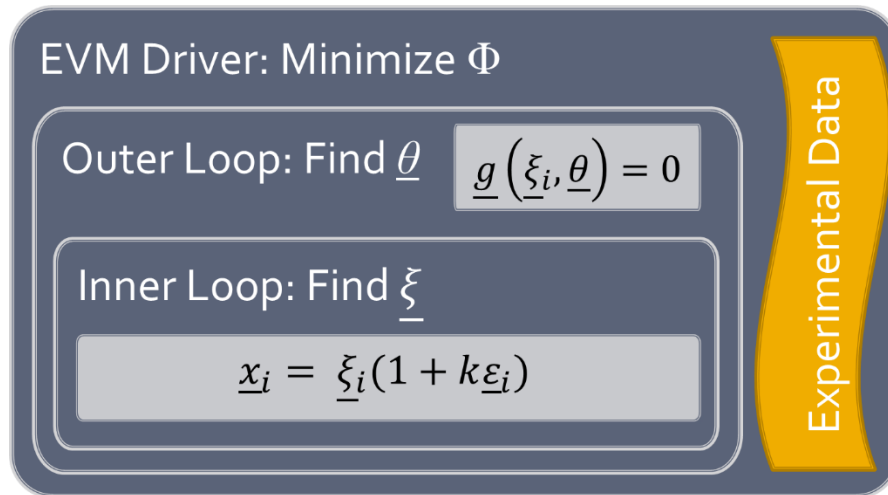


Figure 2.9: Nested-Iterative Algorithm for the Error-in-Variables-Model (EVM)

From a statistical perspective, the program uses this nested-iterative approach to minimize the sum of squares between the observed and predicted values, both in terms of the error in the independent variables and in terms of the parameter estimates. When the objective function (Equation 2.44) is minimized, the program has found the best estimates for both the independent variables and the parameters (reactivity ratios).

$$\Phi = \frac{1}{2} \sum_{i=1}^n r_i (\bar{\underline{x}}_i - \hat{\underline{\xi}}_i)' \underline{V}^{-1} (\bar{\underline{x}}_i - \hat{\underline{\xi}}_i) \quad 2.44$$

Where n is the number of experimental trials (runs), r_i is the number of replicates for the i^{th} trial, $\bar{\underline{x}}_i$ is the average of the r_i measurements (\underline{x}_i), $\hat{\underline{\xi}}_i$ is an estimate of the true values of the variables ($\underline{\xi}_i$) and \underline{V} is the variance-covariance matrix of the variables (which provides information about measurement error of the variables involved). To gain a better understanding of the magnitude of the error, the error distribution, the relationship between variables and errors (additive versus multiplicative), and potential correlation, independent replication becomes necessary; again, see Appendix B (Section B.2) for more information.

Alternatively, minimizing the objective function can be considered graphically, as in Figure 2.10. Given a model and some measured (independent) data, the inner loop minimizes the horizontal distances between the data points and the model (curve). At the same time, the outer loop minimizes the vertical distances between the data points and the model (that is, the outer loop attempts to reconcile model predictions and measurements).

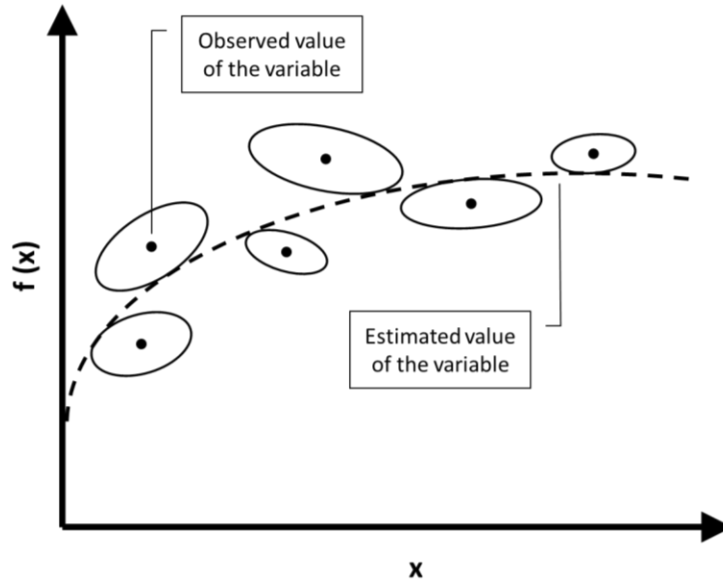


Figure 2.10: Graphical Representation of EVM (inspired by [67])

After estimates are obtained by EVM for both model parameters and model variables, it is important to evaluate the estimation results. This is primarily done by determining the precision of the parameter estimates. In the case of reactivity ratio estimation, several parameters are being estimated simultaneously. Thus, joint confidence regions (JCRs) are invaluable. JCRs are typically elliptical contours that quantify the level of uncertainty in the parameter estimates; as shown previously (in Section 2.3.1.1 and Figure 2.7), smaller JCRs indicate higher precision and therefore more confidence in the estimation results.

To approximate the error with an ellipse (Equation 2.45) requires that the error be normally distributed and that the variance be known. Here, it is important to note that $\hat{\theta}$ represents the vector of parameter estimates that minimize the objective function (Equation 2.44).

$$(\underline{\theta} - \hat{\underline{\theta}})' \underline{G} (\underline{\theta} - \hat{\underline{\theta}}) \leq \chi^2_{p,1-\alpha} \quad 2.45$$

Where $\chi^2_{p,1-\alpha}$ represents the chi-squared distribution for p parameters and a confidence level of $(1-\alpha)$.

An additional advantage of EVM is that it can be used to analyze copolymerization data up to medium-high conversion levels, since either the instantaneous or the cumulative model can be employed (recall Section 2.2). The instantaneous model described previously (Equation 2.21 for copolymerization and Equations 2.31 to 2.33 for terpolymerization) is only applicable to low conversion data, as it assumes that composition drift in the free monomer fraction is negligible (which may be true below 5% or 10% conversion). Assuming that no composition drift occurs (that is, the cumulative and instantaneous mole fractions in the copolymer are about the same) is considered ‘best practice’, and is used throughout the reactivity ratio estimation literature (see, for example, [71-76]).

However, limiting kinetic investigations to low conversion levels presents some fundamental challenges. In spite of our best efforts to validate the ‘lack of composition drift’ assumption, there is almost inevitably some change in feed composition with increasing conversion. From a more practical perspective, collecting low conversion data presents experimental challenges and the collected data are extremely prone to error.

Researchers should be aware of these limitations and should act accordingly. One might choose to include conversion data in the analysis (using a cumulative model and DNI, as per Section 2.2) to account for composition drift. Alternatively (rather, in addition), researchers might use design of experiments and experimental replication to address the inevitable error associated with the data collected. If nothing else, parameter estimation using EVM considers the error present in all variables, which can account for some of the experimental error. Ultimately, though, even the most statistically correct technique cannot compensate for bad data collection! Case studies examining the limitations of low conversion data (Section 2.3.2.2) and the advantages of using a cumulative model for analysis of medium-high conversion data (Section 2.3.2.3) are presented in what follows.

Although all three case studies presented in what follows are for copolymerization systems, the same observations (regarding shortcomings of linear parameter estimation, limitations of low conversion (instantaneous) data analysis, and advantages of full conversion (cumulative) models can be extended to the terpolymer case. Ternary reactivity ratios (that is, reactivity ratios estimated directly from ternary data) are described further in the following chapters, and two studies highlighting the importance of using appropriate estimation procedures are provided in Chapter 5 (Section 5.1).

2.3.2.1 MDO/VAc Case Study: Demonstrating the Shortcomings of Linear Parameter Estimation

This case study was part of the feature paper by Scott and Penlidis published in *Processes* [6], and presents an overview of recent literature [71-73, 77] regarding the copolymerization of 2-methylene-1,3-dioxepane (MDO; monomer 1) and vinyl acetate (VAc; monomer 2) (see also Table

2.3; RR stands for reactivity ratio). This copolymer has gained considerable attention in the past decade, largely due to its degradable properties. Researchers are especially interested in the reactivity ratios for the system, as reactivity ratios provide information about the copolymer microstructure. However, the reactivity ratio estimation (RRE) techniques used in this field are often incorrect. This case study will focus primarily on the issue of linear parameter estimation techniques, but invalid low conversion assumptions (that is, inappropriate use of the instantaneous copolymerization model) and error-prone data cannot be overlooked. Therefore, to demonstrate the advantages of EVM, select data from the literature will be re-evaluated (properly) and comparisons will be conducted.

Table 2.3: Summary of Reactivity Ratio Estimation (RRE) Studies for 2-methylene-1,3-dioxepane (MDO; monomer 1)/Vinyl Acetate (VAc; monomer 2) Copolymerization

| Ref. | RRE Technique | RRE Results | | Comments |
|------|---------------------------------|-------------|-------|--|
| | | r_1 | r_2 | |
| [71] | Kelen-Tüdös (K-T) | 0.47 | 1.56 | <ul style="list-style-type: none"> • Linear RRE technique used • Inappropriate low conversion assumption (reactivity ratios are ‘different enough’ that composition drift is possible) • Low conversion (<20%) data not presented; cannot be re-evaluated with EVM |
| [72] | Non-Linear Least Squares (NLLS) | 1.03 | 1.22 | <ul style="list-style-type: none"> • Non-linear RRE technique used (good!) • Controlled radical polymerization (RAFT) data used for RRE, therefore parameter estimates are ‘apparent’ reactivity ratios (as per Feldermann et al. [74]) |
| [73] | Fineman-Ross (F-R) | 0.14 | 1.89 | <ul style="list-style-type: none"> • Linear RRE technique used • Inappropriate low conversion assumption (as with [71], reactivity ratios are ‘different enough’ that composition drift is possible) • Suggest that low MDO reactivity (compared to other MDO/VAc RRE results in the literature) a result of low temperature; however, effect of temperature on RRs is usually weak |
| [77] | Fineman-Ross (F-R) | 0.93 | 1.71 | <ul style="list-style-type: none"> • Linear RRE technique used • Unequal weighting of experimental data • Instantaneous model applied to high conversion data (58–78% conversion reported) • F-R plot axes unintentionally flipped in original work (which changes RR estimates) • More comments in what follows |

In a recent study by Undin et al. [77], experimental data from six distinct feed compositions were used to estimate reactivity ratios for the MDO/VAc copolymerization. These six (batch) runs were allowed to continue until conversion did not change and the final conversion and composition measurements were reported. Finally, the reactivity ratios for the system were calculated using the Fineman-Ross (F-R) method. However, as mentioned briefly in Table 2.3, the data on the x and y

axes were unintentionally flipped in the analysis; thus, the reactivity ratio estimates originally reported are not representative of the experimental data collected.

Besides this unintended error, there are several other problems with the analysis, including (1) the use of undesigned data (that is, no design of experiments used for the selection of feed compositions); (2) the lack of composition drift considerations (RRE experiments should be performed at low conversion, or a cumulative model should be used); (3) the use of an outdated (and linear!) RRE technique. For the purposes of this discussion, we will focus on the use of the F-R method for RRE but the other important points should also be noted and kept in mind.

As discussed by Hagiopol [78], the F-R method is often justified by its simplicity. However, it has many shortcomings, including unequal weighting of experimental data and symmetry issues (i.e. calculation results depend on which monomer is selected as M_1). The data set presented in [77] is especially vulnerable to these shortcomings, largely due to the undesigned initial feed compositions (collection and use of undesigned data for parameter estimation also induce considerable correlation between the parameters, which is highly undesirable). As shown in Table 2.4, some of the data are obtained under fairly low M_1 comonomer feed fraction; these conditions tend to have the greatest influence on the slope of a line, which ultimately affects reactivity ratio estimates obtained using the F-R method [78].

Table 2.4: RRE Data for the Copolymerization of MDO (Monomer 1)/VAc (Monomer 2) [77]

| Sample | Monomer Feed | | Copolymer Composition | |
|--------|--------------|-----------|-----------------------|-------------|
| | $f_{1,0}$ | $f_{2,0}$ | \bar{F}_1 | \bar{F}_2 |
| MDO70 | 0.70 | 0.30 | 0.66 | 0.34 |
| MDO50 | 0.50 | 0.50 | 0.42 | 0.58 |
| MDO30 | 0.30 | 0.70 | 0.23 | 0.77 |
| MDO10 | 0.10 | 0.90 | 0.06 | 0.94 |
| MDO5 | 0.05 | 0.95 | 0.03 | 0.97 |
| MDO1 | 0.01 | 0.99 | 0.005 | 0.995 |

The more pressing concern with the F-R method (also described by Hagiopol [78]) is the lack of symmetry. Thus, values of r_1 and r_2 depend on which monomer is selected as M_1 . To demonstrate this point, the data collected by Undin et al. [77] are evaluated with $M_1 = \text{MDO}$ (which was performed incorrectly in the original work; see Figure 2.11a) and with $M_1 = \text{VAc}$ (performed herein for the demonstration; see Figure 2.11b).

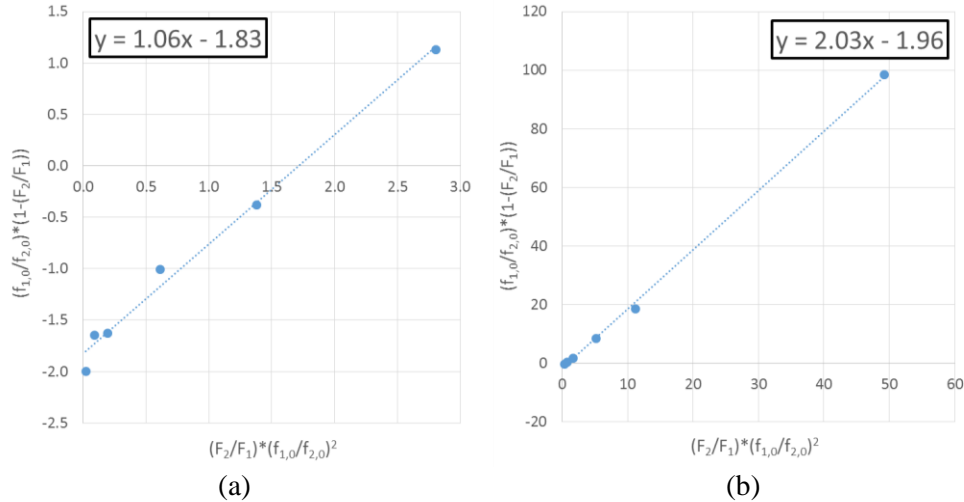


Figure 2.11: Fineman-Ross Plots for the Copolymerization of MDO/VAc with (a) $M_1 = \text{MDO}$ ($r_{\text{MDO}} = 1.06$; $r_{\text{VAc}} = 1.83$) and (b) $M_1 = \text{VAc}$ ($r_{\text{MDO}} = 1.96$; $r_{\text{VAc}} = 2.03$)

It is clear from Figure 2.11 that the reactivity ratio estimates depend on which comonomer is selected as M_1 ; the fact that two reactivity ratio pairs can be obtained from a single estimation technique is problematic. It is also interesting to note that both analyses give $r_1 > 1$ and $r_2 > 1$. While this is physically impossible, it is a side-effect of experimental (and estimation) error. In reality, these results suggest that both reactivity ratios should be close to unity (which agrees with the findings of Undin et al. [77] and Hedir et al. [72]) but that at least one reactivity ratio is < 1 .

The issue of symmetry (combined with the statistical inaccuracy of using linear parameter estimation to evaluate non-linear models) highlights the need for a non-linear parameter estimation technique like EVM. When using EVM for reactivity ratio estimation, the influence of which comonomer is defined as M_1 has no impact on the parameter estimates. (If RR estimates are slightly different based on the choice of M_1 , this is due to experimental error in the data). As shown in Figure 2.12, reactivity ratio estimates are within the JCR, regardless of which monomer is identified as M_1 . That is, slight discrepancies between EVM-obtained reactivity ratio estimates are well within the expected error (1% error in $f_{i,0}$ and 10% error in \bar{F}_i ; more on typical error levels in Appendix B, Section B.2). As expected, using measured/reported values as program inputs (in this case, $f_{\text{MDO},0}$ and \bar{F}_{MDO}) provides a greater degree of confidence in the results; note that the JCR in Figure 2.12a is smaller than that in Figure 2.12b. There is also significantly more parameter correlation visible in Figure 2.12b, as evidenced by the diagonal nature of the (more elongated) JCR. This, again, is as expected; the VAc data set was calculated from the measured MDO composition data, so correlation is inevitable here.

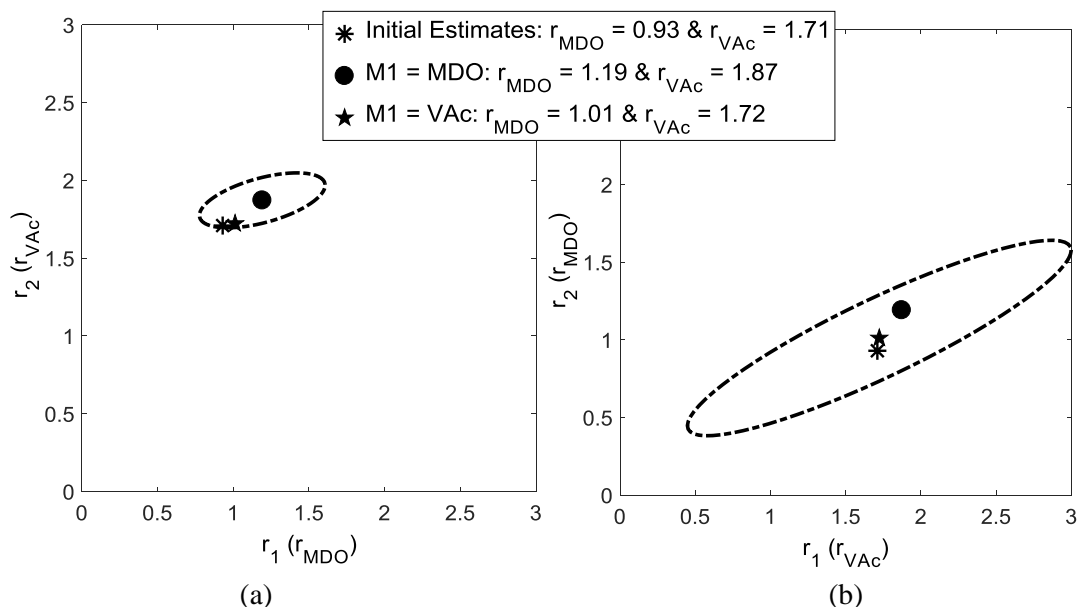


Figure 2.12: EVM-obtained RR Estimates and JCRs for the Copolymerization of MDO/VAc with (a) $M_1 = \text{MDO}$ ($r_{\text{MDO}} = 1.19$; $r_{\text{VAc}} = 1.87$) and (b) $M_1 = \text{VAc}$ ($r_{\text{MDO}} = 1.01$; $r_{\text{VAc}} = 1.72$).

In using EVM to re-analyze the data, $r_1 > 1$ and $r_2 > 1$ is still observed (see again Figure 2.12). This outcome is likely a result of using cumulative composition data in an instantaneous model, since composition drift was not taken into account for this data set and conversion levels up to 80% are reported. Even the most statistically correct technique cannot reconcile cumulative experimental data with an instantaneous model (and, in this case, appropriate conversion data are unavailable for reanalysis with the cumulative EVM program).

The final step is to visually evaluate the prediction performance of the reactivity ratio estimates, which involves comparing the experimental values to those predicted by the instantaneous copolymer composition equation (Equation 2.21). As shown in Figure 2.13, the symmetry issues associated with the Fineman-Ross (F-R) technique have a significant impact on the prediction performance (red curves, Figure 2.13a). In contrast, both of the predictions using EVM-obtained RR estimates (blue curves, Figure 2.13b) are in agreement with each other and with the experimental data. This is compelling evidence to choose non-linear parameter estimation techniques like EVM over the statistically incorrect linear parameter estimation techniques.

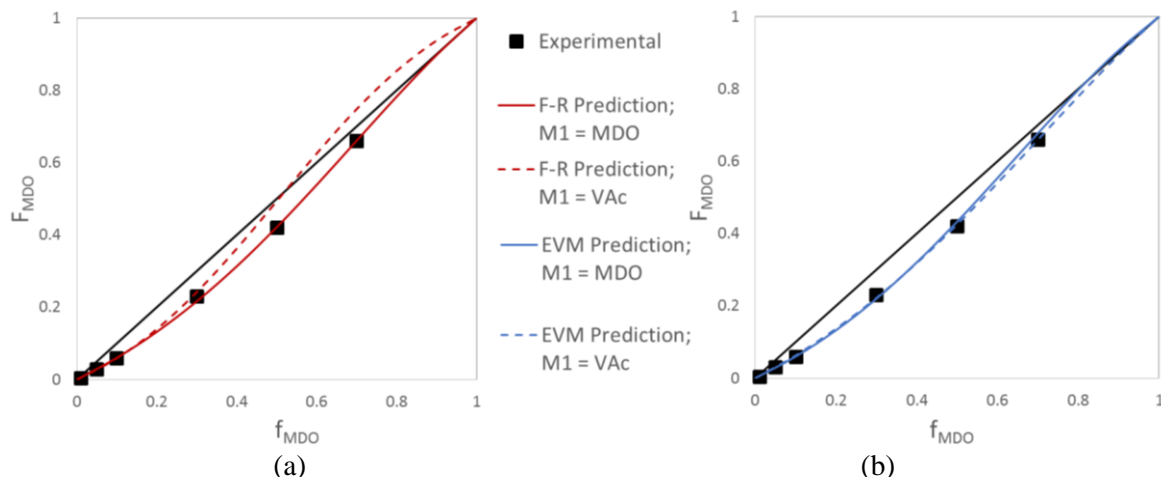


Figure 2.13: Comparison of Prediction Performance for RR Estimates Obtained by (a) F-R and (b) EVM

2.3.2.2 HEA/DCP Case Study: Considering the Limitations of Low Conversion Data Analysis

This case study was part of the same feature paper by Scott and Penlidis described earlier [6].

Since the virtues of EVM over linear parameter estimation techniques have already been established, the goal of the next case study is to emphasize the limitations of low conversion data and demonstrate how they can be addressed using EVM. The data set comes from recent work by Suresh et al. [75], whose work describes the synthesis and reactivity ratio estimation of photosensitive copolymers based on 4-(3-(2,4-dichlorophenyl)-3-oxoprop-1-enyl) phenylacrylate (DCP; monomer 2). In the study, DCP was copolymerized with hydroxyethyl acrylate (HEA; monomer 1) and with styrene and reactivity ratios were determined to better understand copolymerization behaviour. However, as established in the MDO/VAc Case Study (Section 2.3.2.1), researchers often revert back to linear parameter estimation techniques and the authors (incorrectly) used the Fineman-Ross (F-R) and Kelen-Tüdös (K-T) methods for parameter estimation (see Table 2.5).

Table 2.5: Summary of RRE Results for Hydroxyethyl Acrylate (HEA; Monomer 1)/4-(3-(2,4-dichlorophenyl)-3-oxoprop-1-enyl) Phenylacrylate (DCP; Monomer 2) Copolymerization

| Ref. | RRE Technique | RRE Results | |
|------------------|--------------------|-----------------|-----------------|
| | | r_1 | r_2 |
| [75] | Fineman-Ross (F-R) | 1.53 ± 0.10 | 0.76 ± 0.16 |
| [75] | Kelen-Tüdös (K-T) | 1.67 ± 0.13 | 0.58 ± 0.05 |
| [75] | Extended K-T | 1.65 ± 0.13 | 0.60 ± 0.08 |
| Current Work [6] | Instantaneous EVM | 1.28 * | 0.56 * |
| Current Work [6] | Cumulative EVM | 1.32 * | 0.55 * |

* Note: For EVM-obtained reactivity ratio estimates, statistically correct JCRs are presented instead of approximate confidence intervals (derived on a linear hypothesis); see Figure 2.15.

All experimental data that Suresh et al. [75] used for reactivity ratio estimation were kept below 15% conversion, so that the instantaneous copolymerization equation could be used for parameter estimation. But, is ‘below 15% conversion’ enough? As mentioned previously, this is largely considered ‘best practice’, but does not account for composition drift (even at low conversions) nor for experimental error. As shown in Figure 2.14, only five (seemingly unreplicated) data points were collected for reactivity ratio estimation, with obvious discrepancies between the experimental data and the model predictions.

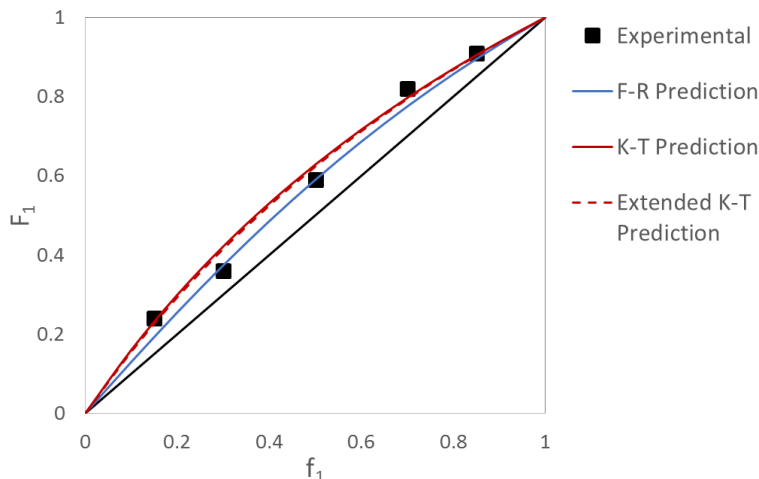


Figure 2.14: Prediction Performance of RR Estimates for HEA/DCP Copolymerization (Obtained by Linear RRE Techniques)

It is likely that these discrepancies are due to experimental error; this type of behaviour is observed very often, especially for low conversion data. In order to address this, researchers should review potential sources of error; they are likely (1) unidentified composition drift and/or (2) experimental difficulties. This case study will demonstrate both of these sources of error (and how to handle them). This is another very important, yet implicit, contribution of EVM. EVM, if nothing else, forces one to think about the possible sources of variation (and quantify them).

To account for composition drift (even at low conversions), the cumulative copolymerization model (Equations 2.22 and 2.23) should be used. Using direct numerical integration to solve this system of equations ensures that the feed composition (f_1) is considered as a function of conversion, thus taking any composition drift into account mathematically. To establish whether unidentified composition drift is the culprit in the current experimental data set, one can evaluate the data using both the instantaneous and cumulative models and compare the results (Figure 2.15, discussed below). In reality, using the cumulative model would also increase the amount of data available for analysis, as the copolymerization would be allowed to go to higher conversion levels (and data would continue to be collected); in addition, the experimental information is enhanced, anyway, since both conversion and copolymer composition data are included; see also Section 2.3.2.3.

Ultimately, this would increase the degree of confidence in the reactivity ratio estimates and decrease the size of the JCR.

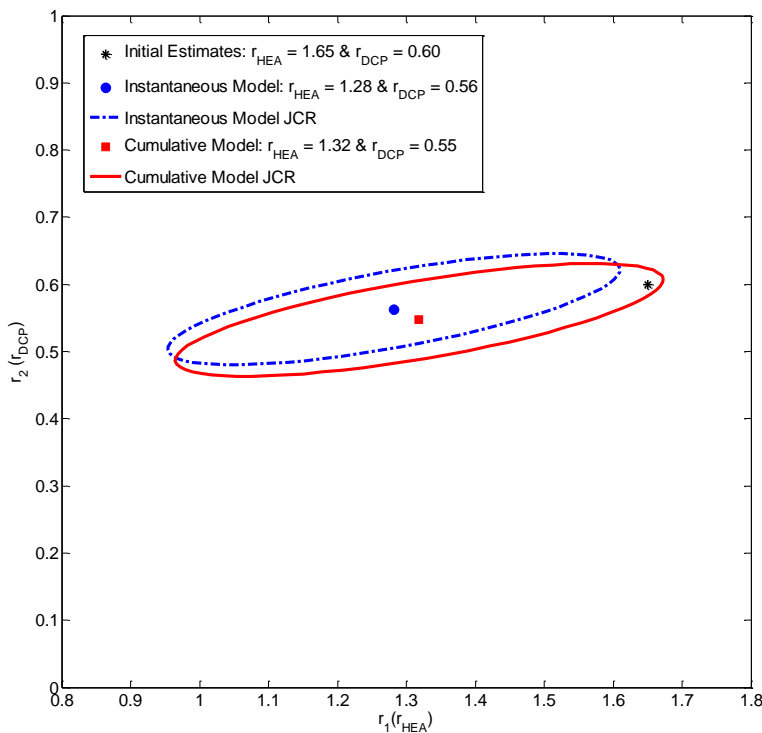


Figure 2.15: EVM-obtained RR Estimates and JCRs for the Copolymerization of HEA/DCP using the Instantaneous Model ($r_{\text{HEA}} = 1.28$; $r_{\text{DCP}} = 0.56$) and the Cumulative Model ($r_{\text{HEA}} = 1.32$; $r_{\text{DCP}} = 0.55$)

Figure 2.15 indicates that the two EVM-obtained reactivity ratio estimates are in good agreement and the JCR sizes and orientations are similar. Thus, in this case, the effect of composition drift is likely minimal. Therefore, we will continue our troubleshooting by investigating the second source of error: experimental difficulties. Since no replicate data are available, it is not possible to calculate the error associated with the composition measurements shown in Figure 2.14. However, as discussed previously, EVM considers the error present in all variables throughout the parameter estimation process. The program default values of 1% error (associated with $f_{1,0}$) and 5% error (associated with \bar{F}_1) were therefore used in the analysis (see Appendix B, Section B.2 for additional information).

The reactivity ratios calculated using the EVM program are as described in Table 2.5 and Figure 2.15. The converged program also provides the best available estimates of ‘true’ values of the variables (recall Equations 2.42 and 2.43). Thus, in Figure 2.16, it is possible to compare the experimental (measured) values to the ‘true’ experimental values and the EVM model predictions (both instantaneous and cumulative).

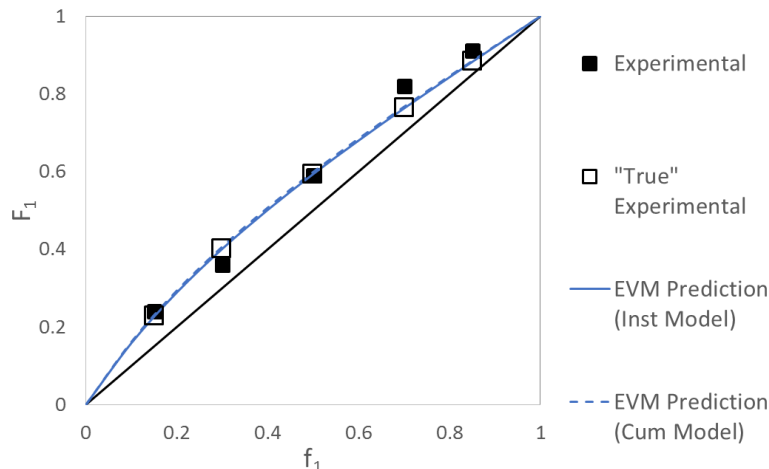


Figure 2.16: Prediction Performance of RR Estimates Obtained using EVM

Figure 2.16 indicates that the experimental data points were subject to some degree of error, especially for $f_{1,0} = 0.3$ and $f_{1,0} = 0.7$. Thus, experimental difficulties are likely the culprit here. The best way to mitigate this type of problem is to design experiments, replicate copolymerization runs and use EVM for parameter estimation. Additionally, using full conversion data with the cumulative model gives a more complete picture of copolymerization kinetics; researchers do not have to struggle with the experimental challenges of collecting low conversion data. This will be discussed in the next case study.

2.3.2.3 BMA/BA Case Study: Exploiting Information Content through Medium-High Conversion Data Analysis

This case study was part of the same feature paper by Scott and Penlidis described earlier [6].

Since medium-high conversion level data are used for parameter estimation in this case, reactivity ratios are estimated by applying the cumulative composition model (using direct numerical integration) to the data through EVM (see again Equation 2.23). Also, because conversion (X) varies with time as the polymerization proceeds, one cannot expect the composition of the polymerizing mixture to remain constant. Therefore, the instantaneous composition of the unreacted (unbound) monomer (f_i) can be evaluated using the differential copolymer composition equation (Equation 2.22). Solving these equations simultaneously makes it possible to minimize the sum of squares between the measured and the predicted values (for both the independent variables and the parameter estimates), which is the main objective of EVM.

The data used for this case study were taken from Ren et al. [79], who recently investigated the copolymerization kinetics of *n*-butyl methacrylate (BMA; monomer 1) and *n*-butyl acrylate (BA; monomer 2). Originally, the group collected copolymerization data at low conversion levels (<10%) so that the instantaneous model (Equation 2.21) could be used for analysis. After

estimating preliminary reactivity ratios using the original RREVM program [70], additional (replicated) designed experiments were completed to improve the quality of the data. This low conversion data set was re-analyzed using the new MATLAB-based EVM program [6]. As with the original investigation, analysis was first performed with the preliminary data only (9 equidistant feed compositions). Then, the analysis was repeated with preliminary data supplemented by the designed replicates (feed compositions selected using the Tidwell-Mortimer criterion [61]). A comparison of reactivity ratio estimates (from the original and current studies) is shown in Table 2.6.

Table 2.6: Summary of RRE Results for *n*-Butyl Methacrylate (BMA; Monomer 1) and *n*-Butyl Acrylate (BA; Monomer 2) Copolymerization

| Ref. | RRE Technique | RRE Results | |
|------------------|---|-------------|-------|
| | | r_1 | r_2 |
| [79] | Preliminary Estimates (RREVM) [70] | 2.100 | 0.489 |
| [79] | Estimates from Tidwell-Mortimer Designed Experiments (RREVM) [67, 70] | 2.008 | 0.460 |
| Current Work [6] | Instantaneous EVM (preliminary data) | 2.109 | 0.492 |
| Current Work [6] | Instantaneous EVM (preliminary data & designed replicates) | 2.012 | 0.462 |
| Current Work [6] | Cumulative EVM | 2.114 | 0.500 |

Good agreement is observed between reactivity ratio estimates, no matter what the amount (or type) of data used. This indicates well-behaved data; the low conversion analysis was done in a methodical and statistically correct manner. The cumulative EVM results (presented in the final row of Table 2.6) are discussed in what follows.

Although low conversion analysis (as performed by Ren et al. [79]) was sufficient for reactivity ratio estimation (especially since design of experiments was included in the investigation), it is interesting to consider the following: what if one had also included additional (medium-high conversion) experimental data? Ren et al. [79] chose to run three feed compositions up to high conversion values; the full conversion experimental data were used to evaluate the prediction performance of the reactivity ratio estimates. The analysis showed good agreement between model predictions and experimental data, thus confirming the reactivity ratio estimates.

We can take this one step further for illustration purposes. Using the cumulative model and direct numerical integration provides us with the opportunity to ‘repurpose’ this cumulative (medium-high conversion) data for improved reactivity ratio estimation. With a cumulative model, there is potential to obtain significantly more information (that is, more data points) from each experiment. Also, since researchers are not limited to low conversion, less experimental tedium is required to obtain the same degree of accuracy, as long as the experiments are well-designed.

A direct comparison of the preliminary analysis (9 feed compositions) and the cumulative analysis (3 feed compositions) results is provided in Figure 2.17. The same initial estimates were used in

both cases to ensure that both of the RRE techniques had the same starting point. It is interesting to note that both the reactivity ratio estimates and the JCR areas are almost identical for the two data sets. This leads to two main conclusions: that the parameter estimation results using the instantaneous and cumulative models are in agreement and that the degree of confidence in the results is approximately the same (regardless of which data set and/or model is being used). Therefore, in this case, 3 full conversion runs have approximately the same information content as 9 runs that are limited to low conversion levels.

This result should motivate researchers to think carefully about their preliminary experimental work. By strategically selecting feed compositions (using design of experiments techniques like Tidwell-Mortimer [61, 62] or EVM [59, 80]) and collecting copolymerization data up to medium or high conversion levels, it is possible to obtain sufficient information about a new system. The results shown herein suggest that preliminary experimental work can almost be reduced to 1/3 of the original load, without any loss of information content. Therefore, researchers should be encouraged to make use of all copolymerization data by employing the cumulative copolymerization model.

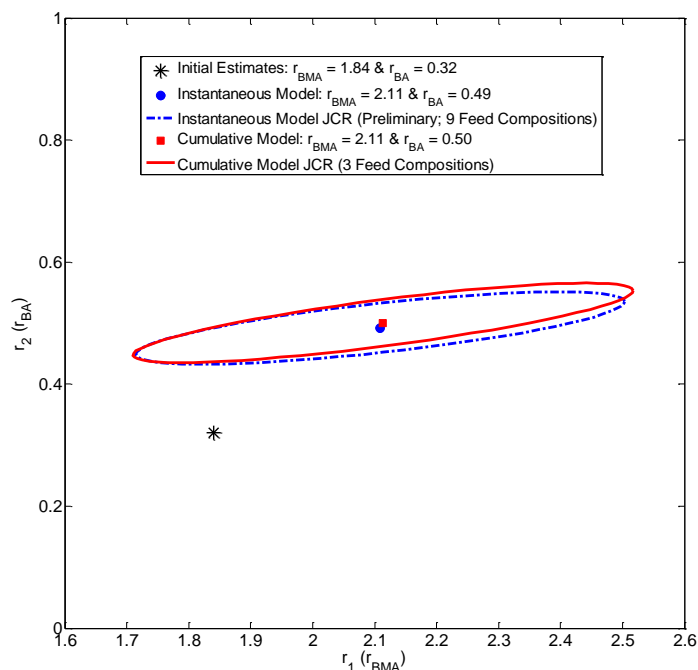


Figure 2.17: Comparison of Results for the Copolymerization of BMA/BA using the Instantaneous Model ($r_{\text{BMA}} = 2.11$; $r_{\text{BA}} = 0.49$) and the Cumulative Model ($r_{\text{BMA}} = 2.11$; $r_{\text{BA}} = 0.50$)

2.4 Terpolymerization Kinetics of AMPS/AAm/AAc

Most of the literature review outlined in this section has been recently published by Scott, Duever and Penlidis [81]; the work examines the effect of various experimental conditions on the

terpolymerization kinetics of 2-acrylamido-2-methylpropane sulfonic acid (AMPS), acrylamide (AAm) and acrylic acid (AAc).

As explained in Section 2.1.3, AMPS/AAm/AAc terpolymers are a promising candidate for enhanced oil recovery (EOR), given the application requirements and the anticipated properties of the terpolymer. AMPS/AAm/AAc has only recently appeared in the literature, with applications ranging from enhanced oil recovery [21] to controlled drug delivery [82]. Typically, existing studies focus on the final properties of the material (swelling behaviour, thermal and mechanical stability, etc.) [21, 48, 50], but investigating the terpolymerization kinetics is equally important [80]. The bulk polymer properties (and, by extension, properties relevant to the final application) depend on the terpolymer microstructure, therefore a clear understanding of the terpolymerization kinetics is invaluable.

The kinetics of an associated copolymer, acrylamide/acrylic acid, have been well-studied. Riahi-zhad et al. [83], among others, have shown that experimental conditions (that is, the pre-polymerization solution properties) can significantly impact polymerization kinetics and the resulting copolymer. Since the AAm/AAc copolymer is a polyelectrolyte, pH, ionic strength and monomer concentration are all influential variables during synthesis [84-87]. AMPS also exhibits polyelectrolyte behaviour, so one might expect that solution properties will also affect AMPS/AAm/AAc terpolymerization.

In looking at extensions from the AAm/AAc copolymer to the AMPS/AAm/AAc terpolymer, it is important to note that binary observations do not always apply to the ternary system [38]; this will be discussed further in Chapter 5 (Section 5.1). In the past, many researchers have used copolymerization results to predict terpolymerization behaviour. Although this may work for some cases, it is an approximation, as it effectively ignores the presence of the third comonomer. A third comonomer will inevitably change the reaction conditions and, by extension, the polymerization kinetics. Therefore, although one might look to the AAm/AAc system for guidance, new terpolymer-specific investigations are needed.

This section describes known effects of various reaction conditions on the polymerization kinetics of AMPS/AAm/AAc and (more often) the effects of those conditions on related homopolymers and copolymers. This background knowledge can help inform decisions about experimental conditions and can provide confirmation that the observed experimental results are reasonable. Therefore, a brief overview about the effects of pH, ionic strength, monomer concentration and feed composition on the polymerization of AMPS/AAm/AAc (and associated systems) is presented herein.

2.4.1 Effect of pH

The terpolymer of AMPS/AAm/AAC is a polyelectrolyte. That is, the macromolecule can contain covalently bound anionic or cationic groups (as a result of dissociation), which ultimately results in a charged polymer. These charges are extremely influential in terms of polymerization kinetics and should therefore be understood for customization purposes.

The comonomers AMPS and AAC are both acidic in nature, which means that dissociation (loss of the H⁺ ion from the carboxylic or sulfonic acid group) occurs as pH increases. The amount of dissociation that occurs is often reported as the degree of ionization, α , and can be calculated according to Equation 2.46.

$$\alpha = \frac{10^{pH-pK_a}}{10^{pH-pK_a} + 1} \quad 2.46$$

Where pK_a is the acid dissociation constant, which varies by compound. Atta et al. [88] have reported that AMPS and AAC have pK_a values of 2.3 and 4.2, respectively.

The rate of polymerization is a strong function of the degree of ionization. As the monomers (and resulting polymer chains) dissociate, they will contain like charges. These charges repel one another, which causes two significant changes in the system. First, the chain is forced to stretch out to separate the charges as much as possible (which eliminates the typical coil conformation of polymer chains). Second, the monomers and the radical chain contain like charges, which decreases the reactivity ratio of said monomers.

The effect of pH on the homopolymerization of AAm and the homopolymerization of AAC have been studied extensively, as have the copolymerization kinetics of AAm/AAC (see, for example, [89-92] for AAm, [93-96] for AAC, and [85, 97-99] for AAm/AAC). To the best of our knowledge, a limited number of homopolymerization studies have been performed for AMPS [100]; it is more frequently used as a comonomer with AAm or AAC (see, for example, [62, 101-105]).

A brief overview of pH effects is presented herein, as this research can help inform the current study. However, it is important to recognize that binary reactivity ratios (and, in general, copolymerization behaviour) do not necessarily extend to terpolymer system [38]. So, by extension, the homopolymerization kinetics reported in literature may not always align with what is observed in terpolymer systems.

A recent study by Beuermann et al. [100] investigated the homopolymerization kinetics for the solution polymerization of AMPS using near-infrared spectroscopy and pulsed laser polymerization. The study included pH effects, as $\langle k_t \rangle/k_p$ values were compared over conversion for both the acid (AMPS) and salt (NaAMPS) forms of the monomer (where $\langle k_t \rangle$ is a mean termination rate coefficient and k_p is the propagation rate constant). Kinetic behaviour was similar

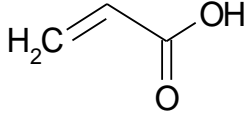
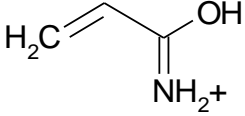
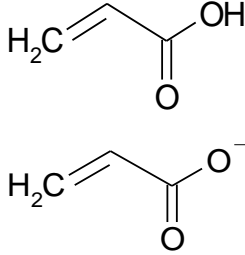
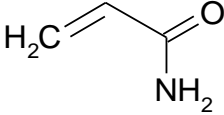
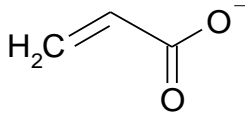
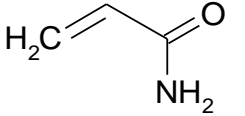
for both the acid form (where pH was very low) and the salt form (where pH = 7), suggesting that pH had no significant effect [100].

The effect of pH on the homopolymerization of poly(acrylamide) has been widely studied for many years (see, for example, [89-92]). The majority of these reports suggest that pH has little effect on acrylamide homopolymerization kinetics, at least over the ranges studied. Some exceptions are an increase in k_p at pH 1 (compared to higher pH levels) reported by Currie et al. [89] and an increased rate of polymerization between pH 6 and pH 7 ([106] as reported by [90]). However, in general, other solution effects and reaction conditions are more influential than the solution pH.

Many poly(acrylic acid) kinetic studies (including these references [93-96]) have experimentally confirmed that the rate of polymerization of acrylic acid is significantly affected by pH. As the solution is neutralized (that is, as pH increases to approximately pH 7 and the degree of ionization, α , increases to 1), repulsion occurs between monomers and around the propagating chain, thus reducing the rate of polymerization for poly(acrylic acid). As the pH is increased beyond pH 7, an increased rate of polymerization is observed, likely due to charge screening effects [93, 96].

The general pH effects on the AAm/AAC copolymerization have also been well studied [97-99] and are summarized in Table 2.7. Copolymerization behaviour at pH 2 (that is, where the acrylamide radical is protonated) has been studied by Cabaness et al. [97] and Paril et al. [98]; although pH effects are minimal in acrylamide homopolymerization studies, both copolymerization studies showed a reduction in AAm incorporation (and, subsequently, increased AAC incorporation) at low pH. Riahinezhad et al. [85] recently confirmed pH effects for the range of pH 3 to pH 7; experimental observations showed that the charged (AAC) monomer (at higher pH values) has lower additivity (that is, a lower reactivity ratio) due to charge repulsion.

Table 2.7: Effect of pH on AAm/AAc Polymerization Kinetics

| pH | Monomer Forms Present | | Effect on Reactivity Ratios (r_i or r_j) |
|------------|---|---|--|
| | Acrylic Acid (AAc) | Acrylamide (AAm) | |
| pH < 2 |  |  | Increased r_{AAc} , decreased r_{AAm} |
| 2 < pH < 6 |  |  | Complex kinetics, since it can technically be considered a terpolymerization; both r_{AAc} and r_{AAm} are similar and close to 1 [99] |
| pH > 6 |  |  | Decreased r_{AAc} , increased r_{AAm} |

For simplicity, the acidic monomers are referred to as AMPS and AAc throughout the thesis; the change in structure is acknowledged in terms of experimental conditions (and not reflected in the monomer name). Based on the above discussion (and on the use of NaOH and NaCl for pH and ionic strength adjustment, respectively), the monomers become sodium salts as the acids dissociate. This will be discussed in more detail in what follows. However, the presence of NaAMPS (2-acrylamido-2-methylpropane sulfonic acid sodium salt) and NaAAc (acrylic acid sodium salt or sodium acrylate) is implied as pH increases.

2.4.2 Effect of Ionic Strength

The polyelectrolyte nature of this terpolymer means that the ionic strength (IS) of the polymerizing mixture must also be considered. To minimize the repulsion between charges (both within the polymer chains and between the monomers and the chains), counter-ions can be added to the system in the form of salt. These counter-ions shield (and effectively neutralize) the charged molecules, which limits repulsion and increases reactivity. The IS of a given solution can be calculated according to Equation 2.47.

$$IS = \frac{1}{2} \sum c_i z_i^2 \quad 2.47$$

Where c_i is the molar concentration of ion i (mol/L) and z_i is the charge of ion i .

Not only does the ion charge number play a role in the ion shielding, but the type of cation does as well; this affects the electrostatic attraction between anions and counter-ions. It has been shown

that the reactivities of both AAm and AAc in copolymerization can be affected by the type of cation [107, 108]. These studies indicate that the counter-ion type affects the reactivity ratios, which are also related to the copolymer composition and the sequence length. In the current work, sodium is the counter-ion of choice (largely due to availability and ease-of-use), but other options can be considered to customize the polymer product.

Ionic strength effects have been evaluated for both acrylamide and acrylic acid homopolymerization kinetics, and have often been studied alongside pH effects (see, for example, [92, 93, 95]). As mentioned in the discussion surrounding pH, a smaller amount of information is available for the AMPS comonomer, since it is less widely used. However, since it is a strong acid, it is expected that the terpolymerization of AMPS/AAm/AAc will also be influenced by the IS of the pre-polymerization mixture.

The effect of NaCl on polyacrylamide synthesis was studied by Lacik et al. [92] alongside their pH investigation. For aqueous polymerization with 5 wt% acrylamide, no change in k_p was observed over the range of 0.001 M to 0.1 M NaCl. Further increasing the NaCl concentration to 1 M resulted in a slight increase of k_p . The effect of NaCl (or other salt) addition on poly(acrylic acid) synthesis is much more pronounced, as the cations from the salt act as counter-ions, providing charge screening and increased reactivity as described previously. The impact of salt addition on poly(acrylic acid) kinetics was first described by Kabanov et al. [93], who described an ‘ion pair mechanism’ that significantly increased the propagation rate and the molecular weights of the product polymers. Since then, similar ionic strength effects have been reported by many other groups for homopolymerization of acrylic acid and copolymerization of acrylic acid with acrylamide [84, 86, 95, 98, 99, 109].

Specifically, copolymerization studies for acrylamide/acrylic acid have shown that ionic strength affects the rate of polymerization and monomer reactivity ratios (see, for example, the recent study by Riahinezhad et al. [84]). When the acrylic acid monomer is partially or fully ionized, the reactivity ratio associated with AAc is low (due to charge repulsion). Experimental results have shown that adding salt (typically NaCl) to the pre-polymerization formulation can provide charge screening, thus increasing the incorporation of AAc (and r_{AAc}) [84, 86, 99].

2.4.3 Effect of Monomer Concentration

In aqueous polymerization, the total monomer concentration ($[M]$) can drastically affect the kinetics. This is especially true for polyelectrolytes, as the monomer concentration can also affect the ionic strength of the polymerizing mixture. The kinetic study for AMPS homopolymerization discussed earlier [100] compared rate constants (k_p and k_t) for aqueous solution polymerization (at 40°C) with 20 wt% AMPS (1.04 M) and 50 wt% AMPS (2.79 M). The analysis indicated that k_p was higher at a lower $[M]$; at the higher $[M]$, a four-fold decrease in k_p was reported. In this case, Beuermann et al. [100] suggested that the reduction in k_p may be due to reduced chain mobility

and repulsion between charged monomers and charges along the macroradical. Similar behaviour has been observed for the homopropagation of acrylamide [92, 110], acrylic acid [111], and methacrylic acid [112-114].

The relationship between monomer concentration, ionic strength and polymerization kinetics studied for poly(methacrylic acid) [113] can provide insight about the poly(acrylic acid) case. Pulsed-laser polymerization results showed that k_p decreased with increasing $[M]$ (as for the AMPS study) for the non-ionized case ($\alpha=0$); there was a four-fold decrease as the concentration changed from 5 wt% (0.59 M) to 40 wt% (4.72 M). Conversely, for the fully ionized case ($\alpha=1$), k_p increased with increasing monomer concentration (three-fold increase over the same range), which may be due to charge screening. In all cases (that is, at all monomer concentration levels), the k_p was higher for the non-ionized monomer than the ionized monomer [113]. This is as expected, since the ionized monomer will repel other monomers and charged macroradicals due to the like charges. Interestingly, polymerizations at lower monomer concentrations exhibited a more drastic change in k_p as the degree of ionization increased. That is, ionization effects were more pronounced at low monomer concentration. This may indicate that a higher monomer concentration (and, therefore, a higher ionic strength for the fully ionized case) stabilizes the system via charge screening.

As mentioned in the discussion of other recipe factor effects, extensions from homopolymerization to multi-component systems (copolymerization or terpolymerization) should be made with caution. The influence of monomer concentration on the copolymerization kinetics of AAm/AAC has been studied recently [85, 86, 99]. In general, copolymerization studies have shown that increased $[M]$ does not have an isolated effect; it is influenced by other factors including pH and ionic strength (as one might expect given the complexity of the system). Riahinezhad et al. [85] reported that the effect of $[M]$ becomes more pronounced at higher pH levels (that is, partially or fully ionized conditions); changing $[M]$ at pH 3 had almost no effect on the reactivity ratios, but had significant effects at pH 7. At higher pH levels, increasing $[M]$ results in a decreased r_{AAm} and an increased r_{AAC} . These results agreed with those reported previously by Rintoul and Wandrey [99]. Riahinezhad et al. [85] also observed that an increase in monomer concentration made reactivity ratios less ‘scattered’ (that is, more consistent over different pH levels). This observation aligns with the stability observed in the poly(methacrylic acid) study described previously [113]; higher monomer concentration seems to provide additional charge screening, thus decreasing the effect of monomer ionization on polymerization kinetics.

It is well-known, but worth acknowledging nonetheless, that adjusting monomer concentration can also have a significant impact on the molecular weight of the polymer product. Molecular weight is directly proportional to $[M]$, which provides researchers with a convenient way to achieve the desired molecular weight for a custom terpolymer.

2.4.4 Effect of Feed Composition

In addition to the overall monomer concentration, the feed composition (that is, the fraction of each comonomer in the recipe) can also influence the polymerization kinetics and product properties. The design of experiments relies on EVM criteria to select optimal feed compositions (see Section 2.3.1), but the feed composition can be varied once relationships are known. Theoretically, the fraction of each comonomer in the recipe affects the cumulative copolymer composition and the sequence length distribution; these relationships are visible in several equations presented previously (see, for example, Equations 2.31 to 2.39 and 2.10 to 2.16).

During AAm/AAC copolymer design work by Riahinezhad et al. [32], high levels of acrylamide showed the best performance for the EOR application. When the fraction of acrylamide was between 65% and 95%, the product exhibited high molecular weights and high shear viscosity (with maximum shear viscosity observed at 70% AAm) [115], both characteristics being desirable in EOR. The same study found that small amounts of acrylic acid improved the polyelectrolyte nature of the copolymer, but too much AAC resulted in brine sensitivity.

These considerations can be extended to the case of the AMPS/AAm/AAC terpolymer. It is expected that high levels of acrylamide will still be necessary, therefore preference should be given to solution conditions that promote high AAm incorporation into the product terpolymer. Ideally, we are also looking for conditions where the terpolymerization exhibits very little composition drift, so that the cumulative terpolymer composition remains approximately constant at any level of conversion.

Chapter 3. Experimental Methodology for Case Study #1 – Enhanced Oil Recovery

The experimental methodology has been presented (at least in part) in several of our publications. These publications provide information about preliminary investigations [80] and screening experiment results [81]. Also, several of the experimental procedures described in what follows will inform an additional paper (recently submitted), in which the optimally designed terpolymers for enhanced oil recovery are evaluated in terms of application performance.

3.1 Materials

Monomers 2-acrylamido-2-methylpropane sulfonic acid (AMPS; 99%), acrylamide (AAM; electrophoresis grade, 99%), and acrylic acid (AAc; 99%) were purchased from Sigma-Aldrich (Oakville, ON, Canada). AAc was purified via vacuum distillation at 30°C, while AAM and AMPS were used as received. Initiator (4,4'-azo-bis-(4-cyanovaleric acid), ACVA), inhibitor (hydroquinone) and sodium hydroxide were also purchased from Sigma-Aldrich. Sodium chloride from EMD Millipore (Etobicoke, ON, Canada) was used as received. In terms of solvents, water was Millipore quality (18 MΩ·cm); acetone (99%) and methanol (99.8%) were used as received. Nitrogen gas (4.8 grade) used for degassing solutions was purchased from Praxair (Mississauga, ON, Canada). Finally, the reference polymers that were used as baseline for comparison of properties were part of the Alcoflood series (254S, 935X, and 955), purchased from BASF, USA.

3.2 Polymer Synthesis

3.2.1 Screening Experiments

The screening experiment study was the first step in examining the effects of reaction conditions on the terpolymerization of AMPS/AAM/AAc. Specifically, optimally designed experiments (using the error-in-variables model (EVM) design [60] as described in Section 2.3.1.2) and a definitive screening design made it possible to select pre-polymerization recipes with high information content so that the entire system could be understood in just a few experimental runs. The experimental data were subsequently used to estimate ternary reactivity ratios, which provide valuable information about the resulting terpolymer properties. A good understanding of how the solution properties affect terpolymer reactivity ratios, composition, microstructure and molecular weight paves the way for the synthesis of custom-made polymers for specific applications.

In general, the experimental techniques described by Riahi-zhad et al. [83] were adopted for these terpolymer systems. As per the EVM design of experiments procedure for terpolymerizations [60], each pre-polymerization recipe was rich in one comonomer ($f_{AMPS,0}/f_{AAM,0}/f_{AAc,0} = 0.8/0.1/0.1, 0.1/0.8/0.1, 0.1/0.2/0.7$). Prior work has shown poor polymerization when the AAc fraction is too

high [62], therefore the constrained design (relative to the general heuristic shown in Figure 2.8) shown in Figure 3.1 was used for this experimental work. Additional experimental conditions (at each of these feed compositions) are described in what follows.

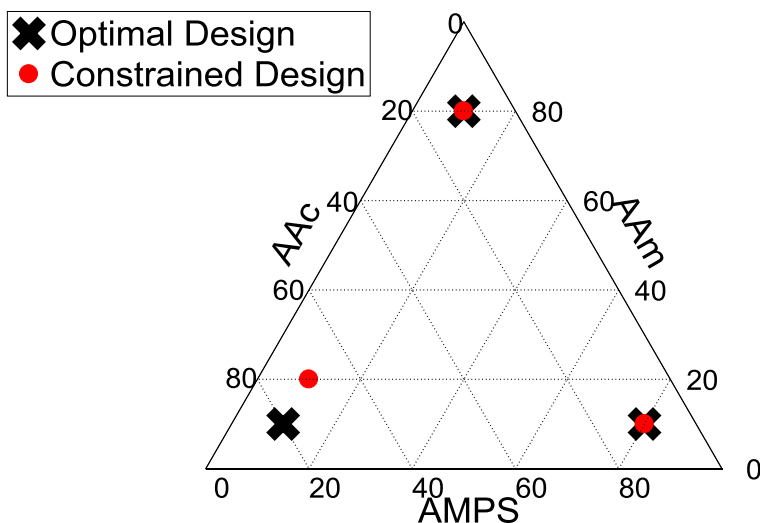


Figure 3.1: Optimally Designed Experiments for Ternary Reactivity Ratio Estimation (Constrained Design for AMPS/AAm/AAC Terpolymerization)

Solutions to be polymerized were prepared with target monomer concentrations (according to the experimental design of Table 3.1) and the initiator (ACVA) concentration was adjusted to maintain a constant $[M]/[I]^{1/2}$ ratio ($=15.8$). Prior to polymerization, solutions were titrated with sodium hydroxide to adjust the solution to the desired pH (± 0.5), and sodium chloride was added to adjust ionic strength among the experiments.

All solutions were purged for two hours under 200 mL/min nitrogen. After degassing, aliquots of ~ 20 mL of solution were transferred to sealed vials using the cannula transfer method. Free-radical solution (aqueous phase) polymerizations were run in a temperature-controlled shaker-bath (OLS200; Grant Instruments, Cambridge, UK) at 40°C and 100 rpm. Vials were removed at selected time intervals, placed in ice and further injected with approximately 1 mL of 0.2 M hydroquinone solution to stop the polymerization. Polymer samples were isolated by precipitating the products in acetone, filtered (paper filter grade number 41, Whatman; Sigma-Aldrich, Oakville, ON, Canada) and vacuum dried for 1 week at 50°C .

pH, ionic strength and monomer concentration are expected to affect the polymerization kinetics and resulting terpolymer properties. Therefore, in preliminary work [80], all variables were kept constant and controlled to the extent possible. In contrast, the current work employs a definitive screening design (using Design Expert software) to adjust four variables (in 3 levels each) simultaneously and glean general information about the system. Level selection was informed by prior work (for the AAm/AAC copolymer [84, 85] and the AMPS/AAm/AAC terpolymer [80]) and

influenced by considering desirable properties for enhanced oil recovery application performance [32]. The definitive screening design is presented in Table 3.1 (Runs S1 through S9). The conditions for two additional runs (Runs S10 and S11) were informed by preliminary results and kept screening variables constant to the extent possible, for comparison purposes. This will be discussed further in Section 4.1.2.

Table 3.1: Definitive Screening Design for Terpolymerization of AMPS/AAm/AAc

| Run # | pH | IS | [M] | Feed Composition ($f_{\text{AMPS},0}/f_{\text{AAm},0}/f_{\text{AAc},0}$) |
|-------|----|-------|-------|--|
| S1 | 7 | 1.5 M | 1.0 M | 0.1/0.2/0.7 |
| S2 | 5 | 1.2 M | 1.0 M | 0.8/0.1/0.1 |
| S3 | 7 | 1.8 M | 1.5 M | 0.8/0.1/0.1 |
| S4 | 7 | 1.2 M | 0.5 M | 0.1/0.8/0.1 |
| S5 | 9 | 1.2 M | 1.5 M | 0.1/0.2/0.7 |
| S6 | 5 | 1.8 M | 0.5 M | 0.1/0.2/0.7 |
| S7 | 9 | 1.8 M | 1.0 M | 0.1/0.8/0.1 |
| S8 | 5 | 1.5 M | 1.5 M | 0.1/0.8/0.1 |
| S9 | 9 | 1.5 M | 0.5 M | 0.8/0.1/0.1 |
| | | | | |
| S10 | 7 | 1.5 M | 1.0 M | 0.8/0.1/0.1 |
| S11 | 7 | 1.5 M | 1.0 M | 0.1/0.8/0.1 |

By combining the definitive screening design with optimal feed compositions (as per the EVM design of experiments for ternary reactivity ratio estimation), different subsets of data for parameter estimation can be analyzed under specific conditions. For example, from Table 3.1, one could use Runs S1, S3 and S4 to estimate (approximate) reactivity ratios for the AMPS/AAm/AAc terpolymer at pH 7. Although [M] and IS are varying, the associated feed compositions for these 3 runs make up an optimal design. Therefore, full conversion data from 3 runs can be used for parameter estimation. It is important to note that these parameter estimates are general; reactivity ratios from these experiments should not be used to predict cumulative terpolymer composition or terpolymer microstructure. Rather, these screening runs can be used to examine how changes in pH, ionic strength and monomer concentration affect general trends (i.e. incorporation of various comonomers, rate of polymerization, molecular weight averages, and so on). These trends inform subsequent runs, with the intent to manipulate pre-polymerization recipes and terpolymerization kinetics to create custom-made materials.

3.2.2 Optimally Designed Experiments

In the optimal design phase of this study, terpolymers were synthesized under consistent solution properties at the levels determined from the definitive screening design results [81]. Sodium chloride was added to adjust ionic strength to 0.9 M, and all monomer solutions were titrated with sodium hydroxide to adjust the pH to approximately 7 (± 0.5). Total monomer concentration was

1.5 M for each synthesis, with 0.009 M initiator (ACVA). Two optimal feed compositions (both rich in acrylamide) were selected to allow for the most desirable terpolymer microstructure (see Table 3.2). These feed compositions were based on predictions made using newly estimated reactivity ratios (from definitive screening design data). A more detailed justification of these ‘optimal’ experimental conditions is provided in Chapter 4 (Section 4.2.1).

Table 3.2: Optimally Designed Experiments for Terpolymerization of AMPS/AAm/AAc

| Run # | pH | IS | [M] | Feed Composition ($f_{\text{AMPS},0}/f_{\text{AAm},0}/f_{\text{AAc},0}$) |
|-------|----|-------|-------|--|
| Opt1 | 7 | 0.9 M | 1.5 M | 0.21/0.69/0.10 |
| Opt2 | 7 | 0.9 M | 1.5 M | 0.10/0.75/0.15 |

As with the screening experiments, all solutions were degassed with 200 mL/min nitrogen for 2h prior to polymerization. After degassing, aliquots of ~20 mL of solution were transferred to sealed vials using the cannula transfer method. Free-radical solution (aqueous phase) polymerizations were run in a temperature controlled shaker-bath (OLS200; Grant Instruments, Cambridge, UK) at 40°C and 100 rpm. Vials were removed at selected time intervals, placed in ice and further injected with approximately 1 mL of 0.2 M hydroquinone solution to stop the polymerization. Polymer samples were isolated by precipitating the products in acetone, filtered (paper filter grade number 41, Whatman; Sigma-Aldrich, Oakville, ON, Canada) and vacuum dried for 1 week at 50°C. Both polymerizations were independently replicated.

3.3 Characterization of Polymer Properties

3.3.1 Conversion

Conversion of all polymer samples was determined using gravimetry. Due to the high ionic strength (and necessarily high salt content), it was observed that sodium chloride remained present in the polymer samples at an approximate 1:1 ratio with acrylamide. This was initially deduced from elemental analysis results and uncharacteristically high conversion calculations, and then independently confirmed for select samples via inductively coupled plasma mass spectrometry (ICP). This is discussed further in Section 4.1.4. As per the recommendation of Riahinezhad et al. [84], the mass of the sodium ions (attracted to the dissociated acids along the polymer chain) was considered in conversion calculations. Sample calculations are available in Appendix C (Section C.1).

3.3.2 Composition

Polymer composition was measured using elemental analysis (CHNS, Vario Micro Cube, Elementar). The machine was calibrated daily (and after every 60 samples) using a sulfanilamide standard and samples were combusted at 1150°C. The content of elemental C, H, N and S in the samples was determined, which allowed for the subsequent calculation of cumulative terpolymer

composition. Composition calculations did not include H measurements, as residual water has been known to affect the determined H content. Sample calculations are provided in Appendix C (Section C.2).

One of the challenges in performing elemental analysis for these terpolymer samples was the high sulfur concentration (especially for the AMPS-rich samples). Initially, sulfur entrapment within the elemental analysis system (and, potentially, poor combustion) resulted in poor repeatability of elemental analysis results. In collaboration with the technical team at Elementar, the following alterations to standard procedures were found to significantly improve the repeatability of the results:

- WO_3 powder was added to each polymer sample (in a 1:1 mass ratio) during the sample preparation stage. This provided additional oxygen during combustion and ensured complete combustion of the polymer sample. Additionally, the presence of WO_3 in the combustion tube required that a ceramic ash crucible (with 5 mm WO_3 in the bottom) be used instead of standard glass. The ceramic crucible is better able to collect sample combustion residue, whereas the WO_3 may leach out of the standard glass tube (which could make the ash crucible stick to the inside of the combustion tube).
- At least four conditioning runs were completed before daily calibration. Occasionally, additional conditioning runs were added, especially if the sulfur content seemed unstable.
- Terpolymer samples were run in triplicate to ensure consistent results. Essentially, the first sample acted as a ‘conditioning’ sample for the terpolymer being analyzed, which was especially important if the sulfur content in the terpolymer was significantly different than the previous sample (or standard).
- Over time, the quartz bridge (linking the combustion tube and the reduction tube) can develop a blue tint, which indicates that wolframic acids have precipitated. In this case, the quartz bridge should be replaced with a clean one, and the contaminated bridge should be thoroughly cleaned and dried.
- The cotton ‘plugs’ in the drying tube are known to trap sulfur-containing compounds (mainly SO_2). An alternative plug to improve gas flow rates (which Elementar calls their poly filter) can minimize the entrapment.
- If sulfur content becomes especially high (noticeable during blank runs, conditioning runs, and/or calibration runs), the adsorption column can be baked out to clean out any debris.

These adjustments significantly improved the repeatability of the elemental measurements (and simultaneously increased confidence in the results).

3.3.3 Molecular Weight

Molecular weight averages were determined using gel permeation chromatography (PL-GPC 50, Agilent, with two columns, type PL aquagel-OH MIXED-H 8 μm , Agilent). To analyze the

AMPS/AAm/AAC terpolymers, four detectors were employed: refractive index, low-angle and right-angle light scattering (LALLS/RALLS), and differential pressure. To minimize the charge interactions between the column and the polymer samples, a buffer solution of pH 7 was used as the mobile phase (flowing at a rate of 1.0 mL/min). The buffer was prepared using sodium nitrate (0.2 M) and sodium phosphate (monobasic and dibasic, 0.1 M) in Millipore quality water. The synthesized polymers were dissolved in the mobile phase (pH 7 buffer) to obtain concentrations of ~1 mg/mL. The solution preparation step required fine grinding prior to dissolving polymers in buffer, and allowing the solutions to sit under ambient conditions (with occasional manual mixing) until the polymer was dissolved. This sometimes took several days, since the material did not dissolve easily. Prior to injection, polymer solutions were filtered through a 0.2 μm filter. Polyacrylic acid – sodium salt calibration standards were obtained from Agilent Technologies and their peak average molecular weight (\overline{M}_p) values ranged from 4.67×10^5 to 2.25×10^6 g/mol.

Calibration was also confirmed using a well-characterized copolymer (poly(acrylamide-co-acrylic acid) partial sodium salt from Aldrich; ~80% acrylamide; $M_w = 520,000$ and $M_n = 150,000$); measurements were in good agreement with the expected results (coefficient of variation <10% for both \overline{M}_w and \overline{M}_n). For a dn/dc of 0.171, $M_w = 456,400$ and $M_n = 160,362$. Additional details are provided in Appendix C, Section C.3.

For all unknown samples, a dn/dc of 0.175 was used (based on the dn/dc of the PAAc-Na standards and verified by laser refractometry). The range of dn/dc values for both polyacrylamide and polyacrylic acid (in salt water) are similar; changing the dn/dc value during analysis had no effect on the reported molecular weight averages. Note, however, that dn/dc values come from a variety of sources, meaning that the mobile phase is not necessarily consistent for measurements reported by different groups. A more complete analysis (like the one done by Leamen et al. [116]) would be necessary to understand the full intricacies of the system.

3.3.4 Sequence Length Distribution

^{13}C -NMR (nuclear magnetic resonance) was conducted on a Bruker AVANCE 500 Ultrashield NMR spectrometer (Nuclear Magnetic Resonance Facility, Department of Chemistry, University of Waterloo). The NMR was run for 12 hours per sample at 68 °C (around 6,000 scans) and employed inverse gated proton decoupling (30 degree pulse) with a pulse delay of 6 s ($D1 = 6$ s).

To prepare the samples for analysis, each terpolymer was dissolved in a pH 7 D_2O /buffer solution (prepared using 0.2 M sodium nitrate and 0.1 M sodium phosphate (monobasic and dibasic) as for GPC, but with D_2O as the mobile phase). Polymer samples were finely ground and slowly added to the buffer to achieve a concentration of 6 wt% (~0.1332 g of polymer in 2 ml of D_2O /buffer). Solutions were injected into NMR tubes using a long-tipped needle and a syringe, and tubes were heated in a 60°C water bath to ensure all bubbles had escaped prior to analysis.

3.3.5 Thermal Stability

Select samples were analyzed using thermal gravimetric analysis (TGA) on a Q500 TGA from TA Instruments (analytical instrumentation lab, Department of Chemical Engineering, University of Waterloo). Small sample quantities (<5 mg) were placed in platinum pans for analysis, and samples were run from 30°C to 600°C with a heating rate of 10°C/min under nitrogen atmosphere. It was especially important to use small amounts of sample (< 5 mg), since entrapped water could result in sample expansion during analysis (see Appendix C, Section C.4).

3.3.6 Additional Characterization

To evaluate whether residual sodium chloride was present in the AMPS/AAm/AAC terpolymer, sodium concentration was measured for select samples using inductively coupled plasma (ICP) mass spectrometry. The instrument used was a Prodigy radial ICP-OES by Teledyne-Leeman (analytical instrumentation lab, Department of Chemical Engineering, University of Waterloo). Samples outside the calibration range (0-100 mg/L) were diluted to fall within the calibration range and dilution factors were applied to the results. All working standard solutions were prepared using Millipore quality water (18 M Ω ·cm), acidified with reagent grade nitric acid to a concentration of 0.3%.

3.4 Characterization of Application-Specific Properties

3.4.1 Rheology

Solutions for rheological analysis were prepared by dissolving finely ground terpolymer samples in Millipore quality water or pH 7 buffer (prepared as described for GPC; Section 3.3.3); solutions were made to have a concentration of 0.01 g/mL. A stress-controlled cone and plate rheometer (AR2000, TA Instruments) was used to measure the viscoelastic properties of the polymer solutions. An environmental test chamber (ETC) steel cone with 40 mm diameter and 1° angle was used for all tests, and all measurements were taken at 25°C. Select independent replicates were performed, and additional details are available in Appendix C, Section C.5.

3.4.2 Enhanced Oil Recovery

The optimal terpolymers designed for enhanced oil recovery were evaluated using specialized equipment (capable of simulating oil reservoir flooding on a lab scale) at the University of New Brunswick, Department of Chemical Engineering. Experimental procedures reported by Riahi-zhad et al. [117] were used as a guideline, and details specific to the current investigation are presented in what follows. Generally speaking, the EOR application performance was evaluated in two phases. Phase I (described in Section 3.4.2.1) measured polymer flow

performance in unconsolidated porous media (that is, the sand-pack simulating an oil reservoir) and Phase II (described in Section 3.4.2.2) determined oil recovery efficiency through polymer flooding experiments.

3.4.2.1 Phase I: Polymer Flow Performance Testing

Phase I provides information about how each polymeric material behaves in solution as it is injected into the reservoir. The lab-scale experimental set-up used to simulate an oil reservoir is called a sand-pack system, and a schematic is shown in Figure 3.2.

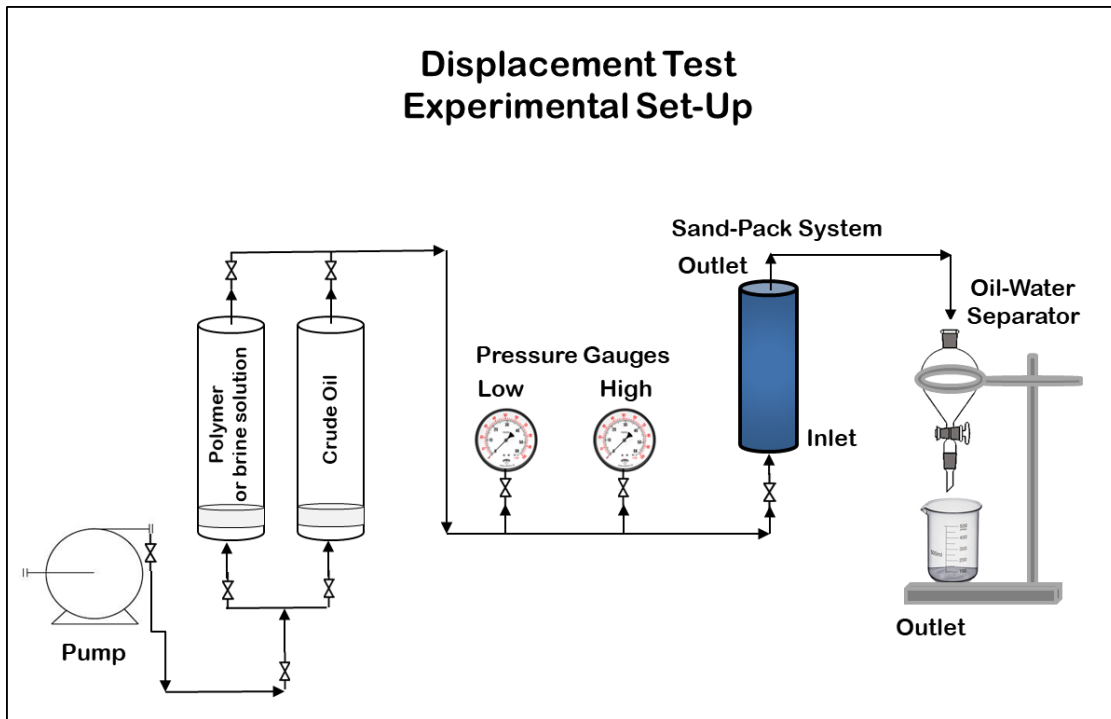


Figure 3.2: Experimental Set-Up for Sand-pack Flooding Tests

The sand-pack system makes it possible to examine polymer flow behaviour through porous media (representative of oil reservoirs). The sand-pack used for this series of investigations contains Quikrete sand, and the particle size distribution of the sand is provided in Figure 3.3.

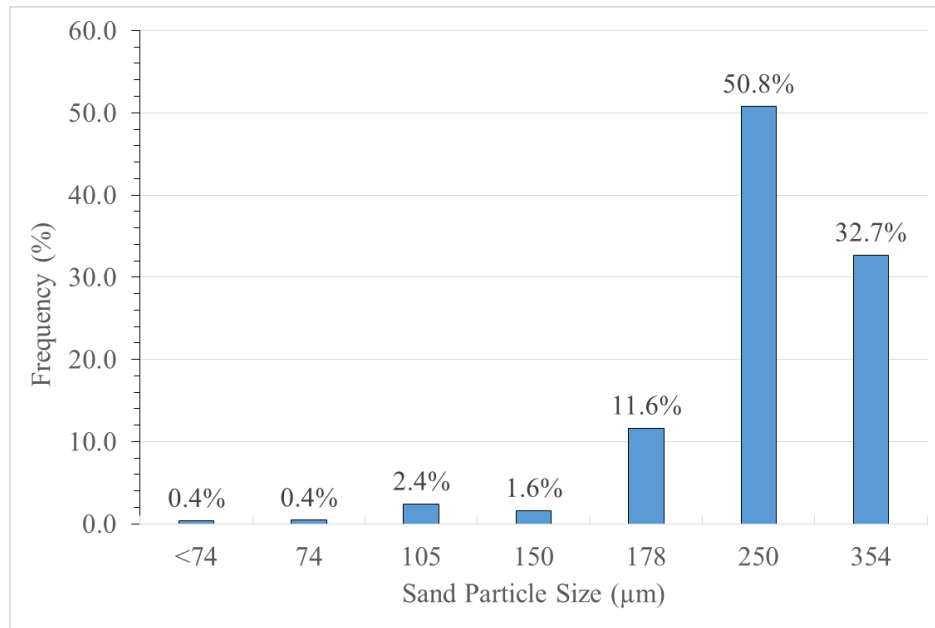


Figure 3.3: Particle Size Distribution of Sand for Sand-pack Flooding Tests

The sand-pack geometry is also an important consideration in this experimental stage and is shown (along with additional experimental conditions) in Table 3.3. The system geometry is relevant to determine the required flow rate and is necessary for determining the porosity and permeability of the sand-pack. The injection flow rate was selected to simulate an average linear velocity of 1 ft/day (similar to real conditions in oil fields); the linear velocity of 1 ft/day is equivalent to the volumetric flow rate of 0.18 ml/min (given the cross-sectional area of the sand-pack cylinder).

Table 3.3: Sand-pack Characteristics and Experimental Conditions

| Property | Value |
|----------------------|----------------------|
| Length | 15.30 cm |
| Diameter | 3.30 cm |
| Cross sectional area | 8.55 cm ² |
| Pump flow rate | 0.18 ml/min |

The procedure for a typical polymer flow performance test is described below. Estimates of volume requirements are provided in Appendix C, Section C.6.

1. Sand-pack preparation and characterization: The rigid cylinder (sand-pack system shown in Figure 3.2) was packed with sand. Then, the characteristics of the sand-pack (pore volume, porosity and permeability) were measured. Brine was injected into the sand-pack until the porous medium was fully saturated. The pore volume (PV) was established as the total volume of brine that could be injected into the system, the porosity was calculated from the total volume of the cylinder, and the permeability was experimentally determined using Darcy's Law.

2. Brine injection #1: 1 pore volume (PV) + 1 dead volume (DV) of brine were injected into the sand-pack system. The synthetic brine that was used in this test (and subsequent polymer flooding tests) had a composition inspired by real conditions in oil reservoirs in Alberta, Canada (see Table 3.4).

Table 3.4: Composition of Synthetic Brine

| Salt | wt % |
|---------------------------------|------|
| NaCl | 1.72 |
| MgCl ₂ | 0.04 |
| CaCl ₂ | 0.33 |
| Na ₂ SO ₄ | 0.01 |
| Total Dissolved Solids | 2.10 |

3. Polymer solution injection: A 1 wt% polymer solution was prepared for polymer flooding. During the preparation of the polymer solution, it was essential that the polymer be ground into a fine powder. Also, adding the polymer gradually ensured that a homogeneous polymer solution was obtained. The required volume for this stage was equivalent to 2 PV + DV, with an additional 10 mL included for expected sample losses.
4. Brine injection #2: After polymer flooding, the sand-pack was further injected with brine. In this case, 4 PV + DV was required to remove the majority of the polymeric material from the sand-pack.

The full procedure was completed at least twice for each of the polymeric materials (Opt1, Opt2 and a reference polymer). The reference polymer used was a combination of two commercially available materials (both in the Alcoflood family); this made it possible to use a reference material with a molecular weight average similar to the designed terpolymers. Characteristics of the reference polymer are provided in Table 3.5.

Table 3.5: Composition of Reference Polymer for EOR Testing

| Polymer | MW (g/mol) | Mass Fraction |
|--|------------|---------------|
| HPAM Alcoflood 254S | 500,000 | 0.81 |
| HPAM Alcoflood 935X | 5,000,000 | 0.19 |
| Average MW (based on terpolymer properties) | 1,370,000 | |

The purpose of Phase I testing was primarily to establish the resistance factor (RF) and the residual resistance factor (RRF) for each polymeric material. The RF provides information about the effective viscosity (mobility control capability) of the polymer solution in porous media relative to water. Therefore, higher RF values typically indicate that polymer flooding will be more successful. The definition of RF is provided in Equation 3.1.

$$RF = \frac{\lambda_w}{\lambda_p} = \frac{k_w/\mu_w}{k_p/\mu_p} \quad 3.1$$

Where λ_w and λ_p are the mobility of the water and polymer solution, respectively. Also, λ_w can be replaced with λ_b (where b is brine), since the flood water used in these experiments was a brine solution. k represents the permeability of the porous media and μ represents the viscosity of the water or the polymer solution. The permeability, k , is calculated from Darcy's Law (Equation 3.2).

$$k = 1000 \frac{L}{A} \mu Q \frac{1}{(P_o - P_i)} \quad 3.2$$

Where Q is the volumetric flow rate (ml/s), P_o and P_i are the outlet and inlet fluid pressures (atm), μ is the fluid dynamic viscosity (centipoise, cP), L is the length of the sand-pack (cm), and A is the cross-sectional area of the sand-pack (cm²).

By combining Equations 3.1 and 3.2 (assuming a fixed flow rate and knowing that the geometry is invariant), the measurement of the RF can be simplified as shown in Equation 3.3.

$$RF = \frac{\Delta P_{polymer\ solution\ injection}}{\Delta P_{brine\ injection\ \#1}} \quad 3.3$$

Where ΔP is the pressure difference across the sand-pack at steady state conditions.

In contrast, the RRF provides information about polymer retention and adsorption onto solid surfaces within the reservoir (adsorption is usually physical in nature; chemisorption is less common). Any retention can lead to permeability reduction within the sand-pack (or, more broadly, the reservoir), and can cause potential injectivity issues. Therefore, lower RRF values are more desirable for EOR.

As shown in Equation 3.4, the RRF is defined as the ratio of the mobility of water (or brine) before polymer injection (that is, brine injection #1) to the mobility of water (or brine) after polymer flooding (that is, brine injection #2). However, it can also be rewritten in terms of the pressure difference across the sand-pack before and after polymer solution injection (Equation 3.5).

$$RRF = \frac{\lambda_{b, \text{ brine injection \#1}}}{\lambda_{b, \text{ brine injection \#2}}} \quad 3.4$$

$$RRF = \frac{\Delta P_{\text{ brine injection \#2}}}{\Delta P_{\text{ brine injection \#1}}} \quad 3.5$$

3.4.2.2 Phase II: Polymer Flooding Tests

Polymer flooding tests were carried out using the same experimental set-up shown in Figure 3.2 and at reservoir conditions similar to real conditions. The major difference in the experimental

process (compared to the tests in Section 3.4.2.1) was the addition of an oil injection step (step 2 below).

During each injection step, injection time, flow rate, pressure readings, and volume of oil produced were recorded. Also, at the end of each stage, the oil and brine saturation in the sand-pack and the oil recovery were calculated. The general procedure for a typical heavy oil displacement test is described in steps 1 through 6 below. Again, experimental details are provided in Appendix C, Section C.6.

1. Sand-pack preparation and characterization: as per step 1 in the Phase I test; see Section 3.4.2.1.
2. Heavy oil injection: 2 pore volumes (PV) + 1 dead volume (DV) of oil were injected into the sand-pack system. The oil used in these tests (provided by Husky Energy, Canada) was diluted with natural condensate (provided by Corridor Resources Inc., Canada) to obtain a viscosity of 3.93 Pa·s at 25°C.
3. Brine injection #1: The first brine injection is essentially a water flooding stage. 4 PV + 1 DV brine (with the composition shown in Table 3.4) were injected into the sand-pack at constant flow rate (0.18 mL/min).
4. Polymer solution injection: In this step, a 1 wt% polymer solution was prepared for polymer flooding. As mentioned in Phase I, using a fine powder and gradually adding it to the solution helped with solution preparation. The total volume injected during this polymer flooding step was 1 PV + DV (flow rate = 0.18 mL/min), with an additional 10 mL included for sample losses.
5. Brine injection #2: This is the post-polymer water flooding stage. Here, additional brine (2 PV + DV) was injected into the sand-pack at 0.18 mL/min. This ensured that as much oil as possible would be produced from the reservoir.
6. Determination of oil production: In order to measure the volume of oil produced, the output fluid was collected from the sand-pack in a separation funnel (of known mass). After several days (usually 4 to 7 days), most of the oil and brine mixture had separated. However, in some cases (if the separation of water was difficult), a known amount of toluene was added to the output fluid to force the rapid removal of residual water. When only oil remained in the funnel, the mass of the oil-containing funnel was measured, which made it possible to calculate the mass and the volume of the oil produced.

The primary objective at this stage is to determine the overall percentage of oil recovery that can be obtained from polymer flooding. This is essentially the sum of the oil recovery after water flooding (step 3 above), polymer flooding (step 4 above) and post-polymer water flooding (step 5 above). It can also be informative to look at the incremental oil recovery. This provides a measure of 'how much more' oil can be recovered from polymer flooding compared to simple water flooding. Therefore, this is a combination of the recovery contributions from the polymer flooding stage (step 4 above) and the post-polymer water flooding stage (step 5 above).

Chapter 4. Results and Discussion for Case Study #1 – *Enhanced Oil Recovery*

4.1 Screening Experiments

The results and discussion provided in this section have largely been published in recent work by Scott, Duever and Penlidis [81].

The screening experiments described in Section 3.2.1 make it possible to examine the effects of important factors (namely, pH, ionic strength and monomer concentration) on the terpolymerization of 2-acrylamido-2-methylpropane sulfonic acid (AMPS), acrylamide (AAM) and acrylic acid (AAc). A good understanding of how these factor levels affect terpolymerization reactivity ratios, and terpolymer composition, microstructure and molecular weight paves the way for the synthesis of custom-made polymers for specific applications.

4.1.1 Effect of pH

As mentioned in Section 2.4.1, changes in solution pH affect the degree of dissociation (and therefore the charge) of acidic monomers and the resulting polymer. By grouping the screening experiments according to pH level (that is, pH level constant with varying ionic strength and monomer concentration), it is possible to estimate ternary reactivity ratios at each pH level. The screening runs (from Table 3.1) used for each analysis and the resulting reactivity ratio estimates (obtained using full conversion data and cumulative terpolymer composition to obtain ternary reactivity ratios) are shown in Table 4.1. Again, note that at each pH, there is a pre-polymerization recipe rich in each of the three comonomers. For all estimation steps, preliminary estimates were taken from recent work [80]; in all cases, monomer 1 is 2-acrylamido-2-methylpropane sulfonic acid (AMPS), monomer 2 is acrylamide (AAM) and monomer 3 is acrylic acid (AAc).

Table 4.1: pH Effects on Ternary Reactivity Ratio Estimates for AMPS/AAM/AAc ($M_1/M_2/M_3$)

| pH | Data from Run # | r_{12} | r_{21} | r_{13} | r_{31} | r_{23} | r_{32} |
|----|-----------------|----------|----------|----------|----------|----------|----------|
| 5 | S2, S6, S8 | 0.96 | 0.53 | 0.25 | 1.22 | 1.55 | 0.51 |
| 7 | S1, S3, S4 | 1.14 | 0.66 | 0.45 | 0.99 | 1.48 | 0.42 |
| 9 | S5, S7, S9 | 1.12 | 0.53 | 0.32 | 1.56 | 2.07 | 0.55 |

The estimation results at varying pH levels do not show any clear correlation between pH and reactivity ratio estimates; most values for a given parameter (say r_{ij} ; ‘vertical’ comparison within Table 4.1) are close together. However, the point estimates only provide part of the story. The joint confidence regions (JCRs, or error ellipses) for the parameter estimates should also be examined, as they provide additional information about possible parameter correlation and degree of

confidence for each estimate. JCRs for all three pH levels and all ternary reactivity ratio pairs are presented in Figure 4.1.

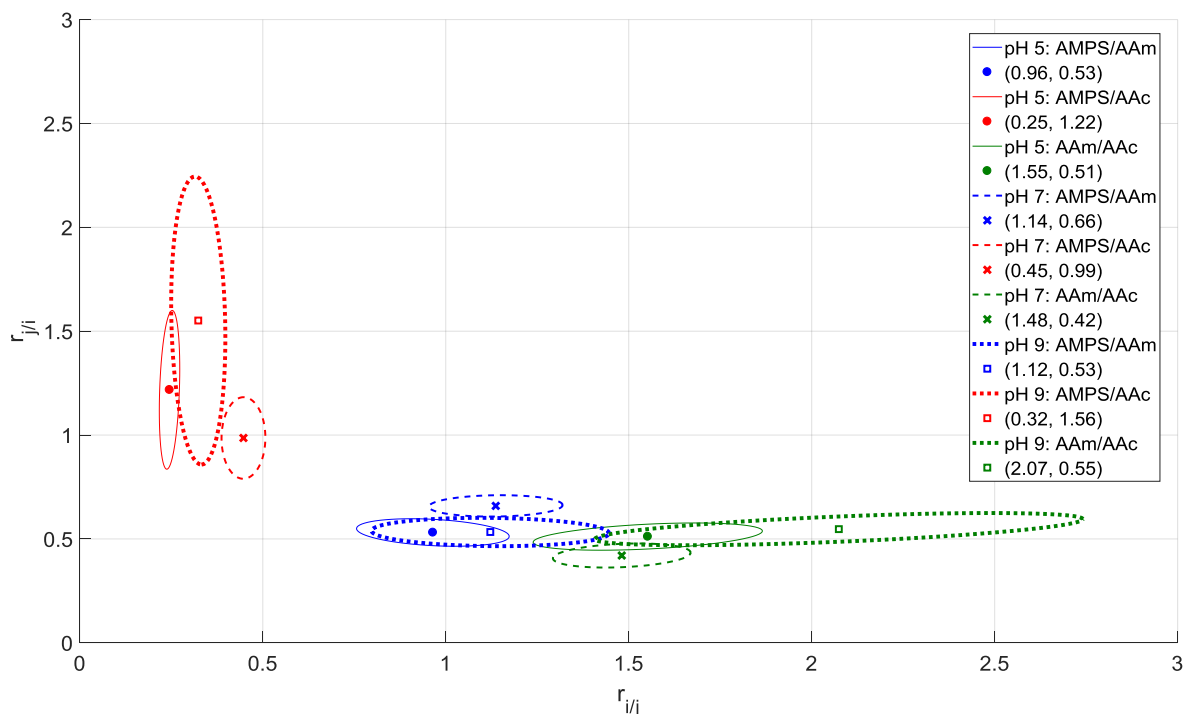


Figure 4.1: Comparison of Reactivity Ratio Estimates for AMPS/AAm/AAC at pH 5, 7 and 9

Figure 4.1 provides significantly more information than the numerical estimates of Table 4.1. First, we can evaluate the area of the JCRs associated with each pH level. At pH 5 and pH 7, the JCRs are small, which indicates a high degree of confidence in the estimates. At pH 9, the JCRs are larger, which suggests more uncertainty. This may be related to the fact that other variables (namely ionic strength and monomer concentration) are not held constant, which affects the precision of the parameter estimates. Alternatively, fewer data points are available for Run S9 as it had an unusually long induction time, so the parameters are being estimated from a smaller (and therefore less informative) data set.

A second observation from Figure 4.1 is related to the overlap in JCRs, especially for the AMPS/AAm and AAm/AAC comonomer pairs. This agrees with the numerical results shown in Table 4.1, which indicate that most parameter estimates are close together. According to Figure 4.1, there is no statistically significant difference between parameter estimates for the AMPS/AAm and AAm/AAC comonomer pairs at pH 5 and pH 9. Distinct JCRs (that is, without overlap) are visible for the AMPS/AAC copolymer pair, which suggests that the acidic comonomers may be more affected by changes in pH. This agrees with physicochemical expectations, as the degree of acid dissociation is likely to be influential in the pH range being studied.

Given prior investigations of pH effects (especially for the AAm/AAC copolymer [85, 97-99]), one might expect bigger differences in the reactivity ratios at different pH levels. However, it is important to keep in mind that these results are under specific conditions, where several variables are being manipulated simultaneously. pH effects are largely due to acid dissociation and charge effects. Therefore, adding sodium chloride to the recipe (to adjust ionic strength) increases charge screening, reducing acrylic acid repulsion and moderating the effect that a pH increase would have in isolation.

The final takeaway from Figure 4.1 is the shape and orientation of the JCRs. All JCRs are somewhat ‘stretched’ in one direction, which indicates more uncertainty associated with one of the parameters. This phenomenon has been described in recent work [6] and is likely related to the absolute value of the parameter estimate; a larger absolute value results in more uncertainty. It is also important to note that the JCRs are either horizontal or vertical (not on a diagonal). This indicates that parameter correlation is minimal, thanks to well-designed experimental runs based on the error-in-variables model.

In referring again to the numerical estimates of Table 4.1, it is interesting to note that at each pH level, the relationship between reactivity ratios for a given comonomer pair remains consistent. That is, for any subset of screening runs, $r_{12} > r_{21}$, $r_{13} < r_{31}$ and $r_{23} > r_{32}$. Therefore, regardless of pH, the degree of incorporation of each comonomer remains relatively constant. This is confirmed by using the reactivity ratio estimates from Table 4.1 to predict the cumulative terpolymer composition at pH 5, pH 7 and pH 9 given the AAm-rich recipe ($f_{\text{AMPS},0}/f_{\text{AAm},0}/f_{\text{AAc},0} = 0.1/0.8/0.1$); see Figure 4.2.

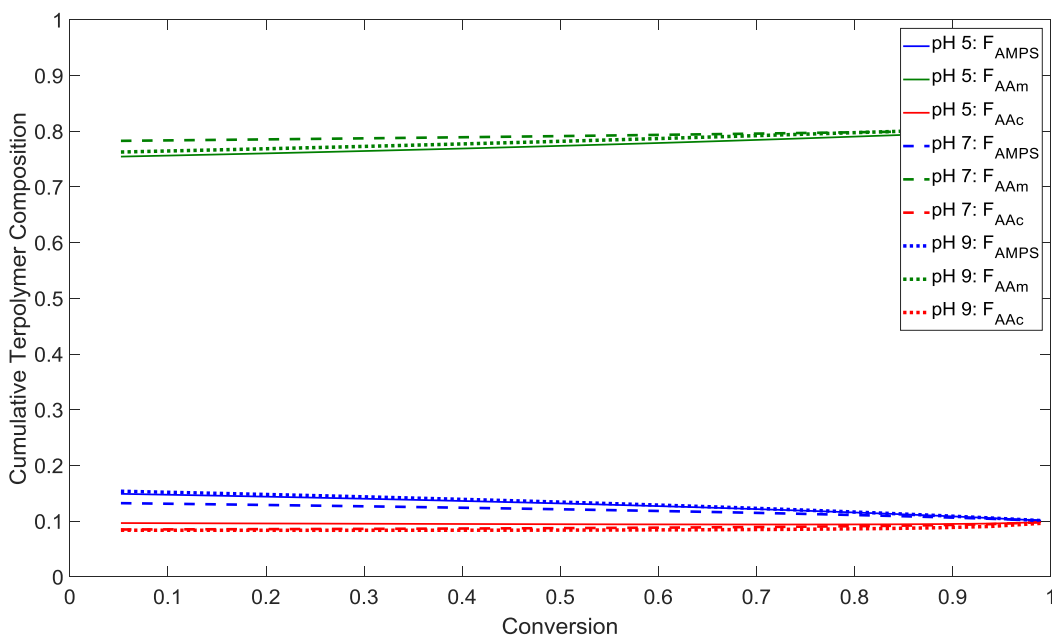


Figure 4.2: Predicted Cumulative Composition from Screening Experiments for AAm-rich Terpolymer at pH 5, 7 and 9

The relationship between reactivity ratios for comonomer pairs becomes even more interesting when the experimental results are compared to the (previously determined [80]) preliminary estimates. Scott et al. [80] estimated ternary reactivity ratios for AMPS/AAm/AAc using data collected at pH 7, with constant ionic strength (IS = 0.9 M) and monomer concentration ([M] = 1.0 M). Therefore, it is straightforward to compare two sets of reactivity ratios from data obtained at pH 7: the current estimates (with varying IS and [M]) versus earlier estimates (with constant IS and [M]).

Table 4.2: Reactivity Ratio Estimates at pH 7 with Varying and Constant IS and [M]

| Experimental Conditions | r₁₂ | | r₂₁ | r₁₃ | | r₃₁ | r₂₃ | | r₃₂ |
|---|-----------------------|---|-----------------------|-----------------------|---|-----------------------|-----------------------|---|-----------------------|
| Current study [81]: pH 7 1.2 M < IS < 1.8 M 0.5 M < [M] < 1.5 M | 1.14 | > | 0.66 | 0.45 | < | 0.99 | 1.48 | > | 0.42 |
| Scott et al. [80]: pH 7 IS = 0.9 M [M] = 1.0 M | 0.66 | < | 0.82 | 0.82 | > | 0.61 | 1.61 | > | 0.25 |

The key takeaway from Table 4.2 is the shift in relationship for two of the comonomer pairs. As discussed already, the current experimental results indicate that $r_{12} > r_{21}$ and $r_{13} < r_{31}$ in all cases (recall Table 4.1). In contrast, the reactivity ratio estimates determined by Scott et al. [80] show the opposite: $r_{12} < r_{21}$ and $r_{13} > r_{31}$. Since the pH is the same for these two data sets, it is possible to conclude that this ‘cross-over’ behaviour is not a result of pH effects. The most significant difference (aside from varying IS and [M] vs. constant IS and [M]) is the increased ionic strength used in the current experiments. This provides further motivation to investigate the effects of ionic strength on ternary reactivity ratios of AMPS/AAm/AAc (see Section 4.1.2). Specifically, if we can learn more about how ionic strength creates a cross-over point (at which $r_{ij} \approx r_{ji}$), we can target specific reaction conditions to create custom-made materials with desirable properties.

In summarizing the effect of pH on the terpolymerization of AMPS/AAm/AAc, the following remarks can be made:

1. No clear correlation exists between pH and reactivity ratio estimates for the range of 5 to 9.
2. The largest JCRs (and therefore the most uncertainty) were observed for reactivity ratio estimation at pH 9.
3. Acidic comonomers (AMPS and AAc) seem to be more affected by changes in pH.
4. pH effects are likely masked by salt addition in this type of screening design.
5. Well-designed experiments (using the error-in-variables model) minimize parameter correlation.
6. Cross-over behaviour was observed for AMPS/AAm and AMPS/AAc comonomer pairs (current designs [81] vs. Scott et al. [80]); both data sets are at pH 7, therefore cross-over behaviour is due to some other factor effect.

4.1.2 Effect of Ionic Strength

Ionic strength is an important factor to consider during the synthesis of polyelectrolytes. As discussed in Section 2.4.2, adding counter-ions (in the form of salt) to a pre-polymerization solution can reduce repulsion between charged monomers and polymer chains. This effectively neutralizes the charged molecules (dissociated AMPS and/or acrylic acid, in this case), which minimizes repulsion and increases the rate of polymerization.

The design of experiments used requires that the ‘low’ (-1) level for ionic strength be 1.2 M. This is the result of high monomer concentration and a high proportion of acidic monomer in a ‘low’ ionic strength run. Specifically, in Run S5 (from Table 3.1), a total monomer concentration of 1.5 M and full dissociation of AMPS and AAc comonomers result in an ionic strength of 1.2 M before any NaCl is added to the recipe. Therefore, the ‘low’ (-1) ionic strength level is necessarily 1.2 M. This imposes a relatively high range for the ionic strength investigation, but this is a consequence of using the specific experimental design for such a complex polymerization.

The data from the experiments were grouped according to ionic strength for reactivity ratio estimation. As explained previously, ternary reactivity ratios were estimated for the AMPS/AAm/AAc terpolymer at each ionic strength level (with varying pH and monomer concentration). The trials used for each analysis and the resulting reactivity ratio estimates (obtained as described in Section 4.1.1) are shown in Table 4.3.

Table 4.3: Ionic Strength (IS) Effects on Ternary Reactivity Ratio Estimates for AMPS/AAm/AAc ($M_1/M_2/M_3$)

| IS | Data from Run # | r_{12} | r_{21} | r_{13} | r_{31} | r_{23} | r_{32} |
|-------|-----------------|----------|----------|----------|----------|----------|----------|
| 1.2 M | S2, S4, S5 | 0.90 | 0.65 | 0.24 | 1.08 | 1.87 | 0.52 |
| 1.5 M | S1, S8, S9 | 13.19 | 0.68 | 0.48 | 27.02 | 7.47 | 0.70 |
| 1.8 M | S3, S6, S7 | 1.11 | 0.54 | 0.46 | 1.35 | 1.65 | 0.55 |

Given the reactivity ratios estimated at all three ionic strength levels, there is an obvious difference at IS = 1.5 M. For each reactivity ratio pair at IS = 1.5 M, the larger parameter estimates (namely r_{12} , r_{31} and r_{23}) are much larger than under the other conditions. These values have likely been overestimated (due to more uncertainty associated with these parameters), and the JCRs will be examined to troubleshoot this aspect (see Figure 4.3). Inaccurate estimation may be due to the effects of non-constant pH and monomer concentration, or (as suggested for the pH 9 analysis, see Section 4.1.1) non-informative experimental data.

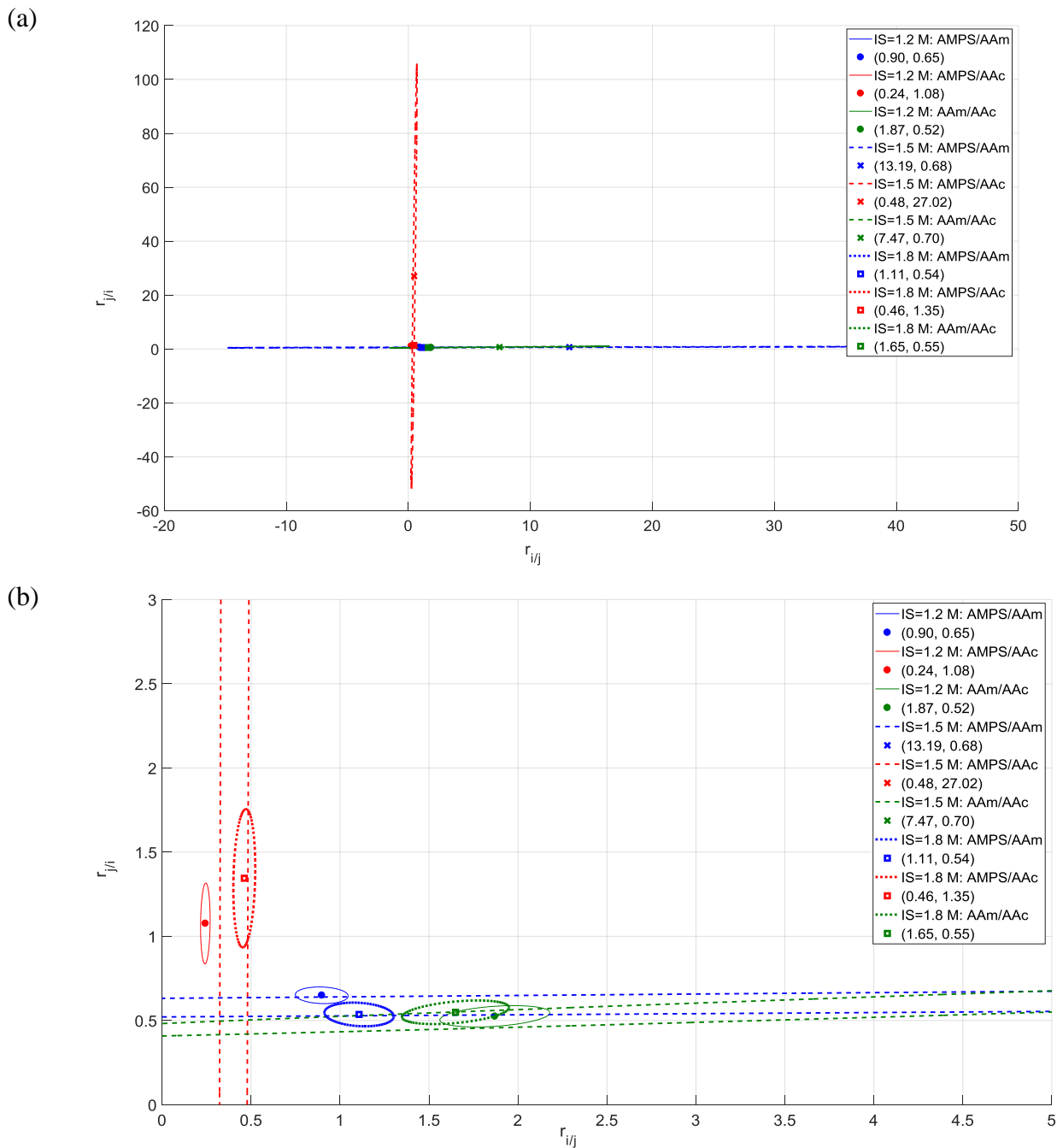


Figure 4.3: Comparison of Reactivity Ratio Estimates for AMPS/AAm/AAC at IS = 1.2 M, IS = 1.5 M and 1.8 M ((a) All Data and (b) Without the IS = 1.5 M Data)

Examining the point estimates and joint confidence regions for these reactivity ratios confirms that there is substantial uncertainty for the IS = 1.5 M data. These long and narrow JCRs emphasize the uncertainty associated with r_{12} , r_{31} and r_{23} ; since the error is associated with all three comonomers, parameter estimates can likely be improved by eliminating the confounding variables (that is, keeping pH and [M] constant during synthesis). If the uncertainty were related

to non-informative data or poor experimental design, one might expect the error to be more clearly associated with one specific comonomer.

4.1.2.1 Ternary Reactivity Ratios for Constant pH and [M]

The most likely cause for the error associated with IS = 1.5 M is the influence of changing pH and [M]. Consideration of non-constant variables is a necessary part of screening design analysis, but it seems that some combinations of runs are more prone to error (that is, more influenced by non-constant variables) than others. Therefore, for improved reactivity ratio estimates at IS = 1.5 M, two supplemental runs were added to the experimental docket: Runs S10 and S11 (recall Table 3.1). Both runs are informed by the EVM design of experiments for ternary reactivity ratio estimation and vary only in feed composition. The data from these runs can be combined with the data from Run S1 for accurate ternary reactivity ratio estimation at IS = 1.5 M, pH 7 and [M] = 1.0 M. As an additional bonus, these runs are under similar conditions to previous work; Scott et al. [80] have reported ternary reactivity ratios for AMPS/AAm/AAC from data collected at IS = 0.9 M, pH 7 and [M] = 1.0 M. Therefore, comparison of reactivity ratios can be performed for IS = 0.9 M and IS = 1.5 M, all else being equal.

First, the data from Runs S1, S10 and S11 are revisited to estimate reactivity ratios at IS = 1.5 M. As before, full conversion data can be analyzed using the cumulative composition model. The point estimates here are much more reasonable (compared to the IS = 1.5 M results of Table 4.3) and the JCR areas have decreased significantly (see Figure 4.4). This confirms that controlling IS, pH and [M] gives more reliable parameter estimates.

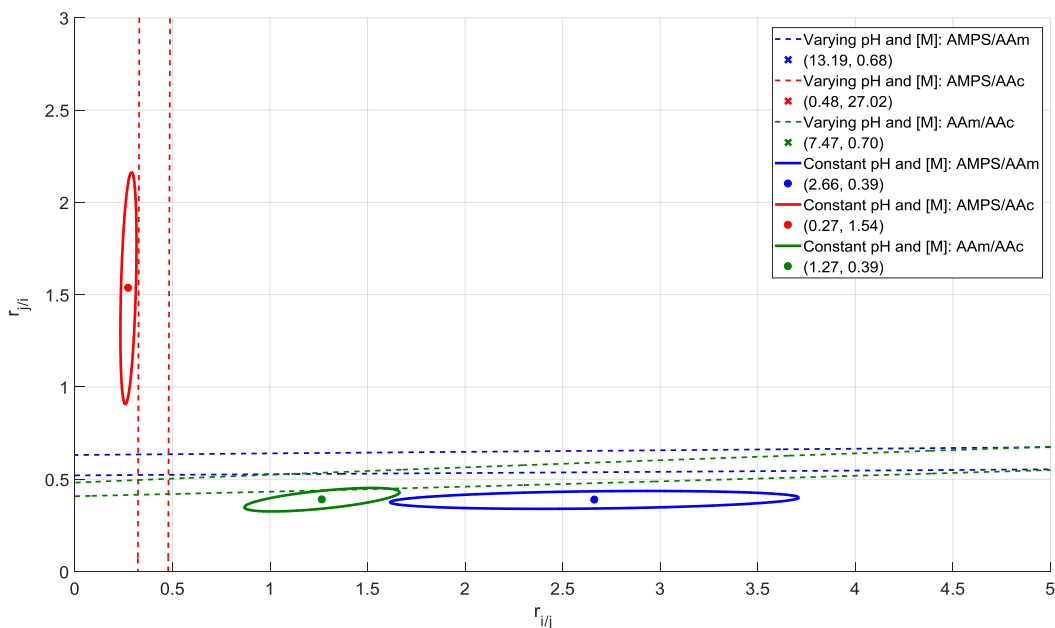


Figure 4.4: Reactivity Ratio Estimates for AMPS/AAm/AAC at IS = 1.5 M; Comparison of Results at Constant/Varying pH and [M]

Table 4.4: Ionic Strength (IS) Effects on Ternary Reactivity Ratio Estimates; Varying and Constant pH and [M]

| Experimental Conditions | r₁₂ | r₂₁ | r₁₃ | r₃₁ | r₂₃ | r₃₂ |
|--|-----------------------|-----------------------|-----------------------|-----------------------|-----------------------|-----------------------|
| IS = 1.5 M 5 < pH < 9 0.5 M < [M] < 1.5 M Data from Run #: S1, S8, S9 | 13.19 | > 0.68 | 0.48 | < 27.02 | 7.47 | > 0.70 |
| IS = 1.5 M pH = 7 [M] = 1.0 M Data from Run #: S1, S10, S11 | 2.66 | > 0.39 | 0.27 | < 1.54 | 1.27 | > 0.39 |
| IS = 0.9 M pH = 7 [M] = 1.0 M Data from Scott et al. [80] | 0.66 | < 0.82 | 0.82 | > 0.61 | 1.61 | > 0.25 |

Aside from the improved degree of confidence associated with the parameter estimates, it is also possible to compare ternary reactivity ratios at IS = 1.5 M (current study [81]) to IS = 0.9 M (Scott et al. [80]), with constant pH and monomer concentration. This comparison, shown in the last two rows of Table 4.4, provides an interesting result: we see the same change in relationship for the AMPS/AAm and the AMPS/AAc comonomer pairs that was observed during the pH analysis (recall the comparison between screening experiments and preliminary estimates in Section 4.1.1). The cross-over behaviour observed for AMPS/AAm and for AMPS/AAc between IS = 0.9 M and IS = 1.5 M must be a result of changing ionic strength; all other variables are controlled. To find the true cross-over point (that is, the ionic strength at which $r_{12} = r_{21}$ and $r_{13} = r_{31}$), additional experiments would need to be performed for $0.9 \text{ M} < \text{IS} < 1.5 \text{ M}$ at pH 7 and $[\text{M}] = 1.0 \text{ M}$. However, this result proves that ionic strength in this range can be manipulated to adjust these reactivity ratios, thus improving control over the degree of incorporation of each comonomer in the product terpolymer. Interestingly, only the comonomer pairs containing AMPS exhibit cross-over behaviour in this range. Therefore, it is only possible to manipulate relationships between AMPS/AAm and AMPS/AAc by adjusting ionic strength. Cross-over behaviour for the AAm/AAc comonomer pair has not been observed under current conditions, but has been observed for the analogous AAm/AAc copolymer by Riahinezhad et al. [85], Cabaness et al. [97] and Rintoul and Wandrey [99]. The crossover point varies slightly from study to study, but ranges from pH 3.77 to pH 5. In all cases, $r_{AAm} > r_{AAc}$ above the crossover point, but $r_{AAm} < r_{AAc}$ in more acidic solutions. It is unwise to make extensions directly from the copolymer case to the terpolymer case [38], but terpolymer synthesis below pH 5 might reveal the AAm/AAc cross-over point. One could conceivably manipulate both solution pH and IS to exploit this cross-over behaviour, in order to influence reactivity ratio ranges for AMPS/AAm/AAc terpolymerization.

4.1.2.2 Cumulative Terpolymer Composition

The change in reactivity ratio estimates (as ionic strength increases) can directly influence cumulative terpolymer composition. As an example, refer to the final two rows of Table 4.4; as ionic strength increases, both r_{21} and r_{23} decrease (from 0.82 to 0.39 and from 1.61 to 1.27, respectively). Physically, this suggests that the likelihood of acrylamide incorporation decreases as ionic strength increases; higher ionic strength (that is, more NaCl added) results in more charge screening, improving incorporation of the charged (acidic) monomers and reducing the incorporation of the acrylamide monomer.

This observation can be confirmed by predicting cumulative terpolymer composition under different experimental conditions. Given ternary reactivity ratio estimates and initial feed compositions, the recast Alfrey-Goldfinger model [57] can be used to predict cumulative terpolymer composition as a function of conversion. As seen in Figure 4.5 and Figure 4.6, it is possible to compare the cumulative composition of different terpolymers of AMPS/AAm/AAC, given reactivity ratios estimated at IS = 0.9 M and IS = 1.5 M. Experimentally speaking, pH and [M] were controlled at 7 and 1.0 M, respectively. Therefore, any changes in composition are primarily due to changes in ionic strength.

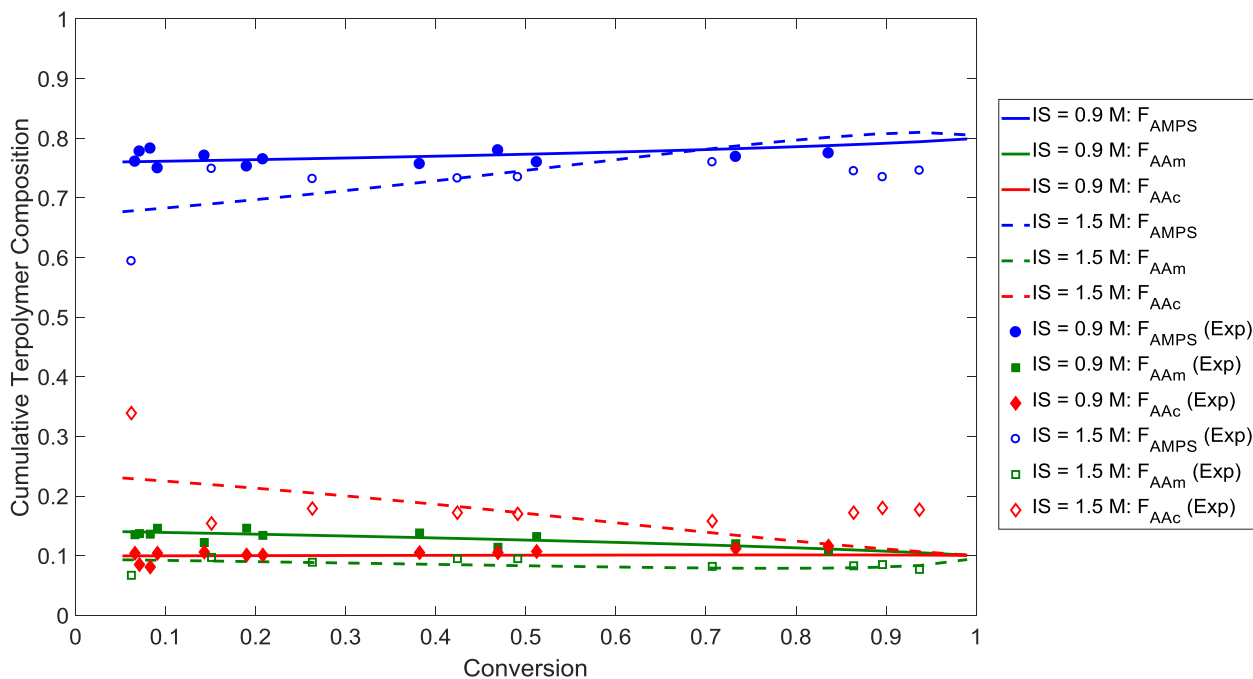


Figure 4.5: Cumulative Composition for AMPS-rich Terpolymer at IS = 0.9 M and 1.5 M

The predicted cumulative composition profiles (confirmed with experimental data) in Figure 4.5 reveal an important result. As ionic strength changes, the composition of the resulting terpolymer changes substantially. For IS = 0.9 M, $\bar{F}_{AAm} > \bar{F}_{AAC}$, but for IS = 1.5 M, $\bar{F}_{AAm} < \bar{F}_{AAC}$. This

agrees with what was observed when evaluating the reactivity ratios: higher ionic strength creates charge screening, reducing repulsion of the charged acrylic acid monomers. Therefore, an increased acrylic acid incorporation and a decreased acrylamide incorporation is visible. This is especially obvious for the AMPS-rich polymer, as the EVM-based design of experiments dictates an initial feed composition of $f_{\text{AMPS},0}/f_{\text{AAm},0}/f_{\text{AAc},0} = 0.8/0.1/0.1$. An equimolar concentration for AAm and AAc (at least initially) emphasizes the fact that solution properties affect the degree of incorporation of each comonomer.

To confirm that the increased ionic strength is reducing the acrylamide content in the product terpolymer, it is also possible to examine the acrylamide-rich terpolymer recipe. As shown in Figure 4.6, the cumulative mole fraction of AAm in the product terpolymer is significantly reduced at IS = 1.5 M, especially at low conversion. Since high acrylamide content and minimal composition drift are both desirable properties for the EOR application, solutions with lower ionic strength (IS = 0.9 M) seem like the more promising candidate for synthesizing AMPS/AAm/AAc terpolymers specifically for EOR.

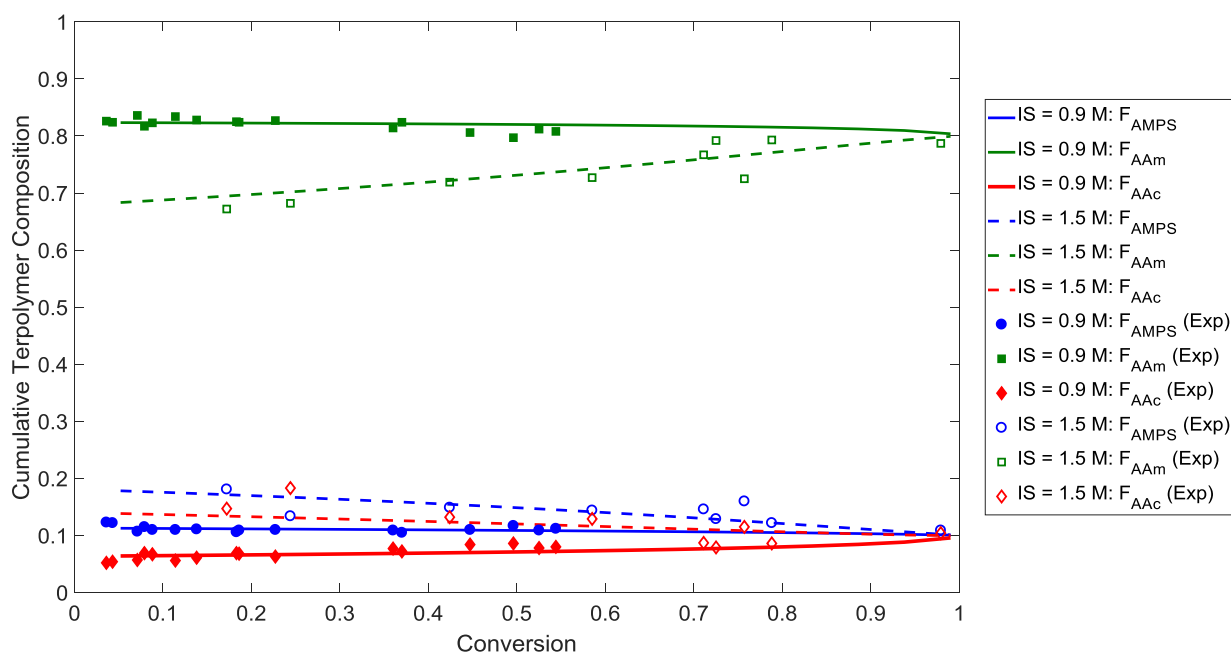


Figure 4.6: Cumulative Composition for AAm-rich Terpolymer at IS = 0.9 M and 1.5 M

Before concluding the discussion about the effect of ionic strength on cumulative terpolymer composition, a brief comment on azeotropy is in order. In this case, the ternary reactivity ratios estimated for IS = 0.9 M do not exhibit an azeotrope. However, those estimated for IS = 1.5 M exhibit azeotropic behaviour at $f_{\text{AMPS},0}/f_{\text{AAm},0}/f_{\text{AAc},0} = 0.26/0.35/0.39$. This further emphasizes the customization potential for AMPS/AAm/AAc as more information is obtained about the solution effects on polymerization kinetics.

4.1.2.3 Terpolymer Microstructure

Terpolymer microstructure, an important property for customization of materials (as explained in Section 2.1.2.1), is only discussed as a function of ionic strength herein. Given two data sets where all solution conditions (pH, IS and [M]) are the same (prior work from Scott et al. [80] and Runs S1, S10, S11 from the current study [81]), it is possible to consider terpolymer microstructure at IS = 0.9 M and 1.5 M more consistently.

The instantaneous triad fractions are calculated for demonstration and in order to get a general understanding about the system. This involves using all possible initial feed compositions ($0 < f_{i,0} < 1$; $\sum_{i=1}^3 f_{i,0} = 1$) and relevant reactivity ratios to calculate 18 possible triad fractions (recall Equations 2.4 to 2.6 and 2.10 to 2.15). As explained previously, 6 triads are centered around each monomer; the full list of triads is shown in Table 4.5.

Since AMPS/AAm/AAC terpolymers are being investigated for enhanced oil recovery, the material should be acrylamide-rich with an equal distribution of anionic charges, as per references [32, 118]. Therefore, given the triad fractions shown in Table 4.5, the goal is to minimize ‘blocky’ homopolymer sections (highlighted in red) and to simultaneously maximize alternating behaviour for acidic (charged) comonomers. For the analysis, it can be assumed that AMPS and AAC are both fully dissociated (which is true for any $\text{pH} > 5$), so they both contribute to the desired charge density. Therefore, any triad fraction for which AMPS or AAC alternates with AAm is desirable; these fractions (the sum of which is to be maximized) are highlighted in green in Table 4.5.

Table 4.5: Possible Triad Fractions for the AMPS/AAm/AAC Terpolymer

| AMPS (1)- centered | AAm (2)-centered | AAC (3)-centered |
|--------------------|------------------|------------------|
| A_{111} | A_{222} | A_{333} |
| A_{212} | A_{121} | A_{131} |
| A_{313} | A_{323} | A_{232} |
| $A_{112+211}$ | $A_{221+122}$ | $A_{331+133}$ |
| $A_{113+311}$ | $A_{223+322}$ | $A_{332+233}$ |
| $A_{213+312}$ | $A_{123+321}$ | $A_{132+231}$ |

To better visualize the instantaneous triad fractions, the likelihood of ‘blocky’ sections occurring in the polymer chain can be plotted as a function of initial feed composition. This is achieved by summing the A_{111} , A_{222} and A_{333} triad fractions at all feed compositions. Since the triad fractions can be predicted using reactivity ratios, the same analysis was completed using reactivity ratios

estimated from data at IS = 0.9 M and at IS = 1.5 M (recall Table 4.4). The results for both analyses are presented in Figure 4.7.

As expected, the most ‘blocky’ behaviour is exhibited for homopolymers ($f_{\text{AMPS},0}/f_{\text{AAm},0}/f_{\text{AAc},0} = 1.0/0.0/0.0, 0.0/1.0/0.0, 0.0/0.0/1.0$). The minimum changes somewhat as the ionic strength shifts from IS = 0.9 M to IS = 1.5 M, but the general trends are the same. In this case, the desire to synthesize a terpolymer and the desire to minimize ‘blocky’ behaviour align: the ‘blocky’ behaviour decreases as we move towards the center of the composition diagram.

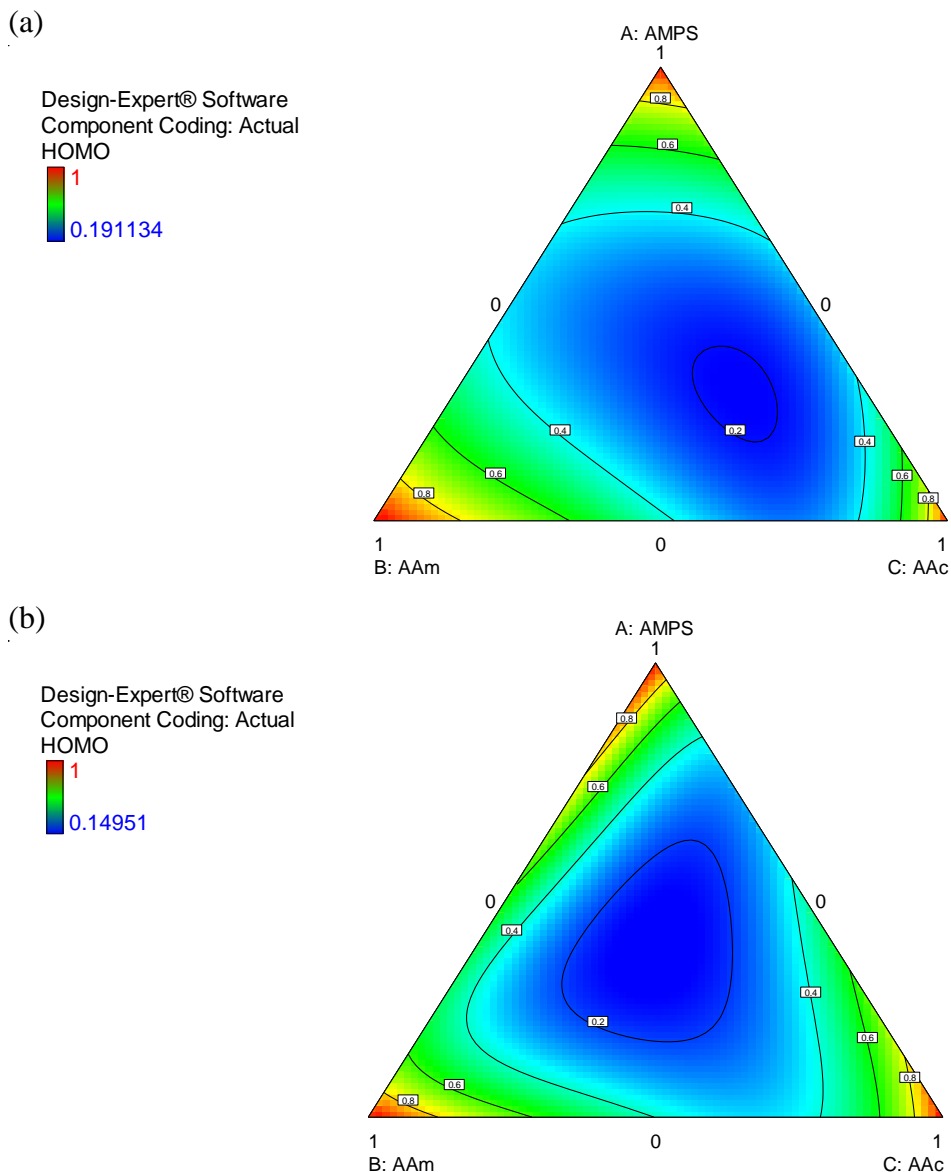


Figure 4.7: Prediction of Instantaneous ‘Blocky’ Triad Fractions at IS = (a) 0.9 M and (b) 1.5 M

The charge distribution along the polymer backbone is considered next. Using Design Expert software, it is possible to minimize the ‘blocky’ triad fractions and maximize the desirable triad fractions (that is, those with alternating behaviour of charged comonomers) simultaneously. Additional composition constraints were added (all $f_{i,0} \geq 0.1$) to ensure that the optimized recipes were, in fact, terpolymers. For both IS = 0.9 M and IS = 1.5 M, several solutions exist. Some feed compositions predict fewer ‘blocky’ fractions, others predict more alternating ion behaviour. Both requirements are equally weighted for the current study, but more tailoring is possible. The results of both optimizations are presented in Table 4.6 and Figure 4.8.

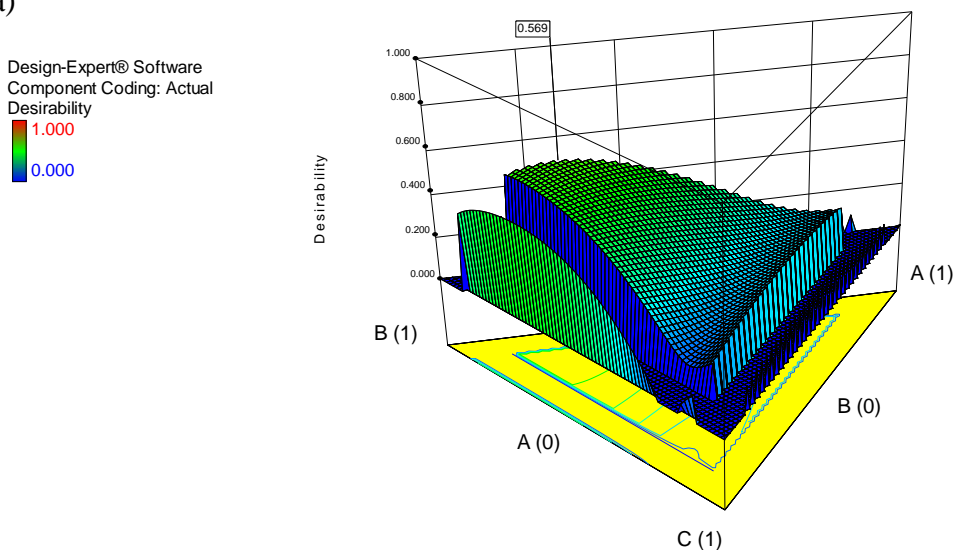
Table 4.6: Optimized Triad Fractions for Enhanced Oil Recovery

| (a) Given Reactivity Ratios Estimated at IS = 0.9 M, pH 7 and [M] = 1.0 M | | | | | | |
|--|--------------|-------------|-------------|-----------------------------------|---------------------------------------|---------------------|
| Solution # | $f_{AMPS,0}$ | $f_{AAm,0}$ | $f_{AAc,0}$ | ‘Blocky’ (to minimize) | Charge Dist. (to maximize) | Desirability |
| 1 | 0.209 | 0.691 | 0.100 | 0.487 | 1.420 | 0.569 |
| 2 | 0.100 | 0.750 | 0.150 | 0.603 | 1.508 | 0.536 |
| 3 | 0.400 | 0.500 | 0.100 | 0.323 | 1.154 | 0.490 |
| 4 | 0.500 | 0.400 | 0.100 | 0.305 | 1.039 | 0.403 |
| 5 | 0.539 | 0.100 | 0.361 | 0.286 | 0.890 | 0.238 |
| 6 | 0.100 | 0.100 | 0.800 | 0.386 | 0.854 | 0.159 |
| (b) Given Reactivity Ratios Estimated at IS = 1.5 M, pH 7 and [M] = 1.0 M | | | | | | |
| Solution # | $f_{AMPS,0}$ | $f_{AAm,0}$ | $f_{AAc,0}$ | ‘Blocky’ (to minimize) | Charge Dist. (to maximize) | Desirability |
| 1 | 0.412 | 0.459 | 0.129 | 0.255 | 1.100 | 0.521 |
| 2 | 0.400 | 0.500 | 0.100 | 0.301 | 1.125 | 0.520 |
| 3 | 0.500 | 0.400 | 0.100 | 0.330 | 1.121 | 0.507 |
| 4 | 0.637 | 0.100 | 0.263 | 0.217 | 0.980 | 0.448 |
| 5 | 0.100 | 0.800 | 0.100 | 0.521 | 1.139 | 0.437 |

According to the low ionic strength results in Table 4.6a (IS = 0.9 M, pH 7 and [M] = 1.0 M), the desirability function is maximized for $f_{AMPS,0}/f_{AAm,0}/f_{AAc,0} = 0.209/0.691/0.100$. This result also aligns with the desire to use an AAm-rich terpolymer; AAm-rich copolymers (with AAc) have been successfully employed for enhanced oil recovery [117]. Alternatively, Solutions 2 and 3 (again from Table 4.6a) also show promise. The exercise predicts that Solution 2 will have more blocky behaviour, but improved charge distribution over Solution 1. In contrast, Solution 3 has less blocky triad fractions, but the negative aspects are the lower AAm content and the poorer charge distribution. Solutions 4 through 6 are not considered further, as the AAm content is likely too low for the EOR application.

The high ionic strength results in Table 4.6b (IS = 1.5 M, pH 7 and [M] = 1.0 M) show lower desirability values for the top two solutions (compared to the IS = 0.9 M results). In general, the reactivity ratios estimated at higher IS predict less ‘blocky’ triad fractions, but the charge distribution is not as good. This is likely due to the lower acrylamide content, both from a feed composition and an incorporation perspective (as shown in Section 4.1.2.2). Along the same line, most optimal feed compositions in Table 4.6b have low $f_{AAm,0}$, which is not ideal for the EOR application. Given the optimized recipes, Solution 5 has the highest (therefore most desirable) AAm fraction, but the overall desirability is lower than for the optimal terpolymerizations at IS = 0.9 M.

(a)



(b)

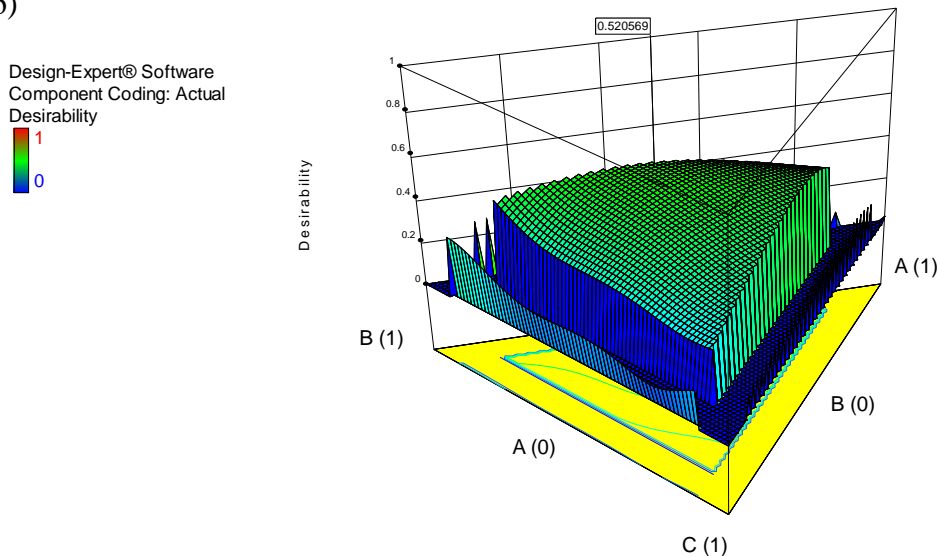
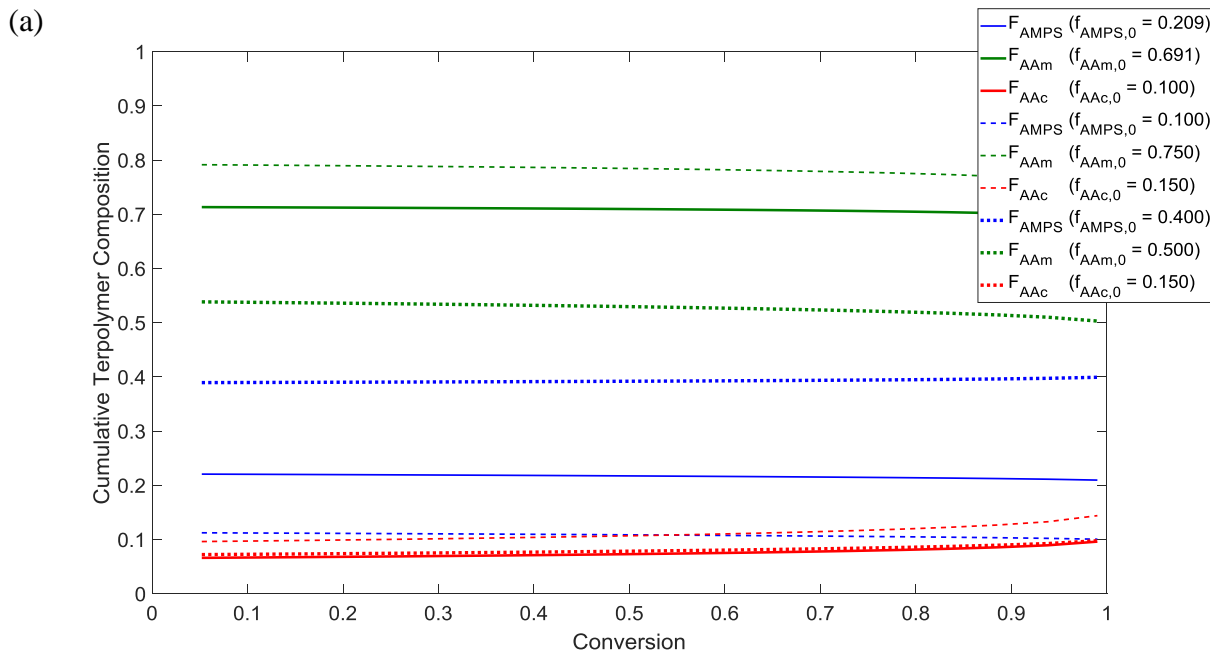


Figure 4.8: Optimized Instantaneous Triad Fractions for Enhanced Oil Recovery at (a) IS = 0.9 M and (b) IS = 1.5 M ($A = f_{AMPS,0}$, $B = f_{AAm,0}$, $C = f_{AAc,0}$)

As mentioned earlier, these instantaneous triad fractions were used to demonstrate the basic principles. Now, the cumulative terpolymer composition can be predicted as a function of conversion, given the most desirable feed compositions from Table 4.6. The most promising optimal recipes are examined for both IS = 0.9 M (Solutions 1, 2 and 3 of Table 4.6a) and IS = 1.5 M (Solutions 1, 2 and 5 of Table 4.6b); corresponding cumulative terpolymer composition profiles are shown in Figure 4.9.

In Figure 4.9a, all three feed compositions exhibit minimal composition drift. Therefore, along with composition, terpolymer triad fractions should remain relatively constant throughout conversion. As per previous EOR studies (for AAm/AAC copolymers), preference is given to materials with higher acrylamide content [32, 117]. Therefore, Solution 1 or Solution 2 of Table 4.6a seem the most promising for future EOR testing.

In Figure 4.9b, the three optimal feed compositions exhibit more composition drift. This is in agreement with earlier results (recall Figure 4.5 and Figure 4.6) but is not a desirable property for this application. Solutions 1 and 2 (from Table 4.6b) give similar results, but both end up being rich in AMPS. The most viable option at high ionic strength is Solution 5 ($f_{AMPS,0}/f_{AAm,0}/f_{AAc,0} = 0.100/0.800/0.100$), since AAm is present in the highest proportion. However, as evidenced in Section 4.1.2.2, the high ionic strength limits AAm incorporation, and therefore the low ionic strength formulation is the better option.



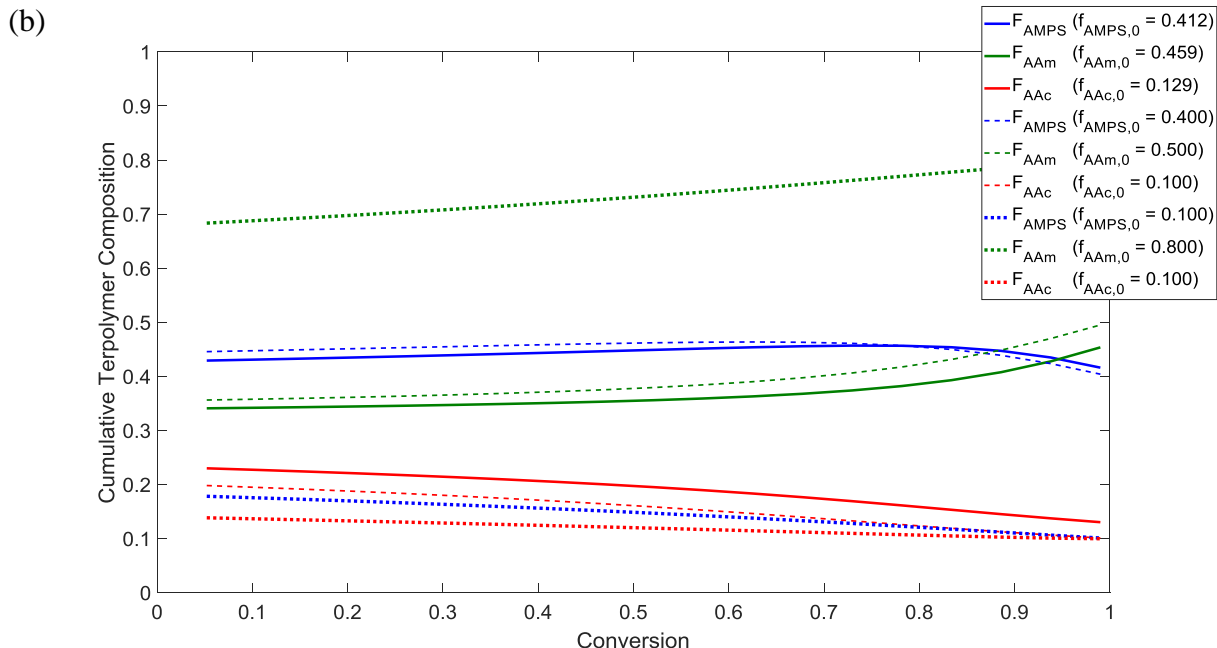


Figure 4.9: Cumulative Terpolymer Composition Predictions from Optimized Triad Fractions at (a) IS = 0.9 M and (b) IS = 1.5 M

In the next step of this enhanced oil recovery study, the most promising materials will be synthesized from acrylamide-rich recipes at IS = 0.9 M ($f_{AMPS,0}/f_{AAm,0}/f_{AAc,0} = 0.209/0.691/0.100$ and $0.100/0.750/0.150$). These are investigated further in what follows; the experimental methodology has been described in Section 3.2.2 and the results are discussed in Section 4.2.

4.1.3 Effect of Monomer Concentration

In Section 2.4.3, the effect of monomer concentration on terpolymerization kinetics was discussed. For related copolymer systems, monomer concentration has an impact on reactivity ratios [85, 86, 99]. This is likely due to the change in monomer concentration influencing the ionic strength; higher monomer concentration results in a higher concentration of charged monomers, thereby influencing the ionic strength and associated charge effects described previously.

Again, in this case, reactivity ratios are estimated (for the sake of completeness), and properties that are expected to be more affected by [M] (namely, molecular weight averages) are evaluated.

Table 4.7: [M] Effects on Ternary Reactivity Ratio Estimates for AMPS/AAm/AAc ($M_1/M_2/M_3$)

| [M] | Data from Run # | r_{12} | r_{21} | r_{13} | r_{31} | r_{23} | r_{32} |
|--------------|-----------------|----------|----------|----------|----------|----------|----------|
| 0.5 M | S4, S6, S9 | 1.05 | 0.65 | 0.30 | 1.14 | 1.81 | 0.54 |
| 1.0 M | S1, S2, S7 | 1.26 | 0.56 | 0.27 | 1.82 | 2.45 | 0.50 |
| 1.5 M | S3, S5, S8 | 1.06 | 0.56 | 0.44 | 0.94 | 1.19 | 0.47 |

In Table 4.7 and Figure 4.10, there are no obvious trends visible; the reactivity ratios do not tend in a particular direction as monomer concentration increases. Many of the reactivity ratio estimates are similar at different $[M]$ levels (at least for the range and conditions considered), especially the AMPS/AAm comonomer pair (r_{12} and r_{21} estimates). As discussed in Section 4.1.1, reactivity ratios associated with acrylic acid seem to have more variability. Again, this may be because the incorporation of acidic comonomers (especially AAc) is more affected by changes in the pre-polymerization solution.

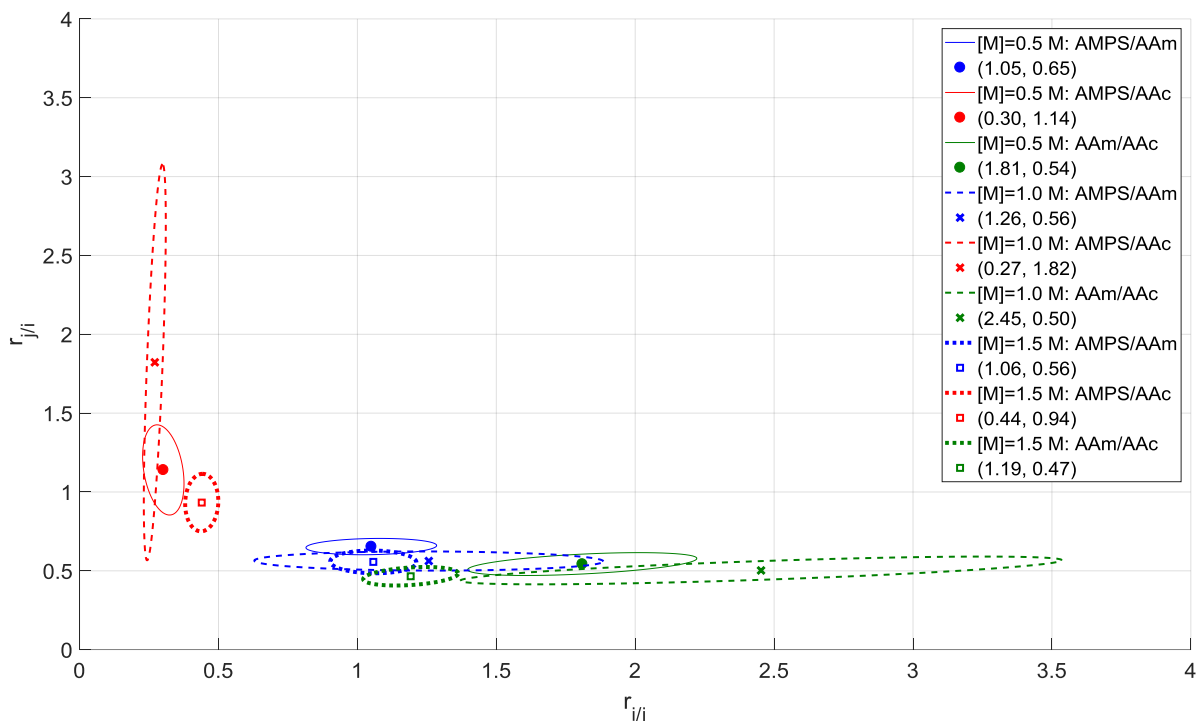


Figure 4.10: Comparison of Reactivity Ratio Estimates for AMPS/AAm/AAc at $[M] = 0.5 \text{ M}$, 1.0 M and 1.5 M

As shown in Figure 4.10, some overlap exists among JCRs for each comonomer pair. In the same way as for the pH effect estimates (Figure 4.1) and the IS effect estimates (Figure 4.3), one set of JCRs is much larger than the other two. In this case, the reactivity ratio estimates obtained from data at $[M] = 1.0 \text{ M}$ show the most uncertainty, especially for r_{12} , r_{31} and r_{23} . Interestingly, the runs used for estimation are Runs S1, S2, and S7 (see Table 4.7, and refer to Table 3.1 for detailed experimental conditions). Therefore, no ‘common denominator’ exists between the three estimations that exhibited higher error. Uncertainty is most likely related to the confounded effects of pH, ionic strength and monomer concentration.

4.1.3.1 Terpolymer Molecular Weights

Finally, the peak average molecular weights (\bar{M}_p) of all trials are examined. Samples at similar conversion levels (~30%) were selected for analysis, which ensures that any variation in molecular weight is a result of synthesis conditions. Again, the polymer samples are influenced by varying pH, ionic strength and monomer concentration. The results are categorized by feed composition and are presented in Figure 4.11.

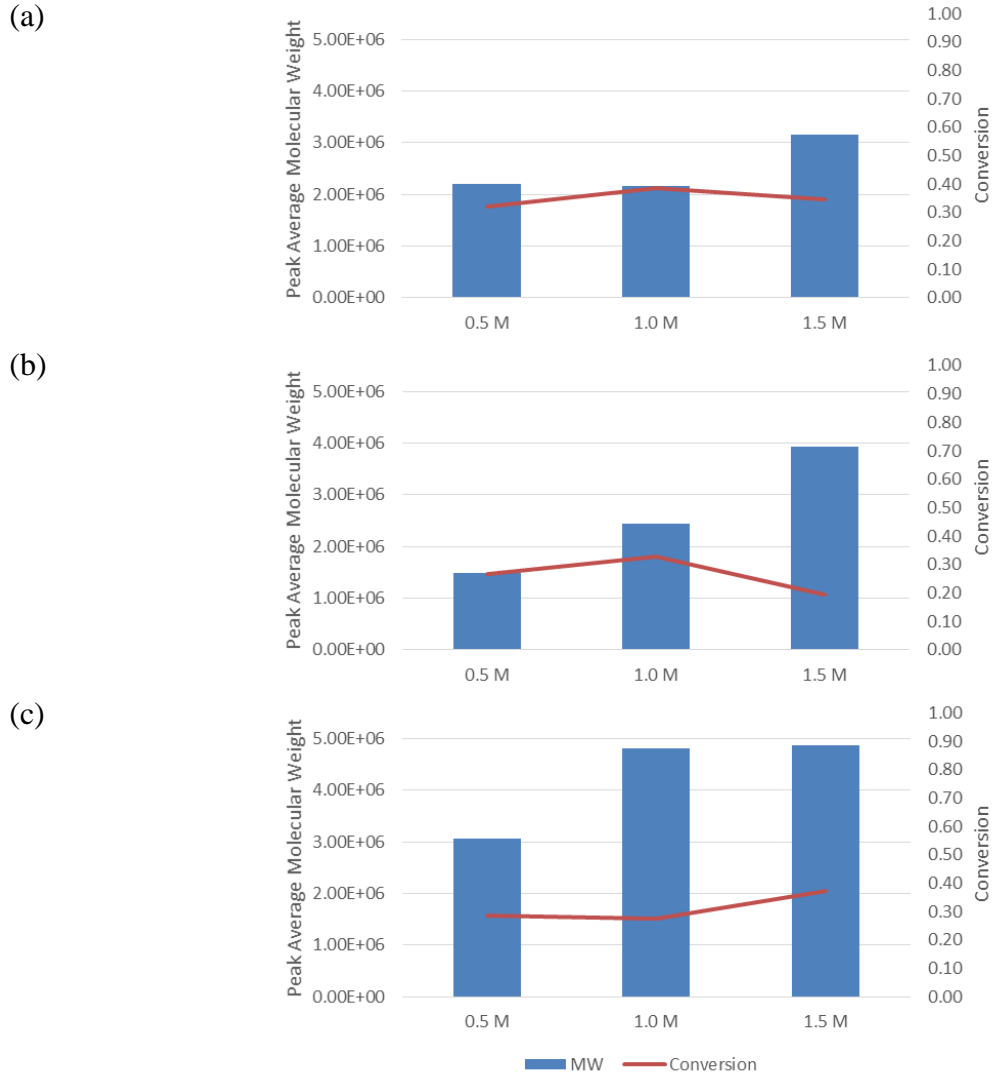


Figure 4.11: Effect of Monomer Composition on Peak Average Molecular Weights for $f_{AMPS,0}/f_{AAm,0}/f_{AAc,0} =$ (a) 0.8/0.1/0.1, (b) 0.1/0.2/0.7 and (c) 0.1/0.8/0.1

As mentioned in Section 3.2.1, the initiator concentration was adjusted alongside the monomer concentration to ensure that a constant $[M]/[I]^{1/2}$ ratio was maintained. This made it possible to target molecular weight averages that are desirable for enhanced oil recovery (on the order of 10^6

g/mol). The effect of $[M]$ on \overline{M}_p is so significant that it is visible despite other confounding variables; even as pH and IS vary, there is still a clear increase in \overline{M}_p as $[M]$ increases for all three feed compositions (Figure 4.11).

It is also interesting to observe the effect of feed composition on \overline{M}_p . The acrylamide-rich system (Figure 4.11c) exhibits the highest molecular weight averages of the three optimal terpolymer recipes, at least for the experimental conditions and conversion levels studied. As discussed earlier, high molecular weights are desirable for the enhanced oil recovery application; once again, the acrylamide-rich material is a promising candidate for EOR.

4.1.4 Effect of High NaCl Content

Due to the high ionic strength (and necessarily high salt content), we observed that sodium chloride remained present in the polymer samples at an approximate 1:1 ratio with acrylamide. This was initially deduced from elemental analysis results and uncharacteristically high conversion measurements, and subsequently independently confirmed for select samples via inductively coupled plasma emission spectrometry (ICP).

4.1.4.1 Conversion as an Indicator

For the AMPS/AAm/AAC screening experiments, the ‘low’ level of ionic strength (IS) was necessarily 1.2 M. In run S5, a total monomer concentration of 1.5 M and full dissociation of the acidic comonomers give an ionic strength of 1.2 M before any NaCl is added to the recipe. This imposes a relatively high range of ionic strength levels, and in some cases a large amount of NaCl was added to the pre-polymerization solution to adjust the ionic strength. The mass of NaCl added to each screening experiment is shown in Table 4.8.

Table 4.8: NaCl Addition for the AMPS/AAm/AAC Terpolymerization Screening Design

| Run # | pH | IS | $[M]$ | Feed Composition ($f_{AMPS,0}/f_{AAm,0}/f_{AAC,0}$) | NaCl Added (g) |
|-------|----|-------|-------|--|----------------|
| S1 | 7 | 1.5 M | 1.0 M | 0.1/0.2/0.7 | 8.20 |
| S2 | 5 | 1.2 M | 1.0 M | 0.8/0.1/0.1 | 3.69 |
| S3 | 7 | 1.8 M | 1.5 M | 0.8/0.1/0.1 | 5.23 |
| S4 | 7 | 1.2 M | 0.5 M | 0.1/0.8/0.1 | 12.85 |
| S5 | 9 | 1.2 M | 1.5 M | 0.1/0.2/0.7 | 0.00 |
| S6 | 5 | 1.8 M | 0.5 M | 0.1/0.2/0.7 | 16.92 |
| S7 | 9 | 1.8 M | 1.0 M | 0.1/0.8/0.1 | 18.70 |
| S8 | 5 | 1.5 M | 1.5 M | 0.1/0.8/0.1 | 14.26 |
| S9 | 9 | 1.5 M | 0.5 M | 0.8/0.1/0.1 | 12.27 |

The mass of NaCl required is not only influenced by the desired ionic strength, but also by the ionic contributions of acidic comonomers in the monomer feed. Since both AMPS and AAc dissociate, they both contribute to the ionic strength of a pre-polymerization solution. Therefore, in general, less salt needs to be added to increase the IS to a target value. In contrast, AAm-rich recipes rely more on NaCl addition to increase the IS to the desired value. This is evidenced in Table 4.8: the average NaCl added for AMPS-rich and AAc-rich recipes are 7.06 g and 8.37 g respectively, whereas the average NaCl added to AAm-rich recipes is 15.27 g.

A side-effect of this high salt content (especially for the AAm-rich recipes) became clear when the conversion levels of polymer samples were measured as a function of time; conversion levels were consistently higher than 100%. Run S7, for example, which has the highest mass of NaCl added, plateaued at a conversion level of 150% (see Figure 4.12). This conversion vs. time profile is contrasted with an equivalent run from Scott et al. [80]; both had an initial feed composition of $f_{AMPS,0}/f_{AAm,0}/f_{AAc,0} = 0.1/0.8/0.1$ and a total monomer concentration of 1.0 M. Ionic strength and pH varied from run to run, but these factors generally have a minor effect on the rate of polymerization.

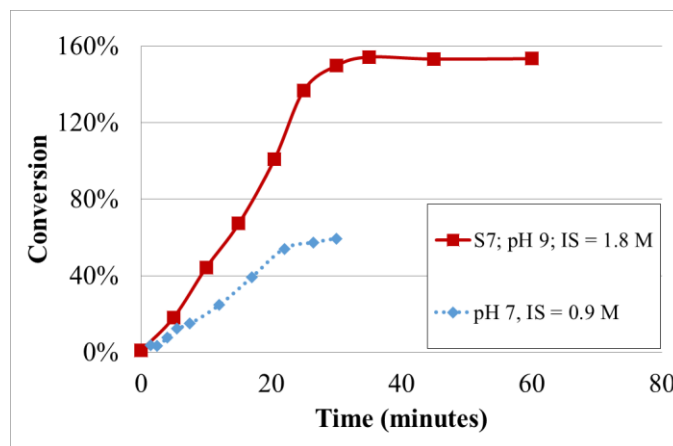


Figure 4.12: Effect of High NaCl Content on the Conversion Level of AMPS/AAm/AAc ($f_{AMPS,0}/f_{AAm,0}/f_{AAc,0} = 0.1/0.8/0.1$ and $[M] = 1.0$ M); with data from Scott et al. [80]

This behaviour, which was also observed for S8 and S11, was the first indication that the mass of NaCl was affecting the final mass (and subsequently, the measured conversion) of acrylamide-rich polymers.

To selectively troubleshoot this unusually high conversion, several additional runs were performed for polyacrylamide homopolymers (PAAm). The experimental conditions were selected such that the NaOH and NaCl addition varied according to Table 4.9, and the monomer concentration was consistently 1.0 M. pH control proved to be much more challenging for the PAAm homopolymer than for the terpolymers. Despite the fact that no acidic monomers were present, the initiator (4,4'-azo-bis-(4-cyanovaleric acid), ACVA) reduced the pre-polymerization solution to pH 3. With and

without the addition of NaCl, a pH decrease was observed throughout the ‘solution preparation’ stage for each recipe. Also, since little or no sodium hydroxide was included in the recipe, dissolution of ACVA took much longer than it did in standard terpolymerization syntheses. Therefore, in some cases, a ‘time 0’ sample was analyzed to check for premature polymerization.

Table 4.9: PAAm Salt Study Experiments

| Run # | NaOH | NaCl | pH | IS |
|-------|------|------|----|-------|
| PAAm1 | | | 3 | 0.0 M |
| PAAm2 | ✓ | | 7 | 0.0 M |
| PAAm3 | ✓ | ✓ | 7 | 1.8 M |
| PAAm4 | ✓ | ✓ | 11 | 1.8 M |
| PAAm5 | | ✓ | 3 | 1.8 M |

Finally, it is important to note that PAAm5 could not be fully evaluated. The addition of ACVA brought the solution to pH 3, but after three hours of mixing the solids had not dissolved (see Figure 4.13; these solutions are normally transparent and colourless). Therefore, this combination of pH and ionic strength was not suitable for the terpolymerization of PAAm.

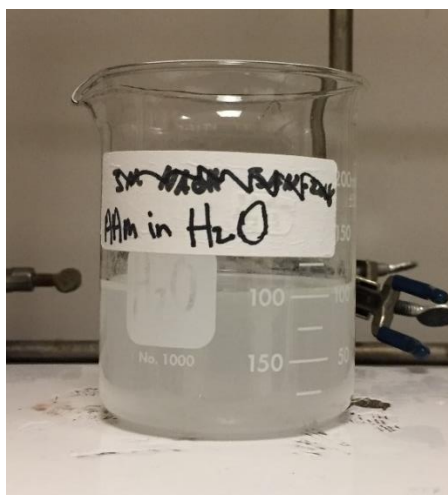


Figure 4.13: Poor Dissolution of Solids in PAAm5

A comparison of conversion vs. time profiles for PAAm with and without NaOH and/or NaCl confirms what was observed during the screening experiments (recall Figure 4.12). In Figure 4.14, both experiments that were performed without NaCl (PAAm1 and PAAm2) plateaued at 100%. The two profiles are similar, which suggests that the NaOH addition (and, by extension, the solution pH) does not affect the rate of polymerization or the mass of the product polymer. This is as expected, as the screening experiments indicated that the incorporation of AAm was less affected by pH (compared to AMPS and AAc).

In contrast, both experiments that had NaCl added to the recipe showed almost 200% conversion. The change in pH (between PAAm3 and PAAm4) may have had a slight effect on the rate of polymerization, but the important observation here is the extraordinarily high conversion values. This validates the high conversion levels calculated earlier; this is in fact due to the combination of acrylamide and high NaCl. Since conversion levels are almost exactly twice the expected values (and NaCl and AAm have similar molecular weights), the most likely explanation is that NaCl is incorporating at a 1:1 molar ratio with acrylamide through a weak physical bond.

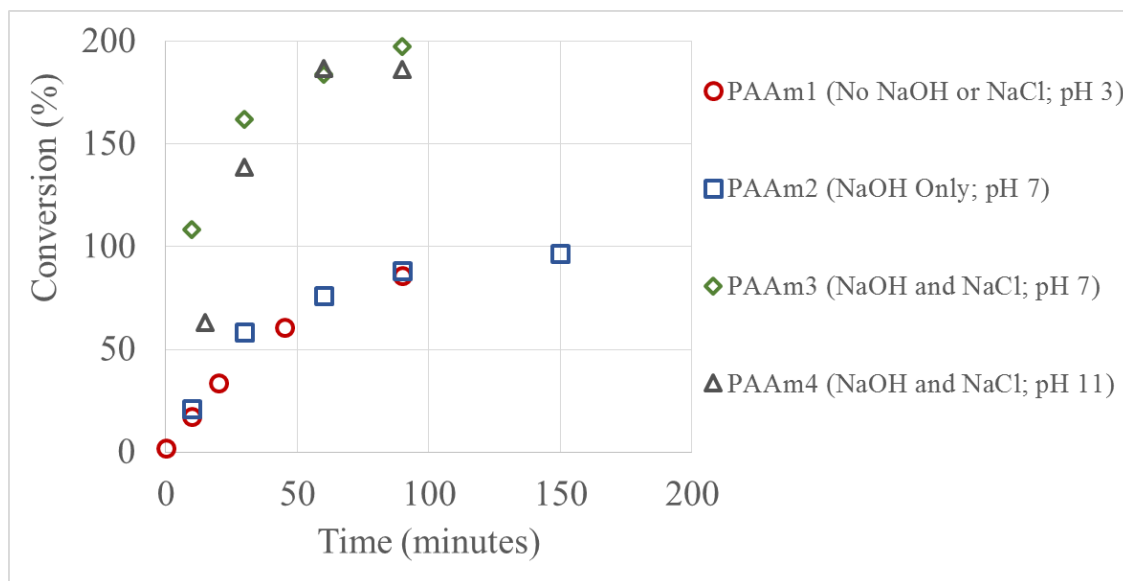


Figure 4.14: Effect of High NaCl Content on the Conversion Level of PAAm at $[M] = 1.0 \text{ M}$

If the mass of each sample is numerically adjusted to include NaCl mass (on a 1:1 molar basis), 45.1wt% of each sample is NaCl and the remainder is PAAm. This effectively reduces the conversion values by a half, providing much more reasonable results as shown in Figure 4.15.

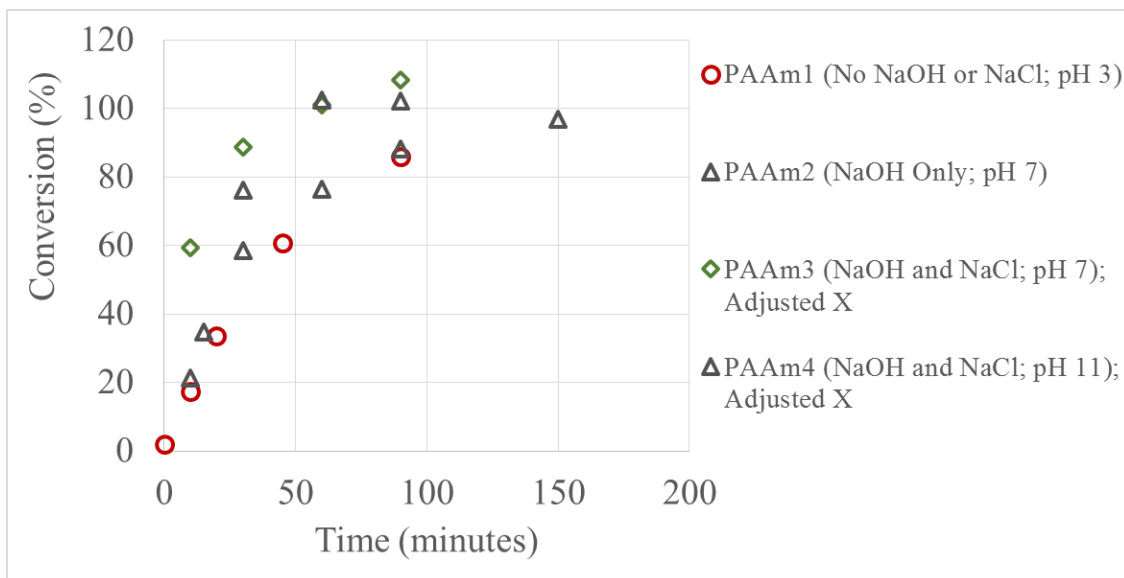


Figure 4.15: Conversion Level Adjustment (NaCl Consideration) for PAAm at $[M] = 1.0 \text{ M}$

For now, this is only a numerical adjustment, but the implications are promising. In what follows, the salt retention assumption was confirmed by looking at the polymer composition. However, as a preliminary check, the S7 profile shown in Figure 4.12 can be revisited. Using the feed composition (80 mol% AAm in this case) as a rough approximation, it is possible to divide the total sample mass into polymer and NaCl contributions; sample conversion calculations for run S7 are shown in Appendix C, Section C.1.

As shown in Equation C.6, the NaCl adjustment gives a calculated conversion of 98.9% for S7-10 (Sample 10 from Run S7). This result is much more reasonable than the “calculation artifact” of 153.5% conversion, which was shown in Figure 4.12. Therefore, taking salt incorporation into account seems reasonable based on these results. The final step, which is typical of all AMPS/AAm/AAC terpolymerization analyses, is to consider the additional Na^+ mass that is bound to dissociated AMPS and AAC comonomers (where the Na^+ ions are present from titration with NaOH; the NaAMPS and NaAAC comonomers are incorporated into the product terpolymer) [84]. The detailed calculations for Na^+ content are presented in Appendix C (specifically Equation C.14). For now, suffice it to say that the presence of Na^+ further (slightly) decreases the total polymer mass, thus decreasing the calculated conversion. The updated conversion vs. time profile for Run S7 is provided in Figure 4.16, and similar behaviour was seen once the same numerical adjustments were made for other screening runs.

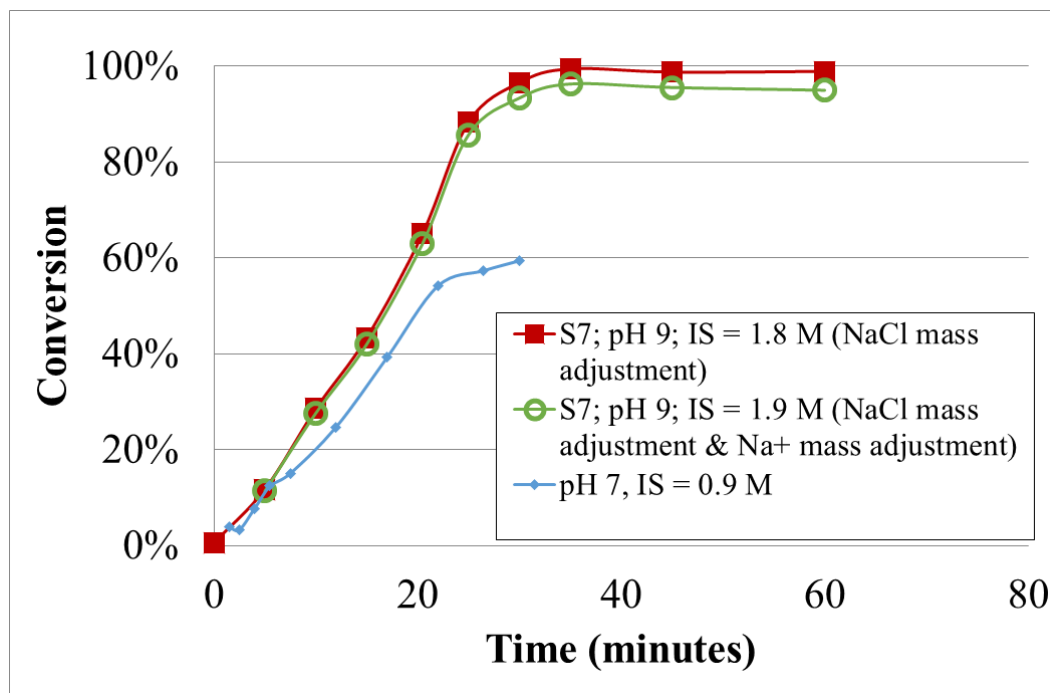


Figure 4.16: High NaCl Mass Adjustment for the Conversion of AMPS/AAm/AAC ($f_{\text{AMPS},0}/f_{\text{AAm},0}/f_{\text{AAc},0} = 0.1/0.8/0.1$ and $[M] = 1.0 \text{ M}$); with data from Scott et al. [80]

4.1.4.2 Composition as an Indicator

Next, the sample composition was investigated (measured through elemental analysis). Nitrogen, carbon, hydrogen and sulfur can be measured, which means that the fraction of any additional expected elements (like oxygen, sodium, etc.) must be inferred. Typically, if the contributions of additional elements are estimated using stoichiometry, the elemental contributions of all components sum to ~100%. Take, for example, Run S5, where no NaCl was added to the recipe; results and sample calculations are shown in Appendix C, Section C.2.

As shown in Table C.1, the sum of elements is almost exactly 100% for all S5 samples. However, for the acrylamide-rich copolymers with high NaCl addition, this was not the case. As discussed previously, Run S7 had 18.70 g NaCl added to the recipe prior to polymerization. In following the same calculations described for Run S5 (in Appendix C, Section C.2), the results of Table 4.10 were obtained.

Table 4.10: Analysis of Elemental Contributions for Run S7

| | wt% N | wt% C | wt% H | wt% S | wt% O (polymer) | wt% O (H ₂ O) | wt% Na | Total wt% |
|--------------|-------|-------|-------|-------|--------------------|-----------------------------|--------|--------------|
| S7-2 | 8.00 | 26.27 | 4.02 | 2.51 | 14.61 | 3.36 | 3.03 | 61.80 |
| S7-3 | 7.37 | 24.66 | 3.74 | 2.75 | 13.94 | 2.80 | 2.98 | 58.24 |
| S7-4 | 7.16 | 23.58 | 3.55 | 2.36 | 13.15 | 2.50 | 2.73 | 55.03 |
| S7-5 | 5.83 | 19.73 | 2.92 | 2.11 | 11.21 | 1.75 | 2.51 | 46.07 |
| S7-6 | 5.04 | 17.08 | 2.51 | 1.95 | 9.74 | 1.36 | 2.16 | 39.84 |
| S7-7 | 5.71 | 19.26 | 2.83 | 2.18 | 10.95 | 1.50 | 2.40 | 44.83 |
| S7-8 | 5.90 | 19.60 | 2.91 | 2.09 | 11.01 | 1.74 | 2.32 | 45.57 |
| S7-9 | 5.72 | 19.15 | 2.94 | 2.06 | 10.81 | 2.52 | 2.34 | 45.54 |
| S7-10 | 7.99 | 26.09 | 3.95 | 2.45 | 14.45 | 2.99 | 2.95 | 60.86 |

Looking at the elemental contributions for samples from Run S7, it is only possible to account for between 40% and 62% of the total mass of each sample. This confirms (as suspected) that there is something else present in the sample, namely residual NaCl. As described earlier, it seems that NaCl is incorporating at a 1:1 molar ratio with acrylamide through a weak physical bond. Taking this into account increases the total elemental contributions to more reasonable values (that is, closer to 100%, as was the case for Run S5 in Table C.1). The evidence is provided in Table 4.11.

Table 4.11: Adjusted Analysis of Elemental Contributions for S7

| | wt% polymer | g polymer in sample | g NaCl in sample | total g sample | wt% NaCl | Total (adjusted) wt% |
|--------------|----------------|------------------------|---------------------|-------------------|----------|-------------------------|
| S7-2 | 61.80 | 0.2054 | 0.1132 | 0.3186 | 35.54 | 97.35 |
| S7-3 | 58.24 | 0.4788 | 0.2640 | 0.7428 | 35.54 | 93.78 |
| S7-4 | 55.03 | 0.7575 | 0.4176 | 1.1751 | 35.54 | 90.57 |
| S7-5 | 46.07 | 1.0808 | 0.5960 | 1.6768 | 35.54 | 81.61 |
| S7-6 | 39.84 | 1.4317 | 0.7894 | 2.2211 | 35.54 | 75.38 |
| S7-7 | 44.83 | 1.7025 | 0.9388 | 2.6413 | 35.54 | 80.37 |
| S7-8 | 45.57 | 1.5520 | 0.8558 | 2.4078 | 35.54 | 81.11 |
| S7-9 | 45.54 | 1.6694 | 0.9205 | 2.5899 | 35.54 | 81.08 |
| S7-10 | 60.86 | 1.8502 | 1.0201 | 2.8703 | 35.54 | 96.40 |

Finally, the residual NaCl content was confirmed with select samples using inductively coupled plasma emission spectrometry (Prodigy radial ICP-OES by Teledyne-Leeman). Samples were run in triplicate, and the results from S7-10 analysis are shown in Table 4.12.

Table 4.12: Analysis of ICP Results for S7-10

| | prepared sample conc. (ppm) | measured Na conc. (ppm) | wt% total Na | wt% Na⁺ ions (calculated; bound to acidic comonomers) | wt% Na in residual NaCl | wt% Cl from residual NaCl | wt% NaCl |
|---|------------------------------------|--------------------------------|---------------------|---|--------------------------------|----------------------------------|-----------------|
| 1 | 9694.51 | 1,715.87 | 17.70 | 2.95 | 14.75 | 22.74 | 37.49 |
| 2 | 9694.51 | 1,686.32 | 17.39 | 2.95 | 14.44 | 22.27 | 36.72 |
| 3 | 9694.51 | 1,686.67 | 17.40 | 2.95 | 14.45 | 22.28 | 36.73 |

In Table 4.12, the wt% total Na is the ratio between the measured Na concentration and the prepared (calculated) sample concentration. This total Na measurement includes the Na⁺ ions bound to acidic comonomers (calculated using elemental analysis and stoichiometry as discussed previously; see Equation C.14). Since any additional Na mass is assumed to be from residual NaCl in the sample, it is straightforward to calculate the total wt% NaCl in sample S7-10. The results of Table 4.12 are in good agreement with each other and are reasonably close to the estimated 35.54 wt% shown in Table 4.11. This further confirms that NaCl incorporates with acrylamide at a 1:1 molar ratio.

4.1.5 Concluding Remarks on Terpolymerization Screening Experiments

A series of nine terpolymerization experiments (from a definitive screening design) and two complementary experiments (Table 3.1) has provided a wealth of information about the terpolymerization kinetics of 2-acrylamido-2-methylpropane sulfonic acid (AMPS), acrylamide (AAM) and acrylic acid (AAc). Solution pH, ionic strength and monomer concentration can all be used to influence the properties of the resulting terpolymer, which ultimately assists with the design of custom materials for enhanced oil recovery and other applications.

Although no clear correlation was observed between pH and reactivity ratio estimates (for $5 \leq \text{pH} \leq 9$), parameter estimation results suggest that the incorporation of acidic comonomers (AMPS and AAc) is affected by pH. More importantly, comparing these parameter estimates to prior work by Scott et al. [80] revealed cross-over behaviour for both AMPS/AAM and AMPS/AAc comonomer pairs. Since all estimates compared were from experiments at pH 7, other solution effects were explored in more detail.

Ionic strength (IS) proved to have the greatest influence on reactivity ratios for the range studied. The two complementary runs confirmed that cross-over behaviour exists between IS = 0.9 M and IS = 1.5 M for AMPS-based reactivity ratios (r_{12} and r_{21} ; r_{13} and r_{31}) at pH 7 and $[M] = 1.0$ M. This shift in reactivity ratios has significant potential for tailoring AMPS/AAM/AAc terpolymer properties. With the enhanced oil recovery application in mind, synthesis at the lower ionic strength (0.9 M) is more desirable, as it allows for increased AAM incorporation and a more

desirable microstructure. Analysis of terpolymer microstructure suggests that the following feed compositions may be of interest for EOR: $f_{\text{AMPS},0}/f_{\text{AAm},0}/f_{\text{AAc},0} = 0.21/0.69/0.10$ and $0.10/0.75/0.15$.

Finally, monomer concentration had a minor influence on reactivity ratio estimates but had a visible impact on molecular weight averages (even when other factors were varied). All samples had peak average molecular weights on the order of 10^6 g/mol, but average molecular weights increased with increasing [M] for all feed compositions. This is as expected from polymerization theory, but these trends provide good experimental confirmation nonetheless.

4.2 Optimally Designed Experiments

4.2.1 Justification of Experimental Conditions

It has been established that the polymerization kinetics of AMPS/AAm/AAc are largely dependent on feed/recipe operating conditions (environment solution properties). It is therefore critical to monitor and/or control the ionic strength, pH, monomer concentration and feed composition of each terpolymer formulation [81]. These variables can impact the rate of polymerization, the degree of incorporation of each comonomer into the terpolymer product, the polymer microstructure, and the molecular weight distribution.

Therefore, at this stage of the investigation, every effort was made so that the terpolymers be synthesized with consistent formulations. In an attempt to synthesize materials that would have desirable properties for the enhanced oil recovery application, the experimental conditions selected were informed by the results of Section 4.1.

The selected pH (at which synthesis occurred) for the optimally designed experiments was pH 7. As described in the screening experiments study (Section 4.1.1), no clear correlation between pH and reactivity ratio estimates was observed for the range of pH 5 to pH 9. However, since acidic comonomers seem to be affected by changes in pH, it is still important to select a pH for synthesis and adjust the pre-polymerization solution accordingly. A solution pH of 7 was selected here because the condition is moderate (neutral) and because it allows for a direct extension of prior work (especially the ionic strength study in Section 4.1.2.1). In Section 4.1, reactivity ratios were generally estimated in a relative way, since experimental conditions were varied (as mentioned earlier, this is the nature of a screening design of experiments). Therefore, the only reactivity ratio estimates that can be used with confidence (for prediction purposes) are from experimental data with constant (and carefully controlled) experimental conditions; this is the case for the reactivity ratios in Table 4.4. In both cases where reactivity ratios are available for AMPS/AAm/AAc under constant experimental conditions, the formulation is with pH 7. Thus, the predictions that are being used to inform these optimally designed experiments can only be guaranteed for new formulations

that are also at pH 7; sodium hydroxide solutions were used to adjust the pH of each optimal formulation to approximately 7 (± 0.5).

The optimal ionic strength (for the range of conditions studied thus far) was found to be 0.9 M. As observed in the previous section (specifically Figure 4.5 and Figure 4.6), lower ionic strength (IS) promotes the increased incorporation of acrylamide. Given the knowledge that high acrylamide content is desirable for the application, the low IS level (0.9 M) is more suitable for the synthesis of AMPS/AAm/AAC terpolymers for EOR. Therefore, sodium chloride was added to each formulation to achieve IS = 0.9 M; since the required NaCl mass (added to each formulation) was more than 5 g, adjustments for high NaCl content were taken into account (as per Section 4.1.4).

In Section 4.1.3, monomer concentration had a limited impact on the reactivity ratios. By association, the terpolymer composition and microstructure were also minimally affected. However, as expected from polymerization kinetics, increasing the monomer concentration led to increased molecular weight averages. As discussed previously (Section 2.1.2.1), polymeric materials with high molecular weights (on the order of 10^6 g/mol) are desirable for the EOR application, so a total monomer concentration of 1.5 M was used for each formulation. As before, the $[M]/[I]^{1/2}$ ratio was maintained, so 0.009 M initiator (ACVA) was used for the optimally designed experiments (see again Section 3.2). The $[M] = 1.5$ M condition was selected because it was the highest level that had been used in our preliminary studies, but higher monomer concentrations may be possible. That said, it is always important to take experimental limitations into account; even at $[M] = 1.5$ M, some of the screening runs exhibited premature polymerization, as the titration of a strong acid like AMPS releases considerable heat and can kick-start the polymerization. Viscosity effects may also play a role at higher monomer concentration, but this has not been considered in great detail.

Finally, two optimal feed compositions (both rich in acrylamide) were selected to allow for the most desirable terpolymer microstructure, as predicted by the recently determined reactivity ratios [81]. The results of Section 4.1.2.3 established that optimal terpolymers for EOR would have minimal ‘blocky’ sections and that the charge (from the acidic comonomers) would be well-distributed along the backbone. Given reactivity ratio estimates for the terpolymerization of AMPS/AAm/AAC at pH 7, IS = 0.9 M and $[M] = 1.0$ M (nearly the same as the current conditions, with the exception of the monomer concentration), the triad fraction model prediction, and the cumulative terpolymer composition prediction, the optimal feed compositions (from Design Expert software) are $f_{\text{AMPS},0}/f_{\text{AAm},0}/f_{\text{AAC},0} = 0.21/0.69/0.10$ and $0.10/0.75/0.15$.

Thus, optimally designed terpolymers of AMPS/AAm/AAC were synthesized as described in Section 3.2.2. The product terpolymers were fully characterized (so that the polymer properties and the application-specific behaviour are well understood), and the results are presented in the following sections.

4.2.2 Investigation of Polymer Properties

Several properties investigated herein are the same characteristics as those for the screening experiments: namely conversion, composition and molecular weight (recall Section 4.1). In this case, consistency of polymer properties (that is, good experimental reproducibility) is extremely important, since several samples must be combined for the application-specific characterization for EOR. As described in Section 3.4.2 and Appendix C (Section C.6), at least 5 grams of polymeric material are needed for a single test, so the polymer product from several vials (or, potentially, from several independent syntheses) must be amalgamated. Therefore, uniform properties are essential for the application.

For both optimal formulations described in Table 3.2, genuine replication was carefully incorporated into the synthesis and subsequent characterization. At the synthesis stage, Opt1 and Opt1R (both of the same formulation) were synthesized from two unique (independently prepared) monomer stock solutions. Similarly, Opt2 and Opt2R were from independently prepared monomer stock solutions, and Opt2RB was synthesized from the same stock solution as Opt2R. Thus, reproducibility between stock solutions (with the same target formulation) and repeatability within a given stock solution (using the same concentrated solution for two separate synthesis procedures) have been considered. In addition, characterization replicates were performed for the evaluation of terpolymer properties described in what follows. A hierarchical design study (related to these two optimal terpolymers and molecular weight analysis) is currently in progress, as part of training a senior undergraduate student for their individual research project.

4.2.2.1 Gravimetry

As shown in Figure 4.17, both optimally designed experiments (shown in part (a) and (b) of the figure) exhibit similar polymerization rates. This is as expected, since influential reaction conditions are similar between the two formulations. Ionic strength and monomer concentration, known to affect the rate of polymerization [84], are the same between the two formulations. Also, although the feed composition varies for these two formulations, both terpolymers are rich in acrylamide. Therefore, the similarity of the two conversion profiles confirms that the syntheses are behaving as anticipated.

In both cases, samples have reached full conversion after ~90 minutes of reaction time. As described previously, conversion values were adjusted to take the high salt content (and residual salt in the product polymer) into account. However, in this case, assuming that NaCl incorporated at a 1:1 molar ratio with acrylamide was unfounded, since there was not enough salt added to the system in the pre-polymerization step. Data analysis and evaluation of conversion and composition (elemental contributions) indicate that NaCl does still incorporate, but that the ratio at which it incorporates is approximately 0.4 mol NaCl to 1.0 mol AAm for Opt1 and 0.5 mol NaCl to 1.0

mol AAm for Opt2. It seems that incorporation at a 1:1 ratio occurs when enough salt is present in the system (that is, when the moles of NaCl outnumber the moles of acrylamide). When NaCl is limited, it incorporates to the extent possible. Therefore, numerical adjustment (or additional sample purification) is required to obtain reasonable conversion levels (below 100%) and to ensure that all sample mass is accounted for (in terms of elemental contributions). Note that, in this case, not all samples were characterized using elemental analysis (which is required to adjust for Na content as it relates to the acidic comonomers; see Section 3.3.1 and Appendix C (Section C.2)), so only the NaCl correction is applied herein. If the adjustment were made for the Na content, all conversion values would fall below 100%.

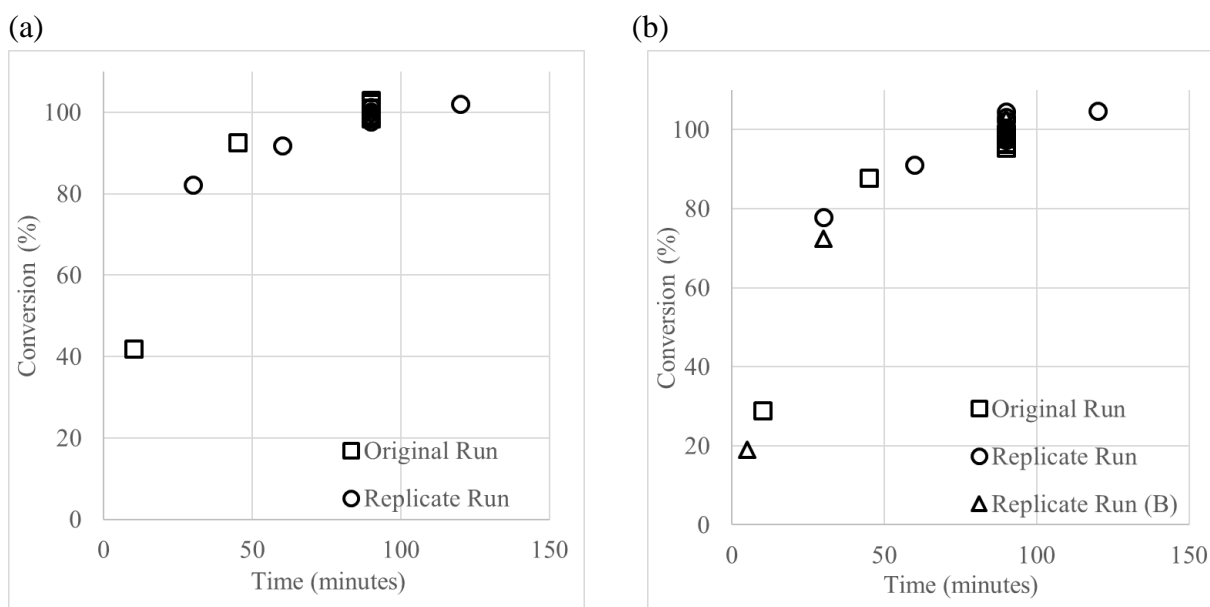


Figure 4.17: Repeatability of Gravimetric Results for Optimal Terpolymers; $f_{AMPS,0}/f_{AA,m,0}/f_{AAc,0} =$ (a) 0.21/0.69/0.10 and (b) 0.10/0.75/0.15

Most samples for both formulations were taken after 90 minutes. This was primarily so that there would be sufficient polymeric material (with nearly identical properties) for subsequent testing. The enhanced oil recovery tests, especially, require large quantities of polymer samples. Having several samples taken at the same time interval also provides additional data for repeatability analysis.

Samples were also collected at lower and higher sampling times (that is, lower and higher conversion levels) to obtain an improved understanding of the conversion effects on other material properties (namely, composition drift and changes in molecular weight averages). For both formulations, the replicate runs were consistent with the original runs in terms of conversion, and the trajectories were as expected. These gravimetry results indicate that the terpolymerization process is consistent through several independent synthesis replicates, and that additional characterization steps can be pursued.

4.2.2.2 Cumulative Terpolymer Composition

The cumulative terpolymer compositions for both optimal formulations were predicted from previously estimated ternary reactivity ratios (recall Figure 4.9a) [80, 81]. Given these predictions, the terpolymers are expected to be rich in acrylamide and to exhibit minimal composition drift throughout conversion. To confirm the cumulative terpolymer composition (and to evaluate the prediction performance of the reactivity ratio estimates), samples throughout the conversion trajectory were analyzed. The results (and comparisons to model predictions) are shown in Figure 4.18 and Figure 4.19.

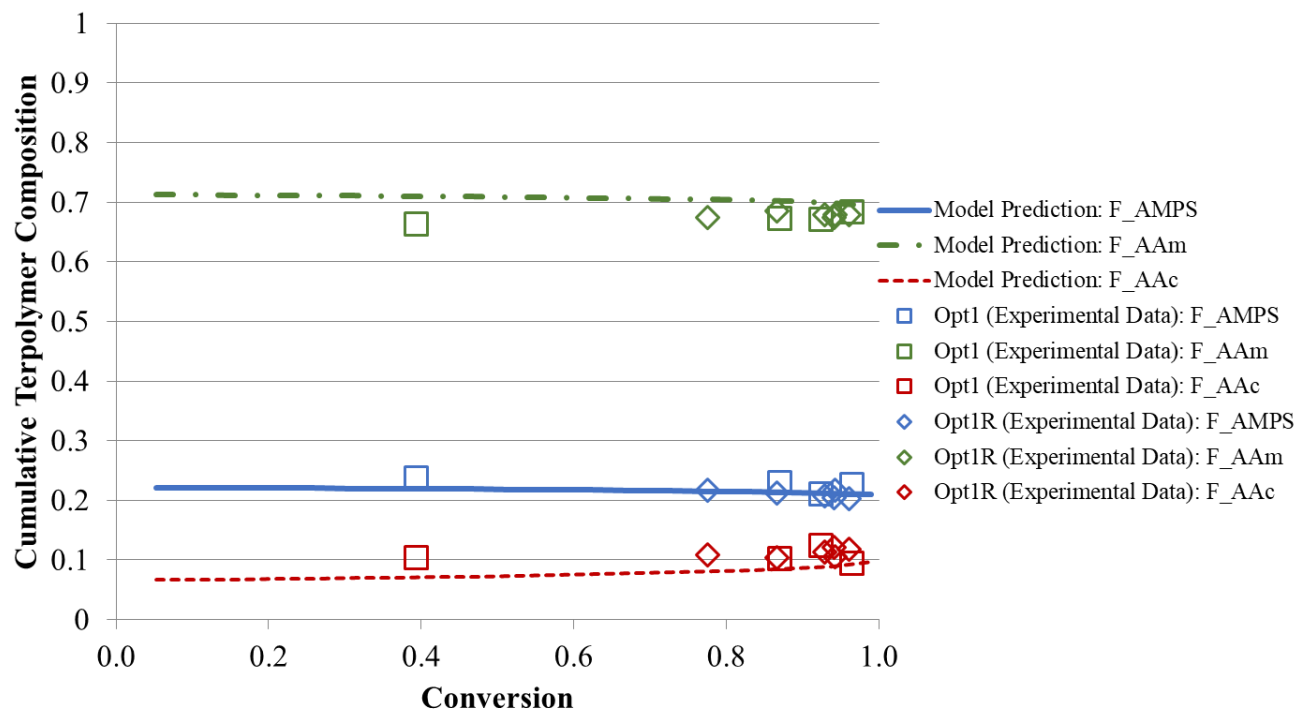


Figure 4.18: Cumulative Terpolymer Composition for Terpolymer Opt1 ($f_{AMPS,0}/f_{AAm,0}/f_{AAc,0} = 0.21/0.69/0.10$)

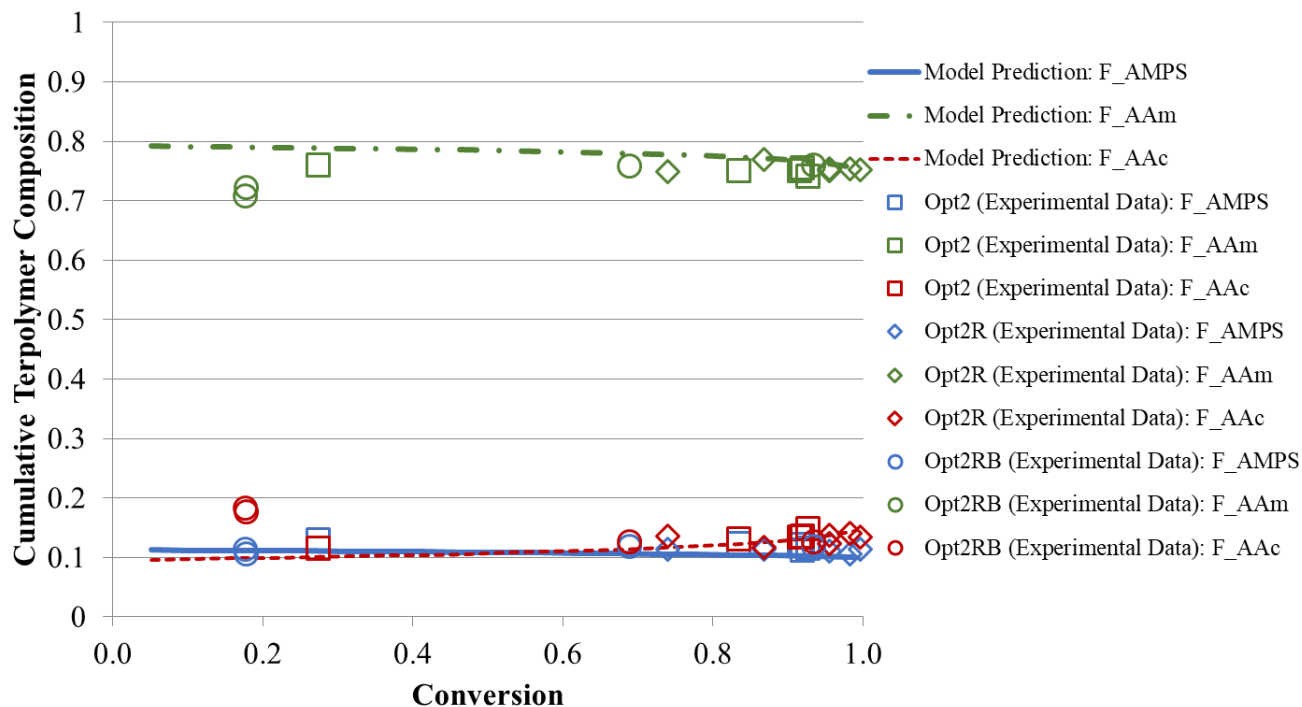


Figure 4.19: Cumulative Terpolymer Composition for Terpolymer Opt2 ($f_{AMPS,0}/f_{AAm,0}/f_{AAc,0} = 0.10/0.75/0.15$)

It is immediately evident that experimental data collected from both formulations are in good agreement with the model predictions. Overall, the composition values are close to the predicted values, and composition drift is minimal. As explained previously, the majority of samples were taken after 90 minutes, which means that the data set is much more comprehensive at higher conversion levels. All composition measurements taken at high conversion levels seem to be in agreement with each other and with the model.

Some specific points at low conversion (at 18% conversion, which was sampled from Opt2RB) are worth examining further. Interestingly, the (repeatable) elemental analysis measurement indicates that the AAc fraction exceeds the AMPS fraction, which conflicts with the model prediction. This could be due to small amounts of experimental error (likely propagating from the synthesis step, since the elemental analysis measurements were replicated). It is also possible that the behaviour of the terpolymerization varies at low conversion levels, and that some composition drift exists early in the polymerization process (below 20% conversion). As outlined earlier (Section 2.3.2.2), this type of behaviour can make instantaneous parameter estimation (solely from low conversion data) unreliable. In this case, though, this discrepancy at 18% conversion is not a major concern. For the application, large quantities of material are desirable, so the polymerization process will typically be taken to higher conversion levels. The main conclusion here is that overall, the model predictions (from ternary reactivity ratios estimated earlier) accurately predict the cumulative terpolymer composition.

4.2.2.3 Molecular Weight Averages

Given the results of the screening experiment study (Section 4.1.3.1 in particular), the expected range for the peak average molecular weights (\overline{M}_p) of these samples was between 1.0×10^6 g/mol and 5.0×10^6 g/mol.

Aqueous GPC analysis is notoriously difficult for multi-component polymers with polyelectrolyte behaviour (like the AMPS/AAm/AAC terpolymer). During this investigation, samples were carefully prepared as described in Section 3.3.3: crushed into a fine powder and given ample time to dissolve in the buffer solution. However, in comparing the ‘expected’ concentration of the polymer solutions (calculated during sample preparation) to the ‘measured’ concentration (obtained during GPC analysis), it was observed that more than 50% (by weight) of each polymer sample was being removed during the filtration step (prior to GPC injection). The comparison of ‘expected’ and ‘measured’ concentrations is available in Appendix C, Section C.3.

Using the GPC-measured concentrations for analysis provides more reliable and repeatable results. For example, analysis of two replicate GPC measurements for Opt2-1 (with both samples taken from the same polymer/buffer solution but filtered into unique GPC vials) demonstrates a significant improvement in repeatability. In Table 4.13, percent error calculations (coefficient of variation, CV) are compared for M_p replicates and M_w replicates, both using the ‘measured’ concentration (from GPC analysis) and the ‘expected’ concentration (from sample preparation) to determine the molecular weight averages.

Table 4.13: Comparison of Molecular Weight Averages for Opt2-1 using ‘Measured’ and ‘Expected’ Sample Concentrations

| Concentration measured during sample prep = 1.02 mg/ml | | | | | |
|--|----------------------------|------------------------------|------------------------------|------------------------------|------------------------------|
| | GPC-Measured Concentration | M_p (using Measured Conc.) | M_p (using Expected Conc.) | M_w (using Measured Conc.) | M_w (using Expected Conc.) |
| Opt2-1 | 0.21 mg/ml | 1.53E+06 | 7.47E+06 | 1.37E+06 | 6.69E+06 |
| Opt2-1 (GPC Replicate) | 0.26 mg/ml | 1.57E+06 | 6.14E+06 | 1.45E+06 | 5.65E+06 |
| % Error (CV) | | 2.13 | 13.87 | 4.05 | 11.96 |

For both samples, the ‘measured’ concentration is much lower than the ‘expected’ concentration: only 20% to 25% of the sample remained in solution for GPC analysis. If this large difference is not taken into account, it can significantly impact the molecular weight averages. First, consider the peak average molecular weight of Opt2-1. When the correct concentration of polymer solution (as measured by the GPC) is used, the measured M_p is 1.53×10^6 g/mol (and the replicate value is reasonably close at $M_p = 1.57 \times 10^6$ g/mol). However, assuming that the sample concentration is still 1.02 mg/ml (and that nothing has been filtered out) results in the recorded peak average molecular weight jumping up to 7.47×10^6 g/mol. In this case, significantly poorer agreement

between the original sample and the replicate analysis is observed (compare 2.13% error when the measured concentration is used to 13.87% error when the expected concentration is used). Given these results, it seems irrational to assume that all of the AMPS/AAm/AAC terpolymer that was dissolved into the buffer solution during sample preparation is still present during the GPC injection (that is, after filtration). Similar comparisons exist for the weight-average molecular weight measurements (also shown in Table 4.13) and for other sample replicates (not shown herein).

There are two main takeaways from this result. First, it is important that GPC-measured concentrations are used when analyzing these types of samples (specifically, multi-component polyelectrolytes, often with high acrylamide content and high molecular weights; these have the potential to significantly increase the solution viscosity and limit polymer dissolution and subsequent filtration). Second, the molecular weight averages (though more consistent) may be underestimated. Since 50% (or more) of the sample is being removed during the filtration phase, it is very possible that the larger polymer chains (higher molecular weights) are being filtered out during sample preparation, thus creating a low bias in the measured molecular weight averages. With that in mind, the molecular weight averages for both optimal formulations will be examined: both the repeatability of the measurements and the measurements themselves (compared to expected values). The main focus here will be on the full conversion samples (taken after 90 minutes of polymerization), since this characterization is valuable for additional (application-specific) experimental work. However, the effect of conversion on the molecular weight averages will also (briefly) be investigated.

For both formulations, excellent repeatability was observed. This is true for a variety of comparisons: between two independently synthesized polymers with the same formulation (for example, Opt1 samples vs. Opt1R samples), between samples independently isolated during a common synthesis (for example, Opt1-4 vs. Opt1-7; both taken after 90 minutes of polymerization), and between characterization tests (two GPC replicates of Opt1-4, completed over several months). Relevant data are shown in Table 4.14 and Table 4.15; in Table 4.14 and Table 4.15, M_p represents peak average molecular weight, M_n represents number average molecular weight, M_w represents weight average molecular weight, and IV represents intrinsic viscosity. ANOVA Tables comparing syntheses, samples and characterization (one for each formulation) are available in Appendix C, Section C.3. No statistically significant differences were observed for any of the comparisons. Therefore, the synthesis replicates and the sampling replicates do not contribute significantly to overall variability.

Table 4.14: Reproducibility/Repeatability of Molecular Weight Averages for Opt1

| | Sample | Mp | Mn | Mw | Bulk IV |
|---|----------------|-----------------|-----------------|-----------------|-------------|
| Original synthesis, sample & characterization | Opt1-4 | 1.54E+06 | 1.33E+06 | 1.36E+06 | 7.76 |
| Original synthesis & sample, characterization (GPC) replicate | Opt1-4 | 1.57E+06 | 1.43E+06 | 1.44E+06 | 8.09 |
| Original synthesis, sample replicate | Opt1-7 | 1.56E+06 | 1.27E+06 | 1.32E+06 | 7.77 |
| Replicate synthesis | Opt1R-3 | 1.56E+06 | 1.37E+06 | 1.39E+06 | 8.23 |
| Replicate synthesis & sample, characterization replicate | Opt1R-3 | 1.61E+06 | 1.36E+06 | 1.40E+06 | 8.04 |
| Replicate synthesis, sample replicate | Opt1R-8 | 1.55E+06 | 1.37E+06 | 1.39E+06 | 8.06 |
| | Average | 1.57E+06 | 1.36E+06 | 1.38E+06 | 7.99 |
| | StDev | 2.31E+04 | 5.26E+04 | 4.16E+04 | 0.19 |
| | % error | 1.47 | 3.88 | 3.00 | 2.33 |

Table 4.15: Reproducibility/Repeatability of Molecular Weight Averages for Opt2

| | Sample | Mp | Mn | Mw | Bulk IV |
|--|----------------|-----------------|-----------------|-----------------|-------------|
| Original synthesis, sample & characterization | Opt2-4 | 1.44E+06 | 1.30E+06 | 1.32E+06 | 7.69 |
| Original synthesis & sample, characterization (GPC) replicate | Opt2-4 | 1.56E+06 | 1.38E+06 | 1.40E+06 | 8.24 |
| Original synthesis, sample replicate | Opt2-10 | 1.54E+06 | 1.32E+06 | 1.35E+06 | 7.21 |
| Replicate synthesis | Opt2R-5 | 1.52E+06 | 1.36E+06 | 1.37E+06 | 7.53 |
| Replicate synthesis & sample, characterization replicate | Opt2R-9 | 1.49E+06 | 1.32E+06 | 1.34E+06 | 7.64 |
| Replicate synthesis & sample, characterization (GPC) replicate | Opt2R-9 | 1.49E+06 | 1.36E+06 | 1.37E+06 | 7.88 |
| | Average | 1.51E+06 | 1.34E+06 | 1.36E+06 | 7.70 |
| | StDev | 4.49E+04 | 2.93E+04 | 2.99E+04 | 0.35 |
| | % error | 2.98 | 2.19 | 2.20 | 4.50 |

Aside from the good repeatability established in Table 4.14 and Table 4.15, the average molecular weights of each sample can also be evaluated. Given the number of replicates available, the average for each formulation is considered. For formulation Opt1 ($f_{AMPS,0}/f_{AAm,0}/f_{AAc,0} = 0.21/0.69/0.10$), the (mean) peak average molecular weight is 1.57×10^6 g/mol. Formulation Opt2 ($f_{AMPS,0}/f_{AAm,0}/f_{AAc,0} = 0.10/0.75/0.15$) is about the same, with a mean Mp of 1.51×10^6 g/mol. The similarity allows for straightforward comparison of other (application-specific) properties; any differences in performance will be due to other factors (such as cumulative terpolymer composition or terpolymer microstructure).

The molecular weight averages reported here are notably on the low end of the anticipated characteristics, but are still within the desired range. As mentioned previously, the molecular

weight averages may be underestimated somewhat, since a considerable portion of each polymer sample was filtered out of the buffer solution prior to analysis. However, these results are well aligned with a reference polymer that is currently used in EOR applications (Alcoflood 955, purchased from BASF, USA). The reference polymer is an acrylamide/acrylic acid copolymer (which had $\bar{F}_{AAm} = 0.91$ and $\bar{F}_{AAC} = 0.09$), and the peak average molecular weight was 1.42×10^6 g/mol (characterized using the same techniques as for the optimally designed terpolymers). Therefore, it is anticipated that the application performance will be as good as (or better than) currently available materials.

For interest, the effect of conversion on molecular weight averages was also examined. Although most data collected were for high conversion samples, the samples taken at low conversion levels indicate that the peak average molecular weight (Figure 4.20a), the weight average molecular weight (Figure 4.20b), and the bulk intrinsic viscosity (IV; Figure 4.20c) are relatively constant over the conversion range analyzed (approximately 15% to 100%). This conflicts with results observed previously for the acrylamide/acrylic acid copolymer [41], but the consistency in molecular weight averages over conversion may be related to the high proportion of each sample removed during the filtration step of the analysis.

All three plots related to the molecular weight analysis (within Figure 4.20) also include the properties of the reference polymer (Alcoflood 955), which was characterized alongside the designed terpolymers. Since the conversion of the reference sample is unknown (but likely very high), the measured value for each property is presented as a horizontal (dashed) line. Both of the newly synthesized (optimal) terpolymers have similar molecular weight characteristics to the reference material, which suggests that the customized (designed) approach led to the development of materials with appropriate and desirable molecular weight characteristics. Also, the molecular weight averages (M_p and M_w) of the new materials are slightly higher than those of the reference material, which could improve the enhanced oil recovery performance.

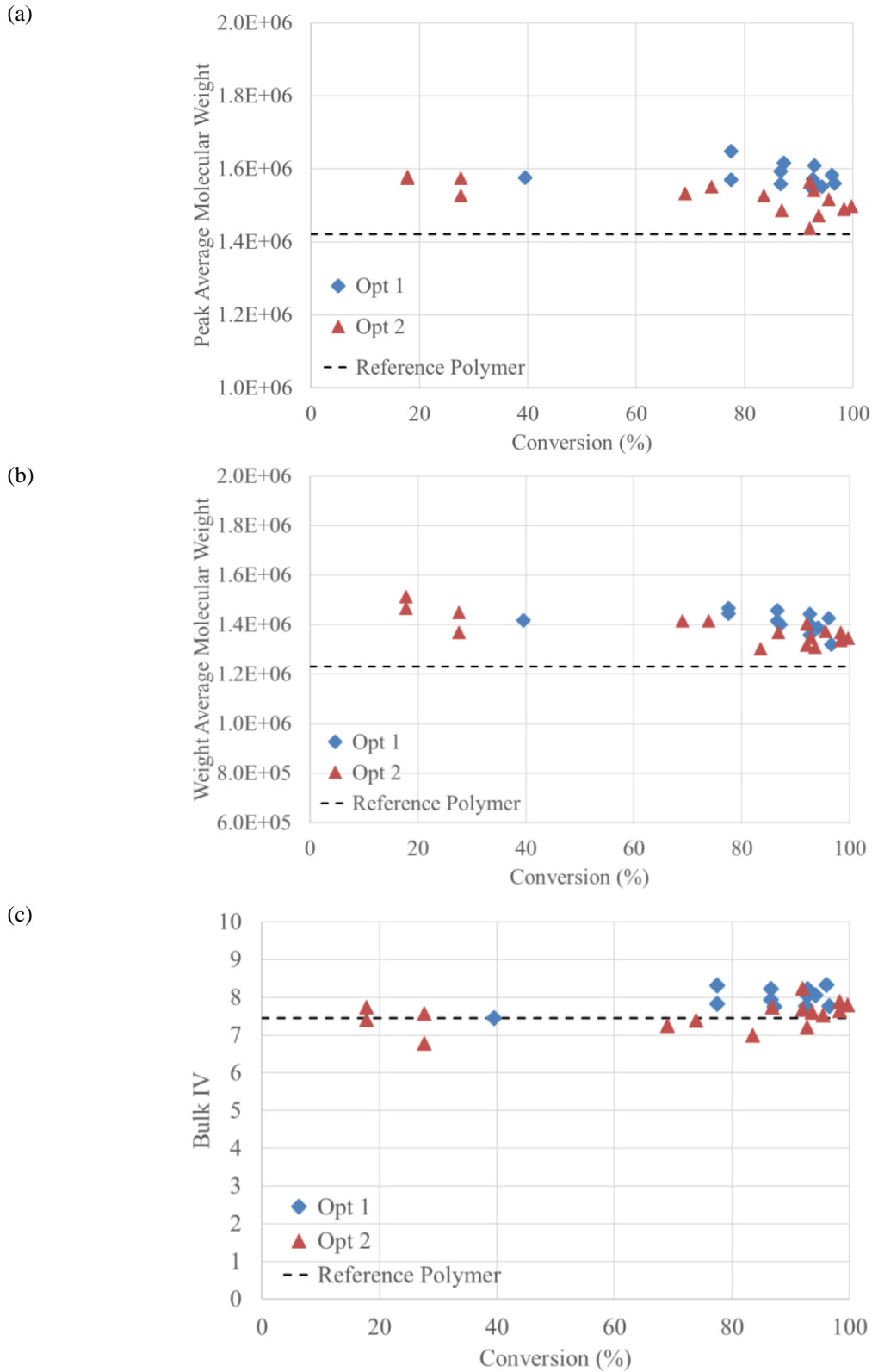


Figure 4.20: Effect of Conversion on (a) Peak Average Molecular Weight, (b) Weight Average Molecular Weight and (c) Bulk Intrinsic Viscosity (and Comparison to Reference Polymer Alcoflood 955) for Optimal Terpolymers

4.2.2.4 Sequence Length Distribution

^{13}C -NMR spectra were measured and analyzed for Opt1 and Opt2 terpolymers, as described in Section 3.3.4. The purpose of these tests was to compare the measured sequence length distributions to those predicted by ternary reactivity ratios in Section 4.1.2.3 (using analysis techniques similar to Randall [119] and Brar and Sunita [120]). However, given the 18 unique monomer triads, the chemical similarity of the comonomers, and the noisy spectra (due to the high viscosity of the samples), sequence length distribution could not be directly determined. What we were able to do was to confirm terpolymer composition from yet another independent source (described shortly below). For reference, ^{13}C -NMR spectra of terpolymer #1 and terpolymer #2 are presented in Figure 4.21 and Figure 4.22, respectively.

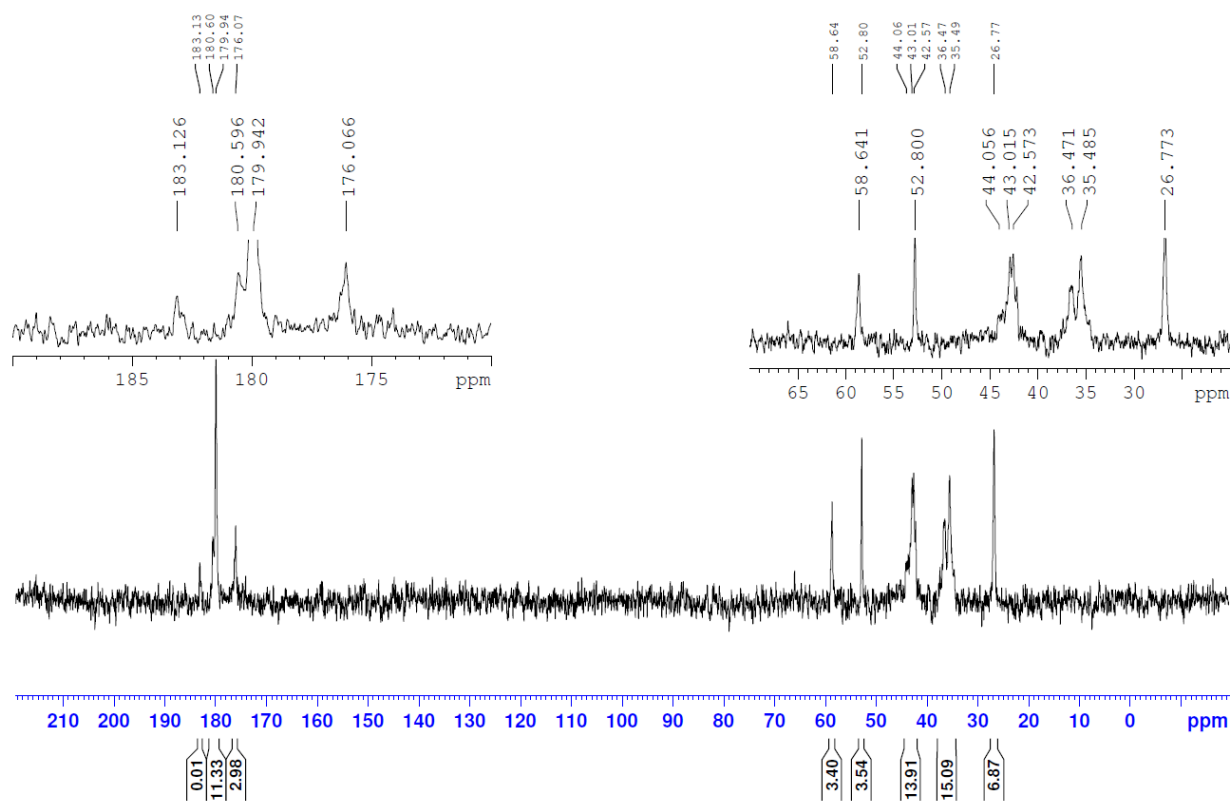


Figure 4.21: ^{13}C -NMR Spectra of Terpolymer #1 in Buffer/ D_2O at 68°C

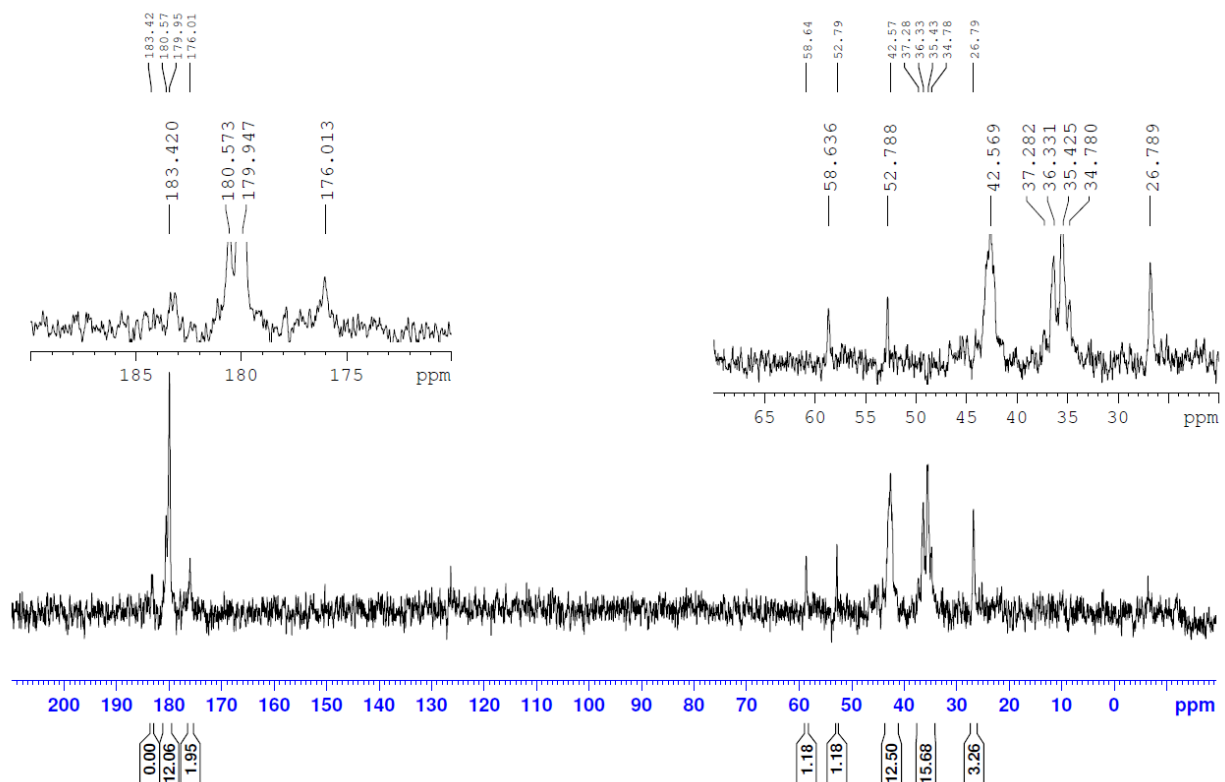


Figure 4.22: ^{13}C -NMR Spectra of Terpolymer #2 in Buffer/ D_2O at 68°C

Although the spectra are not sufficient for the determination of sequence length distribution, they can still be used to calculate the cumulative terpolymer composition. Using the carbonyl carbon responses associated with AMPS ($\delta \approx 176$ ppm), AAm ($\delta \approx 180$) and AAc ($\delta \approx 183$ ppm), it is possible to calculate the mole fraction of each comonomer in the terpolymer sample. These are compared to the (averaged) elemental analysis (EA) results from Section 4.2.2.2 in Table 4.16.

Table 4.16: Comparison of Cumulative Terpolymer Composition from ^{13}C -NMR and EA

| | Cumulative Composition from ^{13}C -NMR | | | Cumulative Composition from Elemental Analysis | | |
|---------------|--|-----------------|-----------------|--|-----------------|-----------------|
| | \bar{F}_{AMPS} | \bar{F}_{AAm} | \bar{F}_{AAc} | \bar{F}_{AMPS} | \bar{F}_{AAm} | \bar{F}_{AAc} |
| Terpolymer #1 | 0.19 | 0.74 | 0.07 | 0.21 | 0.68 | 0.11 |
| Terpolymer #2 | 0.13 | 0.80 | 0.07 | 0.11 | 0.75 | 0.13 |

Composition measurements are in relatively good agreement between ^{13}C -NMR and elemental analysis, especially considering the challenges associated with analyzing viscous polymer samples using nuclear magnetic resonance. NMR results provide adequate confirmation of the elemental analysis results, but the EA results are more trustworthy.

4.2.2.5 Thermal Stability

Thermal gravimetric analysis (TGA) was performed (as described in Section 3.3.5) for Opt1 and Opt2, and included synthesis replicate analysis and characterization replicate analysis. The reference material (Alcoflood 955) and an AAm/AAc copolymer (from Riahinezhad et al. [32]) were also evaluated for comparison. The motivation here was two-fold. First, it was important to ensure that the thermal properties were consistent across synthesis replicates (and to ensure that TGA measurements were consistent for sample replicates). Second, thermal analysis provides an opportunity to confirm that thermal stability is improved (compared to the typically used AAm/AAc copolymer) when AMPS is incorporated into the polymer backbone. As shown previously (Figure 2.4), the majority of oil reservoirs are below 200°C, but behaviour at higher temperatures was evaluated herein as a ‘worst case’ scenario. TGA up to higher temperatures (at least 400°C) made it possible to compare the point at which significant mass loss occurred for each sample; materials that showed degradation at higher temperatures are more thermally stable (and may, therefore, be promising candidates for enhanced oil recovery). Results from synthesis replicates (Opt1 vs. Opt1R and Opt2 vs. Opt2R), the reference material (Alcoflood 955) and the AAm/AAc copolymer are shown in Figure 4.23. Characterization replicates for Opt1 and curve derivatives for all samples are available in Appendix C, Section C.4.

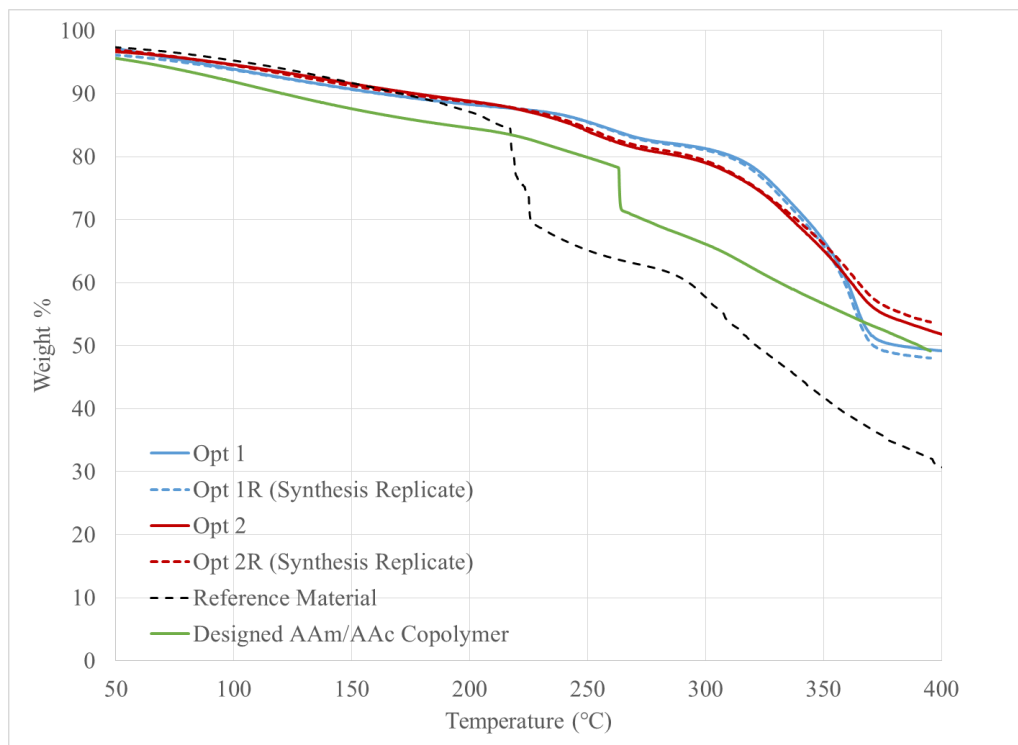


Figure 4.23: Thermal Behaviour (from Thermal Gravimetric Analysis) for Optimally Designed Terpolymers, Reference Material, and a Designed AAm/AAc Copolymer

Examining all six curves on a single plot allows for the direct comparison of all materials. Immediately, excellent agreement is observed between the original terpolymer runs and the synthesis replicates. Both blue curves (for Opt1 and Opt1R) are directly on top of each other, and exhibit two main points of interest. Aside from the gradual decrease in weight initially (which is likely water loss), there are two more obvious transition points. The first transition occurs at 225°C and the second (more significant) transition occurs at 284°C. Thus, any substantial mass loss (degradation) is beyond 200°C. Similarly, excellent repeatability was observed from the independent replication of Opt2. Both red curves exhibit similar behaviour, and the transition points (easily identifiable from the derivatives; see Section C.4 in Appendix C) are identical.

Another important conclusion from Figure 4.23 is the improved thermal behaviour of the terpolymers compared to the reference material and to the AAm/AAc copolymer. Both of these materials show a sudden decrease in sample mass: the reference material at 217°C and the AAm/AAc copolymer at 257°C. The mass reduction for these materials is much more sudden than for the terpolymers; this could have adverse effects in the EOR application.

Table 4.17 provides some key findings from the TGA experimental work. A minor transition (with small mass loss) was only observed for the terpolymer samples, and may be related to water entrapment in the polymer samples. The major transition is the point at which significant mass loss occurs, and is likely related to sample degradation. It is reassuring to note that the major transition occurs at the lowest temperature for the reference material; the (designed) AAm/AAc copolymer can tolerate an additional 40°C before the major transition occurs. Even more improvement is observed when AMPS is added to the material formulation, as both Opt1 and Opt2 exhibit (relatively low) weight loss at 284°C and 281°C, respectively.

It is also enlightening to examine the remaining weight proportion at several (meaningful) temperatures. In Table 4.17, the remaining weight % of each material is listed at 80°C (median reservoir temperature as per Figure 2.4), 120°C (maximum ‘encountered’ reservoir temperature for ~90% of reservoirs worldwide, again as per Figure 2.4), 200°C (maximum reservoir temperature) and 300°C (for interest and to represent a ‘worst case scenario’). For replicated samples, average values are shown.

Table 4.17: Points of Interest from Thermal Gravimetric Analysis Results

| Material | Minor Transition | Major Transition | Weight % at 80°C | Weight % at 120°C | Weight % at 200°C | Weight % at 300°C |
|--------------------------|-------------------------|-------------------------|-------------------------|--------------------------|--------------------------|--------------------------|
| Opt1 | 225°C | 284°C | 95.4% | 92.8% | 88.2% | 80.8% |
| Opt2 | 199°C | 281°C | 95.6% | 93.3% | 88.7% | 79.1% |
| Reference | N/A | 217°C | 96.2% | 94.0% | 87.1% | 57.7% |
| AAm/AAc Copolymer | N/A | 257°C | 93.5% | 90.0% | 84.5% | 66.1% |

All materials exhibit similar thermal behaviour up to 200°C, but the difference in material properties becomes evident at 300°C. In reality, thermal stability up to 300°C is much higher than what the EOR application currently demands, but the contrast in materials shows the improved thermal stability when a terpolymer of AMPS/AAm/AAC is used. Thus, this study has confirmed that the addition of AMPS does, in fact, improve the thermal stability of the polymeric material, as hypothesized in Section 2.1.3.

4.2.3 Investigation of Application-Specific Properties

In evaluating application-specific properties, larger sample volumes are often required (that is, several samples (from one or more synthesis replicate) may be combined for testing purposes). Given that good consistency of polymer properties has been established in the previous section, it is now possible to combine polymer samples (that were synthesized with the same formulation and under the same conditions) and have confidence that the final sample has homogeneous properties. Therefore, in some of the following sections, no distinction is made between synthesis replicates. For example, Opt1 and Opt1R are simply identified as optimal terpolymer #1.

4.2.3.1 Rheological Properties

The rheological properties are critical to the enhanced oil recovery performance. If the materials are not viscous enough, they will not provide the sweep efficiency required (that is, much of the residual oil will remain in the reservoir, even after polymer flooding). In contrast, if they are too viscous, they may cause pressure build-up and plugging in the reservoir. There is potential to adjust the viscosity of a solution by changing the concentration of the polymeric material within the solution [115], but using smaller quantities of the polymer is preferred (for environmental and economic reasons). Therefore, the goal is to create materials with similar properties to the reference material (here Alcoflood 955, described previously). Rheological properties of each optimal terpolymer and the reference polymer (in water and in a saline (pH 7 buffer) solution) were measured as described in Section 3.4.1, and key findings are presented herein.

Frequency sweep tests, performed using a cone and plate rheometer, give information about the viscoelastic properties of the polymer solution. Among the relevant variables are $|n^*|$ (complex viscosity), G' (elastic modulus) and G'' (loss modulus); these measurements and their interpretation are discussed further in what follows. However, prior to completing each frequency sweep test, the linear viscoelastic region (LVR) must be established via a strain sweep test. Strain sweep tests were conducted at a fixed frequency of 10 Hz, ranging from 0.1% to 20%; a representative result for an Opt1 terpolymer sample in water is shown in Figure 4.24. This is representative of most solutions in the present study, and 1% strain was chosen for subsequent frequency sweep testing. As an additional check, for select samples, frequency sweep tests were performed at both 1% strain and 10% strain (both within the linear viscoelastic region), and results

showed excellent agreement (see Figure C.10 in Appendix C, Section C.5). Therefore, as long as the strain level selected is within the linear viscoelastic region, the % strain selected for analysis should not affect results.

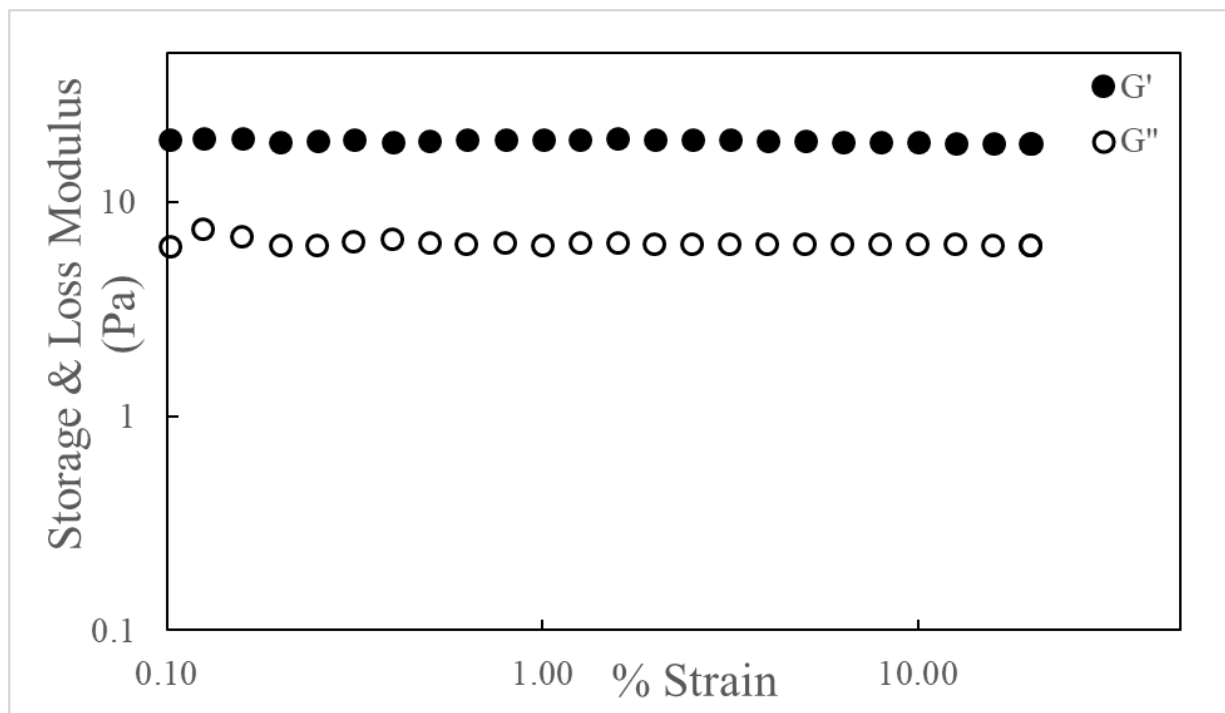


Figure 4.24: Sample Results (from Terpolymer #1) for Strain Sweep Test at 10 Hz (solution concentration of 0.01 g/mL in water)

Representative plots (including replicates) from frequency sweep tests are shown in Figure 4.25. The shear thinning behaviour of the AMPS/AAm/AAC terpolymer solutions is immediately obvious: samples show a decrease in viscosity as angular frequency increases. This makes physicochemical sense, since at higher frequencies (or by analogy, at higher shear rates), the polymers transition from flowing in a coil conformation to flowing in a linear (aligned) arrangement. This decreases the viscosity of the solution, which in turn would decrease the efficiency of the EOR process.

It is also interesting to examine the repeatability of the experimental results (both in terms of synthesis and characterization). For terpolymer #1, the synthesis replicates seem to exhibit more inconsistencies than the characterization replicates (especially for terpolymer #1 in water; Figure 4.25a), but this is often expected. For terpolymer #2, excellent agreement is observed between synthesis replicates.

For the rheological tests done in water, the complex viscosities of both optimal terpolymers were higher than the reference sample at low angular frequencies, and over most of the angular

frequency range studied. However, this distinction became less pronounced at higher angular frequencies (especially for terpolymer #1R (Figure 4.25a) and for terpolymer #2 (Figure 4.25b)).

The change in behaviour between aqueous polymer solutions and polymers in buffer solutions was also examined. For the reference polymer and for the newly synthesized (optimal) terpolymers, the complex viscosity is lower in buffer solutions than in water. Physicochemically, these results are as expected. The terpolymer of AMPS/AAm/AAC is a polyelectrolyte and is therefore very sensitive to ions in solution. When charged molecules (salts, in this case) are added to the environment, charge screening occurs. As a result, previously elongated polymer chains (stretched due to charge repulsion along the macromolecule) reposition themselves into a coil conformation. Of course, this change in polymer conformation impacts the solution viscosity; a smaller radius of gyration will lower the shear viscosity of a given polymer solution.

Interestingly, the designed terpolymers exhibited a larger reduction in complex viscosity (compared to the reference material) when the buffer solution was used rather than water. This is likely due to the addition of AMPS; incorporating a second acidic comonomer into the polymeric material amplifies the charge effects. However, it is anticipated that the presence of AMPS will have additional benefits, including mechanical and chemical stability [21, 23] and as per earlier discussion (recall Section 4.2.2.5). Also, the rheological behaviour of terpolymer #1 and terpolymer #2 is still comparable to the reference material, which makes them good candidates for the enhanced oil recovery application.

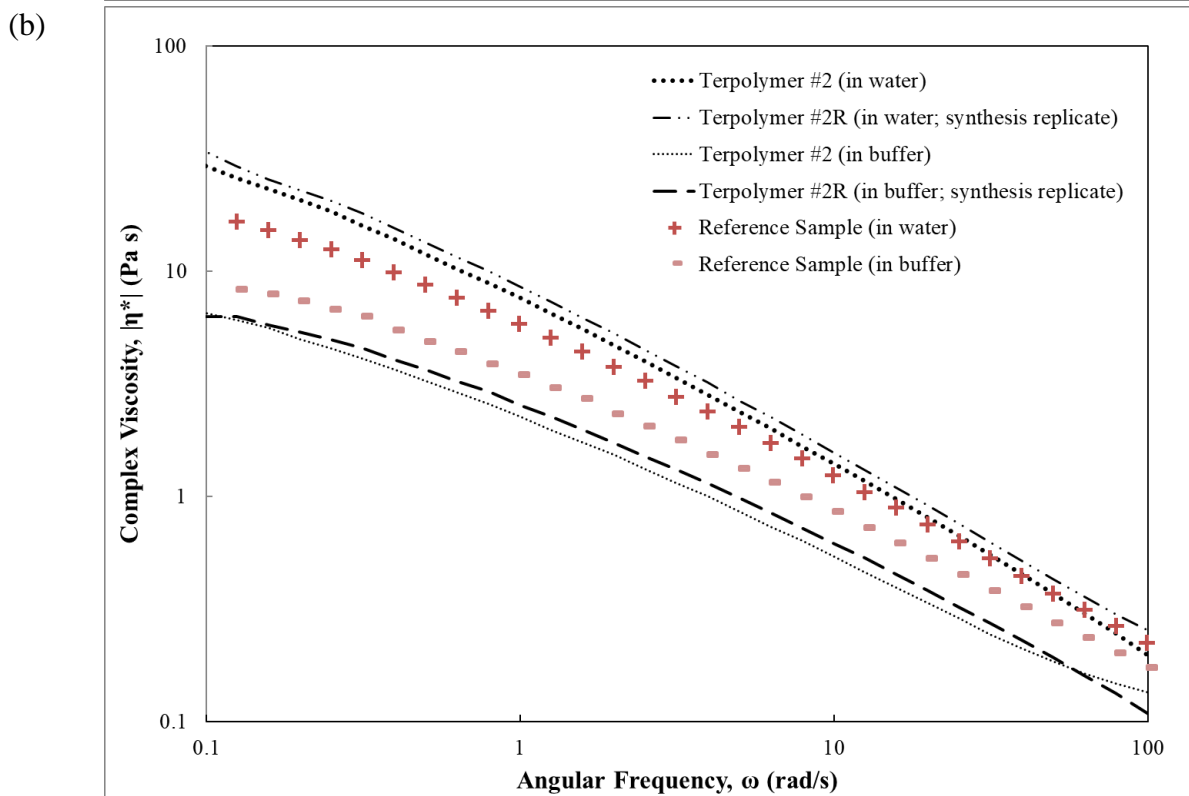
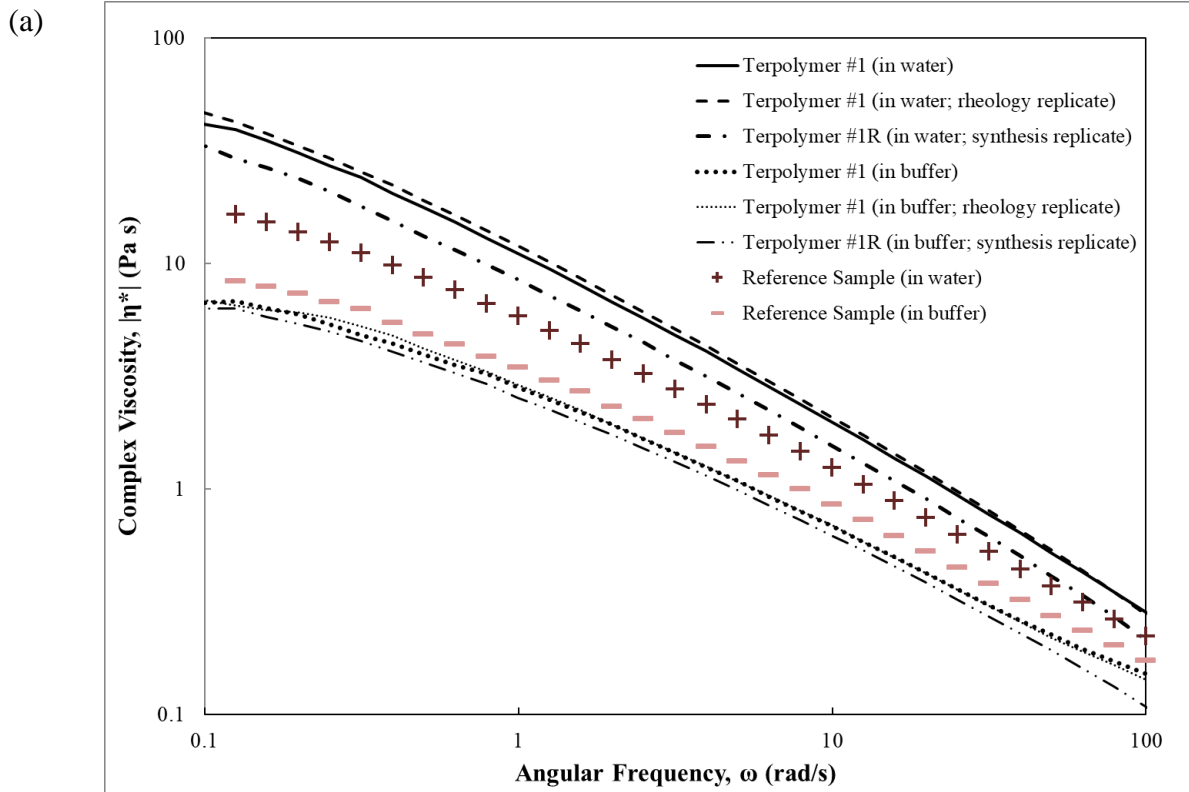


Figure 4.25: Complex Viscosity Profiles for AMPS/AAm/AAC Terpolymers in Water and Buffer for (a) Terpolymer #1 and (b) Terpolymer #2

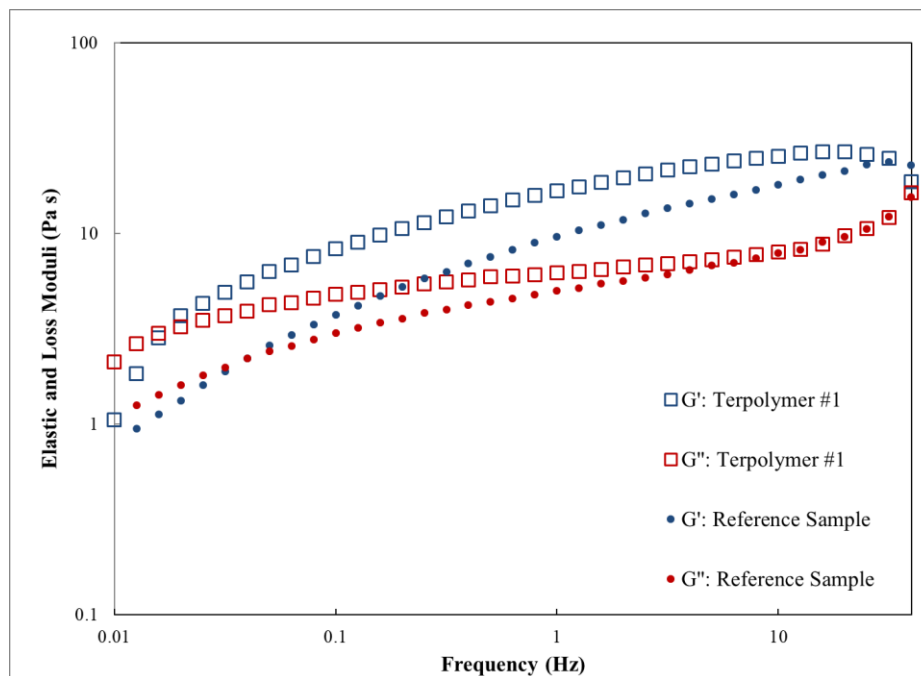
It has been reported that the polymer flood water solutions used in EOR are exposed to a range of shear rates from about 1 s^{-1} to 7 s^{-1} [32]. The Cox-Merz rule makes it possible to assume that the relationship between $|\eta^*|$ and ω is analogous to the relationship between steady state shear viscosity (η) and shear rate ($\dot{\gamma}$). Therefore, shear viscosities for $\dot{\gamma} = 1 \text{ s}^{-1}$, $\dot{\gamma} = 5 \text{ s}^{-1}$ and 7 s^{-1} (specific shear rates of interest for the EOR application) are provided in Table 4.18. Average values for each terpolymer (taken from synthesis and/or characterization replicates, as available) are presented herein, but the full data set is available in Appendix C, Section C.5. This direct comparison shows that the viscosity behaviour of the new terpolymers is generally comparable to the reference copolymer, and hence the designed AMPS/AAm/AAC terpolymers remain viable.

Table 4.18: Summary of Shear Viscosities for Terpolymer Solutions

| In WATER | Shear Viscosity (Pa·s) | | |
|---|-----------------------------------|-----------------------------------|-----------------------------------|
| | $\dot{\gamma} = 1 \text{ s}^{-1}$ | $\dot{\gamma} = 5 \text{ s}^{-1}$ | $\dot{\gamma} = 7 \text{ s}^{-1}$ |
| Terpolymer #1 Average | 10.10 | 3.22 | 2.49 |
| Terpolymer #2 Average | 8.12 | 2.52 | 1.98 |
| Alcoflood (Reference Material) | 5.84 | 2.04 | 1.61 |
| In BUFFER | Shear Viscosity (Pa·s) | | |
| | $\dot{\gamma} = 1 \text{ s}^{-1}$ | $\dot{\gamma} = 5 \text{ s}^{-1}$ | $\dot{\gamma} = 7 \text{ s}^{-1}$ |
| Terpolymer #1 Average | 2.79 | 1.10 | 0.89 |
| Terpolymer #2 Average | 2.41 | 0.93 | 0.74 |
| Alcoflood (Reference Material) | 3.47 | 1.33 | 1.08 |
| AAM/AAC copolymer with best EOR performance (as reported in [115, 117]) | 3.41 | -- | 0.89 |

Viscoelastic properties were also measured during frequency sweep tests. G' , the elastic modulus, provides information about the reversibly stored energy in the system. G'' , the viscous modulus, represents the irreversible energy loss. In general, polymer solutions for enhanced oil recovery with higher G' and G'' values (compared to a standard reference material) offer superior viscoelasticity. This is relevant for EOR, since the viscoelastic behaviour improves the sweep efficiency of the EOR process. The crossover point (that is, the frequency at which the behaviour shifts from predominantly viscous to predominantly elastic) was generally observed at very low frequencies and was occasionally not observed (especially for aqueous solution trials). This value, though commonly used as a measure of viscoelasticity, was not repeatable at these very low frequencies (especially since it was very early in the experimental run), and is therefore only used in a relative way as an indicator of potential EOR performance. Measurements of G' and G'' for both the water and buffer solutions are shown in Figure 4.26 and Figure 4.27.

(a)



(b)

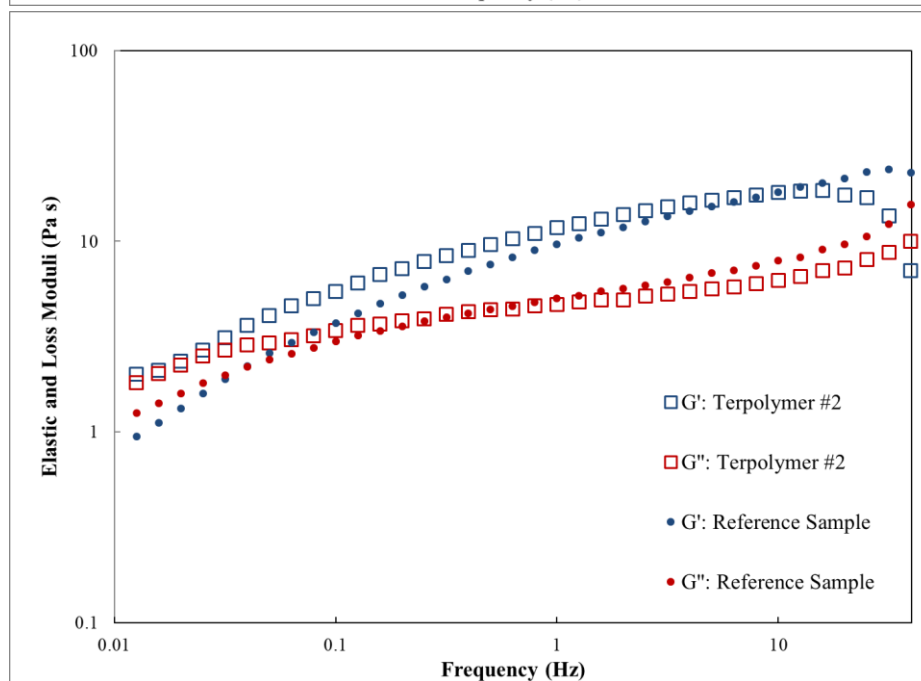
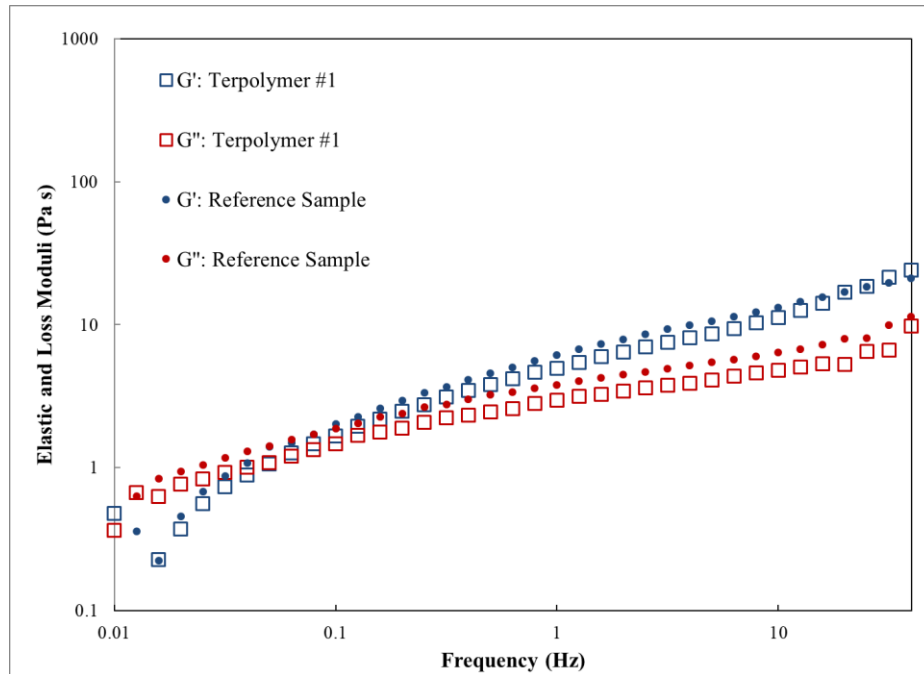


Figure 4.26: Elastic and Loss Modulus for AMPS/AAm/AAC Terpolymers in Water for (a) Terpolymer #1 and (b) Terpolymer #2

(a)



(b)

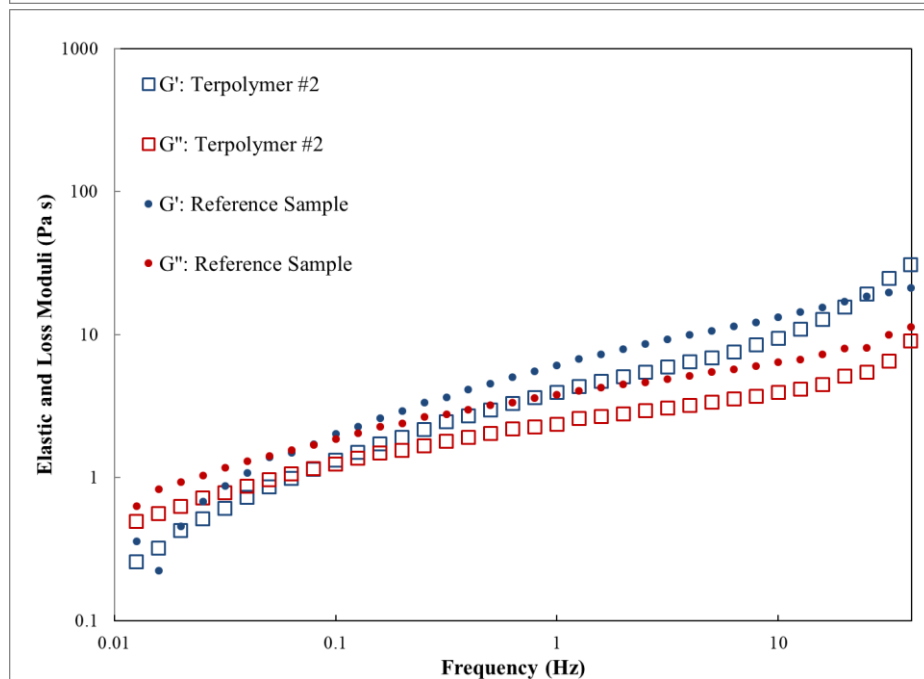


Figure 4.27: Elastic and Loss Modulus for AMPS/AAm/AAC Terpolymers in Buffer for (a) Terpolymer #1 and (b) Terpolymer #2

As demonstrated in Figure 4.26, G' is generally larger than G'' (except at very low frequencies). This indicates that the loss modulus dominates at very low frequencies, but that under normal operating conditions (that is, frequencies characteristic of the EOR application), the solutions are predominantly elastic in nature. A clear crossover point was observed for the reference sample, but the crossover behaviour occurred at very low frequencies (or not at all) for the optimal terpolymers. This predominantly elastic behaviour is desirable for enhanced oil recovery; studies

have shown that polymer solutions with higher elasticity also provide higher oil recovery efficiency [121]. In comparing the newly synthesized (optimal) terpolymers to the reference sample, terpolymer #1 (Figure 4.26a) seems to be somewhat more elastic than the reference material (the moduli are higher, and the crossover point occurs at a lower frequency). However, terpolymer #2 (Figure 4.26b) has characteristics that are very similar to the reference material.

Figure 4.27 shows the viscoelastic behaviour of the same polymeric materials in buffer solution. The properties of the newly synthesized terpolymers are comparable to the reference polymer, but the modulus values are slightly higher for the reference polymer than they are for the optimal terpolymers. For all three materials (terpolymer #1, terpolymer #2 and the reference material) in buffer, the elastic behaviour still dominates, but to a lesser extent than in aqueous polymer solutions. The crossover frequency in buffer is consistently higher than the crossover frequency in water, which suggests that the polymer solution behaviour is more viscous (less elastic) for a wider range of low frequencies.

Information about the storage and loss moduli can be combined by looking at the dynamic mechanical loss tangent ($\tan\delta$), which is the ratio of G'' to G' . When $\tan\delta$ (G''/G') is below unity, elastic behaviour dominates. Low values of $\tan\delta$ (that is, high elasticity) can encourage ‘pulling’ behaviour in an oil reservoir, which assists with the removal of residual oil and increases the displacement efficiency in EOR [22].

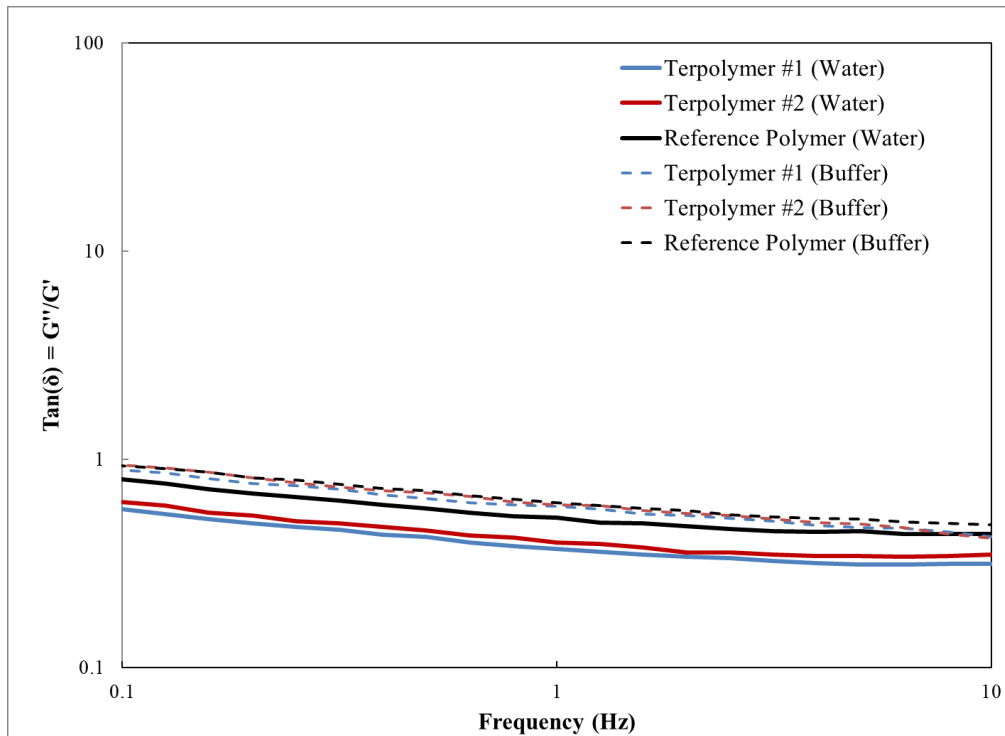


Figure 4.28: Dynamic Mechanical Loss Tangent ($\tan\delta$) for Designed Terpolymers and Reference Polymer

As shown in Figure 4.28, terpolymer #1 and terpolymer #2 have similar $\tan\delta$ profiles. In aqueous solutions, both of the optimally designed terpolymers have a lower $\tan\delta$ (therefore higher elasticity and potentially improved EOR performance) compared to the reference polymer. For the reference polymer, $\tan\delta$ values are closer to the buffer behaviour of the other materials. This indicates that the reference polymer is less affected by salts in solution, which agrees with the complex viscosity results observed previously (Figure 4.25). In any case, all $\tan\delta$ values (over the frequency range presented herein) are below unity, which adds to the increasing list of desirable properties that these terpolymers possess for the enhanced oil recovery application.

4.2.3.2 EOR Phase I: Polymer Flow Performance in Sand-pack Flooding Tests

As described in Section 3.4.2.1, displacement tests (in a sand-pack flooding system) have been performed for three polymers (terpolymer #1, terpolymer #2 and a reference material); this has been pursued in collaboration with Professor Laura Romero-Zerón in the Department of Chemical Engineering at the University of New Brunswick. The purpose of these tests, which have a duration of about two months per material tested, is to compare the flow behaviour of the newly synthesized (optimal) terpolymers to commercially available materials. The process involves flooding a pre-characterized sand-pack system with brine, then with a 1wt% polymer solution, and then with additional brine. Since the system was repacked with sand between each trial (to eliminate any confounding variables that could be introduced during a cleaning step), characteristics of the sand-pack were measured for each run and are reported in Table 4.19.

Table 4.19: Sand-pack Properties for Sand-pack Flooding Tests

| Sample | PV (cm ³) | Porosity | k (mD) |
|------------------------------|-----------------------|----------|--------|
| Terpolymer #1, Trial #1 | 26.97 | 0.2010 | 78,118 |
| Terpolymer #1, Trial #2 | 25.47 | 0.1898 | 85,186 |
| Terpolymer #1, Trial #3 | 23.47 | 0.1749 | 99,383 |
| Terpolymer #2, Trial #1 | 25.47 | 0.1898 | 75,481 |
| Terpolymer #2, Trial #2 | 16.47 | 0.1227 | 98,291 |
| Terpolymer #2, Trial #3 | 25.47 | 0.1898 | 99,383 |
| Reference Material, Trial #1 | 25.97 | 0.1935 | 98,291 |
| Reference Material, Trial #2 | 25.47 | 0.1898 | 85,180 |

In considering the flow behaviour of polymer solutions in an oil reservoir, the two factors of interest are the resistance factor (RF) and the residual resistance factor (RRF). These have been described in Section 3.4.2.1 (see Equations 3.3 and 3.5). Ideally, polymer solutions should have a high RF (indicative of good mobility control and high sweep efficiency) and a low RRF (indicative of polymer entrapment and reservoir plugging).

Since the sand-pack characteristics (permeability and porosity) varied between runs (as evidenced in Table 4.19), differences between runs were normalized by using a modified capillary bundle

parameter (units of volume of fluid injected expressed as a fraction of PV; units of $\text{mD}^{-0.5}$) which is defined by Equation 4.1 [117, 122].

$$\text{Capillary Bundle Parameter} = \frac{1}{4} \frac{F t (1 - \phi) A}{(\phi k)^{0.5} PV} \quad 4.1$$

Where F is flux (cm/min), t is injection time (min), ϕ is porosity (dimensionless), k is permeability (millidarcy, mD), A is the cross-sectional area of the sand-pack (cm^2), and PV is sand-pack pore volume (cm^3).

Figure 4.29 provides a comparison of RF values for all three polymeric materials as a function of volume of polymer injected (expressed as a fraction of pore volume normalized for permeability (i.e., capillary bundle parameter)). Since the polymer flow performance test was performed at least twice for each material, average values are shown herein. For both optimal terpolymers, the RF value increases gradually (as a function of volume of polymer injected) but eventually plateaus. When the RF value stabilizes, it indicates that the polymeric material has propagated throughout the sand-pack, which is a sign of good flow performance. Also, since the tailor-made materials have a higher RF than the reference material, the terpolymers provide better mobility control than the commercially available polymer. This is a promising result, since polymer solutions with higher RF values are typically more effective in recovering oil.

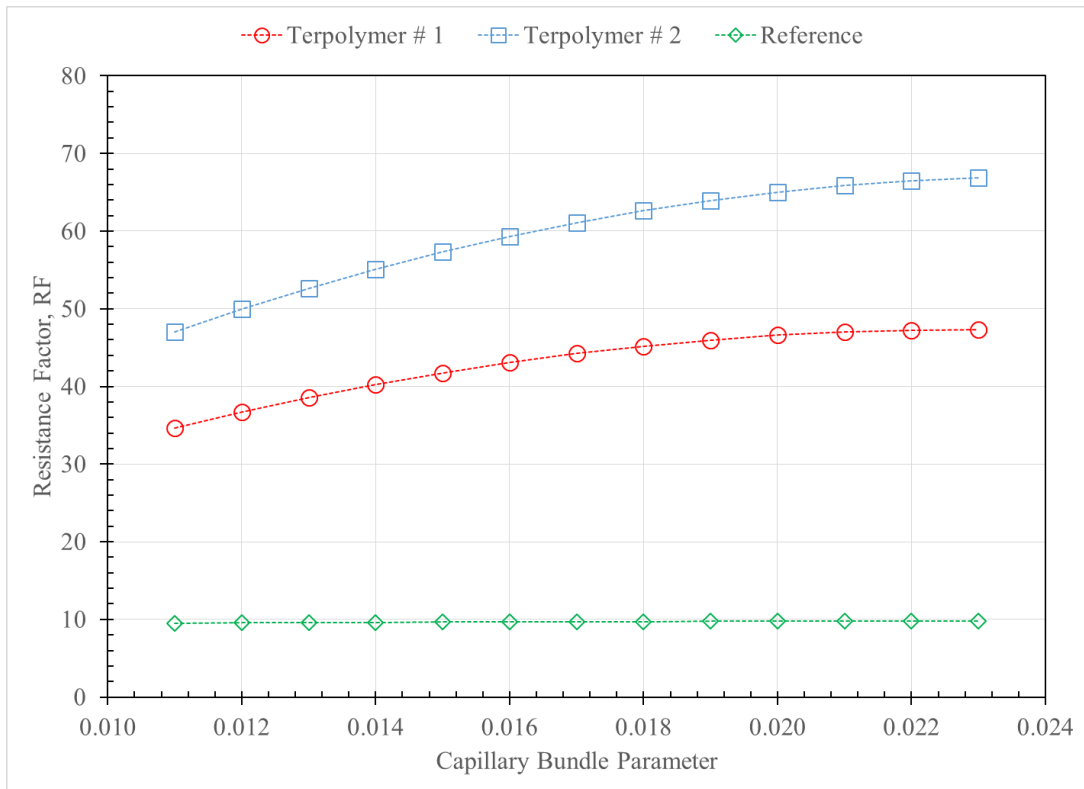


Figure 4.29: Resistance Factor (RF) from Polymer Flow Performance Testing

In Figure 4.30, polymer retention in the reservoir (sand-pack) is evaluated by plotting the residual resistance factor for each material as a function of volume of fluid injected (again normalized for permeability and porosity using the capillary bundle parameter). As before, since at least two runs were performed for each material, average values are presented. All three materials exhibit the same general behaviour, as RRF values decrease with increased brine injection. This is as expected when the definition of RRF is considered (recall Equation 3.5). $\Delta P_{\text{brine injection \#2}}$ is in the numerator for RRF, and is a measure of the pressure difference along the sand-pack column after polymer flooding. Initially (immediately after polymer flooding), there will likely be significant pressure differences, as polymeric material remains entrained in the column. However, as more brine is injected into the system (and, subsequently, more of the polymeric material is recovered), the pressure difference along the sand-pack column will decrease. Therefore, as $\Delta P_{\text{brine injection \#2}}$ decreases, RRF also decreases. The fact that this decrease is observed confirms that entrapped polymeric material is, in fact, being recovered from the system (which is a promising result).

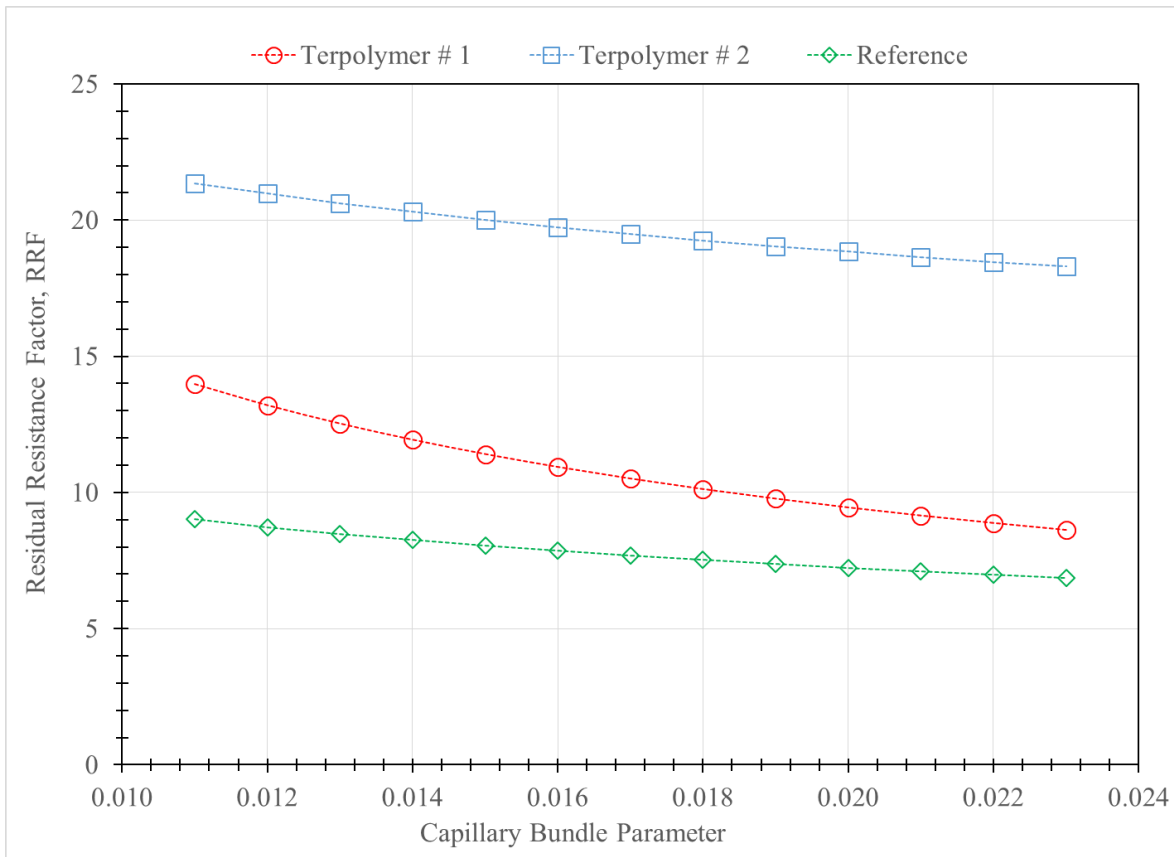


Figure 4.30: Residual Resistance Factor (RRF) from Polymer Flow Performance Testing

Of the three polymeric materials evaluated, terpolymer #2 had the highest RRF values (therefore, it exhibited the most polymer retention). Terpolymer #1 had moderate RRF values, which (initially) decreased more quickly as the capillary bundle parameter increased (compared to terpolymer #2 or the reference material). The initial drop in RRF indicates that the polymer is more

easily recovered as brine is injected after polymer flooding. Since the molecular weight averages of terpolymer #1 and terpolymer #2 are similar, electrostatic effects due to composition differences are the most likely explanation for these different RRF profiles. Terpolymer #1 has a higher proportion of acidic (anionic) monomers along the polymer backbone ($\bar{F}_{AMPs} + \bar{F}_{AAc} = 0.32$ for terpolymer #1 and $\bar{F}_{AMPs} + \bar{F}_{AAc} = 0.25$ for terpolymer #2), and a higher negative charge density would increase the repulsion between the polymer and the negatively charged sand particles. This, in turn, would decrease polymer adsorption on the sand surface (therefore, a steeper initial drop in RRF occurs, which indicates that the polymer is easily recovered as brine is injected after polymer flooding). Finally, the reference material (described in Table 3.5) had the lowest RRF. The lower initial value suggests that polymer entrapment was minimal to begin with, so the RRF plateaued fairly quickly. Although this reference material exhibited the best performance in terms of the RRF, it had the worst mobility control behaviour (from RF measurements in Figure 4.29). Finding a material with optimal EOR properties is a balancing act, since both RF and RRF need to be taken into account.

A summary of reservoir flow properties for the three polymeric materials studied is presented in Table 4.20. Here, RF and RRF values are taken from the end of the corresponding experimental runs and the equivalent percentage of permeability reduction (relative to the original permeability of the corresponding sand-packs) is provided.

Table 4.20: Summary of Reservoir Flow Properties for Terpolymer Solutions

| Polymeric Material | Resistance Factor (RF) | Residual Resistance Factor (RRF) | Permeability Reduction (%) |
|---------------------------|-------------------------------|---|-----------------------------------|
| Terpolymer #1 | 47.3 | 8.6 | 88.3% |
| Terpolymer #2 | 66.9 | 18.3 | 94.5% |
| Reference Material | 9.8 | 6.9 | 85.5% |

Given the RF and RRF values shown in Table 4.20, terpolymer #2 seems like the most promising candidate of the materials being evaluated herein. The fact that the RF values were high suggests that a polymer solution containing terpolymer #2 will exhibit good mobility control and, by extension, superior oil recovery efficiency. It is also important to note that the RF values in Figure 4.29 were ‘leveling out’ (towards a plateau), which suggests that proper propagation of polymeric material through the sand-pack system was achieved (and reservoir plugging did not occur). Also, the RRF for terpolymer #2 plateaued around RRF = 18.3, which indicates that the sand-pack experienced a permeability reduction of 94.5% compared to the original permeability. A recent study by Riahi-zhad et al. [117] reported successful oil recovery behaviour for a material with 88% permeability reduction, so the properties of terpolymer #2 are reasonable. Also, there would be potential to inject post-polymer flooding brine for a longer period of time, which would remove additional residual polymer from the porous media. Therefore, reservoir plugging is not expected to be a concern for this polymer solution.

Terpolymer #1 is also an excellent candidate for further EOR testing, since it has a very good RF value and slightly better permeability reduction. Because it contains a higher proportion of AMPS (recall Section 4.2.2.2), it has improved properties in terms of thermal and mechanical stability. Also, as observed earlier, a higher proportion of anionic monomers along the backbone reduced the polymer retention within the reservoir. Therefore, both optimally designed terpolymers will be evaluated further (along with the reference material) in the following section.

4.2.3.3 EOR Phase II: Heavy Oil Displacement in Sand-pack Flooding Tests

Heavy oil displacement tests were performed for the two optimally designed terpolymers and the reference material, as per the experimental procedure described in Section 3.4.2.2. As described previously, heavy oil displacement tests use four consecutive injection stages: oil injection, water flooding (brine injection #1), polymer flooding (polymer solution injection), and chase water flooding (brine injection #2). Table 4.21 summarizes the sand-pack characteristics and initial test conditions for each experimental run; terpolymer #1 was characterized in triplicate, and the other materials were evaluated twice. Also, the initial oil saturation (S_{oi}) and the irreducible water saturation (S_{wi}) were determined after the oil injection stage and are provided in the table. These allow for an initial understanding of the sand-pack saturation composition (that is, the fraction of pore space occupied by oil and by water). Also, knowing the initial oil saturation makes it possible to monitor the oil saturation in the sand-pack as more oil is incrementally recovered.

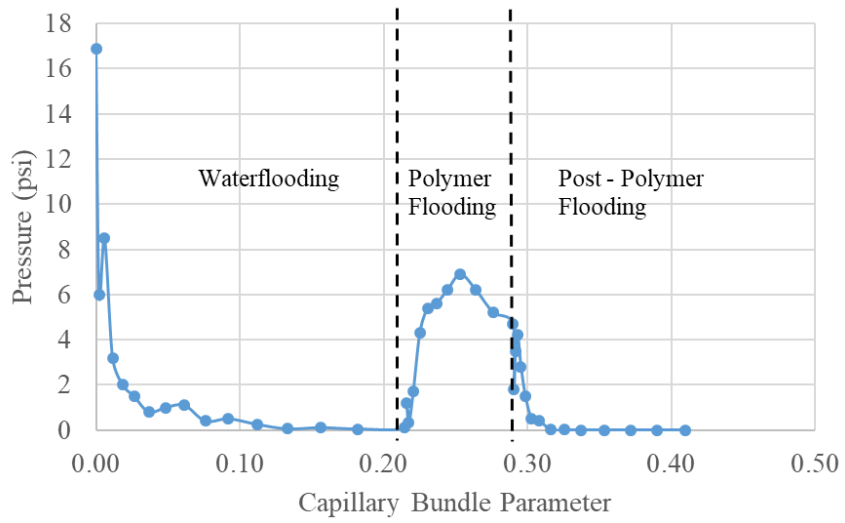
Table 4.21: Sand-pack Properties and Initial Conditions for Heavy Oil Displacement Tests

| Sample | PV (cm ³) | Porosity | k (mD) | F (cm/min) | S _{oi} (%) | S _{wi} (%) |
|------------------------------|-----------------------|----------|---------|------------|---------------------|---------------------|
| Terpolymer #1, Trial #1 | 26.19 | 0.1952 | 110,426 | 0.0208 | 79.20 | 20.80 |
| Terpolymer #1, Trial #2 | 22.19 | 0.1654 | 98,834 | 0.0203 | 89.47 | 10.53 |
| Terpolymer #1, Trial #3 | 22.19 | 0.1466 | 116,922 | 0.0205 | 89.47 | 10.53 |
| Terpolymer #2, Trial #1 | 20.19 | 0.1560 | 129,631 | 0.0193 | 98.00 | 2.00 |
| Terpolymer #2, Trial #2 | 20.94 | 0.1560 | 102,223 | 0.0198 | 91.82 | 8.18 |
| Reference Material, Trial #1 | 20.69 | 0.1542 | 104,006 | 0.0207 | 88.71 | 11.29 |
| Reference Material, Trial #2 | 20.19 | 0.1505 | 117,691 | 0.0206 | 90.23 | 9.77 |

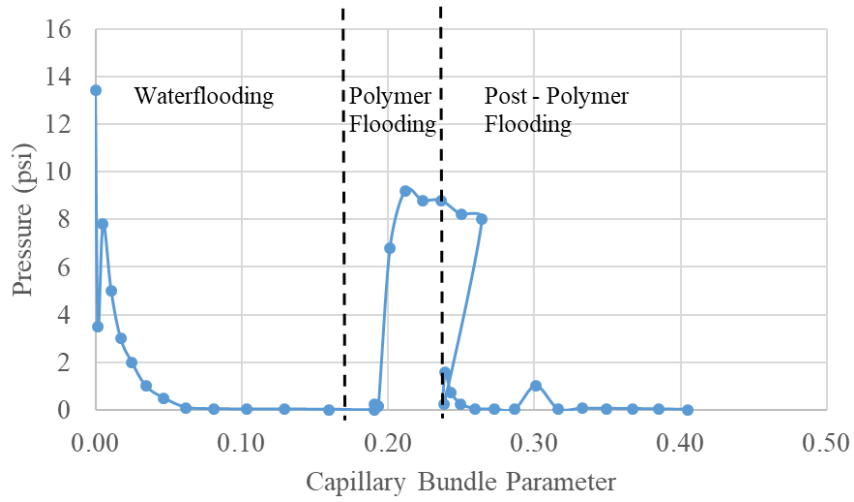
Properties were generally similar from one trial to the next, but any discrepancies have been normalized by using the capillary bundle parameter described earlier (Equation 4.1).

Once the initial conditions (or baseline values) were established for each trial, the flooding steps for oil recovery were performed consecutively. Throughout the oil recovery steps, the pressure in the sand-pack was recorded as a function of injection volume (again, reported as a fraction of PV and normalized using the capillary bundle parameter). Representative pressure graphs are shown in Figure 4.31.

(a)



(b)



(c)

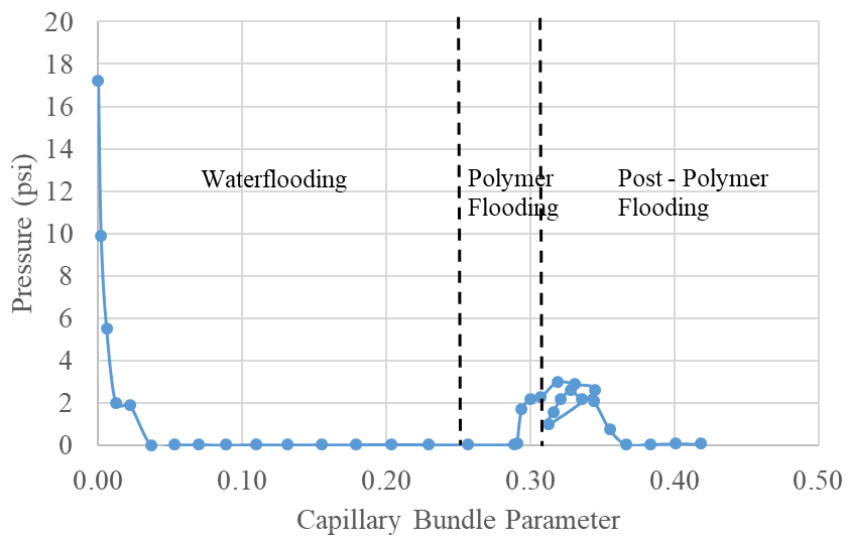


Figure 4.31: Sand-pack System Pressure throughout Heavy Oil Displacement Testing for (a) Terpolymer #1, (b) Terpolymer #2 and (c) the Reference Material

The plots shown in Figure 4.31 provide us with a more detailed understanding of how polymer solutions affect flow through the sand-pack. Initially, during the water flooding stage (that is, as brine is injected into the system), the fluid finds the path of least resistance and flows easily through the reservoir. However, at the polymer flooding stage, the polymer solution sweeps through the entire reservoir. While this improves the oil recovery efficiency, it can also significantly increase the pressure in the system. Therefore, it is extremely important to continue monitoring the pressure in the sand-pack to ensure that plugging does not occur. As expected, injecting a solution of terpolymer #2 results in the largest pressure increase (the highest recorded value during polymer flooding is nearly 10 psi), whereas terpolymer #1 only reaches 7 psi and the reference material remains below 4 psi. However, in all cases, the pressure measurements return to the baseline during the final injection stage (post-polymer flooding, or brine injection #2). This is an excellent result; given the results of the displacement tests (Section 4.2.3.2), some polymeric material is expected to remain in the sand-pack. However, these pressure profiles confirm that no plugging has occurred, and any residual polymer present in the sand-pack does not affect the system pressure.

Finally, perhaps the most important results from these tests are the oil recovery efficiencies at each stage and for each material. In Table 4.22, the oil recovery efficiency (that is, the proportion of oil removed from the sand-pack relative to the original oil in place) is provided for each recovery stage. Also, since at least two trials were performed for each material, the average results are presented for each polymer.

Table 4.22: Oil Recovery Efficiency Results from Heavy Oil Displacement Tests

| Sample & Trial | Water Flooding (%) | Polymer Flooding (%) | Post-Polymer Water Flooding (%) | Incremental Oil Recovery (%) | Overall Oil Recovery (%) |
|-----------------------------------|---------------------------|-----------------------------|--|-------------------------------------|---------------------------------|
| Terpolymer #1, Trial #1 | 24.7 | 37.3 | 16.3 | 53.6 | 78.3 |
| Terpolymer #1, Trial #2 | 22.8 | 35.8 | 17.6 | 53.4 | 76.2 |
| Terpolymer #1, Trial #3 | 28.6 | 35.3 | 15.9 | 51.2 | 79.8 |
| Average Terpolymer #1 | 25.4 | 36.1 | 16.6 | 52.7 | 78.0 |
| Terpolymer #2, Trial #1 | 24.8 | 47.5 | 15.2 | 62.7 | 87.5 |
| Terpolymer #2, Trial #2 | 25.9 | 49.3 | 14.7 | 64.0 | 89.9 |
| Average Terpolymer #2 | 25.4 | 48.4 | 14.9 | 63.3 | 88.7 |
| Reference Material, Trial #1 | 24.2 | 23.0 | 10.8 | 33.9 | 58.1 |
| Reference Material, Trial #2 | 23.6 | 26.0 | 12.1 | 38.0 | 61.6 |
| Average Reference Material | 23.9 | 24.5 | 11.4 | 35.9 | 59.8 |

As described previously (Section 3.4.2.2), water flooding (brine injection #1) was performed first. As expected, the oil recovery from water flooding was similar for all materials (since the polymeric material is not a factor at this stage). The slight variation in water flooding performance would likely be due to subtle changes in sand-pack characteristics between trials.

Clearer differences are observed at the polymer flooding stage, since the nature of the polymeric material can significantly affect the enhanced oil recovery performance. Here, we have confirmed that the designed terpolymers of AMPS/AAm/AAC show a significant improvement over the commercial reference. Terpolymer #2 has the best EOR performance, and 48.4% (nearly half of the original oil volume) is recovered during the polymer flooding stage. This is an excellent result, and is aligned with what was expected based on the displacement test results (recall the high RF values in Figure 4.29). Also, the % oil recovery from the polymer flooding is approximately twice as much for terpolymer #2 as it is for the reference material. Therefore, it is a significant improvement over currently available commercially standard materials. Terpolymer #1 also performs very well at this stage, recovering (on average) 36.1% of the original oil in place. This, too, is much higher than the recovery achieved by the commercially available reference material.

The final experimental stage during heavy oil displacement experiments is post-polymer water flooding (or brine injection #2). Here, more brine is added to the sand-pack system so that any residual oil or polymeric material can be flushed from the reservoir. At the beginning of this stage, it can be advantageous to have some polymeric material entrained in the sand-pack; as it is removed from the system, it will sweep residual oil with it and promote further oil recovery. Trials for all three polymer solutions exhibited some oil recovery during post-polymer water flooding, but the terpolymers allowed for better recovery at this stage compared to the reference material. This further confirmed that both designed terpolymers are excellent materials for the enhanced oil recovery application.

The recovery data from each stage can be summarized by calculating the incremental oil recovery and the overall oil recovery. Incremental oil recovery measures the contributions of the polymeric material compared to standard water (or brine) flooding. Therefore, incremental oil recovery is the sum of the recovery values from polymer flooding and post-polymer water flooding. The overall oil recovery, as one might expect, is the sum of the % oil recovered throughout the three recovery stages. As shown in the last two columns of Table 4.22, the incremental oil recovery was much higher for both terpolymers relative to the reference material. By using terpolymer #1, an additional 52.7% of the original oil in place was recovered; this valuable oil would have remained in the reservoir if only water flooding had been used. Thus, polymer flooding with terpolymer #1 led to a total oil recovery of 78.0%. An even more impressive result was observed when terpolymer #2 was injected. An additional 63.3% of the original oil in place was recovered during the polymer flooding and post-polymer flooding stages, which ultimately made it possible to achieve an overall recovery of 88.7%. This excellent result was achieved through careful design of materials, a good understanding of product requirements, and careful manipulation of polymer formulations (informed by kinetic understanding) to achieve the desired material properties.

4.2.4 Concluding Remarks on Optimally Designed Terpolymers for EOR

Two optimally designed terpolymers were selected based on the results of the screening experiments of Section 4.1. The formulations were selected so that the resulting AMPS/AAm/AAC terpolymers would have high molecular weight averages (on the order of 10^6 g/mol), high AAm content, and a desirable microstructure (with anions well-distributed along the backbone). Given an improved understanding of polymerization recipes and operating factors on the polymerization kinetics and resulting terpolymer characteristics, the two optimally designed terpolymers were synthesized at pH 7, ionic strength = 0.9 M, and monomer concentration = 1.5 M. The feed compositions selected were $f_{\text{AMPS},0}/f_{\text{AAm},0}/f_{\text{AAC},0} = 0.21/0.69/0.10$ and $0.10/0.75/0.15$.

Thorough characterization confirmed that the terpolymer properties were as expected and were well aligned with the properties of a commercially available reference material. Several independent experiments confirmed that synthesis replicates and characterization replicates showed excellent repeatability. This is hardly ever done in the polymerization literature. We also found that the cumulative terpolymer compositions were as predicted from ternary reactivity ratio estimates, molecular weight averages were of the expected order of magnitude, and thermal stability was improved with the addition of AMPS. Thus, investigation of several unique polymer properties confirmed the validity of the designed formulations.

Given these confirmatory results, application-specific properties were evaluated. The rheological properties of the newly designed terpolymers were evaluated in aqueous solution and in buffer, and behaviours were similar to the reference material. The terpolymer solutions had higher shear viscosities in water (compared to the reference material), but the reference material was less affected by the presence of salt. Also, both terpolymers had lower $\tan\delta$ profiles than the reference material, indicating higher elasticity (which often translates to improved EOR performance).

Finally, two phases of sand-pack flooding experiments were conducted to mimic the performance of each polymeric material in an oil reservoir. Here, both terpolymers were evaluated, and a new reference material (as described in Table 3.5) was used for comparison purposes. In the first phase of testing, polymer flow performance was established with displacement tests. Terpolymer #2 had the highest resistance factor (therefore highest potential for mobility control), but also the highest residual resistance factor, which indicates that residual polymeric material could cause injectivity issues within the reservoir. Terpolymer #1 also exhibited good flow performance, and would be an improvement over the reference material.

In the second phase of testing, oil was injected into the sand-pack system to evaluate the oil recovery efficiency (especially in the polymer flooding stage). For all three materials, the pressure within the sand-pack system was at reasonable levels and controllable throughout testing, so no plugging occurred. Terpolymer #2 was an excellent polymer for EOR; the incremental oil recovery

(that is, the percentage of original oil in place that was removed after water flooding) was 63.3%, and the total oil recovery was 88.7%. Terpolymer #1 also performed exceptionally well, averaging a total oil recovery of 78.0%. Both optimally designed terpolymers performed much better than the reference material, which was able to recover 59.8% of the original oil in place.

Thus, the design approach was successfully employed to synthesize, characterize and test optimal materials for enhanced oil recovery. We have acquired a wealth of information about the AMPS/AAm/AAC terpolymer, our model predictions were accurate, and our hypotheses for further performance were valid. Therefore, we can be confident in the application performance of these optimally designed terpolymers and the excellent oil recovery results.

Chapter 5. An Aside: Comparison of Binary and Ternary Reactivity Ratio Estimates

5.1 Using Appropriate Estimation Procedures

Section 5.1 has been recently published in European Polymer Journal [38]; the distinction between binary and ternary reactivity ratio estimates is an important part of this research, and is described in what follows.

A big issue associated with ternary systems is a widely accepted analogy between copolymerization and terpolymerization mechanisms. Many researchers [123-134] have used binary reactivity ratios (obtained from copolymerization experiments) in models dealing with terpolymerizations. Although this approximation has been successfully used in some instances (see, for example, [127-129, 134]), it is not always accurate [123-125, 131]. Using binary reactivity ratios to describe ternary systems effectively ignores the presence of the third comonomer, which will inevitably change the reaction conditions (and may ultimately affect the polymerization kinetics). The effect of the third comonomer ultimately depends on its chemical identity and the overall polymerization ‘recipe’ to which it is being added. At the very least, monomer concentration may vary, potentially affecting rate of polymerization and molecular weight averages. For recipes similar to the AMPS/AAm/AAC terpolymer (described previously and in Section 5.1.2), there can also be a significant electrostatic effect (consider how an additional charged monomer can change the ionic strength of the system). Incorporation (propagation) of a particular monomer may have occurred quickly and easily in an associated copolymer system, but the introduction of a third monomer may result in competitive monomer addition. Thus, using this type of binary analogy for ternary systems calls into question the accuracy of the reactivity ratios, which in turn affects model prediction performance of terpolymer product characteristics.

Previously, it has been suggested that ternary reactivity ratios should be estimated directly from terpolymer composition data, as opposed to using the related binary copolymer reactivity ratios [57]. However, direct comparison between binary and ternary systems has never been possible; differences in reactivity ratios may have been due to numerous other factors including reaction conditions and parameter estimation methods. Now, experimental binary and ternary data are directly compared for the 2-acrylamido-2-methylpropane sulfonic acid (AMPS)/acrylamide (AAm)/acrylic acid (AAc) system, based on recent copolymerization studies by Riahinezhad et al. [84] and Scott et al. [62], and an associated terpolymerization study [80]. To our knowledge, this is the first time that binary and ternary reactivity ratios have been compared directly, for the same system, with all other variables kept constant; to the extent possible, only the number of comonomers (two or three) and the feed composition were varied. Therefore, a direct comparison of binary and ternary reactivity ratios is finally possible.

5.1.1 Case Study: Terpolymerization of AN/Sty/MA

Estimating accurate reactivity ratios for multi-component systems is an important aspect of polymer reaction engineering, as the reactivity ratios are used to predict composition and sequence length properties of the polymer product. Hence, it is important to check the reliability of the model by evaluating, for instance, agreement between experimentally determined composition data and predicted terpolymer compositions. Many of the research groups who have used binary reactivity ratios to describe ternary systems have observed serious deviations between their experimental data and model predictions, which has led them to question the credibility of the Alfrey-Goldfinger terpolymerization model (see, for example, [123, 125, 131], with a more detailed discussion in [57]). In reality, it is the accuracy of the reactivity ratios (as parameter estimates used within the model) that should be questioned.

As an example (first exhibited by Kazemi [135] and re-evaluated for the current work), the terpolymerization of acrylonitrile (AN, M_1), styrene (Sty, M_2) and maleic anhydride (MA, M_3) was studied by Kressler et al. [125]. In the original investigation, the corresponding binary reactivity ratios (for each of the possible copolymer systems) were obtained from the literature (see Table 5.1), and were used to predict terpolymerization composition. As shown in Figure 5.1a, there was a significant disagreement between the experimental data and the model predictions when binary reactivity ratios were used.

By applying the EVM methodology to their (instantaneous) terpolymerization data, it is possible to estimate ternary reactivity ratios for the system (see again Table 5.1). Figure 5.1b shows that using these ternary reactivity ratios significantly improves the prediction performance of the A-G model. These excellent results can be attributed to (1) choosing to include the third comonomer in the estimation process and (2) using the EVM methodology for reactivity ratio estimation.

Table 5.1: Comparison of Binary and Ternary Reactivity Ratio Estimates AN(M_1)/Sty(M_2)/MA(M_3)

| Reactivity Ratios | r_{12} | r_{21} | r_{13} | r_{31} | r_{23} | r_{32} |
|--------------------------|----------------------------|----------------------------|----------------------------|----------------------------|----------------------------|----------------------------|
| Binary | 0.04 | 0.41 | 6.00 | 10^{-4} | 0.04 | 10^{-4} |
| Ternary | 0.14 | 0.58 | 0.40 | 2.40 | 0.05 | 0.07 |

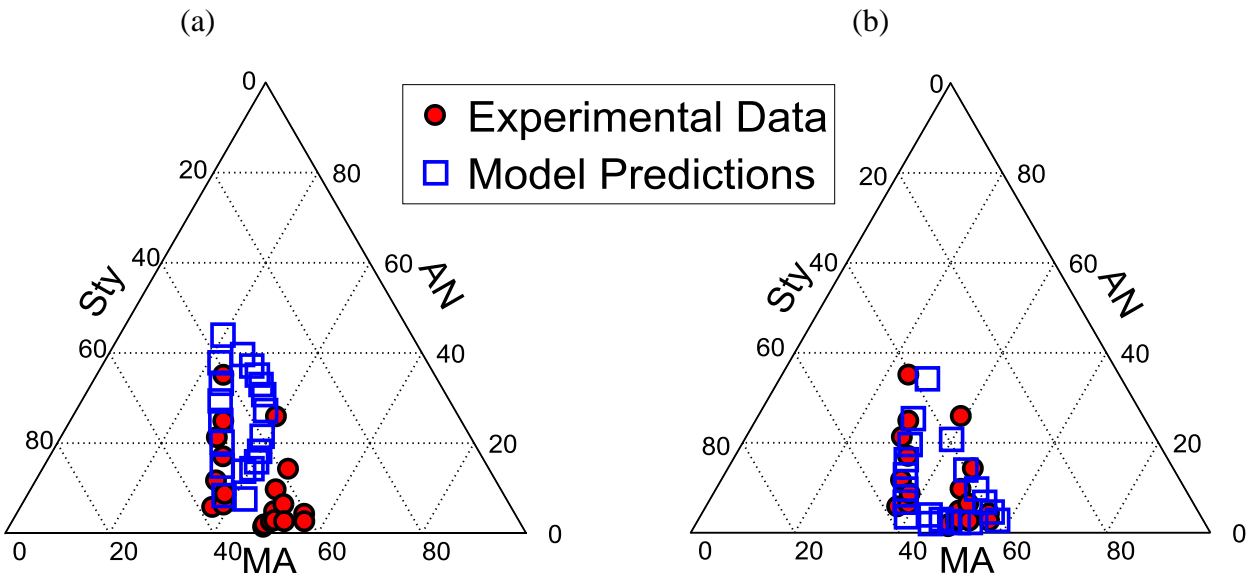


Figure 5.1: Experimental [125] and Predicted Terpolymer Composition for the AN/Sty/MA Terpolymer, using (a) Binary and (b) Ternary Reactivity Ratio Estimates for Prediction (Inspired by [135])

These results confirm the hypothesis that binary and ternary reactivity ratios can differ significantly for a given system, and therefore should not be used interchangeably. However, since the binary reactivity ratios used for the original analysis were taken from literature (and would have been estimated using various techniques), the accuracy of the binary values was rather questionable. For a direct and fair comparison of binary and ternary reactivity ratio estimates, it is necessary to collect dependable experimental data from both terpolymerization experiments and (the so-called analogous) copolymerization experiments. This ensures experimental consistency as well as statistically sound parameter estimation (using EVM) for both the binary and ternary systems. Thus, in what follows, the terpolymer of 2-acrylamido-2-methylpropane sulfonic acid/acrylamide/acrylic acid will be compared to the associated copolymers, based on recent studies by Riahinezhad et al. [84] and Scott et al. [62].

5.1.2 Direct Comparison of Binary and Ternary Systems (AMPS/AAm/AAC)

In what follows, the error-in-variables-model (EVM) is used to estimate reactivity ratios for the copolymerizations and the terpolymerization associated with the AMPS/AAm/AAC system. Data sets containing monomer feed composition, conversion and cumulative copolymer composition are fed to a MATLAB-based EVM program to obtain the best possible reactivity ratio estimates (and associated joint confidence regions, JCRs) [57, 67]. However, the goal here is to investigate more than just the reactivity ratios themselves. For the first time (to our knowledge), it is possible to do a direct comparison of binary and ternary systems, all else (polymerization conditions, reactivity ratio estimation techniques, etc.) being equal.

Thus, in Section 5.1.2.1, there will be a comparison of point estimates and the estimated degree of precision associated with the reactivity ratio estimates (JCRs) for binary and ternary systems. To complement these results, Section 5.1.2.2 will provide an in-depth look at composition prediction performance (using binary and ternary reactivity ratio estimates to predict cumulative terpolymer composition).

5.1.2.1 Comparison of Reactivity Ratios

Experimental information and data used for reactivity ratio estimation have been presented previously by Riahinezhad et al. [84] and Scott et al. [62, 80]. Now, it is finally possible to show a direct comparison of the binary reactivity ratios (for three distinct copolymerizations) and the ternary reactivity ratios (for the AMPS/AAm/AAc terpolymer). A numerical comparison is provided in Table 5.2, and joint confidence regions for each comonomer pair are presented in Figure 5.2 through Figure 5.4.

It is important to note that three distinct data sets were used to estimate the binary reactivity ratios (one for each comonomer pair). In contrast, all six ternary reactivity ratio estimates were obtained from a single data set (experimental terpolymerization data). However, the JCRs have been split into comonomer pairs (in Figure 5.2 through Figure 5.4) for straightforward comparison. The main focus of this investigation is to compare copolymerization and terpolymerization data for ternary reactivity ratio estimation, but a second (more practical) observation cannot be ignored: using copolymerization data to describe a ternary system requires double the experimental work (2 optimal copolymer feed compositions \times 3 comonomer combinations (6 polymerizations in total) vs. 3 optimal terpolymer feed compositions (3 polymerizations in total)). This advantage becomes even more significant in considering replication and/or evaluation of model prediction performance: the binary reactivity ratios would need a minimum of four additional runs (each of the 3 comonomer pairs plus 1 terpolymerization). Conversely, 1 terpolymerization run would provide enough data to confirm the ternary reactivity ratio estimates and demonstrate the accuracy of the terpolymerization model prediction.

Table 5.2: Comparison of Binary and Ternary Reactivity Ratio Estimates AMPS/AAm/AAc

| Reactivity Ratios | $r_{AMPS/AAm}$ | $r_{AAm/AMPS}$ | $r_{AMPS/AAc}$ | $r_{AAc/AMPS}$ | $r_{AAm/AAc}$ | $r_{AAc/AAm}$ |
|--------------------------|----------------|----------------|----------------|----------------|---------------|---------------|
| Binary | 0.18 | 0.85 | 0.19 | 0.86 | 1.06 | 0.22 |
| Ternary | 0.66 | 0.82 | 0.82 | 0.61 | 1.61 | 0.25 |

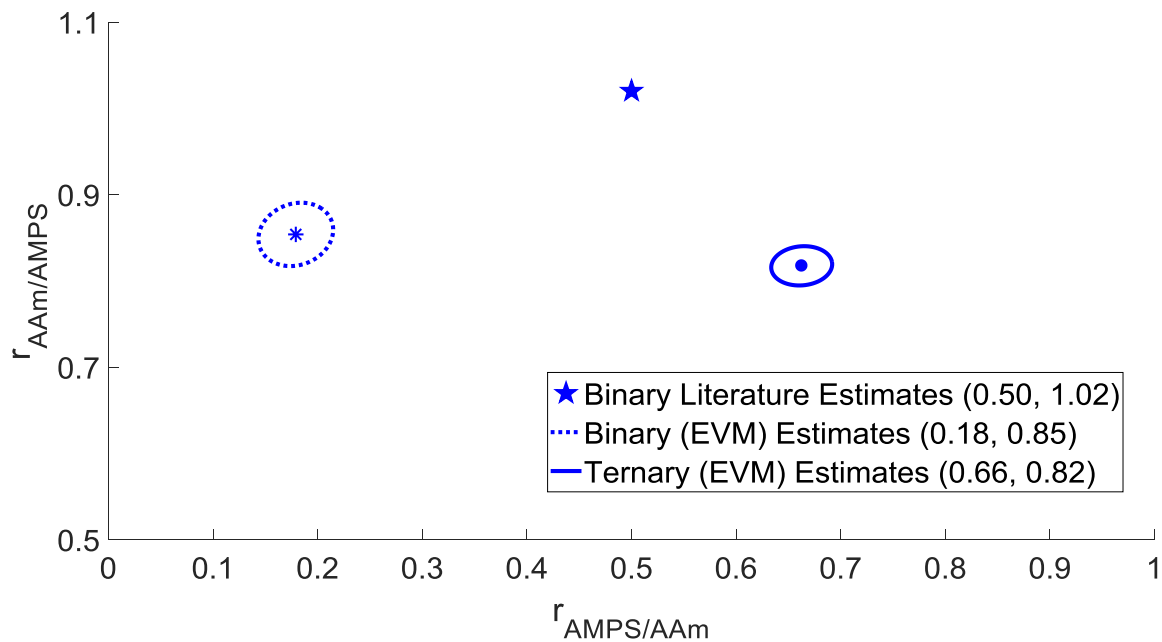


Figure 5.2: Comparison of Reactivity Ratio Estimates for Comonomers AMPS/AAm using Copolymerization Data (Binary Estimates) and Terpolymerization Data (Ternary Estimates)

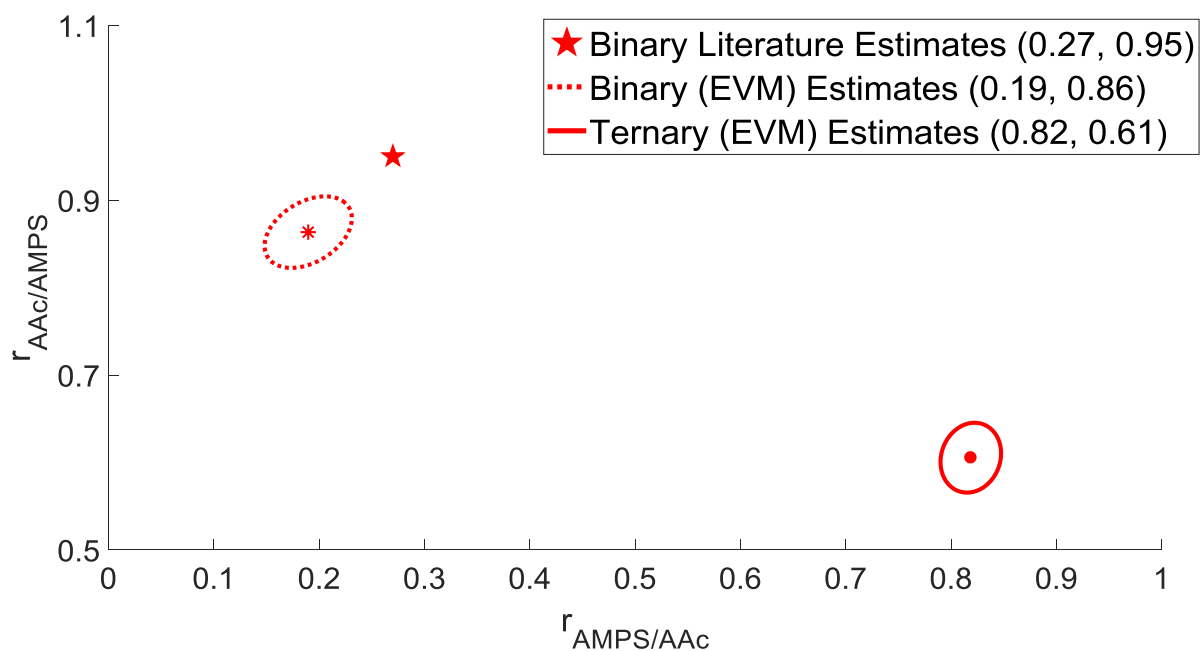


Figure 5.3: Comparison of Reactivity Ratio Estimates for Comonomers AMPS/AAc using Copolymerization Data (Binary Estimates) and Terpolymerization Data (Ternary Estimates)

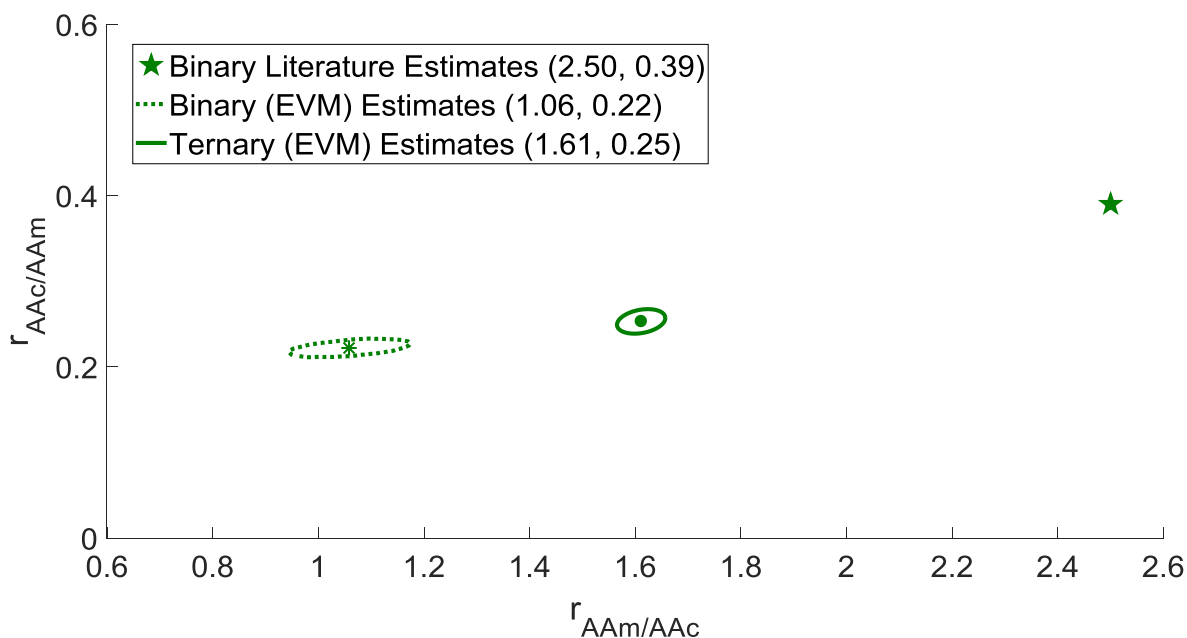


Figure 5.4: Comparison of Reactivity Ratio Estimates for Comonomers AAm/AAc using Copolymerization Data (Binary Estimates) and Terpolymerization Data (Ternary Estimates)

The most important observation from Figure 5.2 through Figure 5.4 is the following: binary and ternary reactivity ratios for a given comonomer pair differ significantly, even under the same reaction conditions. For all three comonomer pairs, no overlap of JCRs is observed. Although individual reactivity ratio estimate values are similar (between binary and ternary systems) for $r_{AAm/AMPS}$ and $r_{AAc/AAm}$, they should not be evaluated without their corresponding counterparts (that is, one cannot make statements about r_{ij} without also considering r_{ji}). Thus, point estimates are statistically different when the binary and ternary estimates are compared.

In Figure 5.2 and Figure 5.3, the size and orientation of the binary and ternary JCRs are similar, which represents a similar degree of confidence in both the binary reactivity ratio estimates and ternary reactivity ratio estimates. Also, the fact that the JCRs are fairly round (and not inclined) indicates that there is little correlation between the parameter estimates. This is largely due to the fact that EVM-based design of experiments was used to select feed compositions for both the copolymerization and terpolymerization studies. In Figure 5.4, the uncertainty in $r_{AAm/AAc}$ seems to be much larger than the uncertainty in $r_{AAc/AAm}$ (notice how the JCR is somewhat ‘stretched’ horizontally). However, this is partially due to the relative values of $r_{AAm/AAc}$ and $r_{AAc/AAm}$. Since $r_{AAm/AAc}$ is almost 6 times larger than $r_{AAc/AAm}$, the absolute error is necessarily larger in the horizontal direction; this phenomenon has also been addressed by Scott and Penlidis [6]. This behaviour is visible for the copolymer because the analysis is evaluating the AAm/AAc relationship in isolation. When the full terpolymerization data set is used for analysis, additional information content helps to improve the precision of all reactivity ratio estimates.

The data can also be evaluated by looking at the three comonomer pairs herein, as they are divided into Figure 5.2 through Figure 5.4. One might expect that if $r_{ij} > r_{ji}$ for the binary system, the same would be true for the ternary system. However, this is not always the case! As shown in the case study of Section 5.1.1 (with data from Kressler et al. [125]), relationships between comonomers may change between the binary and ternary systems; see again Table 5.1.

In the current study, only two of the three comonomer pairs have consistent trends between the binary and ternary reactivity ratio estimates (see again Table 5.2). In looking at the combination of AMPS and AAm, $r_{AAm/AMPS} > r_{AMPS/AAm}$ for both co- and terpolymerization. The trend is also consistent for AAm/AAc. Thus, it is reasonable to conclude that acrylamide is more reactive than the other comonomers (under these experimental conditions), regardless of whether a copolymer or a terpolymer is being synthesized.

In examining the AMPS/AAc comonomer pair, the relationship between reactivity ratios is not so predictable. While $r_{AAc/AMPS} > r_{AMPS/AAc}$ for the binary system, the opposite is true for the ternary system. The reactivity ratio estimates are also (numerically) closer together for the terpolymerization than they are for the copolymerization. We would postulate that this is due to the presence of acrylamide in the recipe; a non-ionized monomer in the presence of two ionized monomers would influence electrochemical interactions (and reduce repulsion) between AMPS and AAc.

More generally, it is also important to recognize the increase in AMPS reactivity for the terpolymerization. Table 5.2 indicates that $r_{AMPS/i}$ is noticeably larger for the ternary system than for the binary system, where i can be either AAm or AAc. This would suggest that the low reactivity of AMPS in the binary systems is not due to steric hindrance, but rather due to charge effects.

Direct comparison of binary and ternary reactivity ratios for the AMPS/AAm/AAc system has shown significant numerical differences, as well as some shifts in behaviour. However, point estimates are only one part of the story. It is equally important to evaluate the prediction performance when binary and ternary reactivity ratio estimates are used in the terpolymerization model.

5.1.2.2 Comparison of Composition Predictions

As mentioned previously, binary reactivity ratios are often used to predict terpolymer composition using the Alfrey-Goldfinger (A-G) model. However, for more accurate results, the recast A-G model (Equations 2.31 to 2.33) can be used in combination with recently determined ternary reactivity ratios [57]. In what follows, the recast A-G model is used to predict terpolymer composition using both the binary and ternary reactivity ratio estimates of Table 5.2.

Experimentally determined composition measurements (obtained using elemental analysis; see Section 3.3.2) are also included for evaluation of the model.

Ternary composition diagrams for the AMPS/AAm/AAC terpolymer are shown in Figure 5.5. The three optimal feed compositions used for reactivity ratio estimation (established using EVM design of experiments) are close to the corners of the triangle, since each is rich in one comonomer. The initial feed compositions, along with the measured and predicted terpolymer compositions, are shown in Figure 5.5 for both the binary and ternary reactivity ratio estimates. One should note that these compositions have been measured over the full conversion range, so scatter is due to composition changes (as a function of conversion) and should not be taken as poor reproducibility.

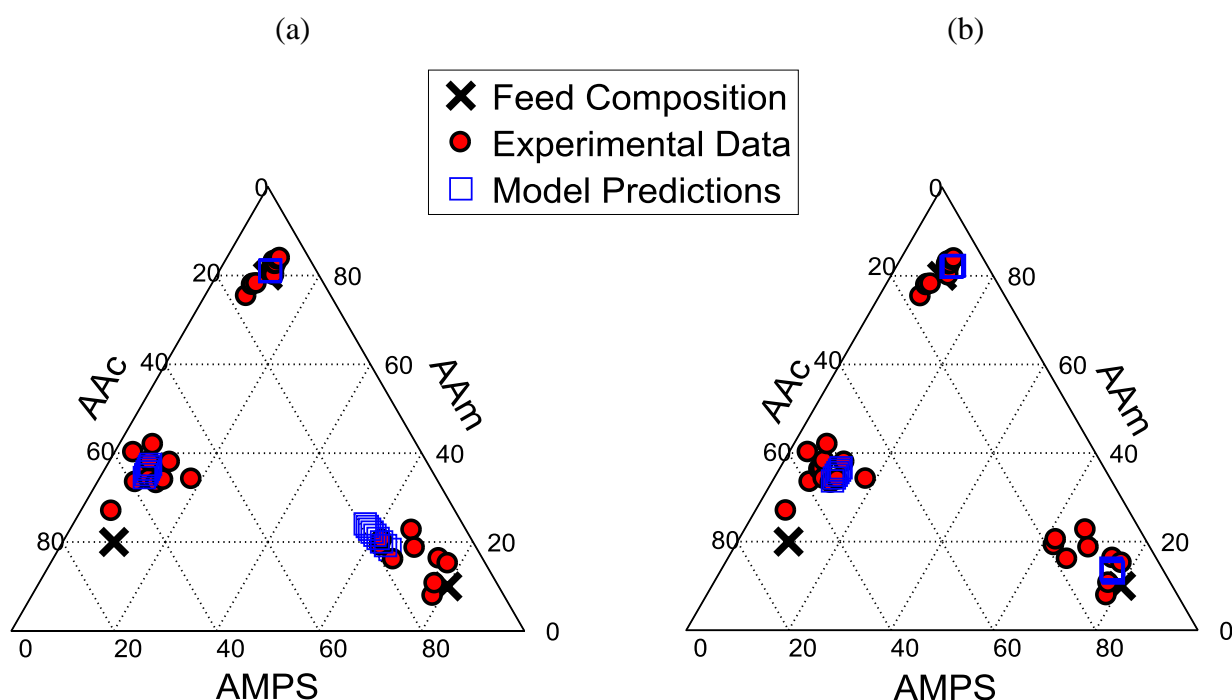


Figure 5.5: Experimental [80] and Predicted Terpolymer Composition for the AMPS/AAm/AAC Terpolymer using (a) Binary and (b) Ternary Reactivity Ratio Estimates for Prediction

The ternary composition diagrams show fairly good agreement between the predicted and measured cumulative terpolymer compositions. However, closer examination of the prediction performance of the binary reactivity ratio estimates reveals that the AMPS-rich terpolymer composition is not well predicted (especially compared to the prediction performance of the ternary reactivity ratio estimates for the same recipe).

This motivates closer examination of the AMPS-rich system. In Figure 5.6, the cumulative terpolymer compositions for all three comonomers (AMPS, AAm and AAC) are plotted against conversion, and the stark contrast between binary and ternary predictions is clearly visible. The

experimental data are in much better agreement with the ternary-based model. This is to be expected (as per previous discussion) and confirms the importance of using ternary reactivity ratios to describe/model terpolymer systems.

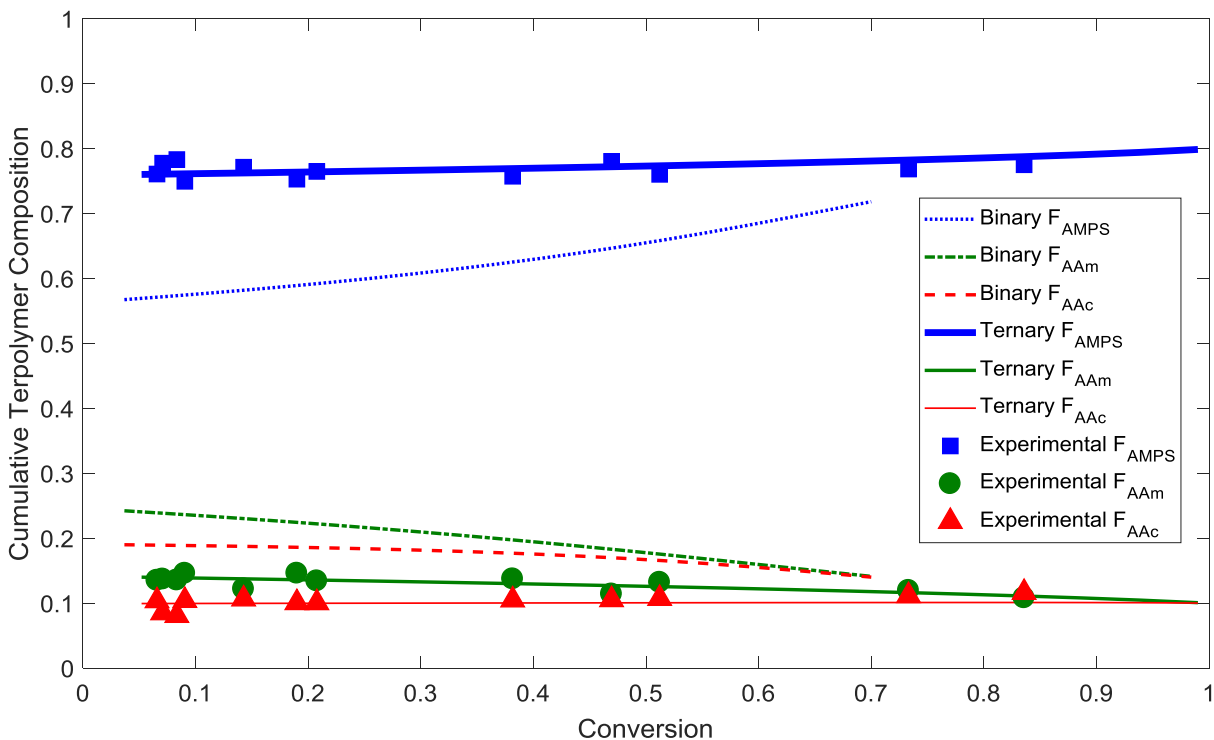


Figure 5.6: Experimental [80] and Predicted Terpolymer Composition for the AMPS-rich Terpolymer ($f_{AMPS,0}/f_{AAm,0}/f_{AAc,0} = 0.8/0.1/0.1$)

It is always good to confirm that model predictions (after parameter estimation) agree with experimental data. However, models are typically evaluated using the same experimental data that were used for parameter estimation [80]. It is important, then, to confirm that the model still holds when the behaviour of new recipes (that is, feed compositions not included in the design data) is being predicted. As mentioned previously, three optimal recipes were chosen for reactivity ratio estimation using EVM design of experiments; these were described in Section 2.3.1.2 and in previous work by Scott et al. [80]. Due to the nature of the design, all three points are near the corners of the composition triangle; they are rich in one comonomer and have low quantities of the other two comonomers. It is interesting to evaluate whether the model obtained from these three points still holds when the operating conditions are closer to the ‘middle’ of the triangle. That is, do the reactivity ratio estimates discussed in Section 5.1.2.1 apply to the entire composition range?

To establish whether the reactivity ratio estimates (and subsequent terpolymer composition predictions) hold for all compositions, three sub-optimal terpolymerization recipes were evaluated. The same synthesis and characterization procedures were used as described previously (see

Section 3.2 and previous work by Scott et al. [80]; synthesis conditions were pH 7 ± 0.5 , IS = 0.9 M; $[M] = 1.0$ M), but the results were not used for reactivity ratio estimation. Therefore, the reactivity ratio estimates are entirely independent of this sub-optimal region of experimental data. Figure 5.7 compares the experimentally measured terpolymer compositions and associated predicted (cumulative) terpolymer compositions for three additional recipes ($f_{\text{AMPS},0}/f_{\text{AAm},0}/f_{\text{AAc},0} = 0.5/0.1/0.4$; $0.2/0.4/0.4$; $0.3/0.5/0.2$).

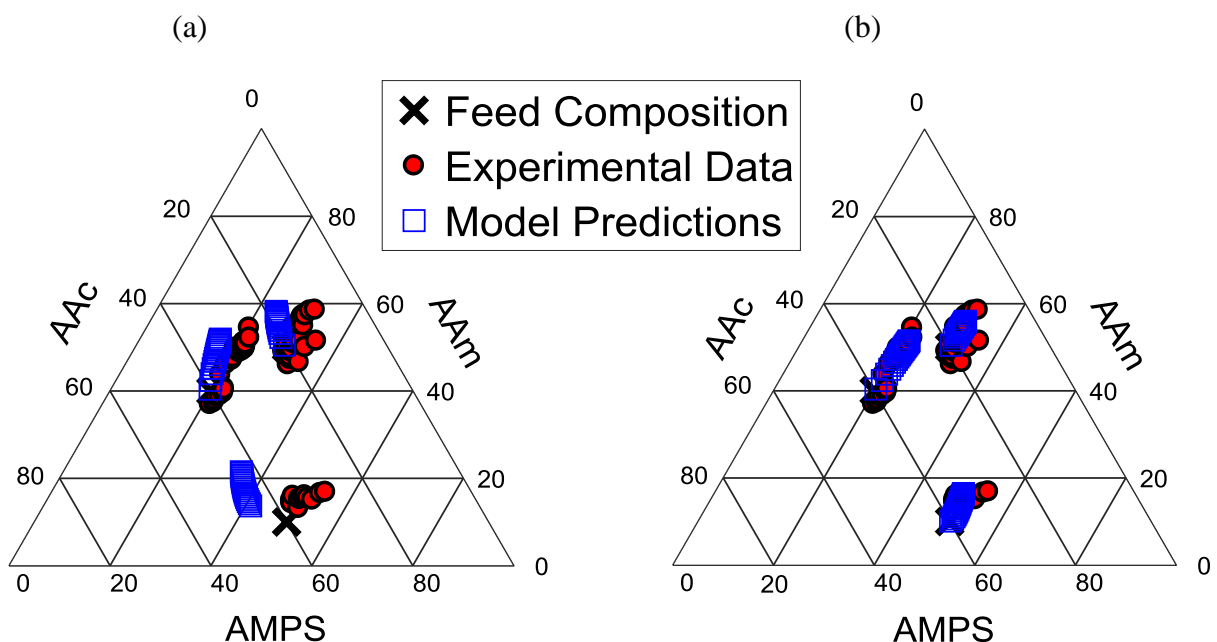


Figure 5.7: Experimental and Predicted Terpolymer Composition for Sub-Optimal AMPS/AAm/AAc Terpolymerizations, using (a) Binary and (b) Ternary Reactivity Ratio Estimates for Prediction

For comparison (and to return to the main goal of the current study), we can again look at the prediction performance of both the binary and ternary reactivity ratio estimates. The binary estimates were lacking for the optimally designed experiments (recall Figure 5.5), but they are even worse for the sub-optimal experiments. In Figure 5.7a, the biggest prediction discrepancy is for $f_{\text{AMPS},0}/f_{\text{AAm},0}/f_{\text{AAc},0} = 0.5/0.1/0.4$ (which is graphically the lowest feed composition in the triangle). The other two predictions (both containing more AAm) are in the right general region, but the direction of the prediction (that is, the slope of the predicted composition) does not agree with the experimental data.

These results can be contrasted with the model prediction using ternary reactivity ratio estimates, as shown in Figure 5.7b. The ternary prediction performance is much better than the binary prediction performance, which again highlights the importance of using ternary reactivity ratio estimates to describe/model/predict terpolymerization behaviour. From these results, it is also possible to confirm/conclude that ternary reactivity ratios obtained from optimally designed

experiments [60] apply to the whole composition range; the recast A-G model holds for any initial feed composition.

Though the ternary model has excellent prediction performance for all three feed compositions, the trend is not entirely correct for $f_{\text{AMPS},0}/f_{\text{AAm},0}/f_{\text{AAc},0} = 0.5/0.1/0.4$. The experimental data points seem to vary horizontally (physically, this indicates that \bar{F}_{AAm} shows very little drift). However, the model shows a different trend, suggesting that \bar{F}_{AMPS} is the comonomer fraction that remains approximately constant. For the sake of completeness, we can also look back to the binary prediction; because it varies in the opposite direction, it is predicting that \bar{F}_{AAc} will exhibit the least drift. Obviously, any one of these comonomer fractions are related to the other two ($\sum \bar{F}_i = 1$), but the model predictions and the experimental data seem to be in disagreement. Thus, the cumulative terpolymer composition can be examined as a function of conversion (Figure 5.8).

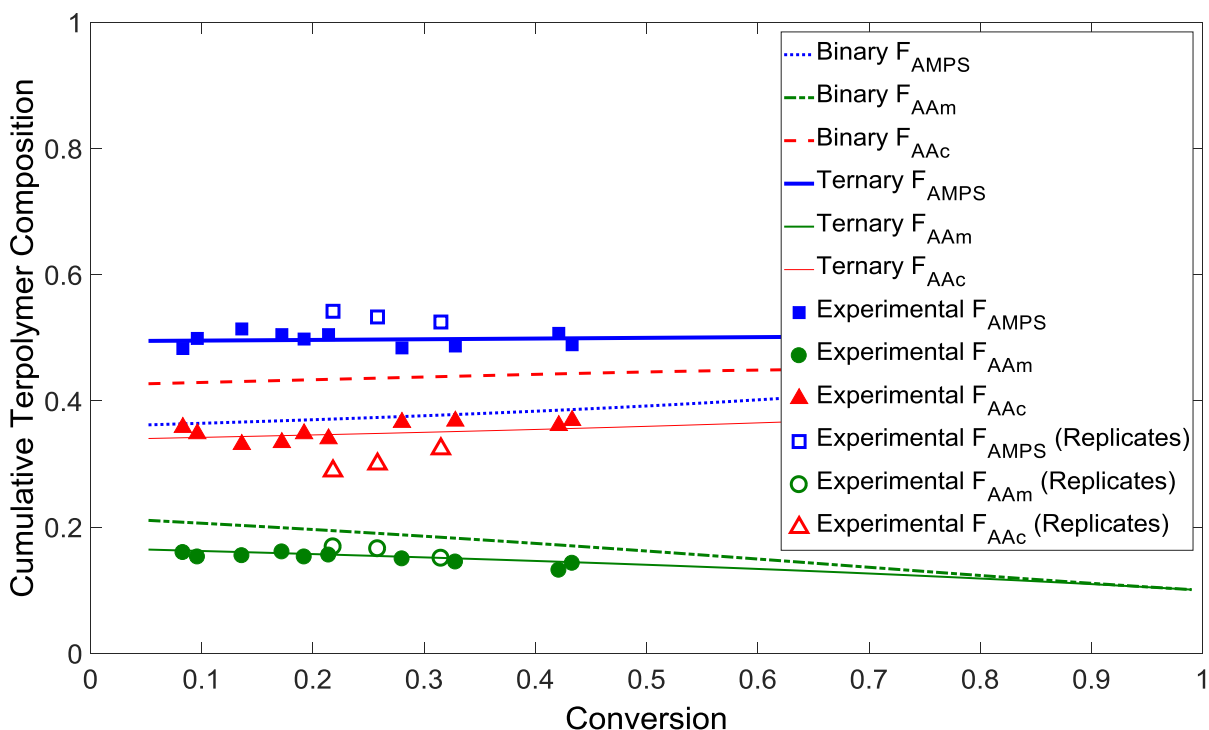


Figure 5.8: Experimental and Predicted Terpolymer Composition for the Sub-Optimal Terpolymer ($f_{\text{AMPS},0}/f_{\text{AAm},0}/f_{\text{AAc},0} = 0.5/0.1/0.4$)

As mentioned earlier (in the discussion surrounding Figure 5.7b), the ternary plot indicated that there may be some discrepancies between the experimentally observed trends and trends predicted by the model (specifically for $f_{\text{AMPS},0}/f_{\text{AAm},0}/f_{\text{AAc},0} = 0.5/0.1/0.4$). One might think that this variation is a result of composition drift changing with conversion, but it is actually due to slight differences between runs. Figure 5.8 confirms that any concerns about prediction performance are unfounded; the experimentally determined cumulative terpolymer composition and the ternary model

prediction are in very good agreement. The inconsistency observed in Figure 5.7b was not a result of bad prediction performance. Rather, a replicate run was ‘biased high’ (in terms of $\overline{F}_{\text{AMPS}}$ measurements) and created a false impression. This variability between runs is not a cause for concern; the replicate run was performed entirely independently (from stock solution preparation to synthesis to characterization), so some experimental error is perfectly normal.

Another important take-away from Figure 5.8 is the terrible prediction performance when binary reactivity ratios are used in the model. It has already been noted that the incorporation of AMPS changes considerably when the system changes from a copolymerization to a terpolymerization. This has been observed both in the change of reactivity ratio estimates (recall Table 5.2) and prediction performance for the optimally designed feed compositions (especially $f_{\text{AMPS},0}/f_{\text{AAm},0}/f_{\text{AAc},0} = 0.8/0.1/0.1$; see Figure 5.6). Previously, in Figure 5.6, using binary reactivity ratios in the recast Alfrey-Goldfinger model severely underestimated $\overline{F}_{\text{AMPS}}$, which in turn affected the prediction performance for the other comonomer fractions. Now, for a sub-optimal recipe, this problem is amplified.

The initial feed composition, again, is $f_{\text{AMPS},0}/f_{\text{AAm},0}/f_{\text{AAc},0} = 0.5/0.1/0.4$. It is important to restate this here, because the fractions of AMPS and AAc in the recipe are close, but $f_{\text{AMPS},0} > f_{\text{AAc},0}$. In the product terpolymer, the cumulative fraction of AMPS remains greater than that of AAc; $\overline{F}_{\text{AMPS}} > \overline{F}_{\text{AAc}}$ is measured throughout the polymerization (at least up to ~50% conversion). When the ternary reactivity ratio estimates are used in the recast A-G model, the model prediction supports these experimental observations, as it should. In contrast, when binary reactivity ratio estimates are used in the model, $\overline{F}_{\text{AAc}} > \overline{F}_{\text{AMPS}}$ for up to about 85% conversion. This inconsistency is a major disadvantage of using binary reactivity ratio estimates to describe a ternary system. Imagine trying to synthesize an AAc-rich terpolymer (given inappropriate binary data), and finding that the end product is actually AMPS-rich! This would only result in frustration and wasted resources. It is therefore preferable, when possible, to use ternary reactivity ratios to obtain information about terpolymerization systems.

5.1.3 Concluding Remarks on Appropriate Estimation Procedures

Terpolymerization kinetics are complex. Historically, binary reactivity ratios have been used to predict terpolymerization behaviour (with some success), but this work shows that this binary-ternary analogy is not always applicable. These results suggest that terpolymerization kinetics should not be oversimplified by applying binary reactivity ratios to ternary systems. When researchers use copolymerization data to describe a terpolymerization, they are essentially ignoring the presence of the third comonomer (and any possible interactions with the other two comonomers) and doubling the amount of experimental work required for reactivity ratio estimation.

In directly comparing the binary and ternary reactivity ratios for the AMPS/AAm/AAC system, significant differences in reactivity ratio estimates (numerically speaking) and in related trends were observed. This ultimately affects model prediction performance; binary reactivity ratios applied to the (recast A-G) terpolymerization model did not agree with experimentally measured composition data. In contrast, ternary reactivity ratios gave very good predictions.

Through this study, it has been shown that three optimally designed feed compositions (selected using EVM-based design of experiments) provide enough information to accurately estimate ternary reactivity ratios. Not only do these three experiments provide better ternary reactivity ratio estimates (and subsequent prediction performance) than their so-called analogous binary estimates, but they also give equally good prediction performance for independent sub-optimal feed compositions.

Thus, whenever possible, researchers should be motivated to use terpolymerization data to estimate ternary reactivity ratios. Design of experiments and the error-in-variables-model make data collection and parameter estimation straightforward and (perhaps more importantly) kinetically and statistically accurate.

5.2 Terpolymer Troubleshooting Tips

Section 5.2 has been recently published in a Special Issue of Processes regarding “Computational Methods for Polymers” [136]; the article includes a series of case studies highlighting the advantages and challenges of estimating ternary reactivity ratios directly from terpolymerization data. A portion of the original article is presented in what follows.

When terpolymerization experiments are selected with parameter estimation in mind (that is, using an error-in-variables model (EVM)-based design of experiments for ternary systems [60]), it can be straightforward to estimate ternary reactivity ratios using the information-rich data set. However, in using historical data (which may not be designed for parameter estimation), experimental terpolymerization data may not be sufficient for analysis. Common limitations in terpolymerization studies include composition restrictions or a lack of experimental information content (minimal replication, formulations selected targeting final properties rather than information collection, etc.). Since working with historical (previously collected) data has some challenges, the case studies presented herein address those challenges and aim to improve ternary reactivity ratio prediction to the extent which is possible. For example, additional targeted experiments (i.e., the sequential selection of experiments based on an existing data set), experimental replication, and full-conversion (cumulative) analysis can supplement a pre-existing terpolymerization data set. While additional targeted experiments and replication may require revisiting the lab (or simulating additional data), full-conversion data are often already available

from earlier runs. Cumulative analysis can provide greater information content from fewer experimental runs [54].

Despite the fact that binary reactivity ratios are only a numerical approximation for ternary systems, several cases have reported that model predictions using binary reactivity ratios seem to be in good agreement with terpolymerization data (most recently [137]). In these cases, although binary reactivity ratios provide good prediction performance, there are still benefits associated with using ternary reactivity ratios directly [38]. First, this ensures that no unfounded assumptions are made about the nature of the terpolymerization, where the addition of the third comonomer (and any interactions it might have with the other two comonomers) is carefully evaluated. Second, it reduces the experimental load required to characterize the system (e.g., two designed formulations of three copolymers require six experiments for binary reactivity ratios, compared to three designed formulations per single terpolymer requiring three experiments for ternary reactivity ratios). This is especially important if a new (unknown) combination of comonomers is being investigated. Third, and perhaps most importantly, the kinetic and statistical accuracy of using ternary reactivity ratio estimation in terpolymerization studies ensures accurate model predictions for the system being studied.

Several case studies are revisited herein to explore the advantages (and challenges) of directly estimating ternary reactivity ratios from terpolymerization data. In the first two case studies (Section 5.2.1), common challenges in parameter estimation are addressed, such as process constraints (experimental/composition limitations) and numerical estimation constraints (ill-conditioned systems). Additional case studies (Section 5.2.2) are then presented to provide a direct comparison between binary and ternary reactivity ratio estimates. When the above-mentioned challenges are not a factor, the advantages of estimating ternary reactivity ratios are evident.

5.2.1 Addressing Composition Restrictions & Ill-Conditioned Systems

In some cases, system limitations and/or product requirements do not necessarily allow for statistically designed experiments, such as those described in Section 2.3.1.2 (each rich in a single comonomer). This paucity of data presents a challenge for researchers, especially when they hope to estimate reactivity ratios for subsequent microstructural predictions. The question is: What does one do when a terpolymer system has composition restrictions? How can a limited data set be analyzed in such a way that researchers are confident in their parameter estimates? In what follows, we take a closer look at the challenges associated with two such systems and provide some suggestions for overcoming the experimental limitations.

5.2.1.1 Case Study: HOST/EAMA/PAG

In a recent study, Pujari et al. [138] synthesized a terpolymer of 4-hydroxystyrene (HOST; monomer 1), 2-ethyl-2-adamantyl methacrylate (EAMA; monomer 2), and a photoacid generator (PAG; monomer 3) to use in chemically amplified resists. Specifically, the PAG used for terpolymerization was triphenylsulfonium salt 4-(methacryloxy)-2,3,5,6-tetrafluorobenzene sulfonate (F4 PAG).

Pujari et al. [138] provided an interesting contrast between the copolymerization and terpolymerization behaviour for the same comonomers. The authors reported that of the three comonomers, only HOST would homopolymerize. The HOST/EAMA copolymers were easily synthesized and HOST/PAG copolymers were achievable when the feed composition of PAG was below 10 mol%. However, their attempts to synthesize an EAMA/PAG copolymer were entirely unsuccessful (at a variety of distinct feed compositions). Finally, they synthesized HOST/EAMA/PAG terpolymers from several different feed compositions, in spite of their inability to synthesize some of the analogous copolymers. This is an example of a system where binary (copolymerization) data would not be suitable for predicting terpolymerization behaviour.

Since Pujari et al. [138] had a specific application in mind, all terpolymer formulations had similar initial compositions. In the feed, mole fractions were selected within the following ranges: $0.25 \leq f_{1,0} \leq 0.40$, $0.50 \leq f_{2,0} \leq 0.75$, and $0.01 \leq f_{3,0} \leq 0.10$ (with $\sum f_i = 1.0$). Of particular interest for the current investigation is the very low mole fraction of PAG. At most, the PAG content in the feed was only 10 mol%. These experiments are not designed with reactivity ratio estimation in mind, rather, application requirements take precedence. However, these (low conversion) terpolymerization data were still used to estimate reactivity ratios and predict terpolymer properties.

Pujari et al. [138] were able to estimate ternary reactivity ratios using Procop 2.3 [139]. However, because this data set has minimal information content, the results exhibit a multiplicity of solutions. Table 5.3 compares the reactivity ratio estimates reported by Pujari et al. [138] with three successive estimations (labelled A through C) using the instantaneous model via the EVM (with the preliminary estimate that $r_{ij} = 0.500$ for all parameters).

Table 5.3: Reactivity Ratio Estimates for HOST(1)/EAMA(2)/PAG(3) (Data from [138])

| | r_{12} | r_{21} | r_{13} | r_{31} | r_{23} | r_{32} |
|--|----------|----------|----------------|----------|----------|----------------|
| Reported by Pujari et al. [138] | 0.05 | 0.12 | 0.81 | 0.12 | 0.05 | 0.79 |
| Current Study (EVM Estimation) | | | | | | |
| Inst. Estimation (A) | 0.1063 | 0.2155 | 0.6754 | 0.0001 | 0.0877 | 0.0307 |
| Inst. Estimation (B) | 0.1767 | 0.2394 | 99.9721 | 0.0002 | 0.0897 | 0.7035 |
| Inst. Estimation (C) | 0.0003 | 0.1753 | 2.5329 | 0.0001 | 0.0728 | 99.9997 |

Clearly, the estimation stage and results using the instantaneous model with EVM are numerically unstable (and therefore unreliable). There are multiple solutions for this estimation. This is a limitation of using a data set that only contains limited process information arising from PAG-poor formulations. Although common sense suggests that a reactivity ratio pair of $(r_{13}, r_{31}) = (99.9721, 0.0002)$ seems unlikely, as seen in estimation (B), it is numerically possible. This is a numerical artefact, as reactivity ratios reach the ‘upper bound’ (UB) of the parameter estimation program (UB = 100 for all parameter values during estimation).

All reactivity ratios presented in Table 5.3 give almost identical prediction performance when the PAG fraction is low. As shown in Figure 5.9, all model predictions ‘fit’ the experimental data (reported at one conversion level) equally well. The model predictions using the original reactivity ratio estimates reported by Pujari et al. [138] are not shown here, but they also ‘fit’ the experimental data well and fall within the ranges of Figure 5.9.

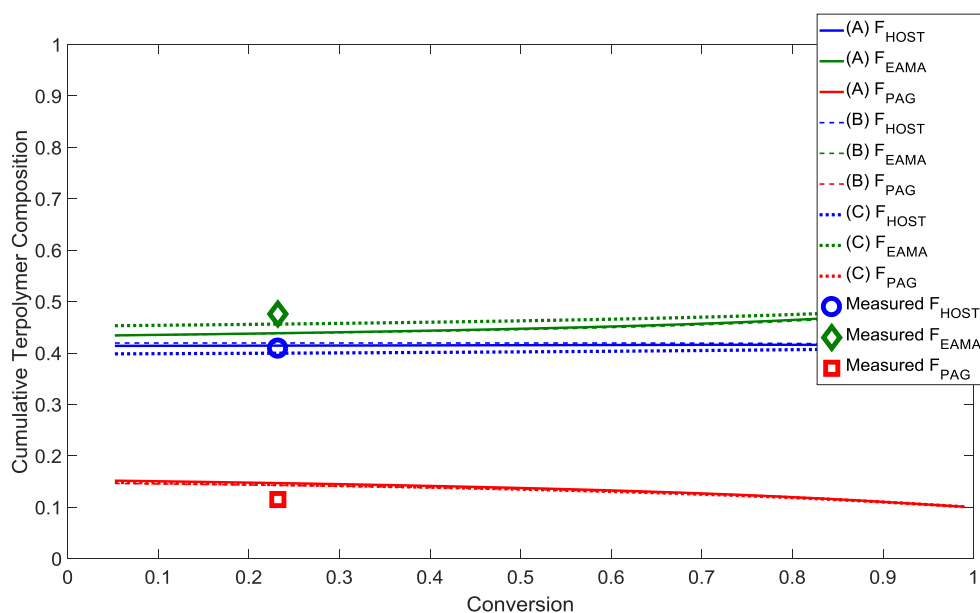


Figure 5.9: HOST/EAMA/PAG Terpolymer Composition Prediction for $f_{1,0}/f_{2,0}/f_{3,0} = 0.4/0.5/0.1$ (Experimentally Measured Composition for TPF10 from Pujari et al. [138])

In contrast, if terpolymerization behaviour is predicted beyond the available experimental data (e.g., a PAG-rich formulation: $f_{1,0}/f_{2,0}/f_{3,0} = 0.1/0.1/0.8$), these considerably different reactivity ratio estimates give distinctly different results (see Figure 5.10). This is an extreme case, selected for demonstration purposes, and may not be achievable experimentally. However, this inconsistent prediction performance is observed for any PAG-rich recipe (with $f_{3,0}$ as low as 0.4).

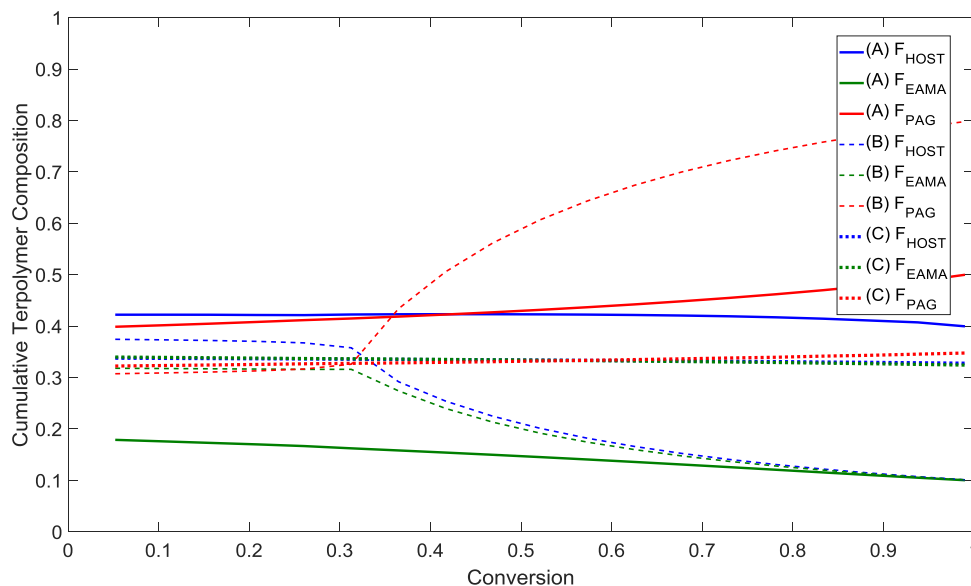


Figure 5.10: HOST/EAMA/PAG Terpolymer Composition Prediction for $f_{1,0}/f_{2,0}/f_{3,0} = 0.1/0.1/0.8$

The predictions shown in Figure 5.10 highlight the importance of statistically well-designed experiments. In spite of the experimental limitations in this case (limiting the PAG content to 10 mol%), introducing a run with as much PAG as possible would likely eliminate the numerical instabilities (and therefore improve the reliability of these estimation results).

5.2.1.2 Case Study: BA/BMA/limonene

Another terpolymerization case that is subject to composition restrictions (as well as ill-conditioning) is the terpolymerization of n-butyl acrylate (BA; monomer 1), butyl methacrylate (BMA; monomer 2), and D-limonene (lim; monomer 3), recently studied by Ren et al. [134]. D-limonene, a renewable monoterpene, is advantageous in terms of its polymer sustainability. When used as a comonomer it reduces the polymerization rate and molecular weight averages. Therefore, no more than 40 mol% lim was used in any feed composition for the study. The feed compositions used in the original investigation [134] are shown in Figure 5.11.

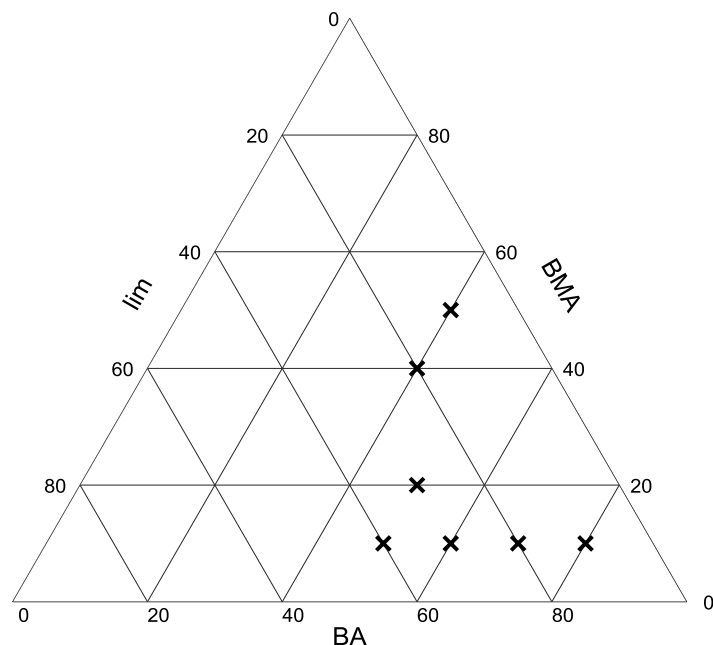


Figure 5.11: Feed Compositions for the BA/BMA/lim Terpolymer, as Reported by Ren et al. [134]

Given that most experimental data are collected under lim-poor conditions, one might expect more error in the reactivity ratio estimates associated with the limonene comonomer. For both the instantaneous model (using low conversion data) and the cumulative model (using all available data), ternary reactivity ratio estimation was performed three times (always with $M_1 = \text{BA}$, $M_2 = \text{BMA}$ and $M_3 = \text{lim}$). The results of each estimation are shown in Table 5.4. In this case, the binary reactivity ratio estimates (as reported by Ren et al. [134], collected from previous work by Dubé and colleagues [79, 140, 141]) were used as the preliminary estimates.

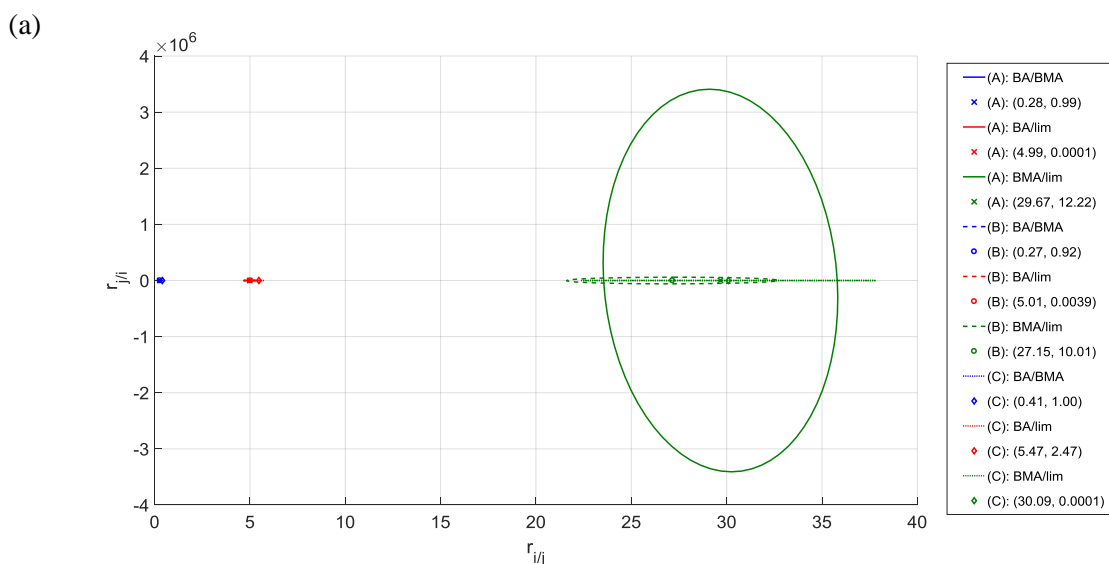
Table 5.4: Reactivity Ratio Estimates for Terpolymerization of BA(1)/BMA(2)/lim(3) with Experimental Data from Ren et al. [134]

| | r_{12} | r_{21} | r_{13} | r_{31} | r_{23} | r_{32} |
|---|----------|----------|---------------|----------------|----------------|----------------|
| Reported by Ren et al. [134] | 0.46 | 2.008 | 6.08 | 0.007 | 6.096 | 0.046 |
| Current Study (EVM Estimation with Low Conversion Data) | | | | | | |
| Inst. Estimation (A) | 0.3729 | 1.4350 | 5.0098 | $<10^{-3}$ | 35.5943 | 13.0409 |
| Inst. Estimation (B) | 0.4986 | 1.4982 | 5.2291 | 27.9826 | 52.3811 | $<10^{-3}$ |
| Inst. Estimation (C) | 0.3729 | 1.4350 | 5.0098 | $<10^{-3}$ | 35.5924 | 36.9594 |
| Current Study (EVM Estimation with Full Conversion Data) | | | | | | |
| Cum. Estimation (A) | 0.2787 | 0.9949 | 4.9888 | 0.0001 | 29.6738 | 12.2200 |
| Cum. Estimation (B) | 0.2733 | 0.9214 | 5.0104 | 0.0039 | 27.1517 | 10.0072 |
| Cum. Estimation (C) | 0.4081 | 0.9987 | 5.4698 | 2.4651 | 30.0914 | 0.0001 |

As observed for the HOST/EAMA/PAG system, the estimation is numerically unstable. However, in general, the cumulative estimation results seem less ill-conditioned than in the instantaneous analysis. This is likely due to the increased information content provided when analyzing composition data over the full conversion range with a cumulative model [6].

Looking closer at the instantaneous estimation results, relatively good agreement is obtained between instantaneous estimations A and C. However, in both cases, the r_{23} and r_{32} estimates are both much greater than 1. Such a case has not been observed in free-radical copolymerization. There are some reports in the literature that have shown both estimates >1 , but this is likely due to experimental error or a different copolymerization model being active. In this case, it is likely due to error, but the degradative chain transfer mechanism (due to the presence of limonene) may also contribute here. The uncertainty in this system is confirmed by comparing instantaneous estimations A and C to instantaneous estimation B. The fact that estimation results based on the same data set have considerable convergence issues (likely due to local optima) suggests that there is not sufficient information for reactivity ratio estimation directly from the terpolymerization data.

Similar behaviour is observed for the cumulative case. Here, cumulative estimations A and B are similar, whereas the third estimation, estimation (C), shows more variation. Again, the estimation results indicate that two reactivity ratios (for a given comonomer pair) are both greater than 1. The same comonomer pairs are of concern here: The BMA/lim comonomer pair (r_{23} and r_{32}) in cumulative estimations A and B, and the BA/lim pair (r_{13} and r_{31}) in cumulative estimation C. This behaviour can be examined further by plotting the joint confidence regions (JCRs, or error ellipses) for each of the point estimates obtained using cumulative analysis (Figure 5.12).



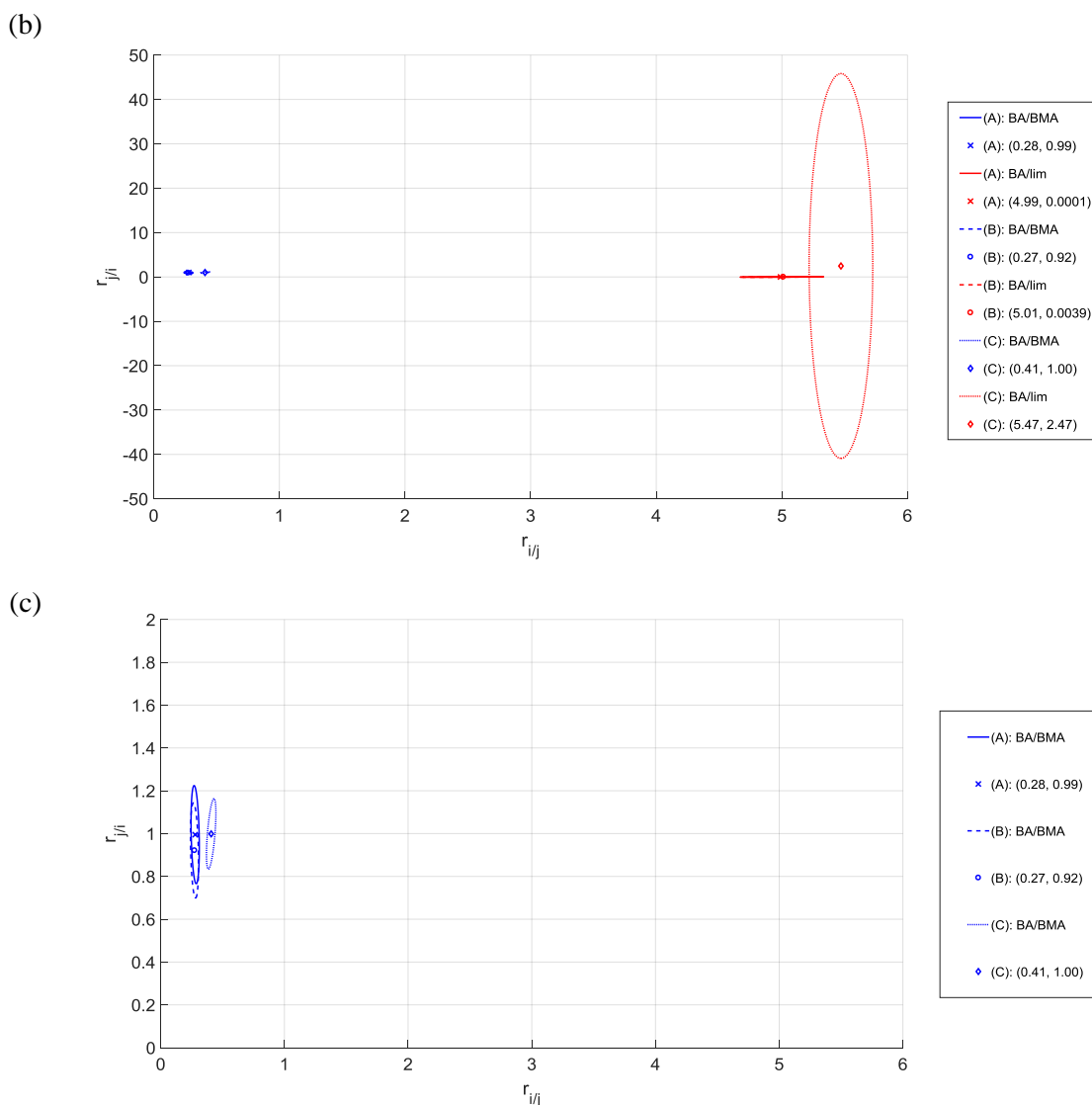


Figure 5.12: Ternary Reactivity Ratio Estimates for the Terpolymerization of BA(1)/BMA(2)/lim(3), with Data from Ren et al. [134]

As shown in Figure 5.12a, the JCRs associated with r_{23} and r_{32} are very large. The largest uncertainty was for estimation A, but subsequent estimations showed similar results. In comparison, the JCRs for the other parameters look like point estimates! This indicates substantial and disproportionate uncertainty in the estimates, especially for the BMA/lim comonomer pair.

As we focus in on the other parameter estimates (for the BA/BMA pair and the BA/lim pair), the JCRs become much smaller (note the change in scale between Figure 5.12a and Figure 5.12b). Comparing BA/BMA to BA/lim, the most uncertainty is clearly for the BA/lim comonomer pair (especially for estimation (C)). In comparison, the JCRs for BA/BMA are very small, which gives a much higher degree of certainty compared to the other estimates (see Figure 5.12c).

The more precise estimation of r_{12} and r_{21} (that is, for the BA/BMA pair) is not coincidental. As mentioned earlier, the experimental data collected (Figure 5.11) only included formulations with low mole fractions of limonene. Therefore, we would suggest that a lack of lim-rich data has contributed to poor estimation performance for the BA/BMA/lim terpolymer. This agrees with previous copolymerization observations reported by Scott and Penlidis [6].

To demonstrate the importance of using well-designed data for ternary reactivity ratio estimation, supplemental data have been simulated for the BA/BMA/lim system. Experimental data were simulated using the binary reactivity ratio estimates (which, as per the original investigation, give acceptable predictions of terpolymer behaviour up to full conversion levels [134]). Two feed compositions, $f_{1,0}/f_{2,0}/f_{3,0} = 0.1/0.8/0.1$ and $f_{1,0}/f_{2,0}/f_{3,0} = 0.1/0.1/0.8$ (that is, BMA-rich and lim-rich formulations) were selected to supplement the original data set. In both cases, the total conversion range was divided into 19 points (between 0 and 0.99 in steps of 0.052) and the corresponding monomer composition mole fractions were calculated via direct numerical integration. Then, the cumulative terpolymer compositions were calculated using the Skeist equation ([142] as per [54]). Random error was added to all data to mimic real experimental observations: A 1% error was added to conversion and feed composition ($f_{i,0}$) data, while a 2% error was added to the cumulative terpolymer composition (\bar{F}_i) data. (Note that typically 5% error is standard for \bar{F}_i data, but using those levels for this system would occasionally make the simulated limonene content negative, given the low incorporation of limonene).

For the instantaneous case, three low conversion data points from each (simulated) feed composition were added to the data set. As shown in Table 5.5, the addition of these data ‘stabilized’ the estimation, and reactivity ratio estimates obtained were now almost well-behaved. However, the newly estimated parameters still pose a concern: For the r_{23} and r_{32} pair (BMA/lim comonomers), both reactivity ratios were much greater than 1 for the low conversion case (instantaneous). In fact, r_{32} was estimated at 100.00 from three consecutive assessments. As explained previously (in Section 5.2.1.1), this is a numerical artefact, where the parameter has reached the ‘upper bound’ of the estimation program. However, the consistency of this result invites further investigation.

It is our understanding that the $r_{32} = 100.00$ result is due to the ill-conditioned nature of the terpolymer system. Physically, we can explain it as follows: The limonene incorporation is very low at low conversion levels, such that k_{32} (the rate constant for terminal limonene radicals adding BMA monomer units) is tending to 0. Given the reactivity ratio definition, $r_{32} = k_{33}/k_{32}$, and as $k_{32} \rightarrow 0$, $r_{32} \rightarrow \infty$. With this logic, we can explain the observation that r_{32} is continually hitting the upper bound of the estimation program.

Table 5.5: Reactivity Ratio Estimates for Terpolymerization of BA(1)/BMA(2)/lim(3) with Supplemental Data (Experimental Data from [134] and Simulated Data from Current Work)

| | r_{12} | r_{21} | r_{13} | r_{31} | r_{23} | r_{32} |
|--|----------|----------|----------|----------|----------------|---------------|
| Reported by Ren et al. [134] | 0.46 | 2.008 | 6.08 | 0.007 | 6.096 | 0.046 |
| Current Study (EVM Estimation with Experimental and Simulated Low Conversion Data) | | | | | | |
| Inst. Estimation (A) | 0.3663 | 1.4317 | 7.5324 | 0.1003 | 10.1289 | 100.00 |
| Inst. Estimation (B) | 0.3662 | 1.4317 | 7.5293 | 0.1004 | 10.1307 | 100.00 |
| Inst. Estimation (C) | 0.3663 | 1.4317 | 7.5324 | 0.1003 | 10.1289 | 100.00 |
| Current Study (EVM Estimation with Experimental and Simulated Full Conversion Data) | | | | | | |
| Cum. Estimation (A) | 0.3009 | 2.4961 | 6.5236 | 0.0009 | 8.1873 | 0.0106 |
| Cum. Estimation (B) | 0.3167 | 1.9085 | 5.7962 | 0.0017 | 5.9647 | 0.0087 |
| Cum. Estimation (C) | 0.2876 | 1.5613 | 8.5751 | 0.0315 | 7.7202 | 0.1240 |

In contrast, the cumulative analysis (which uses the composition data, both experimental and simulated, over the full conversion range) gives more stable results. Specifically, the estimation results show that $r_{32} < 1$. Clearly, supplementing the terpolymerization data set with optimal formulations (as per the EVM framework) significantly improves the stability and trustworthiness of ternary parameter estimates. Ideally, even more experimental data would be collected for the lim-rich system to offset the error associated with low limonene incorporation.

5.2.2 Improved Performance with Ternary Data

The above examples present a variety of challenges: data sets with low information content or ill-conditioned systems (with reactivity ratios of different orders of magnitude) can make estimation difficult. If the estimation steps are unstable, then one does not have confidence in the final estimates. Unfortunately, even with many data points, researchers do not always have all the required information. Therefore, design of experiments for reactivity ratio estimation is key!

In the cases that follow, we present some case studies that highlight the advantages of analyzing terpolymerization data directly using ternary reactivity ratio estimation. All three case studies were originally modelled using analogous binary reactivity ratios; the terpolymerization data have been revisited and reanalyzed.

5.2.2.1 Case Study: BA/MMA/EHA

A recent study by Gabriel and Dubé [137] investigated the terpolymer of butyl acrylate (BA; monomer 1), methyl methacrylate (MMA; monomer 2) and 2-ethylhexyl acrylate (EHA; monomer 3), which is a material of interest for pressure sensitive adhesives. First, the authors determined the reactivity ratio pairs for two of the associated copolymers (BA/EHA and MMA/EHA), and subsequently used these binary reactivity ratios, along with literature values for the BA/MMA

reactivity ratios, to predict terpolymer composition. The terpolymer model prediction (using binary reactivity ratios) showed good agreement with the collected data, as described in the original work [137].

In spite of the good results achieved using binary reactivity ratios, ternary reactivity ratio estimation directly from terpolymerization data presents some additional advantages. First, consider the experimental load: rather than nine experimental runs described by Gabriel and Dubé [137] (and additional prior work for estimating the BA/MMA reactivity ratios [63]), only three different feed compositions are required. Since Gabriel and Dubé [137] selected ternary feed compositions according to the EVM ‘rule-of-thumb’ for ternary reactivity ratio estimation [60], their data can be used to re-estimate reactivity ratios directly from terpolymerization data.

First, only the low conversion data were used for an instantaneous analysis. Now, because these data points were collected for model validation (not necessarily parameter estimation), only 7 data points are available below 20% conversion. These data were used for ternary reactivity ratio estimation using the recast Alfrey-Goldfinger equation (recall Equations 2.31 to 2.33) and EVM (Equations 2.42 to 2.44). There are two observations of note here: (1) the estimation is stable, much more so than the case studies presented in Section 5.2.1, and (2) the estimation is symmetrical. That is, regardless of which monomer is defined as monomer 1, monomer 2 or monomer 3, the estimated parameters are the same. As an example, two variations are shown below and compared to the original (binary) estimation. Here, reactivity ratios are labelled according to the monomer name (rather than monomer number) for further clarity. Also, the colors shown in Table 5.6 are associated with the colors of the JCRs in Figure 5.13.

Table 5.6: Reactivity Ratio Estimates for Terpolymerization of BA/MMA/EHA from Low Conversion Data (Experimental Data from [137])

| | $\Gamma_{BA/MMA}$ | $\Gamma_{MMA/BA}$ | $\Gamma_{BA/EHA}$ | $\Gamma_{EHA/BA}$ | $\Gamma_{MMA/EHA}$ | $\Gamma_{EHA/MMA}$ |
|---|-------------------|-------------------|-------------------|-------------------|--------------------|--------------------|
| Reported by Gabriel and Dubé [137] (binary reactivity ratio estimates) | 0.34 | 2.02 | 0.99 | 1.62 | 1.50 | 0.32 |
| Inst. Estimation ($M_1/M_2/M_3 = BA/MMA/EHA$) | 0.41 | 1.49 | 1.21 | 8.52 | 0.81 | 0.36 |
| Inst. Estimation ($M_1/M_2/M_3 = MMA/EHA/BA$) | 0.41 | 1.49 | 1.20 | 8.45 | 0.81 | 0.36 |

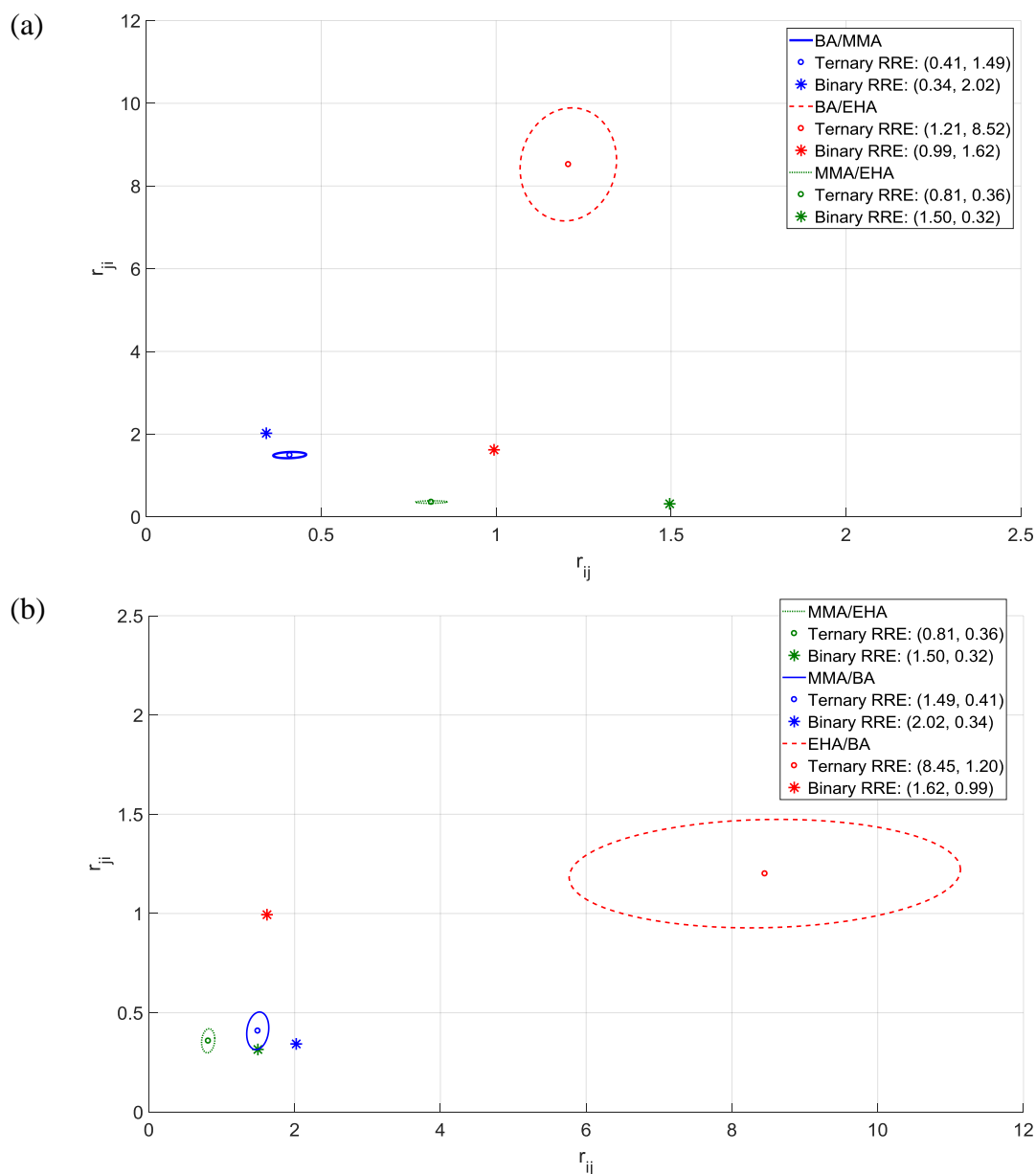


Figure 5.13: Ternary Reactivity Ratio Estimates for the Terpolymerization of BA/MMA/EHA for (a) $M_1/M_2/M_3 = \text{BA/MMA/EHA}$ and (b) $M_1/M_2/M_3 = \text{MMA/EHA/BA}$, with Instantaneous Data from [137]

In general, the ternary reactivity ratios follow the same trends as the original (binary) reactivity ratio estimates (that is, if $r_{ij} > r_{ji}$ for the binary case, the same relationship holds for the ternary case). However, $r_{\text{MMA/EHA}}$ falls below 1.00 when estimated directly from terpolymerization data. This suggests that $k_{\text{MMA/MMA}} > k_{\text{MMA/EHA}}$ in the binary case (homopropagation of MMA is preferable to cross-propagation of MMA and EHA), but that $k_{\text{MMA/MMA}} < k_{\text{MMA/EHA}}$ in the ternary case (homopropagation becomes dominated by cross-propagation of MMA/EHA).

Another notable difference is the significant error present for the BA/EHA system. This is shown in both plots (of Figure 5.13), as the JCR for BA/EHA is much larger than the other JCRs. This may be related to the absolute value of the parameter estimates. As shown in a recent study [6], uncertainty becomes much greater for larger parameter values. Since $r_{\text{EHA/BA}}$ is larger than the other reactivity ratio estimates (by as much as 20 times, in some cases), the same relative error (assumed to be 5% for this system) will have a much larger absolute value in $r_{\text{EHA/BA}}$ compared to the other parameter estimates. This behaviour has been described for the copolymer case [6], but the difference in parameter estimates was observed within a single JCR (that is, the elliptical JCR was stretched in the direction of the larger parameter estimate). In this, a terpolymer case, the JCR associated with the comonomer pair containing larger parameter estimates is greater in both directions. The absolute value of the error seems magnified, likely because most other reactivity ratio estimates for the system are around or below 1.00. Another item of note is that both reactivity ratios for the BA/EHA pair are again >1 ; this may be for the same reasons discussed earlier for the BA/BMA/lim system. An additional reason may be related to the fact that the copolymerization of BA and EHA may lead to branched molecule formation and even microgel formation, which would complicate analysis further.

Next, the full conversion data set is considered; ternary reactivity ratios can be estimated using the EVM and the cumulative terpolymerization model. All terpolymerization data from the original study [137] were used herein, and results are shown in Table 5.7 (and Figure 5.14). Again, the estimation is stable and symmetrical, which can be attributed to carefully designed data. As an aside, the estimation program also converged much more quickly; parameters were estimated in under an hour (on an Intel(R) Core™ i7-860 processor) compared to (on average) 50 hours of computation for the ill-conditioned system described earlier.

Table 5.7: Reactivity Ratio Estimates for Terpolymerization of BA/MMA/EHA from All Terpolymerization Data (Experimental Data from [137])

| | $r_{\text{BA/MMA}}$ | $r_{\text{MMA/BA}}$ | $r_{\text{BA/EHA}}$ | $r_{\text{EHA/BA}}$ | $r_{\text{MMA/EHA}}$ | $r_{\text{EHA/MMA}}$ |
|---|---------------------|---------------------|---------------------|---------------------|----------------------|----------------------|
| Reported by Gabriel and Dubé [137] (binary reactivity ratio estimates) | 0.34 | 2.02 | 0.99 | 1.62 | 1.50 | 0.32 |
| Cum. Estimation (M₁/M₂/M₃ = BA/MMA/EHA) | 0.41 | 1.60 | 2.01 | 7.59 | 0.74 | 0.35 |
| Cum. Estimation (M₁/M₂/M₃ = MMA/EHA/BA) | 0.41 | 1.60 | 2.06 | 7.66 | 0.74 | 0.35 |

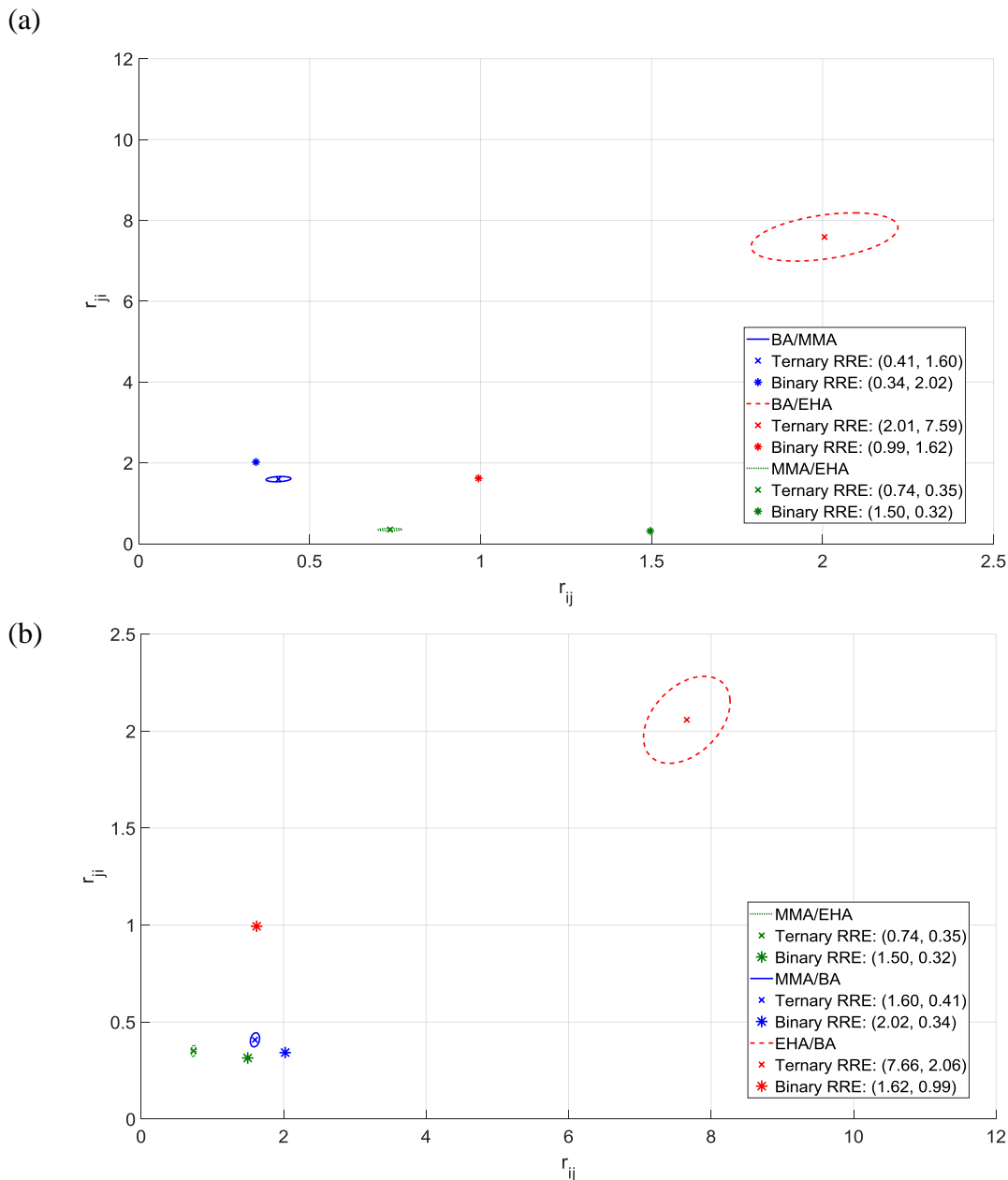


Figure 5.14: Ternary Reactivity Ratio Estimates for the Terpolymerization of BA/MMA/EHA for (a) $M_1/M_2/M_3 = \text{BA/MMA/EHA}$ and (b) $M_1/M_2/M_3 = \text{MMA/EHA/BA}$, with Cumulative Data from [137]

The values estimated using all terpolymerization data (full conversion) are similar to the results of the instantaneous parameter estimation (compare Table 5.6 to Table 5.7). Also, in comparing Figure 5.13 to Figure 5.14, the JCR areas are reduced when the full conversion data set is used for analysis (note that scales are the same for easy comparison of Figure 5.13a to Figure 5.14a and of Figure 5.13b to Figure 5.14b). This is in agreement with previous studies [54, 57] and makes sense physically. Since more experimental data are available for analysis (18 data points over all conversion levels instead of 7 low conversion data points), the uncertainty associated with the

parameter estimates is reduced. Also, since the instantaneous analysis used low conversion data up to 20%, the requisite assumption that no composition drift occurs may not be valid for all of the data [54]. Interestingly, a direct comparison of Figure 5.13 and Figure 5.14 shows little or no JCR overlap (between the instantaneous and cumulative analysis), in spite of the fact that trends remain consistent. Additional replication or sequential design of experiments could be used to further supplement this data set, as has been described for the previous case studies (recall Section 5.2.1).

As for the instantaneous case, the most error associated with the cumulative analysis is present in the BA/EHA comonomer pair, and both reactivity ratios are greater than 1 (which is physically unlikely for any given comonomer pair). Again, this is likely due to the large values of the parameter estimates, which translate to a higher absolute value of the error (since the same relative error is assumed for all experimental data and resulting parameter estimates). Also, as mentioned in the evaluation of the instantaneous results, other copolymerization mechanisms (branching, etc.) may be active specifically for the BA/EHA comonomer pair. However, without further analysis, no specific conclusions can be drawn about this system.

Finally, the prediction performance of these reactivity ratios can be evaluated (compared to the original binary reactivity ratio estimates). Since some of the more substantial differences in reactivity ratios were related to the EHA monomer (especially $r_{\text{EHA/BA}}$ and $r_{\text{MMA/EHA}}$), the model prediction for the EHA-rich terpolymer is of particular interest. The model predictions (using both binary and ternary reactivity ratios) and a comparison to the experimental data from Gabriel and Dubé [137] are shown in Figure 5.15. Only the prediction performance of the cumulative analysis (for ternary reactivity ratio estimation) is provided in Figure 5.15; despite slight differences between the instantaneous and cumulative analysis results, the model prediction performance was very similar for both sets of reactivity ratio estimates.

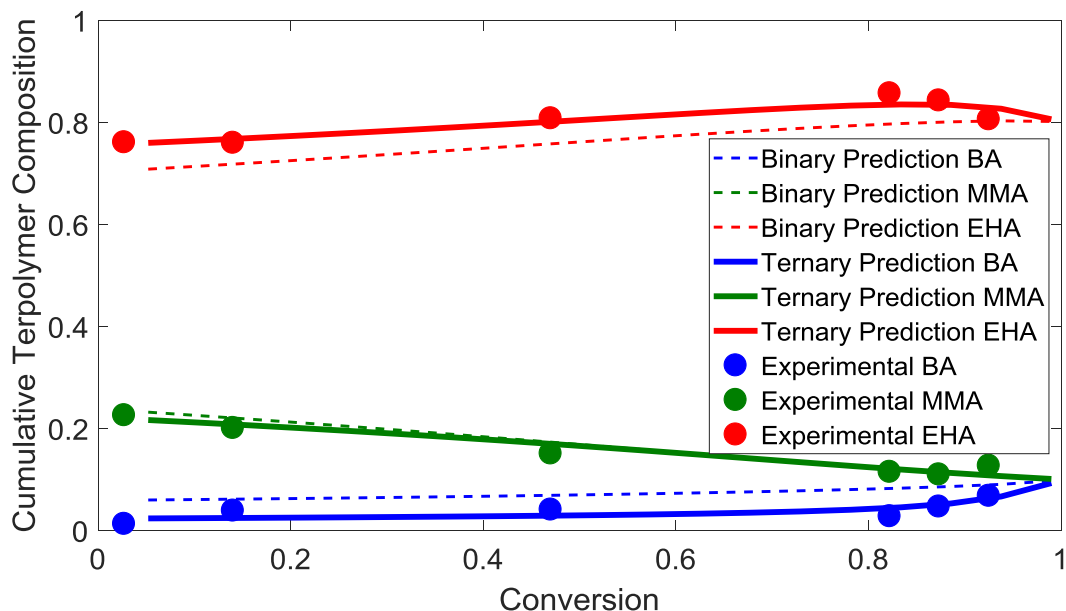


Figure 5.15: Prediction of Cumulative Terpolymer Composition for BA/MMA/EHA ($f_{BA,0}/f_{MMA,0}/f_{EHA,0} = 0.1/0.1/0.8$) (Experimental Data and Binary Predictions from [137])

A direct comparison reveals that while the binary predictions are acceptable, the ternary reactivity ratios further improve the prediction performance of the cumulative terpolymer composition model. In fact, a statistical comparison of the EHA-rich data (experimental data vs. the two model predictions) shows that using the ternary reactivity ratio estimates in the model leads to an 85% reduction in prediction error (total sum of square errors). Similar results were observed for the other terpolymer formulations, but are not shown herein for the sake of brevity. These differences in prediction performance may further be accentuated if the estimated reactivity ratios are used in the sequence length part of the model.

This case study has shown that when experiments are well-designed, ternary reactivity ratio estimates can be obtained from small(er) data sets. This allows for more resources to be directed towards careful replication and supplemental data collection. The results also suggest that binary and ternary reactivity ratio estimates may be similar when the comonomers have similar structures and the polymerization is not affected by solution properties. However, binary reactivity ratios are not always applicable to terpolymer systems (as has been shown recently [38, 57]). In this case, the binary reactivity ratios gave reasonable prediction performance, but the ternary reactivity ratios showed even better prediction performance based on fewer experimental data (and, hence, less effort overall).

5.2.2.2 Case Study: Sty/MMA/MA

A study by Schoonbrood et al. [128] looked at terpolymerization kinetics for the styrene/methyl methacrylate/methyl acrylate (monomer 1/monomer 2/monomer 3 = Sty/MMA/MA) terpolymer.

Again, according to standard practice, binary reactivity ratios (obtained from copolymerizations in the literature) were used to predict terpolymerization behaviour. During this study, only low conversion data were reported. At the time (1994), this was ‘best practice’, where low conversion (instantaneous) data were typically used for parameter estimation. Parameter estimation from cumulative composition data was not part of typical practice, especially with this more complex system of equations representing terpolymerization kinetics. Low conversion data allow for a computationally simpler parameter estimation process but require some assumptions about a lack of composition drift in the system [54].

The experimentally determined (assumed instantaneous) terpolymer compositions were compared to the model prediction. As reported in the original work, good agreement was observed between the predicted and measured values [128]. Given the available terpolymerization data, the recast Alfrey-Goldfinger model (with the EVM) can be used to re-estimate terpolymer reactivity ratios directly from terpolymerization data. The estimation is stable and symmetrical. A comparison of reactivity ratio estimates is presented in Table 5.8, and prediction performance is evaluated in Table 5.9.

Table 5.8: Reactivity Ratio Estimates for Terpolymerization of Sty(1)/MMA(2)/MA(3) (Experimental Data from [128])

| | r_{12} | r_{21} | r_{13} | r_{31} | r_{23} | r_{32} |
|---|----------|----------|----------|----------|----------|----------|
| Reported by Schoonbrood et al. [128] (binary reactivity ratio estimates) | 0.48 | 0.42 | 0.73 | 0.19 | 2.49 | 0.29 |
| Instantaneous Estimation (current work) | 0.57 | 0.51 | 1.82 | 0.20 | 2.49 | 0.23 |

Table 5.9: Comparison of Model Predictions for the Sty/MMA/MA Terpolymerization (Experimental Data and Original Predictions from [128])

| Feed Composition | | | Experimental Data | | | Original Predictions | | | Current (EVM) Predictions | | |
|------------------|-------------|------------|-------------------|-----------------|----------------|----------------------|-----------------|----------------|---------------------------|-----------------|----------------|
| $f_{sty,0}$ | $f_{MMA,0}$ | $f_{MA,0}$ | \bar{F}_{sty} | \bar{F}_{MMA} | \bar{F}_{MA} | \bar{F}_{sty} | \bar{F}_{MMA} | \bar{F}_{MA} | \bar{F}_{sty} | \bar{F}_{MMA} | \bar{F}_{MA} |
| 0.10 | 0.10 | 0.80 | 0.27 | 0.28 | 0.45 | 0.26 | 0.19 | 0.55 | 0.26 | 0.23 | 0.51 |
| 0.10 | 0.20 | 0.70 | 0.24 | 0.38 | 0.38 | 0.24 | 0.33 | 0.44 | 0.23 | 0.37 | 0.40 |
| 0.10 | 0.30 | 0.60 | 0.21 | 0.45 | 0.33 | 0.23 | 0.43 | 0.34 | 0.21 | 0.48 | 0.31 |
| 0.20 | 0.10 | 0.70 | 0.44 | 0.18 | 0.39 | 0.37 | 0.16 | 0.47 | 0.40 | 0.20 | 0.41 |
| 0.20 | 0.20 | 0.60 | 0.37 | 0.39 | 0.24 | 0.35 | 0.28 | 0.37 | 0.36 | 0.33 | 0.31 |
| 0.20 | 0.30 | 0.50 | 0.33 | 0.39 | 0.28 | 0.34 | 0.38 | 0.28 | 0.34 | 0.43 | 0.23 |
| 0.20 | 0.50 | 0.30 | 0.29 | 0.60 | 0.11 | 0.32 | 0.53 | 0.15 | 0.31 | 0.57 | 0.12 |
| 0.30 | 0.20 | 0.50 | 0.42 | 0.27 | 0.31 | 0.43 | 0.26 | 0.31 | 0.46 | 0.31 | 0.24 |
| 0.30 | 0.30 | 0.40 | 0.40 | 0.39 | 0.20 | 0.42 | 0.35 | 0.23 | 0.43 | 0.40 | 0.17 |
| 0.30 | 0.40 | 0.30 | 0.41 | 0.44 | 0.15 | 0.40 | 0.43 | 0.16 | 0.41 | 0.47 | 0.12 |
| 0.30 | 0.50 | 0.20 | 0.39 | 0.54 | 0.07 | 0.39 | 0.50 | 0.10 | 0.39 | 0.54 | 0.07 |
| 0.40 | 0.30 | 0.30 | 0.48 | 0.34 | 0.18 | 0.48 | 0.34 | 0.18 | 0.50 | 0.38 | 0.12 |
| 0.40 | 0.40 | 0.20 | 0.50 | 0.36 | 0.14 | 0.47 | 0.42 | 0.11 | 0.47 | 0.45 | 0.08 |
| 0.50 | 0.20 | 0.30 | 0.56 | 0.24 | 0.21 | 0.55 | 0.25 | 0.21 | 0.59 | 0.28 | 0.13 |
| 0.50 | 0.40 | 0.10 | 0.50 | 0.49 | 0.01 | 0.52 | 0.42 | 0.06 | 0.53 | 0.43 | 0.04 |
| 0.50 | 0.30 | 0.20 | 0.52 | 0.43 | 0.06 | 0.53 | 0.34 | 0.13 | 0.56 | 0.36 | 0.08 |

Although the prediction performance looks similar, the current (EVM) prediction shows a decrease in the sum of square errors for all three comonomer compositions, especially \bar{F}_{MMA} and \bar{F}_{MA} . In evaluating the total sum of square errors, the current work provides a 32% decrease in prediction error over the original analysis. To supplement this result, the residuals for both the original and current predictions can also be examined. As shown in Figure 5.16, the spread (that is, the vertical distance from 0) is reduced for the current predictions; residuals are smaller overall.

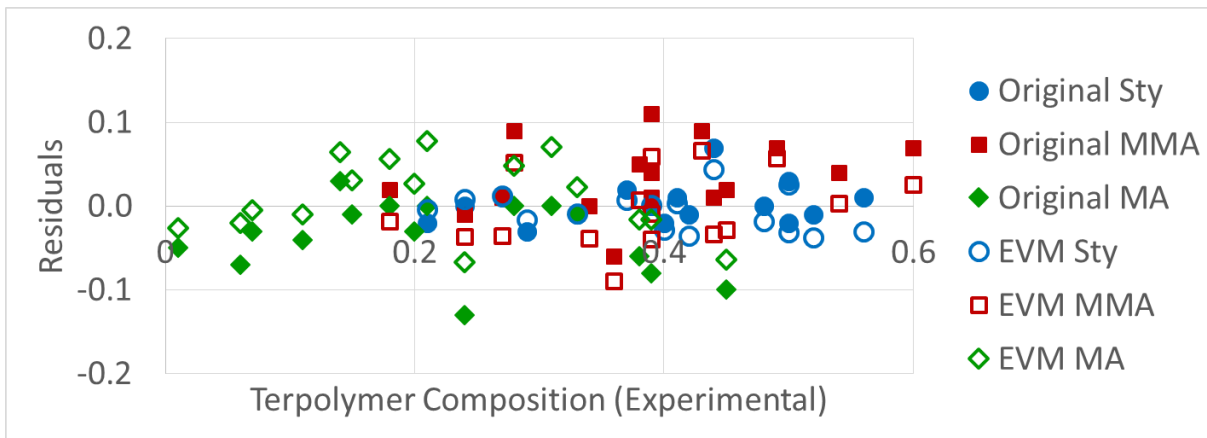


Figure 5.16: Comparison of Residuals for Sty/MMA/MA Terpolymer Composition Predictions

Given these results (and those discussed previously), there is clearly an advantage of estimating ternary reactivity ratios directly from terpolymerization data. If medium-high conversion data were available, they could have been used to supplement the data set or to reduce the number of experiments required. However, even with this low conversion data set, estimating ternary reactivity ratios directly from terpolymerization data is feasible and preferable to using binary data.

5.2.2.3 Case Study: AN/Sty/MMA

The terpolymerization of acrylonitrile (AN; monomer 1), styrene (Sty; monomer 2) and methyl methacrylate (MMA; monomer 3) studied by Brar and Hekmatyar [143] provides interesting experimental data. In addition to reporting terpolymer composition data, they also reported microstructural (triad fraction) information. Thus, there is potential to re-estimate the ternary reactivity ratios for AN/Sty/MMA and evaluate their ability to predict composition and sequence length distribution.

The original investigation used six experiments (no replication is mentioned) and the feed compositions selected provide a good amount of experimental information. As shown in the triangular diagram of Figure 5.17, there are three ‘outer’ formulations further along the outside of the triangle (designated with circles in Figure 5.17). Although (to the best of our knowledge) these were not statistically designed experiments, the fact that there is one formulation rich in each comonomer provides useful data for reactivity ratio estimation [60]. In fact, when reactivity ratios are estimated using only these three trials, parameter estimation results are as expected.

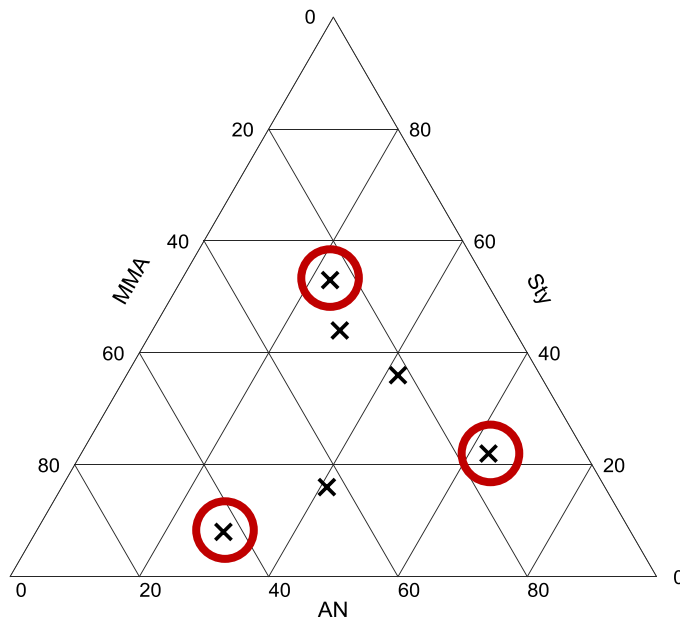


Figure 5.17: Terpolymerization Feed Compositions for AN/Sty/MMA (Data from [143])

Ideally, additional replication would be performed for all six formulations (perhaps even to higher conversion levels), but these results certainly represent carefully measured experimental (process) data (hence, good information content/lower experimental error), leading to a numerically stable estimation situation, thus ensuring that reactivity ratios can be successfully estimated even from a limited data set.

Figure 5.18 shows a comparison of estimation results from these three (more optimal) points to estimation results from the full (six) trial set. Clearly, the three ‘internal’ data points supplement the composition data, but do not significantly alter the reactivity ratio estimation results. Also, the ternary reactivity ratio estimates are in good agreement with previously reported binary reactivity ratios for associated copolymers.

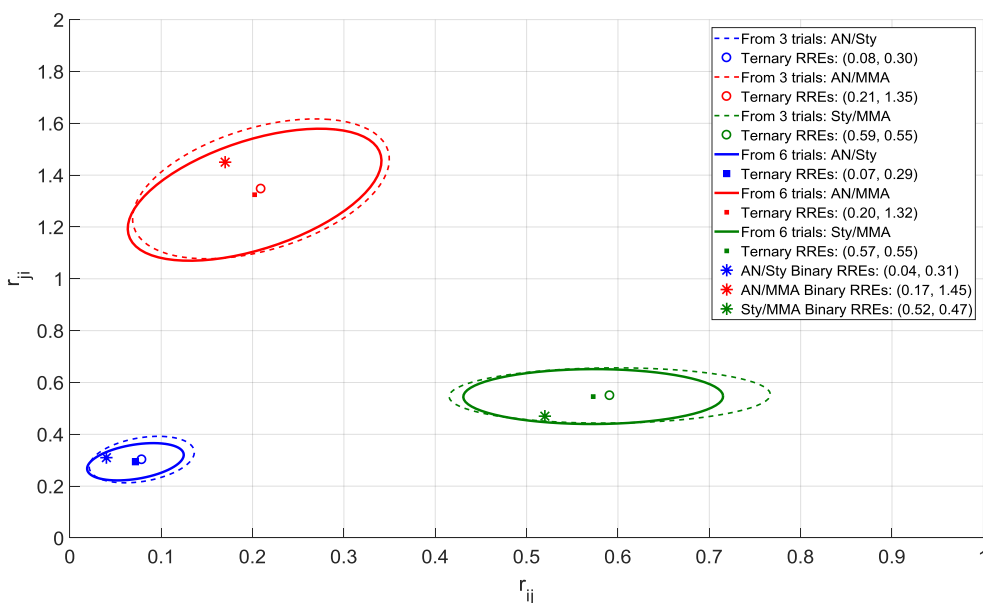


Figure 5.18: Ternary Reactivity Ratio Estimates (RREs) for the Terpolymerization of AN/Sty/MMA with Data from Brar and Hekmatyar [143]

For all three comonomer pairs, the binary reactivity ratios are within the JCRs for the ternary estimates. Thus, the prediction performance (for both terpolymer composition and microstructure) will be similar, regardless of which parameters are used. For the purposes of demonstration, analysis of the composition and microstructure of one terpolymer sample (experimentally determined by Brar and Hekmatyar [143]) is summarized in Table 5.10. Note that triad fractions are defined only by the first letter of the monomer name; for example, triad fraction ASM represents the AN-Sty-MMA triad sequence.

Table 5.10: Analysis of (a) Composition and (b) Microstructure for AN/Sty/MMA
(Experimental Data from [143])

(a)

| Monomer | Experimental [143] | Original prediction (from binary RREs) [143] | Current prediction (from ternary RREs) |
|---------|--------------------|---|---|
| AN | 0.30 | 0.28 | 0.30 |
| Sty | 0.48 | 0.48 | 0.48 |
| MMA | 0.22 | 0.24 | 0.22 |

(b)

| Triad | Experimental [143] | Original prediction (from binary RREs) [143] | Current prediction (from ternary RREs) |
|-------|--------------------|---|---|
| AAA | 0.01 | 0.01 | 0.00 |
| SAS | 0.69 | 0.73 | 0.63 |
| MAM | 0.03 | 0.00 | 0.03 |
| AAS | 0.06 | 0.04 | 0.06 |
| AAM | 0.01 | 0.00 | 0.01 |
| SAM | 0.20 | 0.22 | 0.27 |
| SSS | 0.05 | 0.05 | 0.05 |
| ASA | 0.21 | 0.25 | 0.27 |
| MSM | 0.08 | 0.08 | 0.06 |
| SSA | 0.27 | 0.22 | 0.24 |
| SSM | 0.16 | 0.12 | 0.12 |
| ASM | 0.23 | 0.28 | 0.26 |
| MMM | 0.05 | 0.04 | 0.04 |
| AMA | 0.05 | 0.02 | 0.03 |
| SMS | 0.42 | 0.40 | 0.39 |
| MMA | 0.04 | 0.06 | 0.07 |
| MMS | 0.21 | 0.26 | 0.26 |
| AMS | 0.23 | 0.22 | 0.21 |

5.2.3 Concluding Remarks on Terpolymer Troubleshooting Tips

Through a series of case studies, we have demonstrated with examples and counter-examples both the challenges and advantages of estimating ternary reactivity ratios directly from terpolymerization data. We highlighted some difficulties that may arise when studying multi-component polymerizations due to the nature of such systems and related experimental limitations. These limitations are usually translated to the paucity of experimental information content. The lack of sufficient information on polymer composition, combined with uncertain levels of experimental error (since independent replication is usually non-existent) usually leads to numerically ill-conditioned systems during the estimation steps. This in its turn results in a multiplicity of (and related confusion with) reactivity ratio values. Now, if the above already important limitations are superimposed to a lack of experimental design (i.e., the optimal selection

of feed compositions), the problem is compounded with the extra dimension of added pitfalls with the use of undesigned (happenstance) data.

When experimental design is employed right from the outset and is combined with appropriate parameter estimation techniques using carefully measured (and replicated) data, i.e., when every effort is made to make the terpolymerization system numerically ‘well-behaved’, then accurate and reliable estimates of ternary reactivity ratios can be obtained. The case studies examined gave examples of both instantaneous (low conversion) and cumulative (medium-high conversion) data analysis and demonstrated the advantages of using the cumulative model. Some systems exhibited similarities between the binary and ternary reactivity ratio estimates, and the predictions related to composition and triad fractions were improved.

In some other terpolymerization systems, the reactivity ratios of the binary copolymerization pairs do not apply to ternary systems [38]. Trying to predict terpolymerization behaviour from binary reactivity ratios can require making unfounded assumptions about system-specific polymerization kinetics. Researchers often assume that the presence of the third comonomer is exactly additive via simple superposition, hence the behaviour of the three comonomers is independent of each other. This is the main assumption, akin to assuming that interaction terms are non-existent in a model. Evaluating subsets of the experimental data collected (that is, comonomer pairs) to represent ternary systems can ultimately result in the oversimplification of complex processes. Using appropriate kinetic models can result in better prediction performance and a higher degree confidence in the resulting parameter estimates.

5.3 Concluding Remarks

In studying the terpolymerization kinetics of AMPS/AAm/AAC for the enhanced oil recovery application, it has been impossible to avoid these tangential topics. As described in Section 5.1, the widely accepted analogy between copolymerization and terpolymerization mechanisms is not always valid; reactivity ratios obtained for binary pairs (from copolymerization experiments) cannot blindly be used in models dealing with terpolymerizations. Using the binary-ternary analogy (even as an approximation) requires making considerable assumptions about the system. When binary reactivity ratios are used to describe ternary systems, the consequences may include substantial differences in reactivity ratio estimates, poor composition prediction performance, and incorrect determination of product (terpolymer) characteristics. As shown in this chapter (Section 5.1.2), the inadequacy of binary reactivity ratios for terpolymerization systems is especially true for the AMPS/AAm/AAC terpolymer. This may be a consequence of the solution effects described in Section 4.1, since the addition of a third comonomer can drastically affect the properties of the polymerizing solution.

We have also found it necessary to explore the challenges and advantages associated with estimating ternary reactivity ratios directly from terpolymerization data. Through our estimation work (and through collaborations with other research groups including Yousefi et al. [144]), we have discovered the importance of carefully collected and well-behaved data. Although some adjustments can be made to make use of historical data, there is no substitute for experimental data collected specifically for ternary reactivity ratio estimation. Overall, and as demonstrated in this work [136], ternary reactivity ratio estimation directly from terpolymerization data can provide improved understanding about a complex terpolymer system. Dealing for the first time with a completely unknown terpolymerization system, the current approach offers, if nothing else, a systematic and ‘safe’ approach to accumulating experimental evidence (about the system in question) in fewer experimental trials and hence less experimental effort, but with reliable parameter estimates which can be fine-tuned further later, as one becomes more familiar with the terpolymerization system in a sequential-iterative-optimal manner.

Chapter 6. Literature Background for Case Study #2 – *Polymeric Sensing Materials*

6.1 Polymeric Sensing Materials for Detection of Acetone

Diabetes mellitus, generally called diabetes, is a series of metabolic diseases in which the affected persons experience high blood sugar levels over long periods of time. Type 1 diabetes is caused by the pancreas' inability to produce enough insulin, whereas type 2 diabetes stems from an insulin resistance, which typically builds up over time. According to the most recent report by the International Diabetes Federation, 1 in 11 adults have diabetes (approximately 415 million people worldwide) and 46.5% of those adults are undiagnosed [145]. This organization estimates that a person dies every 6 seconds from diabetes; this may be influenced by the fact that an estimated 75% of people with diabetes live in low- and middle-income countries.

Diabetes research and treatment is very well developed in North America. Diagnosis typically involves taking blood samples to measure blood glucose concentration either (a) after fasting, or (b) two hours after a 'glucose load' [146]. Depending on whether a person has type 1 or type 2 diabetes, it can generally be controlled using insulin injections (type 1) or diet, exercise and medication (type 2). However, there is still a need for low cost, fast responding diagnosis and treatment methods, especially for developing countries.

When blood glucose levels are high, a person's breath often smells sweet. This is largely due to elevated levels of ketones (namely acetone, acetoacetate and 3- β -hydroxybutyrate) that are produced as an alternative energy source, since the body cannot process the glucose that is present (this is a result of low insulin or insulin resistance). All three of the ketones listed above will increase in concentration, but acetone is by far the most volatile. Thus, it can be detected in a person's breath or skin much more easily than acetoacetate or 3- β -hydroxybutyrate [147].

6.1.1 Existing Materials and Methods

Over the past 60 years, a variety of studies have been performed in an attempt to link breath acetone concentration to blood glucose levels. In effect, over 40 different investigations (involving over 3,000 human subjects) have confirmed that breath acetone concentration can be used as a biomarker for diabetes mellitus [148]. In general, type 1 diabetics have shown significantly higher breath acetone concentrations when compared with a (non-diabetic) control group and with type 2 diabetics. For example, in an early study, Rooth and Ostenson [149] measured 4.42 ± 0.71 $\mu\text{g/L}$ in type 1 diabetes patients ($n = 49$), which is much higher than the 1.10 ± 0.88 $\mu\text{g/L}$ observed in the control group ($n = 67$) and 1.70 ± 0.23 $\mu\text{g/L}$ observed in type 2 diabetics ($n = 20$). Similarly, Tassopolous et al. [150] studied the relationship between blood glucose levels and breath acetone concentration, specifically for insulin-treated type 1 diabetics. Their group found that patients with

higher blood glucose levels had much higher breath acetone levels; breath acetone increased (though not entirely linearly) from $1.90 \pm 0.16 \mu\text{g/L}$ to $7.49 \pm 4.90 \mu\text{g/L}$ as blood glucose increased from 51 mg/100 mL to 450 mg/100 mL (patients were divided into four blood glucose level groups, or bins). Other similar studies have shown consistent results (see [148] for a detailed review).

The relationship between breath acetone and type 2 diabetes has also been studied by several groups (see, for example, [151-155]), but a consensus about the trends observed has not yet been reached. Only Deng et al. [151] observed a noticeable difference between the breath acetone concentration of the control group and the type 2 diabetic group (the type 2 diabetic group had consistently higher breath acetone concentration). In most cases, though, there was no significant statistical difference between the breath acetone concentration of the (non-diabetic) control group and the type 2 diabetes group. That being said, increasing acetone breath concentration with increasing blood glucose levels was still observed, as per the type 1 diabetes studies [153, 155].

Two groups have also investigated the relationship between skin acetone concentration and blood glucose. Yamane et al. [156] reported that skin acetone levels were much higher for diabetic test subjects (188 ± 7 ppb, $n = 63$) compared to the control group (87 ± 10 ppb, $n = 32$), and that one patient with ketoacidosis (which is an extreme case that may lead to diabetic coma) had a skin acetone level of 940 ppb. Although their study did not distinguish between type 1 and type 2 diabetics, they found that there was a positive correlation between fasting skin acetone and blood glucose for subjects that used insulin therapy (which are most likely type 1 subjects). In the same way, Turner et al. [157] analyzed five non-diabetic test subjects and found that skin acetone levels increased with breath acetone concentration. Also, both measurements seemed to be somewhat correlated with blood glucose levels.

Increased acetone concentration within the human body can be exploited to develop non-invasive detection techniques for the diagnosis (and potential control) of high blood glucose levels experienced by people with diabetes. Several groups have recently investigated the possibility of using metals and metal oxides as breath acetone sensors, with some success (see Table 6.1, Part A). There have also been a handful of studies done that involved polymeric sensing materials and sensing arrays (see Table 6.1, Part B), but there is still room for improvement. In what follows, design principles (as per [4, 5]) will be used to develop polymeric sensing materials with optimal properties. Polymeric sensing materials typically provide better selectivity than metals and metal oxides [3] and have the added advantage of customization or tailorability.

Table 6.1: Breath Acetone Detection Studies; Summary of Sensing Materials

| Ref. | Sensing Material (and dopant, if applicable) | Sensor Type | Detection Limit | Selectivity |
|--|--|--|-------------------------|--|
| Part A: Metals and Metal Oxides | | | | |
| [158] | Sb-doped SnO ₂ | Resistive | 65.3 ppm | EtOH (1062.5); CO ₂ (27840) |
| [159] | Multi-walled carbon nanotubes with TiO ₂ | Resistive | 1 wt% | -- |
| [160] | Ga ₂ O ₃ nanowires with and without pyruvic acid (PA) | Capacitive | 304 ppm | Nitromethane (very poor with PA); Triethylamine (good selectivity in both cases, better without PA; no numerical values available) |
| [161-163] | Si-doped WO ₃ nanoparticle films | Resistive | 20 ppb | EtOH (4.7 – 6.7) [161] EtOH (8.0 – 16) [162] EtOH, MeOH, isoprene (cannot be calculated) [163] |
| [164] | Pt-doped WO ₃ nanofibres | Resistive | 1 ppm | H ₂ S (0.053) |
| [165] | Pure and Pt-doped SnO ₂ | Resistive | 120 ppb | Pure: Toluene (1.0 – 18); Pt-doped: Toluene (1.0 – 2.7) |
| [166] | WO ₃ microspheres | Resistive | 100 ppm | H ₂ S (2.8); EtOH (2.3); NH ₃ (3.2); NO ₂ (7.3); H ₂ (4.8) |
| [167] | Pt-doped WO ₃ hemitubes | Resistive | 120 ppb | H ₂ S (1.9 – 8.4); Toluene (6.5 – 12.5); EtOH (very high, data not reported) |
| [168] | 'Bumpy' WO ₃ hemitubes (via O ₂ plasma surface mod.) with functionalized graphene | Resistive | 100 ppb | H ₂ S (0.36); EtOH (3.4); NH ₃ (3.9); NO (5.0); CO (6.2); pentane (6.2) |
| [169] | SnO ₂ nanofibres with reduced graphene oxide nanosheets | Resistive | 100 ppb | H ₂ S (2.1); EtOH (4.3); Toluene (7.5); NH ₃ (10.0); CO (10.0) |
| [170] | Nanostructured ZnO film | Resistive | 80 ppm | EtOH (0.50 – 0.75) |
| [171] | SnO ₂ / reduced graphene oxide composite | Resistive | 10 ppm | -- |
| Part B: Polymeric Sensing Materials | | | | |
| [172] | PPy/PMMA blend doped with α -naphthalene sulfonate | Resistive | Saturated (30.3 vol. %) | Acetic Acid (3.9) |
| [173] | PPy sensor arrays: 4 sensing materials varying in thickness & resistance | Resistive | 50 ppm | EtOH S1: 0.95 – 1.4; S2: 1.0 – 1.6 S3: 1.2 – 1.6; S4: 0.93 – 1.3 |
| [174] | 3-enzyme system: secondary alcohol dehydrogenase (s-ADH), lactate dehydrogenase (LDH), pyruvate oxidase (PO) | Amperometric (via formation of H ₂ O ₂) | 0.2 ppm | Good selectivity for ethanol; poor selectivity for 2-pentanone, 3-pentanone, 2-butanone and acetaldehyde (data not reported) |
| [175] | Polyepichlorohydrin (PECH); 2 sensing materials varying in thickness | Mass-based (QCM) | 0.16 ppm | Dimethyl methyl phosphonate (S1: 2.1, S2: 5.2); EtOH (S1: 4.7, S2: 6.3); Hexane (S1: 3.7, S2: 6.8) |

| | | | | |
|--|---|------------------|--|---|
| [176] | PPy deposited by chemical oxidation-casting (COC) or CVD; PPy(COC) doped with α -naphthalene sulfonate | Resistive | PPy(COC): 2983 pm PPy(CVD): 6010ppm | |
| [176] | PANI/PMMA and PANI deposited by chemical oxidation-casting (COC) or impregnated oxidation (IO); PANI/PMMA (COC) doped with ClO_4^- and SO_4^{2-} | Resistive | PANI/PMMA (COC): 132 ppm PANI(IO): 29 ppm | For PANI/PMMA(COC): O_2 , CO_2 , H_2O (cannot be calculated) |
| [177] | NADPH-dependent carbonyl reductase enzyme and Nafion ($\text{C}_7\text{HF}_{13}\text{O}_5\text{S}\cdot\text{C}_2\text{F}_4$) | Amperometric | Enzyme showed no improvement over bare electrode; Nafion showed better response (still quite poor) | For Nafion: EtOH (1.2); Formaldehyde (1.7); MeOH (0.72); NH_4OH (0.34) |
| [178] | Chitosan | Resistive | 0.1 ppm | MeOH (1.2 – 2.0) |
| [179] | OV-275 and P25DMA doped with NiO | Capacitive | 625 ppm for both | Benzene OV-275: 6.7; P25DMA: 0.26 |
| [180] | Polyvinylidene fluoride hexafluoro-propylene (PVDF-HFP) composite sensors with carbon black (C65); S1: PVDF-HFP/C65 S2: multilayer with PVDF-HFP and PVDF-HFP/C65 S3: PVDF-HFP/C65/CNT | Mass-based (QCM) | 42 ppm for all 3 | Ethanol (S1: 9.4, S2: 10.1, S3: 6.0) Isoprene (S1: 17.5, S2: 11.5, S3: 11.9) 2-ethylhexyl acetate (good selectivity, cannot be calculated) |
| Abbreviations: α -NS ⁻ = α -naphthalene sulfonate; C65 = carbon black; CNT = carbon nanotube; COC = chemical oxidation casting; CVD = chemical vapour deposition; DMMP = dimethyl methyl phosphonate; EtOH = ethanol; IO = impregnated oxidation; LDH = lactate dehydrogenase; MeOH = methanol; NADPH = nicotinamide adenine dinucleotide phosphate; OV-275 = highly polar siloxane-based polymer; P25DMA = poly(2,5-dimethyl aniline); PA = pyruvic acid; PANI = polyaniline; PECH = polyepichlorohydrin; PMMA = poly(methyl methacrylate); PO = pyruvate oxidase; PPy = polypyrrole; PVDF-HFP = polyvinylidene fluoride hexafluoropropylene; QCM = quartz crystal microbalance; s-ADH = secondary alcohol dehydrogenase | | | | |

6.1.2 Application Requirements

First, it is important to distinguish between sensing materials and sensors. Sensing materials are the materials that interact with the target analyte (in this case, acetone) through either adsorption or absorption. Adsorption occurs when the gas molecules adhere to the surface of the sensing material, whereas absorption occurs when the gas molecules diffuse into the sensing material. The two most common families of sensing materials are metals and metal oxides, and polymeric

sensing materials. As mentioned previously, most sensing materials used in the field of breath acetone detection have been metals and metal oxides, but some polymeric materials have been used. A summary of these studies has been presented in Table 6.1.

Simply put, sensors are devices that convert non-electrical inputs (physical or chemical) into an electrical output signal (that is a quantifiable response). Three of the most common types of sensors are resistive, capacitive, and mass-based sensors (microcantilevers). Resistive sensors rely on changes in conductivity, normally achieved through the sorption (that is, adsorption or absorption) of the target material onto a sensing material. Metals and metal oxides have historically been used in resistive sensors, but conductive polymers such as polyaniline (PANI) and polypyrrole (PPy) have also been employed successfully (see, for example, the acetone sensing case described by Do and Wang [176]). Capacitive sensors also rely on electrical properties, as the charge-storing ability of the sensing material changes with sorption. If absorption occurs, the sensing material will swell, causing a change in capacitance. Alternatively, if adsorption occurs, the dielectric permittivity of the sensor changes, which also causes a capacitance change. Finally, as the name suggests, mass-based sensors measure changes in mass that occur during sorption; two commonly used mass-based sensors are quartz crystal microbalance (QCM) and microcantilever sensors.

6.1.2.1 Polymer Properties

In the case of polymeric sensing materials, homopolymers or polymer blends are typically used. Therefore, several design considerations (including glass transition temperature, crystallinity, morphology, and the sensing mechanism) should be considered to create tailor-made polymers for the specific application.

The operational temperature dictates what kind of material can be used, or rather eliminates some preliminary options. The glass transition temperature (T_g) of the material is usually preferred to be above the operational temperature of the sensor. If the sensor is to be used repeatedly, mechanical stability should also be considered.

The crystallinity of the sensing material, the surface morphology and the degree of incorporation of any dopants used should also be considered. The influence of these characteristics on the sensor response is not very well studied, as it depends on the specific sensing material and the sensor. However, Sengupta et al. [181] reported that reduced crystallinity in acid-doped PANI (especially at high acid concentration) resulted in reduced conductivity. This observation is in line with a recent ethanol sensing study, in which Stewart [182] reported that poly (2,5-dimethyl aniline) (P25DMA) with lower crystallinity sorbed less of the target analyte.

Surface morphology is a difficult characteristic to quantify, but is very important for sensing materials. Ultimately, the goal is to use thin films, nanorods or nanoparticles to maximize the surface area to volume ratio of the polymer. The morphology of the sensing material is largely

dependent on the synthesis technique used, but surface modification techniques are also fairly common. The degree to which dopants are incorporated into the sensing material (which depends on dopant concentration during synthesis and on dopant/polymer interactions) also affects surface morphology. An additional influence is deposition technique (onto the actual sensor), which is currently beyond the scope of this work.

Finally, and perhaps most importantly, the type of functional groups on the target analyte (here, acetone) must be considered. According to the literature [4], the polarity and the capability for hydrogen bonding should be exploited when selecting a sensing material for ketones. Also, the two lone electron pairs on the oxygen act as a Lewis base, which means that sensing materials that behave as Lewis acids have significant potential. Common electron pair acceptors include NH_4^+ , metal cations, and trigonal planar species like BF_3 and CH_3^+ .

6.1.2.2 Application-Specific Properties

The main evaluation of potential sensing materials depends on their sensing characteristics, namely sensitivity and selectivity. These properties will be described in some detail in what follows.

The sensitivity of a sensor (or sensing material) is related to the lowest discernible concentration that can be measured. Lower concentrations are preferable, indicative of a sensitive sensor or sensing material. In the case of an acetone sensor, the required sensitivity will depend on the source of the analyte being detected. It has been reported previously that breath acetone ranges from 148 ppb to 2744 ppb, and in an extreme case has reached 20 ppm [147]. This gives a general idea of the sensitivity that would be required for breath acetone concentration studies.

A quantifiable measure of sensitivity is the limit of detection, which is the lowest possible signal that can be detected without being influenced by experimental noise. Assuming that a reasonable signal-to-noise ratio is 3, the detection limit can be calculated according to Equation 6.1:

$$\text{Detection Limit} = 3 \times [\text{Response}]_{\text{Noise}} \quad 6.1$$

The challenge is to find materials that have a strong affinity towards the target analyte (that is, show high levels of sorption compared to other materials), but that can also sorb low concentrations (this is the sensitivity aspect). In the current work, the focus is to find materials with a strong affinity toward acetone (therefore, high sorption), with the assumption that materials with high affinity can sorb small quantities. To establish the detection limit, trials at lower gas analyte concentrations would be required.

Another significant property of sensing materials is the selectivity for a given analyte (here, acetone). Selectivity measures how much the sensing material favours acetone over other possible interferents (at equal concentrations), and can be calculated using Equation 6.2.

$$Selectivity = \frac{Acetone_{sorbed}}{Interferent_{sorbed}} \quad 6.2$$

This is an extremely important consideration for this application, since over 3,500 chemical species are present in human breath [183]. Some of the main components that may be considered as interferents (largely due to their concentration in exhaled breath) are nitrogen, oxygen, carbon dioxide, water, ammonia, hydrogen sulfide and carbon monoxide. Of these, the presence of water (that is, the humidity effects on the sensor) will likely be the most problematic. Other, less concentrated interferents include nitric oxide, ethane, pentane, isoprene, methanol, ethanol, acetonitrile, xylene and benzene; some of these are related to whether or not the person in question is a smoker [184]. The most influential interferents for this system will depend on relative concentrations in the human body, and on the structural similarities to acetone. Ultimately, for the interferents studied, the selectivity toward acetone should be as high as possible.

6.1.3 Backbone Selection

Ashby and Johnson's design principles [46] rely on analysis, synthesis, similarity or inspiration. The analysis aspect is extremely important here; the relationship between the target analyte (and any interferents) and the sensing material needs to be carefully considered. Selection by similarity can also be employed, as the literature can be used as a starting point for this and future investigations.

Since acetone has the capacity to hydrogen bond, sensing materials that will promote hydrogen bonding are desirable. Therefore, it may be necessary for the backbone to contain –NH groups or –OH groups. For example, polyaniline or polypyrrole may promote sorption to –NH groups, while poly (vinyl alcohol) or poly (acrylic acid) may promote acetone sorption to –OH groups. However, interferents including water and alcohols also have the ability to hydrogen bond, which may limit the selectivity of the sensing material.

One of the recommended techniques for selecting a sensing material is to examine the solubility parameters of the target analyte and the potential sensing materials. Solubility parameters take many material properties into account, which can help predict both solubility and sorption potential. If the solubility parameters for the analyte and the sensing material are close in value, this indicates that the materials are likely to interact. Table 6.2 presents the solubility parameters of the target analyte (acetone), as well as the solubility parameters of some potential interferents. The table also includes sensing materials of interest, some of which will be discussed further in what follows.

Table 6.2: Hildebrand Solubility Parameters for Target Analyte, Interferents, and Potential Sensing Materials (from [185] unless otherwise stated)

| Analytes | δ (MPa ^{1/2}) | Sensing materials | δ (MPa ^{1/2}) |
|-----------------|--------------------------------|----------------------------------|--------------------------------|
| Acetone | 20.3 | Poly(acrylic acid)* | 18.0 – 21.3 |
| Acetic Acid | 20.7 | Polyaniline* [186] | 22.2 |
| Benzene | 18.8 | Polyisoprene | 16.2 – 20.5 |
| Chloroform | 19.0 | Poly(methyl acrylate) [187] | 19.9 – 21.3 |
| Dichloromethane | 19.8 | Poly(methyl methacrylate)* [187] | 18.6 – 26.2 |
| Ethanol | 26.0 | Polypyrrole* [188] | 25.2 |
| Ethyl Acetate | 18.6 | Poly(vinyl acetate) | 18.0 – 22.6 |
| Hexane | 14.9 | Poly(vinyl alcohol)* [187] | 25.8 – 29.1 |
| Methanol | 29.7 | Poly(vinyl chloride) | 19.2 – 22.1 |
| Toluene | 18.2 | | |
| Water | 47.9 | | |

This preliminary (and very general) assessment suggests that any number of polymeric materials are compatible in terms of solubility. However, solubility parameters should only be used as a general ‘rule-of-thumb’, and should not be approached without critical thought. As mentioned previously, the glass transition temperature (T_g) of the sensing material is extremely important. Poly(vinyl acetate), for example, has a very promising range of solubility parameters relative to acetone. However, the T_g for PVAc is only around 30-35°C [185], which means that it will not be glassy at the operational temperature (human breath is generally around 35°C). Thus, it should not be considered as a candidate for breath acetone sensing.

In what follows, five sensing materials (selected based on previous use in the literature and anticipated performance, marked with a * in Table 6.2) will be reviewed in more detail.

6.1.3.1 Polyaniline

Polyaniline (PANI; $T_g = 100^\circ\text{C}$) is one of the most widely used sensing materials, largely due to its versatility. In fact, five different oxidation states of polyaniline exist, as shown in Figure 6.1. Emeraldine is the most stable form, but any form can be obtained through oxidation or reduction reactions (note that leucoemeraldine is fully reduced, whereas pernigraniline is fully oxidized) [189].

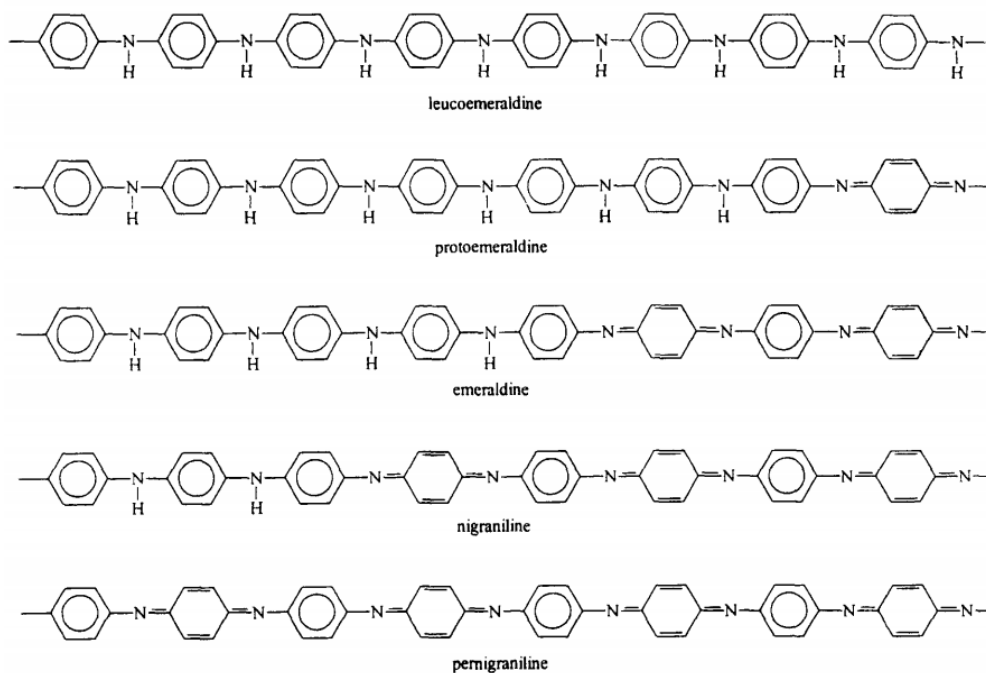


Figure 6.1: Five Oxidation States of PANI (from [189])

Although none of the above forms are conductive, one of the advantages of PANI is that it can be made conductive by protonic acid doping. Essentially, in an acidic (or salt) form, polyaniline becomes conductive without the addition or removal of electrons. A schematic highlighting the two forms of emeraldine is shown in Figure 6.2.

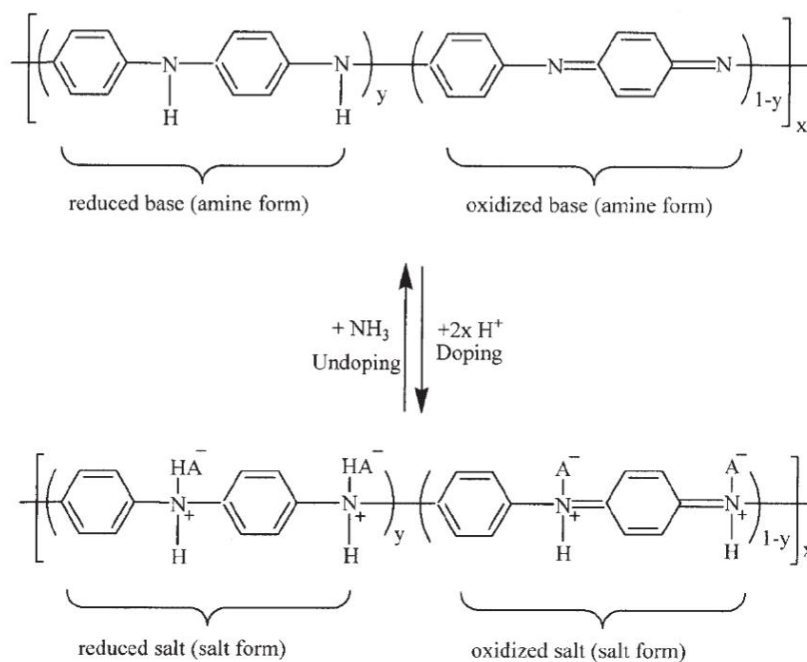


Figure 6.2: Conductive and Non-Conductive Forms of PANI (from [190])

In Figure 6.2, the upper scheme is the ‘undoped’ basic form, which is non-conductive. Conversely, the lower scheme is the ‘doped’ acidic (or salt) form, which is conductive. The doped form of PANI can be achieved by modifying the basic form, or the more common ‘self-doping’ technique can be performed by adding acid to the pre-polymerization recipe in the synthesis phase [190]. The effect of acids in polyaniline synthesis will be discussed further in Section 6.1.4.2.

Previously, PANI has been used to detect several target species besides acetone [176], including ammonia, benzene, carbon monoxide, chloroform, ethanol, hydrogen, hydrogen sulfide, methanol, nitrogen dioxide, toluene, water and xylene [191]. While this may seem like it could cause problems with selectivity, it actually demonstrates the versatility of PANI as the backbone of various tailored sensing materials. PANI can be doped with acids or metal oxides to improve sensing properties like sensitivity and selectivity (this will be discussed further in Section 6.1.4).

Alternatively, derivatives of PANI like poly (*o*-anisidine) (PoANI) and poly (2,5-dimethyl aniline) (P25DMA) can be used. These derivatives maintain many of the desirable sensing characteristics of polyaniline, but also have some improved features like better solubility and processability (due to less dense packing) [182]. A schematic comparing PANI to PoANI and P25DMA is presented in Figure 6.3.

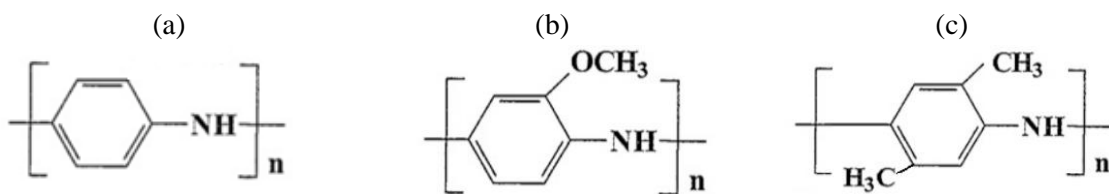


Figure 6.3: Polyaniline and Sample Derivatives (a) PANI, (b) PoANI and (c) P25DMA

These derivatives have recently been investigated for ethanol sensing [182], but could also be tailorable for the detection of other gas analytes. Specific customization techniques will be discussed in Section 6.1.4.

6.1.3.2 Polypyrrole

Polypyrrole (PPy; $T_g = 270^\circ\text{C}$) has also been used in sensing materials, mainly due to its conductive nature. Other favourable characteristics include its strong absorptive properties towards gases and its ability to perform at room temperature [192]. As shown in Table 6.1, it is perhaps the most frequently used polymeric material for acetone detection. Ruangchuay et al. [172], Yu et al. [173], and Do and Wang [176] all chose to use various forms of polypyrrole to construct their acetone sensing materials for resistive sensors.

The structure of PPy is similar to that of PANI, since it contains an –NH group (which promotes hydrogen bonding) and an aromatic ring. It is often produced either by chemical (redox) initiation or by electrochemical activation; both of these techniques have advantages and disadvantages [192]. Chemical polymerization allows for the production of different (and controlled) structures and sizes of PPy particles, including dopants when necessary. The polymerization process can produce large amounts of the polymer, but poor solubility in most solvents makes deposition difficult; chemically prepared PPy often has poor adherence to the sensor surface. Alternatively, electrochemical polymerization relies on an applied current to deposit a thin PPy film on the sensor surface. This technique provides good adherence and conductivity, as well as good control of the material's thickness and morphology. While this method seems to be more common in practice, only very small amounts of polypyrrole are obtained [192].

6.1.3.3 Poly(vinyl alcohol)

Poly (vinyl alcohol) (PVA; $T_g = 85^\circ\text{C}$) has, to our knowledge, not been applied to acetone sensing materials. However, the hydrogen bonding capability of the –OH group makes PVA an interesting option. As mentioned previously, PVA has been used as an additive for PPy sensing materials [193-195] as well as PANI sensing materials [196-199]. The target materials range from methanol [193, 195] and ammonia [194] to humidity [196, 197, 199]. Ultimately, the application (and its success) depends on both the physical properties (thickness, morphology, etc.) and the chemical properties (namely the synthesis techniques, blend ratios and dopants used).

Alone, PVA is most often used for humidity sensing (see, for example, [200-202]). The sensing techniques are varied, and include resistive [200], resonant frequency [201] and optical [202] methods. Penza et al. [201] noted that their sensor was very responsive to water, but was also sensitive to acetone, ethanol, methanol and 2-propanol.

It is expected that breath samples will have high humidity levels, which eliminates the possibility for pure PVA to be used for acetone detection. However, it may be possible to use a sensor array (so that water can be eliminated from the sample earlier) or a modified PVA-based backbone to detect acetone.

6.1.3.4 Poly(acrylic acid)

Poly (acrylic acid) (PAA; $T_g = 106^\circ\text{C}$) shows promise as an acetone gas sensing material, as it has a similar Hildebrand solubility parameter to acetone (see again Table 6.2). However, in the sensing literature, it is generally used to detect ammonia. Chabukswar et al. [203] used acrylic acid-doped PANI in a resistive sensor, while Ding et al. [204] and Lee et al. [205] used PAA as the sensing material with a QCM. While all three studies showed good sensitivity to ammonia, none of them considered the effect of interferents (except for humidity, in one case [204]). Thus, the response of PAA to other analytes (including acetone) is still unknown.

Polymer composites of PAA with polyaniline have also appeared in the literature. Tang et al. [206] and Tiwari et al. [207] both reported the successful detection of ascorbic acid using PANI/PAA composite materials for amperometric sensors. In both studies, dopamine and uric acid were considered as interferents, with no significant response in either case. Ascorbic acid has a more complex structure than acetone, but does contain a double-bonded oxygen atom (as does acetone). Therefore, these studies may be beneficial in establishing a tailor-made polymeric sensing material for acetone.

6.1.3.5 Poly(methyl methacrylate)

As shown in Table 6.1, poly (methyl methacrylate) (PMMA; $T_g = 105^\circ\text{C}$) has been used for acetone detection alongside polypyrrole [172] and polyaniline [176]. In the work by Do and Wang [176], PMMA was only used as a binding agent for PANI. However, Ruangchuay et al. [172] used a PPy/PMMA blend to detect acetone (in the presence of interferents acetic acid and water) using the swelling behaviour of PMMA and the conductivity of PPy. PMMA has similar solubility parameters to both acetone and acetic acid, which limits selectivity. However, the swelling behaviour of the sensing material differs between the two analytes: acetic acid bonds permanently through protonation of the =N (present in $\alpha\text{-NS}^-$ -doped PPy), whereas acetone bonds reversibly via hydrogen bonding (to the -NH group within PPy). Ruangchuay et al. [172] found that the ratio of PMMA to PPy/ $\alpha\text{-NS}^-$ drastically affects the selectivity of the sensing material, and this observation can be used to tailor-make polymeric materials for acetone detection. In general, increasing PMMA increases the response of the sensing material (that is, increases electrical resistance due to swelling) in the presence of both acetone and acetic acid. However, the acetone response dominates when $\text{PMMA}/(\text{PPy}/\alpha\text{-NS}^-) > 1$. In the same study, Ruangchuay et al. [172] reported that the sensing material is insensitive to water when PMMA and PPy/ $\alpha\text{-NS}^-$ are present in equal amounts. Therefore, to optimize the selectivity toward acetone (in the presence of acetic acid and water), a PMMA/(PPy/ $\alpha\text{-NS}^-$) ratio of approximately 1 (or slightly higher) should be maintained.

PMMA is an extremely versatile sensing material, and has been used for resistive, capacitive and mass-based sensors. Most often, PMMA has been used in humidity sensors. Various forms of pure PMMA (linear, crosslinked, surface modified PMMA, etc.) have been used in capacitive sensors, as water sorption in the polymer results in a capacitance change (see, for example, [208-210]). Alternatively, salt-doped PMMA has been used to create resistive humidity sensors, as water sorption promotes dissociation behaviour (and therefore increases ion mobility in the sensing material) [211, 212]. PMMA has also been used for VOC sensing, using resistive [213, 214] and mass-based [215] sensors. In both cases, the sensor response was based on sorption of the target analyte and swelling of the PMMA. Philip et al. [213] investigated the response of a surface modified carbon nanotube/PMMA sensor towards dichloromethane, chloroform, acetone, methanol, ethyl acetate, toluene and hexane. The results showed that the first three VOCs exhibited the highest response, which is largely due to the compatibility of their solubility parameters with

that of PMMA. Lang et al. [215], on the other hand, used a PMMA-coated cantilever sensor to detect four different alcohols (methanol, ethanol, 1-propanol and 1-butanol), with some success.

In an interesting extension, Matsuguchi et al. [208] evaluated the durability of their capacitive humidity sensor by exposing the PMMA to acetone. Since acetone sorbs onto PMMA, their sensor measured high capacitance after exposure to saturated acetone vapour. While the linear PMMA was more sensitive, sorption caused permanent deformation and the sensor could not return to the baseline capacitance. Crosslinked PMMA was not as sensitive to acetone, as sorption was limited to the surface. However, changes in capacitance were still observed, and the capacitance returned to the baseline value.

6.1.4 Product Customization

PANI is perhaps the most attractive backbone, as the polymer product can be tailored and/or modified. The pH of the reaction medium determines whether the resulting polymer is conductive, functional groups and packing can be selected by choosing an appropriate monomer (that is, a derivative of aniline), and doping makes it possible to choose which metal oxides could be incorporated for optimal sensitivity and selectivity. However, beyond these conditions, the reaction is very robust; most polymerization conditions have a limited impact on the properties of polyaniline synthesized via chemical oxidation. Cao et al. [216], for example, investigated a range of synthesis variables including reactant concentrations (and related ratios), initiator type, aqueous solution pH, polymerization solvent (mixtures of organic and aqueous components for the reaction media), polymerization temperature and polymerization time. Some variables had an impact on viscosity (and, by extension, likely had some molecular weight effect). However, yield and conductivity were generally unaffected by the variables considered. Given the results presented by Cao et al. [216], it could be beneficial to target using a molar ratio of initiator/monomer < 1.15 , ammonium persulfate or potassium dichromate as the initiator, aqueous hydrochloric acid solution as the protonic acid medium (concentration range from 1.2 M – 2.0 M), aqueous solution (no organic additives), temperatures between -5°C and 0°C , and a polymerization time between 4 hours and 8 hours to achieve (conductive) PANI samples with high molecular weights.

The PPy structure is largely controlled by the polymerization kinetics, which in turn are affected by the initiator (oxidant) used. Slower polymerization kinetics are generally preferred, since better rate control promotes the production of linear polypyrrole chains [217]. Also, there is a balance that needs to be obtained between the oxidation of pyrrole (to synthesize PPy chains) and the over-oxidation of PPy (which leads to chain degradation). Key control variables, then, are initiator type (specifically the redox potential of the initiator), concentration of initiator, polymerization time and polymerization temperature. It has been shown previously that the conductivity of the sensing material can vary significantly with the Py/initiator ratio and with time (especially when the

polymerization proceeds quickly) [218]. Also, synthesis at higher temperatures (say, above 20°C) can lead to side reactions which are undesirable for the application [219, 220].

Modifying the non-conductive polymers described above (PVA, PAA and PMMA) may require the addition of dopants (likely metal oxides) or comonomers, depending on the desired effect. As described previously, the copolymerization kinetics (specifically, reactivity ratios) provide information about the polymer product (namely copolymer composition and sequence length distribution). Thus, if reactivity ratios are known, the formulation can be tailored to ensure a specific copolymer composition (containing desirable functional groups) and sequence length distribution (which affects steric effects and therefore packing). In some applications, materials like PVA and PMMA are also used as substrates or binders [176]. Therefore, even if these polymers show a poor affinity towards the target analyte, they may still be useful as a stabilizing agent or a backbone (onto which the functional polymer can be grafted).

6.1.4.1 Metal Oxide Dopants

Dopants are additives that can be incorporated into a sensing material to improve its properties. Most dopants are metals and metal oxides, which can improve sensitivity and selectivity, electrical conductivity, thermal stability and mechanical integrity. As mentioned previously, acids can also be used as dopants, especially in the case of polyaniline; adding acid to the polymerization ensures that the resulting polymer will be conductive.

The number of studies surrounding polymeric sensing materials for acetone is limited, so the effectiveness of specific dopants is still relatively unknown. However, the metals, metal oxides, and acid dopants listed in Table 6.1 can be used as a starting point. Potential dopants are listed in Table 6.3 according to previous studies in which they were used for acetone detection. The effects of these materials (as additives) will be researched and evaluated in more detail so that the most promising dopants are selected.

Table 6.3: Potential Dopants, Based on Prior Breath Acetone Studies

| Ref. | Dopant | Sensor Type | Additional Notes |
|-------|--------------------------------|-------------|--|
| [176] | α -NS ⁻ | Resistive | Doping makes PPy more conductive |
| [172] | α -NS ⁻ | Resistive | Doping makes PPy/PMMA blend more conductive |
| [176] | ClO ₄ ⁻ | Resistive | Doping makes PANI/PMMA blend conductive |
| [160] | Ga ₂ O ₃ | Capacitive | Primary sensing material (Ga ₂ O ₃ nanowires) |
| [164] | Ir ₂ O ₃ | Resistive | Doping made material selective toward H ₂ S |
| [179] | NiO | Capacitive | P25DMA with 20% NiO was not selective toward acetone |
| [164] | Pt | Resistive | Doping significantly improved response to both acetone and H ₂ S |
| [165] | Pt | Resistive | Doping lowered selectivity (over toluene) |
| [167] | Pt | Resistive | Doping increased selectivity (over H ₂ S) |
| [160] | PA | Capacitive | Doping lowered selectivity (over nitromethane and triethylamine) |
| [158] | Sb | Resistive | No information about dopant-free response |
| [161] | Si | Resistive | Optimal doping (10 wt%) increased acetone sensitivity and thermal stability; materials with higher dopant levels had no sensitivity to acetone |
| [162] | Si | Resistive | Dopant quantity (10 wt%) selected based on [161]; optimal thermal stability, selectivity and sensitivity (even at high humidity levels) |
| [163] | Si | Resistive | See previous |
| [158] | SnO ₂ | Resistive | Primary sensing material |
| [165] | SnO ₂ | Resistive | Primary sensing material (SnO ₂ nanofibres) |
| [169] | SnO ₂ | Resistive | Primary sensing material (SnO ₂ nanofibres functionalized w reduced graphene oxide) |
| [171] | SnO ₂ | Resistive | Primary sensing material (SnO ₂ /reduced graphene oxide hybrid composite) |
| [176] | SO ₄ ²⁻ | Resistive | Doping makes PANI/PMMA blend conductive |
| [159] | TiO ₂ | Resistive | Dopant acts as 'trapping site' for acetone on multiwall carbon nanotubes; response time increased with doping |
| [161] | WO ₃ | Resistive | Primary sensing material (WO ₃ nanoparticle films) |
| [162] | WO ₃ | Resistive | Primary sensing material (WO ₃ nanoparticle films) |
| [163] | WO ₃ | Resistive | Primary sensing material (WO ₃ nanoparticle films) |
| [164] | WO ₃ | Resistive | Primary sensing material (WO ₃ nanofibres) |
| [166] | WO ₃ | Resistive | Primary sensing material (WO ₃ microspheres) |
| [167] | WO ₃ | Resistive | Primary sensing material (WO ₃ hemitubes) |
| [168] | WO ₃ | Resistive | Primary sensing material (WO ₃ hemitubes) |
| [170] | ZnO | Resistive | Primary sensing material (ZnO film) |

6.1.4.2 Acid Dopants

Acid dopants are especially useful in polyaniline synthesis, since they can be used to increase the protonation of the polymer backbone. Acid-doping polyaniline is typically necessary if the material is to be electrically conductive for a particular application; the charge improves the conductivity of the polymer. For example, emeraldine contains imine and amine sites in

approximately equal proportion along the backbone (recall Figure 6.1). Some studies have indicated that the imine sites are preferentially protonated, but it seems that some amine sites can be protonated as well [221]. The most common approach to obtain partially protonated emeraldine is using an in-situ technique (that is, through the synthesis of an emeraldine salt) [221, 222]. This can be achieved via the oxidative polymerization of aniline in aqueous acidic media. Typically, the oxidizing agent (that is, the initiator) is ammonium persulfate (APS) and the acid used in solution is hydrochloric acid (HCl) [221]. However, many different acids (or mixtures of acids) can be used to dope PANI [222].

The selection of acids for PANI doping can also be extended to organic acids [223, 224]. Kulkarni et al. [223] investigated the chemical oxidative polymerization of PANI in four organic acids (namely, acetic acid, citric acid, oxalic acid and tartaric acid). The experimental results showed that of the four organic acids, oxalic acid provided the highest selectivity in obtaining the conducting (protonated) emeraldine salt phase. In comparing the conductivities of the synthesized materials, the oxalic acid-doped PANI had the highest conductivity, followed by citric acid-doped PANI, tartaric acid-doped PANI and acetic acid-doped PANI. Characterization of the samples also indicated that when acetic acid was used as the dopant, the fully oxidized pernigraniline form of PANI was dominant (see again Figure 6.1).

Some researchers choose instead to dope the polymeric material after synthesis using protonic acid doping or pseudo-protonic acid doping (see, for example, [216, 221, 225]). In this case, to obtain the (protonated) emeraldine salt, one starts with an emeraldine base (non-protonated, as shown in the upper portion of Figure 6.2) and treats it with aqueous protonic acids. Again, HCl is most commonly used as the acid dopant, since it is a strong acid but can easily be removed from the product polymer [221]. With this technique, the degree of protonation can be controlled by changing the pH of the acid solution used for doping. Despite the ease-of-use of this technique, Cao et al. [216] observed a loss of viscosity (which may be indicative of a decreased molecular weight); they concluded that exposure to the strong acid resulted in chain degradation, and recommended protonating PANI with aqueous HCl solution with a low concentration (<0.5 M) for 2 hours.

For most investigations, the motivation to protonate PANI stems from a desire to improve electrical conductivity of the polymeric material, as the emeraldine salt (that is, the protonated form) is significantly more conductive than the (original) emeraldine base [221]. However, in the acetone sensing case, both the conductivity (for possible future sensor applications) and the affinity towards the target analyte are being considered. Using the protonated form of polyaniline should make it possible to take advantage of the polarity of acetone, as the positively charged nitrogen atoms could attract the negative (oxygen) end of gaseous acetone molecules.

Some studies have also investigated the potential to use acids for polypyrrole doping [172, 176]. Ruangchuay et al. [172], for example, evaluated seven different acids in order to find the best PPy dopant for acetone detection. During the study, PPy was synthesized in solutions containing α -naphthalene sulfonic acid (sodium salt), β -naphthalene sulfonic acid (sodium salt), camphor sulfonic acid, dodecylbenzene sulfonic acid (sodium salt), ethane sulfonic acid, perchloric acid, and *p*-aminobenzoic acid. Using α -naphthalene sulfonic acid (sodium salt) or β -naphthalene sulfonic acid (sodium salt) gave the best sensitivity results (for acetone sorption), but no interferent gases were considered.

6.1.4.3 Copolymers and Polymer Blends

One of the main challenges with polymers that are suitable for sensing is that they are not always easily processed. PANI, for instance, has very poor solubility, which makes characterization (molecular weight determination, for example) and processing difficult [216, 226]. Similarly, PPy can be very brittle; the mechanical properties are not sufficient for the demands of the sensing application. Therefore, researchers have been motivated to create copolymers and polymer blends containing these materials. Here, it is important to make a distinction between true copolymers and polymer blends. Copolymers contain both monomer types within a single polymer chain (this occurs during synthesis and has been described in detail in Section 2.2.1), whereas polymer blends are made via mixing techniques (combination of multiple homopolymers, which generally occurs after synthesis) [39].

A customized sensing material (for a particular application) could combine desirable sensing characteristics (especially electrical conductivity in the case of PANI and PPy) of one polymer (or comonomer) and mechanical stability of another. In the current study, the main focus is the sensing capability (not processability), so the mechanical properties are a secondary consideration. However, once optimal sensing characteristics are obtained, there would be the potential to create a copolymer or a polymer blend to incorporate all of the required material properties.

Due to the versatility of PANI and PPy, both materials have been incorporated into many copolymers and polymer blends. For example, for sensing applications, PANI has been grafted onto several different naturally occurring polymers including xanthan gum [227] and chitosan [228, 229]. These investigations reported that the copolymers exhibited increased sensitivity to target analytes and/or good processability (which included improved solubility, appropriate mechanical strength and desirable electrical properties). Similarly, researchers have synthesized a copolymer of polyaniline and poly-*o*-anisidine (recall the various derivatives of aniline shown in Figure 6.1) [190, 230]. The addition of the substituted $-\text{OCH}_3$ functional groups modified the geometry of the polymer backbone, which improved the copolymer's solubility (in common organic solvents like acetone, dimethylformamide (DMF), tetrahydrofuran (THF), and N-

methylpyrrolidinone (NMP)) compared to pure PANI. However, the electrical conductivity decreased in the presence of the side group.

In terms of PANI being incorporated into polymer blends, many investigations have been reported. To adjust the sensing performance of the materials, PANI has been blended with polyvinyl chloride, polystyrene, polyvinyl alcohol, and other polymers (see, for example, [231-233]). As mentioned in Table 6.1, Do and Wang [176] used a PANI/PMMA blend (where PMMA essentially acted as a binder for the sensor electrode) for an acetone sensing study. Also, acid doping of PANI (as described in Section 6.1.4.2) can be beneficial for the formation of polymer blends [226]. By doping PANI with organic acids (like camphorsulfonic acid or *p*-toluenesulfonic acid), the long alkyl chains can act as plasticizers, improving the miscibility of PANI and, subsequently, the processability of polymer blends.

A recent study that proved useful for the current investigation reported the in-situ polymerization of a polyaniline/polypyrrole copolymer using several different techniques [234]. Hammad et al. [234] used conventional chemical oxidation processes to synthesize PANI/PPy copolymers with different morphologies. Two reaction media were employed (synthesis occurred in 0.2 M acetic acid solution or in 0.2 M hydrochloric acid solution) and three synthesis methods were attempted in each medium. Method 1 employed conventional chemical oxidation (similar to what is described in Section 7.2.1) with the dropwise addition of initiator (ammonium persulfate) prior to the 24 hour polymerization. In Method 2, all of the initiator was added at once (rather than gradually) and was rapidly mixed (at 1000 rpm) for the first two hours of the 24 hour polymerization. Finally, Method 3 employed supercritical CO₂ in a 3 hour polymerization process in an attempt to improve the morphology of the product polymer. The results shown by Hammad et al. [234] indicate that the morphology changes drastically from one methodology to the next, and the type of acid used for the reaction medium is also influential.

To ameliorate the mechanical properties of pure polypyrrole, several groups have attempted to blend PPy with other (stronger) polymers such as poly(vinyl chloride) [235-237] and poly(vinyl alcohol) [193-195]. Also, as shown in Table 6.1, a PPy/PMMA blend doped with α -naphthalene sulfonate has already been used for acetone sensing [172]. However, most groups reported that incorporation of the stronger polymer improved the mechanical properties of the sensing material, but decreased the conductivity, response time and recovery time compared to pure PPy. Therefore, the recipe must be optimized to achieve a desirable balance between mechanical and electrical properties.

6.2 Extensions to Detection of Additional VOCs

The same design principles can be applied to other volatile organic compounds. One must consider the application requirements (both in terms of polymer properties and application-specific

behaviour) and consider appropriate candidates for polymeric sensing materials. In parallel to the work described thus far (related to acetone detection), our research group was asked to design and test materials (over a 6-month period) for the detection of formaldehyde and benzene. The details of this work have been presented in an independent internal report entitled “Wearable Chemical Hazard Sensors”, which is available upon request. This project was especially successful not only because it developed and demonstrated technology for wearable sensors, but also because it lay the foundations for detecting surrogates of chemical warfare gases. Two groups collaborated in executing the project:

- 1) The ‘polymer group’ developed detector polymers. The group included myself, Noushin Majdabadifarahani (MASC student) and Nicole A. Francis (MASC student), under the supervision of Professor A. Penlidis.
- 2) The ‘sensor group’ developed the microsensor platform. The group included Mohamed Arabi (PhD student), Alaaedin Ahmed (PhD student), Dr. Nafissi Hamidreza (research associate), Muhammed Kayaharman (MASC student) and Junaid Siddiqui (undergraduate student), under the supervision of Professor E. Abdel-Rahman.

Only a brief overview is presented herein, since the objective is to demonstrate that this design approach can be extended to other gas analytes for novel applications.

6.2.1 Detection of Formaldehyde - Project Background

Chemical similarities between target analytes and simple aldehydes (organic compounds containing a carbonyl group) can be exploited for preliminary testing of sensing materials. Specifically, if the goal is to detect phosgene (a chemical warfare agent), a surrogate gas like formaldehyde can be used; they are chemically similar (they contain a carbonyl group and are similar in size), yet formaldehyde is significantly less toxic. For the preliminary evaluation of materials, formaldehyde was selected as the main surrogate gas, but acetaldehyde (which is slightly larger, as a molecule) could also be used for evaluation.

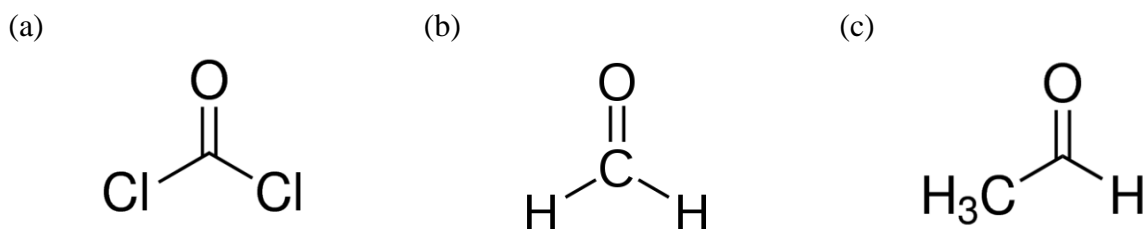


Figure 6.4: Similarity of Chemical Structures of (a) Phosgene, (b) Formaldehyde and (c) Acetaldehyde

Benzene was selected as the interferent gas for this study, as it is representative of aromatic hydrocarbons. It is the least complex aromatic hydrocarbon and is a good representative of interferent (rather large) gases for the application.

As described previously, the goal in designing sensing materials is to promote interactions between the gas analytes and the polymeric materials through various sensing mechanisms. In this case, there is potential to take advantage of the carbonyl group, since it is common to phosgene and (less toxic) aldehydes. Three properties that can be employed are polarity, hydrogen bonding, and Lewis acid-base behaviour.

6.2.2 Significant Contributions

The characteristics of aldehydes (and, by extension, warfare agents like phosgene) described above were considered in the selection of sensing materials. Initially, four polymeric materials were selected and analyzed: polyaniline (PANI), poly(2,5-dimethyl aniline) (P25DMA), poly(4-vinylpyridine) (P4VP) and poly(acrylic acid) (PAAc). Many of the same synthesis, deposition and characterization techniques described in Chapter 7 were used for this study. Through a series of experimental trials, the sensitivity of the selected materials (that is, the affinity of each material toward the target analyte) and the selectivity of the selected materials at various concentrations (with benzene as the interferent gas) were evaluated. Experimental results indicated that most promising materials for the application were PANI and P25DMA.

In collaboration with the ‘sensor group’ (Systems Design Engineering, University of Waterloo), small quantities of these materials were deposited onto functional sensors. To achieve this, 1 g polymer (PANI or P25DMA) was mixed with 50 grams of ethylene glycol (ethylene glycol facilitates polymer dispersion for pumping and subsequent deposition, and is volatile enough that the solvent can evaporate naturally from the sensor-plate). The mixture was then deposited onto the sensor plate using a microfluidic pump ($10 \mu\text{m}^3/\text{min}$) through a pipe-pipette assembly to deposit a $10 \mu\text{m}^3$ droplet on the sensor-plate. The solvent was then allowed to evaporate naturally, leaving the detector polymer on the plate (see Figure 6.5).

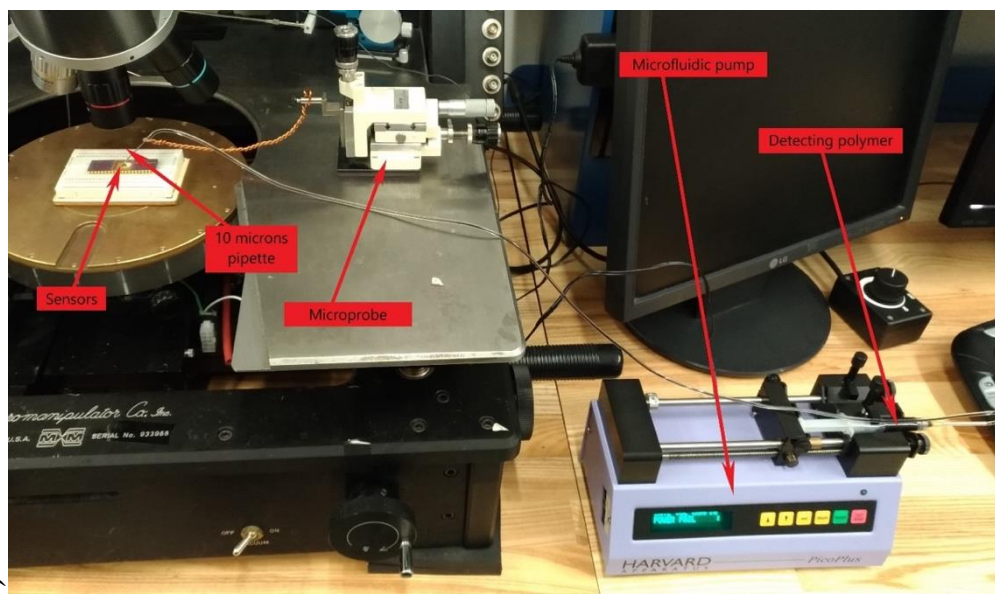


Figure 6.5: Deposition of Polymeric Material onto Sensor Plate

Figure 6.6a shows the sensor before the deposition process, while Figure 6.6b shows the successful deposition of P25DMA onto the sensor; this deposition process was developed by PhD student Mohamed Arabi, with support from our group.

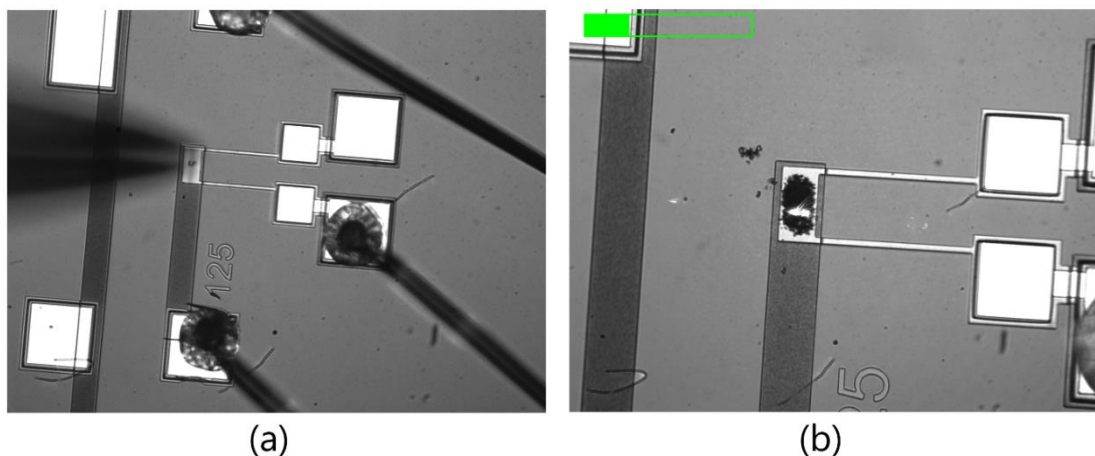


Figure 6.6: Sensor (a) Before and (b) After Polymer Deposition

It is important to provide this additional background information so that the reader can appreciate the eventual application of this work. Although the main focus herein is the design of materials, one can apply the materials to different sensors given a target application. For this formaldehyde detection study, the ‘polymer group’ observed good selectivity of formaldehyde in the presence of benzene (for both PANI and P25DMA) and the ‘sensor group’ was able to develop new microscale and very sensitive gas sensors for the detection of formaldehyde.

6.3 Sensing Material Array for Volatile Organic Compounds

An interesting extension of polymeric sensing materials is their use in sensor arrays. Sensor arrays or electronic noses (e-noses) have been developed for a wide variety of applications, including discrimination between and detection of specific ingredients in food [238, 239] and beverage [240, 241] industries, wastewater assessment [242], disease diagnosis [243, 244], and chemical process analysis [245]. Sensor arrays combine multiple sensing materials into one sensor. The response from each of the sensing materials is incorporated into some algorithm (often an artificial neural network), which analyzes all of the data and provides an output where specific analytes are identified [242]. For an effective sensor array, both the algorithm and the sensing materials are important.

The algorithms are used in principle to discriminate between different analytes through pattern recognition. Fine-tuning an algorithm can improve the selectivity of a sensor array for a specific application [246]. However, as a proof of concept, widely available cluster analysis tools such as principal component analysis (PCA) are used by researchers [247, 248].

When selecting sensing materials, the specific materials do not need to exhibit high selectivity towards different analytes (that is, they do not need to sorb one specific analyte significantly more than other competing or interfering analytes). However, the response pattern should be different from that of the other sensing materials used [249]. A pattern with a larger variation in sensing material response to gas analytes generally means that fewer sensing materials may be needed in a sensor array [250]. In other words, if two materials respond similarly to gas analytes (sorbing approximately equal amounts of a given analyte, showing similar affinity to specific gas mixtures, etc.), incorporating both materials into a sensor array may not show significant improvement in terms of gas analyte separation and/or identification (compared to only using one of the materials in an array). Rather, in developing a sensor array, the goal is to find materials that respond uniquely; if material A preferentially sorbs a different analyte than material B, using the two materials in a sensor array will complement each other and enrich the information content of the array. Therefore, synthesizing, characterizing and evaluating sensing materials for various applications and environments are all important steps/aspects for the development of new sensor arrays.

6.3.1 Case Study: Evaluation of Doped and Undoped PoANI as Materials for a Sensing Array

In a recent paper (written collaboratively with K. M. E. Stewart [251]), three polymeric materials (pure poly-*o*-anisidine (PoANI), PoANI doped with NiO, and PoANI doped with ZnO) were evaluated as sensing materials for methanol, ethanol, acetone, and benzene. In addition, a sensor array (using PCA as the ‘clustering’ algorithm) was assessed using these three sensing materials.

Poly (*o*-anisidine) (PoANI) is a derivative of polyaniline (recall Figure 6.3b) and has been used as a sensing material for a variety of volatile organic compounds (VOCs), including aliphatic alcohols and aldehydes [4, 252, 253]. Since it has been used as a sensing material for multiple VOCs, it has partial selectivity. This means that PoANI can respond somewhat non-discriminately to a range of gases. PoANI's non-specific sorption can be advantageous for sensor arrays, since it shows a partial response to several different gas analytes. However, to provide some specificity (that is, to improve the selectivity of PoANI), the material has been doped with nickel (II) oxide (NiO) and zinc oxide (ZnO) [247, 254].

Principal component analysis (PCA) was used as the data processing algorithm to separate the gas analyte signatures from these three sensing materials. PCA is a well-known multivariate tool, often used to determine the inter-relationships between variables in large data sets. The goal is to explain the variation of a data set with fewer factors than were originally provided. By reducing the number of factors (components) in the data set, PCA simplifies the analysis while retaining the majority of the statistical information. This is useful for providing an understanding of relationships within and between variables and is often useful for troubleshooting and/or process analysis [255]. For example, plotting data often reveals clusters, identifying a collection of experimental runs/trials with similar properties and, in some cases, outlying trials. In addition, PCA can be used to identify influential variables and provide a qualitative idea of the relationships within or between variables.

First, PCA was applied to the responses from the individual gas analytes and two principal components (or factors) were plotted against each other (see Figure 6.7). In Figure 6.7, M stands for methanol, E stands for ethanol, A stands for acetone, and B stands for benzene. It should be noted that for the individual gases, Factor 1 vs. Factor 3 was used, whereas Factor 1 vs. Factor 2 was used for all of the other PCA plots. In general, Factor 1 vs. Factor 2 provides the best separation (since the first two factors contain the most statistical information). However, when using PCA as an algorithm for sensor arrays, these two factors may not always provide the best separation of analyte signatures. It is more important for a sensor array to have good separation of analytes than it is to maximize information content with fewer factors. This motivated the decision to plot Factor 1 versus Factor 3 for the individual gases (Figure 6.7) and Factor 1 versus Factor 2 for the gas mixture analyses (Figure 6.8 through Figure 6.12).

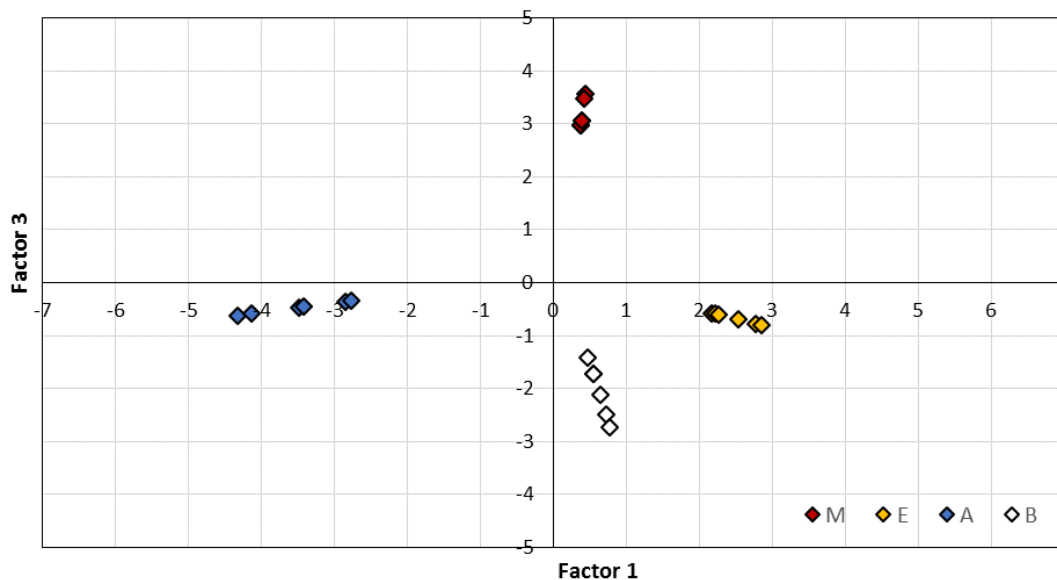


Figure 6.7: Sensor Array for Individual Gases; Methanol (M), Ethanol (E), Acetone (A) and Benzene (B)

For individual gas analytes, these three PoANI-based sensing materials (along with PCA as a clustering algorithm) were able to differentiate between methanol, ethanol, acetone and benzene. However, for real world applications, gas analytes are always present with other gas analytes (interferents). Therefore, all possible mixtures of these four gas analytes must be considered. PCA was applied to all of the related combinations of gas analytes with the goal of using these sensing materials and PCA in a more realistic setting (see Figure 6.8).

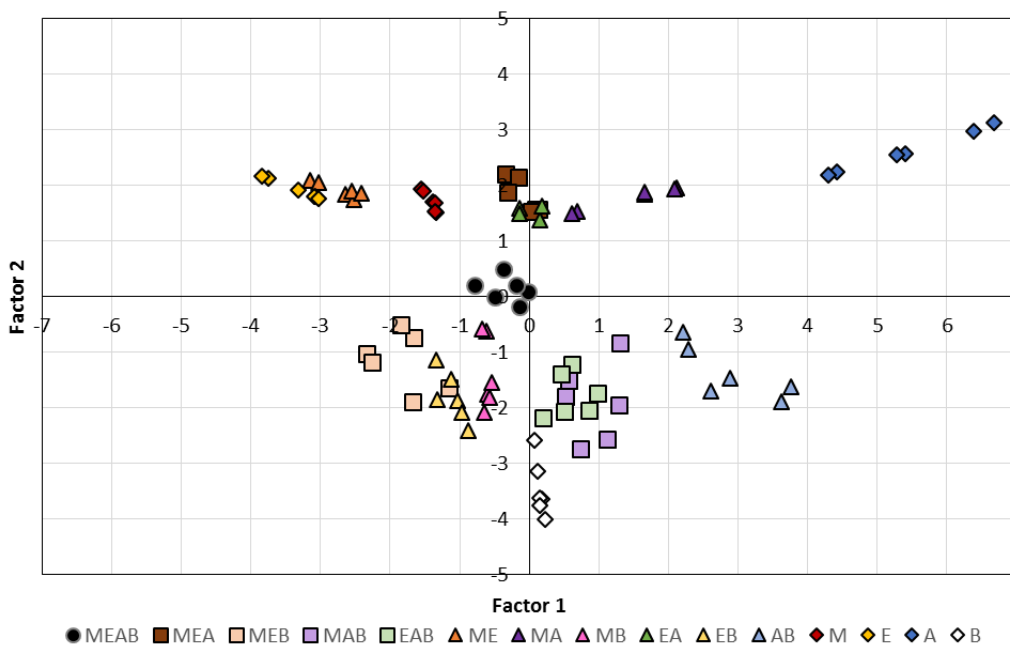


Figure 6.8: Sensor Array for All Possible Gas Mixture Combinations of Methanol (M), Ethanol (E), Acetone (A) and Benzene (B)

Figure 6.8 shows the clustered responses of all four (individual) gas analytes and all of the gas mixtures (composed of two, three or four of the analytes). The individual gas responses (shown as diamonds in Figure 6.8) are generally on the outskirts of the plot; methanol and ethanol are in the top left quadrant, acetone is in the top right quadrant, and benzene is central in the lower half of the plot. The individual gases typically have the highest amount of sorption, and the larger response of the pure gases is somewhat amplified by the PCA projection. Therefore, the clusters related to individual gases are on the periphery in Figure 6.8.

Upon closer inspection, Figure 6.8 also shows the relationship between certain gas analytes and gas mixtures. For example, it is not coincidental that the 4-gas mixture of methanol, ethanol, acetone, and benzene (MEAB, circles in Figure 6.8) is in the centre of the plot. The response to the MEAB mixture is centrally located between each of the individual analytes because it contains attributes of each of the four gases. Similarly, for a simpler case (like a two-gas mixture of methanol and ethanol), the ME response falls in between the pure methanol and the pure ethanol responses. In plotting these factors (Factor 1 and Factor 2 from PCA), methanol and ethanol give similar responses. Because they are close together, there is necessarily some overlap between the individual gases and the ME mixture; as shown in the top left corner, the ethanol (E) response and the ME response overlap somewhat. This overlap could be eliminated if different factors were plotted (Factor 1 vs Factor 3, for example), but at the expense of different analytes and mixtures overlapping elsewhere. To obtain even better separation, one might consider using a different combination of sensing materials (more selective to either methanol or ethanol); this will be discussed further in what follows. However, the fact that methanol and ethanol responses fall in the same quadrant does make physicochemical sense. Since the two analytes are chemically similar, it is likely that they will have a similar ‘footprint’ for this type of analysis.

While the plot shown in Figure 6.8 contains a very large amount of information about individual gases and related gas mixtures, the clusters for each gas combination do not show sufficient separation to use this data as a reference plot for a sensor array for these four gas analytes. To ‘unclutter’ the sensor array plot, new plots can be constructed using the same three sensing materials, but with combinations of up to three gas analytes (Figure 6.9 through Figure 6.12). That is, one gas analyte and all related mixtures are excluded from each plot. Benzene is excluded in Figure 6.9, methanol is excluded in Figure 6.10, ethanol is excluded in Figure 6.11, and acetone is excluded in Figure 6.12. By dropping the number of gas analytes from four to three, the potential combinations drop from fifteen to seven. This results in significantly better separation, especially for the individual gas responses; single gas clusters are almost always independent, with the exception of benzene (which is somewhat overlapping with the MAB three-gas mixture in Figure 6.11).

This simplification of data sets also highlights the relationship between single gases, two-gas mixtures and three-gas mixtures. Take, for example, Figure 6.9: the three individual gases (M, E

and A) are on the periphery (as observed in Figure 6.8), and the two-gas mixture responses fall in between the two related single-gas responses. Similarly, the three-gas mixture response falls in the middle of the 'triangle' that forms between the three single-gas responses.

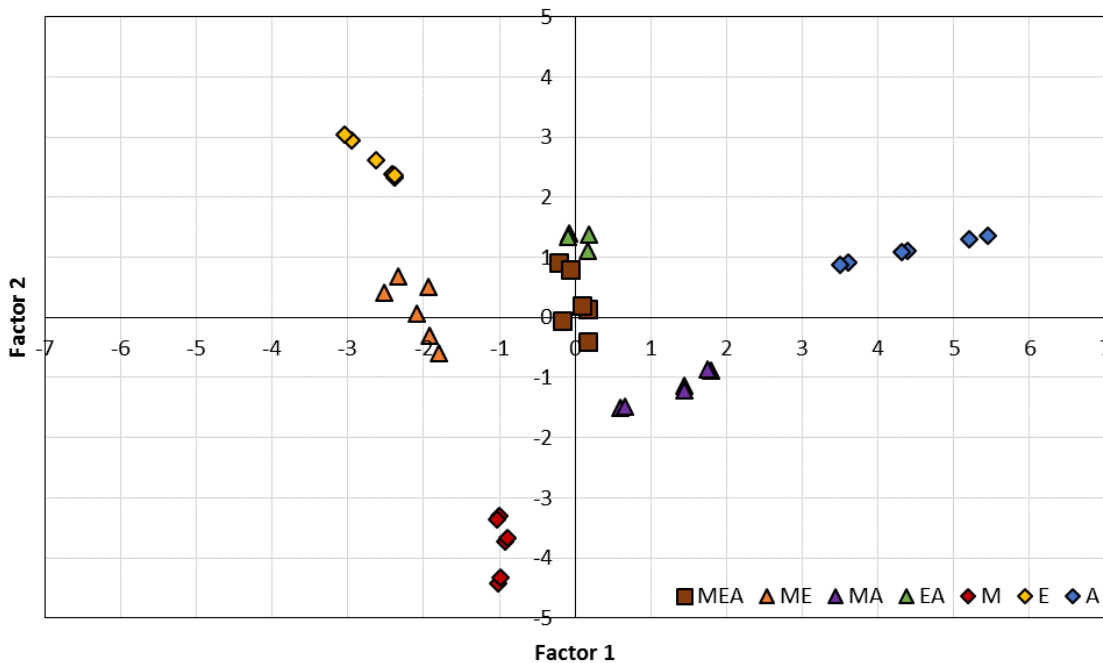


Figure 6.9: Sensor Array for All Gas Combinations of Methanol (M), Ethanol (E) and Acetone (A)

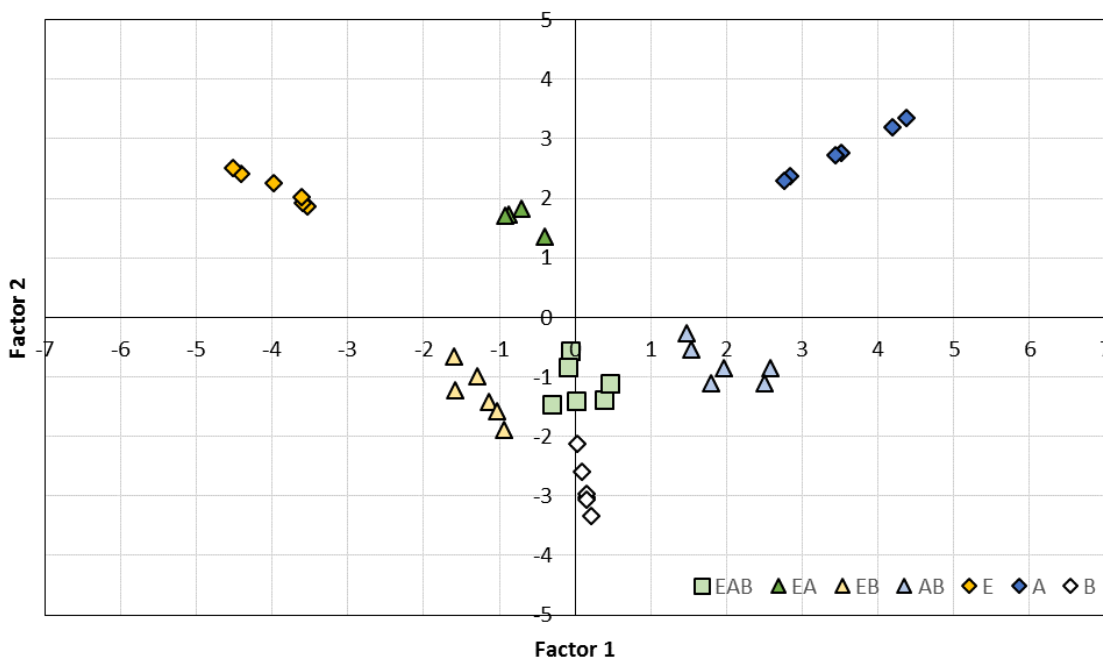


Figure 6.10: Sensor Array for All Gas Combinations of Ethanol (E), Acetone (A) and Benzene (B)

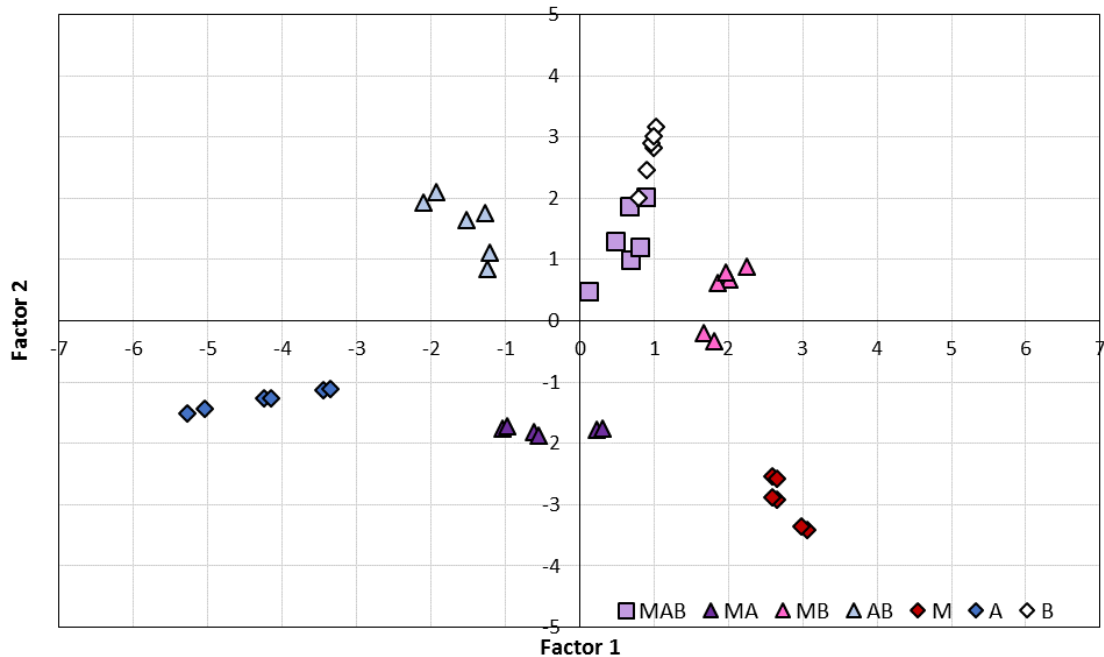


Figure 6.11: Sensor Array for All Gas Combinations of Methanol (M), Acetone (A) and Benzene (B)

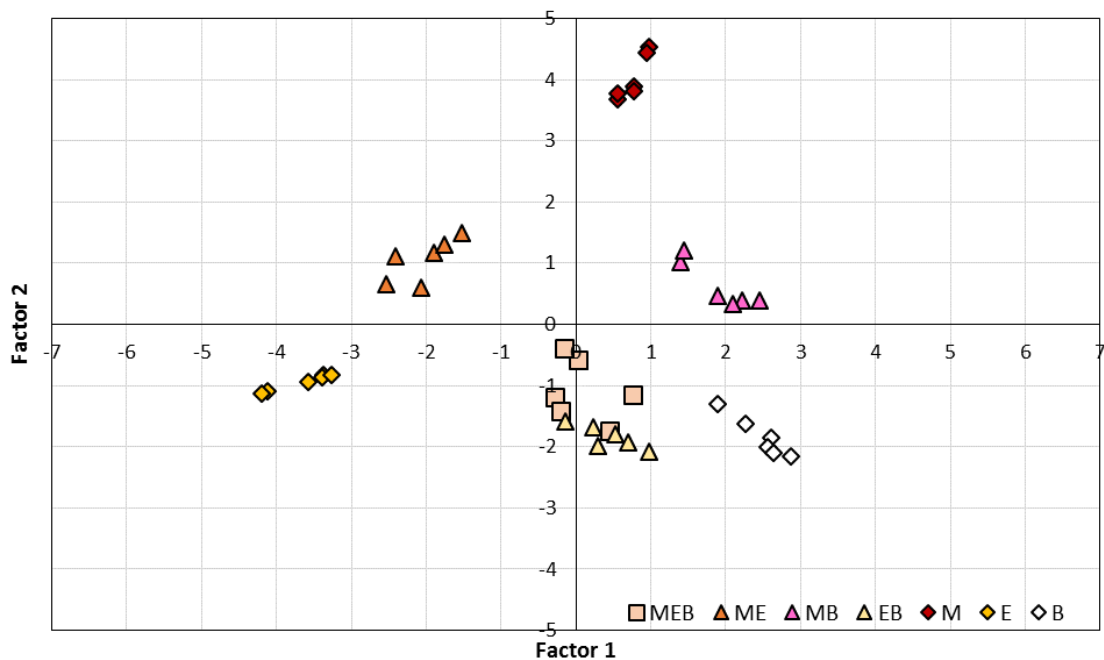


Figure 6.12: Sensor Array for All Gas Combinations of Methanol (M), Ethanol (E) and Benzene (B)

Although these three-gas analyses significantly improve the separation of analytes, some overlapping responses are still observed in Figure 6.11 and Figure 6.12. In Figure 6.11, B and MAB responses overlap in the upper right quadrant of the plot. Similarly, in Figure 6.12, EB and MEB responses overlap in the lower middle portion of the plot. Interestingly, in both cases, the common analyte is benzene. The poor separation observed here may be due to the low sorption of

benzene; low sorption (or low response) from experimental data limits the potential for separation of clusters using an algorithm like PCA. Also, all three PoANI-based sensing materials showed a (similar) poor affinity toward benzene (alone and in analyte mixtures). Therefore, to improve separation in this case, one might consider using a material that has a higher affinity to benzene as part of the sensing material array.

The overlap shown on PCA plots with gas mixture data (especially Figure 6.8, Figure 6.11 and Figure 6.12) may be due to similar responses of the sensing materials to the different analytes in mixtures, the use of PCA as a clustering network, or a combination thereof. Therefore, to improve the usefulness of a sensor array, these PoANI-based sensing materials could be paired with different sensing materials (that is, different polymer backbones). In addition, a sensor array with more sensing materials could have better separation of analyte responses due to more information being included in the pattern recognition of the employed algorithm [256].

For example, such a sensor array could be one consisting of PoANI, poly (vinyl pyrrolidone) (PVP) [5], poly (2,5-dimethyl aniline) (P25DMA) [257], and SXFA (a polymeric sensing material containing trifluoro groups and hydroxyl groups) [258]. These potential sensing materials were chosen because each one has acceptable partial selectivity to one of the four gas analytes evaluated in this investigation: PoANI to acetone, PVP to ethanol, P25DMA to methanol, and SXFA to benzene. This combination of potential sensing materials may resolve the issues by having a wider variation in selectivity (to different gas analytes), as well as a larger number of sensing materials for the sensor array, which would provide more data for the pattern recognition algorithm.

Overall, these three sensing materials in combination with PCA were not ideal for creating a sensor array capable of analyzing all possible combinations of methanol, ethanol, acetone, and benzene. However, sensor arrays that were able to distinguish between three of the four analytes were developed. Since the PoANI-based sensing materials showed affinity to these four gas analytes, there is potential to use them in sensor arrays, especially for a room temperature sensor. To improve these sensor arrays, a different combination of sensing materials could be used (including some of the PoANI-based sensing materials) and/or an improved pattern recognition technique could be employed to improve the separation of the response clusters, which would allow for better identification of the gas analytes.

Chapter 7. Experimental Methodology for Case Study #2 – *Polymeric Sensing Materials*

Based on the background information for material design presented in Chapter 6 (specifically Sections 6.1.3 and 6.1.4), three polymer backbones and three metal oxide dopants were selected for experimental investigation. Polyaniline (PANI), polypyrrole (PPy) and poly(methyl methacrylate) (PMMA) showed promise as polymer backbones, and SnO₂, WO₃ and ZnO were among the most commonly used metal oxides for inorganic sensing materials. Thus, these three polymers (doped with different levels of the three metal oxides) are synthesized and characterized in what follows.

7.1 Materials

All reagents for this study were used as received. For the synthesis of polyaniline and polypyrrole, monomers (aniline and pyrrole) and initiators (ammonium persulfate, APS and iron (III) chloride, FeCl₃) were purchased from Sigma-Aldrich (Oakville, Ontario, Canada). Poly(methyl methacrylate) (PMMA) powder was purchased from Sigma-Aldrich (average Mw ~15,000). Metal oxide (MO) nanoparticles (used for doping) were also purchased from Sigma-Aldrich; SnO₂ and WO₃ came as powders (both <100 nm nanoparticle size). ZnO came in a 50% solution with water, and the nanoparticle diameter was also < 100 nm. Oxalic acid dihydrate (ACS grade) from EMD Millipore was used for acid doping. Finally, in terms of solvents, deionized water was used for PANI and PPy synthesis; acetone (99%) and ethanol (ACS grade) were used as received.

Analyte-containing gases used for sensing material evaluation were purchased from Praxair (Mississauga, Ontario, Canada). Separate gases containing pre-specified concentrations (on the ppm level) of acetaldehyde, ethanol, acetone and benzene were of standard grade, in nitrogen. Pure nitrogen (also from Praxair, 5.0 grade) was used to purge the samples prior to each sorption test.

7.2 Polymer Synthesis for Acetone Detection

Design of experiments was employed for the synthesis of polymeric materials: 3 polymer backbones, 3 metal oxides, and 3 dopant levels (that is, weight percent dopant) were considered. The original design of experiments is shown in Table 7.1 and formulations are numbered for easy reference throughout the discussion.

Table 7.1: Experimental Design of Polymeric Materials for Acetone Detection

| # | Polymer Backbone | Dopant | wt% Dopant in Recipe |
|----|------------------|------------------|----------------------|
| 1 | PANI | -- | -- |
| 2 | PANI | SnO ₂ | 5 |
| 3 | PANI | SnO ₂ | 10 |
| 4 | PANI | SnO ₂ | 20 |
| 5 | PANI | WO ₃ | 5 |
| 6 | PANI | WO ₃ | 10 |
| 7 | PANI | WO ₃ | 20 |
| 8 | PANI | ZnO | 5 |
| 9 | PANI | ZnO | 10 |
| 10 | PANI | ZnO | 20 |
| 11 | PPy | -- | -- |
| 12 | PPy | SnO ₂ | 5 |
| 13 | PPy | SnO ₂ | 10 |
| 14 | PPy | SnO ₂ | 20 |
| 15 | PPy | WO ₃ | 5 |
| 16 | PPy | WO ₃ | 10 |
| 17 | PPy | WO ₃ | 20 |
| 18 | PPy | ZnO | 5 |
| 19 | PPy | ZnO | 10 |
| 20 | PPy | ZnO | 20 |
| 21 | PMMA | -- | -- |
| 22 | PMMA | SnO ₂ | 5 |
| 23 | PMMA | SnO ₂ | 10 |
| 24 | PMMA | SnO ₂ | 20 |
| 25 | PMMA | WO ₃ | 5 |
| 26 | PMMA | WO ₃ | 10 |
| 27 | PMMA | WO ₃ | 20 |
| 28 | PMMA | ZnO | 5 |
| 29 | PMMA | ZnO | 10 |
| 30 | PMMA | ZnO | 20 |

7.2.1 Synthesis of PANI

Polyaniline (PANI) was synthesized by mixing aniline, ammonium persulfate (APS), and the dopant (when applicable) in deionized water. PANI was synthesized in its pure (undoped) form, and doped with 5%, 10%, and 20% (by weight) of the three metal oxides (SnO₂, WO₃ and ZnO).

As per Stewart et al. [259], up to 0.4 g of monomer was added to 20 mL of deionized water and then mixed using a sonicator for 30 minutes. This solution was then cooled to -1°C before the addition of a solution containing 1 g of APS in 5 mL of deionized water. The solution was mixed for one minute, and was then left for 6 hours to polymerize at -1°C. The reaction is extremely exothermic, which is the main motivation for using small quantities and low polymerization temperatures. Upon completion of the reaction, the polymer was filtered out (Whatman #5 filter paper) and the polymer was washed with ethanol or acetone at least three times.

When dopants were added to the sensing material, up to 20% (by weight) of the metal oxide was suspended in the pre-polymerization solution. Then, the solution was cooled to -1°C and APS was added to the system. The rest of the synthesis process is as described previously.

7.2.2 Synthesis of PPy

The synthesis procedure used for PPy was based on the work done by Chitte et al. [260]. Polypyrrole (PPy) was synthesized by mixing pyrrole, FeCl₃, and the dopant (when applicable) in

deionized water. Like PANI, PPy was synthesized in its pure (undoped) form, and doped with 5%, 10%, and 20% (by weight) of the three metal oxides (SnO_2 , WO_3 and ZnO).

Up to 0.4 g of monomer was added to 20 mL of deionized water and then mixed using a sonicator for 30 minutes. This solution was then cooled to 1°C before the addition of a FeCl_3 solution. The FeCl_3 solution was prepared using 5 mL distilled water; the initiator mass was selected such that the molar ratio of initiator to monomer was 2.4:1. The solution was mixed for one minute, and was then left for 4 hours to polymerize at 1°C . Upon completion of the reaction, the polymer was filtered out (Whatman #5 filter paper) and the polymer was washed with ethanol at least three times.

When dopants were added to the sensing material, up to 20% (by weight) of the metal oxide was suspended in the pre-polymerization solution. Then, the solution was cooled to 1°C and FeCl_3 was added to the system. The rest of the synthesis process is as described previously.

7.2.3 Preparation of PMMA

Preliminary evaluation of PMMA as a sensing material for acetone employed PMMA (average molecular weight $M_w \sim 15,000$) purchased from Sigma-Aldrich. PMMA was blended with 5%, 10% and 20% (again by weight) of the metal oxides (MO) described above. PMMA/MO blends were created directly in the round bottom flasks that would later be used for sorption tests (to be described in Section 7.4.2) to ensure that the percentage of metal oxides in each sample was as expected. In these cases, up to 0.1 g PMMA was dissolved in 10 mL acetone and stirred for 90 minutes at 100 rpm. Then, if metal oxides were used, they were weighed (to achieve the desired weight percentage) and rinsed into the PMMA solution. Mixing at 100 rpm continued for another 30 minutes, and then the flask was left (undisturbed) under ambient conditions for approximately 1 week. Once all acetone had evaporated, the samples were further dried at 50°C until a constant mass was reached.

7.2.4 Customized Synthesis: Acid Doping and Copolymerization

After the original investigation with PANI, PPy and PMMA (described in this chapter and in Section 8.1), four additional polymers were synthesized in an attempt to improve the application performance of the sensing materials.

As will be discussed in the following chapter (Section 8.1), PANI and PPy showed the most promise for acetone sensing (of the polymeric materials studied herein). Also, results indicated that adding metal oxides did not appreciably improve the application performance. Therefore, during this part of the investigation, the goal was to improve upon the preliminary performance of PANI and PPy. Therefore, for the customized synthesis, two main modifications were considered:

the potential to acid-dope the polymeric material and the potential copolymerization of aniline with pyrrole. The acid dopant selected for this investigation was informed by the organic acid study done by Kulkarni et al. [223]. The study used a synthesis technique similar to the technique described herein (as per Section 7.2.1), but with solutions of organic acids as the reaction medium. Kulkarni et al. [223] reported that oxalic acid-doping gave the highest yield of protonated emeraldine salt, and that it was the most conductive of the four organic acid-doped materials synthesized. The key motivator in our case was the protonation of the polyaniline; the positively charged polymer backbone should attract the negative end of the polar acetone molecules.

A 2^2 design of experiments (as shown in Table 7.2) was employed to investigate the effectiveness of these modifications. To connect these additional polymers to the earlier formulations (recall Table 7.1), the numbering is continued from Table 7.1.

Table 7.2: Experimental Design of Polymeric Materials for Acetone Detection: Part II

| # | Polymer Backbone | Dopant | # | Polymer Backbone | Dopant |
|----|------------------|-------------|----|------------------|-------------|
| 31 | PANI | -- | 33 | PANI/PPy | -- |
| 32 | PANI | oxalic acid | 34 | PANI/PPy | oxalic acid |

Pure PANI (sample #31) was synthesized as described in Section 7.2.1. The process (and therefore, the product polymer) was the same as sample #1 (from Table 7.1), and was primarily performed as a replicate (confirmation) run. It also allowed for simple, direct comparison to the newly synthesized materials. As before, the polymerization was performed in deionized water, ammonium persulfate was used as the initiator, and the reaction was allowed to continue for 6 hours at -1°C .

Oxalic acid-doped PANI (referred to as ox-PANI or sample #32 herein) followed the same procedure as pure PANI, but the polymerization occurred in an aqueous oxalic acid solution (approximate concentration = 0.5 M). 1.5 g oxalic acid dihydrate was dissolved in 20 mL deionized water, then 0.4 mL of aniline (monomer) was added to the oxalic acid solution. The rest of the procedure was the same as for PANI synthesis in water: the formulation was mixed using a sonicator for 30 minutes and the flask (containing the monomer solution) was cooled to -1°C . Then, the initiator solution (1 g APS in 5 mL of deionized water) was added to the pre-cooled flask, and the complete solution was mixed for one minute. Finally, the polymerization was allowed to occur for 6 hours at -1°C . Upon completion of the reaction, the polymer was filtered out (Whatman #5 filter paper) and washed with deionized water or ethanol at least three times. Interestingly, the ox-PANI required less rinsing (that is, the filtrate ran clear after fewer rinses) than the PANI synthesized in water. Also, distinct colour differences were observed between the pure PANI and the ox-PANI (samples #31 and #32). As shown in Figure 7.1, the synthesis in water (on the left hand side of the image) created a dark blue PANI sample (in the round bottom flask and in the filter paper) and the filtrate was a light brown colour. In contrast, synthesis in oxalic acid (on the right hand side of Figure 7.1) resulted in a much darker green colour, and the filtrate

was a dark purple. This colour difference indicates that the presence of oxalic acid has changed the chemical structure of the product polymer. From the literature [221], emeraldine base has a blue tint and emeraldine salt has a bright green hue. Therefore, it is possible to conclude that sample #32 (that is, the ox-PANI formulation) contains the emeraldine salt, and that PANI was successfully customized through oxalic acid doping.



Figure 7.1: Comparison of Qualitative Observations during PANI (left) and ox-PANI (right) Synthesis

In parallel, the copolymers of PANI/PPy were synthesized in water and in an aqueous oxalic acid solution. Here, the procedures described by Hammad et al. [234] were used as a starting point. To obtain an equimolar concentration of aniline and pyrrole, 0.2 mL of aniline and 0.15 mL pyrrole were added to 20 mL deionized water (or, for the ox-PANI/PPy formulation, monomers were added to an aqueous solution of oxalic acid). All other synthesis steps were completed as before: 1 g APS (in 5 mL deionized water) was used as the initiator, the reaction proceeded at -1°C , and product polymers were filtered out after 6 hours.

Again, in this case, the colour varied between the PANI/PPy copolymer (sample #33) and the ox-PANI/PPy copolymer (sample #34). Sample #33 (left side of Figure 7.2) was brown, while sample #34 (right side of Figure 7.2) had a purple tint. The polymeric materials synthesized are undoubtedly influenced by the presence of pyrrole, as comparison between Figure 7.1 and Figure 7.2 shows clear differences in the colour of the product polymer.



Figure 7.2: Comparison of Qualitative Observations during PANI (left) and ox-PANI (right) Synthesis

The purple colour observed for sample #34 may be due to the presence of pernigraniline (the fully oxidized form of PANI) [222]. Since the initiator concentration remained constant, but the amount of aniline monomer was lowered (since pyrrole was added to the formulation), it is possible that the aniline monomer was entirely consumed and the residual initiator (ammonium persulfate) oxidized the polymer. However, it is difficult to draw concrete conclusions about the form of polyaniline using these qualitative observations. The main result here is that the four different formulations allowed for the synthesis of four unique polymeric materials. These will be characterized further in Chapter 8 using techniques described in what follows.

7.3 Characterization of Polymer Properties

As explained in Section 6.1.2, key properties of the sensing materials include crystallinity, surface morphology, and dopant incorporation.

The crystallinity of select polymer samples (primarily those obtained from customized synthesis) was analyzed using X-ray diffraction (XRD). XRD was performed at the Waterloo Advanced Technology Laboratory (WATLAB) on a PANalytical Material Powder Diffractometer (MPD)-Pro. The source was a Cu tube at 45 kV and 35 mA (K-alpha1 = 1.54060 Å; K-Alpha2 = 1.54443 Å; K-Beta = 1.39225 Å) and scans were performed at 25°C over the range of $2\theta = 5^\circ$ to 90° (step size = 0.0170°). Select independent replicates (both from independently synthesized samples and multiple samples from a single experimental synthesis) were performed.

Surface morphology was evaluated for select samples using scanning electron microscopy (SEM), which provides information about both the topology and the composition by producing images of the sample surface (incidentally, the effect of doping can be qualitatively evaluated using SEM). SEM and energy dispersive X-ray spectroscopy (EDX) were both performed at WATLAB on a Zeiss UltraPlus FESEM. SEM stubs for analysis were prepared by placing small pieces of carbon

tape on each stub, suspending each polymeric material in a small volume of ethanol, pipetting each suspension onto its designated stub, and allowing the ethanol to evaporate off at room temperature (under ventilation). Also, any non-conductive samples were gold-coated prior to analysis.

As in previous studies [182], EDX was performed alongside SEM to determine the composition of the sensing material. This was especially relevant for the polymeric materials doped with metal oxide, since this characterization step provides information about the degree to which each metal incorporated. Dopant incorporation largely depends on the initial composition (percent dopant in the pre-polymerization recipe), but is also affected by chemical and physical interactions between the dopant and the polymer.

7.4 Characterization of Application-Specific Properties

7.4.1 Deposition of Materials for Analysis of Sorption

For PANI, PPy, and all related materials (Samples #1 through #20 and #31 through #34), approximately 0.1 g of the individual polymer samples were deposited into 100 mL round bottom flasks. The polymer was deposited by weighing out the material and rinsing it into the flask with ethanol. Flasks were left to dry under atmospheric conditions until all ethanol had evaporated.

Since PMMA was used as received (for the pure PMMA and for blending with metal oxide nanoparticles), the deposition process included the dissolution of PMMA and the addition of metal oxides in appropriate proportions (as per Table 7.1). This has already been described in some detail in Section 7.2.3).

7.4.2 Experimental Set-Up for Sorption Studies

The test set-up for sorption studies has been described previously by Stewart et al. [261], and the key points are revisited here. Individual polymer samples (each with a mass of ~0.1 g) were deposited into round bottom flasks for the sorption study (as described in the previous section), and each polymer sample was purged with dry nitrogen for at least 1 hour prior to being exposed to the gas analyte. This ensured that any residual analyte sorbed (from previous runs) would be released.

To measure the sorption, each polymeric sensing material was exposed to a gas (containing known concentrations of one or more analytes), and the amount of analyte that sorbed onto the sensing material was measured. If the sensing material being evaluated was sensitive to the target analyte, higher quantities of the analyte were sorbed. All sorption measurements were taken at room temperature (24°C) and approximately 15 psi (slightly above atmospheric pressure).

The set-up uses a difference in gas concentration (before and after exposure to the sensing material) to establish how much of the target analyte has been sorbed. Prior to exposure, a ‘blank’ run can be analyzed by a highly specialized Varian 450 gas chromatograph (GC) (with a photon discharge helium ionization detector (PDHID)) to determine the gas concentration for the case of no sorption. After exposure to the sensing material, the gas concentration is again measured by the GC, but this second measurement represents the amount of gas that did not sorb (residual gas). Therefore, by subtracting the residual analyte concentration from the initial concentration of the analyte, the amount of analyte sorbed can be calculated. The advantage of the highly specialized GC is that it can distinguish between similar analytes and record concentrations down to the ppb level; more details are presented in Appendix D, Section D.1.

For each experimental run (before and after exposure to the sensing material), gas samples were collected at regular intervals until readings remained consistent (this indicated that the system had reached equilibrium). Independent sampling replicates were performed for all samples. A schematic is shown in Figure 7.3.

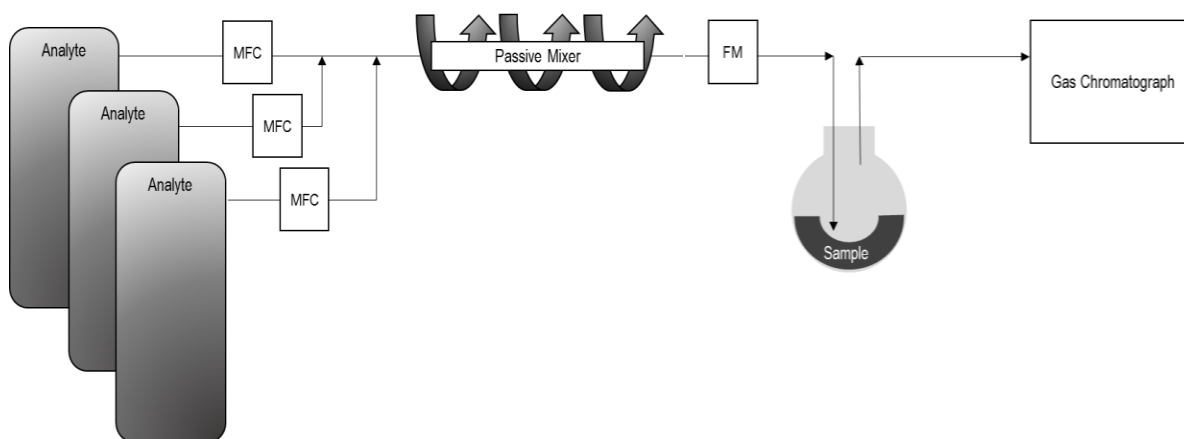


Figure 7.3: Experimental Set-Up for Evaluation of Sensing Materials, where MFC represents Mass Flow Controller and FM represents Flow Meter (adapted from [257])

The most promising materials were further characterized through selectivity studies. Here, polymeric sensing materials were exposed to a mixture of up to four gases (acetone, acetaldehyde, ethanol and benzene) simultaneously, and the response to acetone was measured in the presence of interferent gas analytes.

Chapter 8. Results and Discussion for Case Study #2 – *Polymeric Sensing Materials for Acetone Detection*

8.1 Screening Experiments: Metal Oxide-Doped Polyaniline, Polypyrrole and Poly(methyl methacrylate)

8.1.1 Sensitivity – Acetone Sorption

For the sensitivity study, thirty polymeric materials (listed in Table 7.1) were evaluated, based on their ability to sorb acetone gas. As described in Section 7.4.2, polymers were introduced into the experimental set-up and were exposed to 5 ppm acetone in balance nitrogen. This initial investigation allowed for the identification of the materials with the best sorption (or the strongest affinity towards the target analyte) and provided justification to rule out the most unresponsive polymers. Supplemental data tables are available in Appendix D, Section D.2.

8.1.1.1 Original Polymeric Materials

First, the sorption capabilities of the three (undoped, unmodified) polymer backbones were examined. As explained previously, polyaniline (PANI), polypyrrole (PPy) and poly(methyl methacrylate) (PMMA) were selected as promising candidates given our understanding of the system. The sorption of each material (after exposure to 5 ppm acetone, as described in Section 7.4.2) is shown in Figure 8.1.

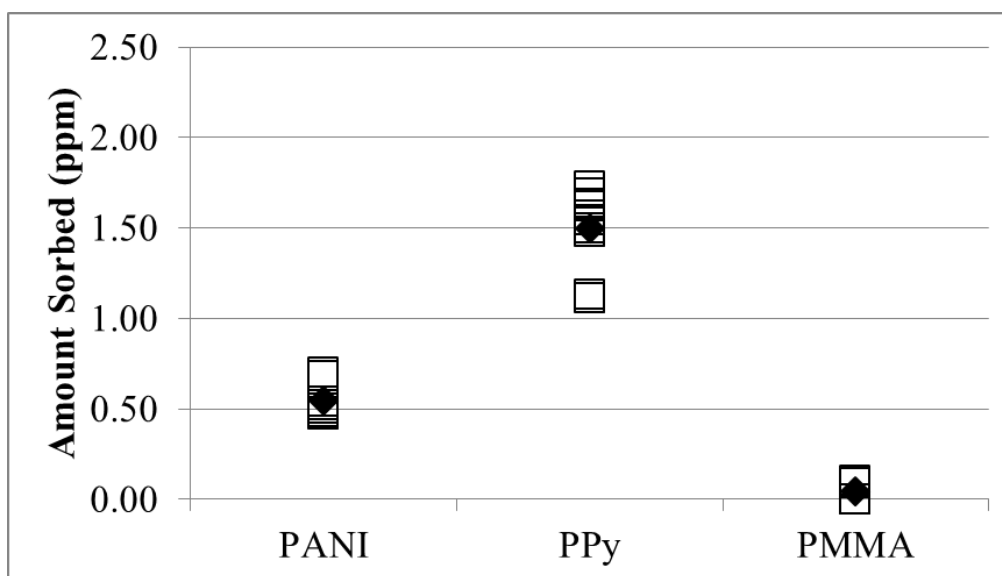


Figure 8.1: Sorption of Acetone for PANI, PPy and PMMA (source: 5 ppm acetone in nitrogen)

The results of Figure 8.1 suggest that PPy has the most acetone sorption, followed by PANI. In contrast, PMMA sorption is negligible. Although it is somewhat surprising that PMMA is not an

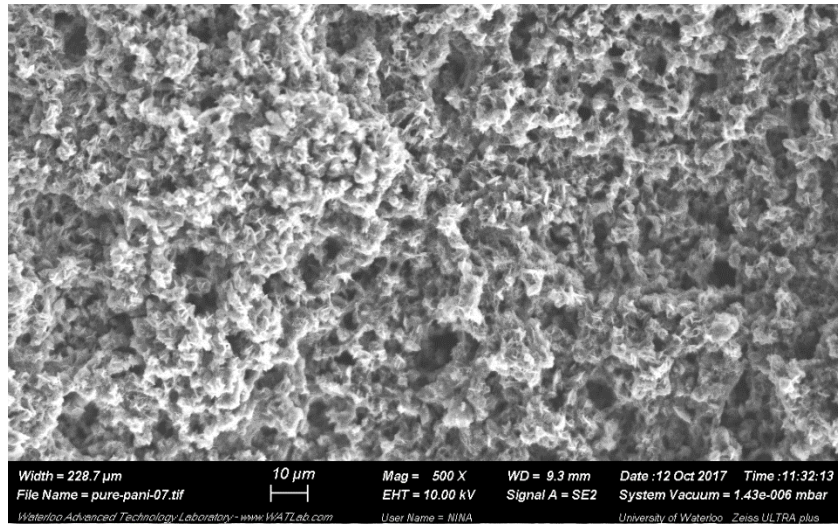
effective sensing material for acetone, it has historically been used in combination with other comonomers (see, for example [172, 176]). Therefore, we can continue to evaluate the potential of PMMA in other capacities.

The sorption capability of the three materials is related to the surface morphology of each polymer. SEM imaging (in Figure 8.2(a) and Figure 8.3(a)) shows that the PANI sample has many ‘cavities’ (well dispersed throughout the sample), and the polymer itself exhibits a fibrous structure, which gives it a large surface area. Similarly, PPy samples are characterized by a large surface area, but in this case it is more due to the granular morphology (see Figure 8.2(b) and Figure 8.3(b)). In both cases, these structures resemble what happens when a catalyst particle accommodates a reaction within it that produces new material. This reaction can cause fragmentation of the (almost spherical) starting particle. This ‘explosion-fragmentation’ in turn creates a large fraction of interstitial space. In other words, more surface area is exposed and thus more area is available for whatever interactions can take place between the sensing material and the analyte in question. Hence, there are many sorption ‘sites’ available for an analyte (like acetone) to sorb (analogous to active sites in a catalytic system that can bind with adsorbing reactant molecules to lead to surface reaction and subsequently desorption of product molecules). Therefore, it makes sense that both PANI and PPy showed good sorption for acetone.

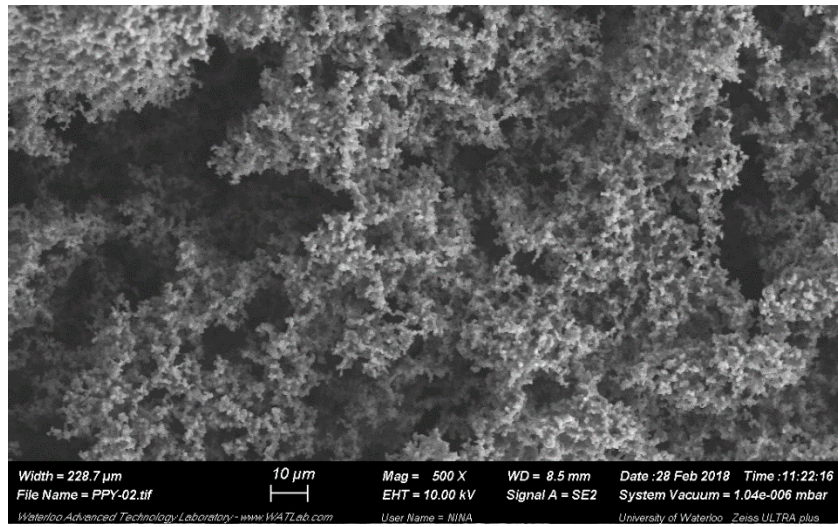
In contrast, Figure 8.2(c) and Figure 8.3(c) provide images of PMMA (at 500X and 5000X magnification, respectively). This is a different material altogether, compared to the other two morphologies discussed above. The image reveals a rather smooth ‘plate-like’ structure. This suggests that the sorption capability of this sample is limited, as the analyte may not sorb as easily to such a uniformly smooth material. Thus, the SEM images further support the sorption measurements: PANI and PPy have more surface area available (compared to PMMA), which is influencing the sorption capabilities.

Thus, based on these preliminary results, PANI and PPy show significantly more promise than PMMA. However, all three polymer backbones are further investigated with the addition of metal oxide dopants, as described in Section 7.2. While PANI and PPy are more likely to be useful for acetone sensing, PMMA is still an interesting material to pursue further. Not only can PMMA act as a substrate for metal oxides, but it may also be useful as a ‘zero baseline’ in future sensing applications.

(a)



(b)



(c)

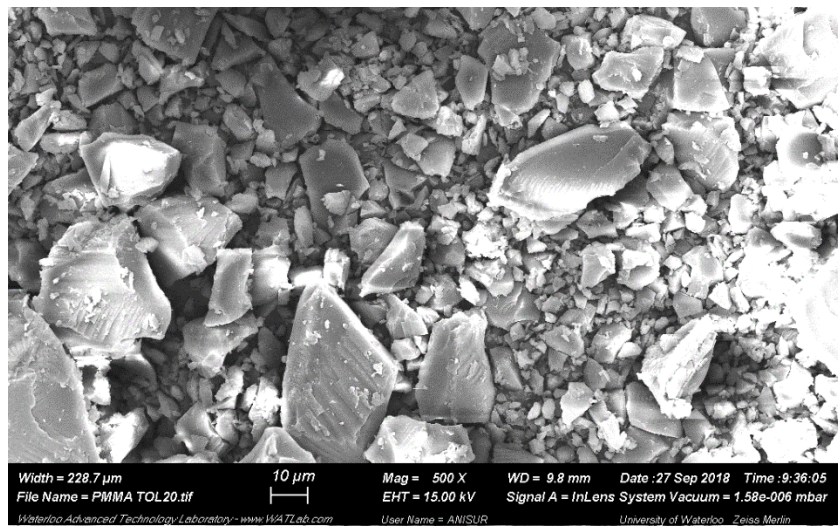
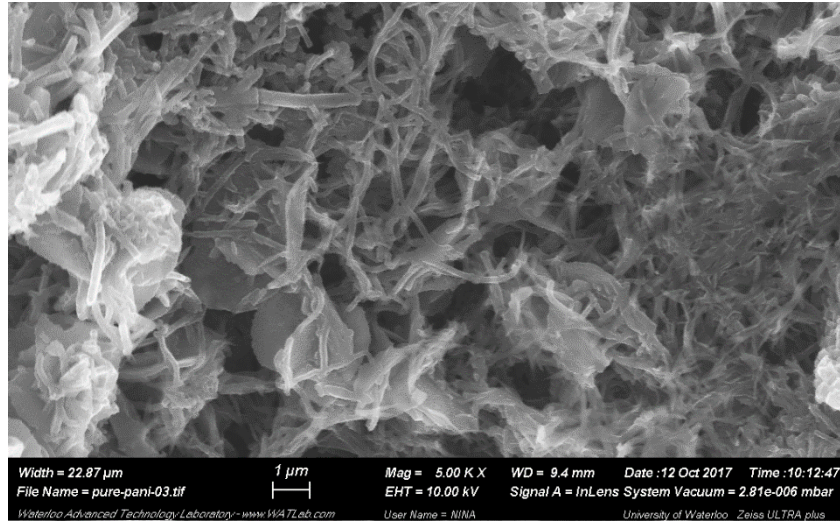
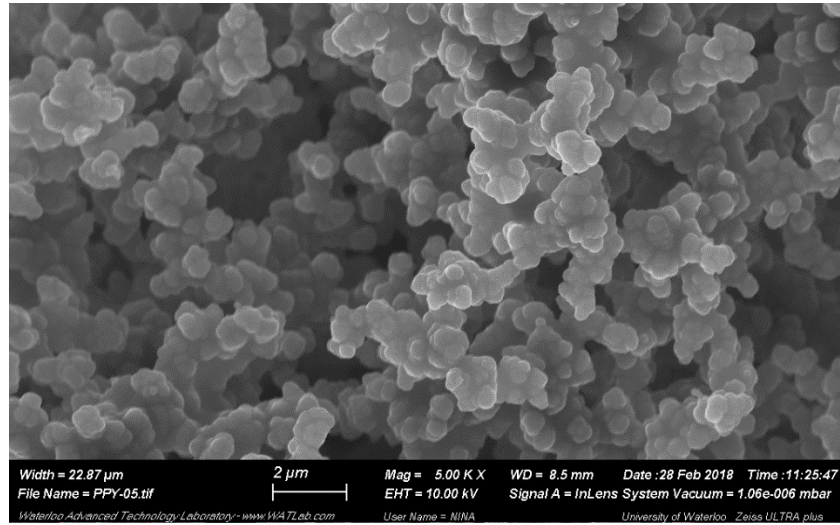


Figure 8.2: Surface Morphology of (a) PANI, (b) PPy and (c) PMMA from SEM at 500X Magnification

(a)



(b)



(c)

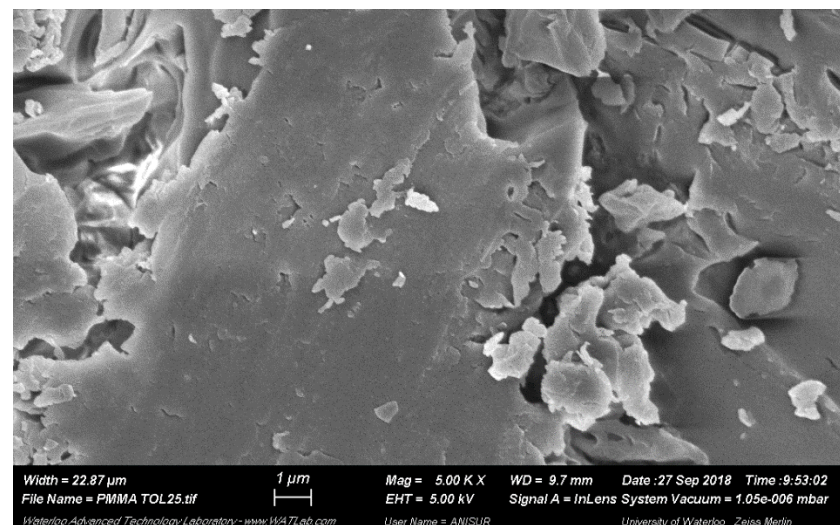


Figure 8.3: Surface Morphology of (a) PANI, (b) PPy and (c) PMMA from SEM at 5000X Magnification

8.1.1.2 PANI-based Polymeric Materials

PANI doped with different levels of SnO₂, WO₃ and ZnO is considered next (formulations #2 through #10 in Table 7.1), and sorption performance is compared to that of pure PANI (formulation #1). First, material properties (namely surface morphology and degree of incorporation of each metal oxide) are evaluated, followed by sorption of acetone from a 5 ppm source (as before).

The degree of incorporation of each metal oxide, as measured by EDX, is shown in Table 8.1. The expected weight percentage of the metal oxide (as calculated for synthesis) is provided in the first column, and the percentage of each metal oxide measured is listed within the table. All measurements took the full imaging area into account so that the measurement would be a good representation of the whole sample. Also, select replicate measurements were taken at different levels of magnification (typically ranging from 500X to 1000X), and showed good repeatability. Where more than one measurement was taken, averages are provided.

Table 8.1: Measured Metal Incorporation for PANI-based Polymeric Materials

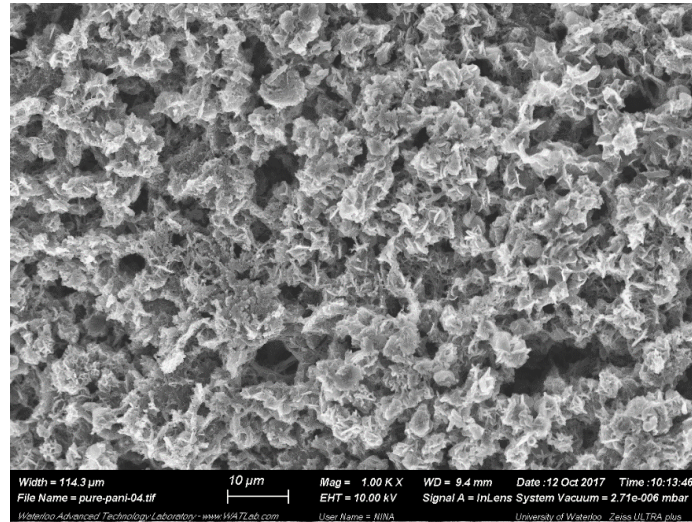
| Polymeric Nanocomposite | wt% of Metal (M) in Product Polymer | | |
|----------------------------|-------------------------------------|-----------------|------|
| | SnO ₂ | WO ₃ | ZnO |
| PANI w 5% MO _x | 7.00 | 0.22 | 0.10 |
| PANI w 10% MO _x | 10.21 | 0.54 | 0.75 |
| PANI w 20% MO _x | 19.57 | 0.77 | 0.94 |

These results indicate that of the three metal oxides investigated, only SnO₂ incorporated into the product polymer. Slight increases in W content and Zn content were observed for the other metal oxides (as the wt% of the metal oxide increased in the recipe), but not by any appreciable amount. Interestingly, while the average measurements for WO₃ were very low, targeted measurements (where metal oxides were clearly visible) showed much higher concentrations of W. These ‘spot’ measurements for different formulations of PANI with WO₃ ranged from 18.79 wt% W to 73.38 wt% W, depending on the area selected. This (along with the SEM images) indicates that WO₃ remains present in the polymer sample, but clumps together in large aggregates (compare Figure 8.4(c) and (d)).

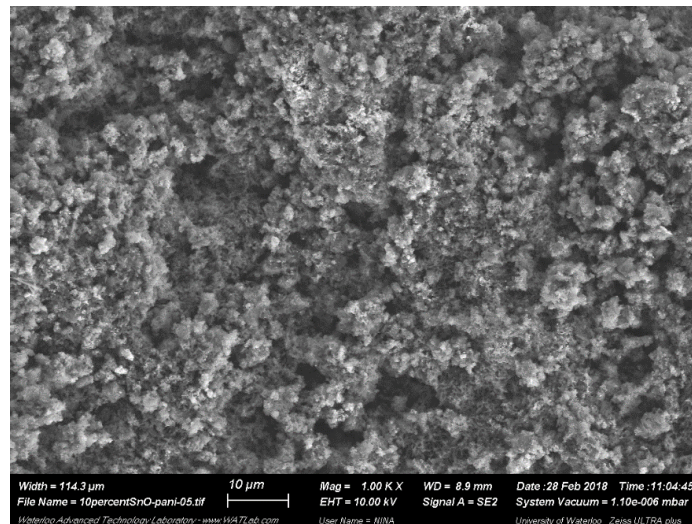
To ensure that WO₃ or ZnO are better incorporated in the future, modifications could be made to the synthesis procedure. For example, one might consider surface modification of the nanoparticles prior to the polymerization, more vigorous mixing during the polymerization, or a multi-step synthesis process. Regardless of the degree of incorporation, the presence of the metal oxides during synthesis may affect the surface morphology of the product polymer. Therefore, representative SEM images are shown in Figure 8.4. Here, the pure (undoped) PANI morphology (Figure 8.4(a)) can be compared to the morphology of the materials doped with 10 wt% of each metal oxide (whether or not large amounts of the metal oxide remain in the final product).

Although the surface morphology of pure PANI has already been shown in Figure 8.2 and Figure 8.3, it is shown again here for comparison at the same level of magnification.

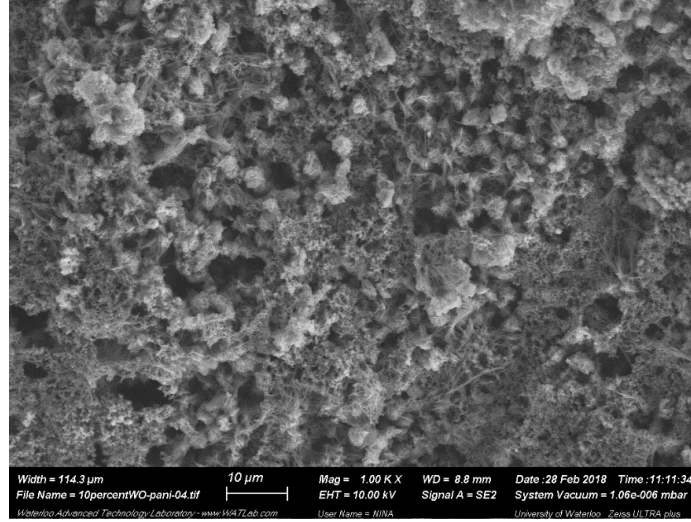
(a)



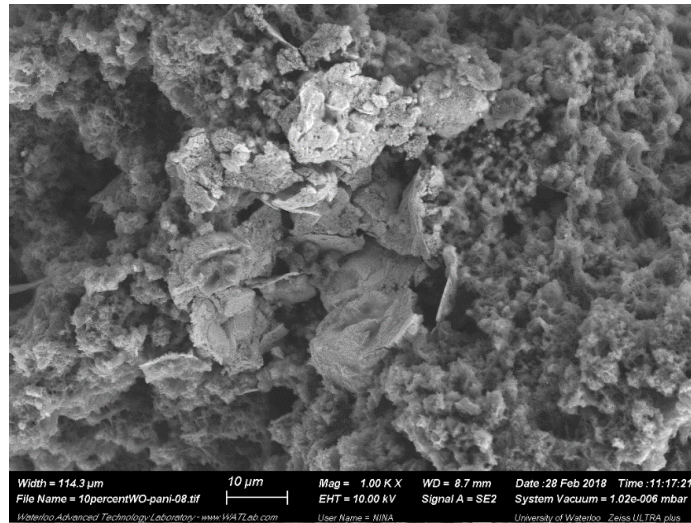
(b)



(c)



(d)



(e)

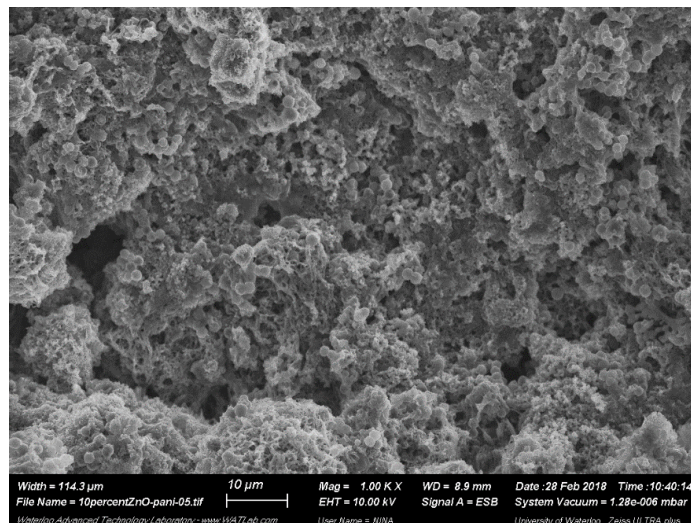


Figure 8.4: Surface Morphology of (a) PANI, (b) PANI doped with 10 wt% SnO_2 , (c) PANI doped with 10 wt% WO_3 (typical result), (d) PANI doped with 10 wt% WO_3 (metal oxide cluster), and (e) PANI doped with 10 wt% ZnO

Figure 8.4(b) is a representative image of SnO₂-doped PANI. There are speckles visible throughout the sample, which indicates that the metal oxide particles are well distributed (as expected given the EDX results of Table 8.1). However, the underlying morphology is very similar to that of the pure PANI (compare Figure 8.4(b) with Figure 8.4(a)). Therefore, although the SnO₂ is well distributed, the surface morphology of the PANI itself remains unchanged.

Figure 8.4(c) and Figure 8.4(d) are both images of WO₃-doped PANI. As discussed earlier, WO₃ nanoparticles tend to form agglomerates during PANI synthesis, thus leaving the majority of the PANI sample with little or no WO₃. In Figure 8.4(c), the WO₃ particles are non-existent. In contrast, Figure 8.4(d) (which is at the same magnification) is dominated by the WO₃ agglomerate. Where WO₃ is absent (in Figure 8.4(c)), the PANI morphology is similar to the pure PANI morphology; one may argue that it has a slightly more granular morphology (which may be due to the presence of WO₃ during synthesis).

Finally, the ZnO-doped PANI is shown in Figure 8.4(e). Given the EDX results of Table 8.1, negligible quantities of ZnO are present in the sample. However, it seems as though the negative space (or ‘cavities’) present in this sample is larger than in the pure PANI. It is possible that the presence of ZnO during synthesis has resulted in a slight deterioration of the morphology; ZnO nanoparticles may have prevented polymer growth in certain locations, only to be rinsed out following polymer synthesis.

Given these observations of the metal oxide effects on the surface morphology, it is interesting to consider how acetone sorption performance has been affected. As before, all sensing materials (formulations #2 through #10) were exposed to 5 ppm acetone in balance nitrogen, and sorption was calculated as described in Section 7.4.2. In this case, different source tanks were used for acetone, which resulted in slight variations in the initial acetone concentration (measured concentrations ranged from 4.64 ppm to 5.98 ppm). Therefore, to account for the tank variation, acetone sorption is normalized and reported as percent sorption ($= [\text{acetone sorbed}]/[\text{initial concentration}] \times 100$). The percent sorption of all 9 materials (and pure PANI, for comparison) is plotted in Figure 8.5.

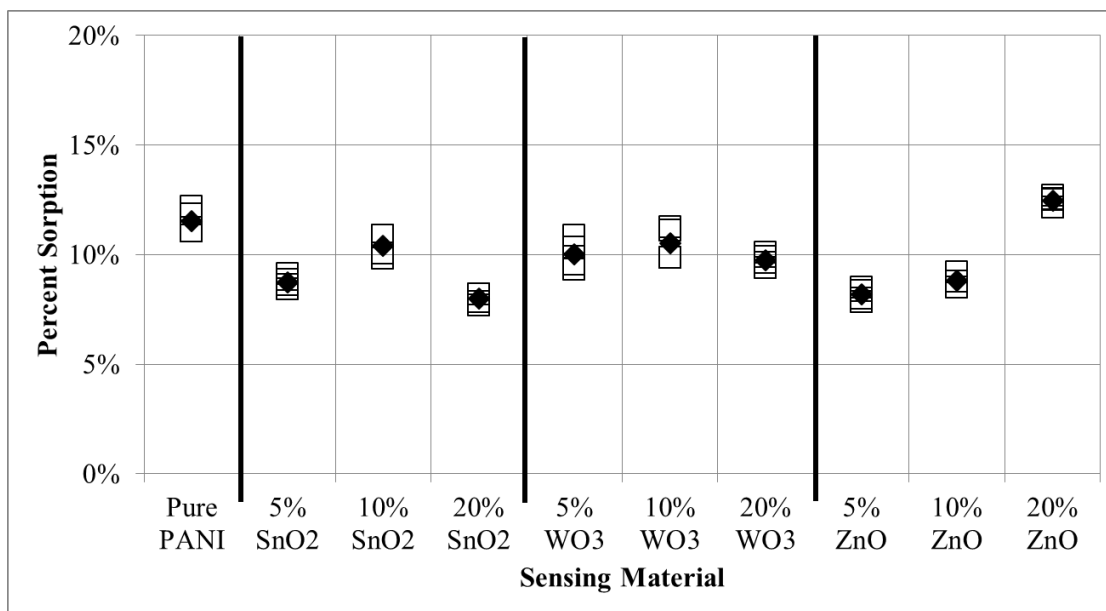


Figure 8.5: Sorption of Acetone for PANI-based Polymeric Materials (formulations #1-#10; source 5 ppm acetone in nitrogen)

Immediately, Figure 8.5 indicates that doping PANI with any metal oxide shows little improvement in the sorption ability; if anything, the sorption of metal oxide-doped materials is lower than the sorption of pure PANI. Statistical comparison of means through Fisher's least significant difference (LSD) test and multiple t-tests (with the Bonferroni correction applied) was used to compare sorption performance within each dopant type (that is, comparing the wt% doped for a given metal oxide); the analysis, shown in Appendix D (Section D.3), is summarized herein:

- For SnO₂-doped materials, sorption averages at the three dopant levels were statistically different. PANI doped with 10% SnO₂ (formulation #3) was found to be statistically better than the other SnO₂-doped materials.
- For WO₃-doped materials, there was no statistical difference between the percentage of acetone sorption at the three dopant levels. PANI doped with 5% WO₃ (formulation #5) is preferred, since it uses the smallest amount of metal oxide and is therefore the least expensive option (if doping is used at all).
- For ZnO-doped materials, sorption averages at the three dopant levels were statistically different. PANI doped with 20% ZnO (formulation #10) was found to be statistically better than the other ZnO-doped materials.

Once the best formulation for each metal oxide was identified, those preferred formulations were compared to each other and to pure PANI (formulation #1). Again, Fisher's LSD and multiple t-tests were performed (see Appendix D, Section D.3). Analysis showed that formulations #1 and #10 (pure PANI and PANI with 20% ZnO) were significantly different (and had better sorption) than formulations #3 and #5 (PANI with 10% SnO₂ and PANI with 5% WO₃). However,

statistically speaking, there was no difference between formulations #1 and #10, and no difference between formulations #3 and #5.

These four materials (formulations #1, #3, #5 and #10) were selected as the best candidates for PANI-based polymeric materials (of the formulations studied thus far), and were therefore considered for the selectivity study. Therefore, the sorption capabilities of these materials will be revisited in Section 8.1.2.

8.1.1.3 PPy-based Polymeric Materials

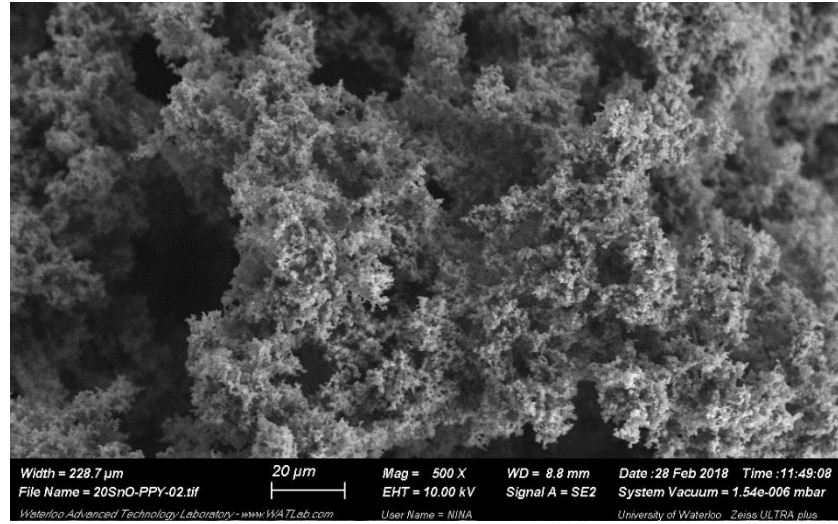
Next, polypyrrole and the metal oxide-doped PPy samples are investigated (formulations #11 to #20 of Table 7.1). Since PPy was the most promising material of the pure polymer backbones studied (recall Section 8.1.1.1), this study examines whether the sorption performance can be improved by incorporating metal oxide nanoparticles. As for the PANI case, surface morphology and degree of incorporation of each metal oxide are evaluated first. Then, the sorption of acetone from a 5 ppm source is measured.

Given the poor incorporation of metal oxides for PANI (and the similar synthesis procedure used for PPy), only PPy doped with 20% of each metal oxide is evaluated herein. As shown in Table 8.2, SnO₂ incorporates better than the other metal oxides, but incorporation is low for all three. Despite low incorporation, the presence of metal oxides may have affected the morphology of the product polymer. Therefore, representative SEM images are provided in Figure 8.6; these can be contrasted with the pure PPy sample imaged at the same magnification, which was shown in Figure 8.2(b).

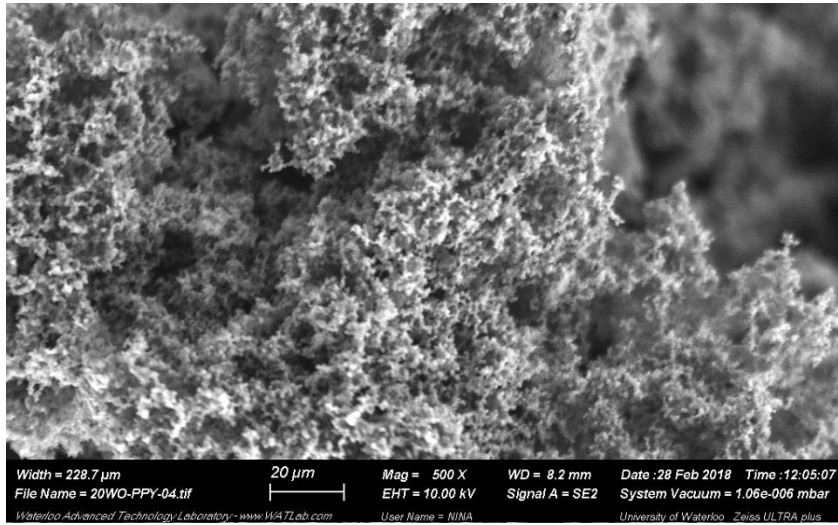
Table 8.2: Measured Metal Incorporation for PPy-based Polymeric Materials

| Polymeric Nanocomposite | wt% of Metal (M) in Product Polymer | | |
|---------------------------|-------------------------------------|-----------------|------|
| | SnO ₂ | WO ₃ | ZnO |
| PPy w 20% MO _x | 8.62 | 2.76 | 0.41 |

(a)



(b)



(c)

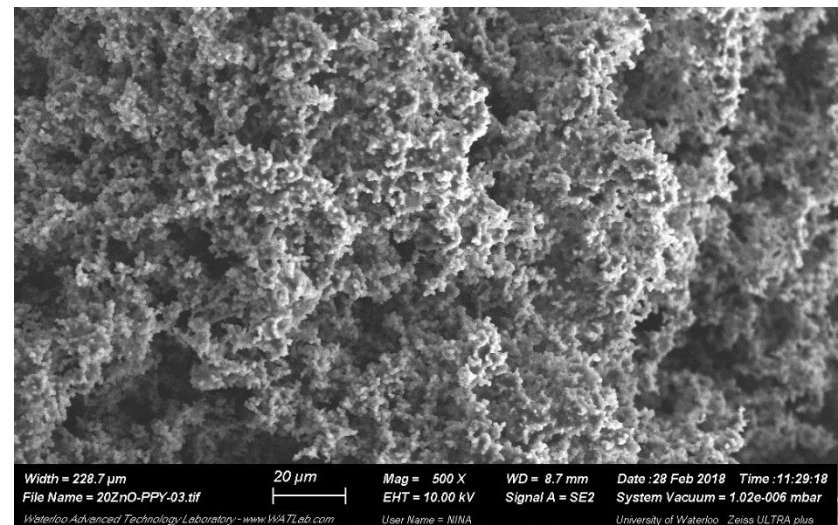


Figure 8.6: Surface Morphology of (a) PPY doped with 20 wt% SnO_2 , (b) PPY doped with 20 wt% WO_3 , and (c) PPY doped with 20 wt% ZnO

The three images in Figure 8.6 are almost identical; the presence of metal oxides during synthesis (even at 20 wt%) seems to have little effect on the PPy surface morphology. One might suggest that Figure 8.6(a) (formulation #14; PPy with 20% SnO₂) has more ‘cavities’ in the sample (compared to the other materials), but the general morphology is the same.

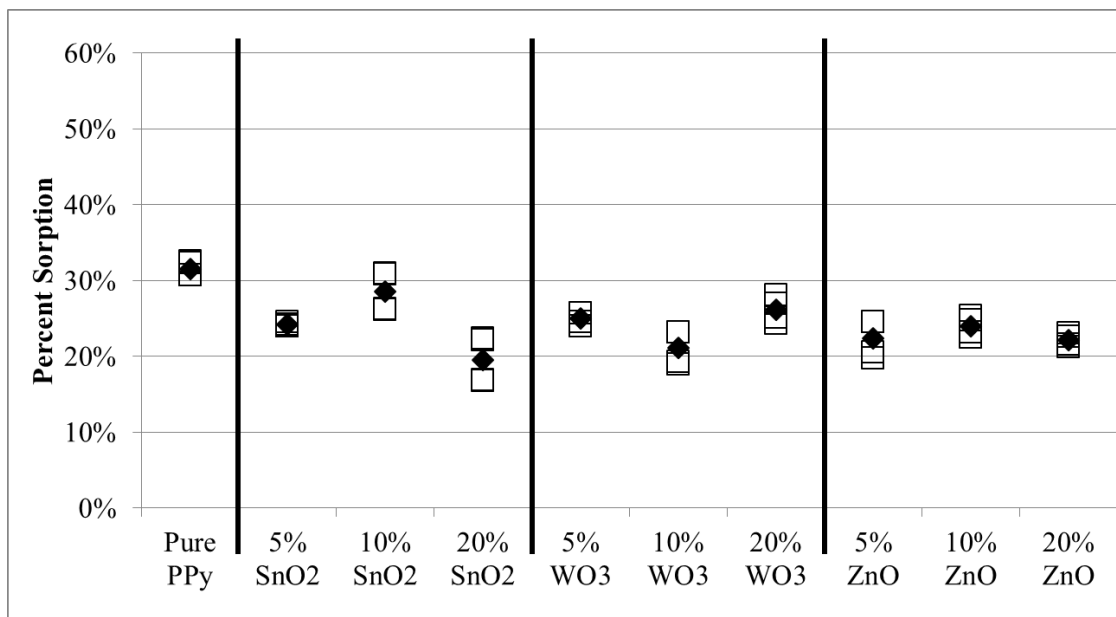


Figure 8.7: Sorption of Acetone for PPy-based Polymeric Materials (formulations #11-#20; source 5 ppm acetone in nitrogen)

In Figure 8.7, the sorption results indicate that the addition of metal oxides reduces polypyrrole’s ability to sorb acetone. This behaviour is similar to what was observed for PANI; the pure polymer (without any dopants) seems to have the highest acetone sorption. Again, though, a full statistical analysis can provide an improved understanding of the materials. Therefore, comparison within each metal oxide (at different levels) is performed first (see again Appendix D, Section D.3), and then the best candidates from each metal oxide grouping are compared to each other and to the pure polymer. The outcomes of the Fisher’s LSD and multiple t-tests are summarized below:

- For SnO₂-doped materials, all three dopant levels showed statistically significant differences in sorption. The best-performing material from this subset was PPy doped with 10% SnO₂ (formulation #13).
- For WO₃-doped materials, statistically significant differences in sorption were detected between 5% and 10%, and between 10% and 20% dopant. In both comparisons, the 10% WO₃-doped material exhibited a lower percentage of sorption, and was therefore ruled out. However, no significant difference was observed in comparing the 5% WO₃ PPy (formulation #15) and the 20% WO₃ PPy (formulation #17). Therefore, for simplicity and to conserve resources, formulation #15 was selected.

- For ZnO-doped materials, no statistical difference was observed as the amount of dopant was varied. Therefore, PPy doped with 5% ZnO (formulation #18) is preferred, since it uses the least metal oxide.
- As before, the final comparison was the ‘best’ performing metal oxide-doped materials relative to the pure (undoped) polypyrrole. Statistically speaking, formulations #11 and #13 were equivalent and exhibited more sorption than the other formulations. Formulations #15 and #18 were not statistically different from one another, but did not perform as well as the other formulations. Therefore, of the formulations shown in Figure 8.7, pure PPy and PPy with 10% SnO₂ show the most potential.

Given these results, formulations #11, #13, #15 and #18 were selected as the best candidates for PPy-based polymeric materials (at least for the formulations studied thus far). Even though #11 and #13 sorbed more acetone under these conditions, the WO₃ and ZnO-doped materials should not be ruled out prematurely. The presence of these other metal oxides (even just during the synthesis step, if not in the product polymers) may provide additional (desirable) properties in terms of selectivity. This will be revisited in Section 8.1.2.

8.1.1.4 PMMA-based Polymeric Materials

As discussed in Section 8.1.1.1, pure (undoped) PMMA showed very low levels of acetone sorption. However, it is worth investigating whether or not it can be used as a substrate for metal oxide nanoparticles (namely, the metal oxides discussed already herein). If the metal oxides promote sorption on their own, we can be further motivated to use them alongside other polymeric materials. That is, if the metal oxides (essentially on their own) show sorption, it may be possible to pursue higher degrees of metal oxide incorporation in the (perhaps more promising) polymer backbones.

In this case (as described in Section 7.2.3), PMMA was purchased directly from the supplier, and the doping involved a mechanical mixing process. Since the sample preparation here did not include any filtration or rinsing, all metal oxides added to the formulation remained within the sample. Given that the amount of metal oxide present in the PMMA sample was known a priori, EDX was not performed.

Select samples were imaged using SEM and a representative image is provided in Figure 8.8. In general, the PMMA did not act as a substrate for the metal oxides. Instead, two separate and distinct components were visible in the sample. In Figure 8.8, for example, the smooth pieces on the left side of the image are PMMA, and the top right corner contains only SnO₂ particles. Thus, incorporation was limited.

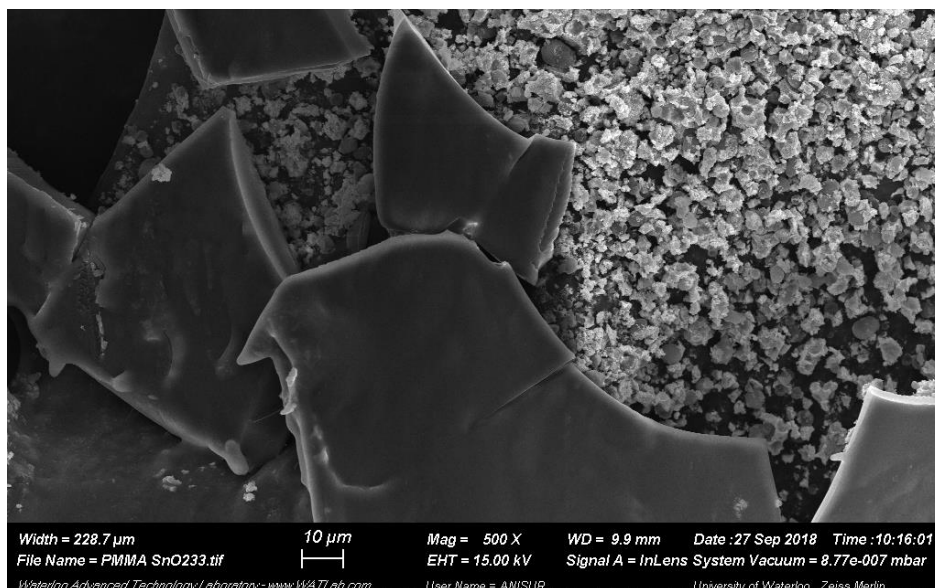


Figure 8.8: Surface Morphology of PMMA doped with 10 wt% SnO₂

For all potential sensing materials that were PMMA-based (formulations #21 to #30 of Table 7.1), the amount of acetone sorbed was negligible. That is, addition of SnO₂, WO₃ or ZnO nanoparticles did not improve the sorption by any appreciable amount. It had already been established that PMMA showed poor sorption on its own, and metal oxide-based sensors often require high temperatures. Additional modifications (including higher molecular weights of PMMA and in situ doping during in-house synthesis) were attempted [262], but similar results were obtained. Therefore, these combinations should not be pursued further for this application. The sorption results for formulations #21 through #30 are shown in Figure 8.9 for the sake of completeness.

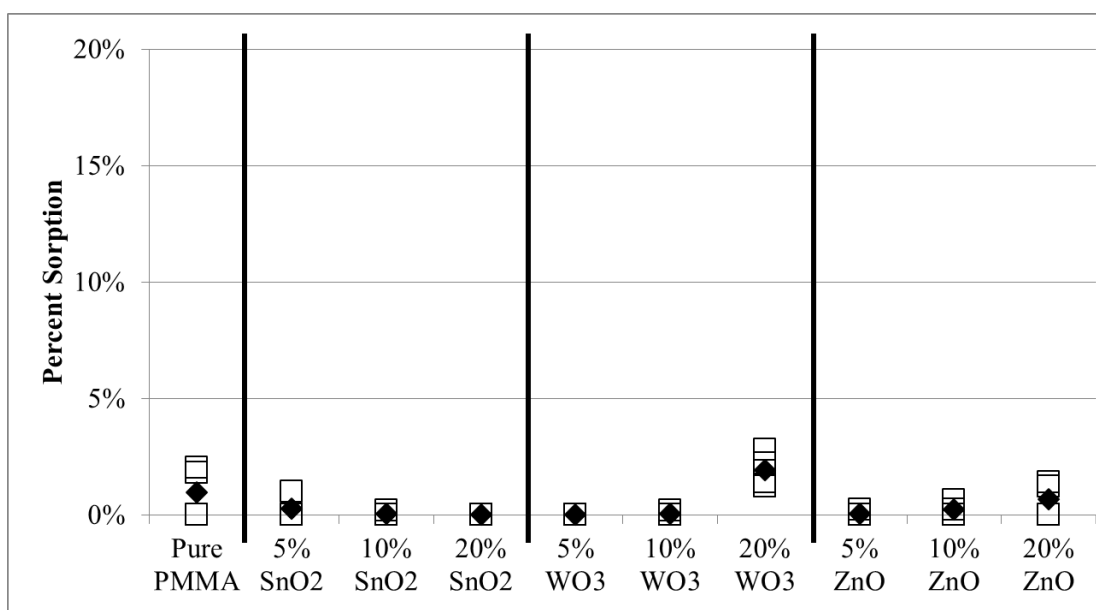


Figure 8.9: Sorption of Acetone for PMMA-based Polymeric Materials (formulations #21-#30; source 5 ppm acetone in nitrogen)

Initially, PMMA was chosen as a sensing material candidate based on previous success in the literature [172, 176] (as well as promising Hildebrand solubility parameters; recall Table 6.2). However, based on the current experimental results, PMMA seems to act more like a substrate for other (more active) polymeric components like PANI and PPy. This makes sense when the sorption mechanisms proposed by Stewart and Penlidis [4, 5] are considered; PMMA does not have the same potential for sorption (through polar effects or hydrogen bonding, for example) compared to PANI or PPy. Also, from the SEM results (Figure 8.8), it is clear that the morphology of PMMA (at least at this molecular weight) is not conducive for sorption, as the sample surface is completely smooth. Polymeric materials that are porous (like both of the sensing materials described earlier) are more readily able to sorb gas analytes. Therefore, due to both the sensing mechanisms and the physical properties of PMMA, it is not a promising material for acetone sorption.

Although PMMA seems incapable of sorbing acetone under these conditions, the observed results are still useful for sensing applications. Zero-sorption materials can be used in sensors or sensor arrays to establish a baseline, which can help reduce the number of false positives in a sensing study [259]. Therefore, this result, though negative with respect to the sorption capabilities of PMMA, can still inform future work, as it is useful in establishing a true zero.

8.1.2 Selectivity – Mixtures of 4 Gases

Following the sensitivity study of Section 8.1.1, a selectivity study was performed for the most promising materials. As described in Section 7.4.2, polymers were introduced into the experimental set-up for evaluation of sensing materials and were exposed to four gas analytes simultaneously. That is, each polymeric material was exposed to a mixture of acetaldehyde, ethanol, acetone and benzene (in balance nitrogen). These analytes were specifically chosen as representatives of different volatile organic compounds, so that the sorption of acetone could be measured in the presence of interfering aldehydes, alcohols and aromatics.

Eight polymeric sensing materials were used for this portion of the study. PANI-based materials and PPy-based materials showed promise in the sensitivity study (Section 8.1.1), but PMMA-based materials were not pursued further. As mentioned previously, statistical comparison of means through Fisher's least significant difference (LSD) test and multiple t-tests (with the Bonferroni correction applied) were used to compare sorption performance of materials. The materials selected as 'most promising' either improved sorption in a statistically significant way (compared to other loadings of a given metal oxide) or, if no statistically significant improvement was observed, the lowest (and therefore most cost effective) metal oxide loading was selected. Therefore, based on the results of Section 0, formulations #1, #3, #5 and #10 (from Table 7.1) were chosen for the selectivity study of PANI-based materials. Similarly, based on the results of Section 8.1.1.3, formulations #11, #13, #15 and #18 (also from Table 7.1) were investigated as representative PPy-based materials. Selectivity results from gas mixtures with equal

concentrations of all analytes (Section 8.1.2.1) and acetone-rich mixtures (Section 8.1.2.2) are presented in what follows.

8.1.2.1 Gas Mixtures with Equal Concentrations of Analytes

To establish each polymeric material's ability to sorb acetone in the presence of other interferent gases, each material was exposed to a 4-gas mixture containing acetaldehyde, ethanol, acetone and benzene (in balance nitrogen). The concentration of each gas in the mixture was $0.9 \text{ ppm} \pm 0.1 \text{ ppm}$, and the total concentration of analytes in the gas mixture ranged from 3.3 ppm to 4.0 ppm. Therefore, the gas mixture is slightly less concentrated than that used for the pure acetone study, and there are several analytes competing for sorption sites. This is essentially mimicking a 'healthy breath' scenario; endogenous volatile organic compound concentrations should generally be fairly low. As reported by Rooth and Ostenson [149], the breath acetone levels for their control group averaged 0.95 ppm (although healthy levels reported by Jones [263] were as high as $4.01 \text{ } \mu\text{g/L}$ (3.46 ppm)). The other gas analytes are also expected to be present in low quantities (assuming the subjects are healthy and no exogenous factors are contributing). Jones [264] reported typical acetaldehyde breath concentrations ranging from 0.2 nmol/L to 0.6 nmol/L (7.6 ppb to 22.8 ppb), with higher levels after the moderate consumption of alcohol. Higher levels of ethanol levels have been reported, again by Jones [263]: breath ethanol measurements ranged from 0.07 to $0.39 \text{ } \mu\text{g/L}$ (60.3 ppb to 336 ppb) when no exogenous alcohol was consumed. Finally, benzene is not expected to be present in breath samples in any appreciable amount (unless the subject is a smoker [265, 266] or has had substantial environmental exposure [267, 268] – these levels are beyond the scope of this work). However, benzene was selected for inclusion in the current study to examine the sorption effects of aromatic compounds and because benzene is a typical 'bulky' interferent.

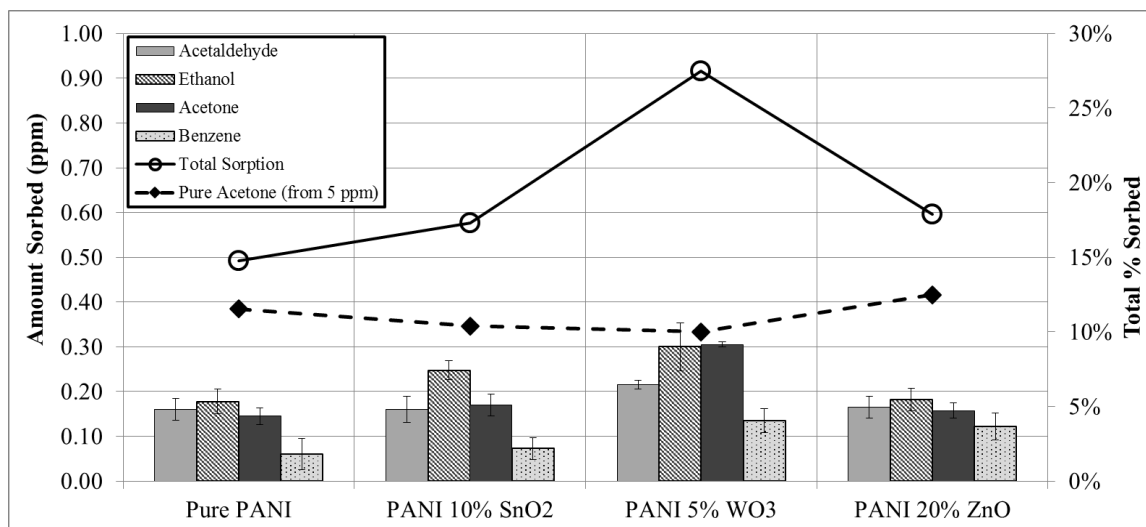


Figure 8.10: Sorption of Acetaldehyde, Ethanol, Acetone and Benzene for PANI-based Polymeric Materials (formulations #1, #3, #5 and #10); source ~1 ppm each analyte in nitrogen)

Figure 8.10 shows the sorption results for each of the most promising PANI-based materials (pure PANI and one representative sample for each of the metal oxides). The bar graph provides the average amount of each analyte sorbed, and is presented in terms of absolute concentration sorbed (in ppm) rather than the (normalized) percent sorption of earlier plots (since very low concentrations are being considered here). In parallel, the line graph provides a comparison of the total percentage sorbed for the combination of analytes and the percentage of acetone sorbed from the 5 ppm source (described in Section 0 for the sensitivity study).

For all PANI-based materials, acetaldehyde, ethanol and acetone show similar amounts of sorption. Thus, all four materials shown in Figure 8.10 have poor selectivity toward acetone. In fact, only the PANI with 5% WO₃ (formulation #5) sorbs acetone in the highest proportion, but statistically speaking there is no difference in sorption between ethanol and acetone. The other three materials sorb ethanol more than acetone, but, again, the selectivity is quite poor. Therefore, these materials would not be used in isolation to sorb low concentrations of acetone, but may be useful as part of a sensor array [251]. This information can also help to establish a baseline for a 'negative' result (that is, breath acetone levels are normal and are not indicative of high blood glucose).

The comparison of line plots shows an increase in the percentage of analyte sorption for the 4-gas mixture (compared to pure acetone at 5 ppm). This is especially evident for the WO₃-doped PANI (formulation #5), which allowed 27.5% sorption (compared to 10.0% sorption for acetone alone). For the 4-gas mixture, both the ethanol sorption and the acetone sorption were fairly high; one might suggest that the presence of ethanol is enhancing acetone sorption, thus increasing the overall analyte sorption. However, a more detailed study (with gas mixtures containing only ethanol and acetone, for example) would be needed to confirm this hypothesis. Regardless, it seems as though some synergistic effect is improving sorption of the gas mixtures on the PANI-based sensing materials.

Next, the same experimental investigation is performed for the most promising PPy-based materials (again, with representative samples doped with each of the three metal oxides). The sorption of each analyte in the 4-gas mixture (acetaldehyde, ethanol, acetone and benzene) is presented in the bar graph portion of Figure 8.11, while the total percentage of sorption (from 5 ppm pure acetone and from the 4-gas mixture) is shown as a line graph.

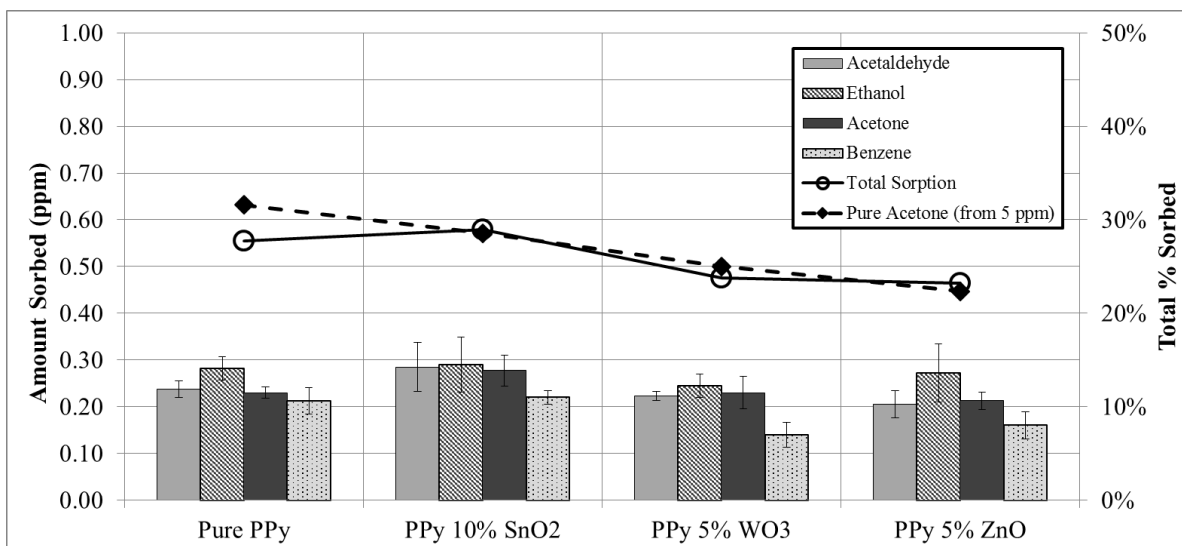


Figure 8.11: Sorption of Acetaldehyde, Ethanol, Acetone and Benzene for PPy-based Polymeric Materials (formulations #11, #13, #15 and #18); source ~1 ppm each analyte in nitrogen)

Again (as observed for the PANI-based materials), there is no appreciable selectivity towards acetone. In fact, ethanol sorption is slightly higher than acetone sorption for all four materials. The same statements made previously (about PANI-based materials) are valid here: one might use these results in establishing a baseline for a ‘negative’ result (normal/healthy breath acetone levels) and these sensing materials may be useful in sensor arrays [251].

The more interesting result for PPy-based materials is related to the comparison of line graphs for total sorption of the 4-gas mixture and the total sorption of 5 ppm acetone (from the sensitivity study of Section 8.1.1.3). As shown in Figure 8.11, the two sets of experiments provide nearly identical sorption results. That is, regardless of whether the PPy-based sensing materials are exposed to pure acetone (at 5 ppm) or a mixture of gas analytes (totaling ~ 4 ppm), the proportion of gas analytes sorbed remains approximately consistent. This suggests that polypyrrole (and metal oxide-doped polypyrrole samples) are indiscriminately sorbing all analytes, and that the materials are not selective towards any particular chemical species. Thus, these polymers may not be useful for detecting one particular target analyte, but (again) could be useful in a sensor array or as a material for air filtration applications.

8.1.2.2 Acetone-Rich Gas Mixtures

While the polymeric sensing materials did not demonstrate good selectivity when exposed to 1 ppm gas mixtures, the results of Section 8.1.2.1 provide information about the behaviour of the sensing materials when all analytes are present in low concentrations. As described in the introduction, several (sometimes conflicting) relationships between breath acetone and blood glucose have been reported. However, these studies have motivated our work to detect (relatively)

high acetone concentrations in gaseous samples, even in the presence of other interfering gas analytes.

For the final stage of this investigation, the acetone concentration in the gas mixture can be increased, thus creating an acetone-rich gas mixture (with acetaldehyde, ethanol and benzene present as interferents). Although the exact (expected) concentration of acetone varies considerably in biological studies, a relatively high acetone concentration was selected herein. If, in reality, breath acetone levels are lower, the sorption response would likely be lower as well. However, as proof of concept, PANI-based materials and PPy-based materials were exposed to a 4-gas mixture of acetaldehyde (1.3 ppm \pm 0.1 ppm), ethanol (1.3 ppm \pm 0.2 ppm), acetone (105 ppm \pm 5 ppm) and benzene (1.4 ppm \pm 0.2 ppm).

For brevity, only the sorption response of pure PANI and pure PPy are shown herein; similar results were obtained for the metal oxide-doped materials. A comparison of sorption performance for the gas mixtures where all analytes had similar concentration levels (labeled 1 ppm gas mixture in Figure 8.12) and the acetone-rich (A-rich) gas mixtures is provided below.

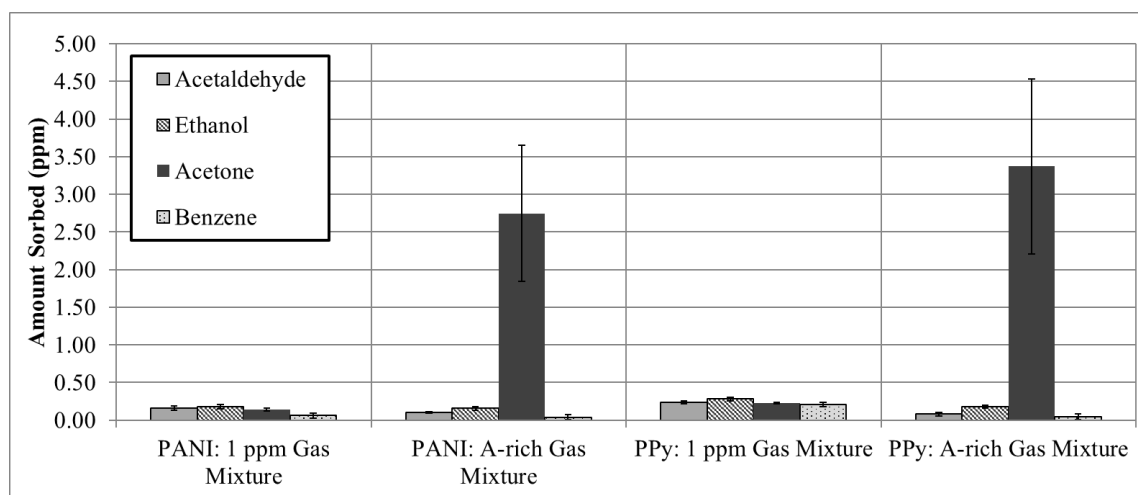


Figure 8.12: Sorption of Acetaldehyde, Ethanol, Acetone (A) and Benzene for Pure PANI and Pure PPy (formulations #1 and #11); source ~1 ppm each analyte in nitrogen or A-rich gas mixture)

The PANI: 1 ppm Gas Mixture and the PPy: 1 ppm Gas Mixture data have been shown previously (in Figure 8.10 and Figure 8.11, respectively), but are shown again herein for direct comparison (and to appreciate the scale of sorption of the acetone-rich gas mixtures. A clear increase in acetone sorption is visible for both pure PANI and pure PPy, which is expected given the significant increase in acetone exposure. In both acetone-rich (A-rich) cases, error bars (representative of standard deviation over 6 replicates) are much wider, but this is due to the larger absolute value of the measurements (especially compared to the non-dominant analytes: acetaldehyde, ethanol and benzene). The results obtained from both PANI and PPy suggest that both polymers show promise as sensing materials for acetone detection, as long as the acetone is present in much larger

concentrations than other interfering gases. However, a better understanding of acetone levels in breath measurements would be needed to quantify the required ratio of acetone to interferents in the source gas. In the current study, acetone was approximately 100x more abundant than the other analytes, which may not be representative of actual conditions.

It is also interesting to note that the amount of acetone sorbed is not proportional to the concentration of acetone in the source gas. That is, when the acetone concentration in the source gas is increased by two orders of magnitude, the same kind of increase is not observed in the sorption response. The same type of behaviour was observed for all PANI-based and PPy-based materials (including the metal oxide-doped polymers) exposed to ~100 ppm acetone in the gas mixture; total acetone sorption was always well below 10 ppm. This could indicate that the polymeric sensing material is saturated, and that no additional analyte units would sorb onto the sample (even at higher concentrations).

A final observation from Figure 8.12 is the decreased sorption of the interferent gases present in the acetone-rich gas mixture. Take PANI, for example: in comparing the sorption of acetaldehyde, ethanol and benzene from the 1 ppm gas mixture to the sorption of those analytes from the acetone-rich mixture, all three analytes sorb more in the 1 ppm gas mixture case. The same relationship can be observed for the PPy case. This is somewhat counterintuitive, as the concentration of each interferent analyte in the source gas is lower for the 1 ppm mixture ($0.9 \text{ ppm} \pm 0.1 \text{ ppm}$ for the equal concentration study, vs. concentrations $> 1.0 \text{ ppm}$ for the acetone-rich study). One might expect that having higher concentrations in the source gas would increase the sorption of each analyte. However, in this case, the high acetone concentration seems to be dominating the system. As a result, the analytes are competing for the sorption sites available on the sensing material; the high concentration of acetone leaves fewer sorption sites available for the interferent analytes. This explains the reduced sorption of acetaldehyde, ethanol and benzene that occurs in spite of increased concentrations in the source gas.

8.1.3 Concluding Remarks on Screening Experiments for Acetone Sensing

In this detailed preliminary study, polyaniline, polypyrrole and poly(methyl methacrylate) were doped with varying levels of metal oxide nanoparticles (namely SnO_2 , WO_3 and ZnO at 5%, 10% and 20% doping by weight). Thirty polymeric materials were characterized (in terms of polymer properties and application-specific behaviour). Only SnO_2 incorporated well into the polymeric materials, but did not appreciably affect the sorption of acetone. WO_3 and ZnO incorporation was poor, and (again) doping had a minimal effect on the concentration of acetone sorbed. In spite of the low incorporation of metal oxides, PANI-based materials and PPy-based materials were found to be the most promising candidates. PMMA-based materials did not show significant sorption, and metal oxide nanoparticles on PMMA (with PMMA essentially acting as a substrate) did not show any sorption under the experimental conditions used for this study.

Eight of the most promising materials (formulations #1, #3, #5, #10, #11, #13, #15 and #18 from Table 7.1) were studied further through two selectivity studies. These formulations represent PANI- and PPy-based polymers, each in its pure form and doped with each metal oxide (dopant levels selected based on sensitivity results). Selectivity studies were performed using a custom-made gas testing system [261]; polymeric sensing materials were exposed to four gas analytes (acetone and three interferent gases). When all four analytes were present in equal concentrations, selectivity was poor (that is, none of the materials could preferentially sorb acetone). However, given an acetone-rich mixture (where the acetone concentration was 100x higher than the concentration of the interferent gases), acetone sorption was much increased.

In comparing the polymer surface morphology to the sorption ability, we would suggest that the materials with the more porous structures sorb more acetone (PPy > PANI > PMMA). However, even the most porous materials are not selective. For PPy, for example, exposure to 5 ppm acetone (in nitrogen) or a mixture of 4 different gas analytes (with the total concentration ~ 5 ppm) led to the same total proportion of analytes sorbed. Therefore, the polypyrrole samples indiscriminately sorb all analytes, and the material is not selective towards any of the four chemical species.

Additional customization of materials is necessary to improve the selectivity of sensing materials. One might consider some (or all) of the following: (1) trying to improve the degree of incorporation of metal oxides, (2) acid-doping polyaniline to change the backbone charge (thereby taking advantage of the polarity of acetone) or (3) creating multi-component polymers containing two or more of the backbones listed in Section 6.1.3. Some of these (especially items (2) and (3)) will be considered in Section 8.2.

8.2 Customized Experiments: Acid-Doped Polymers and Copolymers

8.2.1 Investigation of Polymer Properties

Given the results of the previous section, customized polymeric materials (to further improve sensitivity and selectivity toward acetone) were synthesized as described in Section 7.2.4. These materials either (1) were doped in situ with oxalic acid (to increase protonation of the polymer backbone), (2) were copolymers of the two most promising materials (PANI and PPy), or (3) were acid-doped copolymers (that is, a combination of both modifications (1) and (2)). To ensure that these synthesis modifications affected the polymer product, samples were characterized in terms of crystallinity and surface morphology.

To establish a reference point for XRD results, pure PANI (not doped; synthesized in deionized water as described in Section 7.2.1) is analyzed first (see Figure 8.13; red curve). The XRD pattern shows two main peaks: the first at 18.6° and the second at 25.4°. These are in relatively good agreement with other XRD characterization results reported for PANI [234, 269-271], although

the first peak occurs at a slightly lower angle than expected. Most researchers postulate that the earlier peak (around 20°) is attributed to a periodicity parallel to the polymer chain and the later peak (between 24° and 26°) is attributed to a periodicity perpendicular to the polymer chain [272]. The characteristic peaks shown in Figure 8.13 were obtained from [271], but all references listed above show equivalent agreement with our experimental results. The slight discrepancy in the first peak (comparison from literature and comparison between replicates) may be due to the presence of a different form of PANI (different oxidation state or acid/base form).

Now, the pure PANI (formulation #31, synthesized in water; red curve) can be compared to the acid-doped PANI (formulation #32, synthesized in oxalic acid; green curve); see again Figure 8.13. The peak observed at 25.4° for the PANI sample is also present for the ox-PANI sample, but the earlier peak (at $2\theta = 19.9^\circ$ for ox-PANI) has shifted to the right. In fact, the peak is better aligned with the characteristic peaks from literature, for which the occurrence is at $2\theta = 19.5^\circ$. This result makes sense when we consider that the literature values [271] were measured for PANI samples synthesized in acetic acid. Therefore, the two materials synthesized in acids (our ox-PANI and the PANI characterized by Noby et al. [271]) have more consistent XRD characteristics (compared to PANI synthesized in deionized water). Also, one might postulate that the shift in the first peak is due to acid-doping.

The later peaks in Figure 8.13 (the largest of which is at $2\theta = 43.8^\circ$) are likely related to the sample holder response. Finally, from this preliminary XRD analysis, the characteristic peaks are fairly sharp (especially relative to the XRD results shown in what follows), which suggests that PANI exhibits some crystalline behaviour.

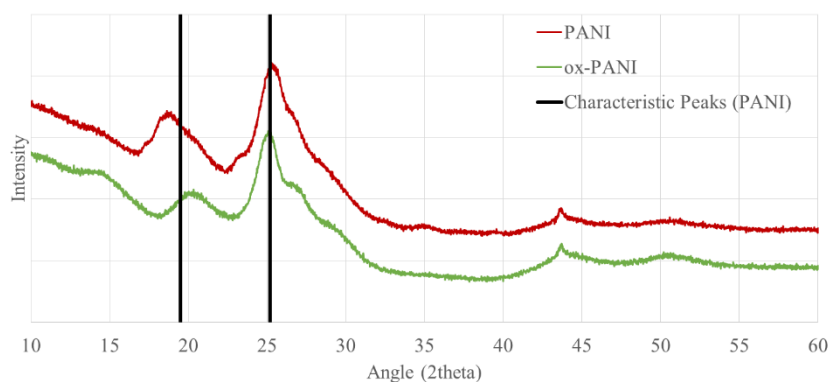


Figure 8.13: XRD for pure PANI (formulation #31) and ox-PANI (formulation #32); characteristic peaks reported by Noby et al. [271]

Before examining the crystallinity of the PANI/PPy copolymer, it is important to characterize samples containing the pure PPy homopolymer (formulation #11). XRD was performed twice for PPy, and samples were independently prepared for XRD from a common synthesis. As shown in Figure 8.14, excellent agreement was observed between the two replicates. Also, from the

literature, the location of the primary characteristic peak ranges from $2\theta = 24^\circ$ [273] to $2\theta = 26^\circ$ [274], which is in good agreement with our experimental result. The broader peaks (especially compared to PANI and ox-PANI in Figure 8.13) indicate that the material is more amorphous, and this result is in agreement with previous studies [273, 274]. Again, the later peak is observed at $2\theta = 43.8^\circ$ (and a broader peak is observed at $2\theta = 50.6^\circ$). These are aligned with peaks identified (at the same angles) in Figure 8.13, which confirms that they are not sample-specific, and are responses from the XRD sample holder.

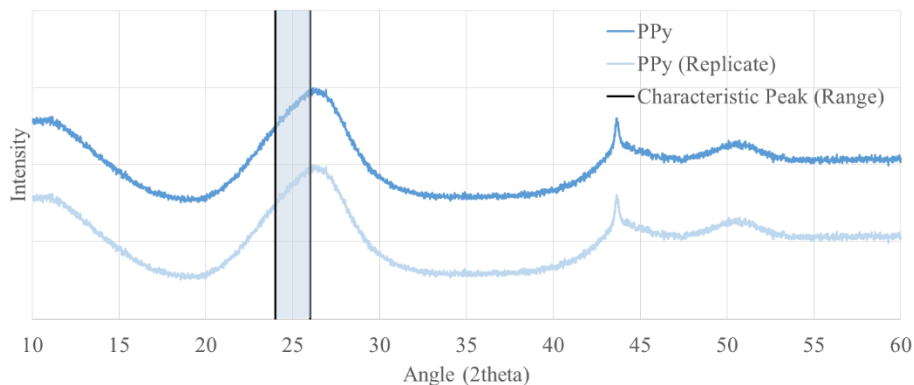


Figure 8.14: Replicated XRD for pure PPy (formulation #11); characteristic peak range reported by Chougule et al. [273] and Waghuley et al. [274]

The analysis of the PANI/PPy copolymer is especially important; a unique scan (that is, a unique XRD pattern) can confirm that a new copolymer has been synthesized. If, for example, the trace for formulation #33 (the PANI/PPy copolymer) was exactly the same as one of the related homopolymers (pure PANI or pure PPy), it would indicate that one monomer was preferentially added during chain propagation and that a homopolymer formed, even in the presence of the second comonomer (recall Section 2.2.1). Also, given the comparison of PANI/PPy synthesis techniques published by Hammad et al. [234], the main diffraction peak should be centred between $2\theta = 20^\circ$ and $2\theta = 24^\circ$.

Figure 8.15 confirms the successful synthesis of a PANI/PPy copolymer. The primary peak for the copolymer (at $2\theta = 22.2^\circ$) falls between the pure PANI and pure PPy peaks, which suggests that it is incorporating properties from both comonomers but is, in fact, a distinct polymer product. Given the broad peak, the copolymer is amorphous in nature, and it seems to be more structurally similar to PPy than to PANI. Also, the peak for the PANI/PPy copolymer falls in the centre of the range reported by Hammad et al. [234]; the expected range for the main diffraction peak is included in Figure 8.15 for reference.

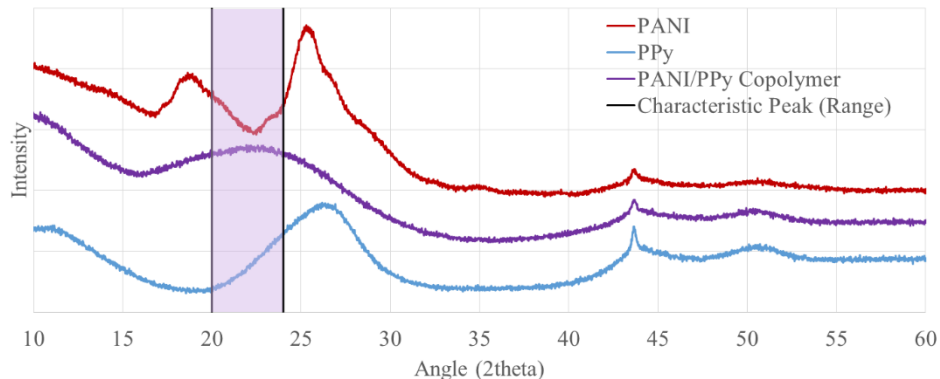


Figure 8.15: XRD for the copolymer of PANI/PPy (formulation #33); characteristic peak range reported by Hammad et al. [234]

The relationship between the PANI/PPy copolymer (formulation #33) and the ox-PANI/PPy copolymer (formulation #34) is examined next (Figure 8.16). This comparison of XRD patterns makes it possible to establish whether the addition of oxalic acid to the formulation had any effect on the product copolymer. The main diffraction peak of the ox-PANI/PPy copolymer is not as broad as that of the PANI/PPy copolymer, which suggests that it is more crystalline. Also, the peak center is shifted to the right for the oxalic acid-doped sample; this behaviour was also observed when the PANI homopolymer was doped with oxalic acid (recall Figure 8.13).

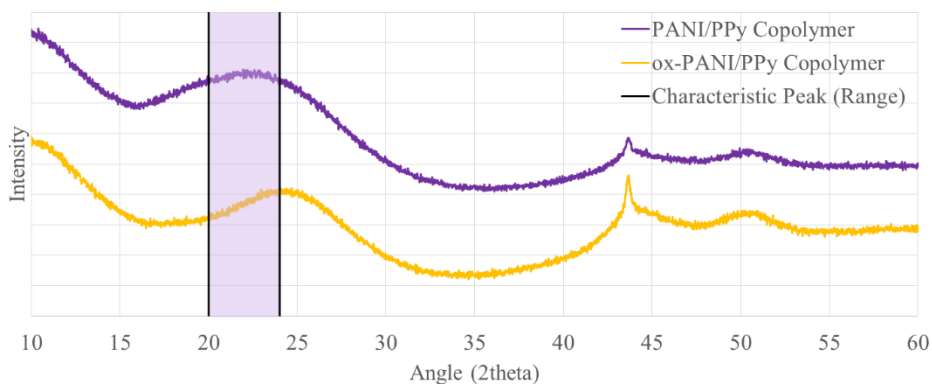


Figure 8.16: XRD for the copolymer of ox-PANI/PPy (formulation #34) compared to PANI/PPy (formulation #33); characteristic peak range (for PANI/PPy copolymer) reported by Hammad et al. [234]

Finally, for comparison, the crystallinity of the pure PMMA (average molecular weight $M_w \sim 15,000$) investigated in Section 8.1 was analyzed (see Figure 8.17). The peaks are much larger than the other samples, which is simply a result of a higher sample loading (PMMA was not synthesized in-house, so larger quantities are available for analysis). The characteristic peaks of PMMA are observed at $2\theta = 15^\circ$, 30.2° and 42.2° [275], and are included in Figure 8.17 for reference. An important observation here is the very broad peak; it is by far the least crystalline sample of the three original polymer backbones (PANI, PPy and PMMA). This indication that the PMMA sample is amorphous, along with the smooth ‘plate-like’ polymer surface shown in Section

8.1.1 (Figure 8.2 and Figure 8.3), can be linked to the poor application performance (that is, negligible acetone sorption). Therefore, the properties of PMMA (low crystallinity and smooth surface morphology) make it unsuitable as a sensing material for acetone.

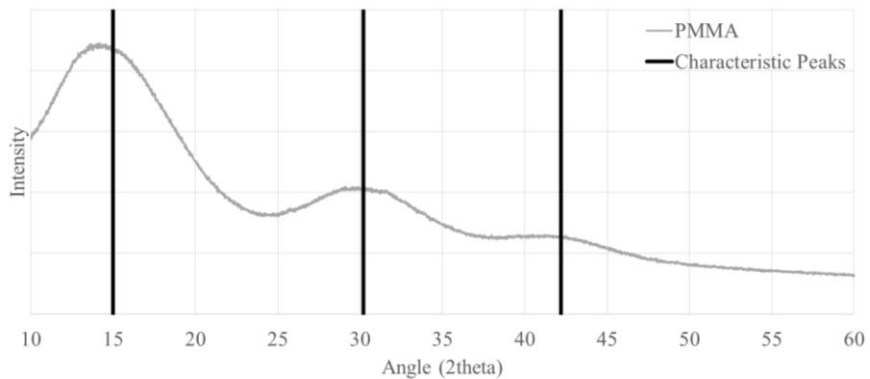
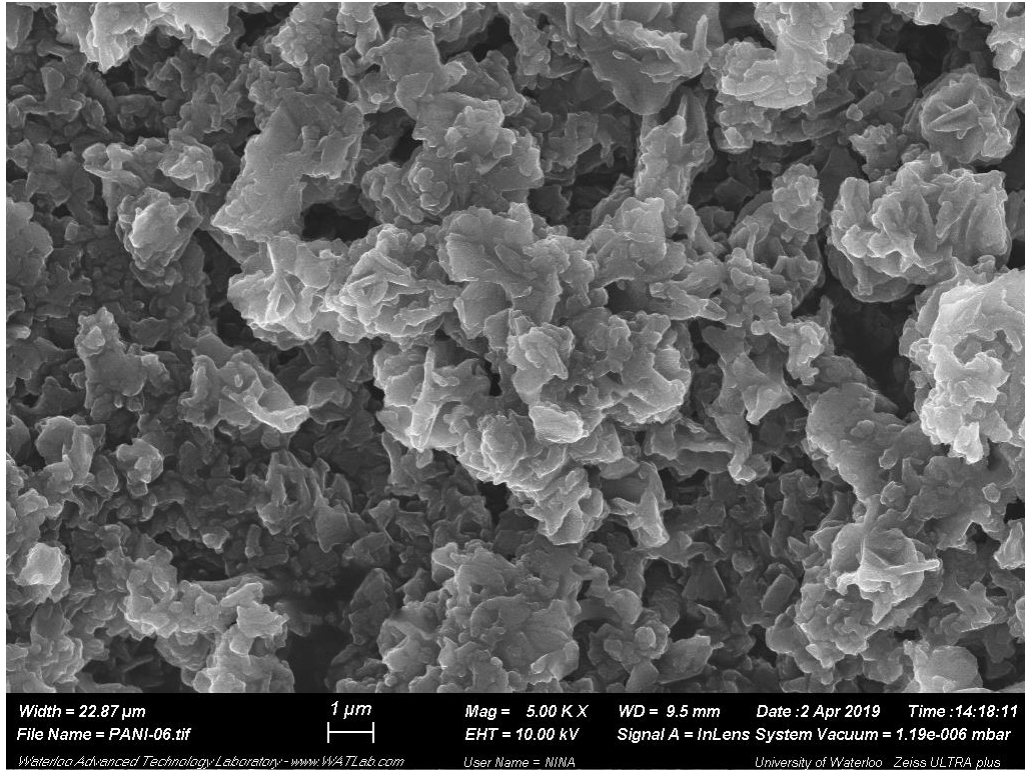


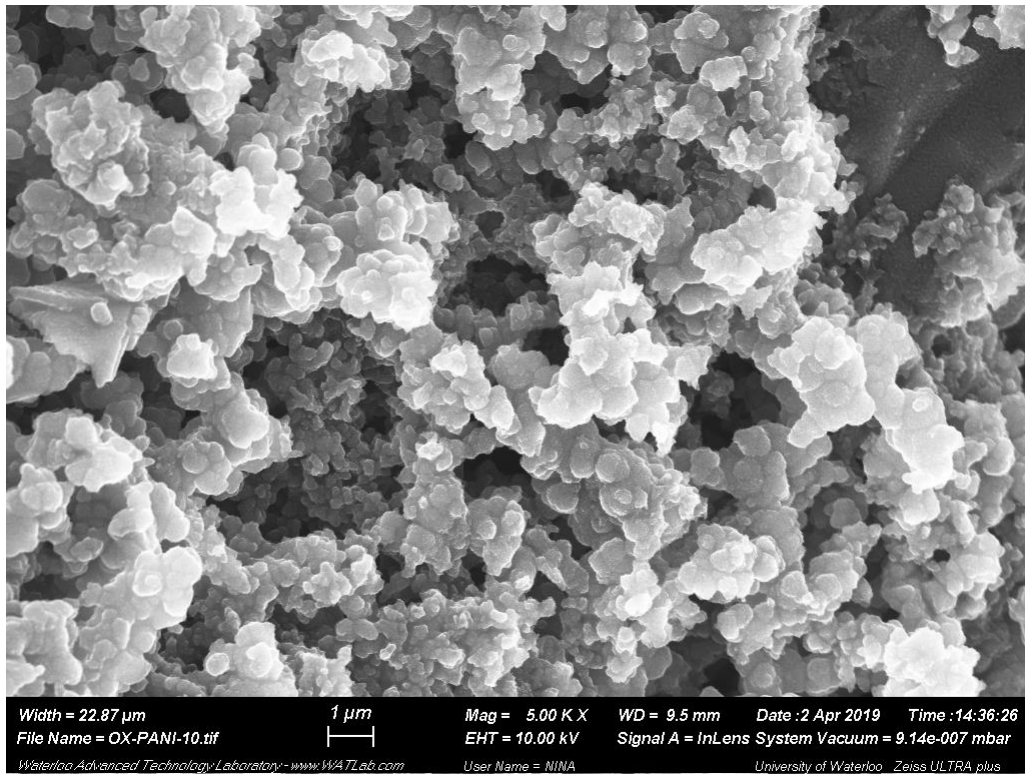
Figure 8.17: XRD for PMMA (formulation #21); characteristic peaks reported by Abdelrazek et al. [275]

The surface morphologies of the customized samples (formulations #32 to #34) were examined and properties were compared to those of pure PANI (formulation #31); see Figure 8.18. Additionally, these samples can be compared to the original polymeric materials (PANI, PPy and PMMA) examined in Section 8.1.1.1.

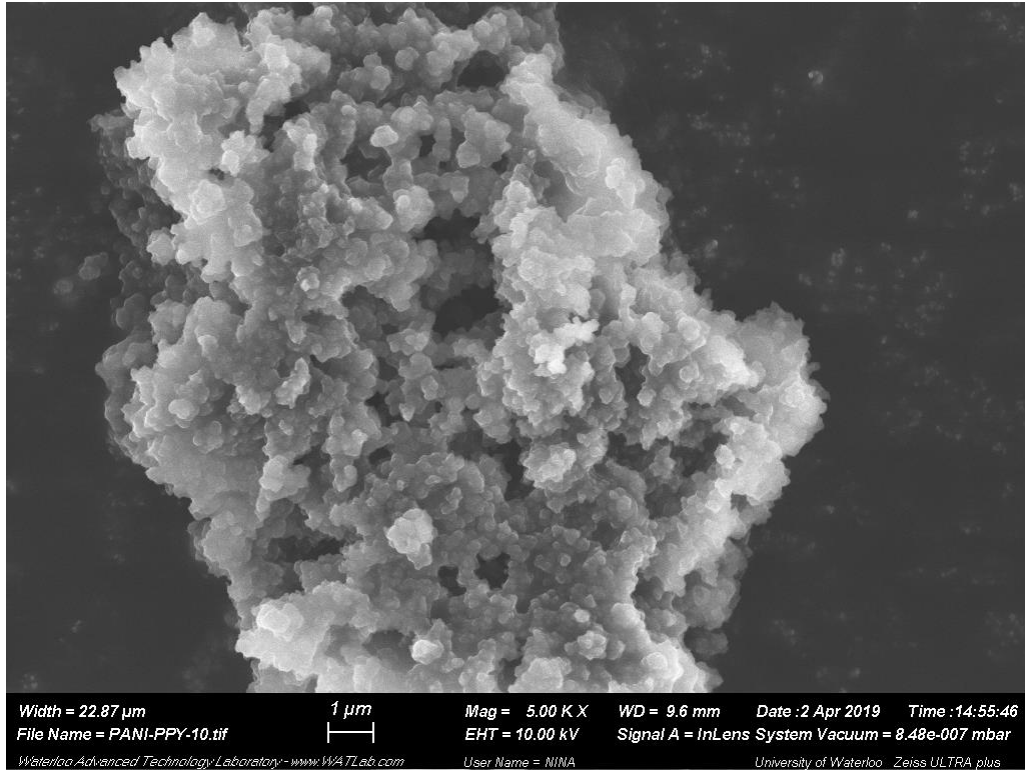
(a)



(b)



(c)



(d)

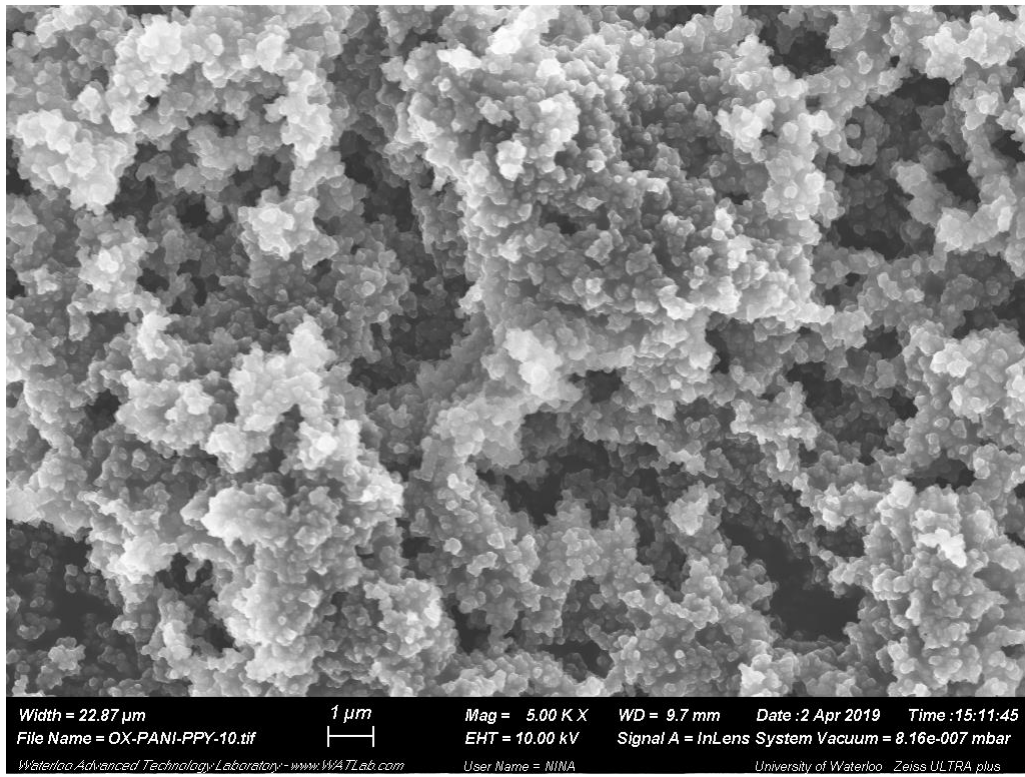


Figure 8.18: Surface Morphology of (a) PANI (b) ox-PANI, (c) PANI/PPy and (d) ox-PANI/PPy from SEM at 5000X Magnification

As observed previously (recall Figure 8.3), pure polyaniline contains many well-dispersed ‘cavities’ throughout the sample, which provides a large surface area for sorption. Interestingly, in this synthesis replicate (Figure 8.18a), the fibrous structure seen earlier (in Figure 8.3a) is less pronounced. Although the fibres are still visible, there is also a layered characteristic here, where polymer ‘sheets’ seem stacked on top of each other. The minor structural variation here may be due to any number of influences, such as slight temperature fluctuations during synthesis or sample preparation for SEM (that is, mounting the polymer sample onto the stub).

Using pure polyaniline (formulation #31) as the benchmark for surface morphology, we can examine the effect of adding oxalic acid as an in situ dopant and/or pyrrole as a comonomer. PANI imaging reveals surface structures that are fibrous and sheet-like, and these features have fairly sharp edges. In contrast, the ox-PANI (Figure 8.18b) exhibits a more rounded polymer surface. Kulkarni et al. [223] described oxalic acid-doped PANI (ox-PANI) as a sponge-like structure resulting from aggregates of small granules; our observations are well-aligned with this account.

Both copolymers of PANI/PPy (synthesized in water and in aqueous oxalic acid; Figure 8.18c and Figure 8.18d, respectively) seem to have increased surface area compared to the homopolymers of PANI or PPy. The materials have the same granular structure observed for the PPy homopolymer (Figure 8.3b), and exhibit a very small average particle size. This allows for a large surface area, which may lead to increased sorption (this hypothesis will be tested in the following section). In comparing the copolymers with and without oxalic acid doping, we would suggest that the ox-PANI/PPy granules (Figure 8.18d) have a more uniform size than the PANI/PPy granules (Figure 8.18c). Also, the ox-PANI/PPy samples has more interstices (and therefore more sorption sites) than ox-PANI.

8.2.2 Investigation of Application-Specific Properties

Equipped with the knowledge that the polymer properties have been successfully modified, the next step involves re-evaluating the application performance of these customized polymeric sensing materials. As before, sensitivity is evaluated first by exposing each candidate sensing material to 5 ppm acetone in balance nitrogen. The sorption results are presented in Figure 8.19 for formulations #31 to #34, and can be contrasted with the sorption measured in the screening stage (recall Figure 8.5, Figure 8.7 and Figure 8.9). For this study, eight replicates were collected for each material (rather than four replicates in the screening study). This increases our confidence in the final experimental results.

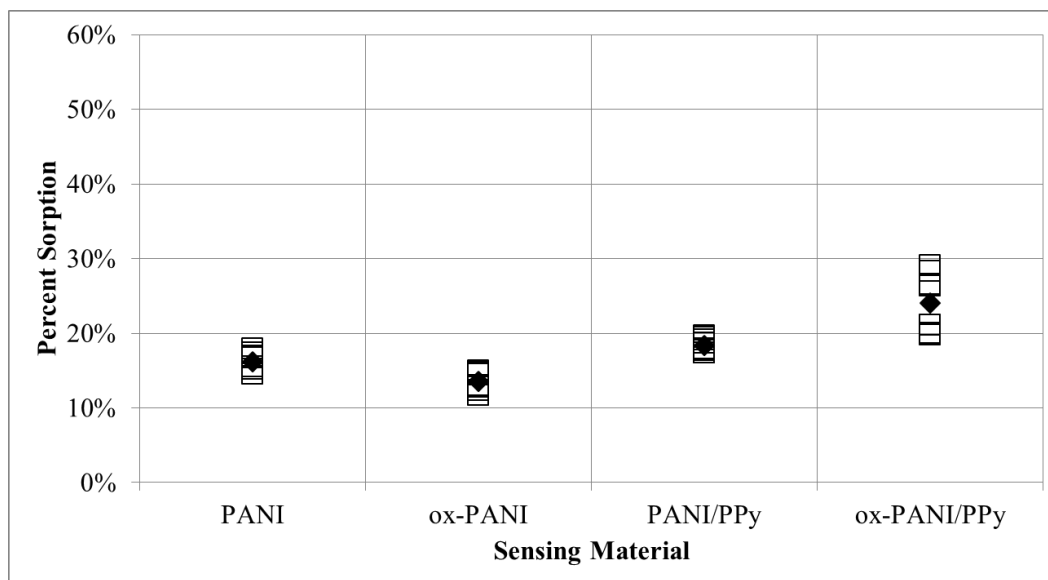


Figure 8.19: Sorption of Acetone for Customized Polymers (source: 5 ppm acetone in nitrogen)

The materials synthesized in this stage are able to sorb more acetone than PANI-based polymers (Figure 8.5) and PMMA-based polymers (Figure 8.9) studied previously. In fact, the pure PANI shown in Figure 8.19 uses the same formulation as the pure PANI shown in Figure 8.5, but the sorption is slightly higher for these later experiments (average 12% in Figure 8.5 vs. 16% in Figure 8.19). Of the four samples shown herein, ox-PANI/PPy (formulation #34) demonstrates the highest percent sorption, but also contains the most variability in results. On the other hand, ox-PANI (formulation #32) provides the lowest amount of sorption, but sorption is only slightly lower than for pure PANI. In comparing the sorption performance of these materials using Fisher's LSD test and multiple t-tests (see Appendix D, Section D.3), the following two conclusions can be made:

- Sorption capabilities of ox-PANI and PANI/PPy are not statistically different than pure PANI. Therefore, adding oxalic acid or pyrrole (as a comonomer) to the synthesis process does not increase the amount of acetone sorbed from a 5 ppm source.
- The copolymer of PANI/PPy synthesized in oxalic acid (ox-PANI/PPy, formulation #34) allows for more sorption than the other three materials, and the improvement is statistically significant in all cases. Thus, the combination of the oxalic acid and the pyrrole comonomer in the formulation does increase the amount of acetone sorbed.

Despite the increase in sorption observed for ox-PANI/PPy, all four materials are still sorbing a lower percentage of the total analyte source compared to PPy-based materials (average acetone sorption of pure PPy was 32%; recall Figure 8.7). This is not unexpected; both PANI and PPy showed promise in terms of sensitivity, but the main motivation at this customization stage was to improve the selectivity. Moderate sorption levels are acceptable for sensing materials, as long as the target analyte sorbs more than any interferent analytes present in the system. Selectivity studies for the customized polymeric materials (using the same interferent gases as in Section 8.1.2) are presented in what follows.

The selectivity analysis performed at this stage was more in-depth than the previous selectivity studies (shown in Section 8.1.2), since each interferent gas was examined individually. That is, acetone was mixed with one interferent gas at a time, and the response of each two-gas mixture was recorded. Also, each combination of gases and sensing materials was evaluated with six replicates. The results are shown in Figure 8.20 through Figure 8.22.

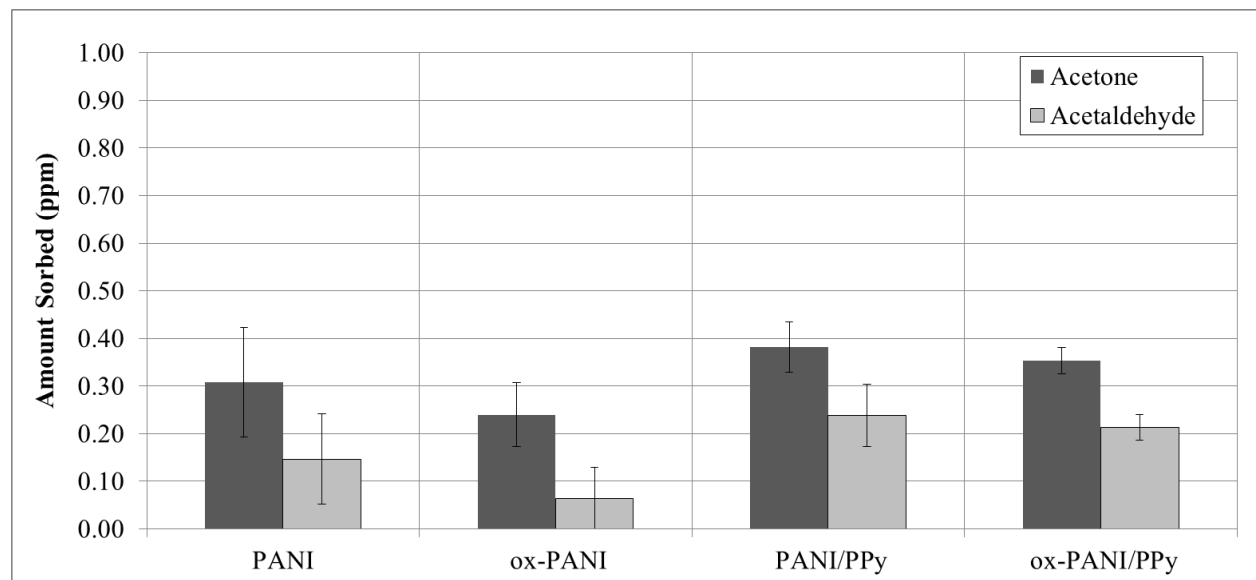


Figure 8.20: Sorption of Acetone in the Presence of Acetaldehyde for Customized Polymeric Materials (formulations #31 to #34); source ~2 ppm each analyte in nitrogen)

As per Figure 8.20, acetone sorbs at a higher concentration than acetaldehyde when the custom sensing materials are exposed to the two-gas mixture; this is the case for all four materials. It is interesting to note that pure PANI (formulation #31) exhibits selectivity towards acetone, especially since acetone and acetaldehyde sorbed in similar amounts when the four-gas mixture was tested previously (recall Figure 8.10). However, given the size of the error bars (representative of the standard deviation over six replicates), the selectivity towards acetone may be slightly less than what was observed during these experimental runs. Of the four materials, the largest experimental error was recorded for PANI and ox-PANI. This error is likely due to the very low concentrations being evaluated by the highly specialized GC and the fact that PANI sorption was affected by humidity. PANI/PPy and ox-PANI/PPy were also moderately selective towards acetone under these conditions. The total concentration of analytes sorbed was higher for the copolymers (compared to PANI and ox-PANI) and the quantitative sorption measurements were more repeatable. A comparison of selectivity values for all four materials is presented in Table 8.3.

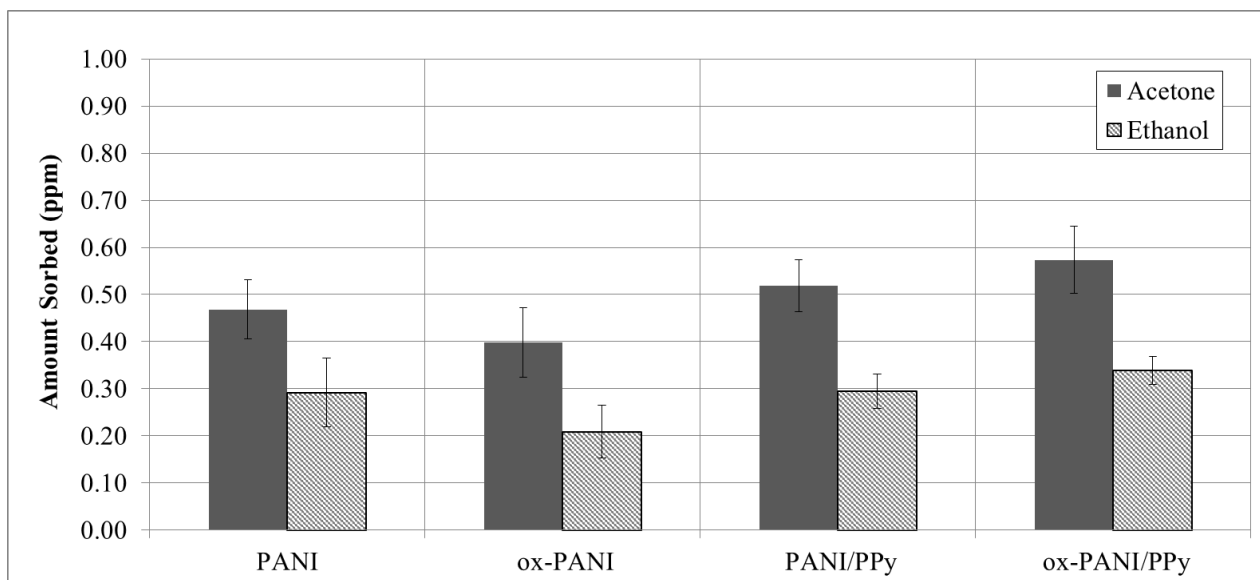


Figure 8.21: Sorption of Acetone in the Presence of Ethanol for Customized Polymeric Materials (formulations #31 to #34); source ~3 ppm each analyte in nitrogen)

For the two-gas mixture of acetone and ethanol, acetone sorbs in a higher proportion for all four polymeric materials (Figure 8.21). Compared to the acetone and acetaldehyde gas mixture, the sorption of acetone is higher for the acetone and ethanol gas mixture (approximately 150% higher in most cases). This may be a result of the higher source gas concentration (~3 ppm rather than ~2 ppm), but it may also be related to the synergistic effects observed previously (recall discussion surrounding Figure 8.10 for the four-gas mixture). That is, it could be that the presence of ethanol in the gas mixture is enhancing acetone sorption. Again, the selectivity of these materials towards acetone in the presence of ethanol is given in Table 8.3.

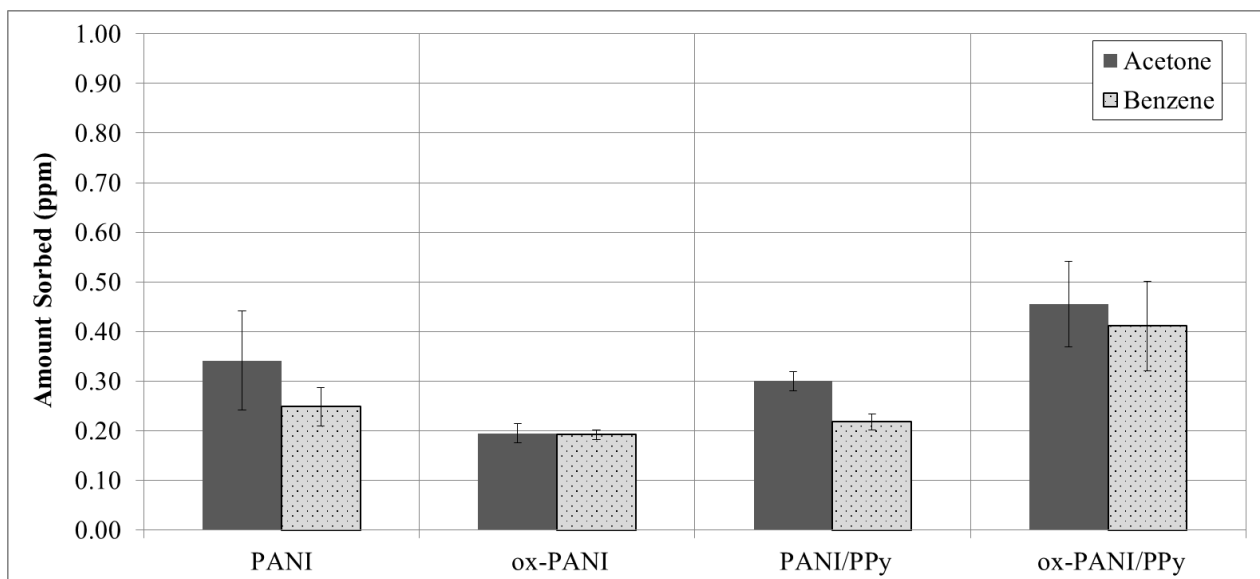


Figure 8.22: Sorption of Acetone in the Presence of Benzene for Customized Polymeric Materials (formulations #31 to #34); source ~ 2 ppm each analyte in nitrogen)

Finally, a two-gas mixture of acetone and benzene was evaluated (Figure 8.22). The low selectivity towards acetone here is surprising, especially since benzene was the least-sorbed analyte when the four-gas mixtures were evaluated during screening experiments (Figure 8.10 through Figure 8.12). It is possible that benzene is interacting with acetone (and subsequently the polymeric sensing materials) since there are no other competing analytes. The fact that the selectivity is close to unity (Table 8.3) may indicate that the benzene is ‘piggy-backing’ onto the acetone before (or during) sorption, which allows the benzene and the acetone to sorb at approximately equal concentrations.

Table 8.3: Average Selectivity of Customized Polymeric Materials for Three Distinct Interferent Gases

| Polymeric Material | Acetaldehyde | Ethanol | Benzene |
|---------------------------|---------------------|----------------|----------------|
| PANI | 2.10 | 1.61 | 1.38 |
| ox-PANI | 3.79 | 1.91 | 1.01 |
| PANI/PPy | 1.60 | 1.76 | 1.37 |
| ox-PANI/PPy | 1.65 | 1.69 | 1.11 |

Due to the unexpectedly high benzene sorption observed in Figure 8.22, the materials were re-evaluated for benzene sorption (without acetone or other interferent gases present). Each material’s sorption from a 5 ppm benzene source (balance nitrogen) was evaluated and compared to sorption from a 5 ppm acetone source (as described earlier; results shown in Figure 8.19). If benzene is sorbing directly onto the polymeric material (that is, competing against acetone for active sorption sites), the percent sorption calculated will be similar to the percent sorption determined for acetone. However, if benzene sorption is ‘enhanced’ in the presence of acetone, the experimentally determined sorption from the 5 ppm benzene source will be lower than those measured from the 5 ppm acetone source.

Figure 8.23 confirms our hypothesis that the polymeric materials are not specifically attracting benzene; the percent sorption is significantly lower than it was for acetone (the acetone sorption is shown again herein for direct comparison). Therefore, benzene sorption is increased in the presence of acetone, and this synergistic effect is most likely responsible for the low selectivity reported in Table 8.3. This relationship could be beneficial in sensing applications: although benzene does not sorb well on its own, it seems to ‘attach’ to acetone (in approximately a 1:1 ratio). Therefore, the acetone response is somewhat amplified in the presence of benzene, and this can improve the detection of acetone. That said, if this behaviour is to be exploited for sensing materials, the potential interaction of benzene with other gas analytes (like ethanol, for example) should also be evaluated. Additional evaluation of gas analyte interactions (between each other and between sensing materials) will reduce the potential for ‘false positives’ in future sensor applications.

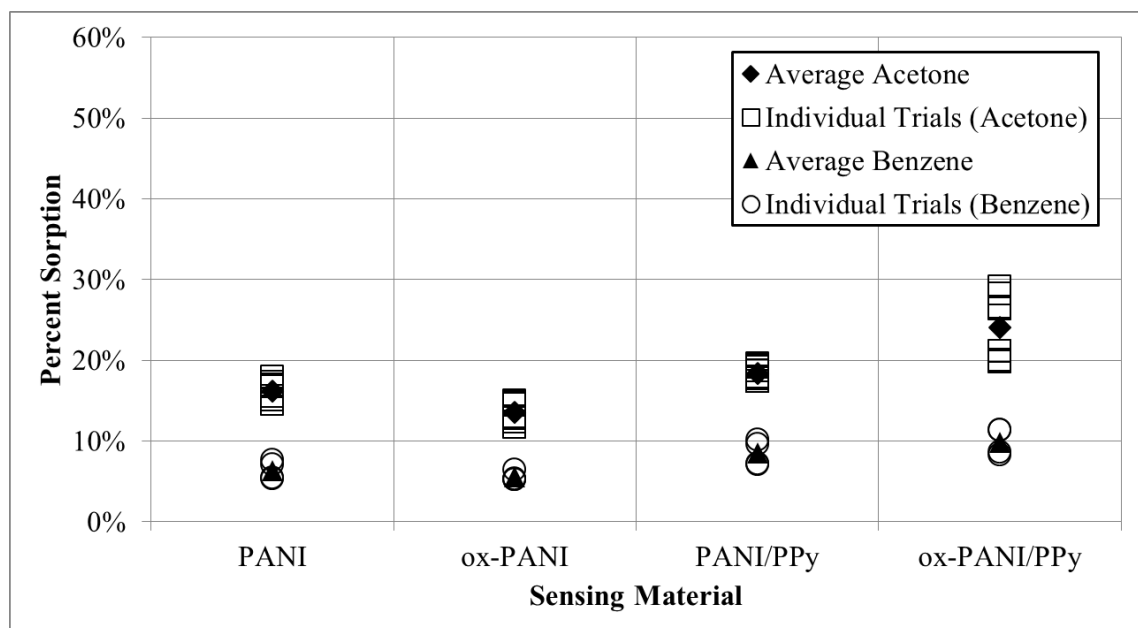


Figure 8.23: Sorption of Acetone and Sorption of Benzene for Customized Polymers (analytes evaluated individually; source: 5 ppm acetone in nitrogen or 5 ppm benzene in nitrogen)

8.2.3 Concluding Remarks on Customized Materials for Acetone Detection

The customized polymeric materials for acetone detection have been evaluated in terms of their polymer properties and their application performance. These materials were selected using the design framework; it was anticipated that the protonation of polyaniline and/or the copolymerization of aniline and pyrrole (combining properties of the two materials) would modify the polymer properties, which in turn would improve the sorption performance (especially towards acetone).

Evaluation of materials through X-ray diffraction and scanning electron microscopy showed the similarities and differences between the original polymeric materials (PANI, PPy, PMMA) and the customized polymeric materials (ox-PANI, PANI/PPy and ox-PANI/PPy). Pure PANI was the most crystalline material, whereas PPy and PMMA were more amorphous in nature. During this analysis, no correlation was observed between the crystallinity of the materials and the sorption capabilities. For example, PPy allowed for the most sorption, but was moderate in terms of crystallinity. In contrast, PANI exhibited moderate sorption potential, but was the most crystalline material. Therefore, although the crystallinity of the polymeric material is an interesting property to characterize, it did not play a major role in the application performance for this study.

Surface morphology (established through scanning electron microscopy) seemed to have a bigger impact on the concentration of analyte sorbed. SEM revealed that polypyrrole (formulation #11) contained aggregates of very small granules, which translated to a very large surface area (many sorption sites for the gas analytes). As a result, PPy exhibited the highest percent sorption of the

materials studied. The oxalic acid-doped copolymer of PANI/PPy (ox-PANI/PPy, formulation #34) was also characterized by a large surface area (small granular aggregates), and in turn sorbed acetone well. PANI, ox-PANI, and PANI/PPy were moderately porous; the available surface area for each sample (upon inspection of SEM images) was poorer than for PPy, but much improved over PMMA. This was reflected in the sorption measurements; the percentage of acetone sorbed was aligned with the (qualitatively evaluated) surface area for each sample.

Despite this perceived relationship between a polymeric sensing material's surface morphology and its ability to sorb, the surface morphology does not impact the selectivity towards a target analyte. This was observed for PPy-based materials in Section 8.1.2.1 (Figure 8.11), where the sensing materials sorbed the same total percentage of analytes under two distinct environments (5 ppm acetone vs. a 4-gas mixture containing 1 ppm of each analyte). This indiscriminate sorption highlighted the need to explore (and exploit) primary sensing mechanisms for selective detection of acetone, and this result motivated the synthesis and characterization of three customized formulations (formulations #32 to #34).

The materials synthesized with sensing mechanisms in mind showed improved selectivity towards acetone. The interferent gases (acetaldehyde, ethanol and benzene) all sorbed to the sensing materials at lower concentrations than acetone, which was an improvement over the selectivity of the screening experiments. The most promising material studied (in terms of selectivity) was ox-PANI: it was selective towards acetone in the presence of acetaldehyde and moderately selective in the presence of ethanol. Although it was not selective when benzene was the interferent gas, an additional sorption test revealed that benzene was likely experiencing some synergistic effect in the presence of acetone. We have postulated that benzene is essentially 'piggy-backing' onto acetone (at a 1:1 ratio) when acetone sorbs onto the sensing material. This can help explain the reduction in the measured concentration of benzene (in the gas mixture) after it is exposed to the polymeric sensing material. It may be possible to exploit this effect to amplify a material's response to acetone, but further investigation would be needed.

Ultimately, the customized materials synthesized and evaluated herein were comparable in terms of sorption capability, but the protonation of the polyaniline backbone (using oxalic acid as a dopant) improved the selectivity towards acetone in the presence of other interferent gases. Therefore, the design methodology allowed for the successful synthesis of a polymeric material that meets the application requirements outlined in Section 6.1.2. Given the iterative nature of design, there is still potential to optimize this material further (especially in terms of increasing the sensitivity and selectivity) given our newfound understanding of material properties and application performance.

Chapter 9. Commonalities between Case Studies – *Design of Polymeric Materials: Synthesis of Design Prescriptions*

9.1 Design Framework

Throughout this research, every effort has been made to consider design principles for the selection, synthesis and subsequent characterization of polymeric materials. Using this targeted approach (and making use of prior knowledge) has helped to create links between polymerization kinetics (and pre-polymerization formulations), the polymer properties, and the application performance for both case studies.

In Case Study #1, there was significant emphasis on reactivity ratios, largely because a multi-component (ternary) system with unique polyelectrolyte behaviour was selected for the application. Since the application performance (that is, enhanced oil recovery efficiency) was not easily evaluated, many polymer properties were studied first to improve our understanding of the material properties. The characterization of the optimally designed materials (determination of conversion, terpolymer composition, molecular weight and so on) provided the confidence necessary to pursue additional (more time-consuming and more resource-intensive) application-specific testing, namely polymer flooding tests and heavy oil displacement tests.

In Case Study #2, the kinetics of the corresponding polymerization were less influential on the application performance. However, using a designed approach ensured that target functional groups, solubility parameters, operational temperature, and product customization were considered in the early stages of the investigation. In this case, relevant links were established between the material properties of each polymer and the sensing ability (both in terms of sensitivity and selectivity).

Both of these case studies were inspired by prior knowledge [41, 182]. In each case, a ‘road map’ was established to clarify the investigation steps and to draw links between different stages of the project. These plans and the related prescriptions (tips) are provided in Figure 9.1 (for a copolymerization study for enhanced oil recovery) and in Figure 9.2 (for selection of sensing materials; specifically ethanol in the original study). However, part of the current project is to create a more generalized framework that can be applied to the design of any custom polymeric material. Therefore, the contents of both Figure 9.1 and Figure 9.2 are taken into account, and a new general design procedure is presented in Figure 9.3.

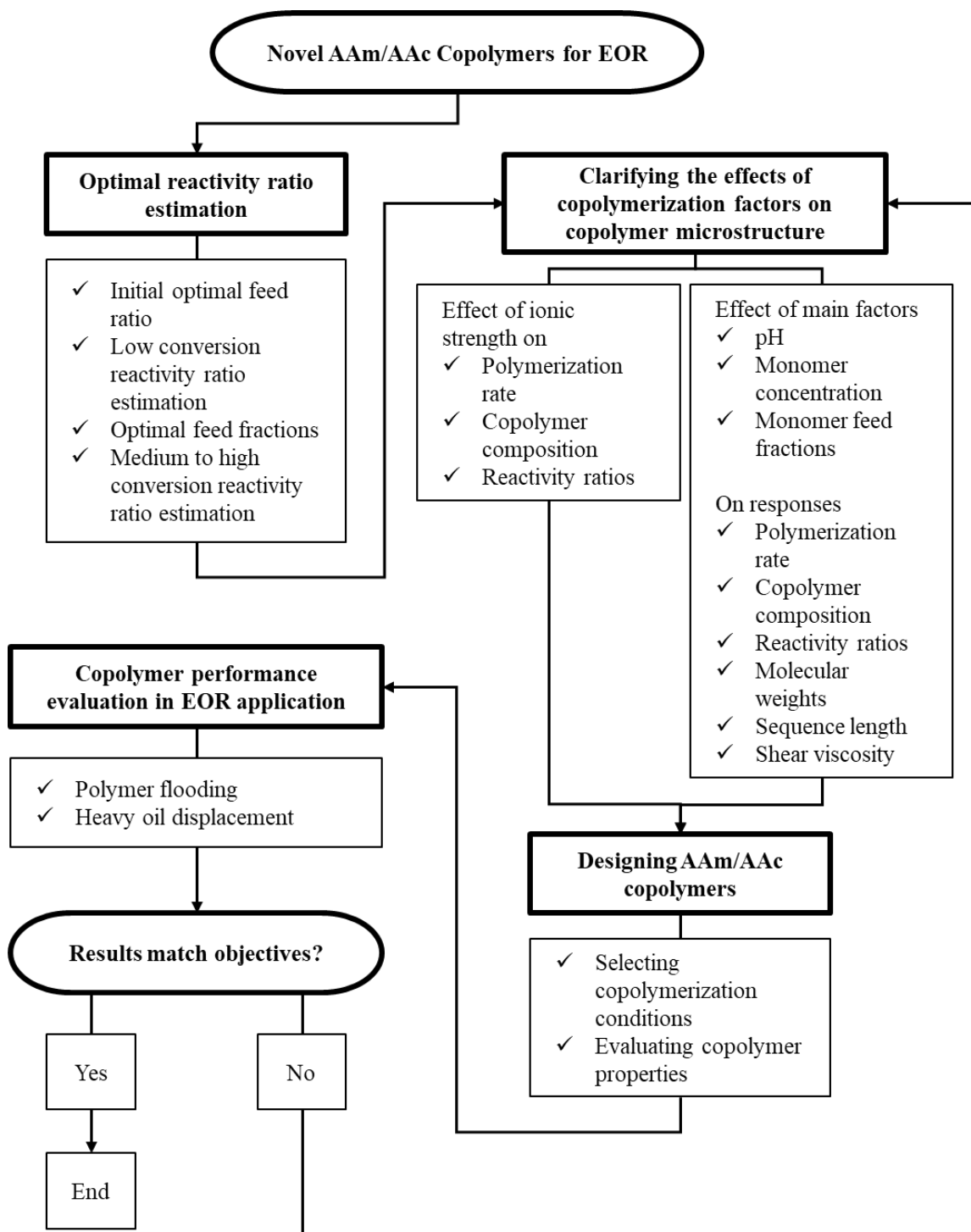


Figure 9.1: Overall Experimental Plan for Related Copolymerization Study (based on [41])

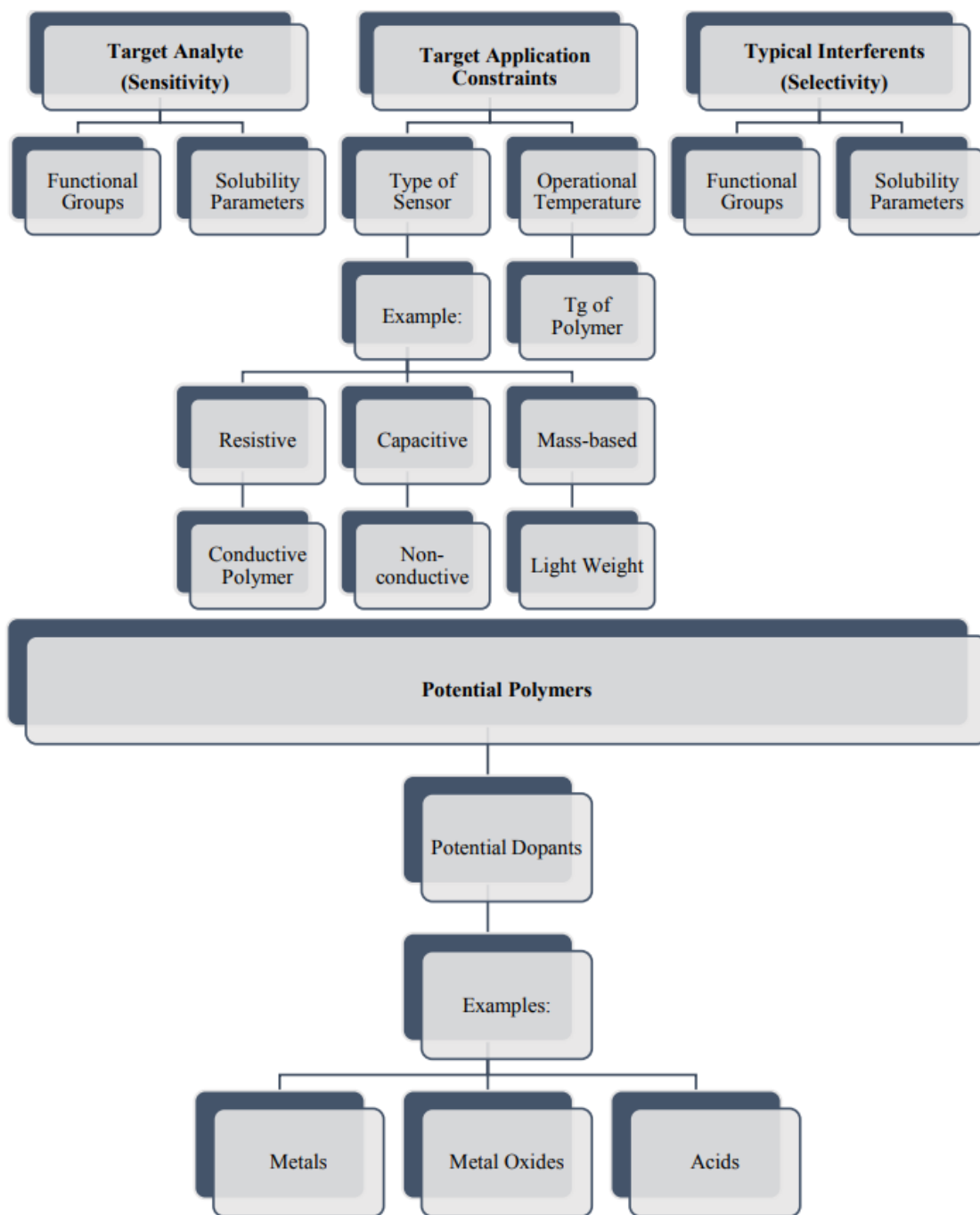


Figure 9.2: Practical Prescriptions for the Selection of Polymeric Sensing Materials (from [182])

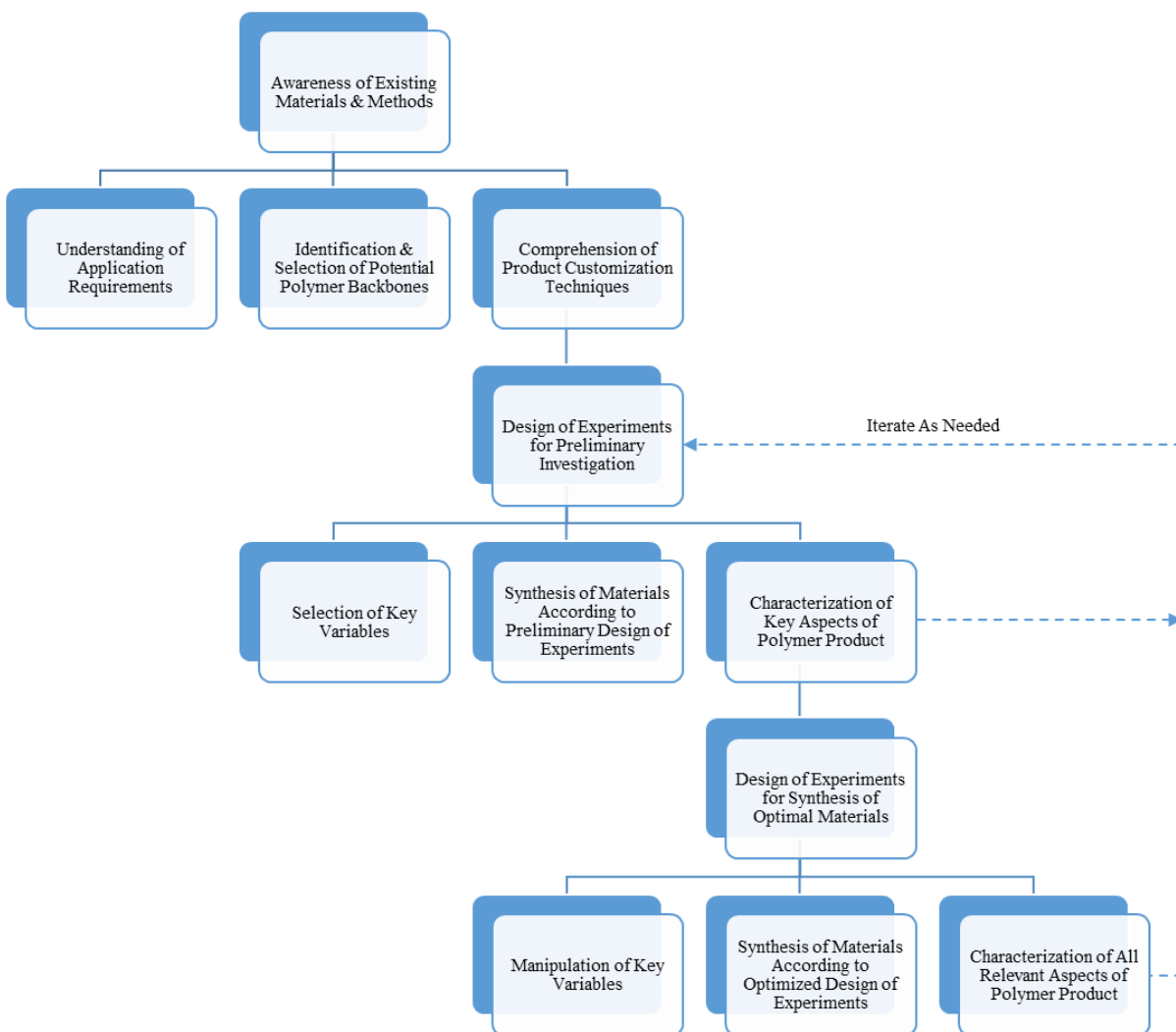


Figure 9.3: General Framework for the Design of Polymeric Materials for Custom Applications

Of course, the framework shown in Figure 9.3 is very general, which ensures that it can be applicable to a wide range of polymeric materials and related applications. This process has been used for both the enhanced oil recovery study and the sensing material investigation within this thesis; the specific steps within the approach of Figure 9.3 will be discussed in more detail in the following sections.

Although this design framework is inspired by the research performed in this thesis, it is aligned with ‘best practices’ for material design (see, for example, [46, 276]). The first stage (Section 9.2) requires a good understanding of product requirements. The middle stage (Section 9.3) allows for an improved awareness of product customization and provides an opportunity for preliminary characterization. Relationships between polymer formulations, structures and properties cannot be

manipulated if they are not first well-understood! The final stage (Section 9.4) moves us towards optimally designed materials, characterizes the most important properties, and still allows for modifications (as needed) to meet the desired specifications. A key aspect of this framework is the sequential and iterative nature of design: the characteristics of the polymer products (either in the preliminary investigation or in the optimal synthesis step) may not always meet the target requirements. In these cases, designing new screening experiments (with different polymer backbones, different customization techniques, etc.) may be the most appropriate path forward in this iterative optimal scenario.

9.2 Awareness of Existing Materials and Methods

Before undertaking any new investigation, it is important to identify (and build upon) prior research in the area. This may seem obvious, but it can be tempting to initiate a new project without a full understanding of existing materials and methods used for the application. The importance of prior knowledge in design cannot be understated; existing work (done either by the current researcher or by other research groups) should always be critically examined and used as building blocks for new studies. Although such strictures may sound like platitudes, the discipline involved in considering/thinking through the purpose of the background of an experimental program is very valuable. If the program involves collaboration, time used in building up knowledge and subsequently clarifying the main objectives is always well spent, and the effort is very informative.

As mentioned briefly in earlier chapters (Sections 2.1.3 and 6.1.3), Ashby and Johnson [46] describe four selection methods for material design: analysis, synthesis, similarity and inspiration. Typically, at least one of these selection methods is applicable to the design of a new material. Selection by similarity was most useful for the enhanced oil recovery application, while selection by analysis was most relevant for sensing materials. That said, research (like thinking) is rarely limited to a single selection method. In fact, several different methods can be used simultaneously to increase the information available for design. A brief overview of the four selection methods is provided herein, and more details are available in the original work [46].

Selection by analysis is primarily motivated by an understanding of the technical requirements for an application. The general principle is to translate the (often non-technical) requirements into a statement of objectives and constraints, analyze and identify important material properties (those that determine performance), and screen a database of materials and their properties (this makes use of existing materials and methods). During the screening process, any materials that do not meet the constraints can be eliminated, and those that remain can be evaluated in terms of anticipated performance. This is the type of approach that was used for the acetone sensing project. Given the objectives and constraints, material properties (solubility parameters, desirable functional groups, glass transition temperature, etc.) were used to screen a database of 50 potential polymeric sensing materials (compiled by Stewart [182]). Preliminary screening led to the list of

nine polymeric materials shown in Table 6.2. Then, the list was reduced to five potential materials (consideration of solubility parameters and glass transition temperature). Finally, based on previous studies (as outlined in Section 6.1.3), the three most promising polymer backbones (PANI, PPy and PMMA) were selected for experimental evaluation trials.

Selection by synthesis takes advantage of prior knowledge and essentially combines desirable properties from several existing technologies. New solutions (that is, new polymeric materials) can be developed by examining materials with desirable features and incorporating those materials (and, therefore, those features) into the new product. This was done, to some extent, in the final stage of the acetone sensing project: PANI and PPy both exhibited desirable characteristics, so a copolymer containing both promising monomers was synthesized (recall Section 8.2). However, true selection by synthesis involves exploiting the knowledge obtained from another problem that has already been ‘solved’; in this case, neither material had ideal properties on their own, which motivated the copolymerization process.

Selection by similarity is exactly as the name suggests: building from existing (or potential) solutions for a given application. This technique is typically used when an established material becomes unavailable or shows room for improvement in one or more aspect. Of course, the new material should have similar properties to the existing (currently used) material, except in the area where we are targeting improvement. This approach was demonstrated in the enhanced oil recovery case study: we built on existing polymeric materials for EOR (namely previously studied copolymers of AAm/AAc [32]) and modified the polymer backbone by adding a third comonomer (AMPS). At several stages of the analysis, we compared the new product properties to reference materials (Alcoflood 955 and AAm/AAc copolymers designed for EOR [32]), which confirmed that the new material was a good candidate for the application.

Selection by inspiration is arguably the least technical approach and was not used in great capacity in the current work. It relies on creative thinking and exploring ideas somewhat randomly [46]. Although the selection of materials by inspiration does not rely as heavily on the design principles described previously, it is important to leave some room for creativity in the process of designing new materials. In this case, flexibility is important, and an element of luck is intimately involved in successful applications.

Regardless of the primary selection technique employed, all selection methods require databases of materials, methods and products (or at least a good understanding of current best practices). This is especially critical to aid in the understanding of specific application requirements. As demonstrated for both case studies, requirements exist both in terms of polymer properties and application performance. Key polymer properties that have been considered include composition (either for multi-component polymeric materials or metal oxide-doped materials), microstructure, molecular weight averages, glass transition temperature, crystallinity and surface morphology. For

both case studies, we also considered the presence of specific functional groups (contributing to stability, flow behaviour, or analyte affinity) along the polymer backbone. Most of these microstructural and bulk polymer properties are intrinsically related to the application performance. For example, molecular weight averages of the AMPS/AAm/AAC terpolymer affect the rheology (and subsequent flow behaviour and oil recovery ability) of the terpolymer solution. Similarly, the surface morphology of candidate sensing materials influences the ability to sorb gas analytes. A good understanding of these requirements (both for the material itself and for the end-use application) allows for informed (targeted) selection of potential polymer backbones.

Identifying promising polymer backbones for a given application can require a significant amount of exploration. As described already, researchers can make use of analysis, synthesis, similarity, or inspiration during this design stage. However, for any of these approaches, some prior work (or databases, if available) must be referenced so that the researcher can become familiar with the relevant properties of each candidate backbone. Again, this highlights the importance of having a solid background (both technical and of the prior work): here, the goal is to combine information about existing materials and methods, knowledge of product requirements, and relevant data for polymeric materials to create a ‘short-list’ of potential polymers for the target application.

Finally, as evidenced in both case studies, comprehension of product customization techniques can be extremely beneficial for design. Since new materials are typically being developed, the possibility to customize said materials is largely based on theoretical knowledge. For example, in the enhanced oil recovery project, we were aware of the potential effects of solution conditions (pH, ionic strength, monomer concentration, etc.) on related homopolymerization and copolymerization systems, but the solution effects on the AMPS/AAm/AAC terpolymerization had not yet been evaluated. In contrast, the customization of polyaniline (through metal oxide or acid doping) was well-established. However, the success of the modification (the degree of incorporation of various metal oxides, for example) was unknown. Also, the specific effects of these customization steps on the application performance were hypothesized from theory. Determining the effectiveness of specific polymer backbones and product customization requires moving from theory to practice. Therefore, the next step is to move to preliminary (screening) experiments.

9.3 Design of Preliminary Experiments

The main purpose of the preliminary experimental investigation is to establish relationships between key variables and the most relevant polymer properties. This is accomplished using statistically designed experiments, which makes it possible to obtain the most experimental information in the fewest experimental runs (that is, making the best use of resources). In this thesis, different experimental designs were used for both case studies: a definitive screening design was employed for enhanced oil recovery (recall the experimental runs described in Section 3.2.1

and the results and discussion of Section 4.1), and a 3^3 factorial design was used for the sensing material study (experimental runs described in Section 7.2 and analysis provided in Section 8.1).

The type of design of experiments employed depends on the prior knowledge available and on the desired outcomes from this stage. In Case Study #1, preliminary ternary reactivity ratios for AMPS/AAm/AAC were available from prior work [80]. If they were not, preliminary design of experiments would have focused on reactivity ratio estimation (feed compositions as key variables, designed using the error-in-variables model for reactivity ratio estimation as described in Section 2.3.1). In that case, other (potentially influential) experimental conditions like pH, ionic strength and monomer concentration would be held constant. Then, once reactivity ratios were known for particular conditions, the next iteration of designed experiments would investigate these factor effects (based on the customization potential established in the previous stage of the design framework).

In effect, for Case Study #1, we had prior knowledge (ternary reactivity ratio estimates at pH 7, IS = 0.9 M and $[M] = 1.0$ M) and the desire to estimate new ternary reactivity ratios. We had also identified key variables (pH, ionic strength, monomer concentration and feed composition) that could affect the terpolymer synthesis and product properties (recall Section 2.4). Based on the design of experiments ‘rule-of-thumb’ for optimal ternary reactivity ratio estimation [60], we wanted combinations of experimental runs where each run was rich in one comonomer and operating conditions were varied in a systematic way. This led to the definitive screening design of Table 3.1.

For Case Study #2, we were not constrained by the design of experiments for multi-component polymerization and reactivity ratio estimation. Therefore, we were inspired to do a full factorial design to synthesize (and later characterize) three polymer backbones and three metal oxide dopants (recall Table 7.1). In this case, since we started with limited information, the key variables were the polymer backbones and the quantity/chemical identity of the dopants. Key variables could also delve further into the synthesis conditions: consider reaction temperature and duration, initiator type, reaction solution properties (aqueous vs. acidic, or the type of acid solution), and so on. However, in this case, the preliminary design of experiments was kept relatively simple.

Once the main factors (variables) are identified and the design of experiments is developed, we move to polymer synthesis and characterization. It is important to note that the characterization at this stage is specifically for *key* polymer properties. That is, not all conceivable (relevant) polymer properties are investigated during the preliminary investigation. Carefully selected characteristics (whether polymer properties or application performance) can give us an indication of whether or not the material seems promising for the target application. Also, characterization results can provide some insight on how to further improve the material(s).

In the enhanced oil recovery study, one of the most important aspects in the preliminary stage was the estimation of ternary reactivity ratios. Thus, conversion data (from gravimetry) and composition data (from elemental analysis) were critical. We also evaluated molecular weight averages (using aqueous gel permeation chromatography, GPC) to ensure that we were in an appropriate range, especially compared to the available reference material. The cumulative terpolymer composition, reactivity ratio estimates and molecular weight averages provided us with an excellent starting point for these materials. Not only were we able to establish some relationships between recipe (formulation) effects and the polymer properties, but we were also able to identify optimal feed compositions for the next step of the investigation. An additional advantage of using elemental analysis and GPC at this stage is that both characterization techniques are relatively direct (especially compared to the application-specific characterization). These methods are not overly time-consuming, they can be done using our own equipment, and they require small amounts of polymeric material for characterization. Therefore, it was straightforward to decide on the key characteristics to be analyzed at this stage of the investigation.

Similarly, for the acetone sensing project, only select characteristics were considered in the preliminary stage. In this case, we evaluated sensitivity and selectivity of all 30 candidate polymers. Although this was a time-consuming process, it was relatively uncomplicated, and provided us with a good overview of the materials' performance. Again, the results from this stage (along with additional background information from the literature) helped us to identify the most promising materials and to discern the important variables (i.e., the polymer backbones were more influential than the metal oxides), which ultimately led to the synthesis of more customized materials.

9.4 Design of Optimal Materials

The results obtained from the preliminary experiments inform the design of optimal materials. At this stage of the design process, we have already identified key variables (and their impact on polymer properties) from the preliminary runs, so we can select new formulations that are expected to have desirable properties. The optimal design stage may be the final stage of the investigation, but it is also possible that some 'fine-tuning' will be needed. Therefore, the design cycle can be reiterated as needed until the application requirements are met. Using sequential and iterative procedures lead to optimality.

As observed in Case Study #1, the most influential variables in the screening experiments for EOR polymers were ionic strength and monomer concentration (recall Section 4.1). Ionic strength had a significant impact on reactivity ratios and cumulative terpolymer composition, while monomer concentration influenced molecular weight averages (as expected). Thus, from the screening experiments, we were able to establish that low ionic strength (IS = 0.9 M) and high monomer concentration ($[M] = 1.5 \text{ M}$) would be suitable for the application. Also, once we had estimated

reactivity ratios, we were able to predict (and optimize) average indicators from the sequence length distribution. This optimization step (in Section 4.1.2.3) provided us with feed compositions that were expected to reduce blockiness and yield a good distribution of ions along the polymer backbone (according to model predictions). Therefore, the key variables (ionic strength, monomer concentration and feed composition) were identified and manipulated given the results of the screening experiments, and two optimally designed terpolymers were arrived at and subsequently synthesized accordingly.

Similarly, preliminary experiments in Case Study #2 (Section 8.1) indicated that the polymer backbone was much more influential than the type or quantity of metal oxide dopants. Thus, the customization potential of the two most promising backbones (polyaniline and polypyrrole) was considered. In this case, two new modification techniques (oxalic acid-doping and copolymerization) were investigated, but any number of new formulations could be investigated at this stage.

The final aspect in the design of optimal materials is to evaluate (test) all relevant characteristics of the polymer products. This will likely include re-evaluation of ‘key’ characteristics measured in the preliminary stage as well as the evaluation of new properties that are essential for application performance. For example, in Case Study #1, we predicted the cumulative terpolymer composition of the optimally designed terpolymers. Once the terpolymers were synthesized, it was important to experimentally confirm that the polymer products had the expected cumulative composition. Similarly, in Case Study #2, we evaluated the sorption ability of the customized sensing materials, just as we did in the preliminary study.

Typically, optimally designed polymeric materials should be evaluated in greater detail than those synthesized in the preliminary study. Since this is (often) the final stage, it is important that we know as much as possible about a given material. For example, do material properties match with model predictions? Do the materials perform well for the desired application? Do materials behave better than the (currently available) reference material in the areas we claimed? Sometimes, answering these questions can involve more time-consuming (and more costly) experimental work, so the full evaluation is reserved for the samples that we have designed (and, ultimately, the materials in which we are most confident based on their properties). In Case Study #1, for example, thermal behaviour, rheology, and polymer flooding efficiency were evaluated for the two most promising materials. Similarly, for Case Study #2, selectivity with two-gas mixtures and crystallinity behaviour were measured for the customized materials. This again saves money, time and resources, in contrast to the typically employed trial-and-error approaches. Whichever properties are evaluated should be relevant to the target application and should supplement the available information about the materials. Eventually, these characteristics may even be used as prior knowledge for future (fine-tuning) studies targeting new applications.

9.5 Extensions and Concluding Remarks

The same framework described in this chapter (and illustrated in Figure 9.3) can be applied to any novel polymeric material; extensions from the two main case studies shown herein are evident. Using the enhanced oil recovery project as a guideline, the framework can easily be used to design multi-component polymers for any number of applications. The polyelectrolyte nature of AMPS/AAm/AAC makes it a complex case, so many copolymer and terpolymer systems may be simpler. Consider, for example, the design of multi-component polymers for pressure sensitive adhesives [136, 137] or self-polishing coatings [144]. A good understanding of reactivity ratios (using appropriate estimation procedures) can lead researchers towards optimality.

Similarly, the framework can easily be applied to other sensing materials. In Section 6.2, we briefly discussed extending the project to formaldehyde detection, but any number of target analytes have the potential to be detected using the same approach. As described herein, researchers must consider application requirements (for a specific target analyte) to identify candidate backbones and customization potential. Related work has investigated prospective sensing materials for formaldehyde and ethanol [4, 259, 277], as well as aqueous sensors for the detection of heavy metals [278].

Beyond these two case studies, many more opportunities exist for optimization. This design approach is intended to act as a general framework, which should encourage researchers to make use of prior knowledge, carefully designed experiments and targeted analysis to make the most of their resources. Ultimately, using sequential and iterative techniques, it is possible to converge on an optimally designed material for a specific target application.

The extensions listed above are primarily long-term extensions, but the short-term extensions should not be overlooked. For example, in Case Study #1, we can further characterize the optimally designed terpolymers (and iterate the design steps as needed). Now that we have the optimal materials, it would be beneficial to investigate the thermal stability and brine compatibility (additional application requirements as per Section 2.1.2) and to demonstrate the economic benefits of the materials. Similarly, in Case Study #2, further iteration of the design steps (including additional customization of the selected polymer backbones) could improve the materials' selectivity towards acetone. These extensions, among others, are discussed further in Chapter 10 (Section 10.3).

Chapter 10. Overall Thesis Conclusions, Main Thesis Contributions, and Recommendations

10.1 Overall Thesis Conclusions

The overarching theme of this work was to develop a framework to design polymeric materials with desirable properties. Two case studies were employed to demonstrate the design approach and to refine the framework. Case Study #1 sought optimized polymers for enhanced oil recovery and Case Study #2 demonstrated the design of polymeric sensing materials for acetone detection.

In Case Study #1, design principles were successfully employed to understand and manipulate the properties of a terpolymer for enhanced oil recovery (EOR). The terpolymer composed of 2-acrylamido-2-methylpropane sulfonic acid, acrylamide and acrylic acid (AMPS/AAm/AAC, a synthetic water-soluble terpolymer) was selected ‘by similarity’ [46]. The copolymer of acrylamide and acrylic acid had been well-studied, but the careful selection and addition of the third comonomer (AMPS) improved the polymer properties (in terms of stability, for example) and the application performance (that is, the oil recovery efficiency).

The terpolymerization kinetics for AMPS/AAm/AAC proved to be very complex, largely due to the polyelectrolyte behaviour of the material. From the literature, it was anticipated that operating conditions (pH, ionic strength, monomer concentration and feed composition) would all have significant impacts on the polymerization kinetics and on the properties of the polymer products. Preliminary experiments (synthesis of 11 terpolymer formulations and related characterization) indicated that ionic strength had the most significant effect on terpolymer composition (and ternary reactivity ratios), whereas monomer concentration impacted the molecular weight averages of the product terpolymer. Also, from these screening experiments (and, specifically, reactivity ratio estimates), we were able to model the terpolymer microstructure (triad fractions) and choose feed compositions that would provide desirable microstructural properties.

Two optimally designed formulations were carefully selected (based on the results of the screening experiments) and characterized. Among the properties considered were cumulative terpolymer composition, molecular weight averages, bulk intrinsic viscosity, thermal properties, rheological properties, and application performance (that is, enhanced oil recovery efficiency). Typical studies in the literature, when evaluating polymeric materials for specific applications, usually stop after an investigation of polymerization kinetics; at best, they may go to rheological properties. A significant contribution of the current thesis is that it saw the evaluation of the terpolymer from kinetics all the way to application performance and time-consuming testing of oil recovery efficiency. Both designed terpolymers had similar (or improved) characteristics compared to available reference materials. Ultimately, in terms of application performance, a significant improvement was observed: the newly synthesized terpolymers were able to achieve an overall oil

recovery of (on average) 78.0% for one optimal material and 88.7% for the second optimal material. In contrast, the commercially available reference material (evaluated during the same investigation) achieved an overall oil recovery of 59.8%.

Another significant aspect of this study (which is tangentially related to the enhanced oil recovery project) is the importance of accurately determined reactivity ratios. This is especially true for ternary systems, since we have proven that binary reactivity ratios are not always appropriate to describe terpolymerization kinetics. Using binary reactivity ratios for ternary systems is ill-advised, as it requires ignoring the presence of the third comonomer and doubling or tripling the amount of experimental work required. Also, there can be significant numerical differences in the reactivity ratio estimates for terpolymerizations and their analogous (binary) copolymerizations, which can drastically impact model predictions (of composition, sequence length distribution, and so on). This work has shown that researchers should aim to use terpolymerization data to estimate ternary reactivity ratios. Design of experiments (feed composition) and the error-in-variables-model allow for straightforward data collection and parameter estimation. More importantly, researchers can be confident that the resulting parameter estimates are kinetically and statistically accurate.

Case Study #2 demonstrated the advantages of using design prescriptions for the development of new polymeric sensing materials. Here, a good understanding of application requirements informed the selection of potential sensing materials ‘by analysis’ [46]. The initial list of candidate materials was reduced by considering various aspects of the polymer properties including target functional groups, solubility parameters, operational temperature, and product customization potential. The five possible polymer backbones that made the ‘short-list’ were further considered (through additional background research) and ultimately three polymeric materials were selected.

Preliminary analysis of polyaniline (PANI), polypyrrole (PPy), and poly(methyl methacrylate) (PMMA) doped with metal oxide nanoparticles (SnO_2 , WO_3 and ZnO) involved a full factorial design of experiments. Thirty materials were synthesized (varying polymer backbone, dopant type, and dopant quantity) and were characterized in terms of sensitivity and selectivity (that is, ability to sorb acetone alone (5 ppm pure acetone in balance nitrogen) and in the presence of other interferent gases (namely acetaldehyde, ethanol and benzene)). In some cases, additional properties (such as surface morphology and polymer composition) were evaluated to better understand and explain the experimental results. At this stage of the study, most metal oxides did not incorporate well into the polymer products, nor did they improve acetone sorption. The most influential variable was determined to be the polymer backbone type: PPy sorbed the highest concentrations of acetone (but was non-selective) and PANI also exhibited acceptable acetone sorption. However, PMMA did not sorb any acetone, whether or not metal oxide dopants were present.

In the customization stage, additional experiments were designed in an attempt to improve the two most promising materials (PANI and PPy). Oxalic acid doping (in situ) was employed to protonate the polymer backbone (thus taking advantage of the polarity of acetone) and copolymers of PANI/PPy were synthesized in an effort to combine the desirable properties of the two polymeric materials. These customized materials performed well in terms of acetone sorption and some improvement was observed in the selectivity (again, with respect to acetaldehyde, ethanol and benzene). Further improvement is still possible here, since a higher selectivity would be more desirable. This highlights the sequential iterative nature of the design framework, which leads to optimal materials.

As we began investigating these two distinct (yet related) case studies, we hypothesized that design of polymeric materials (using a targeted approach and exploiting existing knowledge) is an important aspect of polymer research. Employing a design framework allows for the synthesis and evaluation of polymeric materials with desirable (optimized) properties for specific applications. We have shown that this framework is useful and relevant for design of polymeric materials. The effectiveness is visible throughout the research process, but it is especially evident when we see the application performance of the final (optimal) product. Therefore, we have demonstrated the importance of having a generalized design framework that researchers can use to guide their pursuit of optimal polymeric materials. Essentially, there is nothing more innovative and efficient than following a systematic plan.

10.2 Main Thesis Contributions

To appreciate the main contributions of this thesis, we revisit the objectives outlined in Chapter 1 (Section 1.3):

(1) We have identified important attributes of synthetic polymeric materials for improved enhanced oil recovery performance and selected the terpolymer of AMPS/AAm/AAC for the application. This was provided in Chapter 2, Section 2.1. This overview will also be presented in an upcoming manuscript in December 2019 (currently in production for a special issue invitation in Processes).

(2) We have researched, characterized and exploited relationships between (experimental) synthesis conditions and properties of the AMPS/AAm/AAC terpolymer through a series of screening experiments. The literature background (anticipating the effect of synthesis conditions on the terpolymerization of AMPS/AAm/AAC) has been presented in Chapter 2 (specifically, Section 2.4). Similarly, experimental research (using screening experiments and appropriate characterization techniques) has been described in Chapter 3 (especially Section 3.2.1 for synthesis and parts of Section 3.3 for the characterization of screening experiments). The results of the screening experiments (and the relationships available to be exploited) are described in Chapter 4,

Section 4.1. These chapter subsections (all related to understanding and exploiting factor effects) have been presented at an international polymer conference (Polymer Reaction Engineering X, Punta Cana, Dominican Republic, May 20-25, 2018; by invitation only) and have been published in two parts: “AMPS/AAm/AAC Terpolymerization: Experimental Verification of the EVM Framework for Ternary Reactivity Ratio Estimation” [80] and “The Role of pH, Ionic Strength and Monomer Concentration on the Terpolymerization of 2-Acrylamido-2-Methylpropane Sulfonic Acid, Acrylamide and Acrylic Acid” [81].

(3) We have designed, synthesized, characterized and tested two optimal terpolymers of AMPS/AAm/AAC for the enhanced oil recovery application. The design was informed by the results of the screening experiments, and the justification of experimental conditions was presented in Section 4.2.1. The synthesis, characterization and application-specific testing techniques used are described in Chapter 3 (Sections 3.2.2, 3.3 and 3.4). All experimental results (showing the successful production of two optimally designed materials with improved polymer properties and excellent enhanced oil recovery performance) were presented in Chapter 4, Section 4.2. These results and the surrounding discussion are part of two manuscripts (in progress): one about the design of terpolymers with optimal polymer properties and one specifically about the enhanced oil recovery application performance (to be co-authored with Prof. Laura Romero-Zerón, Department of Chemical Engineering, at the University of New Brunswick).

(4) The ‘aside’ in Chapter 5 demonstrated the importance of statistically correct experimental techniques and subsequent analyses, especially as they relate to copolymers and terpolymers. Chapter 5 is based on two papers related to appropriate procedures for reactivity ratio estimation. Most of Section 5.1 has been published in European Polymer Journal under the title “Binary vs. Ternary Reactivity Ratios: Appropriate Estimation Procedures with Terpolymerization Data” [38]. Similarly, most of Section 5.2 has been published in collaboration with researchers at the University of Ottawa, in a paper entitled “Making the Most of Parameter Estimation: Terpolymerization Troubleshooting Tips” [136]. Although the majority of the reactivity ratio estimation performed for this thesis was for ternary systems, a tangential project was to develop a ‘user-friendly’ MATLAB code for binary reactivity ratio estimation. The related publication, “Computational Package for Copolymerization Reactivity Ratio Estimation: Improved Access to the Error-in-Variables-Model”, was published in Processes [6], and is receiving considerable interest from researchers. Select case studies from the project were shown (for background) in Chapter 2 (Section 2.3) and additional details were provided in Appendix B.

(5) & (6) We have identified the important attributes of synthetic polymeric materials for sensing applications, primarily for acetone sensing (and, as an extension, for formaldehyde sensing as well). These considerations have been described in Chapter 6 (especially Section 6.1). We have also researched and characterized relationships between polymeric sensing materials and dopants as they relate to analyte sensitivity and selectivity; the experimental steps necessary to develop

these relationships were explained in Chapter 7 and preliminary experimental results were presented in Chapter 8 (Section 8.1). This screening investigation is summarized in a manuscript entitled “Design of Polymeric Sensing Materials for Acetone Detection”, currently under review [279]. As part of this project, we also developed a sensing material array (using a variety of different sensing materials for the detection of four different gas analytes). This tangential study, briefly described in Section 6.3, is part of a paper entitled “Evaluation of Doped and Undoped Poly (o-anisidine) as Sensing Materials for a Sensor Array for Volatile Organic Compounds”, which has been accepted for publication in *Polymers for Advanced Technologies* [251].

(7) We have designed, synthesized, characterized and tested customized polymers for detection of acetone gas. The customized materials have not yet been optimized (that is, there is still room for improvement in terms of selectivity), but the design framework has been successfully applied. There is still potential to use sequential iterative techniques to further improve the selectivity of the candidate sensing materials. However, the experimental process has been described in Chapter 7, and relevant results and discussion for the customized materials are in Chapter 8 (Section 8.2).

(8) Finally, we have demonstrated the advantages of a design framework (considering physicochemical behaviour, statistical design principles, and product requirements) for polymer synthesis and application performance. The design approach is infused throughout the thesis, but key aspects are revisited in Chapter 9.

Over the course of my PhD, I have contributed to the publication of 10 refereed papers (first author for 7 of the 10 items). In addition, a paper related to sensing materials (described above) is currently under review. Finally, as alluded to in this section, at least 4 more publications are anticipated (an enhanced oil recovery overview, a paper about the design of optimal AMPS/AAm/AAC terpolymers for EOR, a paper about the enhanced oil recovery application performance, and a paper describing the customized sensing materials for acetone detection). Several of these manuscripts are already in progress.

10.3 Recommendations for Future Work

10.3.1 Short-Term Recommendations

For Case Study #1 (enhanced oil recovery), the following short-term recommendations have been considered:

- A more in-depth ionic strength study (expanding from Section 4.1.2) is recommended. It has been established that a cross-over point exists between $IS = 0.9\text{ M}$ and 1.5 M , but it is unclear exactly where the shift occurs (that is, the exact ionic strength at which $r_{12} = r_{21}$ and $r_{13} = r_{31}$ is still unknown). To find the true cross-over point, additional experiments

would need to be performed for $0.9 \text{ M} < \text{IS} < 1.5 \text{ M}$ at pH 7 and $[\text{M}] = 1.0 \text{ M}$. A better understanding of the ionic strength effect could allow for the manipulation of feed formulation components and properties to control the degree of incorporation of each comonomer in the terpolymer product. This is related to a long-term recommendation in the following section.

- The addition of AMPS to the polymer formulation for enhanced oil recovery has improved the application performance and we anticipate that it will also improve the mechanical and thermal stability of the polymer flooding solution. Mechanical stability has been evaluated using rheological measurements and thermal stability has been evaluated using TGA. However, it is also recommended that high temperature rheological testing be performed. This would provide additional information about the impact of increased temperature on polymer flow behaviour, which is relevant for the EOR application. This is related to the consideration of oil reservoir conditions, which is discussed further in the long-term recommendations.
- The synthesis replicates and sampling replicates obtained for both Opt1 and Opt2 terpolymers are suitable for a more detailed hierarchical design study. With these samples (and a hierarchical design approach), it is possible to evaluate the variability associated with synthesis, sampling, sample preparation, and characterization. Although some hierarchical (nested) analysis concepts have already been applied for molecular weight analysis (Section 4.2.2.3), it is not a full hierarchical study. Therefore, a complete hierarchical design project could be performed (evaluating the variability of molecular weight average measurements along with the other error contributions described earlier). This project is currently in progress.

For Case Study #2 (polymeric materials for acetone detection), the foremost short-term recommendation is to further improve the selectivity towards acetone in the presence of other interferent gases. This involves reiterating the design sequence described in Chapter 9 (recall Figure 9.3). Three specific possibilities are described below:

- Oxalic acid doping improved the sorption performance of the PANI/PPy copolymer, but there is still more room for improvement. It is recommended that other acids (like hydrochloric acid, for example) be considered to improve protonation of the polymer backbone.
- The metal oxides considered in the preliminary investigation did not incorporate well, nor did they improve sorption performance. It may be beneficial to investigate techniques to improve metal oxide incorporation through a modified synthesis procedure or via pre-treatment of the metal oxide nanoparticles.

- The two lone electron pairs on acetone's carbonyl group act as a Lewis base. It would be worthwhile to investigate the addition of Lewis acids to the polymer backbone.

10.3.2 Long-Term Recommendations

For Case Study #1 (enhanced oil recovery), the following long-term recommendations have been considered:

- As mentioned earlier (in the short-term recommendations and in Section 4.1.2), manipulation of terpolymerization solution properties can allow for customized terpolymer products. In determining the ternary reactivity ratios for AMPS/AAm/AAc at different ionic strength levels, only the comonomer pairs containing AMPS exhibited cross-over behaviour within the range considered. Thus, once the exact cross-over point is established (as per the short-term recommendations above), it would be possible to manipulate relationships between AMPS/AAm and AMPS/AAc by adjusting ionic strength. For the third comonomer pair (AAm/AAc), cross-over behaviour was not observed in the current study, but has been reported for the analogous AAm/AAc copolymer [85, 97, 99]. Although it is unwise to make extensions directly from the copolymer case to the terpolymer case, terpolymer synthesis below pH 5 may reveal the cross-over point for AAm/AAc. Therefore, one could conceivably manipulate both solution pH and ionic strength to exploit cross-over behaviour and influence reactivity ratios (and, by extension, related terpolymer properties) for AMPS/AAm/AAc terpolymerization.
- The polymer flooding tests and heavy oil displacement tests (described in Section 3.4.2) require fairly large quantities of terpolymer samples (especially relative to the amount synthesized in a typical experiment). Of course, extensions to field reservoirs will require substantially more material. Therefore, there is a need to investigate the scale-up potential of the AMPS/AAm/AAc terpolymer synthesis. Preliminary investigations (in a 450 mL bench scale reactor) have already been performed, but more work is needed to ensure consistency of polymer properties. This item has as its target the lowering of manufacturing cost.
- Considering extensions to field reservoirs necessitates the evaluation of the terpolymer performance in a variety of reservoir conditions. Specifically, solution rheology, polymer flow performance, and subsequent heavy oil displacement should be evaluated when there is high salinity, a high degree of hardness, and/or high temperatures. This type of study would benefit from a design of experiments, since the concentration and chemical nature of ions present (Na^+ , Mg^{2+} , Ca^{2+} , Cl^- , SO_4^- and others) could significantly impact the application performance of the polymeric material. In addition, high temperatures could impact performance, and temperature effects may be influenced by the salinity or degree

of hardness of the flood water (that is, there is potential for the confounding of factor effects, especially in terms of polymer precipitation [17]). Finally, the polymer concentration used in the polymer flooding solution can be varied widely, and should be optimized (minimize polymer concentration required for economic reasons and simultaneously maximize the degree of oil recovery). Therefore, a fractional factorial design of experiments investigating concentration and chemical nature of ions, temperature and polymer solution concentration is recommended. Given conditions typically reported in the literature [8, 23, 28], one might consider designing a series of experiments within the following ranges: $0 \text{ ppm} < [\text{NaCl}] < 15,000 \text{ ppm}$; $0 \text{ ppm} < [\text{CaCl}_2] < 2,000 \text{ ppm}$; $25^\circ\text{C} < T < 200^\circ\text{C}$; $1,000 \text{ ppm} < [\text{polymer}] < 10,000 \text{ ppm}$.

- All pH and ionic strength adjustments performed in the current work relied on sodium ions (Na^+). However, it is well-established that the type of cation can impact the polymerization kinetics [107, 108]. Therefore, an interesting extension would be to evaluate the presence of different cations (consider, for example, potassium or calcium ion effects). This may also be helpful in addressing the following item (related to terpolymer purification).
- As described in the main text, the AMPS/AAm/AAC samples contain residual NaCl and H_2O . Ideally, especially if the material is to be used for the EOR application, the final product should only contain the ‘active ingredient’ (that is, the terpolymer). Therefore, it would be worthwhile to investigate additional purification techniques for NaCl removal and sample drying that could be used in post-processing. However, if this route is explored, it will be extremely important to avoid any harsh treatments that could alter microstructure (and subsequent EOR performance) of the terpolymer product.
- Finally, in considering the kinetics aspect of this case study, there is still more to explore in terms of reactivity ratio estimation. Two interesting extensions are as follows: (1) development of a user-friendly MATLAB code for ternary reactivity ratio estimation (inspired by the binary reactivity ratio estimation program shown in Appendix B [6]) and (2) investigation of experimental error associated with low conversion data (and, specifically, how error-prone low conversion data affect instantaneous reactivity ratio estimation).

For Case Study #2 (polymeric materials for acetone detection), the following long-term recommendations have been considered:

- As described in the short-term recommendations section, there is still potential to improve the sensing material in terms of selectivity. If the ‘customization’ approaches listed in the short-term recommendations are insufficient, there is potential to reiterate the preliminary selection step. The two most promising polymer backbones that have been identified are

PANI and PPy, but other options are also available. For example, some functionalized polyaniline derivatives (e.g., poly-*o*-anisidine, poly-*o*-aminobenzoic acid, poly-*m*-aminobenzoic acid, poly-*m*-nitroaniline) may be useful for acetone sensing. Similarly, although the three most promising metal oxides (based on the literature review) were evaluated herein, there are many more candidates for doping. There is always the potential to return to the literature for new inspiration.

- It would be interesting to look at varying the composition of the PANI/PPy copolymers for property modification and improved kinetic understanding. If the copolymer composition were available, it would be possible to establish whether the copolymer product contains 50% aniline and 50% pyrrole. On a related note, there is also potential to estimate reactivity ratios for the PANI/PPy copolymerization; one would need to perform additional runs (with designed formulations) to collect enough data for reactivity ratio estimation.
- The sensing data presented herein could be useful within a sensing material array (as per Section 6.3). Given the large amount of information that has been collected (for individual gases and gas mixtures in the presence of many different sensing materials), there is a wealth of information that could be used as a ‘filtering algorithm’ for detection and identification of specific target analytes.
- The prescriptions and the general framework used for designing polymeric materials for acetone sensing could also be extended to the detection of additional compounds. One area of interest is the detection of pollutant gases (benzene, nitrogen oxides, sulfur oxides, carbon monoxide, and so on). Benzene contributes to poor indoor air quality, and is often a by-product of industrial processes and vehicle exhaust. Similarly, NO_x, SO_x and CO are released from a variety of industrial processes and contribute significantly to air pollution. Thus, using the same general procedure demonstrated in this thesis, new polymeric materials could be developed to detect one or more of these gas components.
- Polymeric sensing materials can also be designed for the detection of toxic aqueous analytes. This can be significantly more challenging than gaseous analytes, since the water effects must also be considered. However, preliminary work in this area has led to the development of a polymeric sensing material (and the design of a functional electrostatic Micro-Electro-Mechanical Systems (MEMS) sensor) to identify mercury acetate in water [278].

References

- [1] "Three Phases Of Oil Recovery," China Oilfield Technology Services Group Limited, 2007. [Online]. Available: <http://www.chinaoilfieldtech.com/oilrecovery.html>. [Accessed 1 August 2016].
- [2] "What Is EOR, and How Does It Work?," Rigzone, 2016. [Online]. Available: http://www.rigzone.com/training/insight.asp?insight_id=313. [Accessed 1 August 2016].
- [3] G. Korotcenkov, "Metal Oxides for Solid-State Gas Sensors: What Determines Our Choice?," *Materials Science and Engineering: B*, vol. 139, pp. 1-23, 2007.
- [4] K. M. E. Stewart and A. Penlidis, "Designing Polymeric Sensing Materials for Analyte Detection and Related Mechanisms," *Macromolecular Symposia*, vol. 360, pp. 123-132, 2016.
- [5] K. M. E. Stewart and A. Penlidis, "Designing Polymeric Sensing Materials: What Are We Doing Wrong?," *Polymers for Advanced Technologies*, vol. 133, no. 42, 2016.
- [6] A. J. Scott and A. Penlidis, "Computational Package for Copolymerization Reactivity Ratio Estimation: Improved Access to the Error-in-Variables-Model," *Processes*, vol. 6, no. 1, p. 8, 2018.
- [7] J. Speight, "Chapter 6: General Methods of Oil Recovery," in *Introduction to Enhanced Recovery Methods for Heavy Oil and Tar Sands, 2nd Edition*, Gulf Professional Publishing, 2016, pp. 253-322.
- [8] S. Kokal and A. Al-Kaabi, "Enhanced Oil Recovery: Challenges & Opportunities," *World Petroleum Council: Official Publication*, vol. 64, 2010.
- [9] E. M. A. Mokheimer, M. Hamdy, Z. Abubakar, M. R. Shakeel, M. A. Habib and M. Mahmoud, "A Comprehensive Review of Thermal Enhanced Oil Recovery: Techniques Evaluation," *The American Society of Mechanical Engineers Journal of Energy Resources Technology*, vol. 141, no. 3, p. 030801, 2018.
- [10] J. Speight, "Chapter 8: Nonthermal Methods of Recovery," in *Introduction to Enhanced Recovery Methods for Heavy Oil and Tar Sands, 2nd Edition*, Gulf Professional Publishing, 2016, pp. 369-386.
- [11] C. Gao, J. Shi and J. Zhao, "Successful Polymer Flooding and Surfactant-Polymer Flooding Projects at Shengli Oilfield from 1992 to 2012," *Journal of Petroleum Exploration and Production Technology*, vol. 4, no. 1, pp. 1-8, 2014.
- [12] D. Wang, R. S. Seright, Z. Shao and J. Wang, "Key Aspects of Project Design for Polymer Flooding at the Daqing Oilfield.," *SPE Reservoir Evaluation & Engineering*, vol. 11, no. 6, pp. 1-117, 2008.
- [13] R. Ryles, "Chemical Stability Limits of Water-Soluble Polymers Used in Oil Recovery Processes," in *SPE Reservoir Engineering*, Phoenix, 1988.
- [14] B. Wei, L. Romero-Zerón and D. Rodrigue, "Mechanical Properties and Flow Behavior of Polymers for Enhanced Oil Recovery," *Journal of Macromolecular Science, Part B: Physics*, vol. 53, p. 625–644, 2014.

- [15] A. O. Gbadamosi, R. Junin, M. A. Manan, A. Agi and A. S. Yusuff, "An Overview of Chemical Enhanced Oil Recovery: Recent Advances and Prospects," *International Nano Letters*, vol. 9, no. 3, pp. 171-202, 2019.
- [16] A. Z. Abidin, T. Puspasari and W. A. Nugroho, "Polymers for Enhanced Oil Recovery Technology," *Procedia Chemistry*, vol. 4, pp. 11-16, 2012.
- [17] M. S. Kamal, A. S. Sultan, U. S. Al-Mybaiyedh and I. A. Hussein, "Review on Polymer Flooding: Rheology, Adsorption, Stability, and Field Applications of Various Polymer Systems," *Polymer Reviews*, vol. 55, pp. 491-530, 2015.
- [18] D. Wever, F. Picchionia and A. Broekhuis, "Branched Polyacrylamides: Synthesis and Effect of Molecular Architecture on Solution Rheology," *European Polymer Journal*, vol. 49, no. 10, p. 3289–3301, 2013.
- [19] Y. Y. Zhu, W. L. Luo, G. Q. Jian, C. A. Wang, Q. F. Hou and J. L. Niu, "Development and Performance of Water Soluble Salt-Resistant Polymers for Chemical Flooding," *Advanced Materials Research*, vol. 476, pp. 227-235, 2012.
- [20] A. Sabhapondit, A. Borthakur and I. Haque, "Characterization of Acrylamide Polymers for Enhanced Oil Recovery," *Journal of Applied Polymer Science*, vol. 87, pp. 1869-1878, 2003.
- [21] A. Zaitoun, P. Makakou, N. Blin, R. Al-Maamari, A. Al-Hashmi, M. Abdel-Goad and H. Al-Sharji, "Shear Stability of EOR Polymers," in *Society of Petroleum Engineers International Symposium*, The Woodlands, Texas, 2011.
- [22] J. J. Sheng, *Modern Chemical Enhanced Oil Recovery - Theory and Practice*, Elsevier, 2011.
- [23] A. Sabhapondit, A. Borthakur and I. Haque, "Water Soluble Acrylamidomethyl Propane Sulfonate (AMPS) Copolymer as an Enhanced Oil Recovery Chemical," *Energy & Fuels*, vol. 17, pp. 683-688, 2003.
- [24] J. J. Sheng, B. Leonhardt and N. Azri, "Status of Polymer-Flooding Technology," *Journal of Canadian Petroleum Engineering*, pp. 116-126, 2015.
- [25] C. Zhong, P. Luo, Z. Ye and H. Chen, "Characterization and Solution Properties of a Novel Water-soluble Terpolymer For Enhanced Oil Recovery," *Polymer Bulletin*, vol. 62, pp. 79-89, 2009.
- [26] M. Han, X. Zhou, A. B. Fuseni, B. H. Al-Zahrani and A. M. AlSofi, "Laboratory Investigation of the Injectivity of Sulfonated Polyacrylamide Solutions into Carbonate Reservoir Rocks," in *SPE EOR Conference at Oil and Gas West Asia*, Muscat, 2012.
- [27] Z. Ye, M. Feng, S. Gou, M. Liu, Z. Huang and T. Liu, "Hydrophobically Associating Acrylamide-Based Copolymer for Chemically Enhanced Oil Recovery," *Journal of Applied Polymer Science*, vol. 130, pp. 2901-2911, 2013.
- [28] Z. Ye, G. Gou, S. Gou, W. Jiang and T. Liu, "Synthesis and Characterization of a Water-Soluble Sulfonates Copolymer of Acrylamide and N-Allylbenzamide as Enhanced Oil Recovery Chemical," *Journal of Applied Polymer Science*, vol. 128, pp. 2003-2011, 2013.
- [29] A. El-Hoshoudy, S. Desouky, A. Al-Sabagh, M. El-kady, M. Betiha and S. Mahmoud, "Synthesis and Characterization of Polyacrylamide Crosslinked Copolymer for

- Enhanced Oil Recovery and Rock Wettability Alteration," *International Journal of Oil, Gas and Coal Engineering*, vol. 3, pp. 47-59, 2015.
- [30] A. El-Hoshoudy, S. Desouky, A. Al-Sabagh, M. Betiha, M. El-kady and S. Mahmoud, "Evaluation of Solution and Rheological Properties for Hydrophobically Associated Polyacrylamide Copolymer as a Promised Enhanced Oil Recovery Candidate," *Egyptian Journal of Petroleum*, vol. 26, pp. 779-785, 2017.
- [31] R. R. Ujjwal, T. Sharma, J. S. Sangwai and U. Ojha, "Rheological Investigation of a Random Copolymer of Polyacrylamide and Polyacryloyl Hydrazide (PAM-ran-PAH) for Oil Recovery Applications," *Journal of Applied Polymer Science*, vol. 134, p. 44648, 2017.
- [32] M. Riahinezhad, L. Romero-Zerón, N. T. McManus and A. Penlidis, "Design of Tailor-Made Water-Soluble Copolymers for Enhanced Oil Recovery Polymer Flooding Applications," *Macromolecular Reaction Engineering*, vol. 11, p. 1600020, 2017.
- [33] G. Wu, L. Yu and X. Jiang, "Synthesis and Properties of an Acrylamide-Based Polymer for Enhanced Oil Recovery: A Preliminary Study," *Advances in Polymer Technology*, vol. 37, pp. 2763-2773, 2018.
- [34] A. A. Olajire, "Review of ASP EOR (Alkaline Surfactant Polymer Enhanced Oil Recovery) Technology in the Petroleum Industry: Prospects and Challenges," *Energy*, vol. 77, pp. 963-982, 2014.
- [35] J. J. Sheng, "A Comprehensive Review of Alkaline-Surfactant-Polymer (ASP) Flooding," *Asia-Pacific Journal of Chemical Engineering*, vol. 9, pp. 471-489, 2014.
- [36] W. Pu, C. Shen, B. Wei, Y. Yang and Y. Li, "A Comprehensive Review of Polysaccharide Biopolymers for Enhanced Oil Recovery (EOR) from Flask to Field," *Journal of Industrial and Engineering Chemistry*, vol. 61, pp. 1-11, 2018.
- [37] J. Glass, "Water-Soluble Polymers," in *Kirk-Othmer Encyclopedia of Chemical Technology*, John Wiley & Sons, Inc., 2014, pp. 1-21.
- [38] A. J. Scott and A. Penlidis, "Binary vs. Ternary Reactivity Ratios: Appropriate Estimation Procedures with Terpolymerization Data," *European Polymer Journal*, vol. 105, pp. 442-450, 2018.
- [39] A. J. Scott and A. Penlidis, "Copolymerization," *Elsevier Reference Module*, 2017.
- [40] J. Koenig, *Chemical Microstructure of Polymer Chains*, New York: John Wiley & Sons, 1980.
- [41] M. Riahinezhad, "PhD Thesis: Clarifying Multi-Component Polymerization Kinetics for Tailoring Properties of Acrylamide/Acrylic Acid Copolymers for Enhanced Oil Recovery," Department of Chemical Engineering, University of Waterloo, Waterloo, 2016.
- [42] R. Seright, M. Seheult and T. Talashek, "Injectivity Characteristics of EOR Polymers," in *Research and Development of Polymer Enhanced Oil Recovery*, Denver, 2008.
- [43] D. Wever, F. Picchioni and A. Broekhuis, "Polymers for Enhanced Oil Recovery: A Paradigm for Structure-Property Relationship in Aqueous Solution," *Progress in Polymer Science*, vol. 36, pp. 1558-1628, 2011.

- [44] S. Mishra, A. Bera and A. Mandal, "Effect of Polymer Adsorption on Permeability Reduction in Enhanced Oil Recovery," *Journal of Petroleum Engineering*, vol. 2014, p. 395857, 2014.
- [45] P. A. Bjørkum and P. H. Nadeau, "Temperature Controlled Porosity/Permeability Reduction, Fluid Migration, and Petroleum Exploration in Sedimentary Basins," *APPEA Journal*, vol. 38, pp. 453-464, 1998.
- [46] M. Ashby and K. Johnson, *Materials and Design: The Art and Science of Material Selection in Product Design*, Burlington: Elsevier, 2002.
- [47] Q. Li, W. Pu, Y. Wang and T. Zhao, "Synthesis and Assessment of a Novel AM-co-AMPS Polymer for Enhanced Oil Recovery (EOR)," in *International Conference on Computational and Information Sciences*, 2013.
- [48] Y. Bao, J. Ma and N. Li, "Synthesis and Swelling Behaviors of Sodium Carboxymethyl Cellulose-g-poly(AA-co-AM-co-AMPS)/MMT Superabsorbent Hydrogel," *Carbohydrate Polymers*, vol. 84, pp. 76-82, 2011.
- [49] J. Ma, H. Zheng, M. Tan, L. Liu, W. Chen, Q. Guan and X. Zheng, "Synthesis, Characterization, and Flocculation Performance of Anionic Polyacrylamide P(AM-AA-AMPS)," *Journal of Applied Polymer Science*, vol. 129, no. 4, pp. 1984-1991, 2013.
- [50] T. S. Anirudhan and S. R. Rejeena, "Poly(Acrylic Acid-co-Acrylamide-co-2-Acrylamido-2-Methyl-1-Propanesulfonic Acid)-Grafted Nanocellulose/Poly(Vinyl Alcohol) Composite for the In Vitro Gastrointestinal Release of Amoxicillin," *Journal of Applied Polymer Science*, vol. 131, no. 17, 2014.
- [51] B. Peng, S. Peng, B. Long, Y. Miao and W.-Y. Guo, "Properties of High-Temperature-Resistant Drilling Fluids Incorporating Acrylamide/(Acrylic Acid)/(2-Acrylamido-2-Methyl-1-Propane Sulfonic Acid) Terpolymer and Aluminum Citrate as Filtration Control Agents," *Journal of Vinyl & Additive Technology*, vol. 16, no. 1, pp. 84-89, 2010.
- [52] G. Odian, *Principles of Polymerization*, Hoboken, New Jersey: Wiley-Interscience, 2004.
- [53] F. R. Mayo and F. M. Lewis, "Copolymerization. I. A Basis for Comparing the Behavior of Monomers in Copolymerization; The Copolymerization of Styrene and Methyl Methacrylate," *Journal of the American Chemical Society*, vol. 66, no. 9, pp. 1594-1601, 1944.
- [54] N. Kazemi, T. A. Duever and A. Penlidis, "Reactivity Ratio Estimation from Cumulative Copolymer Composition Data," *Macromolecular Reaction Engineering*, vol. 5, pp. 385-403, 2011.
- [55] V. E. Meyer and G. G. Lowry, "Integral and Differential Binary Copolymerization Equations," *Journal of Polymer Science, Part A*, vol. 3, pp. 2843-2851, 1965.
- [56] T. Alfrey and G. Goldfinger, "Copolymerization of Systems of Three and More Components," *Journal of Chemical Physics*, vol. 12, pp. 322-323, 1944.
- [57] N. Kazemi, T. A. Duever and A. Penlidis, "Demystifying the Estimation of Reactivity Ratios for Terpolymerization Systems," *AIChE Journal*, vol. 60, pp. 1752-1766, 2014.

- [58] N. Kazemi, T. A. Duever and A. Penlidis, "A Powerful Estimation Scheme with the Error-in-Variables Model for Nonlinear Cases: Reactivity Ratio Estimation Examples," *Computers and Chemical Engineering*, vol. 48, pp. 200-208, 2013.
- [59] N. Kazemi, T. A. Duever and A. Penlidis, "Design of Experiments for Reactivity Ratio Estimation in Multicomponent Polymerizations Using the Error-In-Variables Approach," *Macromolecular Theory and Simulations*, vol. 22, pp. 261-272, 2013.
- [60] N. Kazemi, T. A. Duever and A. Penlidis, "Design of Optimal Experiments for Terpolymerization Reactivity Ratio Estimation," *Macromolecular Reaction Engineering*, vol. 9, no. 3, pp. 228-244, 2015.
- [61] P. W. Tidwell and G. A. Mortimer, "An Improved Method of Calculating Copolymerization Reactivity Ratios," *Journal of Polymer Science, Part A: Polymer Chemistry*, vol. 3, no. 1, pp. 369-387, 1965.
- [62] A. J. Scott, M. Riahinezhad and A. Penlidis, "Optimal Design for Reactivity Ratio Estimation: A Comparison of Techniques for AMPS/Acrylamide and AMPS/Acrylic Acid Copolymerizations," *Processes*, vol. 3, no. 4, pp. 749-768, 2015.
- [63] M. A. Dubé and A. Penlidis, "A Systematic Approach to the Study of Multicomponent Polymerization Kinetics—The Butyl Acrylate/Methyl Methacrylate/Vinyl Acetate Example: 1. Bulk Copolymerization," *Polymer*, vol. 36, no. 3, pp. 587-598, 1995.
- [64] N. Grassie, B. Torrance, J. Fortune and J. Gemell, "Reactivity Ratios for the Copolymerization of Acrylates and Methacrylates by Nuclear Magnetic Resonance Spectroscopy," *Polymer*, vol. 6, no. 12, pp. 653-658, 1965.
- [65] Y. Bard, *Nonlinear Parameter Estimation*, New York: Academic Press, 1974.
- [66] T. A. Duever, S. Keeler, P. Reilly, J. Vera and P. Williams, "An Application of the Error-in-Variables-Model Parameter Estimation from Van Ness-Type Vapour-Liquid Equilibrium Experiments," *Chemical Engineering Science*, vol. 42, no. 3, pp. 403-412, 1987.
- [67] A. L. Polic, T. A. Duever and A. Penlidis, "Case Studies and Literature Review on the Estimation of Copolymerization Reactivity Ratios," *Journal of Polymer Science: Part A: Polymer Chemistry*, vol. 36, pp. 813-822, 1998.
- [68] L. H. Garcia-Rubio, M. G. Lord, J. F. MacGregor and A. E. Hamielec, "Bulk Copolymerization of Styrene and Acrylonitrile: Experimental Kinetics and Mathematical Modelling," *Polymer*, vol. 26, pp. 2001-2013, 1985.
- [69] P. Reilly and H. Patino-Leal, "A Bayesian Study of the Error-in-Variables Model," *Technometrics*, vol. 23, no. 3, pp. 221-231, 1981.
- [70] M. A. Dubé, R. Amin Sanayei, A. Penlidis, K. F. O'Driscoll and P. M. Reilly, "A Microcomputer Program for Estimation of Copolymerization Reactivity Ratios," *Journal of Polymer Science, Part A: Polymer Chemistry*, vol. 29, pp. 703-708, 1991.
- [71] S. Agarwal, R. Kumar, T. Kissel and R. Reul, "Synthesis of Degradable Materials Based on Caprolactone and Vinyl Acetate Units Using Radical Chemistry," *Polymer Journal*, vol. 42, no. 8, pp. 650-660, 2009.
- [72] G. Hedir, C. Bell, N. Jeong, E. Chapman, I. Collins, R. O'Reilly and A. Dove, "Functional Degradable Polymers by Xanthate-Mediated Polymerization," *Macromolecules*, vol. 47, pp. 2847-2852, 2014.

- [73] D. Ding, X. Pan, Z. Zhang, N. Li, J. Zhu and X. Zhu, "A Degradable Copolymer of 2-methylene-1,3-dioxepane and Vinyl Acetate by Photo-Induced Cobalt-Mediated Radical Polymerization," *Polymer Chemistry*, vol. 7, pp. 5258-5264, 2016.
- [74] A. Feldermann, A. Toy, H. Phan, M. Stenzel, T. Davis and C. Barner-Kowollik, "Reversible Addition Fragmentation Chain Transfer Copolymerization: Influence of the RAFT Process on the Copolymer Composition," *Polymer*, vol. 45, pp. 3997-4007, 2004.
- [75] J. Suresh, S. Karthik and A. Arun, "Photocrosslinkable Polymer based on 4-(2,4-dichlorophenyl)-3-oxoprop-1-enyl) Phenylacrylate: Synthesis, Reactivity Ratio, and Crosslinking Studies," *Materials Science - Poland*, vol. 34, no. 4, pp. 834-844, 2016.
- [76] G. Zhang, L. Zhang, H. Gao, I. Konstantinov, S. Arturo, D. Yu and J. B. L. Torkelson, "A Combined Computational and Experimental Study of Copolymerization Propagation Kinetics for 1-Ethylcyclopentyl Methacrylate and Methyl Methacrylate," *Macromolecular Theory and Simulations*, 2016.
- [77] J. Undin, T. Illanes, A. Finne-Wistrand and A. Albertsson, "Random Introduction of Degradable Linkages into Functional Vinyl Polymers by Radical Ring-Opening Polymerization, Tailored for Soft Tissue Engineering," *Polymer Chemistry*, vol. 3, pp. 1260-1266, 2012.
- [78] C. Hagiopol, *Copolymerization: Toward a Systematic Approach*, New York: Plenum Publishers, 1999.
- [79] S. Ren, L. Hinojosa-Castellanos, L. Zhang and M. A. Dubé, "Bulk Free-Radical Copolymerization of n-Butyl Acrylate and n-Butyl Methacrylate: Reactivity Ratio Estimation," *Macromolecular Reaction Engineering*, vol. 11, p. 1600050, 2017.
- [80] A. J. Scott, N. Kazemi and A. Penlidis, "AMPS/AAm/AAC Terpolymerization: Experimental Verification of the EVM Framework for Ternary Reactivity Ratio Estimation," *Processes*, vol. 5, no. 1, p. 9, 2017.
- [81] A. J. Scott, T. A. Duever and A. Penlidis, "The Role of pH, Ionic Strength and Monomer Concentration on the Terpolymerization of 2-Acrylamido-2-Methylpropane Sulfonic Acid, Acrylamide and Acrylic Acid," *Polymer*, vol. 177, pp. 214-230, 2019.
- [82] T. Anirudhan and S. Rejeena, "Biopolymer-Based Stimuli-Sensitive Functionalized Graft Copolymers as Controlled Drug Delivery Systems," in *Surface Modification of Biopolymers*, Hoboken, John Wiley & Sons, Inc., 2015, pp. 291-334.
- [83] M. Riahinezhad, N. Kazemi, N. T. McManus and A. Penlidis, "Optimal Estimation of Reactivity Ratios for Acrylamide/Acrylic Acid Copolymerization," *Journal of Polymer Science, Part A: Polymer Chemistry*, vol. 51, pp. 4819-4827, 2013.
- [84] M. Riahinezhad, N. Kazemi, N. T. McManus and A. Penlidis, "Effect of Ionic Strength on the Reactivity Ratios of Acrylamide/Acrylic Acid (Sodium Acrylate) Copolymerization," *Journal of Applied Polymer Science*, vol. 131, p. 40949, 2014.
- [85] M. Riahinezhad, N. T. McManus and A. Penlidis, "Effect of Monomer Concentration and pH on Reaction Kinetics and Copolymer Microstructure of Acrylamide/Acrylic Acid Copolymer," *Macromolecular Reaction Engineering*, vol. 9, pp. 100-113, 2015.
- [86] C. Preusser, I. Ezenwajiaku and R. Hutchinson, "The Combined Influence of Monomer Concentration and Ionization on Acrylamide/Acrylic Acid Composition in

- Aqueous Solution Radical Batch Copolymerization," *Macromolecules*, vol. 49, no. 13, p. 4746–4756, 2016.
- [87] E. Fischer, D. Cuccato, G. Storti and M. Morbidelli, "Effect of the Charge Interactions on the Composition Behavior of Acrylamide/Acrylic Acid Copolymerization in Aqueous Medium," *European Polymer Journal*, vol. 98, pp. 302-312, 2018.
- [88] A. M. Atta, G. A. El-Mahdy, H. A. Allohedan and M. M. S. Abdullah, "Synthesis and Application of Poly Ionic Liquid-Based on 2-Acrylamido-2-Methyl Propane Sulfonic Acid as Corrosion Protective Film of Steel," *International Journal of Electrochemical Science*, vol. 10, pp. 6106 - 6119, 2015.
- [89] D. J. Currie, F. S. Dainton and W. S. Watt, "The Effect of pH on the Polymerization of Acrylamide in Water," *Polymer*, vol. 6, no. 9, pp. 451-453, 1965.
- [90] V. F. Kurenkov and V. A. Myagchenkov, "Effects of Reaction Medium on the Radical Polymerization and Copolymerization of Acrylamide," *European Polymer Journal*, vol. 16, no. 12, pp. 1229-1239, 1980.
- [91] H.-R. Lin, "Solution Polymerization of Acrylamide using Potassium Persulfate as an Initiator: Kinetic Studies, Temperature and pH Dependence," *European Polymer Journal*, vol. 37, pp. 1507-1510, 2001.
- [92] I. Lacik, A. Chovancova, L. Uhelska, C. Preusser, R. Hutchinson and M. Buback, "PLP-SEC Studies into the Propagation Rate Coefficient of Acrylamide Radical Polymerization in Aqueous Solution," *Macromolecules*, vol. 49, pp. 3244-3253, 2016.
- [93] V. A. Kabanov, D. A. Topchiev and T. M. Karaputadze, "Some Features of Radical Polymerization of Acrylic and Methacrylic Acid Salts in Aqueous Solutions," *Journal of Polymer Science: Symposium*, vol. 42, pp. 173-183, 1973.
- [94] R. A. Scott and N. A. Peppas, "Kinetic Study of Acrylic Acid Solution Polymerization," *AIChE Journal*, vol. 43, no. 1, pp. 135-144, 1997.
- [95] H. Çatalgil-Giz, A. Giz, A. M. Alb and W. F. Reed, "Absolute Online Monitoring of Acrylic Acid Polymerization and the Effect of Salt and pH on Reaction Kinetics," *Journal of Applied Polymer Science*, vol. 91, no. 2, pp. 1352-1359, 2004.
- [96] I. Lacik, S. Beuermann and M. Buback, "PLP-SEC Study into the Free-Radical Propagation Rate Coefficients of Partially and Fully Ionized Acrylic Acid in Aqueous Solution," *Macromolecular Chemistry and Physics*, vol. 205, no. 8, pp. 1080-1087, 2004.
- [97] W. Cabaness and T. P. C. Lin, "Effect of pH on the Reactivity Ratios in the Copolymerization of Acrylic Acid and Acrylamide," *Journal of Polymer Science, Part A: Polymer Chemistry*, vol. 9, no. 8, pp. 2155-2170, 1971.
- [98] A. Paril, A. Alb, A. Giz and H. Catalgil-Giz, "Effect of Medium pH on the Reactivity Ratios in Acrylamide Acrylic Acid Copolymerization," *Journal of Applied Polymer Science*, vol. 103, no. 2, pp. 968-974, 2007.
- [99] I. Rintoul and C. Wandrey, "Polymerization of Ionic Monomers in Polar Solvents: Kinetics and Mechanism of the Free Radical Copolymerization of Acrylamide/Acrylic Acid," *Polymer*, vol. 46, no. 13, pp. 4525-4532, 2005.

- [100] S. Beuermann, M. Buback, P. Hesse, T. Junkers and I. Lacik, "Free-Radical Polymerization Kinetics of 2-Acrylamido-2-methylpropanesulfonic Acid in Aqueous Solution," *Macromolecules*, vol. 39, pp. 509-516, 2006.
- [101] S. Durmaz and O. Okay, "Acrylamide/2-Acrylamido-2-methylpropane Sulfonic Acid Sodium Salt-Based Hydrogels: Synthesis and Characterization," *Polymer*, vol. 41, pp. 3693-3704, 2000.
- [102] C. L. McCormick and G. S. Chen, "Water-Soluble Copolymers. IV. Random Copolymers of Acrylamide with Sulfonated Comonomers," *Journal of Polymer Science: Polymer Chemistry Edition*, vol. 20, pp. 817-838, 1982.
- [103] J. Travas-Sejdic and A. Eastal, "Study of Free-Radical Copolymerization of Acrylamide with 2-Acrylamido-2-methyl-1-propane Sulphonic Acid," *Journal of Applied Polymer Science*, vol. 75, pp. 619-628, 2000.
- [104] A.-A. A. Abdel-Azim, M. S. Farahat, A. M. Atta and A. A. Abdel-Fattah, "Preparation and Properties of Two-Component Hydrogels Based on 2-Acrylamido-2-methylpropane Sulphonic Acid," *Polymers for Advanced Technologies*, vol. 9, pp. 282-289, 1998.
- [105] R. G. Ryles and R. E. Neff, "Thermally Stable Acrylic Monomer for Profile Modification Applications," in *Water-Soluble Polymers for Petroleum Recovery*, G. A. Stahl and D. N. Schulz, Eds., New York, Springer Science + Business Media, 1988.
- [106] V. F. Gromov, P. M. Homikovskiy and A. D. Abkin, "Vysokomolek. Soedin.," *B12*, p. 767, 1970.
- [107] K. Plochocka and T. Woknarowski, "The Effect of Li, Na and K Cations on the Reactivities of Acrylic Acid Salts and Acrylamide in Copolymerization in Aqueous Medium," *European Polymer Journal*, vol. 7, pp. 797-804, 1971.
- [108] K. Plochocka and T. Wojnarowski, "The Effect of Ca, Sr and Ba Cations on the Reactivities of Acrylic Acid Salts and Acrylamide in Copolymerization in Aqueous Medium," *European Polymer Journal*, vol. 8, pp. 921-926, 1972.
- [109] S. Ponratnam and S. L. Kapur, "Reactivity Ratios of Ionizing Monomers in Aqueous Solution: Copolymerization of Acrylic and Methacrylic Acids with Acrylamide," *Makromolekular Chemie*, vol. 178, pp. 1029-1038, 1977.
- [110] S. A. Seabrook, M. P. Tonge and R. G. Gilbert, "Pulsed Laser Polymerization Study of the Propagation Kinetics of Acrylamide in Water," *Journal of Polymer Science, Part A: Polymer Chemistry*, vol. 43, no. 7, pp. 1357-1368, 2005.
- [111] I. Lacik, S. Beuermann and M. Buback, "Aqueous Phase Size-Exclusion-Chromatography Used for PLP-SEC Studies into Free-Radical Propagation Rate of Acrylic Acid in Aqueous Solution," *Macromolecules*, vol. 34, pp. 6224-6228, 2001.
- [112] F. Kuchta, A. M. van Herk and A. L. German, "Propagation Kinetics of Acrylic and Methacrylic Acid in Water and Organic Solvents Studied by Pulsed-Laser Polymerization," *Macromolecules*, vol. 33, pp. 3641-3649, 2000.
- [113] I. Lacik, L. Ucnova, S. Kukuckova, M. Buback, P. Hesse and S. Beuermann, "Propagation Rate Coefficient of Free-Radical Polymerization of Partially and Fully

- Ionized Methacrylic Acid in Aqueous Solution," *Macromolecules*, vol. 42, pp. 7753-7761, 2009.
- [114] E. Fischer, G. Storti and D. Cuccato, "Aqueous Free-Radical Polymerization of Non-Ionized and Fully Ionized Methacrylic Acid," *Processes*, vol. 5, no. 2, p. 23, 2017.
- [115] M. Riahi-zhad, N. T. McManus and A. Penlidis, "Shear Viscosity of Poly (Acrylamide/Acrylic Acid) Solutions," *Macromolecular Symposia*, vol. 360, pp. 179-184, 2016.
- [116] M. J. Leamen, N. T. McManus and A. Penlidis, "Refractive Index Increment (dn/dc) using GPC for the α -Methyl Styrene/Methyl Methacrylate Copolymer at 670 nm in Tetrahydrofuran," *Journal of Applied Polymer Science*, vol. 94, no. 6, pp. 2545-2547, 2004.
- [117] M. Riahi-zhad, L. Romero-Zerón, N. T. McManus and A. Penlidis, "Evaluating the Performance of Tailor-Made Water-Soluble Copolymers for Enhanced Oil Recovery Polymer Flooding Applications," *Fuel*, vol. 203, pp. 269-278, 2017.
- [118] A. Thomas, N. Gaillard and C. Favero, "Some Key Features to Consider When Studying Acrylamide-Based Polymers for Chemical Enhanced Oil Recovery," *Oil & Gas Science and Technology – Rev. IFP Energies nouvelles*, vol. 67, no. 6, pp. 887-902, 2012.
- [119] J. C. Randall, "Monomer Distributions and Number-Average Sequence Lengths in Hydrogenated Butadiene-Styrene Copolymers from Carbon-13 Nuclear Magnetic Resonance," *Journal of Polymer Science: Polymer Physics Edition*, vol. 15, pp. 1451-1473, 1977.
- [120] A. S. Brar and Sunita, "Compositional Sequence Determination of Acrylonitrile-Butyl Acrylate Copolymers by ¹³C-NMR Spectroscopy," *Polymer*, vol. 34, pp. 3391-3396, 1993.
- [121] B. Wei, L. Romero-Zerón and D. Rodrigue, "Oil Displacement Mechanisms of Viscoelastic Polymers in Enhanced Oil Recovery (EOR): A Review," *Journal of Petroleum Exploration and Production Technology*, vol. 4, pp. 113-121, 2014.
- [122] R. S. Seright, "Potential for Polymer Flooding Reservoirs with Viscous Oils," *SPE Reservoir Evaluation and Engineering*, vol. 13, pp. 730-740, 2010.
- [123] S. Iwatsuki, M. Shin and Y. Yamashita, "Radical Terpolymerization of Dodecyl Vinyl Ether, Fumaronitrile and Chloroethyl Acrylate," *Die Makromolekulare Chemie*, vol. 102, no. 2197, pp. 232-244, 1967.
- [124] K. Saric, Z. Janovic and O. Vogl, "Terpolymerization of Acrylonitrile, Styrene, and 2,3-Dibromopropyl Acrylate," *Journal of Polymer Science, Part A: Polymer Chemistry*, vol. 21, no. 7, pp. 1913-1928, 1983.
- [125] J. Kressler, W. Bieger, B. Horvath and G. Schmidt-Naake, "Experimental Investigation of Ternary Azeotropy in the Copolymerization of Acrylonitrile, Styrene and Maleic Anhydride," *Journal of Macromolecular Science, Part A: Chemistry*, vol. 24, no. 6, pp. 681-687, 1987.
- [126] G. Luft, F. Stein and M. Dorn, "The Free-Radical Terpolymerisation of Ethylene, Methyl Acrylate and Vinyl Acetate at High Pressure," *Die Angewandte Makromolekulare Chemie*, vol. 211, no. 3677, pp. 131-140, 1993.

- [127] A. Urretabizkaia and J. M. Asua, "High Solids Content Emulsion Terpolymerization of Vinyl Acetate, Methyl Methacrylate, and Butyl Acrylate. I. Kinetics," *Journal of Polymer Science, Part A: Polymer Chemistry*, vol. 32, no. 9, pp. 1761-1778, 1994.
- [128] H. Schoonbrood, R. van Eijnatten, B. van den Reijen, A. van Herk and A. German, "Emulsion Co- and Terpolymerization of Styrene, Methyl Methacrylate, and Methyl Acrylate. I. Experimental Determination and Model Prediction of Composition Drift and Microstructure in Batch Reactions," *Journal of Polymer Science, Part A: Polymer Chemistry*, vol. 34, no. 6, pp. 935-947, 1996.
- [129] R.-C. Beauchemin and M. A. Dubé, "Bulk Terpolymer Composition Prediction from Copolymer Reactivity Ratios," *Polymer Reaction Engineering*, vol. 7, no. 4, pp. 485-499, 1999.
- [130] A. Jukic, M. Rogosic, E. Vidovic and Z. Janovic, "Terpolymerization Kinetics of Methyl Methacrylate or Styrene/Dodecyl Methacrylate/Octadecyl Methacrylate Systems," *Polymer International*, vol. 56, pp. 112-120, 2007.
- [131] H. F. Naguib, S. M. Mokhtar, N. Z. Khalil and M. Z. Elsabee, "Polymerization Kinetics of Indene, Methyl Methacrylate and Acrylonitrile and Characterization of their Terpolymer," *Journal of Polymer Research*, vol. 16, no. 6, pp. 693-702, 2009.
- [132] I. Soljic, A. Jukic and Z. Janovic, "Terpolymerization Kinetics of N,N-Dimethylaminoethyl Methacrylate/Alkyl Methacrylate/Styrene Systems," *Polymer Engineering & Science*, vol. 50, no. 3, pp. 577-587, 2010.
- [133] M. Zelzer and A. Heise, "Terpolymerization Kinetics of Amino Acid N-Carboxy Anhydrides," *Journal of Polymer Science Part A: Polymer Chemistry*, vol. 52, no. 9, pp. 1228-1236, 2014.
- [134] S. Ren, L. Zhang and M. A. Dubé, "Free-Radical Terpolymerization of n-Butyl Acrylate/Butyl Methacrylate/D-Limonene," *Journal of Applied Polymer Science*, vol. 132, p. 42821, 2015.
- [135] N. Kazemi, "Reactivity Ratio Estimation in Multicomponent Polymerization Systems Using the Error-in-Variables-Model (EVM) Framework," PhD Thesis, University of Waterloo, Waterloo, Ontario, 2014.
- [136] A. J. Scott, V. A. Gabriel, M. A. Dubé and A. Penlidis, "Making the Most of Parameter Estimation: Terpolymerization Troubleshooting Tips," *Processes*, vol. 7, no. 7, p. 444, 2019.
- [137] V. A. Gabriel and M. A. Dubé, "Bulk Free-Radical Co- and Terpolymerization of n-Butyl Acrylate/2-Ethylhexyl Acrylate/Methyl Methacrylate," *Macromolecular Reaction Engineering*, p. 1800057, 2018.
- [138] N. S. Pujari, M. Wang and K. Gonsalves, "Co and Terpolymer Reactivity Ratios of Chemically Amplified Resists," *Polymer*, vol. 118, pp. 201-214, 2017.
- [139] R. Mao and M. Huglin, "A New Linear Method to Calculate Monomer Reactivity Ratios by using High-Conversion Copolymerization Data: Penultimate Model with $r_2=0$," *Polymer*, vol. 35, no. 16, pp. 3525-3529, 1994.
- [140] Y. Zhang and M. A. Dubé, "Copolymerization of n-Butyl Methacrylate and D-Limonene," *Macromolecular Reaction Engineering*, vol. 8, pp. 805-812, 2014.

- [141] S. Ren, E. Trevino and M. A. Dubé, "Copolymerization of Limonene with n-Butyl Acrylate," *Macromolecular Reaction Engineering*, vol. 9, no. 4, pp. 339-349, 2015.
- [142] I. Skeist, "Copolymerization: the Composition Distribution Curve," *Journal of the American Chemical Society*, vol. 68, no. 9, pp. 1781-1784, 1946.
- [143] A. S. Brar and S. K. Hekmatyar, "Microstructure Determination of the Acrylonitrile-Styrene-Methyl Methacrylate Terpolymers by NMR Spectroscopy," *Journal of Applied Polymer Science*, vol. 74, pp. 3026-3032, 1999.
- [144] F. K. Yousefi, A. Jannesari, S. Pazokifard, M. R. Saeb, A. J. Scott and A. Penlidis, "Terpolymerization of Triisopropylsilyl Acrylate, Methyl Methacrylate, and Butyl Acrylate: Reactivity Ratio Estimation," *Macromolecular Reaction Engineering*, p. 1900014, 2019.
- [145] International Diabetes Federation, "IDF Diabetes Atlas - 7th Edition," Karakas Print, 2015.
- [146] K. Alberti and P. Zimmet, "Definition, Diagnosis and Classification of Diabetes Mellitus and its Complications: Part 1: Diagnosis and Classification of Diabetes Mellitus Provisional Report of a WHO Consultation," *Diabetic Medicine*, vol. 15, pp. 539-553, 1998.
- [147] C. Turner, "Potential of Breath and Skin Analysis for Monitoring Blood Glucose Concentration in Diabetes," *Expert Review of Molecular Diagnostics*, vol. 11, pp. 497-503, 2011.
- [148] Z. Wang and C. Wang, "Is Breath Acetone a Biomarker of Diabetes? A Historical Review on Breath Acetone Measurements," *Journal of Breath Research*, vol. 7, p. 037109, 2013.
- [149] G. Rooth and S. Ostenson, "Acetone in Alveolar Air and the Control of Diabetes," *The Lancet*, vol. 288, pp. 1102-1105, 1966.
- [150] C. Tassopoulos, D. Barnett and T. Russell Fraser, "Breath-Acetone and Blood-Sugar Measurements in Diabetes," *The Lancet*, vol. 293, pp. 1282-1286, 1969.
- [151] C. Deng, J. Zhang, X. Yu, W. Zhang and X. Zhang, "Determination of Acetone in Human Breath by Gas Chromatography–Mass Spectrometry and Solid-Phase Microextraction with On-Fiber Derivatization," *Journal of Chromatography B*, vol. 810, pp. 269-275, 2004.
- [152] M. Greiter, L. Keck, T. Siegmund, C. Hoeschen, U. Oeh and H. Paretzke, "Differences in Exhaled Gas Profiles between Patients with Type 2 Diabetes and Healthy Controls," *Diabetes Technology & Therapeutics*, vol. 12, pp. 455-463, 2010.
- [153] I. Ueta, Y. Saito, M. Hosoe, M. Okamoto, H. Ohkita, S. Shirai, H. Tamura and K. Jinno, "Breath Acetone Analysis with Miniaturized Sample Preparation Device: In-Needle Preconcentration and Subsequent Determination by Gas Chromatography–Mass Spectroscopy," *Journal of Chromatography B*, vol. 877, pp. 2551-2556, 2009.
- [154] M. Storer, J. Dummer, H. Lunt, J. Scotter, F. McCartin, J. Cook, M. Swanney, D. Kendall, F. Logan and M. Epton, "Measurement of Breath Acetone Concentrations by Selected Ion Flow Tube Mass Spectrometry in Type 2 Diabetes," *Journal of Breath Research*, vol. 5, p. 046011, 2011.

- [155] C. Wang, A. Mbi and M. Shepherd, "A Study on Breath Acetone in Diabetic Patients using a Cavity Ringdown Breath Analyzer: Exploring Correlations of Breath Acetone with Blood Glucose and Glycohemoglobin A1C," *IEEE Sensors Journal*, vol. 10, pp. 54-63, 2010.
- [156] N. Yamane, T. Tsuda, K. Nose, A. Yamamoto, H. Ishiguro and T. Kondo, "Relationship Between Skin Acetone and Blood β -hydroxybutyrate Concentrations in Diabetes," *Clinica Chimica Acta*, vol. 365, pp. 325-329, 2006.
- [157] C. Turner, B. Parekh, C. Walton, P. Spanel, D. Smith and M. Evans, "An Exploratory Comparative Study of Volatile Compounds in Exhaled Breath and Emitted by Skin using Selected Ion Flow Tube Mass Spectrometry," *Rapid Communications in Mass Spectrometry*, vol. 22, pp. 526-532, 2008.
- [158] N. Makisimovich, V. Vorotyntsev, N. Nikitina, O. Kaskevich, P. Karabun and F. Martynenko, "Adsorption Semiconductor Sensor for Diabetic Ketoacidosis Diagnosis," *Sensors and Actuators B*, vol. 35, pp. 419-421, 1996.
- [159] R. Guirado-Lopez, M. Sanchez and M. Rincon, "Interaction of Acetone Molecules with Carbon-Nanotube-Supported TiO₂ Nanoparticles: Possible Applications as Room Temperature Molecular Sensitive Coatings," *Journal of Physical Chemistry C*, vol. 111, pp. 57-65, 2007.
- [160] L. Mazeina, F. Perkins, V. Bermudez, S. Arnold and S. Prokes, "Functionalized Ga₂O₃ Nanowires as Active Material in Room Temperature Capacitance-Based Gas Sensors," *Langmuir*, vol. 26, pp. 13722-13726, 2010.
- [161] M. Righettoni, A. Tricoli and S. Pratsinis, "Si:WO₃ Sensors for Highly Selective Detection of Acetone for Easy Diagnosis of Diabetes by Breath Analysis," *Analytical Chemistry*, vol. 82, pp. 3581-3587, 2010.
- [162] M. Righettoni, A. Tricoli, S. Gass, A. Schmid, A. Amann and S. Pratsinis, "Breath Acetone Monitoring by Portable Si:WO₃ Gas Sensors," in *The 14th International Meeting on Chemical Sensors*, Nuremberg, 2012.
- [163] M. Righettoni, A. Schmid, A. Amann and S. Pratsinis, "Correlations Between Blood Glucose and Breath Components from Portable Gas Sensors and PTR-TOF-MS," *Journal of Breath Research*, vol. 7, p. 037110, 2013.
- [164] J. Shin, S. Choi, D. Youn and I. Kim, "Exhaled VOCs Sensing Properties of WO₃ Nanofibers Functionalized by Pt and IrO₂ Nanoparticles for Diagnosis of Diabetes and Halitosis," *Journal of Electroceramics*, vol. 29, pp. 106-116, 2012.
- [165] J. Shin, S. Choi, I. Lee, D. Youn, C. Park, J. Lee, H. Tuller and I. Kim, "Thin-Wall Assembled SnO₂ Fibers Functionalized by Catalytic Pt Nanoparticles and their Superior Exhaled-Breath-Sensing Properties for the Diagnosis of Diabetes," *Advanced Functional Materials*, vol. 23, pp. 2357-2367, 2013.
- [166] Y. Zhang, W. He, H. Zhao and P. Li, "Template-Free to Fabricate Highly Sensitive and Selective Acetone Gas Sensor Based on WO₃ Microspheres," *Vacuum*, vol. 95, pp. 30-34, 2013.
- [167] S. Choi, I. Lee, B. Jang, D. Youn, W. Ryu, C. Park and I. Kim, "Selective Diagnosis of Diabetes Using Pt-Functionalized WO₃ Hemitube Networks As a Sensing Layer of Acetone in Exhaled Breath," *Analytical Chemistry*, vol. 85, pp. 1792-1796, 2012.

- [168] S. Choi, F. Fuchs, R. Demadrille, B. Grevin, B. Jang, S. Lee, J. Lee, H. Tuller and I. Kim, "Fast Responding Exhaled-Breath Sensors Using WO_3 Hemitubes Functionalized by Graphene-Based Electronic Sensitizers for Diagnosis of Diseases," *Applied Materials and Interfaces*, vol. 6, pp. 9061-9070, 2014.
- [169] S. Choi, B. Jang, S. Lee, B. Min, A. Rothschild and I. Kim, "Selective Detection of Acetone and Hydrogen Sulfide for the Diagnosis of Diabetes and Halitosis Using SnO_2 Nanofibers Functionalized with Reduced Graphene Oxide Nanosheets," *Applied Materials and Interfaces*, vol. 6, pp. 2588-2597, 2014.
- [170] C. Shao, Y. Chang and Y. Long, "High Performance of Nanostructured ZnO Film Gas Sensor at Room Temperature," *Sensors and Actuators B: Chemical*, vol. 204, pp. 666-672, 2014.
- [171] D. Zhang, A. Liu, H. Chang and B. Xia, "Room-Temperature High-Performance Acetone Gas Sensor Based on Hydrothermal Synthesized SnO_2 -Reduced Graphene Oxide Hybrid Composite," *RSC Advances*, vol. 5, pp. 3016-3022, 2015.
- [172] L. Ruangchuay, A. Sirivat and J. Schwank, "Polypyrrole/Poly(methylmethacrylate) Blend as Selective Sensor for Acetone in Lacquer," *Talanta*, vol. 60, pp. 25-30, 2003.
- [173] J. Yu, H. Byun, M. So and J. Huh, "Analysis of Diabetic Patient's Breath with Conducting Polymer Sensor Array," *Sensors and Actuators B*, vol. 108, pp. 305-308, 2005.
- [174] B. Landini and S. Bravard, "Breath Acetone Concentration Measured Using a Palm-Size Enzymatic Sensor System," *IEEE Sensors Journal*, vol. 9, pp. 1802-1807, 2009.
- [175] Z. Ying, Y. Jiang, H. Qin, L. Zheng and X. Du, "A Study on QCM Sensor for Identification of Acetone Vapor," *COMPEL - The international journal for computation and mathematics in electrical and electronic engineering*, vol. 29, pp. 477-483, 2010.
- [176] J. Do and S. Wang, "On the Sensitivity of Conductimetric Acetone Gas Sensor Based on Polypyrrole and Polyaniline Conducting Polymers," *Sensors and Actuators B: Chemical*, vol. 185, pp. 325-329, 2013.
- [177] N. Hausmann, M. Meredith and S. Minter, "Towards the Design of an Acetone Breath Biosensor," *ECS Transactions*, vol. 45, pp. 1-17, 2013.
- [178] T. Nasution, I. Nainggolan, S. Hutagalung, K. Ahmad and Z. Ahmad, "The Sensing Mechanism and Detection of Low Concentration Acetone using Chitosan-Based Sensors," *Sensors and Actuators B*, vol. 177, pp. 522-528, 2013.
- [179] W. Chen, K. M. E. Stewart, R. Mansour and A. Penlidis, "Polymeric Sensing Material-Based Selectivity-Enhanced RF Resonant Cavity Sensor for Volatile Organic Compound (VOC) Detection," in *IEEE MTT-S International Microwave Symposium*, Phoenix, 2015.
- [180] A. Daneshkhah, S. Shrestha, M. Agarwal and K. Varahramyan, "Poly(vinylidene fluoride-hexafluoropropylene) Composite Sensors for Volatile Organic Compounds Detection in Breath," *Sensors and Actuators B*, vol. 221, pp. 635-643, 2015.
- [181] P. Sengupta, S. Barik and B. Adhikari, "Polyaniline as a Gas-Sensor Material," *Materials and Manufacturing Processes*, vol. 21, pp. 263-270, 2006.

- [182] K. M. E. Stewart, "PhD Thesis: Design of Polymeric Sensing Materials for Volatile Organic Compounds: Optimized Material Selection for Ethanol with Mechanistic Explanations," Department of Chemical Engineering, University of Waterloo, Waterloo, 2016.
- [183] T. Popov, "Human Exhaled Breath Analysis," *CME Review*, vol. 106, pp. 451-456, 2011.
- [184] A. Bikov, "PhD Thesis: Methodological and Physiological Aspects of Exhaled Breath Analysis," Doctoral School of Clinical Medicine, Semmelweis University, Budapest, 2013.
- [185] J. Brandrup, E. Immergut and E. A. Grulke, *Polymer Handbook*, 4th ed., New York: John Wiley & Sons, Inc., 1999.
- [186] L. Shacklette and C. Han, "Solubility and Dispersion Characteristics of Polyaniline," in *MRS Proceedings, Volume 328*, 1993.
- [187] D. van Krevelen and K. te Nijenhuis, "Cohesive Properties and Solubility," in *Properties of Polymers: Their Correlation with Chemical Structure; their Numerical Estimation and Prediction from Additive Group Contributions*, Elsevier, 2009, pp. 201-222.
- [188] F. Bradner, J. Shapiro, H. Bowley, D. Gerrard and W. Maddams, "Some Insights into the Microstructure of Polypyrrole," *Polymer*, vol. 30, pp. 914-917, 1989.
- [189] W. Feast, J. Tsibouklis, K. Pouwer, L. Groenendaal and E. Meijer, "Synthesis, Processing and Material Properties of Conjugated Polymers," *Polymer*, vol. 37, pp. 5017-5047, 1996.
- [190] C. Ozdemir, H. Can, N. Colak and A. Guner, "Synthesis, Characterization, and Comparison of Self-Doped, Doped, and Undoped Forms of Polyaniline, Poly(o-anisidine), and Poly[aniline-co-(o-anisidine)]," *Journal of Applied Polymer Science*, vol. 99, pp. 2182-2192, 2006.
- [191] I. Fratoddi, I. Venditti, C. Cametti and M. Russo, "Chemiresistive Polyaniline-Based Gas Sensors: A Mini Review," *Sensors and Actuators B*, vol. 220, pp. 534-548, 2015.
- [192] A. Ramanavicius, A. Ramanaviciene and A. Malinauskas, "Electrochemical Sensors Based on Conducting Polymer—Polypyrrole," *Electrochimica Acta*, vol. 51, pp. 6025-6037, 2006.
- [193] C. Lin, B. Hwang and H. Lee, "Methanol Sensors Based on the Conductive Polymer Composites from Polypyrrole and Poly (vinyl alcohol)," *Materials Chemistry and Physics*, vol. 55, pp. 139-144, 1998.
- [194] R. Gangopadhyay and A. De, "Conducting Polymer Composites: Novel Materials for Gas Sensing," *Sensors and Actuators B*, vol. 77, pp. 326-329, 2001.
- [195] L. Jiang, H. Jun, Y. Hoh, J. Lim, D. Lee and J. Huh, "Sensing Characteristics of Polypyrrole–Poly(vinyl alcohol) Methanol Sensors Prepared by In Situ Vapor State Polymerization," *Sensors and Actuators B*, vol. 105, pp. 132-137, 2005.
- [196] K. Ogura, T. Saino, M. Nakayama and H. Shiigi, "The Humidity Dependence of the Electrical Conductivity of a Soluble Polyaniline-Poly(vinyl alcohol) Composite Film," *Journal of Material Chemistry*, vol. 7, pp. 2363-2366, 1997.

- [197] S. McGovern, G. Spinks and G. Wallace, "Micro-Humidity Sensors Based on a Processable Polyaniline Blend," *Sensors and Actuators B*, vol. 107, pp. 657-665, 2005.
- [198] M. Irimia-Vladu and J. Fergus, "Suitability of Emeraldine Base Polyaniline-PVA Composite Film for Carbon Dioxide Sensing," *Synthetic Metals*, vol. 156, pp. 1401-1407, 2006.
- [199] N. Misra, S. Bharti, G. Kapusetti, D. Upadhyay, S. Jaiswal, H. Panda and R. Prakash, "Polyaniline-Poly(vinyl alcohol) IPN-Composite Prepared from Potassium Dichromate Embedded PVA Film: A Material for Humidity Sensing Application," *Indian Journal of Physics*, vol. 85, pp. 703-712, 2011.
- [200] M. Yang and K. Chen, "Humidity Sensors using Polyvinyl Alcohol Mixed with Electrolytes," *Sensors and Actuators B*, vol. 47, pp. 240-247, 1998.
- [201] M. Penza and G. Cassano, "Relative Humidity Sensing by PVA-Coated Dual Resonator SAW Oscillator," *Sensors and Actuators B*, vol. 68, pp. 300-306, 2000.
- [202] A. Gaston, F. Perez and J. Sevilla, "Optical Fiber Relative-Humidity Sensor with Polyvinyl Alcohol Film," *Applied Optics*, vol. 43, pp. 4127-4132, 2004.
- [203] V. Chabukswar, S. Pethkar and A. Athawale, "Acrylic Acid Doped Polyaniline as an Ammonia Sensor," *Sensors and Actuators B*, vol. 77, pp. 657-663, 2001.
- [204] B. Ding, M. Yamazaki and S. Shiratori, "Electrospun Fibrous Polyacrylic Acid Membrane-Based Gas Sensors," *Sensors and Actuators B*, vol. 106, pp. 477-483, 2005.
- [205] S. Lee, N. Takahara, S. Korposh, D. Yang, K. Toko and T. Kunitake, "Nanoassembled Thin Film Gas Sensors. III. Sensitive Detection of Amine Odors Using TiO₂/Poly(acrylic acid) Ultrathin Film Quartz Crystal Microbalance Sensors," *Analytical Chemistry*, vol. 82, pp. 2228-2236, 2010.
- [206] Y. Tang, K. Pan, X. Wang, C. Liu and S. Luo, "Electrochemical Synthesis of Polyaniline in Surface-Attached Poly(acrylic acid) Network, and its Application to the Electrocatalytic Oxidation of Ascorbic Acid," *Microchimica Acta*, vol. 168, pp. 231-237, 2010.
- [207] I. Tiwari, K. Singh, M. Singh and C. Banks, "Polyaniline/Polyacrylic Acid/Multi-Walled Carbon Nanotube Modified Electrodes for Sensing Ascorbic Acid," *Analytical Methods*, vol. 4, pp. 118-124, 2012.
- [208] M. Matsuguchi, Y. Sadaoka and Y. Sakai, "A Capacitive-Type Humidity Sensor Using Cross-Linked Poly(methyl methacrylate) Thin Films," *Journal of The Electrochemical Society*, vol. 138, pp. 1862-1865, 1991.
- [209] A. Ralston, J. Tobin, S. Bajikar and D. Denton, "Comparative Performance of Linear, Cross-Linked, and Plasma-Deposited PMMA Capacitive Humidity Sensors," *Sensors and Actuators B*, vol. 22, pp. 139-147, 1994.
- [210] R. Dabhade, D. Bodas and S. Gangal, "Plasma-Treated Polymer as Humidity Sensing Material—A Feasibility Study," *Sensors and Actuators B*, vol. 98, pp. 37-40, 2004.
- [211] P. Su, Y. Sun and C. Lin, "Humidity Sensor Based on PMMA Simultaneously Doped with Two Different Salts," *Sensors and Actuators B*, vol. 113, pp. 883-886, 2006.

- [212] P. Su and C. Wang, "In Situ Synthesized Composite Thin Films of MWCNTs/PMMA Doped with KOH as a Resistive Humidity Sensor," *Sensors and Actuators B*, vol. 124, pp. 303-308, 2007.
- [213] B. Philip, J. Abraham, A. Chandrasekhar and V. Varadan, "Carbon Nanotube/PMMA Composite Thin Films for Gas-Sensing Applications," *Smart Materials and Structures*, vol. 12, pp. 935-939, 2003.
- [214] J. Abraham, B. Philip, A. Witchurch, V. Varadan and C. Reddy, "A Compact Wireless Gas Sensor Using a Carbon Nanotube/PMMA Thin Film Chemiresistor," *Smart Materials and Structures*, vol. 13, pp. 1045-1049, 2004.
- [215] H. Lang, R. Berger, F. Battiston, J. Ramseyer, E. Meyer, C. Andreoli, J. Brugger, P. Vettiger, M. Despont, T. Mezzacasa, L. Scandella, H. Guntherodt, C. Gerver and J. Gimzewski, "A Chemical Sensor Based on a Micromechanical Cantilever Array for the Identification of Gases and Vapors," *Applied Physics A: Materials Science & Processing*, vol. 66, pp. S61-S64, 1998.
- [216] Y. Cao, A. Andreatta, A. J. Heeger and P. Smith, "Influence of Chemical Polymerization Conditions on the Properties of Polyaniline," *Polymer*, vol. 30, pp. 2305-2311, 1989.
- [217] C. Sasso, D. Beneventi, E. Zeno, D. Chaussy, M. Petit-Conil and N. Belgacem, "Polypyrrole and Polypyrrole/Wood-Derived Materials Conducting Composites: A Review," *BioResources*, vol. 6, pp. 3585-3620, 2011.
- [218] J. Thiblemont, J. Gabelle and M. Planche, "Polypyrrole Overoxidation during its Chemical Synthesis," *Synthetic Metals*, vol. 66, pp. 243-247, 1994.
- [219] W. Liang, J. Lei and C. R. Martin, "Effect of Synthesis Temperature on the Structure, Doping Level and Charge-Transport Properties of Polypyrrole," *Synthetic Metals*, vol. 52, pp. 227-239, 1992.
- [220] R. E. Myers, "Chemical Oxidative Polymerization as a Synthetic Route to Electrically Conducting Polypyrroles," *Journal of Electronic Materials*, vol. 15, no. 2, pp. 61-69, 1986.
- [221] A. G. MacDiarmid and A. J. Epstein, "Polyanilines: A Novel Class of Conducting Polymers," *Faraday Discussions of the Chemical Society*, vol. 88, pp. 317-332, 1989.
- [222] H. S. O. Chan, P. K. H. Ho, E. Khor, M. M. Tan, K. L. Tan, B. T. G. Tan and Y. K. Lim, "Preparation of Polyanilines Doped in Mixed Protonic Acids: Their Characterization by X-Ray Photoelectron Spectroscopy and Thermogravimetry," *Synthetic Materials*, vol. 31, pp. 95-108, 1989.
- [223] M. V. Kulkarni, A. K. Viswanath, R. Marimuthu and T. Seth, "Synthesis and Characterization of Polyaniline Doped with Organic Acids," *Journal of Polymer Science, Part A: Polymer Chemistry*, vol. 42, pp. 2043-2049, 2003.
- [224] S. Jain, S. Chakane, A. B. Samui, V. N. Krishnamurthy and S. V. Bhoraskar, "Humidity Sensing with Weak Acid-Doped Polyaniline and its Composites," *Sensors and Actuators B: Chemical*, vol. 96, pp. 12-129, 2003.
- [225] V. J. Babu, S. Vempati and S. Ramakrishna, "Conducting Polyaniline-Electrical Charge Transportation," *Materials Sciences and Applications*, vol. 4, pp. 1-10, 2013.

- [226] M. Jaymand, "Recent Progress in Chemical Modification of Polyaniline," *Progress in Polymer Science*, vol. 38, pp. 1287-1306, 2013.
- [227] S. Pandey and J. Ramontja, "Rapid, Facile Microwave-Assisted Synthesis of Xanthan Gum Grafted Polyaniline for Chemical Sensor," *International Journal of Biological Macromolecules*, vol. 89, pp. 89-98, 2016.
- [228] A. Tiwari and H. Singh, "Synthesis and Characterization of Electrical Conducting Chitosan-graft-Polyaniline," *eXPRESS Polymer Letters*, vol. 1, no. 5, p. 308–317, 2007.
- [229] C. S. Kushwaha, P. Singh, S. K. Shukla and G. C. Dubey, "Electrochemical Urea Sensing Over Polyaniline Grafted Chitosan Copolymer," *MaterialsToday: Proceedings*, vol. 5, no. 7, pp. 15253-15260, 2018.
- [230] S. S. Pandey, S. Annapoorni and B. D. Malhotra, "Synthesis and Characterization of Poly (aniline-co-o-anisidine): A Processable Conducting Copolymer," *Macromolecules*, vol. 26, pp. 3190-3193, 1993.
- [231] J. Laska, K. Zak and A. Proń, "Conducting Blends of Polyaniline with Conventional Polymers," *Synthetic Metals*, vol. 84, pp. 117-118, 1997.
- [232] S. T. McGovern, G. M. Spinks and G. G. Wallace, "Micro-Humidity Sensors Based on a Processable Polyaniline Blend," *Sensors and Actuators B: Chemical*, vol. 107, pp. 657-665, 2005.
- [233] J. Bhadra, N. J. Al-Thani, N. K. Madi and M. A. Al-Maadeed, "Effects of Aniline Concentrations on the Electrical and Mechanical Properties of Polyaniline Polyvinyl Alcohol Blends," *Arabian Journal of Chemistry*, vol. 10, pp. 664-672, 2017.
- [234] A. S. Hammad, H. Noby, M. F. Elkady and A. H. El-Shazly, "In-situ Polymerization of Polyaniline/Polypyrrole Copolymer using Different Techniques," *IOP Conference Series: Materials Science and Engineering*, vol. 290, p. 012001, 2018.
- [235] M. De Paoli, R. Waltman, A. Diaz and J. Bargon, "An Electrically Conductive Plastic Composite Derived from Polypyrrole and Poly(Vinyl Chloride)," *Journal of Polymer Science: Polymer Chemistry*, vol. 23, pp. 1687-1698, 1985.
- [236] V. Mano, M. Felisberti, T. Matencio and M. De Paoli, "Thermal, Mechanical and Electrochemical Behaviour of Poly(vinyl chloride)/ Polypyrrole Blends (PVC/PPy)," *Polymer*, vol. 37, pp. 5165-5170, 1996.
- [237] S. Hosseini and A. Entezami, "Conducting Polymer Blends of Polypyrrole with Polyvinyl Acetate, Polystyrene, and Polyvinyl Chloride Based Toxic Gas Sensors," *Journal of Applied Polymer Science*, vol. 90, p. 49–62 , 2003.
- [238] J. E. Haugen, K. Rudi, S. Langsrud and S. Bredhol, "Application of Gas-Sensor Array Technology for Detection and Monitoring of Growth of Spoilage Bacteria in Milk: A Model Study," *Analytica Chimica Acta*, vol. 565, pp. 10-16, 2006.
- [239] C. Di Natale, A. Macagnano, F. Davide, A. D'Amico, R. Paolesse, T. Boshi, M. Faccio and G. Ferri, "An Electronic Nose for Food Analysis," *Sensors and Actuators B*, vol. 44, pp. 521-526, 1997.
- [240] P. E. Acuña-Avila , R. Calavia, E. Vigueras-Santiago and E. Llobet, "Identification of Tequila with an Array of ZnO Thin Films: A Simple and Cost-Effective Method," *Sensors*, vol. 17, p. 2943, 2017.

- [241] H. Li, B. Zhang, W. Hu, Y. Liu, C. Dong and Q. Chen, "Monitoring Black Tea Fermentation using a Colorimetric Sensor Array-Based Artificial Olfaction System," *Journal of Food Processing and Preservation*, vol. 42, p. 13348, 2018.
- [242] L. Guz, G. Łagód, K. Jaromin-Gleń, Z. Suchorab, H. Sobczuk and A. Bieganski, "Application of Gas Sensor Arrays in Assessment of Wastewater Purification Effects," *Sensors*, vol. 15, pp. 1-21, 2015.
- [243] A. D'Amico, R. Bono, G. Pennazza, M. Santonico, G. Mantini, M. Bernabei, M. Zarlenga, C. Roscioni, E. Martinelli, R. Paolesse and C. Di Natale, "Identification of Melanoma with a Gas Sensor Array," *Skin Research and Technology*, vol. 14, pp. 226-236, 2008.
- [244] A. P. F. Turner and N. Magan, "Electronic Noses and Disease Diagnostics," *Nature Reviews Microbiology*, vol. 2, no. 2, pp. 161-166, 2004.
- [245] L. Feng, C. J. Musto, J. W. Kemling, S. H. Lim, W. Zhong and K. S. Suslick, "Colorimetric Sensor Array for Determination and Identification of Toxic Industrial Chemicals," *Analytical Chemistry*, vol. 82, no. 22, pp. 9433-9440, 2010.
- [246] C. Deng, K. Lv, D. Shi, B. Yang, S. Yu, Z. He and J. Yan, "Enhancing the Discrimination Ability of a Gas Sensor Array Based on a Novel Feature Selection and Fusion Framework," *Sensors*, vol. 18, p. 1909, 2018.
- [247] K. M. E. Stewart and A. Penlidis, "Sensor Array for Volatile Organic Compounds Based on Doped Poly (2,5-dimethyl aniline)," *Macromolecular Symposia*, vol. 370, pp. 120-127, 2016.
- [248] Y. Lu, C. Partridge, M. Meyyappan and J. Li, "A Carbon Nanotube Sensor Array for Sensitive Gas Discrimination using Principal Component Analysis," *Journal of Electrochemical Chemistry*, vol. 593, pp. 105-110, 2006.
- [249] P. Sun, Z. Ou and X. Feng, "Combustible Gas Discrimination by Pattern Recognition Analysis of Responses from Semiconductor Gas Sensor Array," *Applied Mechanics and Materials*, Vols. 303-306, pp. 876-879, 2013.
- [250] R. A. Potyrailo, "Polymeric Sensor Materials: Toward an Alliance of Combinatorial and Rational Design Tools?," *Angewandte Chemie*, vol. 45, pp. 702-723, 2006.
- [251] K. M. E. Stewart, A. J. Scott and A. Penlidis, "Evaluation of Doped and Undoped Poly (o-anisidine) as Sensing Materials for a Sensor Array for Volatile Organic Compounds," *In Press*.
- [252] A. A. Athawale and M. V. Kulkarni, "Polyaniline and its Substituted Derivatives as Sensor for Aliphatic Alcohols," *Sensors and Actuators B*, vol. 67, no. 1-2, pp. 173-177, 2000.
- [253] T. Itoh, I. Matsubara, W. Shin, N. Izu and M. Nishibori, "Preparation of Layered Organic-Inorganic Nanohybrid Thin Films of Molybdenum Trioxide with Polyaniline Derivatives for Aldehyde Gases Sensors of Several Tens ppb Level," *Sensors and Actuators B*, vol. 128, no. 2, pp. 512-520, 2008.
- [254] C. W. Na, H.-S. Woo and J.-H. Lee, "Design of Highly Sensitive Volatile Organic Compound Sensors by Controlling NiO Loading on ZnO Nanowire Networks," *RCS Advances*, vol. 2, pp. 414-417, 2012.

- [255] J. E. A. Jackson, *A User's Guide to Principal Component Analysis*, New York: Wiley, 1991.
- [256] J. W. Gardner, P. Boilot and E. L. Hines, "Enhancing Electronic Nose Performance by Sensor Selection using a New Integer-based Genetic Algorithm Approach," *Sensors and Actuators B*, vol. 106, pp. 114-121, 2005.
- [257] K. M. E. Stewart and A. Penlidis, "Evaluation of Polymeric Nanocomposites for the Detection of Toxic Gas Analytes," *Journal of Macromolecular Science, Part A*, vol. 53, no. 10, pp. 610-618, 2016.
- [258] W. T. Chen, K. M. E. Stewart, R. R. Mansour and A. Penlidis, "Novel Undercoupled Radio-frequency (RF) Resonant Sensor for Gaseous Ethanol and Interferents Detection," *Sensors and Actuators A: Physical*, vol. 230, pp. 63-73, 2015.
- [259] K. M. E. Stewart, W. Chen, R. Mansour and A. Penlidis, "Doped Poly (2,5-dimethyl aniline) for the Detection of Ethanol," *Journal of Applied Polymer Science*, vol. 132, p. 42259, 2015.
- [260] H. K. Chitte, N. V. Bhat, V. E. Walunj and G. N. Shinde, "Synthesis of Polypyrrole Using Ferric Chloride (FeCl₃) as Oxidant Together with Some Dopants for Use in Gas Sensors," *Journal of Sensor Technology*, vol. 1, pp. 47-56, 2011.
- [261] K. M. E. Stewart and A. Penlidis, "Novel Test System for Gas Sensing Materials and Sensors," *Macromolecular Symposia*, vol. 324, p. 11-18, 2013.
- [262] N. Majdabadifarahani, "Evaluating Polymeric Materials as Potential Sensing Materials for Gaseous Analytes," MASC Thesis, Department of Chemical Engineering, University of Waterloo, 2019.
- [263] A. W. Jones, "Excretion of Low-Molecular Weight Volatile Substances in Human Breath: Focus on Endogenous Ethanol," *Journal of Analytical Toxicology*, vol. 9, no. 6, pp. 246-250, 1985.
- [264] A. W. Jones, "Measuring and Reporting the Concentration of Aldehyde in Human Breath," *Alcohol and Alcoholism*, vol. 30, no. 3, pp. 271-285, 1995.
- [265] L. Wallace, E. Pellizzari, T. Hartwell, R. Perritt and R. Ziegenfus, "Exposures to Benzene and Other Volatile Compounds from Active and Passive Smoking," *Archives of Environmental Health: An International Journal*, vol. 42, no. 5, pp. 272-279, 1987.
- [266] R. C. Wester, H. I. Maibach, L. D. Gruenke and J. C. Craig, "Benzene Levels in Ambient Air and Breath of Smokers and Nonsmokers in Urban and Pristine Environments," *Journal of Toxicology and Environmental Health, Part A: Current Issues*, vol. 18, no. 4, pp. 567-573, 1986.
- [267] R. J. Sherwood, "Evaluation of Exposure to Benzene Vapour during the Loading of Petrol," *Occupational and Environmental Medicine*, vol. 29, pp. 65-69, 1972.
- [268] M. A. G. Wallace, J. D. Pleil, K. D. Oliver, D. A. Whitaker, S. Mentese, K. W. Fent and G. P. Horn, "Targeted GC-MS Analysis of Firefighters' Exhaled Breath: Exploring Biomarker Response at the Individual Level," *Journal of Occupational and Environmental Hygiene*, vol. 16, no. 5, pp. 355-366, 2019.
- [269] Z. Zhang, Z. Wei and M. Wan, "Nanostructures of Polyaniline Doped with Inorganic Acids," *Macromolecules*, vol. 35, pp. 5937-5942, 2002.

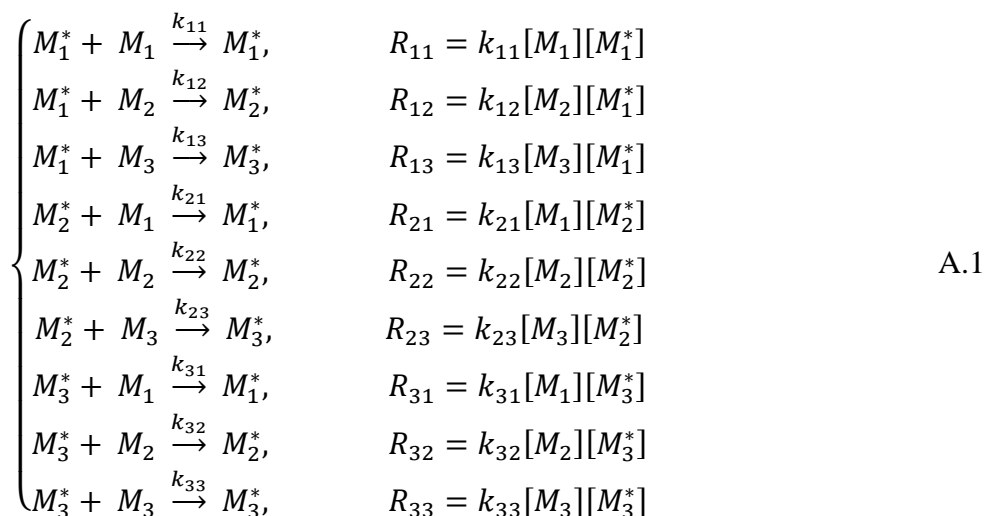
- [270] L. Ai, J. Jiang and R. Zhang, "Uniform Polyaniline Microspheres: A Novel Adsorbent for Dye Removal from Aqueous Solution," *Synthetic Metals*, vol. 160, pp. 762-767, 2010.
- [271] H. Noby, A. H. El-Shazly, M. F. Elkady and M. Ohshima, "Investigation of the Parameters affecting CO₂-Assisted Polyaniline," *MATEC Web of Conferences*, vol. 69, p. 04001, 2016.
- [272] J. P. Pouget, M. E. Jozefowicz, A. J. Epstein, X. Tang and A. G. MacDiarmid, "X-ray Structure of Polyaniline," *Macromolecules*, vol. 24, pp. 779-789, 1991.
- [273] M. A. Chougule, S. G. Pawar, P. R. Godse, R. N. Mulik, S. Sen and V. B. Patil, "Synthesis and Characterization of Polypyrrole (PPy) Thin Films," *Soft Nanoscience Letters*, vol. 1, pp. 6-10, 2011.
- [274] S. A. Waghuley, S. M. Yenorkar, S. S. Yawale and S. P. Yawale, "Application of Chemically Synthesized Conducting Polymer - Polypyrrole as a Carbon Dioxide Gas Sensor," *Sensors and Actuators B: Chemical*, vol. 128, pp. 366-373, 2007.
- [275] E. M. Abdelrazek, A. M. Hezma, A. El-khodary and A. M. Elzayat, "Spectroscopic Studies and Thermal Properties of PCL/PMMA Biopolymer Blend," *Egyptian Journal of Basic and Applied Sciences*, vol. 3, no. 1, pp. 10-15, 2016.
- [276] E. L. Cussler and G. D. Moggridge, *Chemical Product Design*, Cambridge: Cambridge University Press, 2001.
- [277] K. M. E. Stewart, N. T. McManus, E. Abdel-Rahman and A. Penlidis, "Doped Polyaniline for the Detection of Formaldehyde," *Journal of Macromolecular Science, Part A*, vol. 49, pp. 1-6, 2012.
- [278] M. Al-Ghamdi, R. Saritas, K. M. E. Stewart, A. J. Scott, M. Khater, A. Alneamy, A. Abdel-Aziz, H. Nafissi, E. Abdel-Rahman and A. Penlidis, "Aqueous Media Electrostatic MEMS Sensors," in *20th International Conference on Solid-State Sensors, Actuators and Microsystems & Eurosensors XXXIII (TRANSDUCERS & EUROSENSORS XXXIII)*, 2019.
- [279] A. J. Scott, N. Majdabadifarahani, K. M. E. Stewart, T. A. Duever and A. Penlidis, "Design of Polymeric Sensing Materials for Acetone Detection," *Submitted*, 2019.
- [280] N. T. McManus and A. Penlidis, "A Kinetic Investigation of Styrene/Ethyl Acrylate Copolymerization," *Journal of Polymer Science, Part A: Polymer Chemistry*, vol. 34, p. 237-248, 1996.
- [281] P. J. Rossignoli and T. A. Duever, "The Estimation of Copolymer Reactivity Ratios: A Review and Case Studies using the Error-in-Variables Model and Nonlinear Least Squares," *Polymer Reaction Engineering*, vol. 3, p. 361-395, 1995.

Appendix A. Derivation of Equations for Multi-Component Polymerization Kinetics

A.1 Derivation of the Alfrey-Goldfinger Model

This appendix contains the derivation of the Alfrey-Goldfinger model, as described in Chapter 2, Section 2.2.2.1 (see Equations 2.27 to 2.29).

As described in the main text, 9 unique propagation steps occur during free radical terpolymerization. These propagation are shown alongside their respective rates of reaction in Equation A.1. These rate equations are used in Equations A.2 through A.4 to calculate the rate of consumption of the three comonomers.



$$\frac{d[M_1]}{dt} = R_{11} + R_{21} + R_{31} \quad \text{A.2}$$

$$\frac{d[M_2]}{dt} = R_{12} + R_{22} + R_{32} \quad \text{A.3}$$

$$\frac{d[M_3]}{dt} = R_{13} + R_{23} + R_{33} \quad \text{A.4}$$

Using Equations A.2 through A.4, employing the long chain approximation (LCA) assumption for the free radicals (Equations A.5 through A.7), and knowing the relationship between rate constants and reactivity ratios (Equation 2.30), one can derive the instantaneous terpolymer composition model, also known as the Alfrey-Goldfinger equation (Equation A.8, which has also been shown in Equations 2.27 to 2.29 in the main text).

$$R_{12} + R_{13} = R_{21} + R_{31} \quad \text{A.5}$$

$$R_{21} + R_{23} = R_{12} + R_{32} \quad \text{A.6}$$

$$R_{31} + R_{32} = R_{13} + R_{23} \quad \text{A.7}$$

$$\begin{aligned} d[M_1]:d[M_2]:d[M_3] = & \\ & [M_1] \left(\frac{[M_1]}{r_{31}r_{21}} + \frac{[M_2]}{r_{21}r_{32}} + \frac{[M_3]}{r_{31}r_{23}} \right) \left([M_1] + \frac{[M_2]}{r_{12}} + \frac{[M_3]}{r_{13}} \right) \\ : & [M_2] \left(\frac{[M_1]}{r_{12}r_{31}} + \frac{[M_2]}{r_{12}r_{32}} + \frac{[M_3]}{r_{32}r_{13}} \right) \left([M_2] + \frac{[M_1]}{r_{21}} + \frac{[M_3]}{r_{23}} \right) \\ : & [M_3] \left(\frac{[M_1]}{r_{13}r_{21}} + \frac{[M_2]}{r_{23}r_{12}} + \frac{[M_3]}{r_{13}r_{23}} \right) \left([M_3] + \frac{[M_1]}{r_{31}} + \frac{[M_2]}{r_{32}} \right) \end{aligned} \quad \text{A.8}$$

However, this model relies on ratios of responses, which can cause issues with symmetry during parameter estimation. Therefore, the recast Alfrey-Goldfinger model (shown in what follows) is preferred.

A.2 Original Derivation of the Recast Alfrey-Goldfinger Model (from Ratios)

The derivation of the recast terpolymerization composition model is shown herein, as described in Chapter 2, Section 2.2.2.2 (see Equations 2.31 to 2.33). This was originally demonstrated by Kazemi [135], and uses the original Alfrey-Goldfinger equation (ratios) as a starting point. However, rather than using the monomer concentration form shown in Equation A.8, composition is presented in mole fractions f_i (Equations A.9 to A.11):

$$\frac{df_1}{df_2} = \frac{F_1}{F_2} = \frac{f_1 \left(\frac{f_1}{r_{31}r_{21}} + \frac{f_2}{r_{21}r_{32}} + \frac{f_3}{r_{31}r_{23}} \right) \left(f_1 + \frac{f_2}{r_{12}} + \frac{f_3}{r_{13}} \right)}{f_2 \left(\frac{f_1}{r_{12}r_{31}} + \frac{f_2}{r_{12}r_{32}} + \frac{f_3}{r_{32}r_{13}} \right) \left(f_2 + \frac{f_1}{r_{21}} + \frac{f_3}{r_{23}} \right)} \quad \text{A.9}$$

$$\frac{df_1}{df_3} = \frac{F_1}{F_3} = \frac{f_1 \left(\frac{f_1}{r_{31}r_{21}} + \frac{f_2}{r_{21}r_{32}} + \frac{f_3}{r_{31}r_{23}} \right) \left(f_1 + \frac{f_2}{r_{12}} + \frac{f_3}{r_{13}} \right)}{f_3 \left(\frac{f_1}{r_{13}r_{21}} + \frac{f_2}{r_{23}r_{12}} + \frac{f_3}{r_{13}r_{23}} \right) \left(f_3 + \frac{f_1}{r_{31}} + \frac{f_2}{r_{32}} \right)} \quad \text{A.10}$$

$$\frac{df_2}{df_3} = \frac{F_2}{F_3} = \frac{f_2 \left(\frac{f_1}{r_{12}r_{31}} + \frac{f_2}{r_{12}r_{32}} + \frac{f_3}{r_{32}r_{13}} \right) \left(f_2 + \frac{f_1}{r_{21}} + \frac{f_3}{r_{23}} \right)}{f_3 \left(\frac{f_1}{r_{13}r_{21}} + \frac{f_2}{r_{23}r_{12}} + \frac{f_3}{r_{13}r_{23}} \right) \left(f_3 + \frac{f_1}{r_{31}} + \frac{f_2}{r_{32}} \right)} \quad \text{A.11}$$

The right-hand sides of Equations A.9 to A.11 are summarized as shown in Equation A.12 to simplify subsequent calculations.

$$\frac{F_1}{F_2} = \frac{g_1}{g_2}, \quad \frac{F_1}{F_3} = \frac{g_1}{g_3}, \quad \frac{F_2}{F_3} = \frac{g_2}{g_3} \quad \text{A.12}$$

Since stoichiometry dictates that the sum of the mole fractions of terpolymer composition must be unity (Equation A.13), we can use this relationship as a starting point and make substitutions from the original A-G model (Equation A.14). Further simplification gives Equation A.15 (for the F_1 mole fraction), and the same procedure can be followed for F_2 and F_3 . The entire recast model is shown in Equations A.16 through A.18 (and is equivalent to Equations 2.31 to 2.33).

$$F_1 + F_2 + F_3 = 1 \quad \text{A.13}$$

$$F_1 + \frac{g_2}{g_1} F_1 + \frac{g_3}{g_1} F_1 = 1 \quad \text{A.14}$$

$$F_1 = \frac{g_1}{g_1 + g_2 + g_3} \quad \text{A.15}$$

$$F_1 - \frac{f_1 \left(\frac{f_1}{r_{21}r_{31}} + \frac{f_2}{r_{21}r_{32}} + \frac{f_3}{r_{31}r_{23}} \right) \left(f_1 + \frac{f_2 + f_3}{r_{12} + r_{13}} \right)}{f_1 \left(\frac{f_1}{r_{21}r_{31}} + \frac{f_2}{r_{21}r_{32}} + \frac{f_3}{r_{31}r_{23}} \right) \left(f_1 + \frac{f_2 + f_3}{r_{12} + r_{13}} \right) + f_2 \left(\frac{f_1}{r_{12}r_{31}} + \frac{f_2}{r_{12}r_{32}} + \frac{f_3}{r_{13}r_{32}} \right) \left(f_2 + \frac{f_1 + f_3}{r_{21} + r_{23}} \right) + f_3 \left(\frac{f_1}{r_{13}r_{21}} + \frac{f_2}{r_{23}r_{12}} + \frac{f_3}{r_{13}r_{23}} \right) \left(f_3 + \frac{f_1 + f_2}{r_{31} + r_{32}} \right)} = 0 \quad \text{A.16}$$

$$F_2 - \frac{f_2 \left(\frac{f_1}{r_{12}r_{31}} + \frac{f_2}{r_{12}r_{32}} + \frac{f_3}{r_{13}r_{32}} \right) \left(f_2 + \frac{f_1 + f_3}{r_{21} + r_{23}} \right)}{f_1 \left(\frac{f_1}{r_{21}r_{31}} + \frac{f_2}{r_{21}r_{32}} + \frac{f_3}{r_{31}r_{23}} \right) \left(f_1 + \frac{f_2 + f_3}{r_{12} + r_{13}} \right) + f_2 \left(\frac{f_1}{r_{12}r_{31}} + \frac{f_2}{r_{12}r_{32}} + \frac{f_3}{r_{13}r_{32}} \right) \left(f_2 + \frac{f_1 + f_3}{r_{21} + r_{23}} \right) + f_3 \left(\frac{f_1}{r_{13}r_{21}} + \frac{f_2}{r_{23}r_{12}} + \frac{f_3}{r_{13}r_{23}} \right) \left(f_3 + \frac{f_1 + f_2}{r_{31} + r_{32}} \right)} = 0 \quad \text{A.17}$$

$$F_3 - \frac{f_3 \left(\frac{f_1}{r_{13}r_{21}} + \frac{f_2}{r_{23}r_{12}} + \frac{f_3}{r_{13}r_{23}} \right) \left(f_3 + \frac{f_1 + f_2}{r_{31} + r_{32}} \right)}{f_1 \left(\frac{f_1}{r_{21}r_{31}} + \frac{f_2}{r_{21}r_{32}} + \frac{f_3}{r_{31}r_{23}} \right) \left(f_1 + \frac{f_2 + f_3}{r_{12} + r_{13}} \right) + f_2 \left(\frac{f_1}{r_{12}r_{31}} + \frac{f_2}{r_{12}r_{32}} + \frac{f_3}{r_{13}r_{32}} \right) \left(f_2 + \frac{f_1 + f_3}{r_{21} + r_{23}} \right) + f_3 \left(\frac{f_1}{r_{13}r_{21}} + \frac{f_2}{r_{23}r_{12}} + \frac{f_3}{r_{13}r_{23}} \right) \left(f_3 + \frac{f_1 + f_2}{r_{31} + r_{32}} \right)} = 0 \quad \text{A.18}$$

A.3 New Derivation of the Alfrey-Goldfinger Model (from Kinetics)

This newly derived equation does not use the Alfrey-Goldfinger ratios as a starting point. Instead, it is derived directly from kinetics. The first two steps are similar to what has been described for the original A-G model, since the propagation rates (Equation A.1) and the long chain assumption (LCA; Equations A.5 to A.7) are critical.

Combining the individual rates of reaction (for each propagation step; Equation A.1) and the LCA relationships (Equations A.5 to A.7) gives Equations A.19 through A.21 (note that Equation A.5 is used to obtain Equation A.19, and so on).

$$[M_1^*] = \frac{k_{21}[M_1][M_2^*] + k_{31}[M_1][M_3^*]}{k_{12}[M_2] + k_{13}[M_3]} \quad \text{A.19}$$

$$[M_2^*] = \frac{k_{12}[M_2][M_1^*] + k_{32}[M_2][M_3^*]}{k_{21}[M_1] + k_{23}[M_3]} \quad \text{A.20}$$

$$[M_3^*] = \frac{k_{13}[M_3][M_1^*] + k_{23}[M_3][M_2^*]}{k_{31}[M_1] + k_{32}[M_2]} \quad \text{A.21}$$

Next, consider ϕ_i^* , which represents the fraction of radicals of type i. Given the definition of ϕ_1^* in Equation A.22, the equation can be inverted to obtain Equation A.23. Type 1 radicals are the focus herein, but the same general process applies to the other comonomer radicals.

$$\phi_1^* = \frac{[M_1^*]}{[M_1^*] + [M_2^*] + [M_3^*]} \quad \text{A.22}$$

$$\frac{1}{\phi_1^*} = 1 + \frac{[M_2^*]}{[M_1^*]} + \frac{[M_3^*]}{[M_1^*]} \quad \text{A.23}$$

To eliminate the radical terms (which cannot be directly measured), both ratios in Equation A.23 are considered independently. First, radical terms are eliminated in $[M_2^*]/[M_1^*]$ by combining Equations A.19 and A.20 (and recognizing that $[M_3^*]$ is the same in both equations and therefore ‘cancels out’); see Equation A.24. Similarly, radical terms are eliminated in $[M_3^*]/[M_1^*]$ by combining Equations A.19 and A.21 (now allowing $[M_2^*]$ to be ‘cancelled out’); see Equation A.25.

$$\frac{[M_2^*]}{[M_1^*]} = \frac{k_{12}k_{31}[M_1][M_2] + k_{12}k_{32}[M_2]^2 + k_{13}k_{32}[M_2][M_3]}{k_{21}k_{31}[M_1]^2 + k_{21}k_{32}[M_1][M_2] + k_{23}k_{31}[M_1][M_3]} \quad \text{A.24}$$

$$\frac{[M_3^*]}{[M_1^*]} = \frac{k_{13}k_{21}[M_1][M_3] + k_{12}k_{23}[M_2][M_3] + k_{13}k_{23}[M_3]^2}{k_{21}k_{31}[M_1]^2 + k_{21}k_{32}[M_1][M_2] + k_{23}k_{31}[M_1][M_3]} \quad \text{A.25}$$

In Equations A.24 and A.25, the denominator is the same, which makes substitution into Equation A.23 fairly straightforward:

$$\frac{1}{\phi_1^*} = \frac{\left[\begin{array}{l} k_{21}k_{31}[M_1]^2 + k_{21}k_{32}[M_1][M_2] + k_{23}k_{31}[M_1][M_3] \\ + k_{12}k_{31}[M_1][M_2] + k_{12}k_{32}[M_2]^2 + k_{13}k_{32}[M_2][M_3] \\ + k_{13}k_{21}[M_1][M_3] + k_{12}k_{23}[M_2][M_3] + k_{13}k_{23}[M_3]^2 \end{array} \right]}{k_{21}k_{31}[M_1]^2 + k_{21}k_{32}[M_1][M_2] + k_{23}k_{31}[M_1][M_3]} \quad \text{A.26}$$

$$\therefore \phi_1^* = \frac{k_{21}k_{31}[M_1]^2 + k_{21}k_{32}[M_1][M_2] + k_{23}k_{31}[M_1][M_3]}{\begin{bmatrix} k_{21}k_{31}[M_1]^2 + k_{21}k_{32}[M_1][M_2] + k_{23}k_{31}[M_1][M_3] \\ + k_{12}k_{31}[M_1][M_2] + k_{12}k_{32}[M_2]^2 + k_{13}k_{32}[M_2][M_3] \\ + k_{13}k_{21}[M_1][M_3] + k_{12}k_{23}[M_2][M_3] + k_{13}k_{23}[M_3]^2 \end{bmatrix}} \quad \text{A.27}$$

Similarly, for the other comonomers:

$$\phi_2^* = \frac{k_{12}k_{31}[M_1][M_2] + k_{12}k_{32}[M_2]^2 + k_{13}k_{32}[M_2][M_3]}{\begin{bmatrix} k_{21}k_{31}[M_1]^2 + k_{21}k_{32}[M_1][M_2] + k_{23}k_{31}[M_1][M_3] \\ + k_{12}k_{31}[M_1][M_2] + k_{12}k_{32}[M_2]^2 + k_{13}k_{32}[M_2][M_3] \\ + k_{13}k_{21}[M_1][M_3] + k_{12}k_{23}[M_2][M_3] + k_{13}k_{23}[M_3]^2 \end{bmatrix}} \quad \text{A.28}$$

$$\phi_3^* = \frac{k_{13}k_{21}[M_1][M_3] + k_{12}k_{23}[M_2][M_3] + k_{13}k_{23}[M_3]^2}{\begin{bmatrix} k_{21}k_{31}[M_1]^2 + k_{21}k_{32}[M_1][M_2] + k_{23}k_{31}[M_1][M_3] \\ + k_{12}k_{31}[M_1][M_2] + k_{12}k_{32}[M_2]^2 + k_{13}k_{32}[M_2][M_3] \\ + k_{13}k_{21}[M_1][M_3] + k_{12}k_{23}[M_2][M_3] + k_{13}k_{23}[M_3]^2 \end{bmatrix}} \quad \text{A.29}$$

Finally, the radical fractions (ϕ_i^*) can be used to determine the instantaneous copolymer composition (F_i). The general expression for monomer 1 (F_1) is in Equation A.30; since total radical concentration $[R^*]$ and monomer concentration $[M]$ are in both the numerator and the denominator, they can be eliminated. Replacing the ϕ_i^* terms in Equation A.30 with the expressions derived in Equations A.27 through A.29 (and considering the reactivity ratio definitions shown in Equation 2.30) yields an expression for F_1 that does not require the determination of any radical concentrations (see Equation A.31). Similar expressions can be obtained (following the same process) for F_2 and F_3 ; these are shown in Equations A.32 and A.33 for completeness. These expressions (Equations A.31 to A.33) are equivalent to the recast Alfrey-Goldfinger model shown in Equations 2.31 to 2.33 (and derived in Section A.2), but use terpolymerization kinetics as a starting point (rather than pre-determined ratios from the original Alfrey-Goldfinger model).

$$F_1 = \frac{f_1(k_{11}\phi_1^* + k_{21}\phi_2^* + k_{31}\phi_3^*)}{\begin{bmatrix} f_1(k_{11}\phi_1^* + k_{21}\phi_2^* + k_{31}\phi_3^*) \\ + f_2(k_{12}\phi_1^* + k_{22}\phi_2^* + k_{32}\phi_3^*) \\ + f_3(k_{13}\phi_1^* + k_{23}\phi_2^* + k_{33}\phi_3^*) \end{bmatrix}} \quad \text{A.30}$$

$$F_1 = \frac{f_1 \left(\frac{f_1}{r_{21}r_{31}} + \frac{f_2}{r_{21}r_{32}} + \frac{f_3}{r_{31}r_{23}} \right) \left(f_1 + \frac{f_2}{r_{12}} + \frac{f_3}{r_{13}} \right)}{\left[\begin{aligned} & f_1 \left(\frac{f_1}{r_{21}r_{31}} + \frac{f_2}{r_{21}r_{32}} + \frac{f_3}{r_{31}r_{23}} \right) \left(f_1 + \frac{f_2}{r_{12}} + \frac{f_3}{r_{13}} \right) \\ & + f_2 \left(\frac{f_1}{r_{12}r_{31}} + \frac{f_2}{r_{12}r_{32}} + \frac{f_3}{r_{13}r_{32}} \right) \left(f_2 + \frac{f_1}{r_{21}} + \frac{f_3}{r_{23}} \right) \\ & + f_3 \left(\frac{f_1}{r_{13}r_{21}} + \frac{f_2}{r_{23}r_{12}} + \frac{f_3}{r_{13}r_{23}} \right) \left(f_3 + \frac{f_1}{r_{31}} + \frac{f_2}{r_{32}} \right) \end{aligned} \right]} \quad \text{A.31}$$

$$F_2 = \frac{f_2 \left(\frac{f_1}{r_{12}r_{31}} + \frac{f_2}{r_{12}r_{32}} + \frac{f_3}{r_{13}r_{32}} \right) \left(f_2 + \frac{f_1}{r_{21}} + \frac{f_3}{r_{23}} \right)}{\left[\begin{aligned} & f_1 \left(\frac{f_1}{r_{21}r_{31}} + \frac{f_2}{r_{21}r_{32}} + \frac{f_3}{r_{31}r_{23}} \right) \left(f_1 + \frac{f_2}{r_{12}} + \frac{f_3}{r_{13}} \right) \\ & + f_2 \left(\frac{f_1}{r_{12}r_{31}} + \frac{f_2}{r_{12}r_{32}} + \frac{f_3}{r_{13}r_{32}} \right) \left(f_2 + \frac{f_1}{r_{21}} + \frac{f_3}{r_{23}} \right) \\ & + f_3 \left(\frac{f_1}{r_{13}r_{21}} + \frac{f_2}{r_{23}r_{12}} + \frac{f_3}{r_{13}r_{23}} \right) \left(f_3 + \frac{f_1}{r_{31}} + \frac{f_2}{r_{32}} \right) \end{aligned} \right]} \quad \text{A.32}$$

$$F_3 = \frac{f_3 \left(\frac{f_1}{r_{13}r_{21}} + \frac{f_2}{r_{23}r_{12}} + \frac{f_3}{r_{13}r_{23}} \right) \left(f_3 + \frac{f_1}{r_{31}} + \frac{f_2}{r_{32}} \right)}{\left[\begin{aligned} & f_1 \left(\frac{f_1}{r_{21}r_{31}} + \frac{f_2}{r_{21}r_{32}} + \frac{f_3}{r_{31}r_{23}} \right) \left(f_1 + \frac{f_2}{r_{12}} + \frac{f_3}{r_{13}} \right) \\ & + f_2 \left(\frac{f_1}{r_{12}r_{31}} + \frac{f_2}{r_{12}r_{32}} + \frac{f_3}{r_{13}r_{32}} \right) \left(f_2 + \frac{f_1}{r_{21}} + \frac{f_3}{r_{23}} \right) \\ & + f_3 \left(\frac{f_1}{r_{13}r_{21}} + \frac{f_2}{r_{23}r_{12}} + \frac{f_3}{r_{13}r_{23}} \right) \left(f_3 + \frac{f_1}{r_{31}} + \frac{f_2}{r_{32}} \right) \end{aligned} \right]} \quad \text{A.33}$$

Appendix B. Computational Package for EVM

B.1 Computational Package Demonstration

The following screenshots from the MATLAB-based EVM program are meant to provide an overview of the computational package; more details are provided in the related publication [6]. The analysis of instantaneous copolymerization data is presented herein, but the same general information is relevant to the analysis of cumulative data.

We will start by demonstrating the manual data input option, then we will show the same information using the ‘data file’ option. The prompts contain sample data from McManus and Penlidis [280]. If the user decides to input data using a pre-made data file, the same inputs are required (with slightly different formatting).

Running the program brings up the ‘QuickStart’ menu (Figure B.1), and Figure B.2 through Figure B.4 show the pop-up menus (that is, the required data) for manual input of instantaneous composition data. Typically, only the preliminary reactivity ratio estimates (Figure B.2) and the copolymerization (composition) data (Figure B.3) need to be modified by the user; the form of the data entry can be observed in the screenshots below.

As for Figure B.4, the only default value that may require updating (at the user’s discretion) is the variance-covariance matrix. If necessary, the magnitude of the matrix entries may be modified but the size of the matrix itself should not be changed (that is, it should remain a 2×2 matrix for the instantaneous case).

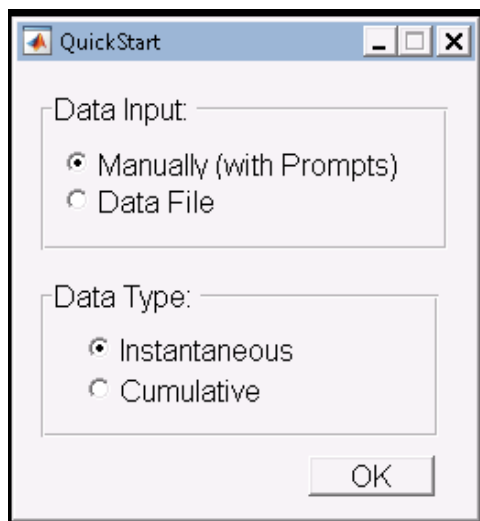


Figure B.1: ‘QuickStart’ Menu

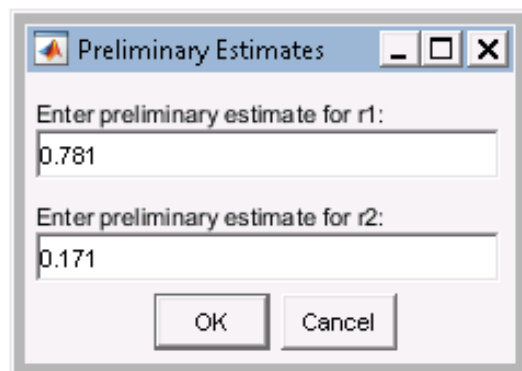


Figure B.2: 'Preliminary Estimates' Prompt

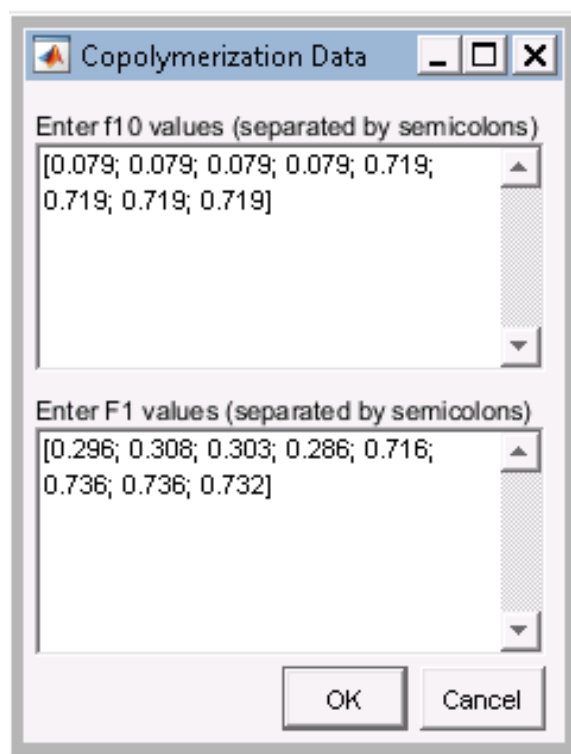


Figure B.3: 'Copolymerization Data' Prompt

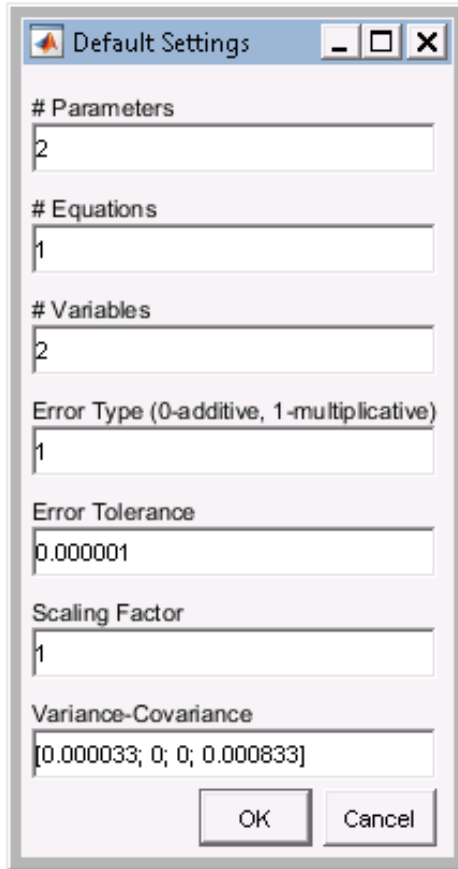


Figure B.4: 'Default Settings' Prompt

An alternative to the step-by-step prompts is to include all the required estimation data in a single “.txt” data file. When a user chooses the data file input option, a pop-up window containing their files appears (that is, any files in the same folder as the ‘QuickStart’ file). Once an appropriate file is selected, the program will access the data and run automatically.

A data file includes all of the same data as the prompts but it can be saved, modified and reused. It can either be created in Notepad or in MATLAB but should have the extension “.txt”. The data file must be prepared prior to running the EVM program, since the program will access the data file ‘behind the scenes’ to obtain the required information. A sample data file (here for the McManus and Penlidis [280] data set) is shown in Figure B.5.

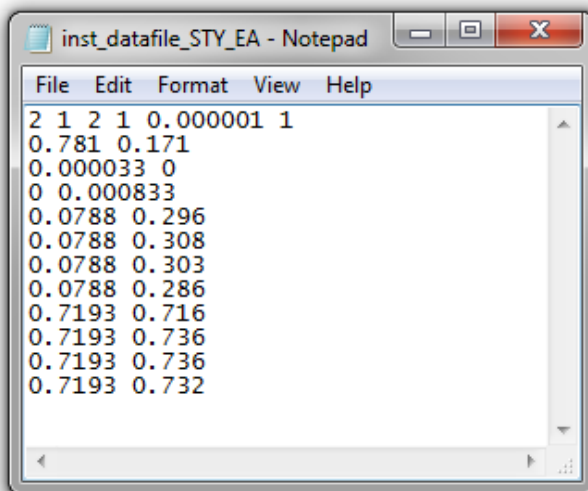


Figure B.5: Sample Data File for Computational Package

In Figure B.5, line 1 provides the ‘Default Settings’ for the program, such as the number of parameters, equations and variables (the reader will notice that these values are the same as in Figure B.4, with slightly different formatting). Line 2 contains preliminary reactivity ratio estimates (recall Figure B.2), while lines 3 and 4 can be combined to form the variance-covariance matrix for the variables. Finally, lines 5 through 12 are the experimental copolymerization data (recall Figure B.3). The first column represents the initial feed composition ($f_{1,0}$) and the second column represents the corresponding measured cumulative copolymer composition (\bar{F}_1).

B.2 Relevant Statistical Principles for the Error-in-Variables Method

Information about relevant statistical principles is presented. This is intended to provide additional insight about ‘behind-the-scenes’ mathematical details. The program user need not have a detailed understanding of the statistical principles used in the error-in-variables-model. However, for the interested reader, some additional information is included in what follows.

B.2.1 Additive and Multiplicative Error

The magnitude (and type) of error associated with the variables can be determined through independent replication. Typically, the relationship between a variable and its error is either additive (absolute) or multiplicative (relative). Multiplicative error is typically assumed because error is presented as a percentage of the measurement (and is, therefore, relative in nature). However, if a user has insight about a system that indicates additive error, it is possible to modify the program accordingly.

The relationships between the ‘true’ value of the variable ($\underline{\xi}_i$) and the measured/recorded values (\underline{x}_i) are shown in Equations B.1 and B.2 for additive and multiplicative error, respectively.

$$x = \xi + k\varepsilon \quad \text{B.1}$$

$$x = \xi(1 + k\varepsilon) \quad \text{B.2}$$

Where k is a constant that reflects the uncertainty of the variables (for example, if 5% error is assumed for the multiplicative case, $k = 0.05$). Error, ε , is a random variable that is typically uniformly distributed between -1 and 1 [281].

When multiplicative error is assumed, it becomes necessary to transform Equation B.2 so that the error term is additive. Taking the natural logarithm of both sides gives Equation B.3. Note that $\ln(1 + k\varepsilon)$ can be replaced by $k\varepsilon$, as long as the magnitude of the error does not exceed 10% ($k \leq 0.10$).

$$\ln(x) = \ln(\xi) + k\varepsilon \quad \text{B.3}$$

Regardless of error structure, the value of k (the degree of uncertainty) manifests itself in the same way in the variance-covariance matrix. This is shown in Equations B.4 through B.7. Equation B.4 gives the variance of x (for the additive case), whereas Equation B.5 gives the variance of $\ln(x)$ (for the multiplicative case).

$$V(x) = V(\xi + k\varepsilon) = k^2V(\varepsilon) \quad \text{B.4}$$

$$V(\ln(x)) = V(\ln(\xi) + k\varepsilon) = k^2V(\varepsilon) \quad \text{B.5}$$

Equations B.6 and B.7 are relevant to both error structures since $V(x) = V(\ln(x))$, as shown above.

$$V(\varepsilon) = E(\varepsilon^2) - [E(\varepsilon)]^2 = \int_{-1}^1 \frac{\varepsilon^2}{2} d\varepsilon = \frac{1}{3} \quad \text{B.6}$$

$$V(x) = V(\ln(x)) = \frac{k^2}{3} \quad \text{B.7}$$

The variance estimate shown in Equation B.7 is applied to different variables, which populate the variance-covariance matrix for the EVM program. The program’s default settings assume 1% error associated with feed composition ($x_1 = f_{1,0}$ and $k_1 = 0.01$) and 5% error associated with cumulative copolymer composition ($x_2 = \bar{F}_i$ and $k_2 = 0.05$). Therefore, the variance-covariance matrix, \underline{V} , for the instantaneous (low conversion) case is shown in Equation B.8.

$$\underline{V} = \begin{bmatrix} V(x_1) & 0 \\ 0 & V(x_2) \end{bmatrix} = \begin{bmatrix} \frac{k_1^2}{3} & 0 \\ 0 & \frac{k_2^2}{3} \end{bmatrix} = \begin{bmatrix} \frac{0.01^2}{3} & 0 \\ 0 & \frac{0.05^2}{3} \end{bmatrix} = \begin{bmatrix} 0.0000\bar{3} & 0 \\ 0 & 0.0008\bar{3} \end{bmatrix} \quad \text{B.8}$$

This can be cross-referenced with the input data shown in Section B.1 (Figure B.4 and Figure B.5).

B.2.2 Calculation of \underline{G} as an EVM Program Output

Only the very basics are presented in what follows. A detailed discussion of the nested-iterative EVM algorithm has been presented by Reilly and Patino-Leal [69] and has more recently been described by Kazemi et al. [54, 58].

Equation B.9 below is the definition of \underline{G} , the second derivative of Φ with respect to the parameters.

$$\underline{G} = E \left[\frac{d^2\Phi}{d\theta_i d\theta_j} \right] = \sum_{i=1}^n r_i \underline{Z}_i' (\underline{B}_i \underline{V} \underline{B}_i')^{-1} \underline{Z}_i \quad \text{B.9}$$

Where r_i is the number of replicates for the i th trial and \underline{V} is the variance-covariance matrix of the variables). \underline{Z}_i is the vector of partial derivatives of the function $\underline{g}(\underline{\xi}_i, \underline{\theta})$ (that is, the model) with respect to the parameters for the m th element (see Equation B.10) and \underline{B}_i is the vector of partial derivatives of the function $\underline{g}(\underline{\xi}_i, \underline{\theta})$ with respect to the variables (Equation B.11).

$$\underline{Z}_i = \left[\frac{\partial \underline{g}(\underline{\xi}_i, \underline{\theta})}{\partial \theta_m} \right] \quad \text{B.10}$$

$$\underline{B}_i = \left[\frac{\partial \underline{g}(\underline{\xi}_i, \underline{\theta})}{\partial (\underline{\xi}_i)} \right] \quad \text{B.11}$$

Appendix C. Relevant Data & Calculations for Case Study #1

C.1 Sample Gravimetry Calculations

These sample calculations are for the high NaCl system described in Section 4.1.4 (specifically, Sample 10 from Run S7). However, the same general principles apply for all terpolymerization analyses described in Chapter 4.

First, the total monomer mass in a given pre-polymerization solution is calculated. In the case of Run S7, both acids are fully dissociated, which means that each mole of AMPS and AAc is actually one mole of NaAMPS and NaAAc (where the Na⁺ ions are introduced during titration with NaOH).

Total m_{monomer} in pre-polymerization solution: C.1

$$\begin{aligned}
 m_{\text{monomer}} &= \left(\sum m_{\text{monomer total from stock solution}} \right) \left(\frac{\text{mL stock solution in pre - polymer solution}}{\text{total mL stock solution}} \right) \\
 &= \left[\left(10.363 \text{ g AMPS} \times \frac{\text{mol AMPS}}{207.24 \text{ g AMPS}} \times \frac{1 \text{ mol NaAMPS}}{1 \text{ mol AMPS}} \times \frac{229.22 \text{ g NaAMPS}}{\text{mol NaAMPS}} \right) \right. \\
 &\quad + 28.439 \text{ g AAm} \\
 &\quad + \left(3.5928 \text{ g AAc} \times \frac{\text{mol AAc}}{72.06 \text{ g AAc}} \times \frac{1 \text{ mol NaAAc}}{1 \text{ mol AAc}} \right. \\
 &\quad \left. \left. \times \frac{94.04 \text{ g NaAAc}}{\text{mol NaAAc}} \right) \text{ in } 250 \text{ mL stock solution} \right] \left(\frac{100 \text{ mL stock solution}}{250 \text{ mL stock solution}} \right)
 \end{aligned}$$

Therefore, in the pre-polymerization solution:

$$m_{\text{monomer}} = 17.8359 \text{ g monomer in } 100 \text{ mL stock solution}$$

$$m_{\text{monomer}} = 17.8359 \text{ g monomer in } 200 \text{ mL pre - polymer solution}$$

With this information, the mass of monomer (represented as NaM) present in each sample flask can be calculated. Generally, since the pre-polymerization solution is an aqueous solution, a solution density of 1 g/ml can be assumed. However, when large amounts of NaCl are used to adjust the ionic strength for a given polymerization, the mass of NaCl must be added to the total ‘recipe’ mass. Not including the NaCl mass would result in the measured monomer mass (that is, the sum of monomer masses from all individual vials) being larger than physically possible given the stock solution calculations.

Specifically for sample S7-10: C.2

$$\begin{aligned}
 &m_{\text{monomer in sample}} \\
 &= \left(\frac{m_{\text{monomer in pre - polymerization solution}}}{\text{mL pre - polymer solution}} \right) \left(\frac{\text{mL pre - polymer solution}}{m_{\text{pre-polymer solution}} + m_{\text{NaCl}}} \right) (m_{\text{recipe in vial}}) \\
 &= \left(\frac{17.8359 \text{ g monomer}}{200 \text{ mL pre - polymer solution}} \right) \left(\frac{200 \text{ mL pre - polymer solution}}{200 \text{ g pre - polymer solution} + 18.7041 \text{ g NaCl}} \right) (22.9319 \text{ g in vial}) \\
 &= 1.8702 \text{ g monomer (or g NaM) in sample S7 - 10.}
 \end{aligned}$$

The sum of monomer masses from all individual vials is 17.1041 g (~96% of calculated mass shown in Equation C.1). However, ignoring the NaCl mass in the above calculation would make the sum of monomer masses from all individual vials equal to 18.7037 g (nearly 1 g more than anticipated given Equation C.1). This confirms the importance of considering NaCl in the monomer mass calculation.

Now that the total monomer mass in each vial is known, the conversion can be calculated using gravimetry. This calculation is the ratio of polymer (sample) mass to monomer mass, and this general formula was used to determine the conversion vs. time results in Figure 4.12. However, as discussed, the sample mass in these (high NaCl) cases should be divided into polymer and NaCl contributions, as shown in Equation C.3.

$$\begin{aligned} \text{Since } \textit{total sample mass} &= \textit{polymer mass} + \textit{NaCl mass} && \text{C.3} \\ \text{and } \textit{NaCl mass} &= \textit{wt\% AAm} \times \frac{MW_{NaCl}}{MW_{AAm}} \end{aligned}$$

$$\text{Specifically for sample S7-10:} \quad \text{C.4}$$

$$\begin{aligned} \textit{polymer mass} &= \frac{\textit{sample mass}}{1 + \textit{wt\% AAm} \times \frac{MW_{NaCl}}{MW_{AAm}}} \\ &= \frac{2.8703 \textit{ g sample}}{1 + \left[\frac{0.8(71.08 \textit{ g/mol})}{0.1 \textit{ mol AMPS}(207.25 \textit{ g/mol}) + 0.8 \textit{ mol AAm}(71.08 \textit{ g/mol}) + 0.1 \textit{ mol AAc}(72.01 \textit{ g/mol})} \right] \left(\frac{58.44 \textit{ g/mol}}{71.08 \textit{ g/mol}} \right)} \\ &= 1.8502 \textit{ g polymer} \end{aligned}$$

$$\text{Therefore:} \quad \text{C.5}$$

$$\begin{aligned} \textit{NaCl mass} &= \textit{total sample mass} - \textit{polymer mass} = 2.8703 \textit{ g} - 1.8502 \textit{ g} \\ &= 1.0201 \textit{ g NaCl} \end{aligned}$$

$$\text{Finally, using gravimetry:} \quad \text{C.6}$$

$$\% \textit{ conversion} = \frac{m_{\textit{polymer}}}{m_{\textit{NaM}}} \times 100 = \frac{1.8502 \textit{ g polymer}}{1.8702 \textit{ g monomer}} \times 100 = 98.93\%$$

As mentioned in the main text (Section 3.3.1), the mass of the sodium ions (attracted to the dissociated acids along the polymer chain) must also be considered in conversion calculations (as per the recommendation of Riahinezhad et al. [84]). The number of moles of each comonomer in the resulting terpolymer was determined using elemental analysis, and sample calculations will be presented in Section C.2. The mass of Na⁺ ions in the system is directly related to the number of moles of AMPS and AAc, as the molar ratio of Na⁺ to both AMPS and AAc is 1:1. Calculations for Na⁺ mass (which is distinct from the NaCl correction shown previously) and corrected conversion are shown below for a representative sample:

Per 100g AMPS/AAm/AAC terpolymer:

$$g \text{ Na}^+ = (0.0763 \text{ mol AMPS} + 0.0520 \text{ mol AAc}) \times \frac{1 \text{ mol Na}}{1 \text{ mol acidic comonomer}} \times \frac{22.989 \text{ g Na}}{\text{mol Na}} = 2.948 \text{ g} \quad \text{C.7}$$

$$\begin{aligned} \text{Corrected Conversion} &= \frac{g \text{ polymer} - (g \text{ polymer})(0.01)(g \text{ Na})}{g \text{ monomer}} \times 100 \quad \text{C.8} \\ &= \frac{1.8502 \text{ g} - (1.8502 \text{ g}) \left(\frac{2.9480 \text{ g}}{100 \text{ g}} \right)}{1.8702 \text{ g}} \times 100 = 96.0\% \end{aligned}$$

C.2 Sample Elemental Analysis Calculations

These sample calculations are also referenced in Section 4.1.4; composition was used as an indicator of residual NaCl in the AAm-rich terpolymer samples. Elemental analysis calculations (and extensions to estimate the elemental contributions for terpolymer samples) were examined for terpolymer ‘recipes’ without NaCl and with NaCl; and the details are shown in this section. These calculations and related principles are applicable to all other terpolymer samples studied herein.

Table C.1: Analysis of Elemental Contributions for S5 (no NaCl added)

| | wt% N | wt% C | wt% H | wt% S | wt% O (polymer) | wt% O (H ₂ O) | wt% Na | Total wt% |
|-------|-------|-------|-------|-------|--------------------|-----------------------------|--------|--------------|
| S5-1 | 4.98 | 36.37 | 5.06 | 3.04 | 27.12 | 7.97 | 14.30 | 98.85 |
| S5-2 | 4.81 | 36.91 | 5.19 | 2.97 | 27.78 | 8.91 | 14.95 | 101.52 |
| S5-3 | 4.44 | 35.96 | 5.11 | 2.99 | 27.36 | 9.26 | 14.94 | 100.06 |
| S5-4 | 4.61 | 36.80 | 4.96 | 2.98 | 27.91 | 7.38 | 15.20 | 99.85 |
| S5-5 | 4.08 | 36.77 | 4.85 | 2.92 | 28.48 | 7.17 | 16.07 | 100.34 |
| S5-6 | 4.93 | 36.75 | 5.13 | 3.16 | 27.53 | 8.21 | 14.60 | 100.31 |
| S5-7 | 4.54 | 36.71 | 4.95 | 3.06 | 27.93 | 7.39 | 15.24 | 99.82 |
| S5-8 | 4.57 | 36.45 | 5.04 | 3.11 | 27.67 | 8.18 | 15.01 | 100.03 |
| S5-9 | 4.72 | 36.27 | 5.10 | 3.09 | 27.33 | 8.61 | 14.66 | 99.77 |
| S5-10 | 4.62 | 36.31 | 5.04 | 3.39 | 27.53 | 7.98 | 14.77 | 99.64 |

Here, wt% of N, C, H and S are as measured by elemental analysis. This provides the data necessary to calculate the mole fraction of AMPS, AAm and AAc in the product terpolymer. A sample calculation is shown below for sample S5-1 in Table C.1. First, the wt% S is used to determine the AMPS content, as S is only present in one comonomer (Equation C.9). Next, the wt% N is used to calculate the AAm content (Equation C.10). Finally, the wt% C can be used to establish how much AAc is present in the sample (Equation C.11).

Per 100g AMPS/AAm/AAC terpolymer:

Since *moles S* = n_{AMPS}

$$n_{AMPS} = \frac{wt\% S}{32.065 \frac{g}{mol}} = \frac{3.04 g}{32.065 \frac{g}{mol}} = 0.0948 mol AMPS \quad C.9$$

Since *moles N* = $n_{AMPS} + n_{AAm}$

$$\begin{aligned} n_{AAm} &= \frac{wt\% N}{14.007 \frac{g}{mol}} - n_{AMPS} = \frac{4.98 g}{14.007 \frac{g}{mol}} - 0.0948 mol AMPS \\ &= 0.2607 mol AAm \end{aligned} \quad C.10$$

Since *moles C* = $7n_{AMPS} + 3n_{AAm} + 3n_{AAC}$

$$\begin{aligned} n_{AAC} &= \frac{\frac{wt\% C}{12.0107 \frac{g}{mol}} - 7n_{AMPS} - 3n_{AAm}}{3} \\ &= \frac{\frac{36.37 g}{12.0107 \frac{g}{mol}} - 7(0.0948 mol AMPS) - 3(0.2607 mol AAm)}{3} \\ &= 0.5275 mol AAC \end{aligned} \quad C.11$$

Now, the mass of additional elements present in the terpolymer sample can be inferred. The only element present in the monomers that has not been measured directly is oxygen. Therefore, stoichiometry can be used to estimate the oxygen content, again using a 100 g polymer basis (Equation C.12).

Since *moles O* = $4n_{AMPS} + n_{AAm} + 2n_{AAC}$

$$\begin{aligned} wt\% O &= (4n_{AMPS} + n_{AAm} + 2n_{AAC}) \times 16 \frac{g}{mol} \\ &= 4(0.0948 mol AMPS) + (0.2607 mol AAm) + 2(0.5275 mol AAC) \\ &\quad \times 16 \frac{g}{mol} = 27.12 \end{aligned} \quad C.12$$

Similarly, the polymer is known to contain small amounts of water. Therefore, oxygen will also be present in the form of H₂O. We can only make a rough approximation here, but it is possible to take advantage of the wt% H measurement from elemental analysis. Subtracting the known wt% H in the polymer (according to stoichiometry) from the measured wt% provides a general idea of how much ‘extra’ H is present in the form of water (Equation C.13). It is also important to note

that the stoichiometric calculations eliminate 1 H⁺ ion for both n_{AMPS} and n_{AAc}, as acid dissociation (and attraction of sodium ions along the polymer chain) is assumed. The incorporation of Na⁺ ions (as described previously by Riahinezhad et al. [84]) is due to titration with NaOH; the wt% Na calculation is shown in Equation C.14.

$$\text{Since moles } H = 12n_{AMPS} + 5n_{AAM} + 3n_{AAc} \quad \text{C.13}$$

$$\begin{aligned} \text{wt\% } O &= \frac{\frac{\text{wt\% } H}{1.008 \frac{g}{mol}} - (12n_{AMPS} + 5n_{AAM} + 3n_{AAc})}{\frac{2 \text{ mol } H}{\text{mol } H_2O} \times \frac{1 \text{ mol } H_2O}{1 \text{ mol } O}} \times 16 \frac{g}{mol} \\ &= \frac{\frac{5.06 \text{ g}}{1.008 \frac{g}{mol}} - (12(0.0948 \text{ mol } AMPS) + 5(0.2607 \text{ mol } AAM) + 3(0.5275 \text{ mol } AAc))}{\frac{2 \text{ mol } H}{\text{mol } H_2O} \times \frac{1 \text{ mol } H_2O}{1 \text{ mol } O}} \\ &\times 16 \frac{g}{mol} = 7.97 \end{aligned}$$

$$\begin{aligned} \text{wt\% } Na &= (n_{AMPS} + n_{AAc}) \times 22.989 \frac{g}{mol} \quad \text{C.14} \\ &= (0.0948 \text{ mol } AMPS + 0.5275 \text{ mol } AAc) \times 22.989 \frac{g}{mol} = 14.30 \end{aligned}$$

As shown in Table C.1, the calculated elemental contribution summed to ~100% for each sample. However, when large quantities of NaCl were included in the terpolymer ‘recipe’, only ~40% to ~60% of the elemental contributions could be identified. This is discussed in more detail in Section 4.1.4.2, and is especially evident in comparing Table C.1 to Table 4.10.

C.3 Molecular Weight Analysis (Supplemental Information)

Molecular weight averages were determined using gel permeation chromatography (as described in Section 3.3.3). A sample chromatogram (and related analysis) is shown herein for a reference copolymer of AAm/AAc (with known properties), which was not used for calibration but was used to confirm the accuracy of the GPC.

Table C.2: Confirmation of GPC Accuracy for Polyelectrolytes using AAm/AAc Reference Copolymer

| | Weight-Average Molecular Weight (Mw) | Number-Average Molecular Weight (Mn) |
|---------------------------------|--------------------------------------|--------------------------------------|
| Expected Values | 520,000 | 150,000 |
| Measured Values | 456,400 | 160,362 |
| Mean | 488,200 | 155,181 |
| Standard Deviation | 44971.99 | 7327.04 |
| Coefficient of Variation | 9.21% | 4.72% |

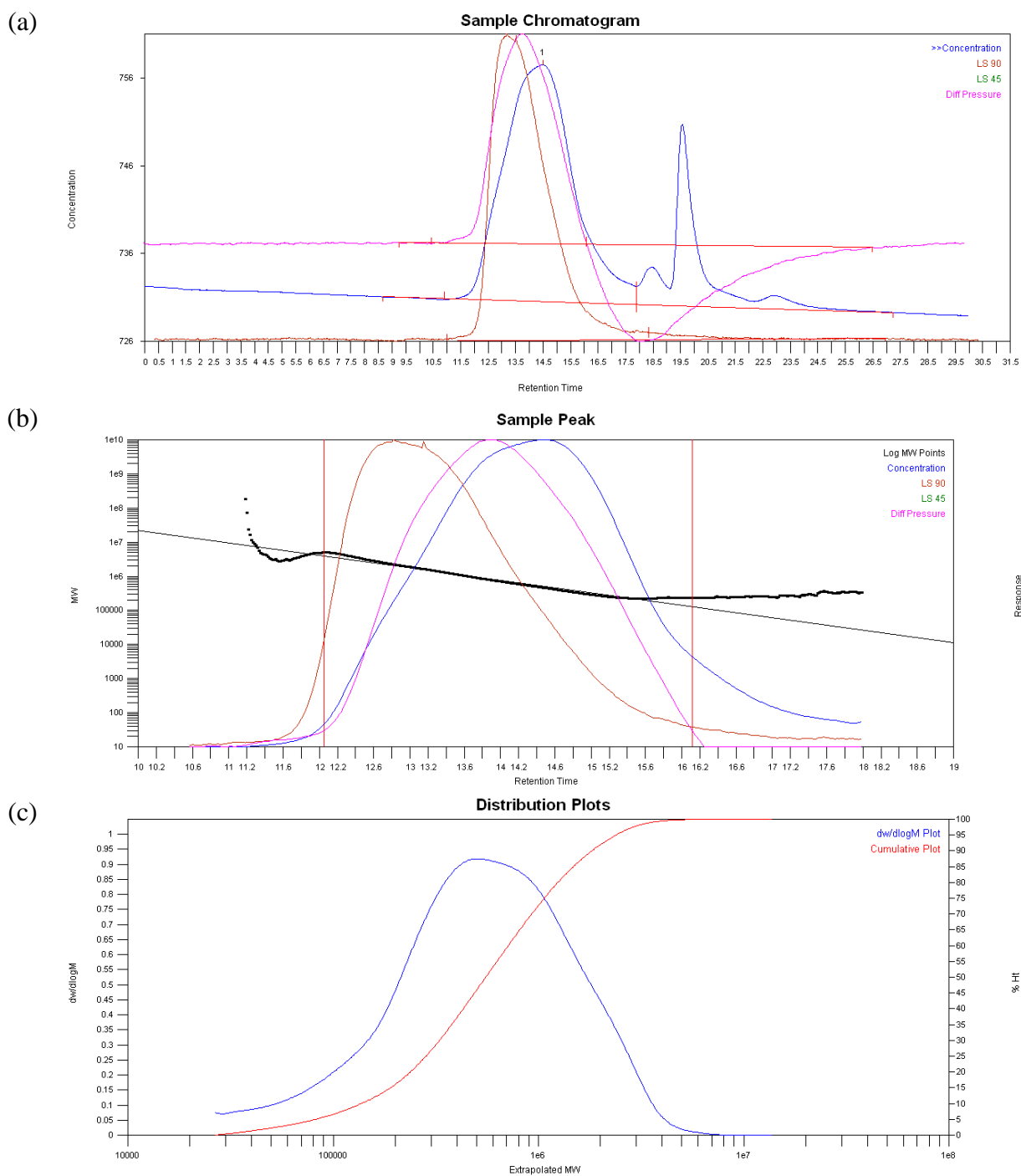


Figure C.1: Sample Analysis from GPC; (a) Sample Chromatograms, (b) Sample Peaks and (c) Distribution Plots for the AAM/AAc Reference Copolymer

As described in Section 4.2.2.3, there were significant discrepancies between the ‘expected’ concentration of the polymer solutions (calculated during sample preparation) and the ‘measured’ concentration (obtained during GPC analysis) for the optimally designed (AAM-rich) terpolymers.

The comparison of ‘expected’ and ‘measured’ concentrations is provided in Table C.3. The repeatability of analysis results was much improved when the GPC-measured concentrations were used, as evidenced by the ANOVA tables in Table C.4 and Table C.5.

Table C.3: Effect of Sample Filtration on Concentration of GPC Samples (see Section 4.2.2.3)

| Sample | Mass Polymer (g) | Mass Buffer (g) | Expected Conc. (mg/ml) | GPC-Measured Conc. (mg/ml) | % Sample Remaining | % Sample Filtered Out |
|---------------|-------------------------|------------------------|-------------------------------|-----------------------------------|---------------------------|------------------------------|
| Opt1-1 | 0.0098 | 10.1086 | 0.9695 | 0.3046 | 31.4 | 68.6 |
| Opt1-1 | GPC Replicate | | 0.9695 | 0.3943 | 40.7 | 59.3 |
| Opt1-2 | 0.0098 | 10.1387 | 0.9666 | 0.3575 | 37.0 | 63.0 |
| Opt1-4 | 0.0108 | 10.1166 | 1.0676 | 0.4060 | 38.0 | 62.0 |
| Opt1-4 | 0.0100 | 10.1391 | 0.9863 | 0.4242 | 43.0 | 57.0 |
| Opt1-7 | 0.0097 | 10.1411 | 0.9565 | 0.4070 | 42.6 | 57.4 |
| Opt1R-1 | 0.0099 | 10.1460 | 0.9758 | 0.3430 | 35.2 | 64.8 |
| Opt1R-1 | 0.0105 | 10.1270 | 1.0368 | 0.2881 | 27.8 | 72.2 |
| Opt1R-1 | GPC Replicate | | 1.0368 | 0.3018 | 29.1 | 70.9 |
| Opt1R-2 | 0.0098 | 10.1286 | 0.9676 | 0.3240 | 33.5 | 66.5 |
| Opt1R-2 | 0.0097 | 10.1332 | 0.9572 | 0.3987 | 41.6 | 58.4 |
| Opt1R-3 | 0.0104 | 10.1435 | 1.0253 | 0.4240 | 41.4 | 58.6 |
| Opt1R-3 | GPC Replicate | | 1.0253 | 0.4480 | 43.7 | 56.3 |
| Opt1R-8 | 0.0108 | 10.1445 | 1.0646 | 0.3780 | 35.5 | 64.5 |
| Opt1R-10 | 0.0109 | 10.1179 | 1.0773 | 0.4230 | 39.3 | 60.7 |
| Opt2-1 | 0.0103 | 10.1324 | 1.0165 | 0.2079 | 20.4 | 79.6 |
| Opt2-1 | GPC Replicate | | 1.0165 | 0.2578 | 25.4 | 74.6 |
| Opt2-2 | 0.0103 | 10.1332 | 1.0165 | 0.2805 | 27.6 | 72.4 |
| Opt2-4 | 0.0107 | 10.1484 | 1.0544 | 0.4370 | 41.4 | 58.6 |
| Opt2-4 | 0.0100 | 10.1225 | 0.9879 | 0.4216 | 42.7 | 57.3 |
| Opt2-4 | GPC Replicate | | 0.9879 | 0.3530 | 35.7 | 64.3 |
| Opt2-10 | 0.0094 | 10.1184 | 0.9290 | 0.4430 | 47.7 | 52.3 |
| Opt2R-1 | 0.0105 | 10.1300 | 1.0365 | 0.3660 | 35.3 | 64.7 |
| Opt2R-2 | 0.0099 | 10.1197 | 0.9783 | 0.3610 | 36.9 | 63.1 |
| Opt2R-5 | 0.0099 | 10.1198 | 0.9783 | 0.4150 | 42.4 | 57.6 |
| Opt2R-9 | 0.0104 | 10.1291 | 1.0267 | 0.3570 | 34.8 | 65.2 |
| Opt2R-9 | GPC Replicate | | 1.0267 | 0.3460 | 33.7 | 66.3 |
| Opt2R-10 | 0.0092 | 10.1400 | 0.9073 | 0.3690 | 40.7 | 59.3 |
| Opt2RB-1 | 0.0101 | 10.1191 | 0.9981 | 0.3288 | 32.9 | 67.1 |
| Opt2RB-1 | GPC Replicate | | 0.9981 | 0.2507 | 25.1 | 74.9 |
| Opt2RB-2 | 0.0097 | 10.1270 | 0.9578 | 0.2979 | 31.1 | 68.9 |
| Opt2RB-6 | 0.0111 | 10.1705 | 1.0914 | 0.3670 | 33.6 | 66.4 |

Table C.4: ANOVA Table for Comparisons between Opt1 Samples (see Section 4.2.2.3)

| | | | | | |
|---|--|-----------|------------|----------|---------------|
| Null: | difference in Mp between runs = 0 | | | | |
| Alternate: | difference in Mp between runs > 0 | | | | |
| Source | df | SS | MSE | F | f_crit |
| Polymerization | 1 | 3.67E+08 | 3.67E+08 | 0.73 | 18.5 |
| Samples | 2 | 1.00E+09 | 5.02E+08 | 0.78 | 19.0 |
| GPC | 2 | 1.29E+09 | 6.46E+08 | | |
| Total | 5 | 2.66E+09 | | | |
| **Note that since this is not a complete hierarchical study, some adjustments were made to the ANOVA calculations. In particular, in considering the number of replicates at the 'GPC' (characterization) stage, $T = 1.5$, since $df_{GPC} = 2 = P \cdot S \cdot (T-1)$. | | | | | |

Table C.5: ANOVA Table for Comparisons between Opt2 Samples (see Section 4.2.2.3)

| | | | | | |
|--|--|-----------|------------|----------|---------------|
| Null: | difference in Mp between runs = 0 | | | | |
| Alternate: | difference in Mp between runs > 0 | | | | |
| Source | df | SS | MSE | F | f_crit |
| Polymerization | 1 | 3.27E+08 | 3.27E+08 | 0.43 | 18.5 |
| Samples | 2 | 1.54E+09 | 7.68E+08 | 0.19 | 19.00 |
| GPC | 2 | 8.15E+09 | 4.07E+09 | | |
| Total | 5 | 1.00E+10 | | | |
| **Again, this is not a complete hierarchical study. For the 'GPC' (characterization) stage, $T = 1.5$, since $df_{GPC} = 2 = P \cdot S \cdot (T-1)$. | | | | | |

The final portion of 'supplemental information' provided herein for molecular weight analysis is a series of relationships between GPC measurements (Mp, Mw and bulk IV) for the two optimal terpolymers and the reference material. These further confirm that the newly synthesized materials exhibit similar properties to the reference material.

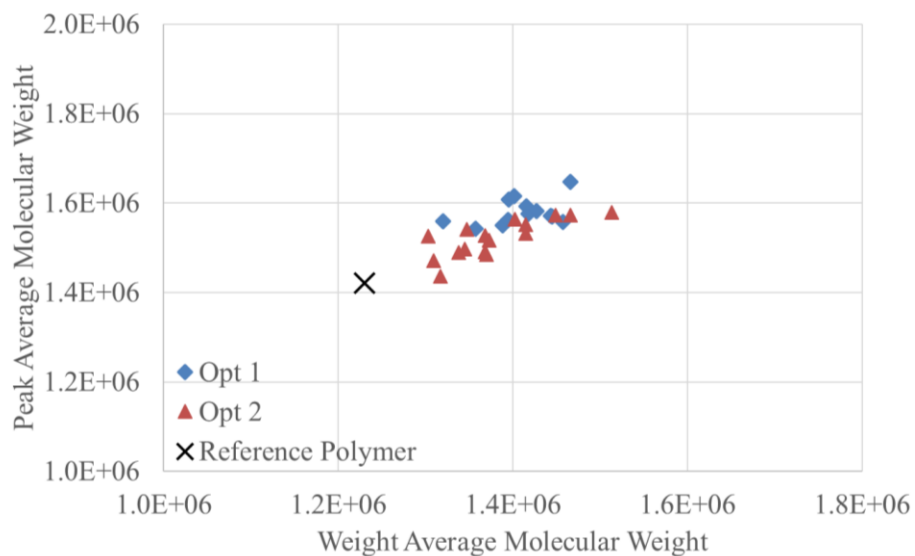


Figure C.2: Peak Average Molecular Weight and Weight Average Molecular Weight for Optimal Terpolymer Samples (compared to Reference Polymer Alcoflood 955)

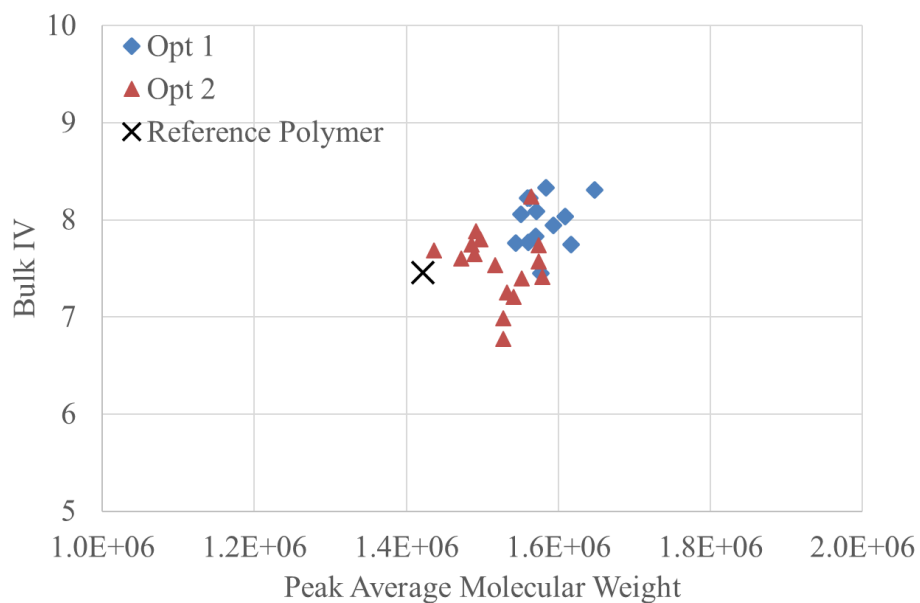


Figure C.3: Bulk Intrinsic Viscosity (IV) and Peak Average Molecular Weight for Optimal Terpolymer Samples (compared to Reference Polymer Alcoflood 955)

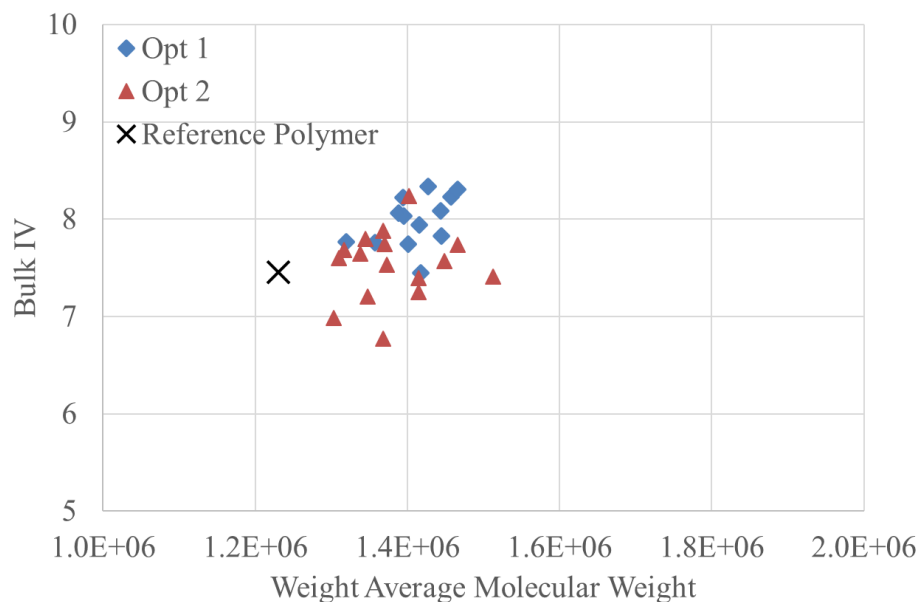


Figure C.4: Bulk Intrinsic Viscosity (IV) and Weight Average Molecular Weight for Optimal Terpolymer Samples (compared to Reference Polymer Alcoflood 955)

C.4 Thermal Gravimetric Analysis (Supplemental Information)

Thermal gravimetric analysis was conducted for the optimally designed terpolymers, the reference polymer (Alcoflood 955) and a representative designed copolymer of AAm/AAc [32]. The experimental methodology was provided in Section 3.3.5 and the most important results were presented in Section 4.2.2.5. Replicate analyses are provided herein for the two terpolymers, and the derivatives of the weight % measurements are presented for all samples.

For terpolymer #1, the characterization replicate shown in Figure C.5 shows good agreement initially, but becomes unreasonable at about 350°C. This was a result of extreme expansion that occurred during heating (20 mg sample shown in Figure C.6), which affected subsequent mass measurements. Similar behaviour was observed for terpolymer #2 and for the reference material (when 20 mg samples were used), but results are not shown herein. Therefore, to obtain reliable results, less than 5 mg of polymeric material was used beyond preliminary analyses.

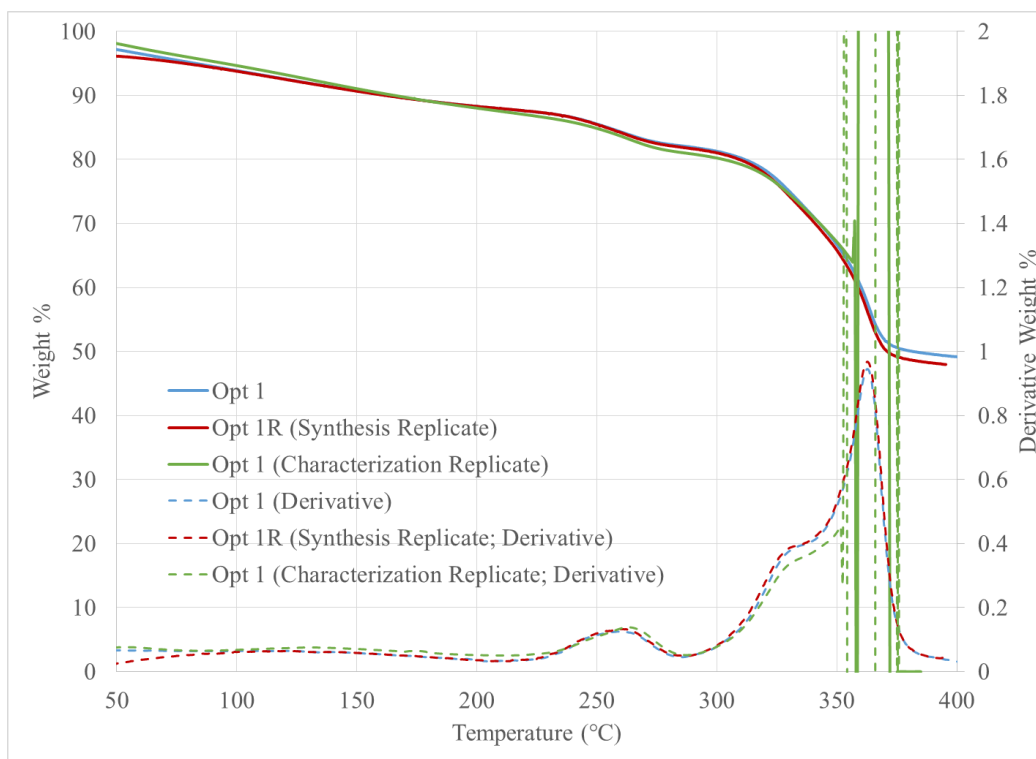


Figure C.5: Synthesis and Characterization Replicates of TGA for Terpolymer #1



Figure C.6: Expansion of Terpolymer #1 Sample during TGA

Good repeatability was also observed for terpolymer #2 (comparison of synthesis replicates). The weight % measurement and related derivatives are provided in Figure C.7. Similar results (with earlier/lower temperature degradation) were observed for the reference material (Alcoflood 955) and a designed AAm/AAc copolymer [32], and are shown in Figure C.8 and Figure C.9, respectively.

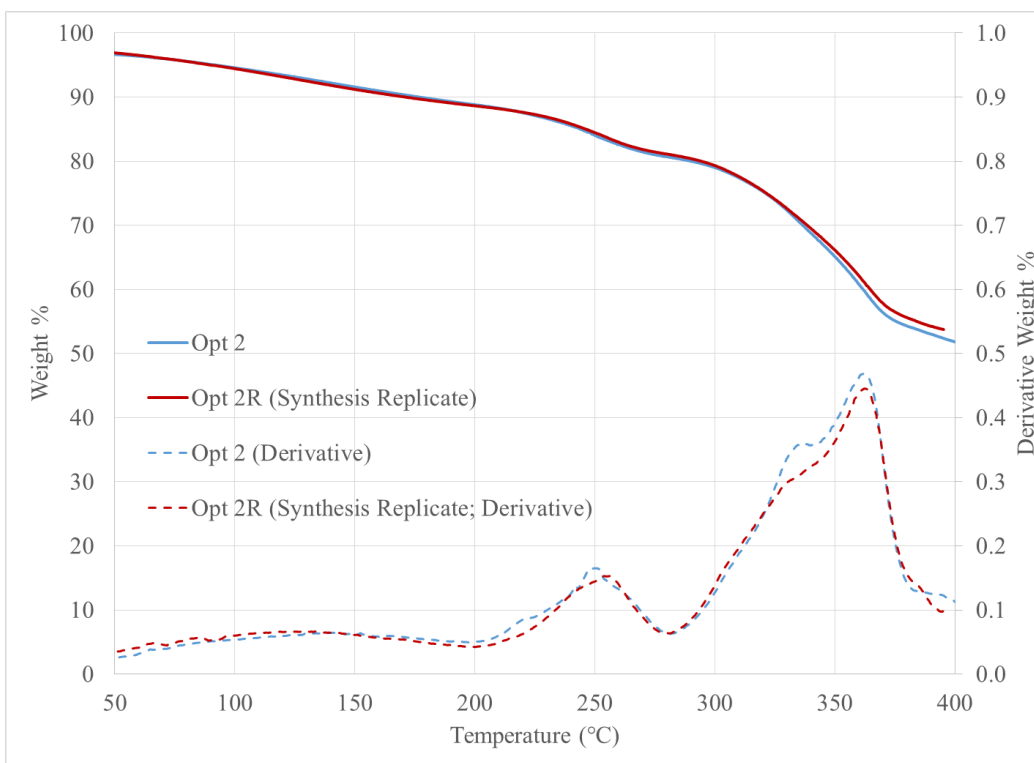


Figure C.7: Synthesis Replicates Analyzed with TGA for Terpolymer #2

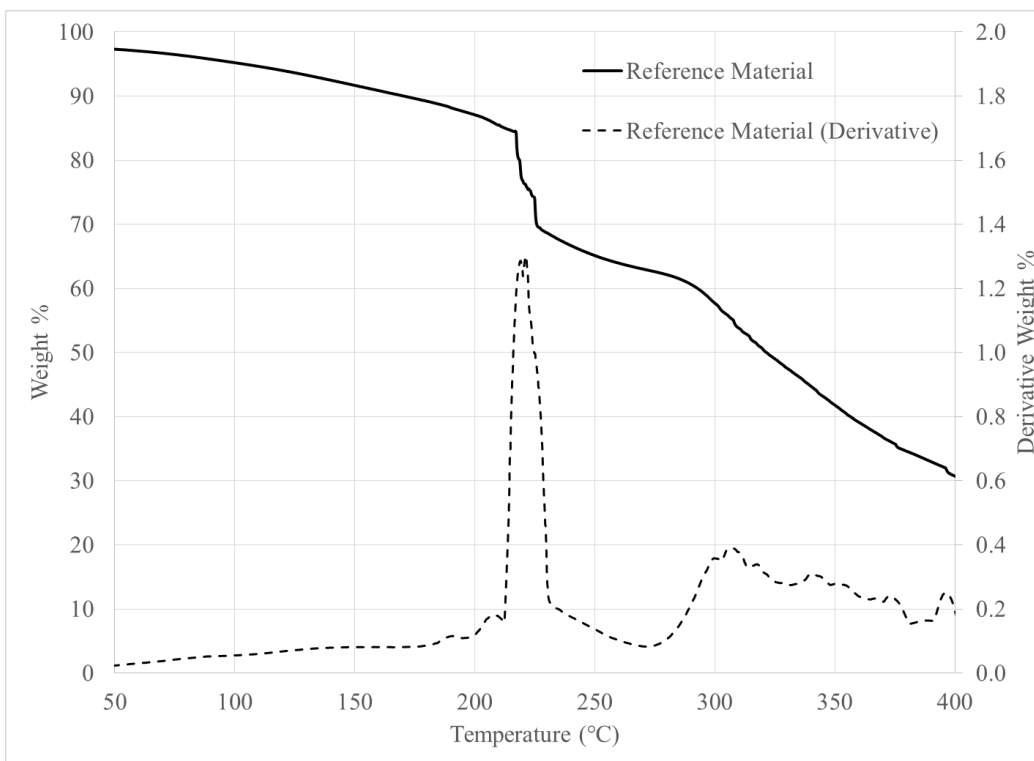


Figure C.8: Thermal Gravimetric Analysis Results for Reference Material (Alcoflood 955)

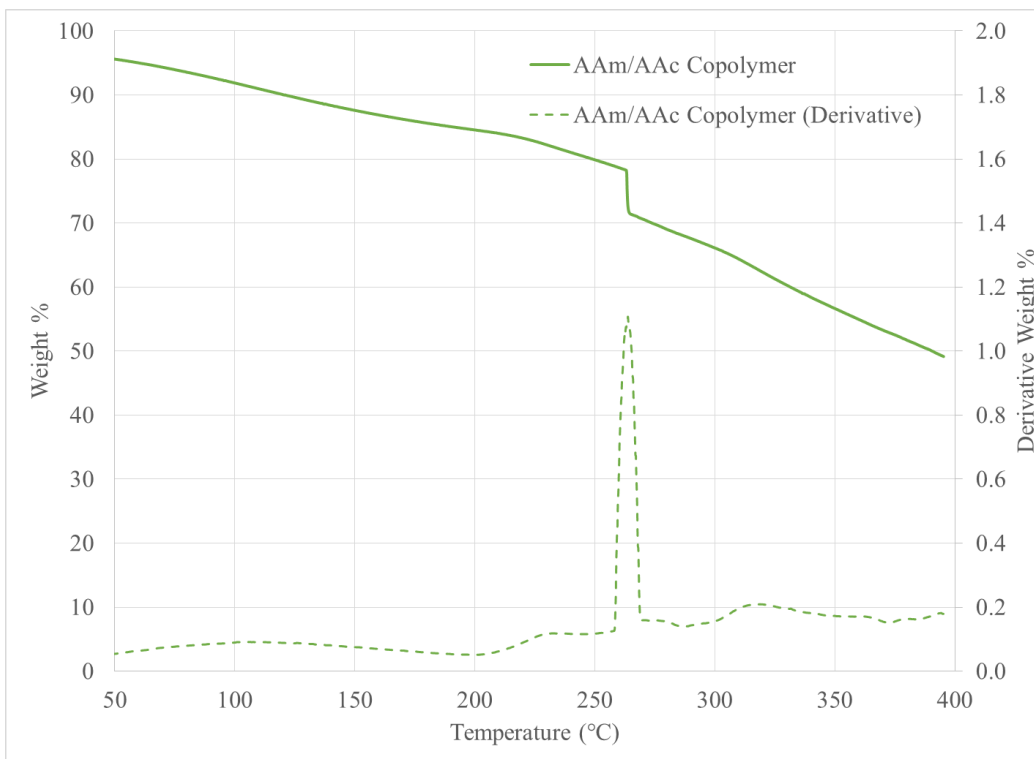


Figure C.9: Thermal Gravimetric Analysis Results for a Designed AAm/AAc Copolymer

C.5 Additional Rheology Data

Rheological properties were measured as described in Section 3.4.1 and as reported in Section 4.2.3.1. The claim was made in Section 4.2.3.1 that any % strain within the linear viscoelastic region will give similar frequency sweep results; this was confirmed by analyzing the reference material at both 1% strain and 10% strain. Results are shown in Figure C.10.

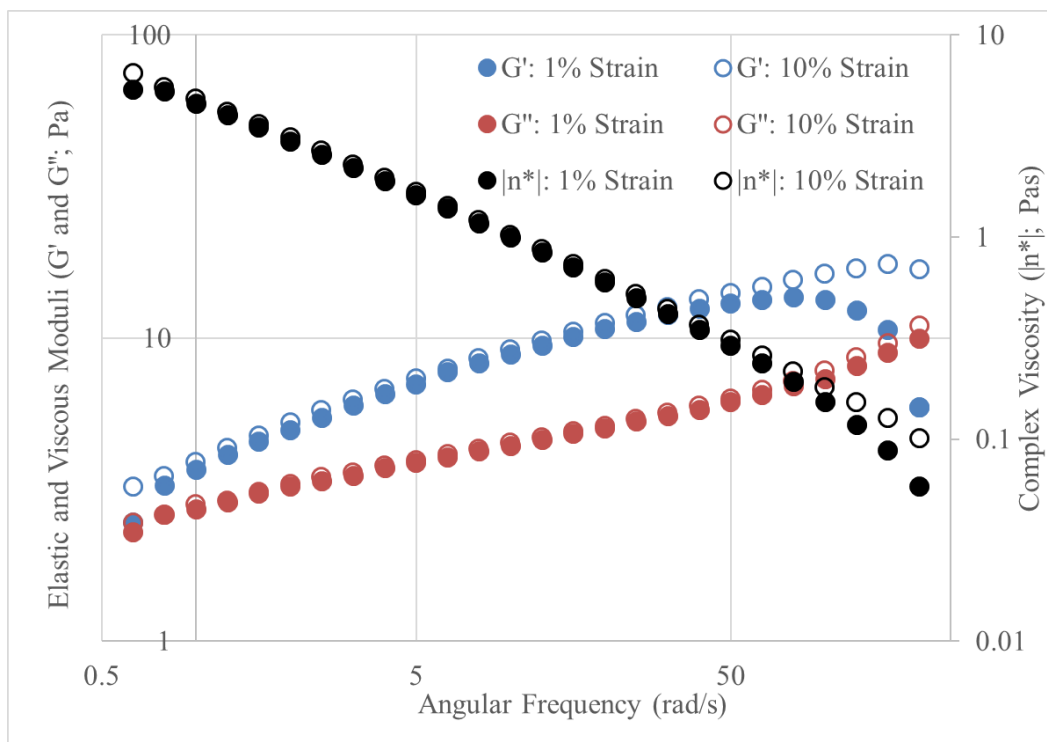


Figure C.10: Comparison of Frequency Sweep Results at 1% Strain and 10% Strain for Reference Polymer (solution concentration of 0.01 g/mL in water)

A summary of shear viscosities at specific frequencies was provided in the main text (recall Table 4.18). However, for brevity, only average values were given for each unique terpolymer formulation. An extended version of the table (with individual trials) is shown herein (see Table C.6).

Table C.6: Summary of Shear Viscosities for Terpolymer Solutions (extended version of Table 4.18)

| In WATER | Shear Viscosity (Pa s) | | |
|---|-----------------------------------|-----------------------------------|-----------------------------------|
| | $\dot{\gamma} = 1 \text{ s}^{-1}$ | $\dot{\gamma} = 5 \text{ s}^{-1}$ | $\dot{\gamma} = 7 \text{ s}^{-1}$ |
| Terpolymer #1 | 11.11 | 3.41 | 2.63 |
| Terpolymer #1 (Rheology Replicate) | 10.68 | 3.60 | 2.78 |
| Terpolymer #1R (Synthesis Replicate) | 8.50 | 2.65 | 2.07 |
| Terpolymer #1 Average | 10.10 | 3.22 | 2.49 |
| Terpolymer #2 | 7.66 | 2.38 | 1.86 |
| Terpolymer #2R (Synthesis Replicate) | 8.57 | 2.66 | 2.09 |
| Terpolymer #2 Average | 8.12 | 2.52 | 1.98 |
| Alcoflood (for reference) | 5.84 | 2.04 | 1.61 |
| In BUFFER | Shear Viscosity (Pa s) | | |
| | $\dot{\gamma} = 1 \text{ s}^{-1}$ | $\dot{\gamma} = 5 \text{ s}^{-1}$ | $\dot{\gamma} = 7 \text{ s}^{-1}$ |
| Terpolymer #1 | 2.82 | 1.09 | 0.87 |
| Terpolymer #1 (Rheology Replicate) | 2.89 | 1.08 | 0.88 |
| Terpolymer #1 (Synthesis Replicate) | 2.67 | 1.12 | 0.91 |
| Terpolymer #1 Average | 2.79 | 1.10 | 0.89 |
| Terpolymer #2 | 2.28 | 0.86 | 0.69 |
| Terpolymer #2R (Synthesis Replicate) | 2.54 | 0.99 | 0.79 |
| Terpolymer #2 Average | 2.41 | 0.93 | 0.74 |
| Alcoflood (for reference) | 3.47 | 1.33 | 1.08 |
| AAm/AAc copolymer with best EOR performance (as reported in [115, 117]) | 3.41 | -- | 0.89 |

C.6 Sand-pack Flooding Experimental Details

Sand-pack flooding experiments were conducted to characterize the polymeric materials in terms of polymer flow performance and oil recovery efficiency. The experimental procedures were described in Section 3.4.2, and results and discussion were presented in Sections 4.2.3.2 and 4.2.3.3. Additional details regarding the experimental plan and the sand-pack set-up are provided herein (see Table C.7 and Table C.8).

The dead volumes used for these calculations varied from one step to the next, since it depends on which flow path is being used for a given experimental step. For reference, the dead volumes (and which stage they are related to) are shown in Table C.9.

Table C.7: Experimental Plan for Phase I of EOR Study

| | Total Volume to Inject (ml) | Injection Time (min) | Injection Time (hr) |
|---|------------------------------------|-----------------------------|----------------------------|
| 1) Prepare the sand-pack | | | |
| 2) Determine pore volume and permeability | | | |
| 3) Brine injection #1. Injection of 1 PV + DV of brine (Flow rate = 0.18103 ml/min) | 56 | 309.34 | 5.16 |
| 4) Polymer injection. Injection of 2 PV + DV of 1 wt% polymer solution (Flow rate = 0.18103 ml/min) | 84 | 464.01 | 7.73 |
| 5) Brine injection #2. Injection of 4 PV + DV of brine (Flow rate = 0.18103 ml/min) | 140 | 773.35 | 12.89 |

**Total volumes to inject were based on approximate values of PV and DV; both were assumed to be 28 mL for preliminary calculations.

Table C.8: Experimental Plan for Phase II of EOR Study

| | Total Volume to Inject (ml) | Injection Time (min) | Injection Time (hr) |
|---|------------------------------------|-----------------------------|----------------------------|
| 1) Prepare the sand-pack | | | |
| 2) Determine pore volume and permeability | | | |
| 3) Heavy oil injection. Injection of 2 PV + DV of heavy oil. (Flow rate = 0.18103 ml/min) | 81.05 | 447.70 | 7.46 |
| 4) Brine injection #1. Injection of 4 PV + DV of brine (Flow rate = 0.18103 ml/min) | 135.56 | 748.82 | 12.48 |
| 5) Polymer injection. Injection of 1 PV + DV of 1 wt% polymer solution (Flow rate = 0.18103 ml/min) | 53.70 | 296.62 | 4.94 |
| 6) Brine injection #2. Injection of 2 PV + DV of brine (Flow rate = 0.18103 ml/min) | 79.56 | 439.48 | 7.32 |

**Total volumes to inject were based on approximate values of PV which was assumed to be 28 mL for preliminary calculations.

Table C.9: Dead Volume Values for Phase II of EOR Study

| Material | Relevant Injection Steps (refer to Table C.8) | Dead Volume (ml) |
|--------------------|--|-------------------------|
| Heavy Oil Metal | Step 3 | 25.05 |
| Brine Metal | Step 4 & Step 6 | 23.56 |
| Polymer Plexiglass | Step 5 | 25.70 |

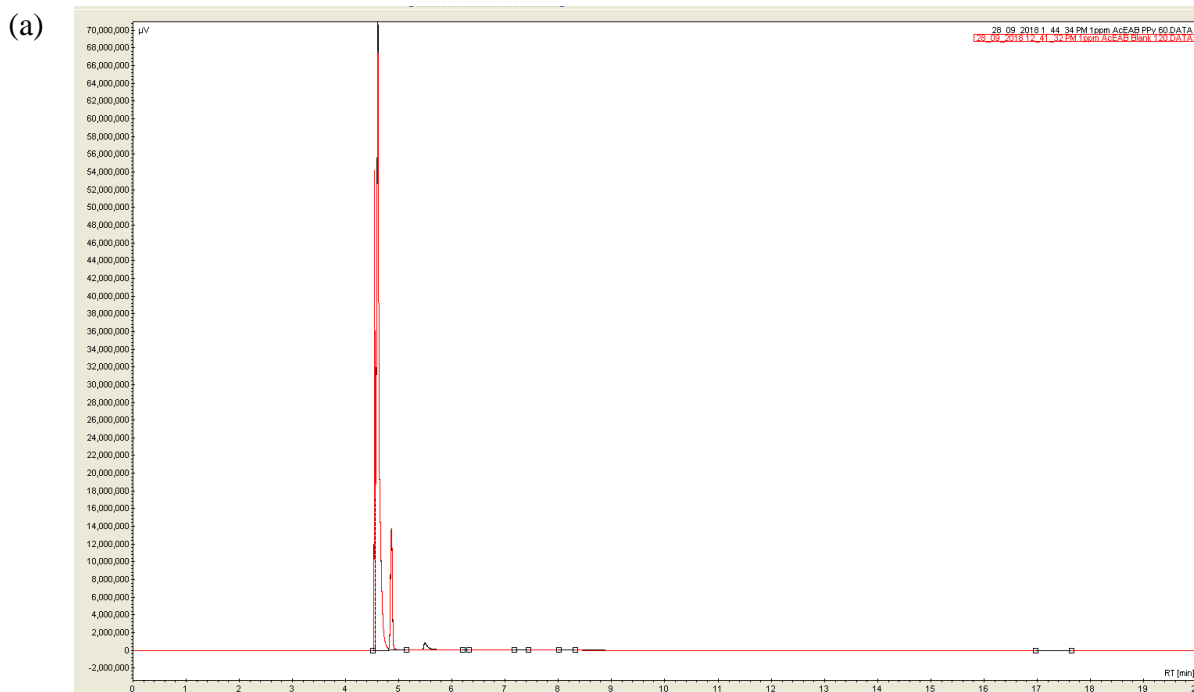
Appendix D. Relevant Data & Calculations for Case Study #2

D.1 Sample Gas Chromatography Analysis

Most experimental data for Case Study #2 were obtained using a carefully designed experimental set-up and a highly specialized gas chromatograph; the details have been presented in Section 7.4.2. In this appendix section, more details about the data acquisition (and some representative data) are presented.

The specialized GC allows for the detection of low concentrations of gas analytes, and can distinguish between chemically similar gases. Typical chromatograms are shown in Figure D.1 for a 4-gas mixture (~1 ppm of each analyte, as described in Section 8.1.2.1). Because such low concentrations are being analyzed, the peaks are not easily identified on the full scale (helium and nitrogen peaks dominate below 5 minutes). Therefore, Figure D.1a shows the full chromatograms (shown here for ~ 1ppm acetaldehyde, ethanol, acetone and benzene), while Figure D.1b through Figure D.1e narrow in on the individual gases, which are identified based on their pre-established retention time. In each case, the red curve represents the ‘blank’ system (no sensing material present) and the black curve is the response when polypyrrole is present in the testing system.

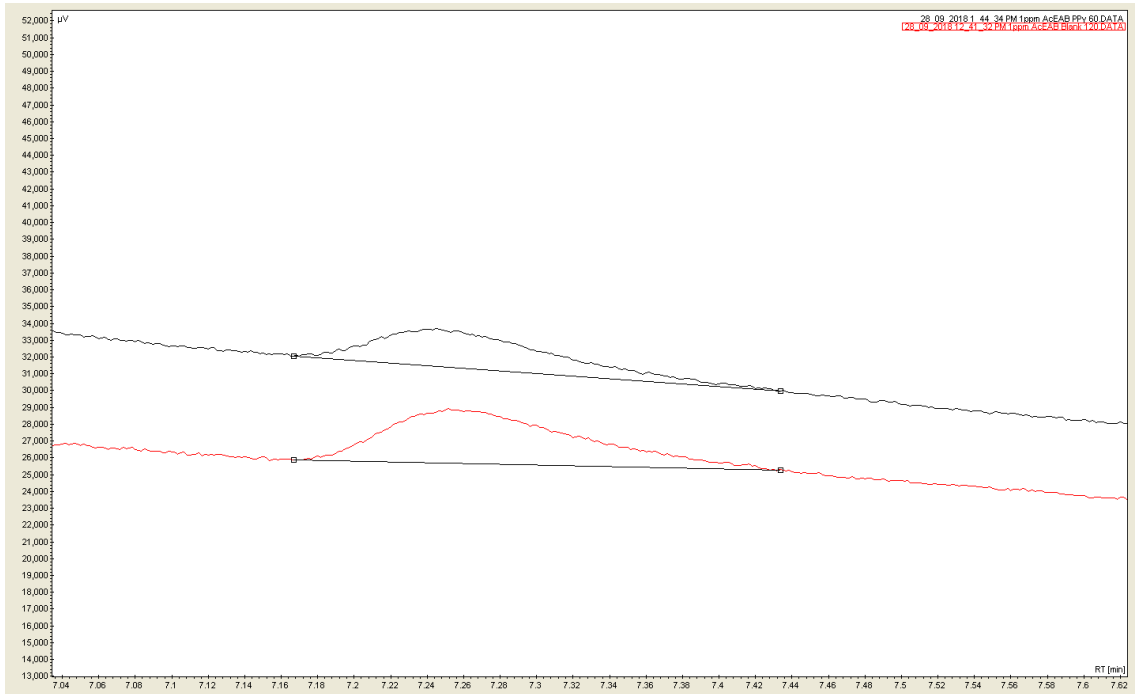
The retention times for the analytes studied (and other components used in related studies) are shown in Table D.1; acetaldehyde, ethanol and acetone all elute before 10 minutes, but benzene (a larger molecule) is retained until almost 18 minutes.



(b)



(c)



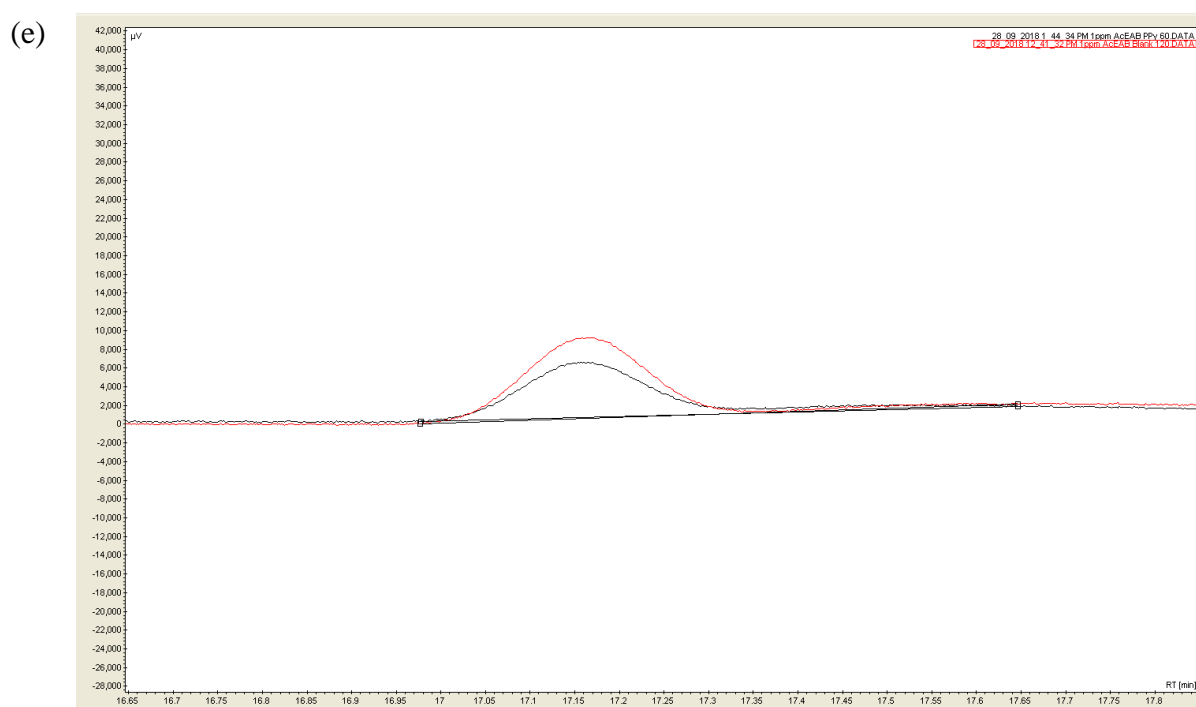
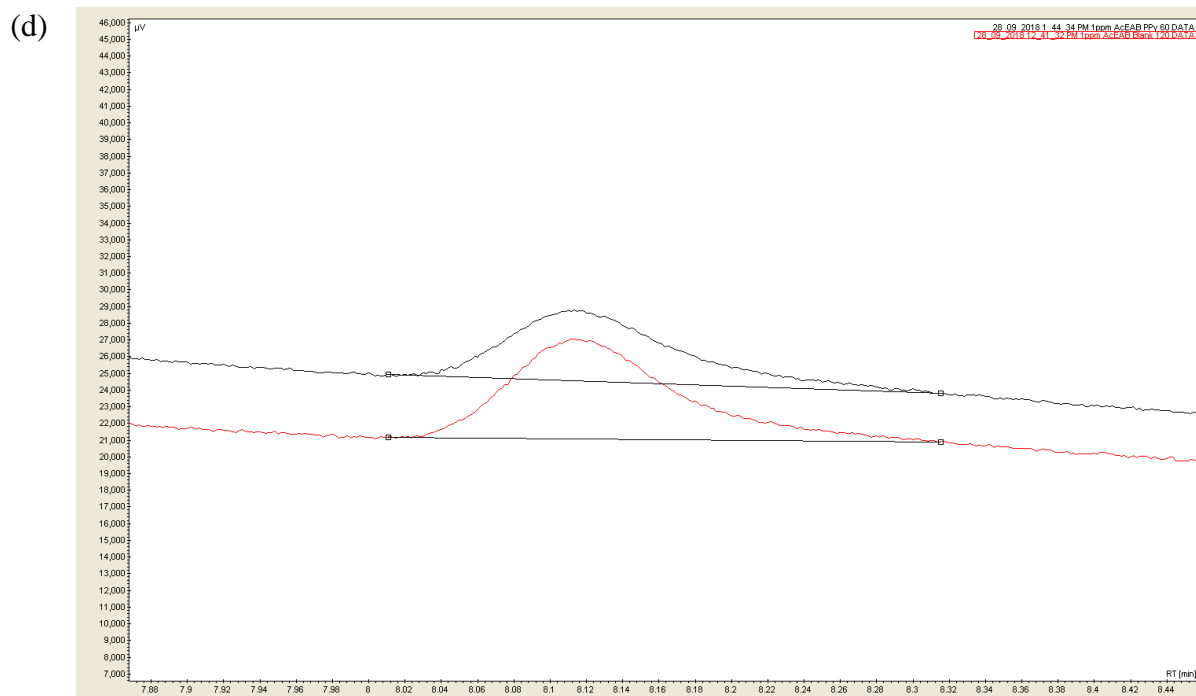


Figure D.1: Sample Chromatograms (red = no sensing material; black = PPy) from GC for ~1 ppm Mixture of Acetaldehyde, Ethanol, Acetone and Benzene; (a) Full Chromatogram, (b) Acetaldehyde Response, (c) Ethanol Response, (d) Acetone Response and (e) Benzene Response

Table D.1: GC Retention Times for Molecules of Interest

| Peak Name | Retention Time (Minutes) |
|--------------|--------------------------|
| Helium | 4.54 |
| Nitrogen | 4.61 |
| Formaldehyde | 5.34 |
| Water | 5.54 |
| Methanol | 6.14 |
| Acetaldehyde | 6.24 |
| Ethanol | 7.20 |
| Acetone | 8.11 |
| Benzene | 17.17 |

As described in Section 7.4.2, the analysis of results involves comparing the concentration of each analyte before and after exposure to the sensing material of interest. Using the data of Figure D.1 as an example, the concentration of each analyte is measured (using the area under the curve and pre-established correlations) for the ‘blank’ run and after PPy has been introduced in the system. The GC software outputs are provided in Figure D.2 for (a) the ‘blank’ run and (b) the PPy-exposure run. Note that helium and nitrogen concentrations are reported as 0.00 ppm because the machine has not been calibrated for those gases.

(a)

| # | Name | Time [Min] | Quantity [ppm] | Height [μ V] | Area [μ V.Min] |
|-------|--------------|------------|----------------|-------------------|---------------------|
| 1 | Helium | 4.54 | 0.00 | 54196127.8 | 781356.8 |
| 2 | Nitrogen | 4.61 | 0.00 | 67562180.6 | 3907832.0 |
| 4 | Acetaldehyde | 6.26 | 0.81 | 7311.0 | 415.8 |
| 7 | Ethanol | 7.26 | 0.86 | 3164.5 | 388.6 |
| 5 | Acetone | 8.12 | 0.86 | 5938.3 | 642.3 |
| 6 | Benzene | 17.16 | 0.85 | 8518.8 | 1428.7 |
| Total | | | 3.38 | 135462068.6 | 5280753.4 |

(b)

| # | Name | Time [Min] | Quantity [ppm] | Height [μ V] | Area [μ V.Min] |
|-------|--------------|------------|----------------|-------------------|---------------------|
| 1 | Helium | 4.54 | 0.00 | 53852753.7 | 790739.6 |
| 2 | Nitrogen | 4.61 | 0.00 | 70984274.6 | 4002538.3 |
| 4 | Acetaldehyde | 6.25 | 0.58 | 5209.2 | 298.9 |
| 5 | Ethanol | 7.25 | 0.57 | 2211.8 | 257.4 |
| 6 | Acetone | 8.12 | 0.62 | 4176.9 | 461.3 |
| 7 | Benzene | 17.16 | 0.63 | 5859.9 | 1063.6 |
| Total | | | 2.40 | 138589628.3 | 5386961.0 |

Figure D.2: Sample GC Results for ~1 ppm Mixture of Acetaldehyde, Ethanol, Acetone and Benzene; (a) Blank System and (b) with Polypyrrole

Given these results, the concentration of each analyte sorbed can easily be calculated by difference. For example, for acetaldehyde:

$$\begin{aligned}
 [\text{Acetaldehyde Sorbed}] &= [\text{Original Acetaldehyde}] - [\text{Residual Acetaldehyde}] && \text{D.1} \\
 &= 0.81 \text{ ppm} - 0.58 \text{ ppm} \\
 &= 0.23 \text{ ppm}
 \end{aligned}$$

Similar calculations can be performed for the other analytes present.

D.2 Experimental Data from Sensitivity and Selectivity Studies

In Chapter 8, the experimental data is generally presented in summary figures; the full experimental data set is shown herein. As mentioned in Section 0, different source tanks were used for acetone throughout the sensitivity study, which resulted in slight variations in the initial acetone concentration (measured concentrations ranged from 4.64 ppm to 5.98 ppm). Therefore, to account for the tank variation, acetone sorption is normalized and reported as percent sorption ($= [\text{acetone sorbed}]/[\text{initial concentration}] \times 100$). All sensitivity data (for both screening experiments and customization experiments) are shown first (Table D.2 through Table D.5), followed by selectivity data (Table D.6 to Table D.10).

Table D.2: Experimental Acetone Sorption Data for PANI-based Polymeric Materials (formulations #1 through #10; supplemental to Figure 8.5)

| Sample | Trial 1A | Trial 1B | Trial 2A | Trial 2B | Average | Coefficient of Variation |
|---------------------------|----------|----------|----------|----------|---------|--------------------------|
| Pure PANI | 11.83% | 12.17% | 11.06% | 11.06% | 11.53% | 4.85% |
| PANI 5% SnO ₂ | 8.42% | 9.11% | 8.84% | 8.62% | 8.75% | 3.37% |
| PANI 10% SnO ₂ | 10.86% | 10.86% | 10.04% | 9.84% | 10.40% | 5.18% |
| PANI 20% SnO ₂ | 7.85% | 7.68% | 8.19% | 8.19% | 7.98% | 3.20% |
| PANI 5% WO ₃ | 10.86% | 10.34% | 9.32% | 9.53% | 10.02% | 7.15% |
| PANI 10% WO ₃ | 11.09% | 11.27% | 9.85% | 9.85% | 10.51% | 7.33% |
| PANI 20% WO ₃ | 9.91% | 10.09% | 9.61% | 9.41% | 9.75% | 3.11% |
| PANI 5% ZnO | 8.52% | 8.35% | 7.83% | 8.00% | 8.17% | 3.87% |
| PANI 10% ZnO | 8.76% | 8.76% | 9.18% | 8.51% | 8.81% | 3.15% |
| PANI 20% ZnO | 12.71% | 12.54% | 12.50% | 12.16% | 12.48% | 1.85% |

Table D.3: Experimental Acetone Sorption Data for PPy-based Polymeric Materials (formulations #11 through #20; supplemental to Figure 8.7)

| Sample | Trial 1A | Trial 1B | Trial 2A | Trial 2B | Average | Coefficient of Variation |
|--------------------------|----------|----------|----------|----------|---------|--------------------------|
| Pure PPy | 32.53% | 32.34% | 30.74% | 30.74% | 31.59% | 3.11% |
| PPy 5% SnO ₂ | 23.97% | 23.97% | 24.60% | 24.20% | 24.18% | 1.23% |
| PPy 10% SnO ₂ | 26.33% | 26.13% | 31.00% | 30.80% | 28.56% | 9.45% |
| PPy 20% SnO ₂ | 16.96% | 16.77% | 22.36% | 22.16% | 19.56% | 15.93% |
| PPy 5% WO ₃ | 25.74% | 25.74% | 24.61% | 24.02% | 25.02% | 3.43% |
| PPy 10% WO ₃ | 18.93% | 19.33% | 23.15% | 23.15% | 21.14% | 11.01% |
| PPy 20% WO ₃ | 25.15% | 24.36% | 26.95% | 28.14% | 26.15% | 6.56% |
| PPy 5% ZnO | 19.76% | 20.55% | 24.55% | 24.55% | 22.35% | 11.44% |
| PPy 10% ZnO | 25.40% | 24.80% | 22.55% | 23.15% | 23.98% | 5.60% |
| PPy 20% ZnO | 21.22% | 21.61% | 23.03% | 22.64% | 22.12% | 3.85% |

Table D.4: Experimental Acetone Sorption Data for PMMA-based Polymeric Materials
(formulations #21 through #30; supplemental to Figure 8.9)

| Sample | Trial 1A | Trial 1B | Trial 2A | Trial 2B | Average |
|---------------------------|----------|----------|----------|----------|---------|
| Pure PMMA | 1.81% | 2.01% | 0.00% | 0.00% | 0.96% |
| PMMA 5% SnO ₂ | 0.00% | 1.00% | 0.00% | 0.00% | 0.25% |
| PMMA 10% SnO ₂ | 0.00% | 0.20% | 0.00% | 0.00% | 0.05% |
| PMMA 20% SnO ₂ | 0.00% | 0.00% | 0.00% | 0.00% | 0.00% |
| PMMA 5% WO ₃ | 0.00% | 0.00% | 0.00% | 0.00% | 0.00% |
| PMMA 10% WO ₃ | 0.00% | 0.20% | 0.00% | 0.00% | 0.05% |
| PMMA 20% WO ₃ | 2.80% | 2.20% | 1.40% | 1.20% | 1.90% |
| PMMA 5% ZnO | 0.21% | 0.00% | 0.00% | 0.00% | 0.05% |
| PMMA 10% ZnO | 0.21% | 0.62% | 0.00% | 0.00% | 0.21% |
| PMMA 20% ZnO | 1.40% | 1.20% | 0.00% | 0.00% | 0.65% |

Table D.5: Experimental Acetone Sorption Data for Customized Polymeric Materials
(formulations #31 through #34; supplemental to Figure 8.19)

| Sample | PANI | ox-PANI | PANI/PPy | ox-PANI/PPy |
|---------------------------------|--------|---------|----------|-------------|
| Trial 1A | 14.54% | 14.54% | 19.12% | 21.12% |
| Trial 1B | 15.14% | 14.54% | 18.73% | 21.12% |
| Trial 2A | 17.33% | 14.79% | 19.42% | 20.04% |
| Trial 2B | 17.95% | 15.00% | 19.62% | 19.83% |
| Trial 3A | 16.91% | 12.32% | 17.75% | 29.09% |
| Trial 3B | 16.70% | 11.72% | 17.95% | 28.28% |
| Trial 4A | 15.15% | 12.97% | 17.37% | 26.55% |
| Trial 4B | 15.56% | 12.77% | 17.37% | 26.35% |
| Average | 16.16% | 13.58% | 18.42% | 24.05% |
| Coefficient of Variation | 7.57% | 9.40% | 4.98% | 16.18% |

Table D.6: Experimental Selectivity Data from ~1 ppm Analyte Gas Mixture ((a) Acetaldehyde, (b) Ethanol, (c) Acetone and (d) Benzene; supplemental to Figure 8.10 and Figure 8.11)

(a) Acetaldehyde Sorption (ppm)

| | Pure | | SnO ₂ -doped | | WO ₃ -doped | | ZnO-doped | |
|-----------------|------|------|-------------------------|------|------------------------|------|-----------|------|
| PANI | 0.19 | 0.16 | 0.20 | 0.16 | 0.21 | 0.21 | 0.20 | 0.16 |
| | 0.16 | 0.13 | 0.13 | 0.15 | 0.23 | 0.21 | 0.15 | 0.15 |
| Average | 0.16 | | 0.16 | | 0.22 | | 0.17 | |
| St. Dev. | 0.02 | | 0.03 | | 0.01 | | 0.02 | |
| PPy | 0.26 | 0.24 | 0.33 | 0.33 | 0.23 | 0.23 | 0.24 | 0.21 |
| | 0.22 | 0.23 | 0.25 | 0.23 | 0.22 | 0.21 | 0.20 | 0.17 |
| Average | 0.24 | | 0.29 | | 0.22 | | 0.21 | |
| St. Dev. | 0.02 | | 0.05 | | 0.01 | | 0.03 | |

(b) Ethanol Sorption (ppm)

| | Pure | | SnO ₂ -doped | | WO ₃ -doped | | ZnO-doped | |
|-----------------|------|------|-------------------------|------|------------------------|------|-----------|------|
| PANI | 0.21 | 0.16 | 0.26 | 0.27 | 0.26 | 0.25 | 0.18 | 0.21 |
| | 0.15 | 0.19 | 0.23 | 0.23 | 0.33 | 0.36 | 0.15 | 0.19 |
| Average | 0.18 | | 0.25 | | 0.30 | | 0.18 | |
| St. Dev. | 0.03 | | 0.02 | | 0.05 | | 0.03 | |
| PPy | 0.25 | 0.28 | 0.35 | 0.33 | 0.24 | 0.28 | 0.31 | 0.34 |
| | 0.31 | 0.29 | 0.23 | 0.25 | 0.24 | 0.22 | 0.22 | 0.22 |
| Average | 0.28 | | 0.29 | | 0.25 | | 0.27 | |
| St. Dev. | 0.03 | | 0.06 | | 0.03 | | 0.06 | |

(c) Acetone Sorption (ppm)

| | Pure | | SnO ₂ -doped | | WO ₃ -doped | | ZnO-doped | |
|-----------------|------|------|-------------------------|------|------------------------|------|-----------|------|
| PANI | 0.17 | 0.13 | 0.19 | 0.16 | 0.30 | 0.30 | 0.18 | 0.16 |
| | 0.15 | 0.13 | 0.19 | 0.14 | 0.31 | 0.31 | 0.15 | 0.14 |
| Average | 0.15 | | 0.17 | | 0.31 | | 0.16 | |
| St. Dev. | 0.02 | | 0.02 | | 0.01 | | 0.02 | |
| PPy | 0.24 | 0.22 | 0.30 | 0.31 | 0.20 | 0.20 | 0.21 | 0.24 |
| | 0.22 | 0.24 | 0.24 | 0.26 | 0.26 | 0.26 | 0.20 | 0.20 |
| Average | 0.23 | | 0.28 | | 0.23 | | 0.21 | |
| St. Dev. | 0.01 | | 0.03 | | 0.03 | | 0.02 | |

(d) Benzene Sorption (ppm)

| | Pure | | SnO ₂ -doped | | WO ₃ -doped | | ZnO-doped | |
|-----------------|------|------|-------------------------|------|------------------------|------|-----------|------|
| PANI | 0.03 | 0.03 | 0.07 | 0.04 | 0.14 | 0.12 | 0.13 | 0.15 |
| | 0.09 | 0.09 | 0.10 | 0.08 | 0.17 | 0.11 | 0.13 | 0.08 |
| Average | 0.06 | | 0.07 | | 0.14 | | 0.12 | |
| St. Dev. | 0.03 | | 0.03 | | 0.03 | | 0.03 | |
| PPy | 0.23 | 0.17 | 0.24 | 0.21 | 0.18 | 0.13 | 0.13 | 0.15 |
| | 0.23 | 0.22 | 0.21 | 0.22 | 0.12 | 0.13 | 0.20 | 0.16 |
| Average | 0.21 | | 0.22 | | 0.14 | | 0.16 | |
| St. Dev. | 0.03 | | 0.01 | | 0.03 | | 0.03 | |

Table D.7: Experimental Selectivity Data from Acetone-Rich Analyte Gas Mixture (containing Acetaldehyde, Ethanol, and Benzene; supplemental to Figure 8.12)

| | Pure PANI | | Pure PPy | |
|---------------------|-----------|------|----------|------|
| Acetaldehyde | 0.11 | 0.11 | 0.07 | 0.04 |
| | 0.10 | 0.08 | 0.10 | 0.09 |
| | 0.12 | 0.10 | 0.09 | 0.09 |
| Average | 0.10 | | 0.08 | |
| St. Dev. | 0.01 | | 0.02 | |
| Ethanol | 0.18 | 0.14 | 0.19 | 0.20 |
| | 0.18 | 0.12 | 0.16 | 0.15 |
| | 0.17 | 0.16 | 0.19 | 0.17 |
| Average | 0.16 | | 0.18 | |
| St. Dev. | 0.02 | | 0.02 | |
| Acetone | 2.35 | 1.67 | 3.49 | 1.77 |
| | 4.07 | 2.37 | 3.92 | 2.77 |
| | 3.61 | 2.41 | 5.22 | 3.05 |
| Average | 2.75 | | 3.37 | |
| St. Dev. | 0.90 | | 1.16 | |
| Benzene | 0.00 | 0.00 | 0.00 | 0.00 |
| | 0.06 | 0.03 | 0.06 | 0.08 |
| | 0.07 | 0.07 | 0.07 | 0.07 |
| Average | 0.04 | | 0.05 | |
| St. Dev. | 0.03 | | 0.04 | |

Table D.8: Experimental Selectivity Data from ~2 ppm Analyte Gas Mixture of Acetone and Acetaldehyde; supplemental to Figure 8.20

| | PANI | | ox-PANI | | PANI/PPy | | ox-PANI/PPy | |
|---------------------|------|------|---------|------|----------|------|-------------|------|
| Acetone | 0.46 | 0.45 | 0.19 | 0.20 | 0.39 | 0.37 | 0.39 | 0.38 |
| | 0.25 | 0.26 | 0.34 | 0.31 | 0.45 | 0.43 | 0.32 | 0.33 |
| | 0.22 | 0.21 | 0.20 | 0.20 | 0.33 | 0.32 | 0.36 | 0.34 |
| Average | 0.31 | | 0.24 | | 0.38 | | 0.35 | |
| St. Dev. | 0.12 | | 0.07 | | 0.05 | | 0.03 | |
| Acetaldehyde | 0.26 | 0.26 | 0.00 | 0.00 | 0.22 | 0.21 | 0.24 | 0.25 |
| | 0.12 | 0.14 | 0.14 | 0.15 | 0.32 | 0.32 | 0.20 | 0.20 |
| | 0.04 | 0.06 | 0.05 | 0.04 | 0.17 | 0.19 | 0.21 | 0.18 |
| Average | 0.15 | | 0.06 | | 0.24 | | 0.21 | |
| St. Dev. | 0.10 | | 0.07 | | 0.07 | | 0.03 | |

Table D.9: Experimental Selectivity Data from ~2 ppm Analyte Gas Mixture of Acetone and Ethanol; supplemental to Figure 8.21

| | PANI | | ox-PANI | | PANI/PPy | | ox-PANI/PPy | |
|-----------------|------|------|---------|------|----------|------|-------------|------|
| Acetone | 0.49 | 0.47 | 0.41 | 0.39 | 0.51 | 0.52 | 0.68 | 0.63 |
| | 0.55 | 0.51 | 0.32 | 0.31 | 0.45 | 0.47 | 0.57 | 0.56 |
| | 0.39 | 0.40 | 0.47 | 0.49 | 0.60 | 0.56 | 0.50 | 0.50 |
| Average | 0.47 | | 0.40 | | 0.52 | | 0.57 | |
| St. Dev. | 0.06 | | 0.07 | | 0.06 | | 0.07 | |
| Ethanol | 0.24 | 0.25 | 0.15 | 0.14 | 0.33 | 0.30 | 0.35 | 0.33 |
| | 0.37 | 0.40 | 0.21 | 0.21 | 0.25 | 0.25 | 0.37 | 0.37 |
| | 0.24 | 0.25 | 0.27 | 0.27 | 0.33 | 0.31 | 0.31 | 0.30 |
| Average | 0.29 | | 0.21 | | 0.30 | | 0.34 | |
| St. Dev. | 0.07 | | 0.06 | | 0.04 | | 0.03 | |

Table D.10: Experimental Selectivity Data from ~2 ppm Analyte Gas Mixture of Acetone and Benzene; supplemental to Figure 8.22

| | PANI | | ox-PANI | | PANI/PPy | | ox-PANI/PPy | |
|-----------------|------|------|---------|------|----------|------|-------------|------|
| Acetone | 0.47 | 0.47 | 0.22 | 0.20 | 0.28 | 0.29 | 0.38 | 0.39 |
| | 0.28 | 0.28 | 0.18 | 0.18 | 0.32 | 0.31 | 0.56 | 0.57 |
| | 0.27 | 0.28 | | | 0.28 | 0.32 | 0.41 | 0.42 |
| Average | 0.34 | | 0.20 | | 0.30 | | 0.46 | |
| St. Dev. | 0.10 | | 0.02 | | 0.02 | | 0.09 | |
| Benzene | 0.30 | 0.29 | 0.20 | 0.18 | 0.23 | 0.20 | 0.38 | 0.37 |
| | 0.25 | 0.21 | 0.20 | 0.19 | 0.22 | 0.20 | 0.53 | 0.52 |
| | 0.22 | 0.22 | | | 0.24 | 0.22 | 0.35 | 0.32 |
| Average | 0.25 | | 0.19 | | 0.22 | | 0.41 | |
| St. Dev. | 0.04 | | 0.01 | | 0.02 | | 0.09 | |

D.3 Comparison of Acetone Sorption Performance

This appendix section provides details about the statistical analysis of acetone sorption. ANOVA Tables allow for the comparison of means, which provides information about whether or not the dopant level has a statistically significant effect on the amount of acetone sorption. First, the 3 dopant levels for each metal oxide (5% vs 10% vs 20%) are compared, and then the ‘best performing’ level of metal oxide in each case is compared to pure polymer.

Table D.11: ANOVA Comparing SnO₂ Dopant Levels in PANI

| Source | SS | df | MS | F _{obs} | F _{2,9,0.05} |
|---------|----------|----|----------|------------------|-----------------------|
| Between | 0.001227 | 2 | 6.14E-04 | 41.51 | 4.26 |
| Within | 0.000133 | 9 | 1.48E-05 | | |
| Total | 0.00136 | 11 | | | |

| Mean Comparison | T _{obs} | LSD |
|-----------------|------------------|-------|
| 5-10 | 6.09 | 1.65% |
| 5-20 | 2.83 | 0.77% |
| 10-20 | 8.92 | 2.42% |

STAT DIFF - use 10%

T_{crit} (9,(0.1/3)) = T_{crit} (9,0.033) = use T_{crit} (9,0.025)

| | |
|---------------------|----------|
| T _{crit} = | 2.262 |
| α' = | 0.073141 |
| LSD = | 0.61% |

Table D.12: ANOVA Comparing WO₃ Dopant Levels in PANI

| Source | SS | df | MS | F _{obs} | F _{2,9,0.05} |
|---------|----------|----|----------|------------------|-----------------------|
| Between | 0.000119 | 2 | 5.97E-05 | 1.49 | 4.26 |
| Within | 0.00036 | 9 | 4.00E-05 | | |
| Total | 0.000479 | 11 | | | |

NO STAT DIFF - use 5% (less MO)

Table D.13: ANOVA Comparing ZnO Dopant Levels in PANI

| Source | SS | df | MS | F _{obs} | F _{2,9,0.05} |
|---------|-------------|----|----------|------------------|-----------------------|
| Between | 0.004320958 | 2 | 2.16E-03 | 281.58 | 4.26 |
| Within | 6.90534E-05 | 9 | 7.67E-06 | | |
| Total | 0.004390011 | 11 | | | |

| Mean Comparison | T _{obs} | LSD |
|-----------------|------------------|-------|
| 5-10 | 3.23 | 0.63% |
| 5-20 | 21.98 | 4.30% |
| 10-20 | 18.75 | 3.67% |

STAT DIFF - use 20%

T_{crit} (9,(0.1/3)) = T_{crit} (9,0.033) = use T_{crit} (9,0.025)

| | |
|---------------------|-----------|
| T _{crit} = | 2.262 |
| α' = | 0.0731406 |
| LSD = | 0.44% |

Table D.14: ANOVA Comparing Pure PANI to 'Best' Doped PANI

| Source | SS | df | MS | F _{obs} | F _{3,12,0.05} |
|---------|----------|----|----------|------------------|------------------------|
| Between | 0.001499 | 3 | 5.00E-04 | 17.09 | 3.49 |
| Within | 0.000351 | 12 | 2.92E-05 | | |
| Total | 0.00185 | 15 | | | |

| Mean Comparison | T _{obs} | LSD |
|-----------------------------------|------------------|-------|
| P-ZnO | 2.47 | 0.95% |
| P-WO ₃ | 3.97 | 1.52% |
| P-SnO ₂ | 2.96 | 1.13% |
| ZnO-WO ₃ | 6.44 | 2.46% |
| ZnO-SnO ₂ | 5.43 | 2.08% |
| WO ₃ -SnO ₂ | 1.01 | 0.38% |

T_{crit} (12,(0.1/6)) = T_{crit} (12,0.0167) = use T_{crit} (12,0.01)

| | |
|---------------------|---------|
| T _{crit} = | 2.681 |
| α' = | 0.05852 |
| LSD = | 1.03% |

Table D.15: ANOVA Comparing SnO₂ Dopant Levels in PPy

| Source | SS | df | MS | F _{obs} | F _{2,9,0.05} |
|---------|----------|----|----------|------------------|-----------------------|
| Between | 0.016219 | 2 | 8.11E-03 | 14.24 | 4.26 |
| Within | 0.005124 | 9 | 5.69E-04 | | |
| Total | 0.021344 | 11 | | | |

| Mean Comparison | T _{obs} | LSD |
|-----------------|------------------|-------|
| 5-10 | 2.60 | 4.38% |
| 5-20 | 2.74 | 4.62% |
| 10-20 | 5.34 | 9.00% |

STAT DIFF - use 10%

T_{crit} (9,(0.1/3)) = T_{crit} (9,0.033) = use T_{crit} (9,0.025)

| | |
|---------------------|----------|
| T _{crit} = | 2.262 |
| α' = | 0.073141 |
| LSD = | 3.82% |

Table D.16: ANOVA Comparing WO₃ Dopant Levels in PPy

| Source | SS | df | MS | F _{obs} | F _{2,9,0.05} |
|---------|----------|----|----------|------------------|-----------------------|
| Between | 0.006879 | 2 | 3.44E-03 | 14.81 | 4.26 |
| Within | 0.00209 | 9 | 2.32E-04 | | |
| Total | 0.008969 | 11 | | | |

| Mean Comparison | T _{obs} | LSD |
|-----------------|------------------|-------|
| 5-10 | 3.60 | 3.88% |
| 5-20 | 1.73 | 1.87% |
| 10-20 | 5.33 | 5.75% |

10% is worst, but no difference between 5% & 20%
therefore use 5% (less MO)

T_{crit} (9,(0.1/3)) = T_{crit} (9,0.033) = use T_{crit} (9,0.025)

| | |
|---------------------|------------|
| T _{crit} = | 2.262 |
| α' = | 0.07314063 |
| LSD = | 2.44% |

Table D.17: ANOVA Comparing ZnO Dopant Levels in PPy

| Source | SS | df | MS | F _{obs} | F _{2,9,0.05} |
|---------|-------------|----|----------|------------------|-----------------------|
| Between | 0.000815705 | 2 | 4.08E-04 | 1.35 | 4.26 |
| Within | 0.0027183 | 9 | 3.02E-04 | | |
| Total | 0.003534005 | 11 | | | |

NO STAT DIFF - use 5%

Table D.18: ANOVA Comparing Pure PPy to 'Best' Doped PPy

| Source | SS | df | MS | F _{obs} | F _{3,12,0.05} |
|---------|----------|----|----------|------------------|------------------------|
| Between | 0.019566 | 3 | 6.52E-03 | 16.80 | 3.49 |
| Within | 0.004658 | 12 | 3.88E-04 | | |
| Total | 0.024224 | 15 | | | |

| Mean Comparison | T _{obs} | LSD |
|-----------------|------------------|-------|
| P-ZnO | 6.79 | 9.46% |
| P-WO3 | 4.71 | 6.56% |
| P-SnO2 | 2.17 | 3.02% |
| ZnO-WO3 | 2.08 | 2.90% |
| ZnO-SnO2 | 4.62 | 6.44% |
| WO3-SnO2 | 2.54 | 3.54% |

T_{crit} (12,(0.1/6)) = T_{crit} (12,0.0167) = use T_{crit} (12,0.01)

| | |
|---------------------|---------|
| T _{crit} = | 2.681 |
| α' = | 0.05852 |
| LSD = | 3.74% |

Table D.19: ANOVA Comparing Customized Materials (from Section 8.2)

| Source | SS | df | MS | F _{obs} | F _{3,28,0.05} |
|---------|----------|----|----------|------------------|------------------------|
| Between | 0.047696 | 3 | 1.59E-02 | 33.30 | 2.95 |
| Within | 0.013368 | 28 | 4.77E-04 | | |
| Total | 0.061065 | 31 | | | |

| Mean Comparison | T _{obs} | LSD |
|--------------------------|------------------|--------|
| PANI vs. ox-PANI | 1.67 | 2.58% |
| PANI vs. PANI/PPy | 1.46 | 2.26% |
| PANI vs. ox-PANI/PPy | 5.10 | 7.89% |
| ox-PANI vs. PANI/PPy | 3.13 | 4.83% |
| ox-PANI vs. ox-PANI/PPy | 6.77 | 10.46% |
| PANI/PPy vs. ox-PANI/PPy | 3.64 | 5.63% |

T_{crit} (28,(0.1/6)) = T_{crit} (28,0.0167) = use T_{crit} (28,0.01)

| | |
|---------------------|---------|
| T _{crit} = | 2.467 |
| α' = | 0.05852 |
| LSD = | 3.81% |